

LHC DESIGN REPORT



VOL. III THE LHC INJECTOR CHAIN

© Copyright CERN, Genève, 2004

Propriété littéraire et scientifique réservée pour tous les pays du monde. Ce document ne peut être reproduit ou traduit en tout ou en partie sans l'autorisation écrite du Directeur général du CERN, titulaire du droit d'auteur. Dans les cas appropriés, et s'il s'agit d'utiliser le document à des fins non commerciales, cette autorisation sera volontiers accordée.

Le CERN ne revendique pas la propriété des inventions brevetables et dessins ou modèles susceptibles de dépôt qui pourraient être décrits dans le présent document ; ceux-ci peuvent être librement utilisés par les instituts de recherche, les industriels et autres intéressés. Cependant, le CERN se réserve le droit de s'opposer à toute revendication qu'un usager pourrait faire de la propriété scientifique ou industrielle de toute invention et tout dessin ou modèle décrits dans le présent document.

Literary and scientific copyrights reserved in all countries of the world. This report, or any part of it, may not be reprinted or translated without written permission of the copyright holder, the Director-General of CERN. However, permission will be freely granted for appropriate non-commercial use.

If any patentable invention or registrable design is described in the report, CERN makes no claim to property rights in it but offers it for the free use of research institutions, manufacturers and others. CERN, however, may oppose any attempt by a user to claim any proprietary or patent rights in such inventions or designs as may be described in the present document.

ISSN 0007-8328
ISBN 92-9083-239-8

CERN-2004-003
15 December 2004

ORGANISATION EUROPÉENNE POUR LA RECHERCHE NUCLÉAIRE
CERN EUROPEAN ORGANIZATION FOR NUCLEAR RESEARCH

LHC Design Report
Volume III The LHC Injector Chain

Editorial Board

M. Benedikt, P. Collier, V. Mertens, J. Poole, K. Schindl

GENEVA
2004

Abstract

The LHC Design Report is presented in three volumes: the first concerns the main ring, the second the infrastructure and general services and the third, the injector chain. The conceptual design was published in 1995 and this report provides a snapshot of the detailed design as it stands at the time of writing – between late 2003 and Autumn 2004.

Editorial Note

The editors would like to express their gratitude to the many authors who contributed to this report.

Volume III – Contents

Part 1 The Proton Pre-Injectors

CHAPTER 1: INTRODUCTION AND SUMMARY	3
REFERENCES	4
CHAPTER 2: BEAM REQUIREMENTS AND FUNDAMENTAL CHOICES	5
2.1 LHC AND SPS REQUIREMENTS	5
2.2 SCHEME TO PRODUCE THE LHC PROTON BEAM IN THE PS COMPLEX	7
2.3 EVOLUTION OF LHC BEAM INTENSITY REQUIREMENTS	9
2.4 OVERVIEW OF HARDWARE CHANGES	10
REFERENCES	11
CHAPTER 3: PROTON LINAC FOR LHC INJECTION	13
3.1 LINAC REQUIREMENTS	13
3.2 PROTON SOURCE OPTIMISATION	13
3.3 REPLACEMENT OF THE COCKROFT-WALTON INJECTOR BY RFQ2	13
3.4 LINAC RF IMPROVEMENTS	14
3.5 BUNCH SHAPE MEASUREMENTS AND OPTIMISATION OF THE LINAC SETTINGS	14
3.6 BEAM TRANSPORT TO THE PSB	14
3.7 LINAC2 PERFORMANCE	15
REFERENCES	16
CHAPTER 4: UPGRADING THE PSB TO 1.4 GeV – POWER SUPPLIES	17
4.1 MAIN MAGNET POWER SUPPLY AND REACTIVE POWER COMPENSATOR	17
4.2 MAIN BENDING MAGNETS “TRIM” POWER SUPPLY	20
4.3 PSB-PS/ISOLDE BEAM-LINE POWER SUPPLIES	21
4.4 PULSED POWER CONVERTERS FOR SEPTUM MAGNETS IN THE PSB-PS LINE	24
REFERENCES	26
CHAPTER 5: BOOSTER ENERGY UPGRADE TO 1.4 GeV – OTHER SYSTEMS	27
5.1 PSB-PS LINE SEPTUM MAGNETS	27
5.2 PSB-PS TRANSFER LINE MAGNETS	30
5.3 FAST KICKER SYSTEMS	33
5.4 MORE POWERFUL WATER AND AIR COOLING SYSTEMS FOR THE PSB	36
REFERENCES	38

CHAPTER 6: BOOSTER RF SYSTEMS	39
6.1 NEW PSB RF CAVITIES H = 1 (0.6 – 1.8 MHz)	39
6.2 CONVERTED PSB H = 2 CAVITIES (1.2 – 3.9 MHz)	41
6.3 PSB BEAM CONTROL MODIFICATIONS	42
REFERENCES	44
CHAPTER 7: BUNCH SPLITTING AND BUNCH ROTATION IN THE PS	45
7.1 NOMINAL BUNCH TRAIN SCHEME	45
7.2 ALTERNATIVE BUNCH TRAINS	48
7.3 REPERCUSSION ON OTHER BEAMS	50
7.4 PS BEAM CONTROLS	51
REFERENCES	53
CHAPTER 8: NEW PS RF CAVITIES	55
8.1 TUNABLE CAVITIES 13.3 MHz – 20 MHz	55
8.2 40 MHz AND 80 MHz CAVITIES	57
REFERENCES	64
CHAPTER 9: TRANSVERSE EMITTANCE CONSERVATION AND MEASUREMENT	65
9.1 EMITTANCE CONSERVATION ISSUES	65
9.2 BEAM DIAGNOSTIC UPGRADES IN VIEW OF LHC BEAMS	67
9.3 OTHER BEAM DIAGNOSTICS	69
REFERENCES	71
CHAPTER 10: PERFORMANCE OF THE PRE-INJECTOR COMPLEX	73
10.1 GENERAL ISSUES	73
10.2 THE CASE OF 25ns BUNCH SPACING	73
10.3 THE CASE OF 75ns BUNCH SPACING	74
10.4 PILOT BUNCH BEAMS	75
10.5 ULTIMATE BEAM	76
REFERENCES	77
Part 2 The SPS as LHC Injector	
CHAPTER 11: INTRODUCTION	81
REFERENCES	82
CHAPTER 12: BEAM PARAMETERS AND REQUIREMENTS	83
12.1 CYCLE AND OPERATIONAL REQUIREMENTS	83
12.2 BEAM PARAMETERS	86
REFERENCES	88

CHAPTER 13: THE SPS INJECTION CHANNEL	91
13.1 INTRODUCTION	91
13.2 SYSTEM PARAMETERS AND LAYOUT	91
13.3 MKP MAGNETS	91
13.4 MKP PULSE FORMING NETWORKS	94
13.5 MKP CONTROL SYSTEM	94
13.6 REPLACEMENT OF INJECTION DUMP MAGNET	95
13.7 OPERATIONAL ISSUES	95
REFERENCES	95
CHAPTER 14: THE SPS DAMPER	97
14.1 RE-ENGINEERING THE SPS DAMPER FOR THE LHC BEAM	97
14.2 HARDWARE PARAMETERS AND ELEMENTS OF THE TRANSVERSE DAMPER	97
14.3 PERFORMANCE WITH LHC BEAM	100
14.4 UNFORESEEN ELEMENTS DURING THE UPGRADE AND FUTURE EVOLUTION	101
REFERENCES	103
CHAPTER 15: PRESERVATION OF THE TRANSVERSE EMITTANCE	105
15.1 INTRODUCTION	105
15.2 THE TT2-TT10 TRANSFER LINE FROM PS TO SPS	105
15.3 STATIC INJECTION ERRORS	105
15.4 STATIC ERRORS AFTER INJECTION	113
15.5 DYNAMIC SOURCES OF EMITTANCE GROWTH	115
15.6 ELECTRON CLOUD EFFECTS IN THE SPS	118
REFERENCES	121
CHAPTER 16: RF SYSTEM AND LONGITUDINAL BEAM DYNAMICS	123
16.1 INTRODUCTION	123
16.2 BEAM DYNAMICS CONSIDERATIONS	124
16.3 HARDWARE MODIFICATIONS	128
16.4 OPERATIONAL RESULTS	135
REFERENCES	136
CHAPTER 17: MACHINE IMPEDANCE ISSUES	137
17.1 INTRODUCTION	137
17.2 THE PUMPING PORT SHIELDING PROGRAMME	139
17.3 THE SEPTUM SHIELDING PROGRAMME	146
17.4 THE KICKER TANK SHIELDING	146
17.5 REMOVAL OF OBSOLETE EQUIPMENT AND VACUUM CHAMBER STANDARDISATION	148
17.6 MEASUREMENTS OF THE EFFECT OF THE IMPEDANCE REDUCTION PROGRAMME WITH BEAM	149
17.7 BEAM INDUCED HEATING	153
REFERENCES	157

CHAPTER 18: EXTRACTION TOWARDS THE LHC	159
18.1 INTRODUCTION	159
18.2 REQUIREMENTS	159
18.3 EXTRACTION EQUIPMENT SYSTEMS	160
18.4 TRAJECTORIES	164
18.5 APERTURE	165
18.6 EFFECTS OF MST AND MSE STRAY FIELD	168
18.7 STABILITY AND FIELD ERRORS	169
18.8 INTERLOCKING AND MACHINE PROTECTION	169
REFERENCES	169
CHAPTER 19: BEAM INSTRUMENTATION	171
19.1 TT2/TT10 INSTRUMENTATION	171
19.2 SPS INSTRUMENTATION	172
19.3 EXTRACTIONS	178
REFERENCES	178
CHAPTER 20: THE INTERNAL BEAM DUMPING SYSTEM	181
20.1 SYSTEM DESCRIPTION	181
20.2 RATIONALE FOR A DESIGN UPGRADE	181
20.3 ASSEMBLY AND TESTING	182
20.4 INSTALLATION AND COMMISSIONING	182
REFERENCES	185
Part 3 The LHC Transfer Lines	
CHAPTER 21: INTRODUCTION	189
21.1 SITUATION	189
21.2 OVERALL DESIGN CONSIDERATIONS	190
21.3 STATUS AND PLANNING	191
REFERENCES	191
CHAPTER 22: TRANSFER LINE OPTICS AND LAYOUT	193
22.1 INTRODUCTION	193
22.2 GEOMETRICAL LAYOUT	193
22.3 OPTICS	194
22.4 TRAJECTORY CORRECTION	200
22.5 BEAM STABILITY AT INJECTION INTO THE LHC	201
22.6 APERTURE	202
22.7 INTERLOCKS AND SURVEILLANCE	204
REFERENCES	204

CHAPTER 23: GENERAL SERVICES	205
23.1 WATER COOLING	205
23.2 TUNNEL VENTILATION	206
23.3 ELECTRICAL DISTRIBUTION	208
23.4 POWER RAIL	209
23.5 MONITORING	209
REFERENCES	209
CHAPTER 24: TRANSFER LINE MAGNETS	211
24.1 INTRODUCTION	211
24.2 MAIN DIPOLES, MBI	211
24.3 MAIN QUADRUPOLES, MQI	212
24.4 OTHER MAGNETS	213
24.5 CORRECTOR MAGNETS	216
24.6 SUMMARY AND CONCLUSION	218
REFERENCES	218
CHAPTER 25: TRANSFER LINE POWERING	219
25.1 INTRODUCTION	219
25.2 GENERAL RUNNING	219
25.3 POWER CONVERTER REFURBISHMENT	220
25.4 OVERVIEW OF TI 2	220
25.5 OVERVIEW OF TI 8	220
25.6 GENERAL PERFORMANCE	221
25.7 POWER CONVERTER TOPOLOGIES	221
25.8 DISTINCTIVE FEATURES OF THE TI 8 MBI POWER CONVERTERS	224
25.9 POWER CONSUMPTION AND LOSSES	225
25.10 CONTROLLING THE POWER SUPPLIES FOR TI 2 & TI 8	225
REFERENCES	226
CHAPTER 26: BEAM INSTRUMENTATION	227
26.1 INTRODUCTION	227
26.2 POSITION MEASUREMENT	227
26.3 INTENSITY MEASUREMENT	228
26.4 BEAM-LOSS MEASUREMENT	228
26.5 BEAM-PROFILE MEASUREMENT	229
REFERENCES	231
CHAPTER 27: TRANSFER LINE DUMPS, SAFETY STOPPERS AND COLLIMATORS	233
27.1 EXTERNAL BEAM DUMPS (TED)	233
27.2 EXTERNAL SAFETY BEAM STOPPER (TBSE)	234
27.3 THE TRANSFER LINE COLLIMATION SYSTEM (TCDI)	235
REFERENCES	237

CHAPTER 28: VACUUM SYSTEM FOR LHC TRANSFER LINES TI 2 AND TI 8	239
28.1 INTRODUCTION	239
28.2 VACUUM REQUIREMENTS AND BASIC PRINCIPLE	239
28.3 LAYOUT AND PRESSURE PROFILE	239
28.4 VACUUM COMPONENTS AND VACUUM CONTROL SYSTEM	240
CHAPTER 29: ACCESS AND SAFETY	243
29.1 ACCESS SYSTEMS	243
29.2 SAFETY SYSTEMS	243
29.3 TI 2 ACCESS AND SAFETY	243
29.4 TI 8 ACCESS AND SAFETY	244
CHAPTER 30: INTEGRATION AND INSTALLATION	247
30.1 INTEGRATION ISSUES	247
30.2 TRANSPORT AND INSTALLATION SYSTEM	249
REFERENCES	253
CHAPTER 31: COMMISSIONING	255
31.1 INTRODUCTION	255
31.2 HARDWARE COMMISSIONING OF TI 8	255
31.3 COLD CHECKOUT OF TI 8	255
31.4 BEAM COMMISSIONING OF TI 8	257
REFERENCES	259
Part 4 The LHC Ion Injector Chain	
CHAPTER 32: INTRODUCTION	263
REFERENCES	264
CHAPTER 33: ION BEAM REQUEST AND OVERVIEW	265
33.1 LHC BASELINE BEAM REQUEST	265
33.2 INJECTOR CHAIN: OVERVIEW, LIMITATIONS	266
33.3 EARLY LEAD ION OPERATION SCHEME	269
33.4 INJECTOR CHAIN, OTHER VARIANTS	270
33.5 FUTURE OPTION: LIGHTER IONS	271
REFERENCES	272
CHAPTER 34: SOURCE AND LINAC3	273
34.1 SOURCE UPGRADE (14 – 18 GHz, 100 TO 200 μ A)	273
34.2 LINAC REPETITION RATE TO 5 Hz	274
34.3 ENERGY RAMPING CAVITY	275
34.4 SHIELDING	275
34.5 CONTROLS	276
REFERENCES	276

CHAPTER 35: LEIR	277
35.1 OVERVIEW	277
35.2 LAYOUT AND BEAM DYNAMICS	278
35.3 INJECTION AND EXTRACTION	284
35.4 INJECTION/EXTRACTION SEPTA	287
35.5 INJECTION/EXTRACTION KICKERS AND BUMPERS	291
35.6 ELECTRON COOLING	294
35.7 ACCELERATION AND FEEDBACK SYSTEMS	297
35.8 POWER CONVERTERS	301
35.9 VACUUM SYSTEM	312
35.10 INSTRUMENTATION	318
35.11 CONTROL SYSTEM	321
35.12 INFRASTRUCTURE, SAFETY AND RADIATION PROTECTION	323
35.13 LEIR PARAMETER LIST	326
REFERENCES	327
CHAPTER 36: LINAC3-LEIR-PS LINES	329
36.1 OVERVIEW AND LAYOUT	329
36.2 OPTICS	329
36.3 MAGNETS	333
36.4 POWER CONVERTERS	335
36.5 INSTRUMENTATION	335
REFERENCES	336
CHAPTER 37: THE PS AND TRANSFER LINE TO SPS	337
37.1 INJECTION: TRAJECTORIES AND OPTICS	337
37.2 NEW PULSED INJECTION SEPTUM	340
37.3 UPGRADED INJECTION KICKER AND BUMPERS	341
37.4 PS RF MANIPULATIONS FOR LEAD IONS	342
37.5 PS-SPS LINE STRIPPING WITH LOW-BETA INSERTION	345
37.6 STRIPPING IN THE PS-SPS LINE: HARDWARE ASPECTS	348
REFERENCES	349
CHAPTER 38: SPS	351
38.1 INJECTION	351
38.2 ACCELERATION AND RECOMBINATION OF BUNCHLETS	352
38.3 OTHER ISSUES	355
REFERENCES	356

CHAPTER 1

INTRODUCTION AND SUMMARY

CERN's Large Hadron Collider (LHC) [1] will be supplied with protons from the injector chain Linac2 - Proton Synchrotron Booster (PSB) - Proton Synchrotron (PS) - Super Proton Synchrotron (SPS), shown in Fig. 1.1. These accelerators were upgraded to meet the very stringent needs of the LHC: many high intensity proton bunches (2808 per LHC ring) with small transverse and well defined longitudinal emittances.

The main challenges for the PS complex are (i) the unprecedented transverse beam brightness (intensity/emittance), almost twice that which the PS was able to produce in the past and (ii) the production of a bunch train with the LHC spacing of 25 ns before extraction from the PS (25 GeV).

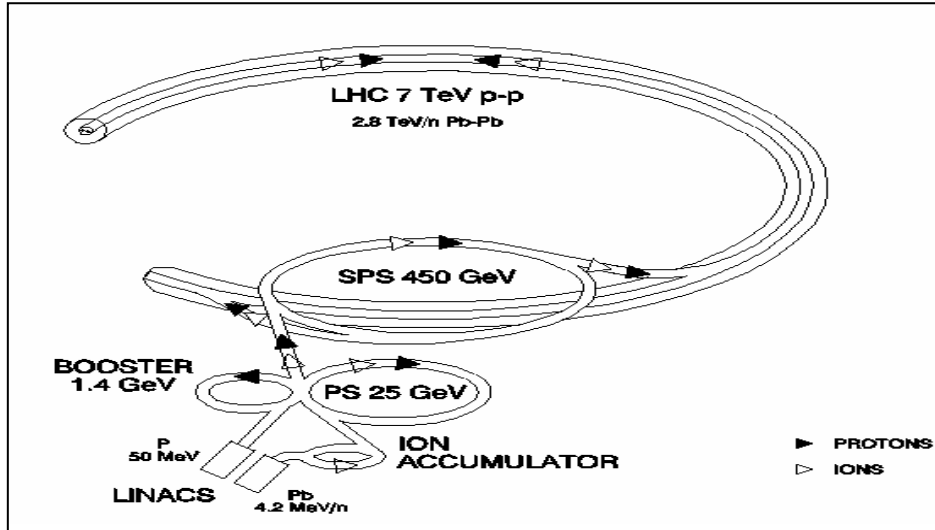


Figure 1.1: The LHC injector complex.

Initially, a scheme requiring new Radio Frequency (RF) harmonics of $h = 1, 2$ in the PSB and $h = 8, 16, 84$ in the PS, an increase of the PSB energy from 1 to 1.4 GeV and two-batch filling of the PS was proposed [2]. After a partial test of the scheme's main ingredients in 1993 [3], a project to convert the PS complex for LHC operation was started in 1995 and completed in 2000 [4]. Major parts of this project were

- (i) new $h = 1$ RF systems in the PSB,
- (ii) upgrading the PSB main magnet supply from 1 GeV operation to 1.4 GeV,
- (iii) new magnets, septa, power supplies, kicker pulsers for the PSB-PS beam transfer,
- (iv) new 40 and 80 MHz RF systems in the PS,
- (v) beam profile measurement devices with improved resolution.

About one quarter of the project resources (funds, manpower) was provided by TRIUMF under the Canada-CERN Co-operation Agreement on the LHC.

During first beam tests with the complete scheme in 1999, difficulties for producing the LHC bunch train at PS extraction were encountered. The problem was an instability of the coasting beam after adiabatic debunching just before recapture with the new 40 MHz RF system. As a consequence the final bunch length at extraction was too large (>5 ns) to fit the SPS 200 MHz RF system. A modified scheme [5], avoiding debunching in the PS while changing the number of bunches by multiple bunch splitting operations was proposed. This method is based on using RF harmonics 7, 21, 42 and 84 in the PS and required the installation of an additional 20 MHz RF system in the PS.

An overview of the PS conversion as well as the beam dynamics issues involved are presented in Chap. 2. A comparison of the initial and modified schemes for producing the LHC bunch train in the PS complex is made and the most important side effects of the new scheme are outlined. Recent beam tests indicate that

assumptions on beam losses throughout the injector chain have been too optimistic. A beam loss inventory is given and the consequences of increased losses are discussed.

Measures that led to a significant increase of proton beam intensity (to ~ 180 mA) and brilliance from Linac2 are outlined in Chap. 3.

Increasing the beam energy of the PSB by 40% (momentum by 26%) to 1.4 GeV called for renewal or overhaul of several systems and components, such as the main magnet supply (including transformers and chokes), the PSB-PS 4-level recombination and transfer line magnets and their DC or pulsed power supplies, the pulsed magnetic septa and fast kicker pulsing systems and the water and air cooling system to tackle the increased power dissipation. Chap. 4 deals with the new or upgraded power supply systems, whereas new magnets, septum magnets, kicker pulsers and water cooling are discussed in Chap. 5.

Operating each of the four PSB rings with just one bunch opened up the way for PS two-batch filling. The new $h = 1$ and converted $h = 2$ cavities as well as the digital beam control systems dealing with the new harmonic numbers in the PSB ($h = 1, 2$) are presented in Chap. 6.

The multiple bunch splitting scheme in the PS, for establishing the LHC bunch train structure, is described in Chap. 7 where all PS beam control modifications are summarised. Chap. 7 also touches on the repercussions of the new RF harmonics in PSB and PS on other operational beams of the complex.

Short (< 4 ns) bunches with 25 ns spacing are produced in the PS by fixed-frequency RF cavities (one at 40 MHz with 300 kV and two at 80 MHz with 300 kV each) which have to withstand the beam loading of much higher intensity beams without perturbing them. The cavities and their driving systems are dealt with in Chap. 8 where the new 13.3 - 20 MHz RF system required for the multiple bunch splitting is also described.

The transverse emittances of the LHC beam have to be maintained at their unusually small size throughout the injector chain. Small amounts of mis-steering and mismatch between the accelerators of the chain, virtually negligible for normal operation, are becoming increasingly important and their effect has to be measurable, calling for high-resolution beam profile monitors. Moreover, various position measurement systems were modified to deal with the new harmonics in the circular machines and to allow bunch-by-bunch observation in TT2. The new or modified diagnostic devices are summarised in Chap. 9 which also deals with work on an injection oscillation damper for the PS.

Finally, Chap. 10 summarises the performance of the PS complex as LHC injector and addresses open issues concerning the ultimate beam.

REFERENCES

- [1] P. Lefèvre, T. Petterson (Editors), *The Large Hadron Collider, Conceptual Design*, CERN/AC/95-05(LHC), Geneva, 1995.
- [2] F. Blas et al., *Conversion of the PS complex as LHC proton pre-injector*, Proc. PAC '97, p. 973, Vancouver, 1997.
- [3] The PS Staff, reported by K. Schindl, *Partial test of the PS complex as LHC proton pre-injector*, Proc. EPAC '94, p. 500, London, 1994.
- [4] M. Benedikt (Editor), *The PS Complex as Proton Pre Injector for the LHC – Design and Implementation Report*, CERN 2000-003, Geneva, 2000.
- [5] R. Garoby, *Status of the nominal proton beam for LHC in the PS*, Proc. of the Chamonix Workshop on LEP-SPS Performance, pp. 94-98, Chamonix, 1999.

CHAPTER 2

BEAM REQUIREMENTS AND FUNDAMENTAL CHOICES

2.1 LHC AND SPS REQUIREMENTS

The figure of merit for colliders such as the LHC is the luminosity

$$L = \frac{k_b N_b^2 f_{\text{rev}} \gamma}{4\pi \epsilon_n \beta^*} ,$$

with k_b the number of bunches per ring, N_b the number of protons per bunch, f_{rev} the revolution frequency, ϵ_n the normalised rms transverse beam emittance (same in both planes), β^* the beta-function at the interaction point. L is proportional to the number of events per second and thus has to be maximised. But more conditions are to be satisfied:

- (i) the beam emittance has to fit into the small aperture of the superconducting LHC magnets;
- (ii) the total intensity $k_b \cdot N_b$ is limited by the thermal energy produced by synchrotron radiation which must be absorbed by the cryogenic system;
- (iii) the beam-beam effect – proportional to the transverse beam brightness N_b/ϵ_n – causing a spread in betatron tunes (“footprint”) when the beams are colliding has to be kept below a certain limit;
- (iv) the space-charge limit in the injectors, which also scales with N_b/ϵ_n .

Conflicting requirements also determine the longitudinal emittance ϵ_L which has to be small at injection (small $\Delta p/p$ to ease beam transport from the SPS through the two ~ 2.5 km long lines), but larger at collision to avoid transverse emittance blow-up by intra-beam scattering.

An elaborate optimisation procedure, taking into account these boundary conditions, has resulted in the LHC beam parameter set [1] compiled in Tab. 2.1. The “ultimate” performance level corresponds to the LHC beam-beam limit, whereas the “nominal” performance combines high luminosity with operational margin. Moreover, during the first year of physics running the LHC will be operated at a much lower intensity and luminosity level.

Table 2.1: LHC nominal and ultimate proton beam parameters.

		Injection	Collision	
Energy	[GeV]	450	7000	
Luminosity	nominal ultimate	[cm ⁻² s ⁻¹]	10 ³⁴ 2.5 × 10 ³⁴	
Number of bunches			2808	3564 bunch places
Bunch spacing	[ns]		24.95	
N_b intensity per bunch	nominal ultimate	[p/b]	1.15 × 10 ¹¹ 1.70 × 10 ¹¹	
Beam current	nominal ultimate	[A]	0.58 0.86	
ϵ_n (transverse emittance, rms, normalised), nominal & ultimate	[μm]	3.5	3.75	Emittances equal in both planes, small blow-up allowed in LHC
Longitudinal emittance, total	[eVs]	1.0	2.5	Controlled blow-up during accel.
Bunch length, total (4σ)	[ns]	1.7	1.0	has to fit into 400 MHz buckets
Energy spread, total (4σ)	[10 ⁻³]	1.9	0.45	

Much like the PS complex, the SPS is an “old” machine and was not optimised for its future function as LHC injector. The intensity the SPS is able to accelerate ($\sim 4 \times 10^{13}$ protons per cycle, particularly difficult if concentrated on a fraction of its circumference) limits the number of PS pulses per SPS cycle to a maximum of four. The momentum spread acceptance of the PS-SPS line (TT2, TT10) is about $\pm 0.2\%$ in $\Delta p/p$, while the total bunch length has to be below 4 ns to fit into the buckets of the SPS 200 MHz accelerating system, meaning a longitudinal emittance of 0.35 eVs per PS bunch. While the longitudinal emittance will be increased (hopefully in a controlled way) from 0.35 to 1 eVs during SPS acceleration, there is little margin for transverse emittance blow-up in this machine.

The LHC and SPS requirements define the beam characteristics at PS extraction, summarised in Tab. 2.2 (assuming 100% transmission from PS to LHC). The filling sequence PS-SPS-LHC is sketched in Fig. 2.1.

Table 2.2: Beam characteristics at extraction from the PS.

Proton kinetic energy	[GeV]	25	
Number of PS batches to fill SPS		3 or 4	Limited by SPS peak intensity
PS repetition time	[s]	3.6	PS 2-batch filling from PSB
Number of bunches in PS		72	$h=84$, 12 empty buckets for extraction kicker
Bunch spacing	[ns]	24.97	
Number of protons/bunch N_b – <i>ultimate nominal</i>		1.70×10^{11} 1.15×10^{11}	100% transmission assumed from PS to LHC
Transverse normalised rms emittance ϵ_n	[μm]	3.0	
Bunch area (longitudinal emittance) ϵ_L	[eVs]	0.35	
Bunch length (total)	[ns]	4	Limited by SPS 200 MHz buckets
Relative momentum spread $\Delta p/p$ total (4 σ)		0.004	Limited by TT2-TT10 acceptance

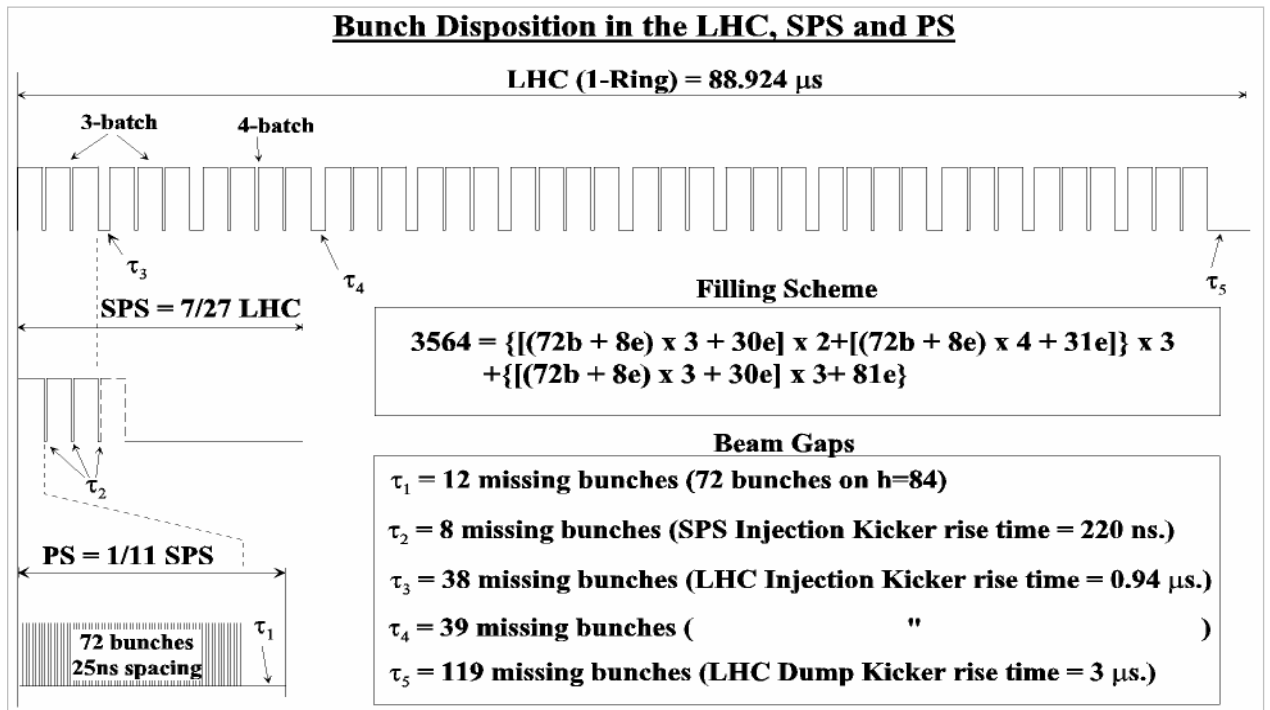


Figure 2.1: Proton bunches in the PS, SPS and one LHC ring. Note the partial filling of the SPS (3/11 or 4/11) and the voids due to kicker rise-time. One LHC ring is filled in ~ 3 min.

2.2 SCHEME TO PRODUCE THE LHC PROTON BEAM IN THE PS COMPLEX

2.2.1 Space charge issues in PSB and PS

While the intensity required for the LHC is well within the capabilities of the PS complex, the transverse emittance is very small, yielding a beam brightness N_b/ϵ_n about 1.6 times higher than was hitherto achievable. Low-energy synchrotrons suffer from space charge which can be quantified by the tune shift

$$\Delta Q \propto -\frac{N}{(\beta\gamma^2)_{\text{rel}} \epsilon_n},$$

where N is the number of protons in the synchrotron. This tune shift would become unmanageable in the PSB at 50 MeV (almost -1) and in the PS at 1 GeV. The measures to overcome this fundamental limitation are (i) filling the PS with two consecutive PSB pulses, thus significantly reducing the intensity per pulse and thus ΔQ at 50 MeV; (ii) raising the PS injection energy from 1 to 1.4 GeV, thus decreasing ΔQ in the PS by a factor 1.5, $(1/\beta\gamma^2)_{\text{rel}}$.

The four PSB rings, $\frac{1}{4}$ of the PS circumference each, are normally ejected and transferred sequentially to fill the PS in one go, e.g. for the SPS Physics beam with two bunches per ring (5 bunches per ring until 1997). However, with only one bunch per ring, up to four bunches can be squeezed into $\sim\frac{1}{2}$ of the PS, thus leaving space for a second PSB batch 1.2 seconds later. Fig. 2.2 shows the standard filling scheme for SPS physics and the LHC two batch filling scheme where three and three (or alternatively four and two) bunches from the PSB are transferred to the PS on consecutive PSB cycles.

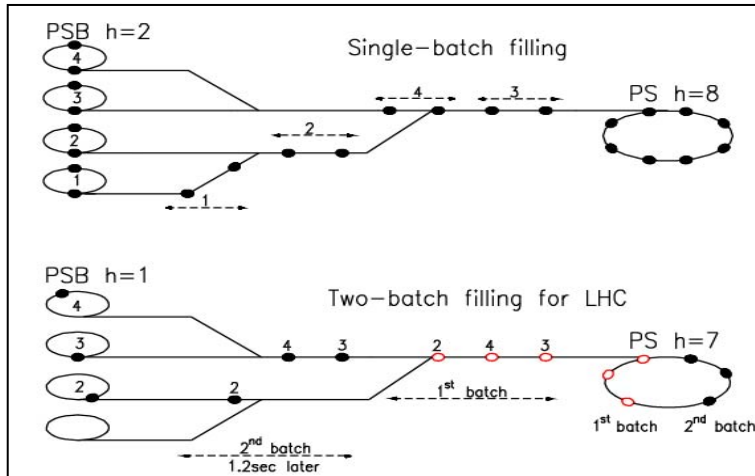


Figure 2.2: PSB-PS transfer: single-batch filling for SPS physics (top), two-batch filling for LHC (bottom).

To operate with RF harmonic 1 instead of the former 5, the PSB is now equipped with new RF cavities featuring a frequency range of 0.6 to 1.7 MHz and the former $h = 5$ systems have been modified to work on $h = 2$. Also the PS has to cope with new RF harmonics – an opportunity to equip both machines with Digital Beam Control.

To raise the PSB ejection and PS injection energy from 1 to 1.4 GeV (+26.3% in momentum), the PSB main power supply has been upgraded to cope with the higher magnet currents. The elements of the PSB-PS beam transport have to provide higher field levels, which meant renewal of most of the magnets (dipoles, quadrupoles, septa, kickers) and their power supplies.

2.2.2 LHC Bunch Train Generation in the PS

Initial debunching-rebunching scheme

The initially proposed scheme was for the injection of two times four PSB bunches (two PSB batches) on harmonic 8 in the PS. The bunches were then split in two and accelerated on harmonic 16 to 25 GeV. The

25 ns bunch spacing was achieved by debunching and rebunching the beam on $h=84$, followed by bunch rotation with the new 40 MHz ($h=84$) and 80 MHz RF systems. Out of the 84 bunches, 81 were transferred to the SPS, 3 were supposed to be lost due to the PS extraction kicker rise-time.

However, when testing the scheme in 1999, microwave instabilities due to the longitudinal impedance of the PS blew up the momentum spread during the delicate debunching process: at nominal intensity there was no way to make the bunches shorter than 5 ns. The decision was then taken to change to a newly proposed scheme using multiple splitting techniques [2] which avoided this instability, provided a gap without particles for the rise-time of the ejection kicker and introduced flexibility in the bunch train time structure.

Multiple splitting scheme

For the generation of the LHC bunch train with 25 ns spacing in the PS, a multiple splitting scheme is employed. Six PSB bunches (two PSB batches of 3 + 3 or 4 + 2 bunches) are captured on harmonic 7 in the PS. The bunches are then split in three at 1.4 GeV using appropriate amplitude and phase parameters on three groups of cavities operating on harmonics 7, 14 and 21, respectively [3]. Bunched on harmonic 21, the beam is accelerated up to 25 GeV where each bunch is split twice in two using the process which has been demonstrated in regular operation. The new 20 MHz and 40 MHz RF systems are required at that stage. Finally each of the six original bunches has been split in 12 and 72 bunches are created on harmonic 84. The 80 MHz systems finally shorten the bunches to ~ 4 ns so as to fit into the SPS 200 MHz buckets. Injecting only 6 bunches, the final bunch train contains 72 bunches and 12 consecutive empty buckets, providing a gap of ~ 320 ns (13×25 ns) for the rise-time of the ejection kicker. The change from the debunching-rebunching scheme to the multiple splitting scheme required the installation of a 20 MHz RF system that was not part of the “PS for LHC” conversion project [4].

The new scheme, though indispensable for longitudinal beam dynamics, has one drawback: 72 LHC bunches are produced from 6 PSB bunches (instead of initially 84 from 8). Therefore the intensity per PSB bunch and consequently, due to the fixed emittance, the beam brightness have to be 14% higher than with the debunching-rebunching scheme. The consequence is that the ultimate beam, which was already at the limit of the achievable brightness, can no longer be provided by the PSB due to the increase in intensity (2.04×10^{12} , 2.5 μm). Initially it was thought that by using up parts of the PS emittance budget and with some more experience one could still achieve the required beam characteristics – this possibility has now been ruled out following the observation of beam losses (Sec. 2.3). Alternative ways to produce the ultimate beam are sketched in Sec. 10.5. A comparison of debunching-rebunching and multiple splitting schemes is given in Tab. 2.3 (the intensities quoted assume 100% transmission from PSB to LHC).

Table 2.3: PS complex operation for filling LHC: debunching-rebunching and multiple splitting.

	Debunching-rebunching	Multiple splitting
No. of bunches per PSB ring	1	1
No. of PSB cycles per PS cycle	2	2
No. of bunches from PSB per PS cycle	8	6
h at PS injection	8	7
Bunch splitting at 1.4 GeV	1=>2	1=>3
h from 1.4 GeV to 25 GeV	16	21
No. of bunches from 1.4 GeV to 25 GeV	16	18
Gymnastics at 25 GeV	Debunching-rebunching	Double bunch splitting (1=>4)
h at PS extraction	84	84
No. of bunches to SPS per PS cycle	81 (3 bunches lost due to PS extraction kicker rise time)	72 (empty bucket conserved, provides 320 ns for kicker)
PS intensity at 1.4 GeV for 1.15×10^{11} protons per LHC bunch (“nominal”)	9.66×10^{12}	8.28×10^{12}
PSB intensity per ring (“nominal”)	1.21×10^{12}	1.38×10^{12}
PS intensity at 1.4 GeV for 1.7×10^{11} protons per LHC bunch (“ultimate”)	14.28×10^{12}	12.24×10^{12}
PSB intensity per ring (“ultimate”)	1.79×10^{12}	2.04×10^{12}

2.3 EVOLUTION OF LHC BEAM INTENSITY REQUIREMENTS

Since the definition of nominal and ultimate LHC beam intensities in 1993 [5], several changes were made, due to LHC design parameter modifications and also the change of the bunch train production scheme in the PS. In addition, the initial intensity requirements assumed zero beam losses or 100% efficiency from capture in the PSB throughout the complete injector chain (and also the LHC), which turned out to be too optimistic. To compensate for these losses and design changes, the injectors have to provide more intensity to keep the LHC luminosity at the required level.

Any increase of beam intensity also increases the brightness of the beam that has to be produced by the PSB because of the fixed transverse emittance budget. It is therefore mandatory to review the required intensities since the brightness that can be provided by the PSB is limited by space charge effects at injection. Of course the space charge effects at PS injection flat bottom are increased by the same factor due to the bunch to bucket transfer between PSB and PS.

The different ingredients leading to an intensity increase on the LHC side were:

- LHC crossing angle change from 200 to 285 μrad (1995): requiring an intensity increase by a factor 1.10.
- LHC β^* change from 0.5 to 0.55 m (2003): requiring an intensity increase by 1.05.

On the PS side:

- The change from debunching-rebunching to multiple splitting scheme (2000): requiring an intensity increase by 1.14.

It is important to note that compensation of crossing angle and β^* changes is only required for the nominal beam and not for the ultimate, where the intensity is fixed by the LHC beam-beam limit. The factor 1.14 to compensate for the scheme change in the PS is required for both beams.

Extensive beam tests with nominal and ultimate intensities allowed a beam loss inventory to be established. With the present performance an overall efficiency of 0.85 is realistic for the nominal beam whereas the figure for the ultimate beam is only around 0.8. The major part of the beam losses ($\sim 10\%$ for nominal and $\sim 15\%$ for ultimate beams) appears at start of acceleration in the SPS; studies to understand the mechanism leading to these losses and hopefully to reduce them are being made at the time of writing.

Tab. 2.4 compares PSB bunch intensities estimated in 1993 and 2003 to obtain the nominal and ultimate beams in the LHC, taking into account the observed losses and all modifications to the LHC and the injectors.

Table. 2.4: PSB beam intensities required for nominal and ultimate beams in 1993 and 2003.

	1993	2003	Correction factor
LHC nominal bunch	1.00×10^{11}	1.15×10^{11}	1.10·1.05
PSB nominal bunch	10.50×10^{11}	16.25×10^{11}	1.10·1.05·1.14/0.85
LHC ultimate bunch	1.70×10^{11}	1.70×10^{11}	1.00
PSB ultimate bunch	17.85×10^{11}	25.50×10^{11}	1.14/0.80

In conclusion it can be stated that the nominal beam is well within reach but the intensity and brightness required from the PSB are moving closer to what was defined as ultimate beam in 1993. There is no longer a comfortable margin left over from the emittance budget, which will make operation more critical. In fact, the ultimate beam is currently not feasible in the PSB. Potential solutions are sketched in Chap. 10.

2.4 OVERVIEW OF HARDWARE CHANGES

The project to convert the PS complex to an LHC pre-injector was launched in 1995, based on a project proposal which included budget and manpower estimates [5]. Also in 1995, Canada offered in-kind contributions for the LHC machine (via TRIUMF/Vancouver) which soon developed into an efficient collaboration, with TRIUMF providing ~1/4 of the resources needed for the PS upgrading project. Major systems and their hardware components are listed in Tab. 2.5, together with Canadian contributions and installation dates. The project was essentially finished by 2001.

Table 2.5: Major hardware components of the “PS Conversion for LHC” project.

System	Components	Installation	TRIUMF contribution	Comments
Linac	Inter-tank beam shape monitors (2)	1999, 2000		study very high intensities (180 mA)
50 MeV line	laminated quadrupoles	1997	two magnets	correct optics for protons and ions
PSB RF $h=1$	RF cavities “C02” (4), tune range 0.6-1.7 MHz	1998	ferrites, HV power supplies	one cavity per ring
PSB RF $h=2$	RF cavities “C04” (4), tune range 1.2-3.9 MHz	1998		bunch flattening and/or splitting
PSB main magnet supply	double-transformers (5), VAR compensator, quadrupole trim supplies, control circuitry	1998	all transformers, VAR compensator	26% increase of magnet current on PSB main magnets
PSB water cooling	closed-circuit demineralised water	2000		copes with more heating at 1.4 GeV
PSB instrumentation	fast wire scanners (4 rings, H+V, + 2 spares)	2001-2003	10 units, design and fabrication.	standard PS beam profile meas. device
	Q-measurement: electronics, kicker pulser	1999/2000		all four beams are kicked
PSB-PS beam transport	ejection/recombination kicker pulsers (6)	1998, 1999		26% more kick to cope with 1.4 GeV
	ejection, recombination, PS injection septa + power supplies (8)	1997, 1998, 1999		half-sine-wave pulses of 3.5 ms
	15 laminated magnets (vertical bending magnets, quadrupoles, correction dipoles)	1997, 1998	all 15 magnets all (+spare) power supplies	allow pulse-to-pulse modulation between 1.4 GeV (PS) and 1 GeV
PS RF $h=84$	300 kV fixed-frequency (40 MHz) cavities (1+1 spare installed) “C40”	1996, 1999	model studies, tuners, higher-order-mode dampers, HV supplies	for generating LHC bunch spacing of 25 ns at 25 GeV
PS RF $h=168$	300 kV fixed-frequency (80 MHz) cavities (2+1 spare installed) “C80”	1998, 1999		for shortening the LHC bunches to 4 ns
PS transverse feedback	new amplifiers, deflector, electronics	2003-2005		damping injection oscillations and instabilities
PS instrumentation	wide-band position monitors (2) in line TT2	1998		bunch-by-bunch position measurement
PS RF $h=28, 42$	15 kV dual frequency 13.3 or 20 MHz cavity, (1+1 spare installed) “C20”	2003-2004		for various bunch splitting operations in the PS

REFERENCES

- [1] P. Lefèvre, T. Petterson (Editors), *The Large Hadron Collider, Conceptual Design*, CERN/AC/95-05(LHC), Geneva, 1995.
- [2] R. Garoby, *Status of the nominal proton beam for LHC in the PS*, Proc. of the Chamonix Workshop on LEP-SPS Performance, pp. 94-98, Chamonix, 1999.
- [3] R. Garoby, S. Hancock, J.-L. Vallet, *Demonstration of bunch triple splitting in the CERN PS*, 7th EPAC Vienna, 2000.
- [4] M. Benedikt (Editor), *The PS Complex as Proton Pre Injector for the LHC – Design and Implementation Report*, CERN 2000-003, Geneva, 2000.
- [5] K. Schindl, *Conversion of the PS complex as LHC proton pre-injector: Project proposal*, PS/DI/Note 94-17, Geneva, 1994.

CHAPTER 3

PROTON LINAC FOR LHC INJECTION

3.1 LINAC REQUIREMENTS

Linac2 has been the primary source of protons for the CERN accelerator complex for the last 25 years and over the past few years the machine performance has been steadily improved in anticipation of the demands that will be made on it in the LHC era [1]. The nominal LHC requirement will be for a beam of 180 mA in 30 μ s at the entrance of the PSB, i.e. 20% higher proton current from the Linac2 than the design value of 150 mA and inside the same emittances. Fig. 3.1 shows the increase of the Linac2 operational current and of the high intensity test current delivered to the PSB over recent years, with the corresponding steps taken. A description of these improvements is presented in the following paragraphs.

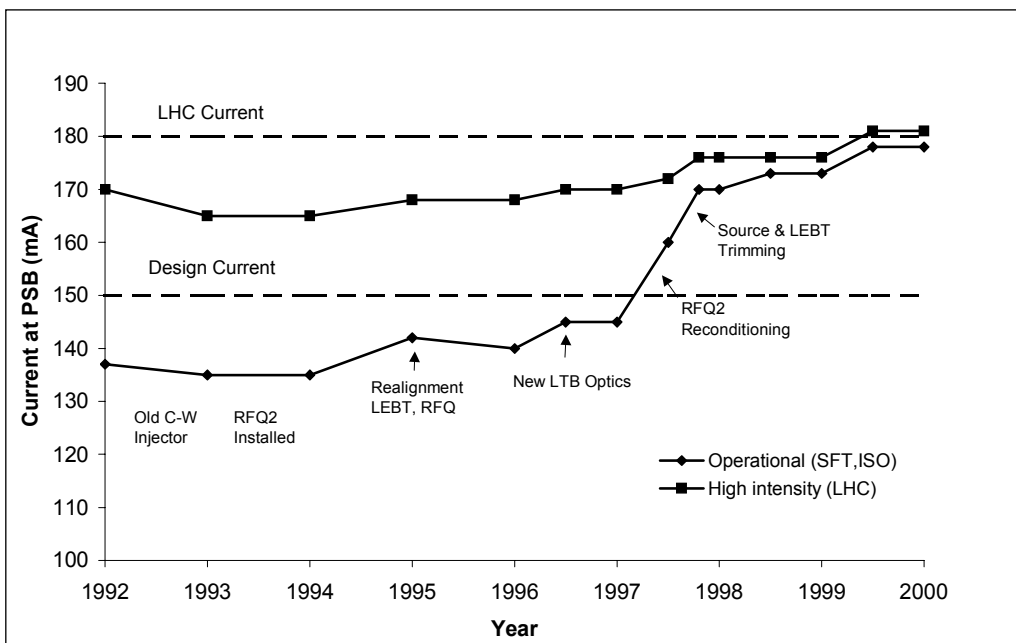


Figure 3.1: Evolution of Linac2 operational and high intensity beam current measured at PSB entry.

3.2 PROTON SOURCE OPTIMISATION

The total beam from the Linac2 duoplasmatron source is around 350 mA with a hydrogen consumption of about 4 ml/min. The gauge pressure of approximately 3.5×10^{-5} mbar in the source housing falls to the mid 10^{-7} level in the RFQ. With this relatively high pressure in the beam transport section between source and RFQ neutralisation is very high, making the effective focusing strength of the solenoids in the line highly dependent on the gas flow from the source. Once this process was understood, gains in intensity of around 10% were obtained by iterative re-optimisation of source parameters and solenoid focusing strengths.

3.3 REPLACEMENT OF THE COCKROFT-WALTON INJECTOR BY RFQ2

The main intensity bottlenecks in the original layout of Linac2 were the space charge limited 750 keV Cockcroft-Walton injector with its long transfer line to the linac. In 1993 they were replaced by a new 90 kV platform and a 750 keV RFQ (RFQ2) designed for 200 mA current with compact (<1 m long) beam matching lines. After the RFQ installation, the linac was immediately able to provide 135 mA for the normal operation and a beam of 165 mA with standard emittances for high intensity studies [2].

A first increase in the RFQ2 current was obtained in 1995 with a careful realignment of the system. After a complete set of source emittance measurements, the source was re-aligned on the measured beam axis instead of the mechanical axis and then the solenoids between the source and the RFQ were also aligned on their magnetic axes [3]. After this, the RFQ could be properly aligned and its transmission increased by about 5%. The number of RF sparks (induced by ions hitting the electrodes) was also reduced.

The next step towards higher RFQ current was a slow re-conditioning of the RFQ cavity during operation at the linac. In order to accelerate a space charge dominated beam of 200 mA, the RFQ was designed for a high electrode voltage, 178 kV, resulting in a peak surface electric field of more than twice the Kilpatrick limit [4]. The operation at this high field level was initially plagued by a high RF sparking rate and the RFQ could only operate reliably up to 92% of the design level which resulted in a 10% reduction in beam transmission. The origin of the breakdowns was finally traced to back-streaming oil vapours from a defective drag pump in the RFQ vacuum system that enhanced field emission from the electrodes and finally started the breakdowns. After replacement of the pump, steady operation at high field level in the following years slowly eliminated the hydrocarbon from the electrodes and the RFQ was reconditioned in small steps from 92% up to 100% of the nominal level during normal operation [5]. As a result, the current delivered by the linac increased from 145 to 160 mA.

3.4 LINAC RF IMPROVEMENTS

Allowing for 5% beam losses in the transfer line, 180 mA at the PSB entry correspond to 190 mA out of the linac. Adding up the beam power corresponding to this current, the copper power and a margin for phase and amplitude control, tuning precision and amplifier balancing, about 2.7 MW per Linac2 final RF amplifier will be needed, i.e. 10% more than their design power. An upgrade programme has been gradually applied to the RF chains to increase their output power. In fact, the final amplifier tubes (TH170R), rated at 2.5 MW for a duty cycle greater than that used at Linac2, can deliver more provided that enough drive power is available. For this, an additional amplifier stage was added in the Tank 1 chain, which suffers the heaviest beam loading and modern 4.5 kW solid state amplifiers replaced ageing tube pre-amplifiers in all chains. These more reliable semi-conductor amplifiers also contribute to a decrease in the linac fault rate. Great attention has also been given to the correct adjustment of the feedback loops, which have not only to compensate for an increased beam loading but also have to stabilise amplifiers that are often working in the non-linear region close to saturation.

3.5 BUNCH SHAPE MEASUREMENTS AND OPTIMISATION OF THE LINAC SETTINGS

Particular care was given to minimising the losses inside the linac tanks. This required a complete set of measurements for the re-optimisation of the working point (phase and amplitude setting) for the three linac tanks. These measurements were performed using the longitudinal emittance measurement line and the new bunch shape monitors that give the bunch density distributions in the three geometrical planes and their variations along the beam pulse [6]. Some careful optimisation of the quadrupole setting was also necessary. An example of a measurement is shown in Fig. 3.2.

3.6 BEAM TRANSPORT TO THE PSB

The 80 m long high current beam line between the Linac2 and PSB uses 20 quadrupoles, 2 bending magnets, 8 steering magnets and a debuncher cavity together with eight position pick-ups and two emittance measurement lines. This line has been simulated and re-optimised for the high current beam. The beam is strongly space charge dominated at the beginning of the line and becomes emittance dominated after about 50 metres. The focusing of the line was modified to provide a “quasi” FODO system with constant phase advance per focusing period, an arrangement that turned out to be the most convenient for optimising transmission and beam qualities whilst minimising the sensitivity to steering by the stray field of the PS.

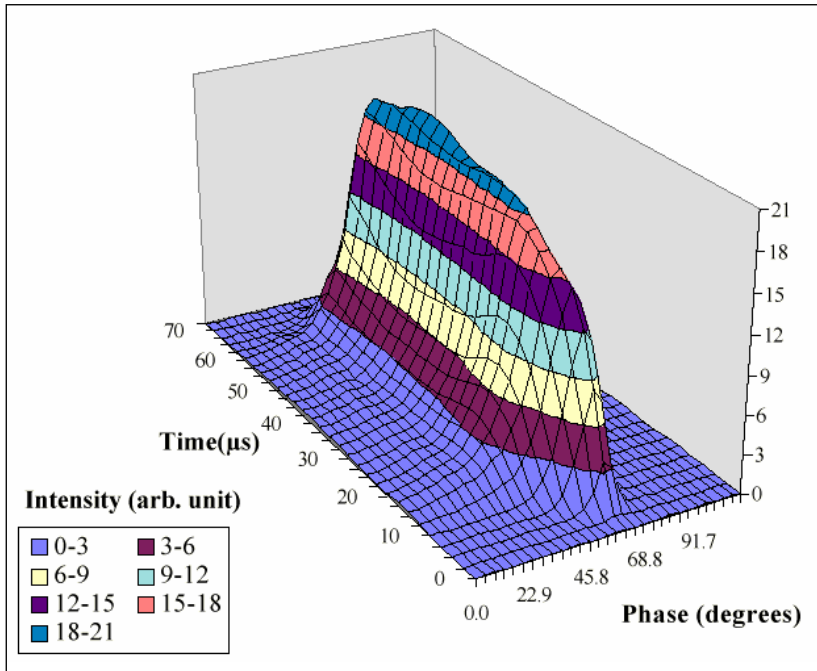


Figure 3.2: Bunch shape evolution along the beam pulse as measured by the Bunch Shape Monitor.

3.7 LINAC2 PERFORMANCE

The result of the installation of the new injector and of many improvements to the source, RF, optics and diagnostics of Linac2 and its transfer lines was the achievement of test currents up to 183 mA and the improvement of the operational current (for SPS and ISOLDE) up to 178 mA. This makes Linac2 the highest intensity ion linear accelerator in the world (peak current). No limitations are observed in the pulse length, making it possible for the linac to produce high intensity beams up to 120 μ s long. The transverse emittances at high intensity are about the same (i.e. within measurement accuracy) as at low intensity (140 mA). A summary of Linac2 beam parameters at 180 mA current is given in Tab. 3.1, while Tab. 3.2 shows the measured beam currents and transmissions for the different elements of the Linac2 accelerator. The losses, mainly concentrated in the RFQ and the first tank of the Linac, are due to space charge effects, as predicted by beam dynamics simulations.

Table 3.1: Characteristics of LHC proton beam from Linac2.

Parameter	LHC Specification	Achieved	
Current during pulse	180	182	mA
Pulse length	30	>100	μ s
Transverse norm. rms emittance	1.2	1.2	μ m
Momentum spread ($\pm 2\sigma$)	$\pm 0.15\%$	$\pm 0.15\%$	

Table 3.2: Output beam current and transmission at high intensity for the different elements of Linac2.

	Output Current	Transmission
Source	360 mA (p^+, H_2^+)	
RFQ	204 mA	~ 86%
Linac tank 1	194 mA	95%
Linac tanks 2 and 3	190 mA	98%
Transfer line to PSB	180 mA	95%

REFERENCES

- [1] C.E. Hill, A.M. Lombardi, E. Tanke, M. Vretenar, *Present Performance of the CERN Proton Linac*, Proc. 1998 Linear Accelerator Conference, ANL-98-28, Chicago, 1998.
- [2] C.E. Hill, A.M. Lombardi, W. Pirkl, E. Tanke, M. Vretenar, *Performance of the CERN Linac2 with a High Intensity Proton RFQ*, Proc. 1994 Linear Accelerator Conference, Tsukuba, 1994.
- [3] E. Tanke, *Realignment of the Linac2 LEBT During the 1994/1995 Machine Shutdown*, CERN PS/HI-Note 95-10 (MD), Geneva, 1995.
- [4] J.L. Vallet, M. Vretenar, M. Weiss, *Field Adjustment and Beam Analysis of the High-Intensity CERN RFQ*, Proc. EPAC '90, Nice, 1990.
- [5] M. Vretenar, *Field Emission Measurements on RFQ2 and Recalibration of the Vane Voltage*, CERN PS/RF/Note 97-11 (MD), Geneva, 1997.
- [6] A.V. Feschenko, A.V. Liiou, P.N. Ostroumov, O. Dubois, H. Haseroth, C. Hill, H. Kugler, A. Lombardi, F. Naito, E. Tanke, M. Vretenar, *Study of Beam Parameters of the CERN Proton Linac using a three dimensional Bunch Shape Monitor*, Proc. 1996 Linear Accelerator Conference, CERN 96-07, Geneva, 1996.

CHAPTER 4

UPGRADING THE PSB TO 1.4 GeV – POWER SUPPLIES

4.1 MAIN MAGNET POWER SUPPLY AND REACTIVE POWER COMPENSATOR

The output energy of the PSB has been increased from 1 to 1.4 GeV. This required an increase of the magnetic field by about 26% to 0.87 T, which was obtained by raising the coil current of the main magnets. The rms current was raised from 2000 A to 2300 A and the peak current from 3300 A to 4050 A at a maximum magnet voltage of nearly 3800 V (the magnet circuits are tested up to 10 kV).

The main magnet power supply has to cope with a significant increase of the peak power (from 8 to 14 MVA for the LHC cycle) which made the redesign of the rectifier transformers and the reactive power compensation system necessary in order to keep the line voltage variations to a minimum.

The upgrade [1] allowed the phasing out of the old polychlorinated biphenyl filled transformers and reactors.

4.1.1 Topology of the Upgraded Main Magnet Supply

The PSB main magnets are powered from the 18 kV line directly without energy storage. A high power fast-pulsed power supply (14 MVA peak power, 1.2 s repetition rate) feeding an inductive load and operated directly from the utility power lines presents a dynamic load that causes voltage and phase variations in the transmission system. The amount of disturbance is directly proportional to the dynamic load and inversely proportional to the short circuit capacity of the power system.

To minimise these effects on the AC lines and to increase the DC performance of the load, the PSB power supply is built as a series connected group of four 12-phase rectifier modules with freewheeling thyristors connected to the star point of the transformers. This circuit arrangement has the advantage of requiring less reactive power on the AC side. With respect to a normal 12-phase-bridge, it significantly reduces the output ripple on the DC load. Therefore, a smaller passive ripple filter can be used. The power system scheme is shown in Fig. 4.1 and the 1.4 GeV magnet cycle in Fig. 4.2.

4.1.2 The Reactive Power Compensation

The scheme described above reduces the line harmonics on the 18 kV side and minimises the reactive power variations, but not sufficiently.

To obtain satisfactory reactive power compensation and sufficiently low total harmonic distortion, an existing 18 MVAR capacitor bank and harmonics filter on the 18 kV level near the Jura substation at the Meyrin site is used [2]. The dynamic compensation is delivered by a set of Thyristor Controlled Reactors (TCR) installed next to the filter. All the filtering and compensating equipment is connected to the power distribution system at the 18 kV level.

Particular care has been taken of the TCR control circuitry to ensure that variations of the network voltage are kept to a minimum. The TCR was specified [3] and installed by the CERN power distribution group and ordered within the Canadian collaboration with TRIUMF.

During the 1.4 GeV cycle the variation of the line voltage on the 18 kV network is of the order of 2.3% without and 0.5% with compensation. The latter figure contains other variations in the network, as it is impossible to do measurements with an ideally stable network (see Fig. 4.2).

4.1.3 The Power Converter Groups

The original rectifier groups (four plus one spare) have been refurbished to deal with the increased rms and peak power for the LHC cycle. However, the water cooling of the freewheeling thyristors had to be upgraded and additional heat sinks for the fuses were installed to decrease their temperature.

The CERN power distribution group installed a complete, new 18 kV switch gear with the connection to the primary of ten new rectifier transformers (two units in one tank, rated 18kV/410V/2x 1.35 MVA). The latter were ordered as part of the Canadian collaboration with TRIUMF. The transformers were specified to be housed in the same position as the former transformers in order to retain the same phase symmetrical connections to the rectifier bridges.

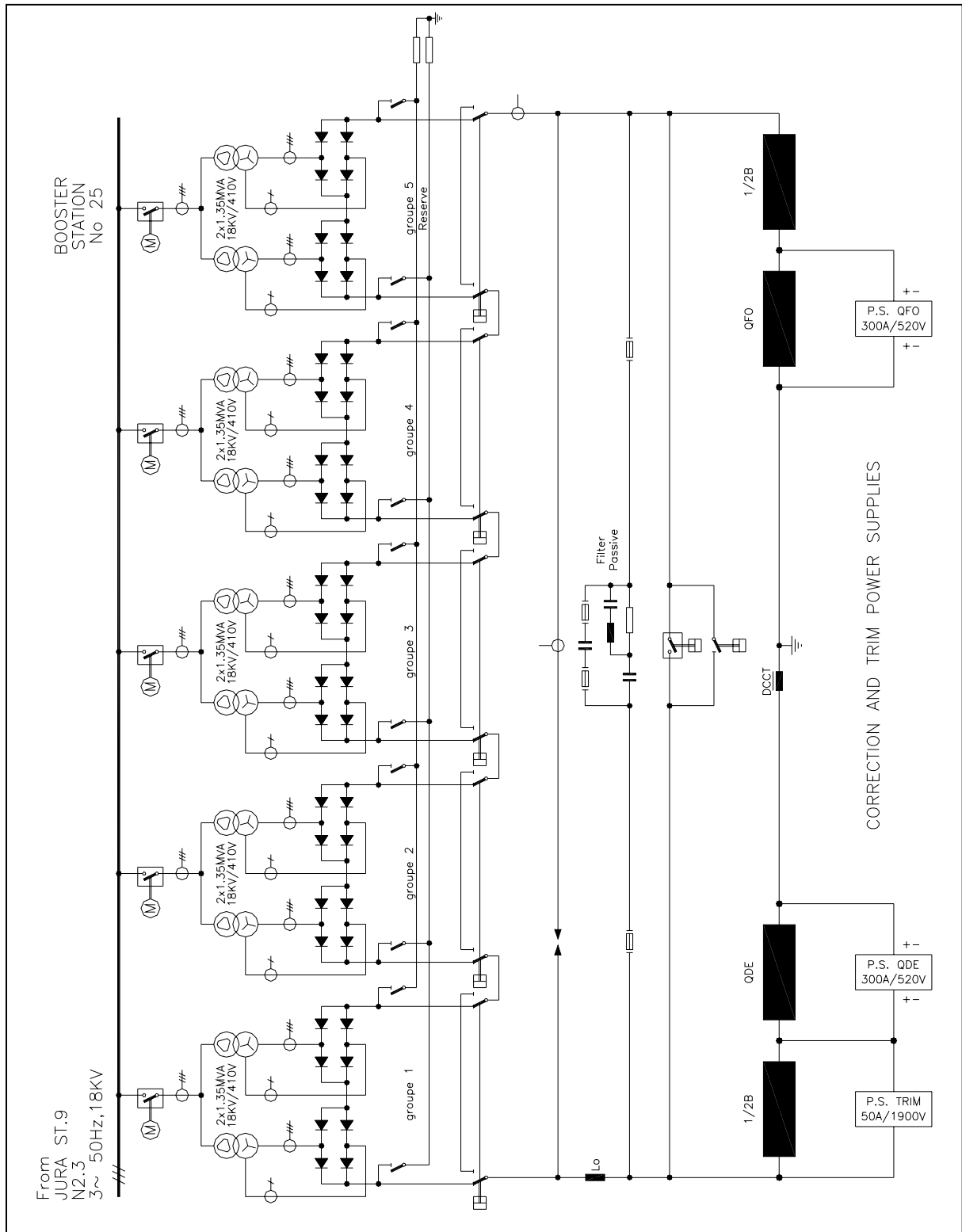


Figure 4.1: PSB main magnets supply electrical diagram.

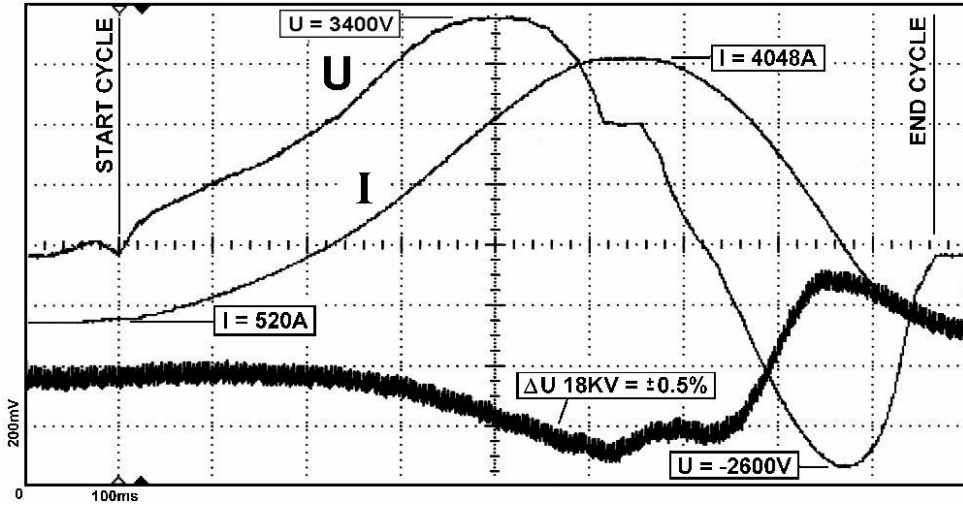


Figure 4.2: Voltage (U) and current (I) of the 1.4 GeV cycle and voltage excursion (ΔU) on the 18 kV network, 100 ms/div.

A polygon-primary to star-secondary coupling was specified for the transformers in order to connect the freewheel thyristors to the neutral point and to have a higher turns ratio for the accuracy of the phase angle ($\pm 15^\circ$ el. with a tolerance of 0.03°). Also much care was taken to ensure that the absolute impedance (4%) of all ten transformers had limited spread within phases and units ($\pm 5\%$). Both efforts were necessary to keep sub-harmonics (50, 100 Hz) as low as possible [4].

The over-voltage protection circuits on the secondary of the transformers were redesigned and adapted to the new layout.

The DC output connections of the rectifier modules (1000 V / 2300 A rms / 4050 A peak), the DC switching circuitry for the series connection of up to four groups, the passive filter and the connections to the magnets have been taken over from the old system.

4.1.4 Regulation and Control Electronics

A magnet cycle editor in the control system allows the creation and storage of cycles for different beam requirements. These cycles are sent to the main magnet supply via the local Device Stub Controller (DSC).

Input to the current regulation electronics is the base current from the PS control interface MIL1553 bus and, via a serial digital function generator, the LdI/dt function. By measuring the magnet current with a DC Current Transformer (DCCT) and using a Digital Signal Processor (DSP) the IR component is added to the LdI/dt component to calculate the reference voltage for the magnet. By integration of the LdI/dt function a current reference is created and compared to the actual current. The difference corrects the reference voltage signal and eliminates the influence from the resistive (thermal) variations of the magnet [5]. A block diagram of the regulation is shown in Fig. 4.3.

The magnet voltage reference signal is distributed to the four rectifier groups and successively controls the groups from zero to full voltage. Each rectifier group has its dedicated voltage feedback loop. This enables the variation of the reactive power consumption to be reduced and to keep the ripple of the voltage of the modules in series as low as possible.

The control of the 12 pulse rectifier-inverter bridges is done by high precision linearised gate control sets with a resolution of 0.1° el.. There are two separate functions for each group: bridge mode and freewheel mode. During start up the firing pulses of the selected groups have to be synchronised and switched from freewheel to bridge mode. In case of a major fault the freewheel thyristors act as a crowbar and thus protect the main magnets.

Disturbances with harmonics of the supply's commutation frequency have been observed on the current and field measurements. The modification of the grounding of the magnet circuit and the installation of a common mode filter at the output of the power supply improved the situation [6].

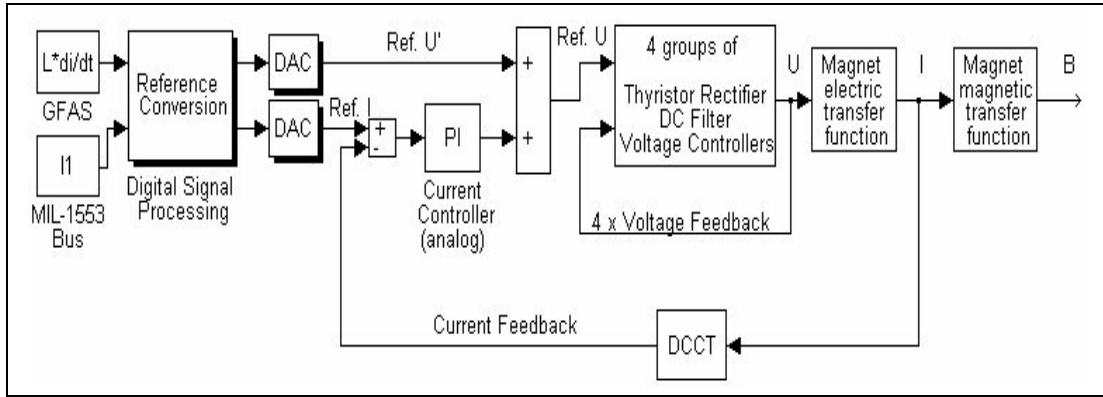


Figure 4.3: Block diagram of voltage and current regulation using digital reference processing.

Most of the control and interlock functions as well as the digital part of the power supply interface to the control system are performed by decentralised Programmable Logic Controllers (PLCs) interconnected by a serial fieldbus. Some vital functions (e.g. overcurrent) are hard wired in parallel to the PLC. The Mimic diagram and local and remote control are also integrated in the PLC system.

4.1.5 Quadrupole Correction Power Supplies, QFO and QDE

All bending and quadrupole magnets of the PSB machine are connected in series. To control the quadrupole magnets separately within a span of 8% of the main current, two correction power supplies are connected in parallel to the quadrupoles (see Fig. 4.1). These power converters are 12-phase thyristor-controlled rectifiers with passive and active fast filters in series with a current precision and tracking error better than 10^{-3} of nominal current and high dynamic capability (4 kA/s). Nominal ratings are 300 A / 520 V / 150 kW. The insulation to ground withstands 10 kV, the same as the entire main magnet circuit [7].

4.2 MAIN BENDING MAGNETS “TRIM” POWER SUPPLY

During the running-in period (in 1998) after the upgrade of the PSB to 1.4 GeV it became clear that the main bending magnets showed more effects of saturation than had been anticipated. The field values for the outer rings (rings 1 and 4) were slightly smaller as the magnet had been shimmed [8] to equalise field values at the former ejection energy of 800 MeV.

To equalise the bending fields the idea of the installation of a trim power supply was developed. Investigations of the cabling of the coils of the bending magnet string showed that the coils for rings 1 and 4 as well for rings 2 and 3 are in series with connection points accessible from the power supply equipment room.

A switch-mode power supply was specified, ordered, constructed, installed and commissioned in a record time of 4 months [9, 10]. The main characteristics are:

- bipolar 1900 V
- current 0 – 50 A with 10 A_{rms}
- total precision $\pm 0.2\%$ (ripple, tracking error, disturbance) relative to the maximum current of the main supply;
- stable operation at zero current;
- radiated and conducted switch noise below 50 mA_{pp}
- insulation to ground 10 kV, as the whole main magnet circuit.

To anticipate a step increase of the main current, the bending magnets voltage signal is used as a feed-forward voltage reference for the trim supply. This allows the tracking error of the trim supply to be reduced to nearly zero.

Control and interlocks of the trim supply are integrated into the PLC system of the main power supply like the QFO- and QDE- supplies (focusing and defocusing quadrupole magnet trim supplies) and they are controlled by the same knobs as the main supply.

4.3 PSB-PS/ISOLDE BEAM-LINE POWER SUPPLIES

The PSB-PS beam transfer line was designed in the late sixties for 800 MeV protons. In mid 1980 the PSB was upgraded to 1 GeV without modifying the transfer line equipment. More recently it was decided to upgrade further to 1.4 GeV for future LHC operation while also making available 1 or 1.4 GeV beams to the ISOLDE facility. Consequently, a number of magnets and power converters of the PSB transfer lines had to be replaced and this work was carried out in co-operation with TRIUMF, taking advantage of the Canadian in-kind contribution to the LHC project.

4.3.1 Requirements

The characteristics of the transfer line magnets and the related power supplies, as well as the operational requirements at 1.4 GeV, are shown in Tab. 4.1 and Tab. 4.2. Some of the magnets are DC while others require modulation during the 600 ms between field values corresponding to 1 and 1.4 GeV or even zero. One magnet (BT.BHZ10), which directs the particles almost symmetrically either to the PS or to the ISOLDE / PSB measurement-line, has to perform a full current reversal at 1 or 1.4 GeV within less than 750 ms. To allow a certain flexibility during operation in the years to come, a suitable margin in voltage and current was provided when specifying the new power supplies.

Table 4.1: Main operational parameters of power converters up to 35 kW and of related magnets (“B” means bending magnet, “D” correction dipole, “Q” quadrupole. “PPM” stands for “Pulse to Pulse current Modulation” every 1.2 s).

Function	Item	Identification	Magnet	DC Resistance (w. cables) (Ω)	Operation at Imax (1.4GeV)	Power Supply	Remarks	Notes
PSB Injection Line	1	BI-BVT	B5 (°)	0.175	250 (*)	44	a2	ppm1
	2	BT1-BVT10	B	0.246	281	70	a2	ppm
	3	BT4-BVT10	B	0.246	281	70	a2	ppm
	4	BT-BVT20	B1	0.442	244	109.5	268 A -118 V	ppm
	5	BT2-DVT10	D	0.09	147	13.5	a1	ppm (+/-)
	6	BT3-DVT10	D	0.09	147	13.5	a1	ppm (+/-)
	7	BT2-DVT20	D	0.09	248	22.5	a1	ppm (+/-)
PSB Transfer Line	8	BT3-DVT20	D	0.09	248	22.5	a1	ppm (+/-)
	9	BT3-DVT40	D	0.09	124	11.5	a1	ppm (+/-)
	10	BT2,3-QNO10	2 X Q	0.35	199	71.5	a2	ppm
	11	BT2,3-QNO20	2 X Q	0.35	189	68	a2	ppm
	12	BT-QNO30	Q	0.18	88	16.5	a1	ppm
	13	BT-QNO40	Q	0.18	259	48	a2	ppm
	14	BT-QNO50	Q1	0.27	197	60	a2	ppm
	15	BTP-QNO10	Q (°)	0.185	150	28	a1	dc (**)
	16	BTP-QNO20	Q (°)	0.185	145	27	a1	dc (**)
PS Injection Line	17	BTP-QNO30	Q (°)	0.2	139	28	a1	dc (**)
	18	BTP-QNO40	Q (°)	0.2	177	35.5	a3	dc (**)
	19	BTP-QNO50	Q	0.2	152	30.5	a1	dc (**)
	20	BTP-QNO60	Q (°)	0.215	176	38	a1	dc (**)
ISOLDE Line	21	BTY-BVT116	B4	0.11	410	45	a3	dc
	22	BTY-QDE209	Q2 (°)	0.23	174	40	a1	dc
	23	BTY-QFO210	Q2 (°)	0.23	221	51	a2	dc
GPS Line	24	BTY-DHZ212	D	0.1	243	24.5	a1	dc (+/-)
	25	BTY-DVT212	D	0.1	243	24.5	a1	dc (+/-)
	26	BTY-BHZ308	B4	0.13	410	53.5	a3	dc
	27	BTY-QDE321	Q2 (°)	0.23	174	40	a1	dc
HRS Line	28	BTY-QFO322	Q2 (°)	0.23	221	51	a2	dc
	29	BTY-DHZ324	D	0.1	243	24.5	a1	dc (+/-)
	30	BTY-DVT324	D	0.1	243	24.5	a1	dc (+/-)

Table 4.2: Main operational parameters of power converters with 100 and 250 kW ratings and of related magnets (“m1-4” means magnet. Other symbols as in Table 4.1).

Function	Item	Identification	Magnet	DC Resistance (with Cables) (Ω)	Operation at I_{max} (1.4 GeV)	Power	Remarks	Magnets: mH / mW / ms
			Type		Current (A)	Voltage (V)	Supply Type	m1: 92 / 480 / 192
			(Ω)					m2: 470 / 200 / 2350
								m3: 370 / 400 / 925
								m4: 205 / 94 / 2180
PSB Transfer Line	1	BT-BVT20	m1	0.5	244	123	b1	ppm
								Power Converter types:
	2	BT-BHZ10	m3	0.42	(+/-) 381	488 (398)	b2	ppm
Switchyards	3	BTY-BVT101	m4	0.11	397	158.5	b1	ppm2
	4	BTY-BHZ301	m4	0.13	397	163.5	b1	ppm3
Measuring Line	5	BTM-BHZ10	m2	0.22	446	161	b1	ppm
								ppm3 = ppm2 for GPS / HRS
								Δt available for ppm: 600 ms (0.75 s for BT-BHZ10)
								(+/-) bipolar power supply b2

4.3.2 Performance Specification

The critical specifications for the new power supplies [11, 12] concern:

- the operational DC precision/stability of current referred to nominal set-point, to be better than $1 \cdot 10^{-4}$ over 8 hours
- the capability of changing the current by $\pm 25\%$, or by 100% in some cases, within 600/750 ms – regulation transients included, on subsequent PSB cycles
- the conformity to the PS control interface (MIL-1553) and to the operator interface in use in the PS complex
- the use of state of the art circuit topologies so as not to become obsolete once the LHC starts operation.

With the view of simplifying the design of the power parts, the operational requirements of the transfer line magnets were met by two sets of power supply ratings: a lower range up to 35 kW (Batch-1) and a higher one up to 250 kW (Batch-2). Consequently the following types of power converters have been specified (Tab. 4.1 and 4.2):

- Batch-1 (38 units): type a1=15 kW (300 A, 50 V) with mechanical output current polarity selector; a2=31.5 kW (350 A, 90 V) and a3=35 kW (500 A, 70 V).
- Batch-2 (8 units): type b1=100 kW (500 A, 200 V) and b2=250 kW (450 A, 550 V).

4.3.3 Technical Solution

Using today’s state of the art technology, Switch Mode Power Supplies (SMPS) have been specified, which have excellent precision/stability, low losses and fast regulation response [13].

As an illustration of the design, a block diagram of the power section of the 100 kW converter is shown in Fig. 4.4. Specifically, the power section of the converter consists of an AC series-parallel input filter to reduce current harmonics and raise the power factor; a rectifier and filter forming the DC link; an Insulated Gate Bipolar Transistor (IGBT) full H-bridge operating at a switching frequency of 16-18 kHz and a ferrite HF transformer with centre tap secondary, feeding a high current rectifier followed by two *LC* passive filter stages. To achieve a 600 ms current fall time despite of a load time constant of over 2 s in some cases an optional regeneration thyristor bridge provides the required negative voltage on the magnet and an IGBT switch isolates the converter from the load when the current is requested to decrease to zero.

The 250 kW converter has three IGBT H-bridges working in parallel and feeding the HF transformer which has its secondary connected to a Graetz-bridge rectifier followed by two *LC* filters. In addition to the regeneration section, this converter has a thyristor selector of the DC current polarity which allows an inversion of the field which directs the protons either to the PS or to the ISOLDE/measurement line. The semiconductor switches and some of the magnetic components are water cooled to obtain the compact assembly required by this type of converter for electromagnetic compatibility reasons.

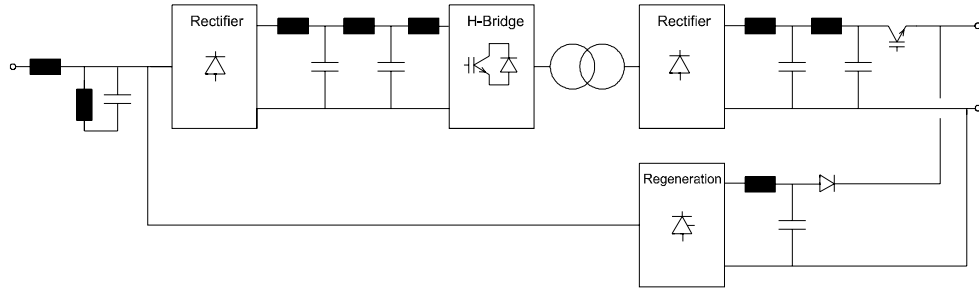


Figure 4.4: Block diagram of a 100 kW switch-mode power converter.

All the voltage and current measurement systems used for monitoring, protection or feedback are insulated. The power supply output current is measured via high precision magnetic sensors (DCCTs).

The regulation of such a SMPS (Fig. 4.5) consists of several cascaded feedback loops:

- A first loop balances the current in the two arms of each IGBT H-bridge to avoid saturation of the HF transformer by any DC component.
- A second loop controls and limits the current I_p on the primary of the HF transformer.
- A third fast loop controls the voltage U_r at the rectifier output.
- Finally the overall feedback loop controls the current and ensures the stability and precision.

The critical components of the current loop are enclosed in a Peltier oven block kept at constant temperature by a separate regulation.

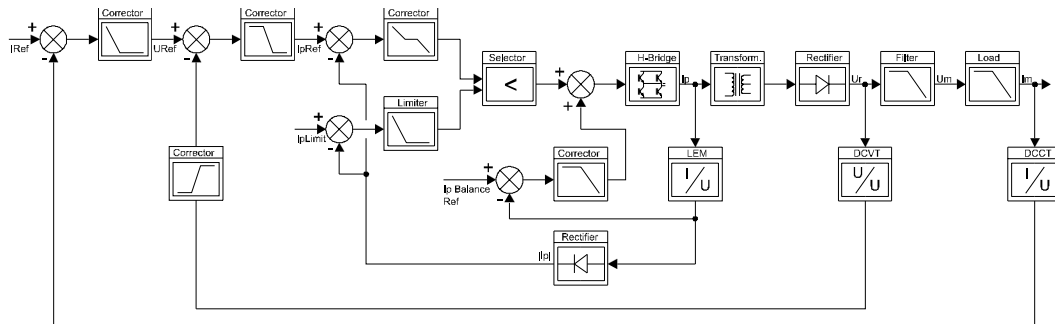


Figure 4.5: Block diagram of final power converter regulation.

As factory tests could not be performed on the actual load, the regulation had to be slightly modified and adjusted during commissioning at CERN. This results in the best possible dynamic and static behaviour over the full current range.

To make the power supply electronics compatible with CERN standard control and operator interfaces, the principle of separating a 6U Euro-crate in two 3U sections was adopted. The upper one was reserved for CERN specific boards and the lower one for the manufacturer's electronic cards. This solution has been shown to work smoothly and to allow a clear definition of responsibilities with a minimum of interfacing conflicts.

4.3.4 Project Wind Up

Having equipment specified at CERN and built in Canada proved difficult. In addition to the distance and time lag, the different workmanship quality standards, work methods and materials in use, as well as the different culture of the North American market, have proved to be quite challenging. From the beginning the arrangement that CERN would prefer to take care of the follow up of technical aspects and of the compliance with the specification and leave TRIUMF the role of managing the contracts and dealing with the suppliers, worked quite well. The power converters were designed, developed and manufactured by firms based in Toronto. Several hundred CERN specific interface boards for all the power supplies were made, stuffed and pre-tested by a specialised firm located in Vancouver.

All supplies have shown excellent performance and availability records. The Batch-1 power supplies have been in operation since March 1998 and the delivery of Batch-2 power supplies was completed in 2001.

4.4 PULSED POWER CONVERTERS FOR SEPTUM MAGNETS IN THE PSB-PS LINE

The upgrading of the PSB-PS recombination and transfer line to 1.4 GeV called for new pulsed septum magnets to replace the unsuitable DC septa (see Chap. 5.1). For the new septa, new pulsed power converters have been designed and installed in the transfer line PSB-PS. To meet the main features such as high current, high precision and duration of the flat-top and to master thermal and magnetic problems owing to the irregular pulses (current and timing modulation), a third harmonic correction of the discharge pulse was added and an active filter inserted [14].

A new electronic crate has been developed at CERN to facilitate the maintenance and to respect different criteria: standardisation, protocol, timing and regulation with active filter. The power parts have been designed at CERN and built in collaboration with industry.

4.4.1 Operational Requirements

In the common part of the transfer line between PSB and PS, the kinetic energy is either 1 GeV (ISOLDE at low energy) or 1.4 GeV (PS and ISOLDE at high energy). The PS supercycle is made of basic cycles (1.2 s length) dependent on the use of different beams. Consequently, pulsed power converters must work with an irregular pulse repetition and with pulse to pulse modulation of their current.

The recombination of the beam in the PSB transfer line uses: four superimposed horizontal septa (BE.SMH with the four magnets in series), three vertical septa (BT1.SMV10, BT4.SMV10, BT.SMV20) and a horizontal septum for the injection in the PS (PI.SMH42).

4.4.2 Pulsed Capacitors Discharge Power Converters

The principle is based on the charge and discharge of capacitors through a resonant circuit between capacitors and load. The charging current of the capacitors is controlled via thyristors on the primary side of a high voltage transformer. The DC voltage and current are measured by voltage dividers and shunt. Once charged, the capacitors are discharged in the magnet via a power thyristor. In order to obtain a better flat top current than the basic sinusoidal discharge current, a third harmonic with parallel *LC* circuit is added. A choke, in series with the discharge circuit, is used for the active filter. The discharge is through a matching transformer whose secondary delivers 4 to 12 times the primary current to the septum magnet.

4.4.3 Matching Transformer and Strip-line

The matching transformer is a specially manufactured device with an air gap and a very low stray inductance. It is installed in the ring and the secondary of the transformer is connected to a magnet vacuum feedthrough via a high current strip-line. This is made of copper plates to minimise the value of inductance and to keep the resistance small relative to the magnet. The current in the septum is monitored by a current transformer between the pulse matching transformer and the high current strip-line.

4.4.4 Regulation and Active Filter

The capacitor voltage is regulated with a charging current internal loop. Temperature variations and magnetic effects caused by irregular repetition rate are regulated by special electronics which slightly increases or decreases the capacitor voltage.

A flat top current stability of 10^{-4} is achieved by an active filter power circuit with a regulation control loop. The principle is to charge the main capacitors slightly more than the value necessary to give the current wanted. The excess current is then pulled through the inductance of the active filter and the system acts in a closed loop through the matching transformer. More details may be found in [14 and 15] and in the specification document [16].

4.4.5 Characteristics of the Power Supplies

The principal characteristics of the power converters are resumed in Tab. 4.3:

Table 4.3: Main parameters of the pulsed septum magnet power supplies.

	BE.SMH	BT1.SMV10	BT4.SMV10	BT.SMV20	PI.SMH42
Peak current septum	A	6000	30000	30000	40000
Transformer turn ratio	n1/n2	4	12	12	12
Charging voltage	V	1200	2100	2100	2100
Peak current primary	A	1500	2500	2500	3333
Total storage capacitors	μF	2500	2000	2000	3000
Energy storage capacitors	J	1800	4410	4410	6 615
Total inductance secondary	μH	22	3	3	2.03
Total resistor secondary	$\mu\Omega$	4020	660	660	620
Current pulse half period	ms	3.6	3.5	3.5	3.6
Current pulse flat top	μs	500	500	500	500
Current flat top precision	ppm	< 100	< 100	< 100	< 100
Pulse to pulse modulation		yes	yes	yes	yes
Irregular pulse repetition		yes	yes	yes	yes
Max. pulse repetition rate	Hz	1	1	1	1
Third harmonic choke	μH	248	370	370	280
Active filter choke	μH	50	50	50	50
Inductance seen by primary	μH	432	503	503	372
Power transformer 3 ph.	kVA	20	63	63	63
Prim./second. voltage effective	V	400/1000	400/2000	400/2000	400/2000

Typical discharge and filter currents are shown in Figs. 4.6 and 4.7, with a current of 33 kA in the PI.SMH42 septum magnet [15].

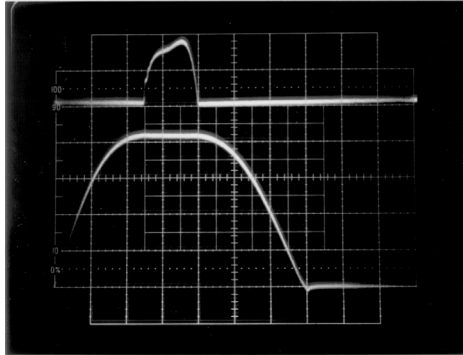


Figure 4.6: Magnet and active filter current at 33 kA
Upper trace: active filter current, 100 A/div,
Lower trace: magnet current, 10 kA/div, 0.5 ms/div.

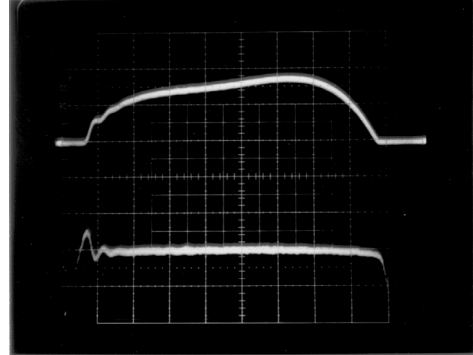


Figure 4.7: Zoom on flat top at 33 kA. The current flat-top precision is in the 10^{-4} range.
Upper trace: active filter current, 100 A/div,
Lower trace: magnet current, 40A/div, 0.1ms/div

The pulsed power supplies for the septum magnets completely fulfil the operational requirements: higher and repetitive currents for 1.4 GeV, pulse to pulse modulation, irregular pulsing and high reliability.

REFERENCES

- [1] H. Ullrich, *Proposal for the upgrade of the Booster main magnet power supply*, CERN PS/PO/Note 95-02(tech.), Geneva, 1995.
- [2] O. Bayard, *Description du filtre d'harmoniques sous station Jura*, CERN LABII/PS/OB/EKK/Tech.Note-72 1, Geneva, 1972.
- [3] J. Pedersen, *Technical specification for a 18 Mvar, 18 kV thyristor controlled reactor*, CERN ST-IE-PI/96-193, Geneva, 1996.
- [4] H. Ullrich, *Rectifier double transformers for upgrading the Booster main magnet supply*, CERN PS/PO/Note 95-23 (Spec.), Geneva, 1995.
- [5] T. Salvermoser, *New electronics for the regulation and timing of the Booster main power converter*, CERN PS/PO/Note 96-23 (Min.), Geneva, 1996.
- [6] H. Fiebiger, F. Gendre, T. Salvermoser, *Modification of Booster magnet circuit grounding layout*, CERN PS/PO Note 97-07(Tech.), Geneva, 1997.
- [7] H. Ullrich, *12 phase thyristor power converters with passive and active filter modulated 0 to 300 A, 520 V*, CERN PS/PO/Note 95-24 (Spec.), Geneva, 1995.
- [8] M. Benedikt, C. Carli, *Operation of the CERN PS-Booster above 1 GeV - Saturation effects in the main bending magnets and required modifications*, CERN/PS 98-059 (OP), Geneva, 1998.
- [9] T. Salvermoser, *Specification of a switch mode power supply*, CERN PS/PO/Note 98-54(Spec), 1998.
- [10] H. Fiebiger, F. Gendre, T. Salvermoser, H. Ullrich, *Commissioning Booster Trim Supply*, CERN Memo 19-3-99, Geneva, 1999.
- [11] F. Völker, *Soft-Switched Mode DC Power Converters for the 1.4 GeV PSB Beam Transfer-line Magnets*, CERN PS/PO Note 96-01 (Spec), Geneva, 1996.
- [12] F. Völker, *Soft-Switched Mode DC Power Converters for the 1.4 GeV PS-Booster Beam Transfer-line magnets*, CERN PS/PO Note 98-08 (Spec), Geneva, 1998.
- [13] M. Georges, G. Simonet, *Les Nouvelles Alimentations des Lignes de Transfert PSB-PS et PSB-ISOLDE*, CERN PS/PO Note 98-44, Geneva, 1998.
- [14] J.P. Royer, *High current with high precision flat-top capacitors discharge power converters for pulsed septum magnets*, CERN/PS/95-13 (PO), Geneva, 1995.
- [15] J.M. Cravero, J.P. Royer, *The new pulsed power converter for the septum magnet in the PS straight section 42*, CERN PS/PO/ Note 97-03, Geneva, 1997.
- [16] J.P. Royer, *Technical specification of the capacitor discharge power supplies for septum magnet of the transfer line PSB-PS*, CERN PS/PO/SPEC94-08, Geneva, 1994.

CHAPTER 5

BOOSTER ENERGY UPGRADE TO 1.4 GeV – OTHER SYSTEMS

5.1 PSB-PS LINE SEPTUM MAGNETS

In the PSB, DC septum magnets that were originally designed for 800 MeV beams, have been used for 1 GeV beams since 1986 without modification. When the PSB energy needed to be increased to 1.4 GeV it required the re-design of all PSB ejection and transfer septa because of the thermal limit of the DC magnets [1]. A single turn pulsed magnet approach which requires less energy and hence less cooling power has been adopted for the construction of these septum magnets. This way they are also less prone to erosion in the cooling circuits. To attain the required vacuum, the laminated yoke of these pulsed magnets must be baked at 200°C, despite the fact that these magnets are installed in non-bakeable accelerators. Therefore, the connecting flanges of the magnet tanks should not exceed 50°C when the magnets are being baked.

In the following paragraphs, the most important details of the modifications will be described for each component.

5.1.1 Vacuum Tanks

To reduce the risk of a leak developing during a bakeout, cylindrical tanks have been fitted with circular ultra high vacuum flanges for diameters < 200 mm and “Wheeler” flanges with copper seals for the bigger diameters (> 375 mm). The connecting flanges of the tanks to the accelerator vacuum chamber are of a conical “quick disconnect” type with aluminium seals, as standard in the CERN PS accelerators. Fig. 5.1 shows a vacuum tank containing two superposed PSB ejection septum magnets.

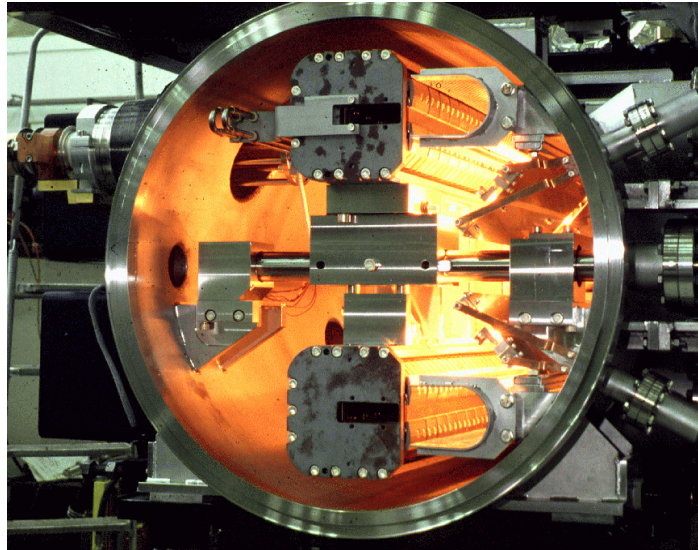


Figure 5.1: Vacuum tank containing two superposed ejection magnets.

5.1.2 Magnets

Because the new septum magnets are a pulsed, they are constructed with laminated yokes. Standard 0.35 mm thickness steel laminations with a 3% silicon content, which are insulated on both sides with a “Carlite” inorganic insulating coating have been used. This solution provides a good inter-laminar resistance and is still bakeable up to 200°C. The laminated yoke is held together in a stainless steel support by ceramic coated endplates and sits on ceramic bars, to ensure the electrical insulation between the yoke and the support.

The single-turn coils have been made of “OFHC” copper. The cooling circuit comprises two thin-walled stainless steel tubes, embedded (and brazed) in pre-machined slots in the septum conductor. This reduces erosion of the cooling circuit due to the high water speeds of up to 10 m/s. To increase the mechanical strength of the 60 mm gap septa conductors, a 0.5 mm thick stainless steel plate is brazed onto the outside of the septum conductor. To reduce the fringe field of the magnets, insulation has been eliminated between magnet yoke and septum conductor, while the return conductor of the coil is insulated with several layers of 0.06 mm and 0.12 mm thermally pre-formed “Kapton” sheet (see Fig. 5.2).

The complete magnet coil is held in the gap by clamping plates which are located outside the magnet yoke. These insulated clamps retain the septum conductor in the gap, while a spring between the septum and rear conductor applies a mechanical force on the return conductor equal to the electromechanical force at the peak current.

The springs, spaced every 45 mm, are made of beryllium copper (5% Be) suitably annealed to obtain the necessary modulus of elasticity (see Fig. 5.3).

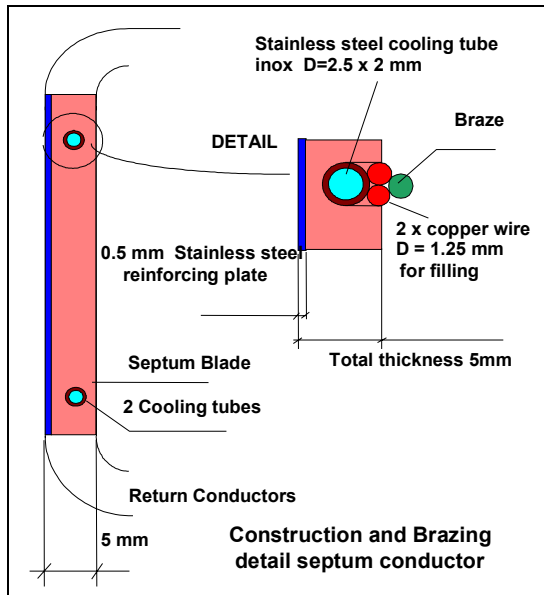


Figure 5.2: Cross section of septum conductor.

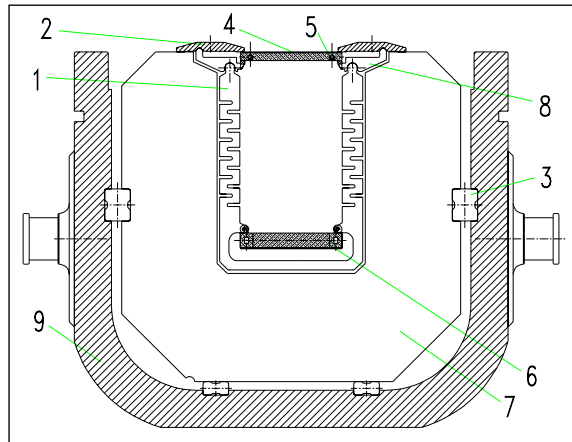


Figure 5.3: Cross section of magnet yoke assembly.

- 1. Damping Spring
- 2. Clamping Plate
- 3. Ceramic Support
- 4. Septum Conductor
- 5. Cooling Tube
- 6. Rear Conductor
- 7. Lamination
- 8. Lever
- 9. Stainless Steel Support.

A water-cooled coaxial power feedthrough, developed for use at 10 kA_{rms}, is used for all new pulsed septum magnets. The coaxial configuration provides the best possible symmetry in mechanical forces, (see Fig. 5.4)

5.1.3 Displacement System

All septum magnets can be moved remotely in the radial (or vertical, in the case of the septa in the transfer line) and angular directions, while their vacuum tanks remain fixed. A variable potentiometer, linked to the mechanical displacement system, provides a measurement of the position of the magnet inside the tank. The resolutions of the radial and angular systems are 0.1 mm and 0.1 mrad, respectively. For the initial installation, the magnet tank is aligned in all directions. In the event of a failure, the entire vacuum tank with septum magnet can be replaced without the need for realignment.

5.1.4 Beam Screen

All septum magnet tanks (except transfer lines) are equipped with RF beam screens for the orbiting beam. These screens ensure the continuity of the RF impedance of the vacuum tanks needed to avoid unwanted harmonics during acceleration. The beam screens are made of perforated stainless steel sheet to improve vacuum pumping speed and are linked to the connecting flanges of the tank by means of RF contacts.

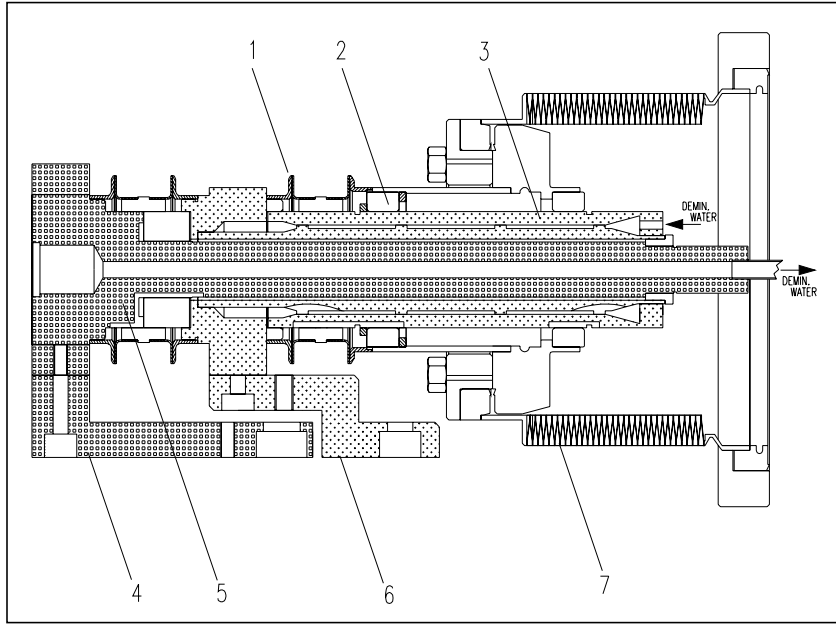


Figure 5.4: Cross section of power feedthrough. 1. Dilver / Stainless steel weld 2. Ceramic support 3. External conductor 4. Main connection 5. Central conductor 6. Main connection 7. Vacuum bellows.

5.1.5 Vacuum Equipment

The vacuum tanks are kept under vacuum with a dedicated set of ion pumps, with additional pumping provided by titanium sublimators for the tanks installed in the accelerator rings. In view of the large surface area of the magnet laminations under vacuum and the pressure level to be obtained, it is necessary to bake out the magnets before commissioning. Standard off-the-shelf infra red lamps with reflectors of electro-polished stainless steel are used inside the vacuum tank. By connecting two reflectors in series, the power consumption is reduced by a factor four, while the expected life time is dramatically increased. The temperature of the magnet is measured with ordinary Cu/Cn (Cn-Constantan) thermocouples and the control and regulation utilises standard temperature regulators.

5.1.6 Calculations

A program was developed in house for the first rough estimation of the septum magnet parameters. To finalise the cross sectional design of the magnet a finite element based program called “FLUX2D” from Cedrat/Magsoft was used. The longitudinal design was determined using the finite element based program “OPERA3D/TOSCA” from Vector Fields, using a technique developed in house to simplify the magnet model without significant loss of precision. For mechanical and thermal calculations the finite element program ANSYS from Swanson Analysis Systems was used, while the cooling requirements were checked with the CERN package TUBE.

5.1.7 Measurement Results and Conclusions

Measurements of magnetic length of the septa confirm theoretical predictions to within 0.5% of the model. The fringe fields measured are less than 1/1000 of the gap field at a 50 mm distance from the septum conductor, or better in case of the BE.SMH (PSB ejection), where a very low fringe field was required. After a bakeout cycle, consisting of a quasi linear temperature increase to 200°C over 12 hours, a 24 hour period at 200°C and an exponential temperature decrease of approximately 48 hours, a vacuum of 6×10^{-10} to 4×10^{-9} mbar is achieved. Since the bakeout lamps are installed with reflectors, the connecting flanges of the vacuum tanks never exceed 50°C, allowing the use of aluminium seals for connecting to the accelerator vacuum chambers. For completeness, the technical specifications of the septum magnets are listed in Tab. 5.1.

Table 5.1: Technical specifications of the septum magnets.

		BESMH	BTSMV10	BTSMV20	PISMH42
L_{eq}	[m]	0.95	1.00	1.00	0.57
B_0	[T]	0.354	0.569	0.525	0.689
$\int B dl$	[Tm]	0.336	0.566	0.523	0.390
I single turn coil	[kA]	7.0	27.3	25.2	33.1
E protons	[GeV]	1.4	1.4	1.4	1.4
Deflection Angle	[mrad]	47	79	73	55
Gap height	[mm]	25	60	60	60
Gap width	[mm]	89	116	116	116
Septum Thickness	[mm]	3.8	5	5	5
Rear conductor thickness	[mm]	7.6	8.8	8.8	8.8
1/2 sine pulse width	[ms]	3.1	3.1	3.1	3.2
Water flow	[l/min]	1.9	3.5	3.5	4.25
Year of installation		1998	1999	1997	1996

5.2 PSB-PS TRANSFER LINE MAGNETS

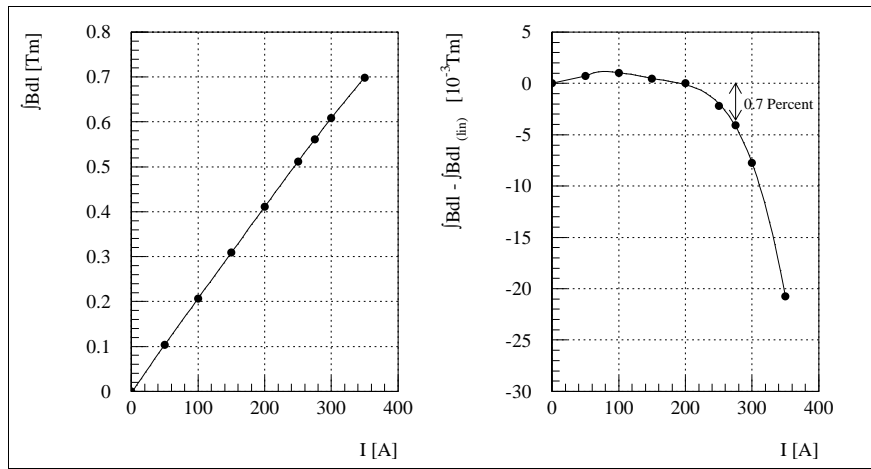
Most of the magnets in the transfer line from the PSB to the PS had to be replaced, for two different reasons. Some of the original magnets were not laminated, thus the induced eddy currents would have hindered pulse to pulse modulation. For some other magnets, the cooling power was no longer sufficient at the higher currents necessary for 1.4 GeV operation. The new magnets are part of the Canadian in-kind contribution to the LHC project.

All the magnet yokes are laminated using low carbon steel sheets of 1.5 mm thickness stacked between non-laminated low carbon steel end plates. The coils are built from rectangular copper conductor with a circular cooling hole. The inter-turn and mass insulation is made with half-lapped glass fibre tape. The coils are vacuum impregnated using radiation resistant epoxy resin.

The BVT10 dipoles are window frame magnets with a single bedstead coil. A yoke extension block compensates the asymmetry caused by the coil head. The BVT20 magnet is similar to the BVT10, but with an aperture of twice the width and two symmetrical bedstead coils which are identical to the BVT10 coils. The DVT correction dipoles are window frame magnets with less bending power. They have two bedstead coils. The yokes of the BT.QNO quadrupoles use a “figure of eight” design. The doublet version is built from two single yokes separated by appropriate spacers. Details about the magnet design and excerpts from the construction drawings can be found in [2, 3] and the references therein.

The quadrupoles were magnetically measured at TRIUMF with a newly built rotating coil system [3] and an existing Hall probe system. The dipoles were field mapped at TRIUMF using a Hall probe system. Details of the measurements, comparisons between different measurement methods and comparisons to magnetic field calculations can be found in [2 – 5] and the references therein.

Tab. 5.2 lists the magnet characteristics. The values given for coolant flow, temperature rise and pressure drop are measured values. Higher currents are possible by increasing the inlet water pressure, the maximum permissible value being 25 bar. Tab. 5.2 also contains the coefficients $\int B dl/I$, $\int G dl/I$; the value for the BVT10 dipoles corresponds to the linear part up to 200 A. At the field necessary for 1.4 GeV operation, a saturation of 0.7% can be seen for this magnet (Fig. 5.5). The polynomial coefficients to describe this curve can be found in [3]. For all other magnets saturation effects are negligible at this field level. All values are averaged over a given magnet type, individual measurements for each magnet are summarised in [3].



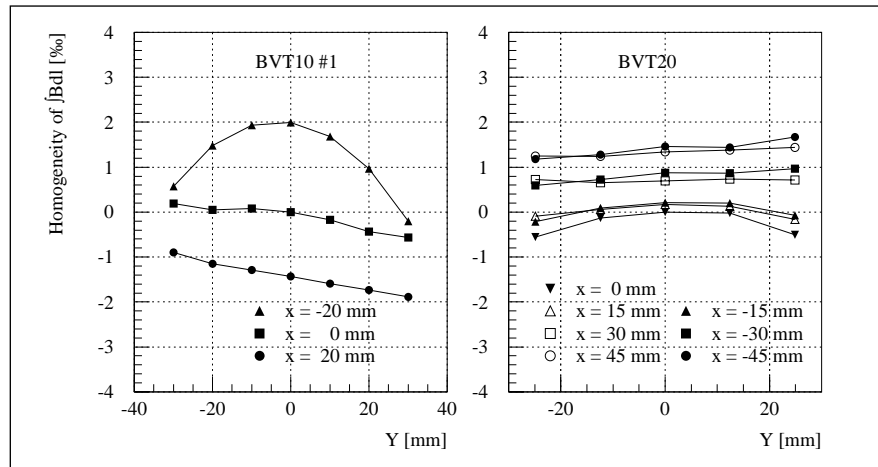


Figure 5.6: Homogeneity of $\int B dl$ of BT.BVT10#1 and BT.BVT20.

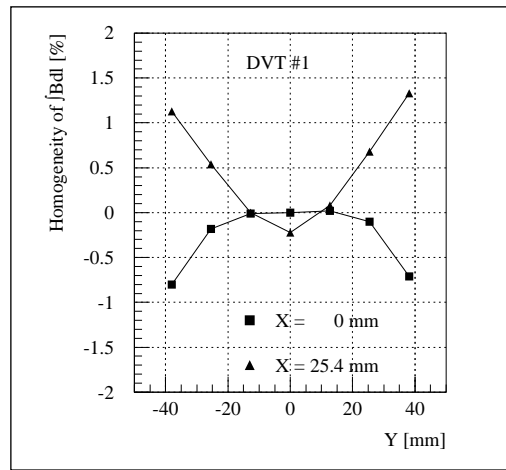


Figure 5.7: Homogeneity of $\int B dl$ of BT.DVT#1.

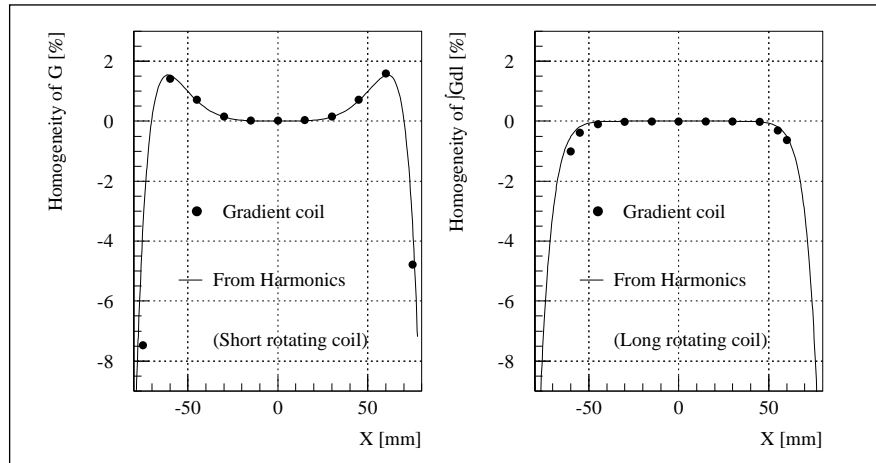


Figure 5.8: Homogeneity of G and $\int G dl$ of BT.QNO#6.

5.3 FAST KICKER SYSTEMS

5.3.1 PSB Ejection BE.KFA14L1 and Recombination Kickers, BT.KFA10 and BT.KFA20

The PSB kicker magnets are used for the horizontal ejection and sequential vertical recombination of the beams from the four PSB rings into one string of bunches, which is guided to the PS. The magnets are of cellular, closed aperture, C-ferrite loaded, transmission line type; they are in the machine vacuum. Ejection and recombination magnets have different apertures to best match the beam dimensions. Given the constraints of the PSB ring and transfer line layout, the original magnets and vacuum tanks were re-used. The particularity of the original PSB kicker system configuration [6] was the insertion of the magnets between the Pulse Forming Network (PFN) and transmission cables, as sketched in Fig. 5.9 below.

The principal advantage of this extremely tailored layout is that the magnets are used in virtual short-circuit mode. The short-circuit current is provided immediately by the thyratron switch and its leading edge travels only once through the magnet. This configuration yields the fastest kick rise-time and highest kick strength for a given PFN voltage. Although the PFNs are resonantly charged in milliseconds, the crucial disadvantage of this configuration, however, is the relatively long exposure of the magnet to the PFN charging voltage, which may precipitate magnet sparking for charging voltages larger than ~ 35 kV. Because of the increase of PSB energy, (the charging voltage for the kicker pulse generators is 26% higher), this (originally air-insulated generator) configuration could not be retained, except for the second recombination kicker BT.KFA20, which operates far below the magnet voltage hold-off. This minimal cost system had other disadvantages:

- The impedance at the main thyratron switch is low (6.25Ω), thus increasing the relative importance of unavoidable inductive mismatches present in such systems.
- Timing and transmission cable length adjustments, possible with independently powered modules, which are very effective to reduce the influence of individual magnet kick rise-time and ripple on the sum kick of the magnets, cannot be made.

During previous PSB energy upgrades, the initially effective, but cumbersome ferrite loaded pulse-steepening lines [7] (Fig. 5.9) were removed. High voltage thyratrons, vacuum feedthroughs and the magnet ferrites were upgraded (except for BT.KFA10) and all PFN and transmission cables were replaced by low loss, SF₆ pressurised high voltage cables.

For the LHC upgrade described here, the PSB kicker equipment (hardware and software) was completely replaced, except for the magnets, vacuum tanks and high voltage cables.

New, oil-insulated pulse generators using two multistage thyratrons, each capable of operating at 60 kV and in two-shot Pulse to Pulse Modulation (PPM), were developed and installed together with their associated electronics and controls for BE.KFA14L1 and BT.KFA10 [8].

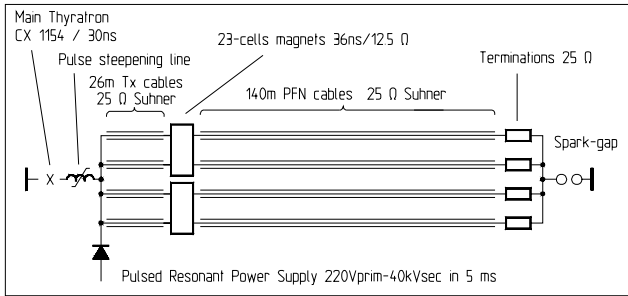


Figure 5.9: Original BT.KFA20 configuration.

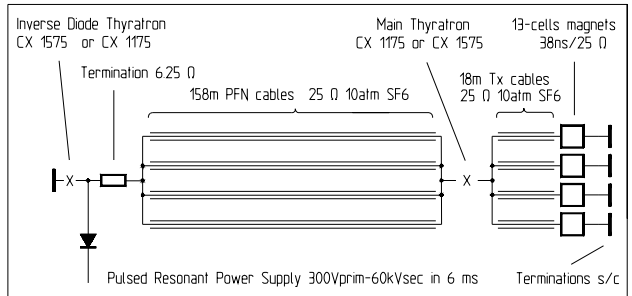


Figure 5.10: BE.KFA 14L1 (1 of 4 rings) for LHC era.

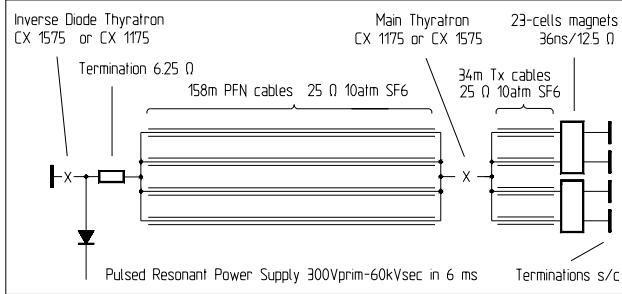


Figure 5.11: BT.KFA 10 configuration for LHC era (1 of 2 lines).

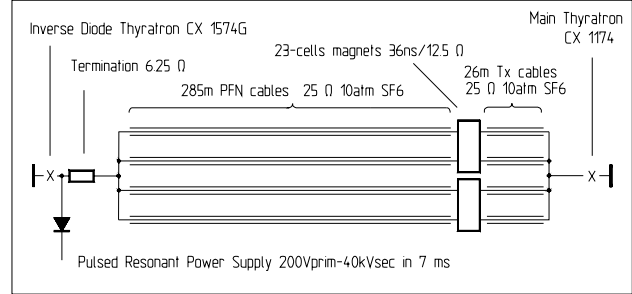


Figure 5.12: BT.KFA 20 configuration for LHC era.

These magnets are now hard short-circuited and pulsed in the more classical configurations of Figs. 5.10 and 5.11. For BT.KFA20, the new hardware developed for the above systems is also used, but the original configuration has been retained in order to achieve the short rise-time without the need of bulky requiring an artifices (Fig. 5.12).

The principal advantage of the new layout is that the short-circuited magnets (and their electrical feed-throughs) are exposed to high voltage for the minimum possible duration, largely obviating the problem of sparking. The intrinsic disadvantage of this new configuration with respect to the previous layout is that the initial switch current has to traverse the magnet twice before the total kick is established, leading to a longer rise-time (~90 ns instead of ~60 ns). However, because of the PSB harmonic number change from 5 to 2 or 1, this longer rise-time can be accepted.

Further development work on the use of saturable inductors involving the mounting of small saturable ferrite loaded inductors improved the kicker rise time. Other complications inherent in this configuration are different lengths of transmission cables to compensate for particle flight time from magnet to magnet. Much of the unavoidable flattop ripple has been reduced by adequate compensation with RC filters.

The main parameters of the PSB kickers can be found in the Tab. 5.3.

Table 5.3: PSB and PS kicker main parameters and performance (kick strengths for I_{\max})

Element	No.of Generators	V_{\max} PFN [kV]	Magnet nominal Z_o [Ω]	Termination Z_o [Ω]	Magnet I_{\max} [kA]	No. of turns	Magnet Aperture $w \times h$ [mm^2]	Magnet length [mm]	Kick strength in SS/ring [Gm]	Rise-time 2-98% [ns]	Flattop length [μs]
BE.KFA14L1	4	60	25	s/c	2.4	1	115×70	450	775	102 ns	1.5
BT.KFA10	2	60	12.5	s/c	4.8	1	53×110	786	862	86 ns	1.5
BT.KFA20	1	30	12.5	s/c	2.4	1	53×110	786	431	80 ns	2.7
PI.KFA45	4	80	26.3	26.3/ 0	1.5 / 3	1	150×53	222	314.2 / 601.5	49 ns	0 - 2.6
PR.KFA71-79	12	80	15	15	2.6	1	147×53	221	1673	85 ns	0 - 2.1
BE.BSW14L4	1	0.5	-	-	0.765	36	141×144	540	946	5.25 ms	100
BE.BSW15L1	1	0.5	-	-	0.845	24	144×72	378	1336	5.25 ms	100
BE.BSW15L4	1	0.5	-	-	0.765	36	141×144	540	946	5.25 ms	100

5.3.2 PSB Ejection Dipoles

For ejection at 1.4 GeV it was necessary to increase the peak current in the bumper magnet from 500 A to 630 A. Whilst it was possible to conserve the existing magnets, their associated pulse generators were limited to 550 A peak current. In addition, the bumpers are now required to operate in PPM between 1 GeV and 1.4 GeV. In view of these new operating conditions, the need to interface to a new DSC-based control system and their advanced age, it was decided to completely replace the existing pulse generators [9].

The existing magnets, in use since 1970, were retained. BE.BSW14L4 and BE.BSW15L4 are PSB type 5 magnets, BE.BSW15L1 is a type 6 magnet. The magnets are connected in a series/parallel configuration which presents an effective impedance equivalent to that of a single magnet. This arrangement is identical for the three straight sections. Each bumper pulse generator excites four vertically superimposed magnets.

The relevant parameters for the three sections are given in Tab. 5.3. For operational purposes, I_{\max} is hardware limited to 690 A for all twelve magnets.

The operating principle is based on a resonant semi-sinusoidal current discharge into the bumper magnet with a freewheel diode/inductor circuit providing a partial recharge of the primary capacitor C1. Fig. 5.13 shows a simplified electrical circuit diagram for one bumper magnet group and its associated power supply.

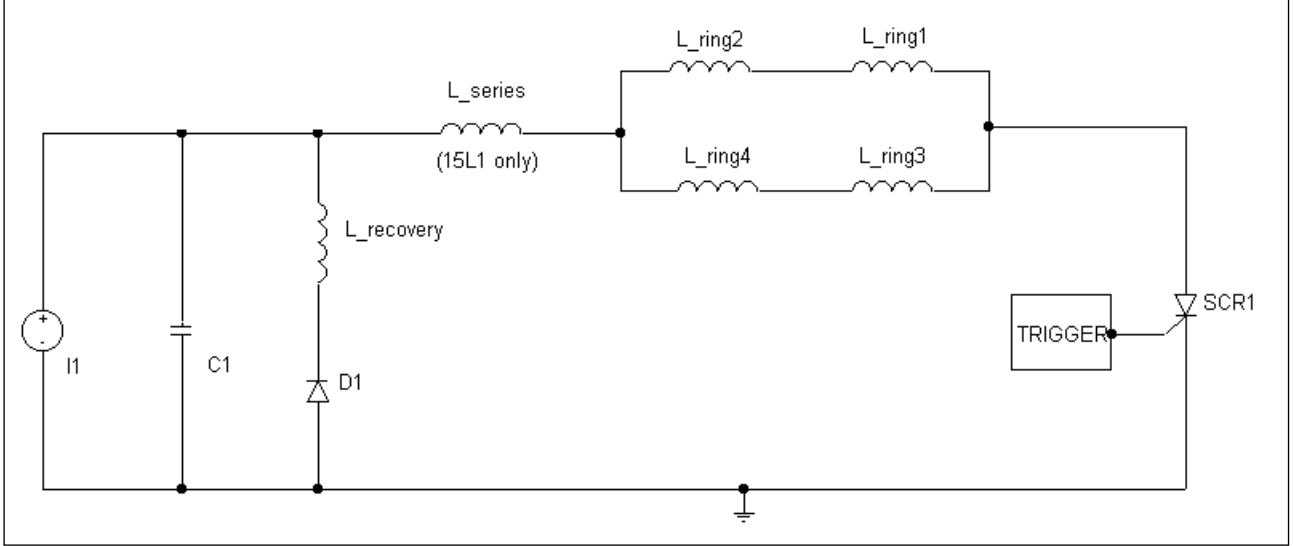


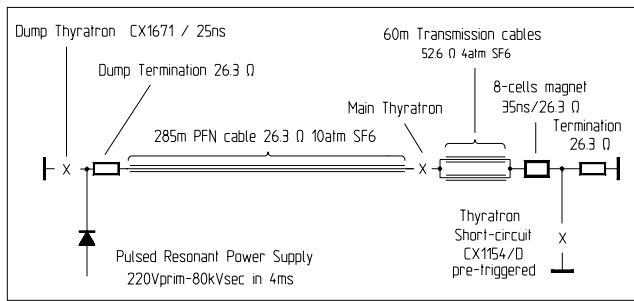
Fig. 5.13: Simplified circuit diagram of one bumper magnet group (four superimposed magnets).

C_1 is charged to a voltage V by a current source I_1 . When the semiconductor switch, SCR1 , is triggered, a resonance is excited between C_1 and the magnet inductances $L_{\text{ring}1}$, $L_{\text{ring}2}$, $L_{\text{ring}3}$ and $L_{\text{ring}4}$. This slightly-damped sinusoidal current is interrupted by the opening of SCR1 at the instance of zero-crossing. Time to peak of the current pulse is 5.25 ms. The free-wheel circuit comprising D_1 and L_{recovery} begins to conduct when the voltage on C_1 goes negative; a secondary, lower-frequency resonance then occurs between L_{recovery} and C_1 which ends when the current in D_1 starts to become negative. This results in C_1 completing the cycle with a positive charge, thereby reducing both the power losses and the post-cycle recharge period. An additional series inductance is required in the 15L1 circuit to compensate for the lower inductance of the type 6 magnets compared to the type 5 magnets.

5.3.3 PS Injection and Ejection Kickers

The PS injection and ejection kickers are re-used in their original configuration because they are sufficiently powerful. The PS injection Kicker PI.KFA45 works in a particular configuration (Fig. 5.14), which permits the doubling of the kick duration by short-circuiting the magnets during PPM and using timing shifts for use with ions. However, as proton injection for LHC is performed in two-batch filling mode, the previous kick rise-time had to be shortened to ~ 95 ns. This improvement was done with saturable inductors and matching elements, which are also very effective for the flatness and fall-time of the kick [10].

The improvement required for the PS ejection kicker KFA 71-79 (Fig. 5.15) was more dramatic. In the (now obsolete) debunching-rebunching scheme [11], 3 out of 84 bunches had to be discarded, which lead to the specified rise-time of 95 ns. However, even if 4 bunches were discarded, the resulting kick rise-time of 120 ns (0.5 - 99.5%) and flat-top stability of $\pm 0.5\%$ were very difficult to achieve. Extensive computer modelling indicated that this requested performance could be obtained. Here as well, the improvement could be achieved by the introduction of saturable ferrite inductors and suitably arranged filters [12]. With the change over to the bunch splitting scheme (Chap. 7), the rise-time requirements are significantly relaxed to 320 ns.



and no longer requires periodic in-situ regeneration of chemical products, except for the final ion exchangers.

It should be noted that the primary water temperature of the new system is subject to seasonal changes of the atmospheric coolant (air temperature, humidity), with concomitant variations of the PSB magnet temperature of up to 7°C. An extensive Machine Development (MD) session in July 1996 demonstrated that this temperature increase does not impair the PSB machine performance [13] at all.

The previous air conditioning system, with an installed power of 1.8 MW, was also adapted to atmospheric coolants, thus saving further 90 m³/h of town water (Tab. 5.5). The new device was also installed in building 237.

Table 5.5: PSB air cooling system, before and after upgrading.

	Old system	New system
Installed cooling power [MW]	1.8	3
Primary water circuit		
Flow rate [m ³ /h]	100	258
Average temperature [°C]	13	24
Town water consumption [m ³ /h]	100 (to drain)	10 (replacement)
Saving in town water consumption [m ³ /h]		90

More detailed information on this upgrading programme may be found in [14]. The overall saving in town water consumption (both systems) amounts to 190 m³/h. The renovated systems became operational for the accelerator start-up in March 2000.

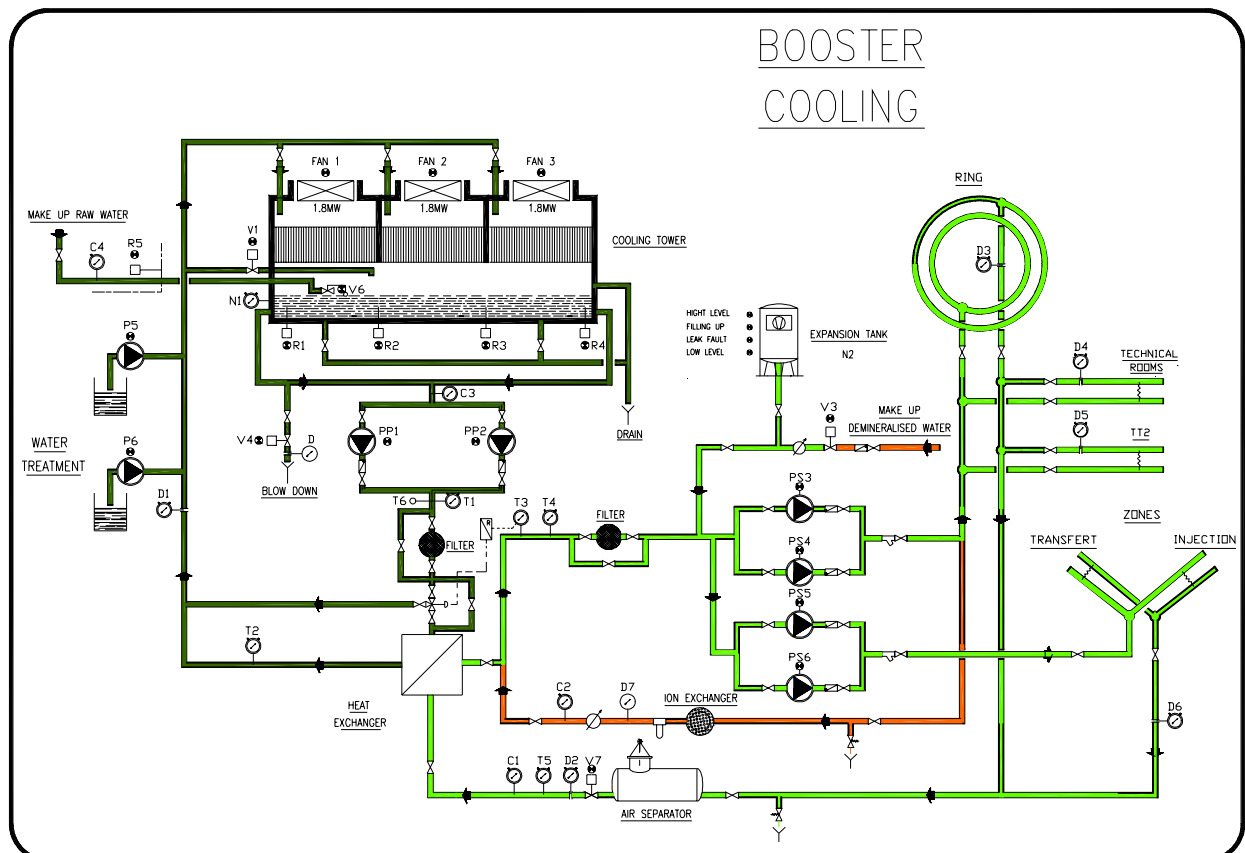


Figure 5.16: Demineralised water cooling system of the PSB after upgrading in March 2000.

REFERENCES

- [1] J. Borburgh, M. Hourican, M. Thievent, *A new set of magnetic septa in the CERN PS Complex*, Proc. PAC '99, New York, 1999.
- [2] G.S. Clark, A.J. Otter, P. Reeve, *Magnets for the CERN PS Booster transfer line*, Proc. PAC '97, Vancouver, 1997.
- [3] M.J. Barnes et al., *New Magnets for the transfer line PSB-CPS*, CERN SL-Note-98-052 MS, Geneva, 1998.
- [4] D. Evans, M.J. Barnes, B. Evans, R. Nussbaumer, *Rotating coil and data acquisition system for measuring CERN beam transferline quadrupole magnets*, Proc. of IMMW 10, Batavia, Illinois, 1999.
- [5] M.J. Barnes, G.S. Clark, M. Sassowsky, *Three dimensional field calculations compared to magnetic measurements for CERN PSB-CPS transfer line magnets*, Proc. PAC '99, New York, 1999.
- [6] A. Brückner, *Kicking protons, fast and cheap*, 1971 US Particle Accelerator Conf., Chicago, 1971.
- [7] A. Brückner, *A non-linear step-pulse steepening delay line*, CERN Report 68-25, Geneva, 1968.
- [8] K.D. Metzmacher, L. Sermeus, *The PSB Ejection and Recombination Kicker Systems for LHC*, PS/CA/Note 2000-004, Geneva, 2000.
- [9] A. Fowler, *The PSB ejection bumper system for LHC*, CERN PS-CA Note 99-22, Geneva, 1999.
- [10] K.D. Metzmacher, L. Sermeus, *The PS Injection Kicker KFA45 Performance for LHC*, PS/PO/Note 2002-015 (Tech.), Geneva, 2002.
- [11] M. Benedikt (editor), *The PS Complex as Proton Pre Injector for the LHC – Design and Implementation Report*, CERN 2000-003, Geneva, 2000.
- [12] K.D. Metzmacher, L. Sermeus, *The PS Ejection Kicker KFA71-79 Performance for LHC*, PS/PO/Note 2001-057 (Tech.), Geneva, 2001.
- [13] B. Dumas et al., *PSB ME 10.-19.7.1996: Cooling water in tunnel +7°C*, PS/HI/Note 96-10 (ME), Geneva, 1996.
- [14] W. Van Cauter, *Adaptation des systèmes de refroidissement et climatisation du Booster en vue du LHC*, CERN ST-CV/96.061/WVC/bm, Geneva, 1996.

CHAPTER 6

BOOSTER RF SYSTEMS

6.1 NEW PSB RF CAVITIES $H = 1$ (0.6 – 1.8 MHz)

The addition of cavities accelerating on RF harmonic $h = 1$ and supplemented with a $h = 2$ system, contributed to the reduction of harmful space charge effects and avoided the coupled bunch instabilities observed with the former acceleration scheme on $h = 5$ [1]. These advantages apply equally well for all other proton beams handled in the PS accelerator chain [2]. The system properties are summarised in Tab. 6.1.

A nominal peak RF voltage of 8 kV with ample margin is required, since high-intensity beams beyond 10^{13} particles per pulse and per PSB ring are to be handled. Vertical installation space is scarce due to the construction of the PSB with four superimposed rings which restrict the vertical size of any equipment. For this reason the idea to squeeze four cavities in one PSB straight section was abandoned and a second section had to be sacrificed to allow usage of large size ferrite rings.

Table 6.1: Main parameters of C02 RF system.

Frequency range	MHz	0.6 - 1.8	
Cav. equiv. capacitance ¹	pF	700	
Quality factor ¹ @			
0.6MHz		6.5	
1.2MHz		16	
1.8MHz		28	
Cav. shunt res. ¹ @	kΩ		
0.6MHz		2.5	
1.2MHz		3.0	
1.8MHz		3.4	
Beam impedance at resonance (with FB)	Ω	~ 300	
Ferrite type (Philips)		4A11	
Permeability at remanence		~ 600	
Tuning bias	A · turn	0 - 500	
Power density	mW/cm ³	64	
Magn. RF flux density	mT	4 - 12	
Cooling air flow	m ³ /s	1	
Ferrite ring size	cm	48×24×3	
Total ferrite length	cm	1500	
Nominal gap voltage	kV	8.0	
Max. gap voltage	kV	10.0	
Power loss	kW	13.0	
Peak power	kW	50	
CW power	kW	20	
RF feedback loop gain	dB	20	

6.1.1 Cavity Design

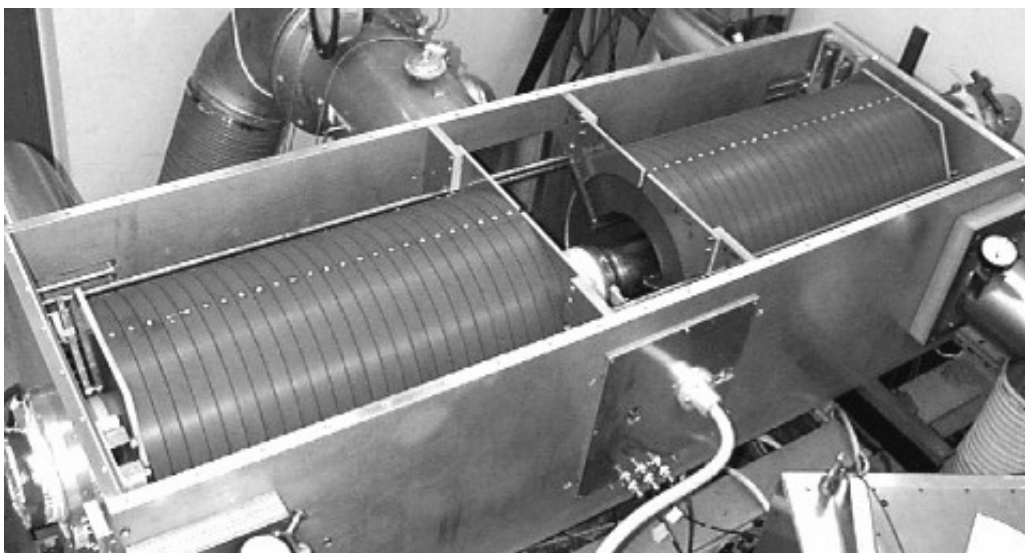


Figure 6.1: Ferrite loaded cavity C02.

¹ As seen across the gap at nominal voltage, with final amplifier and all accessories connected.

A classical and conservative NiZn ferrite-based design was chosen, essentially replicating the design of the one-gap type with virtual ground symmetry in the gap mid plane used for the other two PSB RF system cavities (Fig. 6.1) [3]. Air cooling of the ferrite through 1 mm spacing between rings gives the best ferrite filling factor, keeps the mechanical construction simple and is very cost effective compared with water cooling. The choice of Philips ferrite material grade 4A11 was made after tests on several small size ring samples. The absence of resonant absorption phenomena in the required working area was the main criterion.

PSB operation implies synchronisation of the four rings with the PS cycle on a magnetic flat top (duration up to 60 ms) at constant or very slowly changing RF frequency around 1.8 MHz. It is known that under such conditions ferrite can jump into the so-called High Loss Mode (HLM) at critical excitation and disturb the servo control of the RF voltage amplitude [4]. The onset of HLM appears to arrive earlier at higher DC saturation of the ferrite, i.e. towards the high frequency end of the tuned cavities. Fig. 6.2 shows the measured effect. The ferrite volume and cross section was chosen to stay safely below HLM onset at nominal RF voltage (8 kV_p). The ferrite grade selected exhibits a smooth and fairly stable transition into HLM and experience has shown that safe operation well beyond nominal voltage is possible. A temperature check of the individual rings in the operational cavities replaced laborious ferrite reception testing.

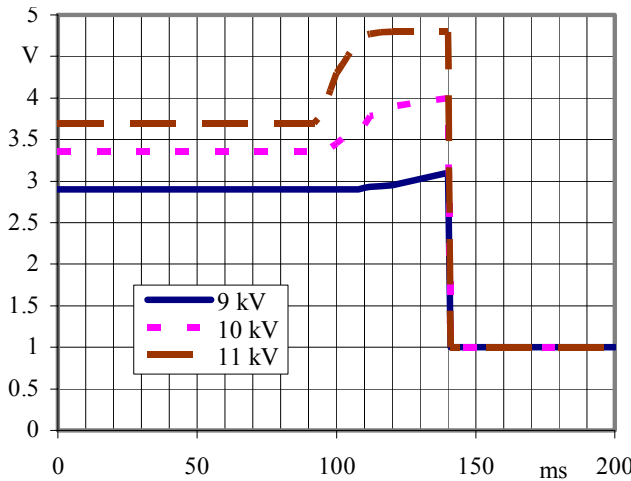


Figure 6.2: Final cathode current vs. time and gap voltage at $f = 1.8 \text{ MHz}$.

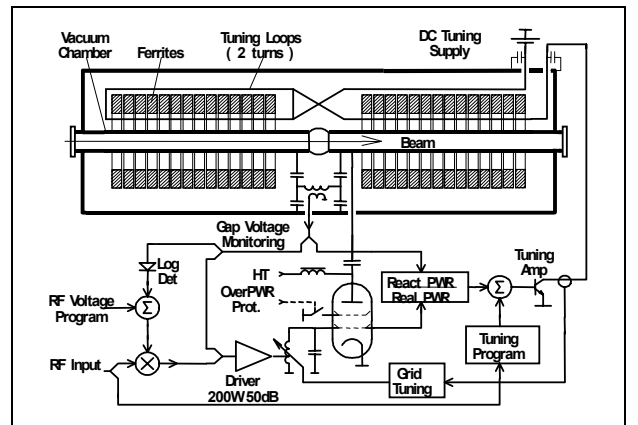


Figure 6.3: C02 system layout.

6.1.2 RF amplifier Chain

A conservatively-rated power amplifier was developed using the tetrode RS1084CJ, already widely used in the PS 10 MHz RF systems. Two newly developed wide-band transistor amplifiers plus a power combiner (100 kHz...100 MHz) serve both as driver and fast feedback amplifier. The whole unit is water-cooled. Feedback of the gap RF signal provides reduction of the cavity impedance to the beam by about 20 dB. Higher values are possible when needed. A particularity of the design is the use of a tuned low- Q resonant grid circuit [5], synchronised with the DC tuning current of the cavities. Advantages are higher gain, smaller drive power and the possibility to program phase response for increased feedback loop stability. The movable amplifiers are placed near to the cavities and can be easily replaced in case of a repair. The system layout is sketched in Fig. 6.3.

6.1.3 System Electronics Layout

The system electronics were developed to cover the frequency range of 0.5-20 MHz and are used in all PSB RF systems. Servo control of RF voltage amplitude is provided by logarithmic detector and modulator electronics (Fig. 6.3). The detector has a 70 dB dynamic range and ~0.5 dB absolute precision in the working range. Frequency response to modulation is 200 kHz for the detector and 40 kHz for the voltage control loop. The cavity tuning uses a novel IGBT linear current amplifier, which is controlled by a reactive power detection module. Maximum current is 400 A and tuning loop response to small perturbations extends to 500 Hz. The frequency to tuning current relationship is pre-programmed in a memory; fine tuning is handled

in the analogue feedback loop which automatically turns on when the gap voltage exceeds ~ 100 V. An RF over-power detector acts rapidly on the final tube screen grid to prevent system trips. Two systems like those shown in Fig. 6.4 are installed in PSB straight sections 10L1 and 7L1.



Figure 6.4: C02 test mount for PSB rings II and IV.

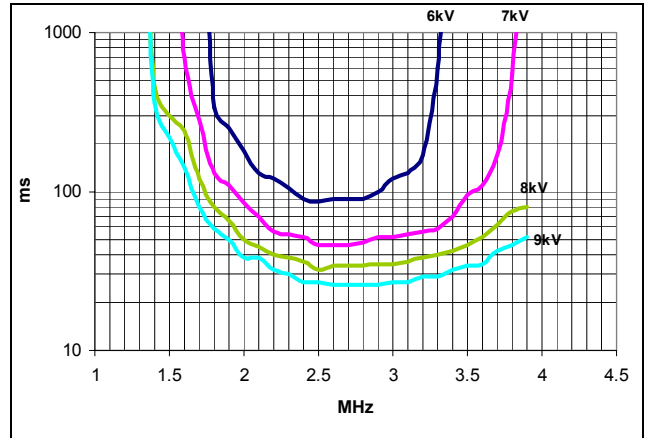


Figure 6.5: High loss mode on-set time.

6.2 CONVERTED PSB $H = 2$ CAVITIES (1.2 – 3.9 MHz)

With the abandoning of RF harmonic $h = 5$ it became possible to modify the existing equipment for $h = 2$ operation at little cost. Cavity modifications mainly consisted in increasing the gap equivalent capacitance, to shift the working frequency range to 1.2 – 3.9 MHz and replacing the gap voltage divider with a calibrated, wide-band unit.

Although the gap voltage required for $h = 2$ operation is only 2/3 of the previously used voltage at $h = 5$ (8 kV instead of 12 kV), the frequency decrease by a factor 2/5 results in an RF induction increase given by the ratio of the two factors (~ 1.7). This pushes the ferrite (Philips 4L2) more to its limits and the nominal RF voltage is reached without much margin. Ferrite entering into HLM, which with this ferrite grade appears to be unstable, is the critical parameter. Operation at constant frequency (~ 3.5 MHz) for synchronisation of the four rings with the PS RF system, has to be limited in duration as shown in Fig. 6.5.

The existing push-pull power amplifiers, using two RS2012CL tetrodes, have been retained without modifications. They are air-cooled and share the cooling system with the cavities (Fig. 6.6).

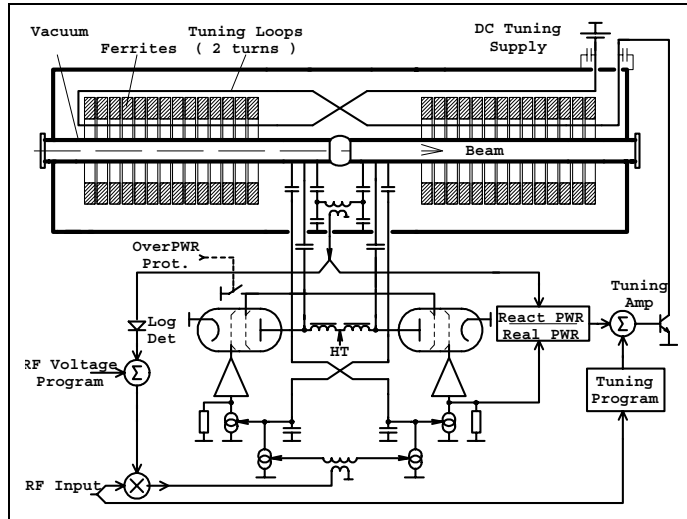


Figure 6.6: C04 system layout.

Standard 100 W wide band amplifiers already used in the C02 systems have been added as fast feedback power drivers. Feedback of the gap RF signal provides reduction of the cavity impedance to the beam by 26–32 dB.

Although most of the heavy hardware has been retained, control and servo electronics have been replaced with the new, wide-band standard electronics developed for the C02 system. The system properties are therefore similar to those already described in the previous section. The system properties are summarised in Tab. 6.2.

Table 6.2: Main parameters of C04 RF system.

Frequency range	MHz	1.2 – 3.9	Tuning bias	A · turn	0 – 1800
Cav. equiv. capacitance	pF	650	Power density	mW/cm ³	31
Quality Factor @			Magn. RF flux dens.	mT	3.2 – 9.4
1.2 MHz		85	Cooling air flow	m ³ /s	1
2.5 MHz		130	Ferrite ring size	cm	20×35×3
3.9 MHz		190	Total ferrite length	cm	1500
Cav. shunt res. @	kΩ		Nominal gap voltage	kV	8.0
1.2 MHz		17.5	Max. gap voltage	kV	9.0
2.5 MHz		12.5	Power loss	kW	3.0
3.9 MHz		12.0	Peak power	kW	20.0
Beam Impedance (with FB):	Ω		CW power	kW	10.0
1.2 MHz		< 440	Feedback loop gain @	dB	
2.5 MHz		< 440	1.2 MHz		> 32
3.9 MHz		< 600	2.5 MHz		> 29
Ferrite Type (Philips)		4L2	3.9 MHz		> 26
Permeability at remanence		~200			

6.3 PSB BEAM CONTROL MODIFICATIONS

The PSB is composed of four superimposed rings, each having three cavities described in Tab. 6.3.

Table 6.3: PSB cavities.

Cavity	Frequency range	Maximum voltage	Use (for protons)	Use (for ions)
C02	0.6 → 2 MHz	8 kV	Acceleration on $h=1$	Acceleration $h=4$ up to 1.8 MHz ($f_{\text{rev}}=450$ kHz)
C04	1.2 → 3.9 MHz	8 kV	Bunch flattening Bunch splitting ($h=1 \rightarrow 2$) at 1.4 GeV Acceleration on $h=2$	Acceleration on $h=4$ from 1.8 MHz ($f_{\text{rev}} = 450$ kHz) up to 3.86 MHz ($f_{\text{rev}} = 965$ kHz)
C16	5 → 16 MHz	6 kV	Controlled longitudinal blow-up during acceleration	Acceleration of 4 bunches of Indium on $h=8$ up to $f_{\text{rev}}=1.13$ MHz

The present beam control was installed in 1998 within the framework of the harmonic change from $h = 5$ to $h = 1$ and/or $h = 2$. Its structure is based on one digital frequency synthesiser per cavity, each digital frequency word being directly derived from the main magnetic field measurement (B to f conversion). The present architecture is represented in Fig. 6.7. For one PSB ring, LHC beam parameters are:
one single proton bunch, 190 ns long, obtained with longitudinal blow-up (momentum spread), $\Delta p/p = \pm 2.5 \times 10^{-3}$ ($\pm 2\sigma$).

6.3.1 Hardware Layout

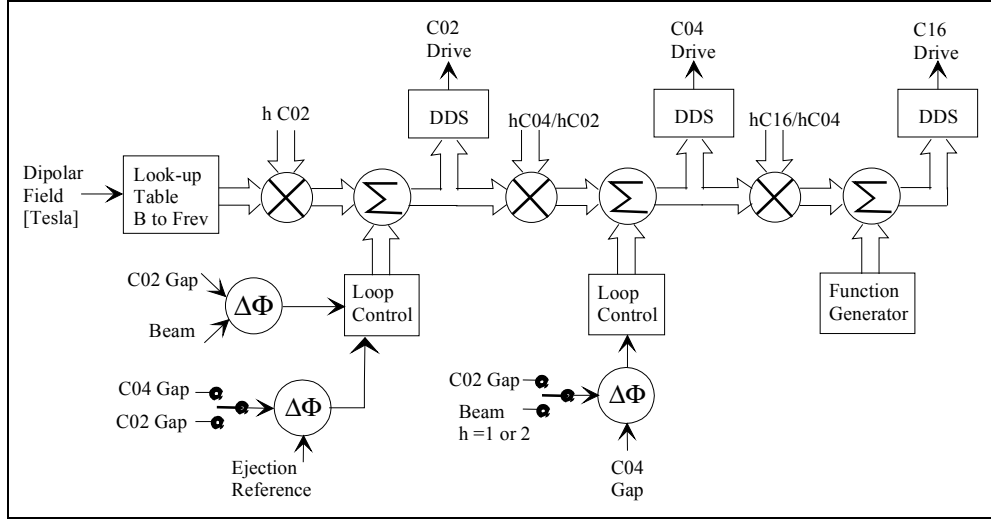


Figure 6.7: PS Booster Beam Control layout.

Fig. 6.7 shows that the measured value of the bending field (“*B*-train”) is used for generating the frequency words feeding all three cavities. The revolution frequency (f_{rev}) is obtained from a look-up table (typically a read only memory) and multiplied by the harmonic number aimed for C02 ($h = 1$ for LHC beams). The resulting frequency is summed with the loop (phase and synchronisation) error signals, to obtain the actual C02 RF value sent to the cavities via a digital synthesiser.

C16, when used as a “controlled blow-up” cavity, is not included in any loop. Its harmonic value is just set to different integer values during acceleration so as to be the highest possible. A phase modulation (at a rational multiple of f_S) is then applied to obtain the desired emittance growth in the same way as in the PS or SPS [6]. When accelerating Indium on $h = 4$, the required RF-frequency at extraction (4.52 MHz) is above the limit of the C04 system, while still below the C16 frequency range. Therefore, the $h = 4$ beam, held by C04, is captured (hand-over process) in every second $h = 8$ bucket of C16 and accelerated until extraction.

The main advantages of the digital structure are:

- The look-up-table on the left-hand side of Fig. 6.7 sets the RF frequency to keep the beam on orbit for any magnetic field. This feature makes it possible to accelerate a beam with all loops open (albeit with some losses and instabilities). In the previous (analogue) version, only the radial loop could establish the required frequency to keep the beam centred but the position detectors were quite hard to run with low intensity beams (e.g. lead ions).
- All cavities are naturally locked in frequency even with loops open; this avoids the presence of an integrating type of corrector in the different phase loops (simplified correctors and more stability margins).
- In the old system, the loss of beam led to saturation of the different loops and erratic behaviour of the frequency and voltage programmes necessitating security interlocks to protect the power equipment which were quite heavy to handle. In the new system the loops only have to act on a small frequency range and do not provoke cavity trips.

6.3.2 The Transition to $h = 1$

Since its running-in period in 1972, the PSB machine was subject to many improvements. The most important was the introduction of a second harmonic cavity on each ring in 1983. The peak accelerated intensity levelled off from that time at about 3.4×10^{13} protons per pulse (ppp) with all four rings (1.1×10^{13} on ring 2). The introduction of a fast feedback on the cavities in 1985 improved the reliability of operation, but did not improve the record value.

During the first $h = 1$ run in 1998, operation was disturbed by the impedance of the vacuum flanges around the ring. The resonances of these flanges gave a total (integrated around the ring) longitudinal coupling impedance of 450Ω at 750 kHz [7] which is the RF frequency range at the beginning of the cycle. The return voltage generated by the beam current was coupling to different electronic devices which therefore had to be

equipped with common mode rejection circuits. Some coupling between rings remained, implying adjustment of the radial position to avoid beating between cavities near the synchrotron frequency. After some flanges had been short-circuited during the 1998-99 shutdown the total impedance was lowered to about 200Ω (still higher than the maximum value for $h = 5$ which was 130Ω). This eliminated the frequency beating from one ring to the other as a source of trouble and helped to reach a new intensity record in September 1999: 4.1×10^{13} protons per pulse accelerated in the PSB with 1.2×10^{13} in ring 2. New RF decoupling flanges were introduced in the 1999-2000 machine shut-down to further reduce the impedance [7].

The transition to $h = 1$ eliminated the coupled bunch mode instabilities (not present with a single bunch) and thus made the complex feedback system as well as the “Hereward” damping system (tackling quadrupolar bunch-shape oscillations) superfluous. This last effect, not formally studied, might be explained by a criterion given in [8, 9] that relates the loss of Landau damping to the beam current. The current threshold, proportional to V_{RF}/h , has been improved by a factor 3.3 when moving from $h = 5$ to $h = 1$. The absence of the quadrupolar loop indirectly permitted an increase of the $h = 2$ versus $h = 1$ voltage ratio limited to 50% in the former system where beam amplitude detection was misled by double peaked bunches.

Another improvement came from the C04 ($h = 2$) cavities. These were obtained from the conversion of the older C08 cavities that were used as the main $h = 5$ drive cavities. They have more voltage and power margin than the previous C16 cavities used at $h = 10$ and thus run more reliably whenever the phase relationship between $h = 1$ (C02) and $h = 2$ (C04) is critical in terms of power demand from $h = 2$.

All these improvements certainly contributed to the record intensity increase. In summary, the main advantages of the $h = 5$ to $h = 1$ conversion are:

- Feasibility of two-batch filling of the PS as required for the LHC beam.
- Increase of longitudinal acceptance (proportional to $\sqrt{V_{\text{rf}}/h}$).
- No need of coupled bunch mode feedback system.
- Less longitudinal space charge effect \Rightarrow no need for Hereward damping at present intensities.

REFERENCES

- [1] F. Blas et al., *Conversion of the PS complex as LHC proton pre-injector*, Proc. of PAC '97, Vancouver, 1997.
- [2] R. Cappi, R. Garoby, S. Hancock, M. Martini, J.P. Riunaud, K. Schindl, H. Schönauer, *Beams in the PS complex during the LHC era*, CERN/PS 93-08 (DI), Geneva, 1993.
- [3] U. Bigliani et al, The RF Accelerating System for the CERN PS Booster, IEEE Trans. Nucl. Sci. NS-18, No3, 1971.
- [4] J.E. Griffin, G. Nicholls, *A review of Some Dynamic Loss Properties of NiZn Accel. RF System Ferrite*, IEEE Trans. Nucl. Sci., Vol. NS-26, No.3, 1979.
- [5] R. Garoby et al, *RF System for High Beam Intensity Acceleration in the CERN PS*, CERN/PS 89-28 (RF), Geneva, 1989.
- [6] T. Bohl, T. Linnecar, E. Shaposhnikova, W. Sinclair, U. Wehrle, *Study of controlled longitudinal blow-up in the SPS using the 800 MHz rf system*, CERN SL-MD Note 221, Geneva, 1996.
- [7] A. Blas, C. Carli, M. Chanel, C. Lacroix, *Reduction of the Impedance Created by the Insulated Vacuum Flanges in the PS Booster*, Proc. EPAC 2000, Vienna, 2000.
- [8] A. Hofmann, F. Pedersen, *Bunches with local elliptic energy distributions*, IEEE transactions on nuclear science, Vol. NS-26, No.3, June 1979.
- [9] F. Pedersen, F. Sacherer, *Theory and performance of the longitudinal active damping system for the CERN PS Booster*, CERN/PS/BR/77-8, Geneva, 1977.

CHAPTER 7

BUNCH SPLITTING AND BUNCH ROTATION IN THE PS

7.1 NOMINAL BUNCH TRAIN SCHEME

In the nominal mode of operation for filling LHC, the PS delivers beam every 3.6 s in batches of 72 bunches spaced by 25 ns. This interval between bunches is preserved up to the LHC. To prepare this beam from the 6 bunches supplied by the PSB in two batches, specially developed splitting schemes are used [1].

Moreover, for a proper capture by the 200 MHz RF in the SPS, a bunch rotation process is applied just before ejection from the PS to reduce the 0.35 eVs bunches to 4 ns length.

Many different LHC filling schemes can be applied [2], the most favourable ones requiring the SPS to capture and accelerate 4 batches of 72 bunches from the PS.

7.1.1 Bunch Splittings

The complete process is sketched in Fig. 7.1. Six bunches delivered in two batches by the PSB are captured on harmonic $h = 7$ in the PS. Triple splitting is started as soon as the second batch is received, which provides 18 consecutive bunches on $h = 21$. The beam is then accelerated on this harmonic up to the 25 GeV flat-top, where each bunch is twice split in two to give 72 consecutive bunches on $h = 84$. This leaves a 320 ns gap in the bunch train for the rise-time of the ejection kicker.

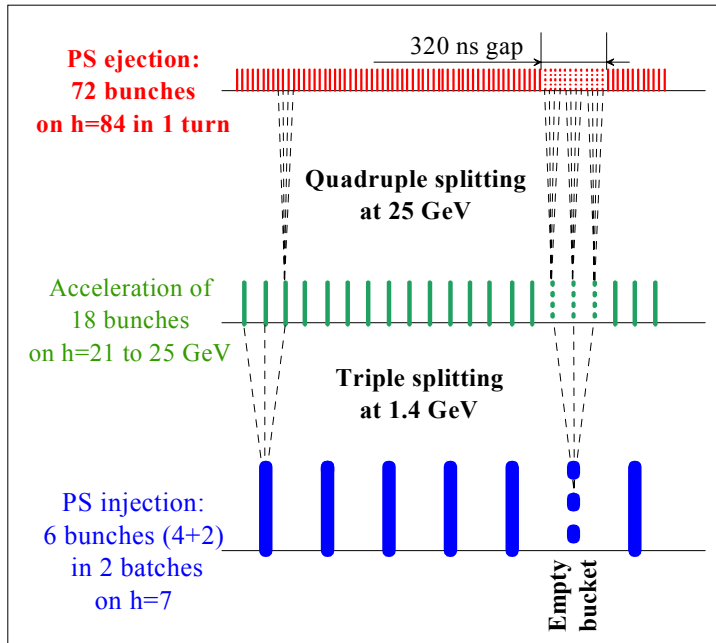


Figure 7.1: Generation of the nominal bunch train for LHC (25 ns bunch spacing).

Triple splitting requires three simultaneous RF harmonics ($h = 7, 14$ and 21). The voltages of these three components and the corresponding evolution of the distribution of particles in the longitudinal phase plane are represented in Fig. 7.2. A stable phase on $h = 21$ and an unstable phase on $h = 14$ coincide with the stable phase on $h = 7$. Starting with $h = 7$ alone, the effect of increasing the voltages on $h = 14$ and 21 is to flatten the bunch ($t=7$ ms in Fig. 7.2). In phase space, two new stable points emerge close to the initial one, encircled by 3 buckets. If the rate of change of the voltages is sufficiently slow, the particles of the initial bunch are gradually captured in these new buckets, whose area grows as the voltage decreases on $h = 7$ and increases on $h = 21$ ($t=14$ ms in Fig. 7.2). Using numerically determined laws of variation, the three areas

are kept equal throughout the process, so that layers of increasing emittance in the initial bunch are progressively peeled off and accumulated evenly into the three new buckets. Three equal bunches are finally obtained, each with the same distribution of particle density as the initial one ($t=25$ ms in Fig. 7.2). A beam phase loop is active during the whole process (see Sec. 7.4). It controls the phase of the sum of all harmonics, whose relative phase is rigidly fixed. Avoiding collective beam oscillations with respect to the RF is essential to preserve the total longitudinal emittance and obtain equal bunches (Fig. 7.3).

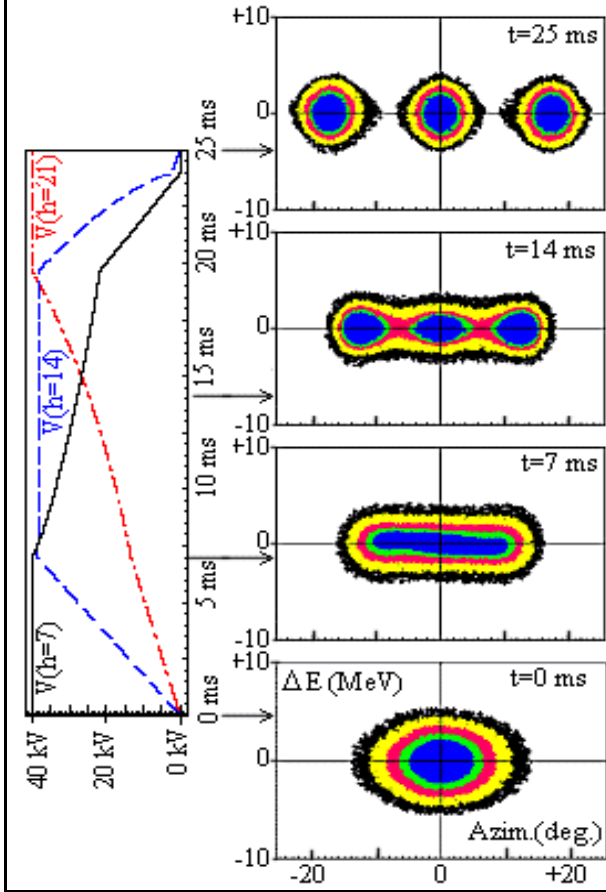


Figure 7.2: Simulation of triple splitting at 1.4 GeV in the PS.

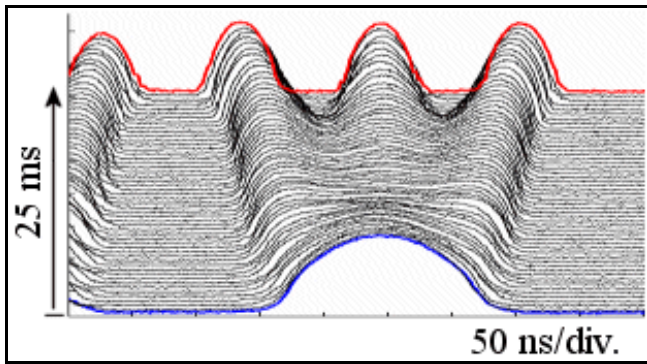


Figure 7.3: Triple splitting for the nominal beam (initial PSB bunch $\sim 1.35 \times 10^{12}$ protons).

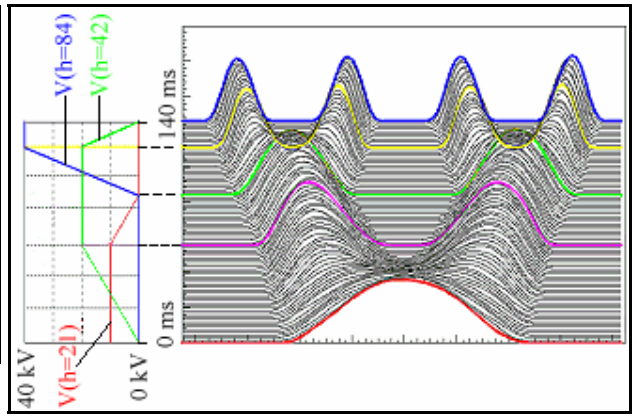


Figure 7.4: Quadruple splitting in the PS (ESME simulation).

For quadruple splitting at 25 GeV three groups of cavities, also operating on harmonics 21, 42 and 84 are employed. New 20 and 40 MHz RF systems have been installed in the PS for these last two harmonics (see

Chap. 8). This scheme is a duplication of the splitting in two process which is extensively used in regular operation. The relative phase between harmonics is rigidly fixed and a beam phase loop suppresses collective oscillations with respect to the RF sum voltage. Simulation (Fig. 7.4) predicts that the longitudinal emittance will not increase and this is also approximately observed in reality (Fig. 7.5). Performance degrades as intensity increases, because of coupled bunch instabilities which give different initial conditions for the different bunches and lead to discrepancies between the bunches.

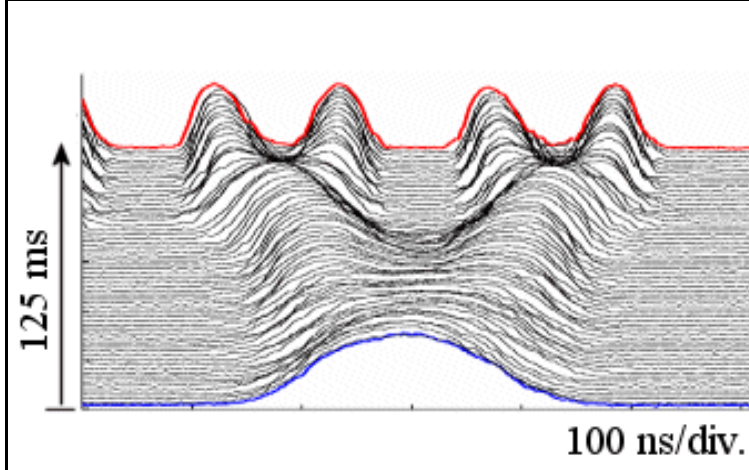


Figure 7.5: Splitting of a bunch of $\sim 0.45 \times 10^{12}$ protons at 25 GeV in the PS.

The parameters of the overall process are summarised in Tab. 7.1 (the intensities quoted assume 100% transmission from PSB to the LHC). The only disadvantage with the nominal bunch train scheme is that, since it uses only 7/8 of the total PSB intensity, the intensity per ring and the beam brightness in that machine have to be 14% higher than for the original scheme [3]. As a consequence, the PSB can no longer achieve the brightness and intensity required for the ultimate beam in the LHC (see Sec. 2.3 and 10.5). This is however counter-balanced by the fact that the beam is always under control of the RF, so that phase oscillation damping loops can be active and the necessary performance can be reliably attained. In addition there are the following features:

- The beam is never debunched, so that the microwave instability threshold is less of a concern.
- The gap without particles corresponding to the missing PSB bunch is preserved. This empty gap of 320 ns at ejection gives ample space for the rise-time of the kicker.

Table 7.1: Nominal PS complex operation for filling LHC.

No. of bunches per PSB ring	1
No. of PSB cycles per PS cycle	2
No. of bunches from PSB per PS cycle	6
h at PS injection	7
Bunch splitting at 1.4 GeV	$1 \Rightarrow 3$
h between 1.4 and 25 GeV	21
No. of bunches between 1.4 and 25 GeV	18
Gymnastics at 25 GeV	Double bunch splitting ($1 \Rightarrow 4$)
h at PS extraction	84
No. of bunches to SPS per PS cycle	72
PS intensity at 1.4 GeV for $1.15 \cdot 10^{11}$ p/LHC bunch (nominal)	8.28×10^{12}
Intensity per PSB ring	1.38×10^{12}

7.1.2 Bunch Rotation

At the end of the splitting process at 25 GeV, each of the 72 bunches, held by 100 kV of RF on $h = 84$ (40 MHz), is 11 ns long. The following non-adiabatic procedure is then applied to reduce it to 4 ns:

- 290 μ s before ejection, the voltage on $h = 84$ is stepped up to 300 kV in approximately 20 μ s,
- 180 μ s later, the voltage on $h = 168$ (80 MHz) is stepped up to 300 kV in approximately 20 μ s.
- 110 μ s later, ejection is triggered when the bunches are at their shortest.

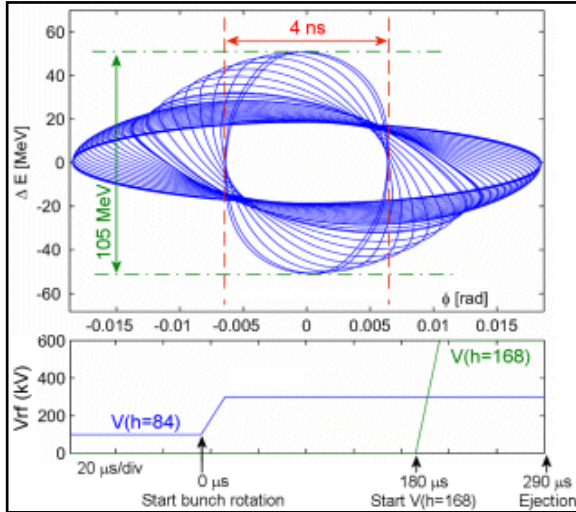


Figure 7.6: RF voltages (bottom) and bunch contour (top) during bunch rotation at 25 GeV.

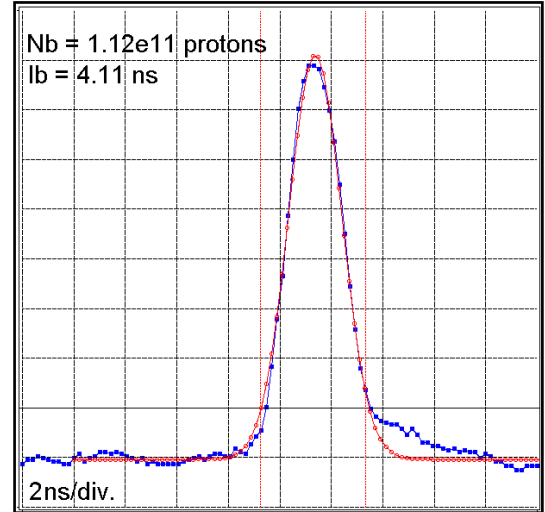


Figure 7.7: Nominal bunch at ejection to the SPS.

This is illustrated in Fig. 7.6, together with the computed result in the longitudinal phase space. No distortion is visible on the final contour. The experimental result measured with a nominal intensity beam is shown in Fig. 7.7.

7.2 ALTERNATIVE BUNCH TRAINS

Electron multipactoring (manifesting itself as the electron cloud effect) has recently been diagnosed as a dominant contributor to the heat load to the LHC cryogenic system, potentially limiting drastically the machine performance [4]. Among the many actions envisaged to solve the problem, a number of them require the beam time structure to be modified, either doubling the distance between bunches or introducing more gaps in the bunch train.

The multiple splitting technique is extremely flexible and offers several possibilities of changing the bunch train in ways which could not be achieved using the initial, more conventional debunching-rebunching technique.

7.2.1 75 ns Bunch Spacing

Keeping the same intensity per bunch, but changing the separation between bunches from 25 to 75 ns, the electron cloud problem can be drastically reduced, both in the SPS and in the LHC, while providing one third of the luminosity in all interaction points of the collider. To generate such a train, a scheme based on two double splittings in the PS is being used (Fig. 7.8).

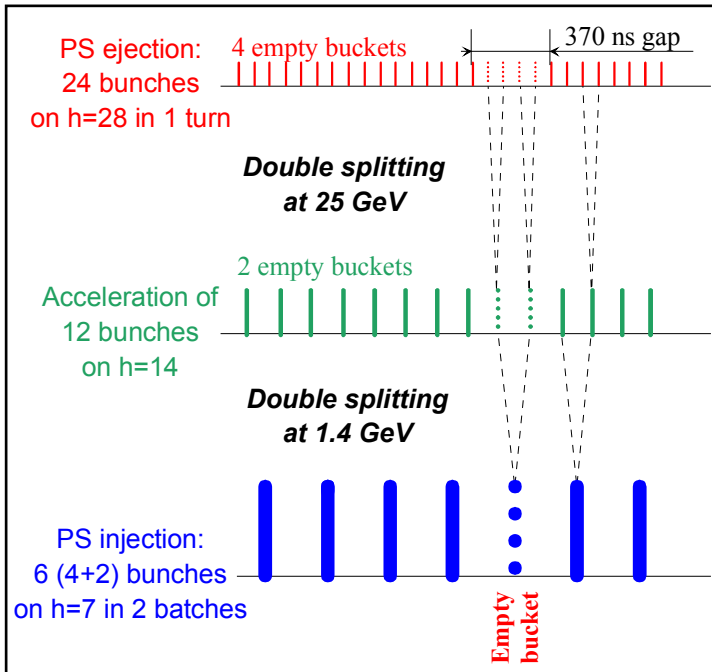


Figure 7.8: Generation of a 75 ns bunch train.

Six bunches delivered in two batches by the PSB are captured on harmonic $h = 7$ in the PS. Double splitting is started as soon as the second batch is received, which provides 12 consecutive bunches on $h = 14$. The beam is then accelerated on this harmonic up to the 25 GeV flat-top, where each bunch is again split in two to give 24 consecutive bunches on $h = 28$. They are then captured on $h = 84$ without any further splitting and the bunch rotation process is triggered with the same initial conditions as in the nominal scheme. This leaves a 370 ns gap in the bunch train for the rise-time of the ejection kicker. The 15 kV necessary on $h = 28$ (13.3 MHz) are delivered by the new RF system which was prepared for operation on $h = 42$ (20 MHz) but which has been made tuneable (Sec. 8.1).

Typical results when delivering the nominal intensity per bunch are shown in Fig. 7.9 and Fig. 7.10.

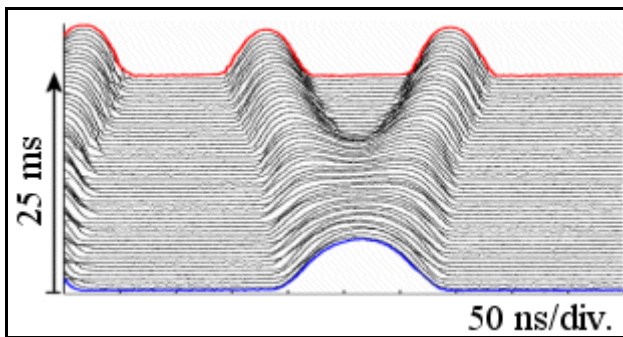


Figure 7.9: Splitting from $h = 7$ to $h = 14$ of a bunch of $\sim 5 \times 10^{11}$ protons at 1.4 GeV in the PS.

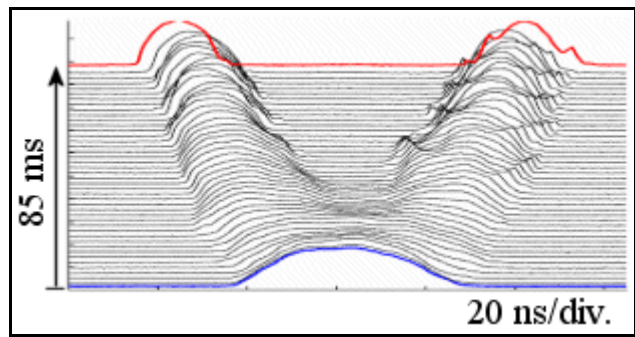


Figure 7.10: Splitting from $h = 14$ to $h = 28$ of a bunch of 2.3×10^{11} protons at 25 GeV in the PS.

7.2.2 50 ns Bunch Spacing

Bringing the separation between bunches from 25 to 50 ns, with the same intensity per bunch, the electron cloud problem will also be reduced, although by a smaller factor than with 75 ns spacing. Luminosity in the LHC, will reach one half of the nominal value, but not simultaneously in all three interaction regions. Such a train is obtained with the process described in Sec. 7.1.1 for the nominal beam, but without the second

splitting in two at 25 GeV. The RF on $h = 84$ is turned on with opposite phase, so that the bunches are more focused by the action of this harmonic instead of being split. A total of 36 bunches are finally obtained, spaced by 50 ns and with a 345 ns gap without particles. Proper operation of this scheme has been demonstrated at the nominal intensity per LHC bunch.

7.2.3 Exotic Bunch Trains

In all the previously described bunch trains, it is operationally simple to create more gaps without beam by suppressing one or more PSB bunches.

Moreover, if necessary, other types of beams can be prepared, for example by changing the phasing between harmonics 7, 14 and 21 at 1.4 GeV (Fig. 7.11) to split bunches in two instead of three. This gives 8 bursts of 7 bunches spaced by 25 ns, separated by 4 empty buckets (120 ns gaps) at 25 GeV.

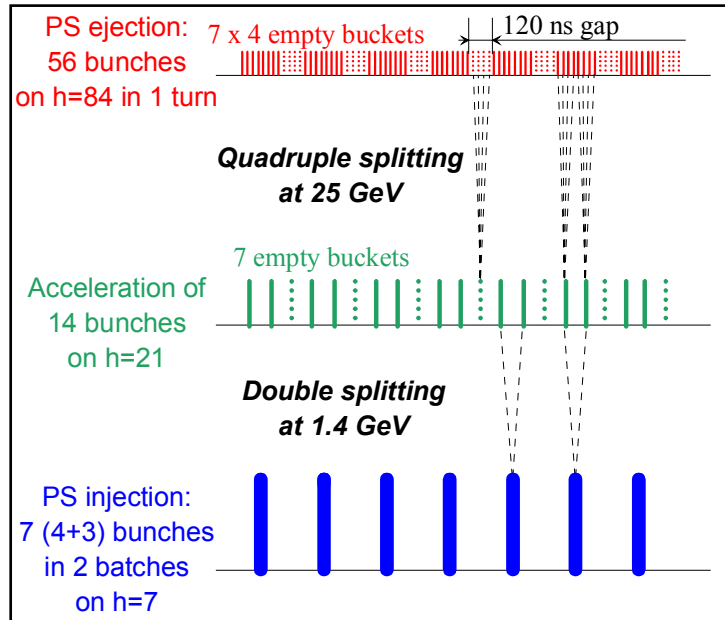


Figure 7.11: Generation of bursts of 25 ns spaced bunches.

7.3 REPERCUSSION ON OTHER BEAMS

The switch of the PSB from a systematic number of five proton bunches per ring to one or two bunches led to a redesign of all RF operations both in the PSB and the PS and renewal of the beam control equipment. Although not fully up-to-date, an extensive analysis of the PS complex' operational beams after the conversion to LHC may be found in [5]. Tab. 7.2 summarises the characteristics and modes of operation in typical cases.

These fundamental changes prove favourable to the quality of most of the beams because of the following main advantages.

In the PSB:

- The longitudinal acceptance is increased by the use of harmonic 1, thus eliminating a long-standing bottleneck.
- Longitudinal coupled bunch instabilities, which were cumbersome to circumvent, are no longer possible with a single bunch per ring.
- Controlled longitudinal blow-up (using the C16 RF system) and bunch splitting (using the C2 and C4 systems) are now possible.
- The rise-times of the PSB ejection, recombination and PS injection fast kicker magnets are now relaxed to at least 90 ns (instead of 60 ns when the PSB was operating with 5 bunches).

In the PS:

- With one bunch per PSB ring, schemes to fill a fraction of the PS with four PSB rings can be designed (LHC, antiproton production beam for the AD, etc.).
- The very long bunches (50 to 100 m in both PSB and PS) cover a narrower frequency spectrum, so that they do not probe potentially harmful impedances at high frequencies.
- With an injection energy of 1.4 GeV, space-charge is reduced for all high intensity beams, such as SPS fixed target physics, AD production, etc.. Moreover, beam losses between PSB and PS are reduced due to the smaller beam size of the highest intensity beams.

Table 7.2: Typical operational beams and ways to produce them.

	ISOLDE	LHC nominal	SPS physics	SPS ion physics	East Hall	AD p-bar production	AD test
Particle	p	p	p	Pb ⁸²⁺	p	p	p
PSB extraction				(Pb ⁵³⁺)			
Energy/nucl. [GeV]	1/1.4	1.4	1.4	0.145	1.4	1.4	1.4
Charges/ring	8×10^{12}		8×10^{12}	5×10^9	$\sim 3 \times 10^{11}$	5×10^{12}	4×10^{10}
Harmonic number	1	1	2	4	1	1	2
Bunch splitting.	no	no	yes	no	no	no	no
Rings used	4	4+2	4	4	1	4	1
PSB batches	1	2	1	1	1	1	1
Bunch spacing at PS injection [ns]			286	259		286	
Bunch length [ns]	190	190	176	90	50-120	190	140
Kicker rise/fall time maximum [ns]	382		110	169		96	
PS injection							
Charges		10^{12}	3×10^{13}	2×10^{10}	$\sim 3 \times 10^{11}$	2×10^{13}	2×10^{10}
Harmonic number		7	8	16	8	8	16
Number of bunches		6	8	16	1	4	1
Bunch splitting at low energy		$h7 \rightarrow h21$ (1.4 GeV)	$h8 \rightarrow h16$ (2.75 GeV)	no	no	no	no
PS extraction							
Energy [GeV]		25.1	13.1	19.1	23.1	25.1	2.74
Harmonic number		84	420	16	debunched	20	16
Number of bunches		72	420	16		4	1
RF gymnastics before extraction		2 double splittings + rotation	debunching rebunching	none	debunching & slow extraction	h sweep from 8 to 20 and rotation	none
Comments			often lower intensity	in-flight transfer C02-C04 in PSB	lower intensity often required		1 bunch discarded at PS injection

7.4 PS BEAM CONTROLS

7.4.1 Capture, low energy splitting and acceleration

For capture at 1.4 GeV and acceleration up to 25 GeV, each of the 10 PS ferrite cavities is driven by its own Direct Digital Synthesizer (DDS), (called Multi-Harmonic Source or MHS), clocked on harmonic 128 of the revolution frequency. The phase and radial loops control the $h = 128$ clock (Fig. 7.12).

The open loop revolution frequency is derived from a look-up table controlled by a real-time B -field measurement (B -train). After digital multiplication by 128, the open loop frequency word is added to a digital correction signal generated by the phase and radial loop to control the main DDS on $h = 128$. The

phase and frequency for each cavity is given by its MHS, driven by the $h = 128$ clock and using the instantaneous value of the harmonic provided by a function generator.

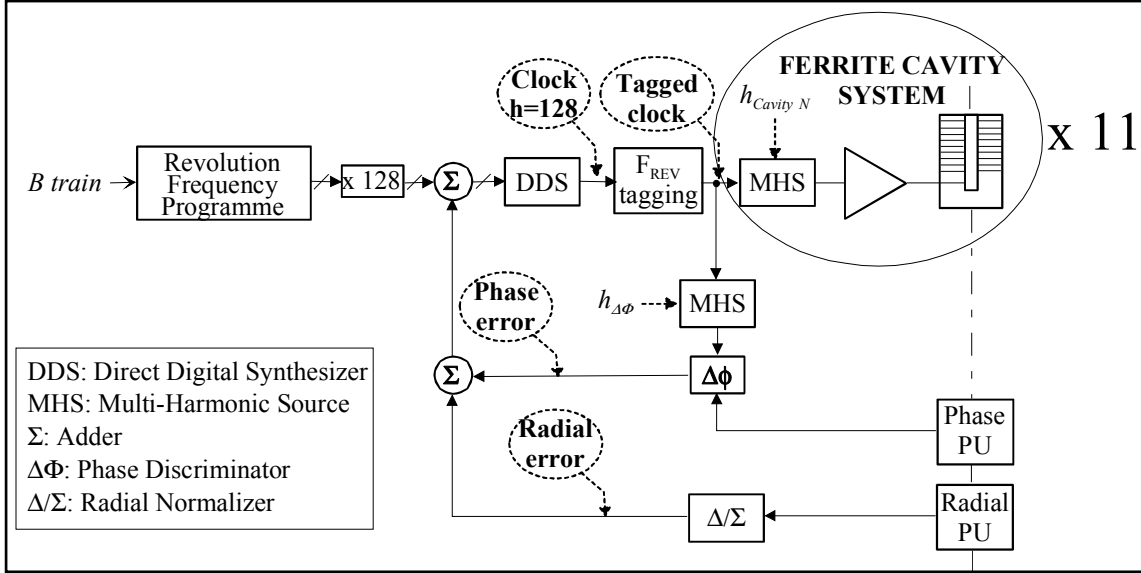


Figure 7.12: PS beam control used from injection till the beginning of the 25 GeV gymnastics.

Phase measurement is done at an harmonic defined by a specific function generator, driving a dedicated MHS. Switching time is negligible with respect to the time response of the loop. Timings control the precise moment when the harmonic number is changed. In these conditions, coherent ($n=0$) bunch phase oscillations are avoided up to the highest intensities required by operational beams, which is essential for reliable performance of the whole process.

7.4.2 Beam Gymnastics at 25 GeV

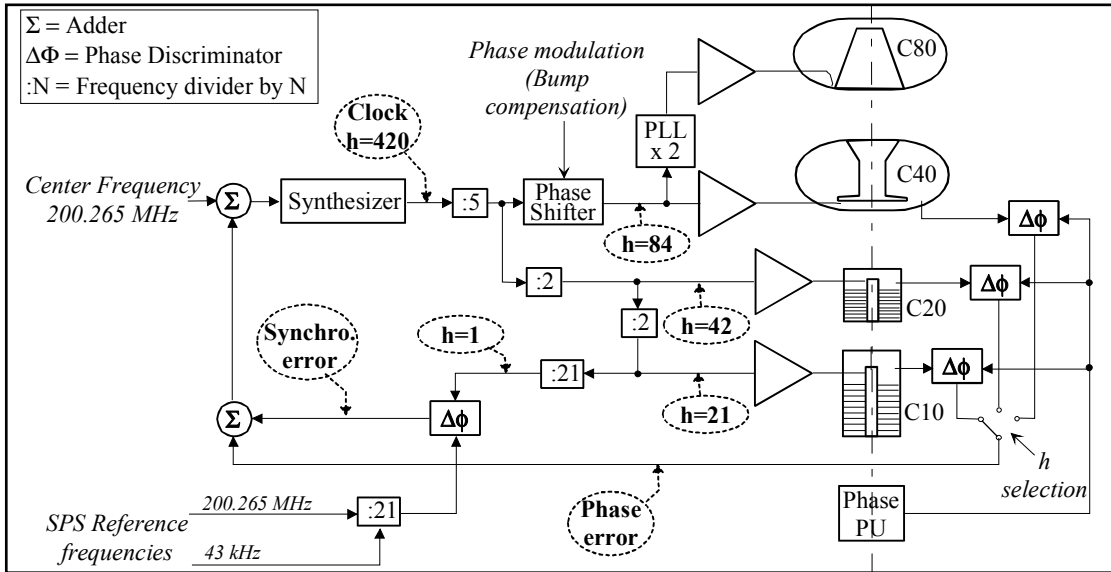


Figure 7.13: PS beam control used during the gymnastics at 25 GeV.

At 25 GeV, a different beam control (Fig. 7.13) takes care of generating the sine waves exciting the 13, 20, 40 and 80 MHz cavities which are outside the frequency range of the beam control used previously in the cycle. The oscillator controlled by the phase loop operates on harmonic 420 of the revolution frequency. The 40, 20 and 13 MHz RF are conveniently derived by division (respectively by 5, 10 and 15), while the 80 MHz is obtained by multiplication by 2 with a Phase Locked Loop (PLL). During all gymnastics, a beam

phase loop is active, which is switched from $h = 21$ to 42 and 84 (25ns bunch spacing) or $h = 14$, 28 and 84 (75 ns bunch spacing).

In the last 7 ms before ejection, a phase shifter serves to keep the beam energy constant while the orbit length is increased by the action of the pulsed extraction bump.

The orbit bump which moves the beam towards the extraction septum has a deleterious effect on the process of bunch rotation. This is compensated by programming the phase of the 40 and 80 MHz RF such that the buckets remain at constant energy while the phase at ejection is kept the same from cycle to cycle (phase modulation with a fixed point at ejection). If the mean radial excursion due to the bump reaches a maximum of ΔR in a time T , the orbit may be assumed to evolve according to

$$R(t) = R_{nom} + \Delta R \cdot \sin\left(\frac{\pi t}{2T}\right).$$

Hence, at constant energy, the (angular) RF frequency differs from its nominal value by

$$\Delta\omega(t) = -\omega_{nom} \cdot \frac{\Delta R}{R_{nom}} \cdot \sin\left(\frac{\pi t}{2T}\right).$$

Integrating gives

$$\Delta\varphi(t) = \omega_{nom} \cdot \frac{\Delta R}{R_{nom}} \cdot \frac{2T}{\pi} \cdot \left[\cos\left(\frac{\pi t}{2T}\right) - 1 \right].$$

This is the form of the function with which the 40 and 80 MHz RF are phase shifted during bunch rotation. Fig. 7.14 shows the result on the beam phase (top trace) of the compensation of the bump (bottom trace) by a suitable phase modulation (middle trace).

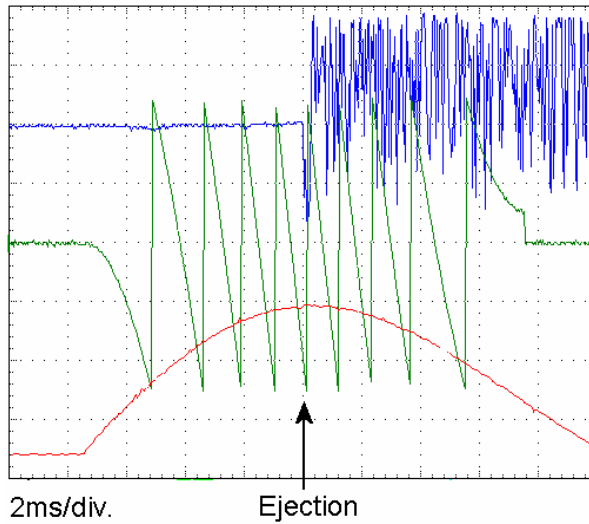


Figure 7.14: Bump compensation before ejection from the PS.

REFERENCES

- [1] R. Garoby, *Bunch Merging and Splitting Techniques in the Injectors for High Energy Hadron Colliders*, CERN/PS 98-048(RF), Proc. of HEACC '98, Dubna, 1998.
- [2] J.M. Jowett, *Collision Schedules and Bunch Filling Schemes in the LHC*, LHC Project Note 179, Geneva, 1999.
- [3] M. Benedikt (editor), *The PS Complex as Proton Pre Injector for the LHC – Design and Implementation Report*, CERN 2000-003, Geneva, 2000.
- [4] V. Baglin et. al., *Beam-induced electron cloud in the LHC and possible remedies*, LHC Project Report 187, Geneva, 1998.
- [5] R. Cappi, R. Garoby, S. Hancock, M. Martini, J.P. Riunaud, K. Schindl, H. Schönauer, *Beams in the PS complex during the LHC era*, CERN/PS 93-08 (DI), 1993.

CHAPTER 8

NEW PS RF CAVITIES

The longitudinal beam manipulations used in the PS to generate the bunch trains for LHC require RF systems operating at 13.3, 20 and 40 MHz (see Chap. 7). In addition, the non-adiabatic bunch compression process, necessary for capture at 200 MHz in the SPS, requires an 80 MHz system.

Along with a small modification of the 10 MHz systems to be fully operational up to $h=21$, the PS now disposes of RF systems which allow to work on harmonics 21, 28, 42, 84 and 168 at top energy – a remarkable flexibility providing the necessary panoply of bunch structure manipulation.

The nominal filling scheme for LHC has bunch trains with 25 ns bunch spacing. The adoption of a 20 MHz RF system ($h=42$), followed by the 40 MHz system ($h=84$), ensures the quadruple splitting at 25 GeV and produces the desired beam pattern [1, 2]. Moreover, the concern about electron cloud induced heating of the LHC vacuum chamber has stimulated the development of an early operation scheme, that requires an RF system to be operated at 13.3 MHz ($h=28$) in order to allow a 75 ns bunch spacing within the LHC bunch train [3]. Two RF systems, tuneable at 13.3 or at 20 MHz, are being installed in the PS ring. While one system is sufficient to generate the nominal LHC beam, the second one represents a “hot spare” and a very valuable performance enhancement, providing the possibility of handling a larger than nominal emittance or generating bunch trains with different bunch spacings in the same PS supercycle.

8.1 TUNABLE CAVITIES 13.3 MHz – 20 MHz

8.1.1 System Requirements

Each system must deliver 16 kV nominal gap voltage¹ and a fast feedback system must ensure a 20 dB reduction of the resonator shunt impedance during the RF pulse (Quality factor < 10). Outside the RF pulse the RF gap must be shorted within maximum 20 ms.

Each cavity should be capable of operating at either 13.3 or 20 MHz, but changing the tune can be made slowly and while the RF is off. A duration of minutes to switch between 13.3 and 20 MHz is acceptable.

8.1.2 Cavity Design

In order to stay safely within the voltage limit (10 kV) for the gap relays that are used to short the accelerating gap outside the RF pulse, each cavity has been split into two resonators, referred to as sections. These two sections are driven in parallel by the common tube amplifier with two short transmission lines. The cavity is shown in Fig. 8.1.

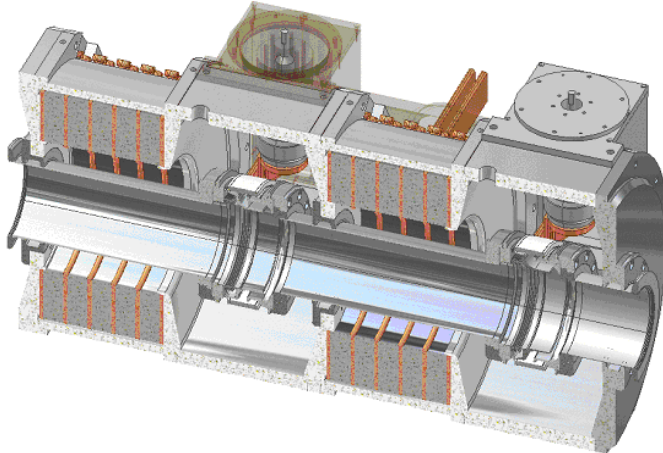


Figure 8.1: The ferrite cavity. The ceramic gaps and the variable capacitors for cavity tuning are visible.

¹ Peak values are used for RF voltages and currents throughout.

The ferrite rings are Ferroxcube standard grade 4E1 and water-cooled copper disks remove heat. This grade has been chosen for its low permeability ($\mu \sim 14$) and low loss at 20 MHz. The ferrite ring size is 440 mm outer diameter, 250 mm inner diameter, 33.3 mm thickness. Each cavity has a total of ten rings.

Tuning is performed by a PLC that moves two variable vacuum capacitors connected in parallel to the gaps. In order to ensure stability during the process, the open loop gain is kept low by disabling the grid pulser of the tetrode and blanking the driver.

Since the cavity is very close to the PS main magnets, a magnetic shield surrounds the ferrite rings to avoid unwanted detuning due to the fringe field. The cavity's main characteristics are summarised in Tab. 8.1.

Table 8.1: Main characteristics of a 13 – 20 MHz cavity.

Parameter / Frequency [MHz]	13.3	20
Quality factor at 20 kV	82	63
Quality factor at 100 V	163	100
Nominal V_{RF} [kV]	15	15
Maximum V_{RF} [kV]	20	20
Shunt resistance at 20 kV [$k\Omega$]	1.7	2
Power dissipation at 20 kV [kW]	25	30
RF magnetic flux density at 20 kV [mT]	9.7	6.7
Peak power density at 20 kV [mW/cm ³]	860	730

8.1.3 Amplifier Chain

The RF system block diagram is shown in Fig. 8.2. A grounded cathode tube power amplifier based on a water-cooled tetrode RS1084CJ (THALES), driven by a 400 W solid-state amplifier has been developed. Feedback from the cavity gap provides reduction of the cavity impedance seen by the beam. Both amplifiers are kept as close as possible to the cavity resonator in order to keep the group delay low. A low- Q (~ 2.5) resonator is implemented in the grid of the tetrode. A coaxial RF switch selects between two shorted coaxial cables to tune the grid resonator at the two frequencies. Fine tuning is obtained using a coaxial line stretcher. The anode dissipation of the tetrode is minimised by pulsing the DC current to 4 A only during operation (10 % maximum duty cycle).

The CERN-made driver amplifier has a gain of 54 dB, a group delay of only 30 ns and a 3 dB bandwidth extending from 0.15 MHz to 80 MHz. The presence of the two transmission lines generates high frequency resonances that limit the overall loop gain. Operating at 20 MHz, the unwanted resonance is located at 56 MHz, when operating at 13.3 MHz, it is located at 71 MHz. The 56 MHz resonance is especially dangerous, because the gain is only 24 dB below the value at 20 MHz. Two notch filters, connected directly to the feedback probe, are used to suppress the two resonances. The main characteristics of a complete RF system are summarised in Tab. 8.2.

Table 8.2: Main characteristics of a 13–20 MHz system.

Parameter / Frequency [MHz]	13.3	20
Feedback gain at 100 V [dB]	25	21
Feedback gain at 20 kV [dB]	20	17
Open Loop Bandwidth [kHz]	75	176
Closed Loop Bandwidth [MHz]	2.6	4.5
Forward Path Gain [dB]	94	95

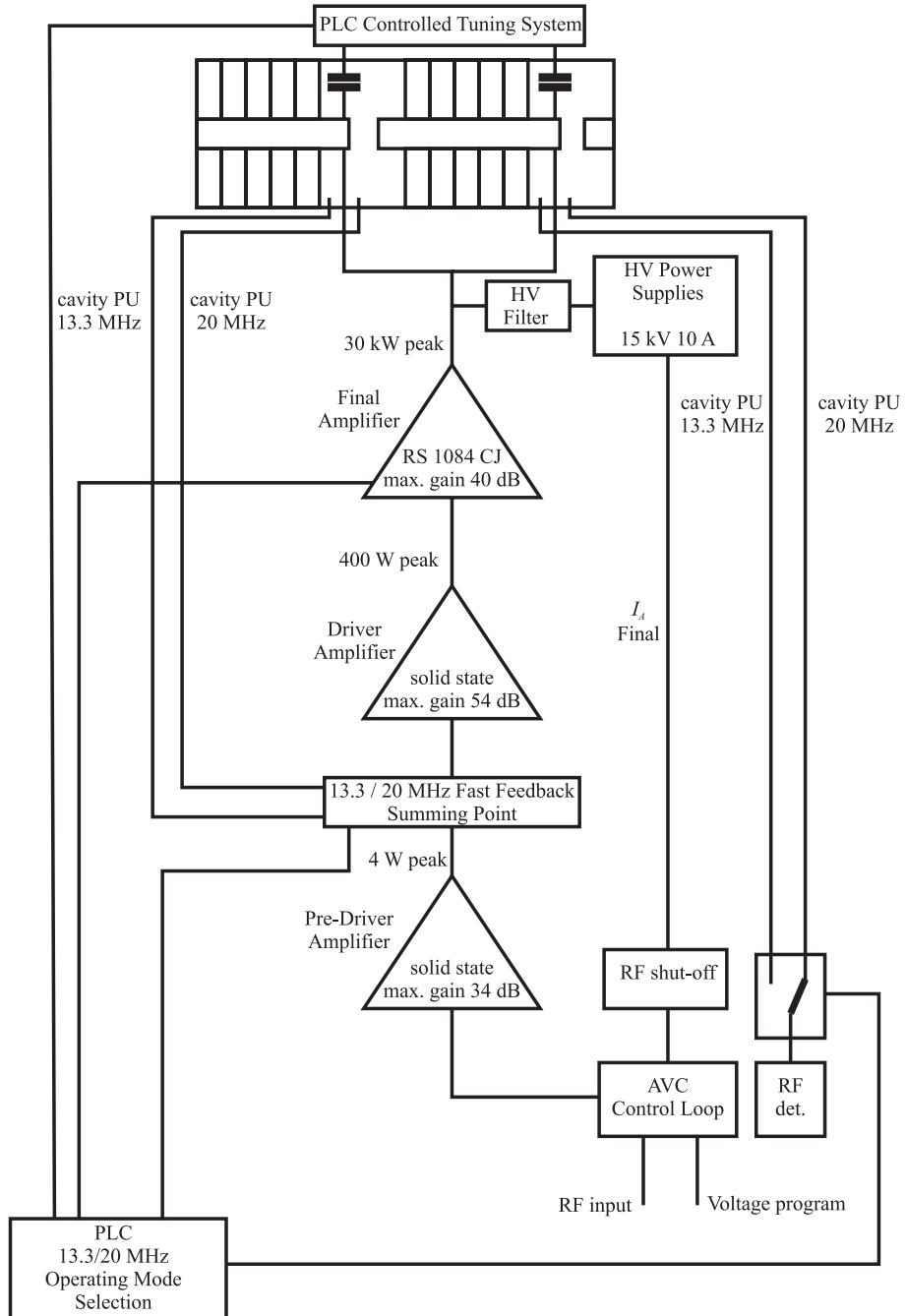


Figure 8.2: Simplified block schematics of the 13.3 – 20 MHz amplifier chain.

8.2 40 MHz AND 80 MHz CAVITIES

8.2.1 Requirements

The bunch compression scheme utilises both adiabatic and non-adiabatic cavity gap voltage variations [4 - 6]. For the quasi-adiabatic part, smooth voltage variations must be possible, i.e. the dynamic range must be free of gap MultiPactor (MP). The dynamic range of the 40 MHz system is required to be 3... 300 kV. For the non-adiabatic part (bunch rotation), both the 40 MHz and the 80 MHz cavities should be able to be filled in $\sim 20 \mu\text{s}$. Short pulses of up to 10 ms at duty cycles below 1 % are required for the 40 MHz system – the 80 MHz system is also capable of delivering long pulses. Beam loading is strong (nominal beam current at 40 MHz: 1.24 A). The impedance must be kept as small as possible in order not to perturb other beams.

8.2.2 Power Considerations

Three somewhat competing requirements determine the power rating of the final amplifiers and the cavities:

- Power loss in the cavity walls, which favours large shunt impedance. Since only short pulses and small duty cycles are needed, this aspect is of minor importance for the 40 MHz cavity. Concerning the 80 MHz cavity, the design includes the option to accelerate leptons, which requires a high average power, so this argument gains importance.
- Instantaneous power needed to fill the cavity to full voltage in a short time. This favours small stored energy, i.e. a high R/Q . This short rise time requirement dominates the dimensioning of the Power Amplifier (PA) for the 40 MHz cavity.
- Reactive power due to transient beam loading: during the whole process of bunching, the voltages in both the 40 MHz and the 80 MHz cavities are kept in quadrature to the beam current. Seen from the amplifier, this is equivalent to an inductive reactance. At steady state, this could in principle be entirely compensated by a parallel capacitance, in other words by detuning the resonance frequency by

$$\frac{\omega - \omega_0}{\omega_0} = \left(\frac{R}{Q} \right) \frac{|I_B|}{2 V_{\text{gap}}}.$$

- It should be noted that the necessary detuning increases with R/Q . However, the detuning depends on both gap voltage and beam current. In order to compensate the reactance both before and after a non-adiabatic voltage variation, one would need a very fast tuner ($\mu\text{s}!$). The possibility to achieve this using perpendicularly biased ferrites has been thoroughly investigated, showing that such a tuner would not be a practicable solution [7].
- Without a fast tuner however, the output of the PA is strongly mismatched either before or after the gap voltage step. Even after balancing this mismatch to limit the absolute value of the generator current, a large complex power must still be delivered by the PA – it must operate as an “electronic tuner”. For a high Q cavity, the lowest maximum generator current (transformed to the gap) can be estimated to be slightly higher than half the beam current (0.7 A at nominal 300 kV). This is a strong effect and it is taken into account in the design of the amplifier.

8.2.3 Cavity Geometry

As a result of the above considerations, the ratio R/Q should be moderately small, requiring a strong capacitive load. The actual parameters are summarised in Tab. 8.3 below. The optimum gap size was determined by MP and voltage breakthrough: The first order band of two point MP at the gap occurs around

$$V = (\omega g)^2 \frac{m_e}{2 e},$$

higher order MP bands will have even lower resonance voltages [8]. Minimising the gap width g will bring the voltage V at which this condition is satisfied to very low values. This will determine the lower limit of the dynamic range of the gap voltage – with the 50 mm gap this value is approximately 0.5 kV at 40 MHz and 2 kV at 80 MHz. The magnetic fringe field of the nearby ring dipoles increases these values: the measured MP band at 40 MHz was 300...1200 V at low magnetic field and 700...3300 V at high field. After conditioning, these bands became somewhat narrower.

The upper gap voltage is limited by vacuum breakdown, which can be conservatively estimated using Kilpatrick's expression [9]. The voltage of 300 kV corresponds, with the chosen gap size of 5 cm, just to Kilpatrick's limit at 40 MHz and to 0.8 Kilpatrick at 80 MHz. Kilpatrick's limit is known to be very conservative and consequently, even at 470 kV, no gap voltage breakdowns have been observed.

The axially asymmetric, re-entrant cavities are machined from forged 316 L+N steel, galvanically copper plated on the inside. Many parts are identical for both systems – the main difference is the capacitive loading of the 40 MHz gap (Fig. 8.3). The outside dimensions of the cavities are approximately: length 1 m, diameter 1.6 m. The asymmetry and the small gap helped accommodate the mechanical short circuit (Fig. 8.4). The 80 MHz cavities are water cooled for lepton operation.

8.2.4 Fast RF Feedback

For beam stability reasons, the impedance seen by the beam (also other beams than for LHC) must be as small as possible. For the accelerating mode, this impedance can be drastically reduced with fast RF feedback. Detecting the gap voltage and feeding this signal back to the input of the amplifier chain will reduce both shunt impedance and Q by the loop gain. The gain characteristics have to be tailored to result in a large gain over a wide band around the operating frequency, a small group delay and stability. Gains of 43 dB (140) at 40 MHz and 41 dB at 80 MHz have been obtained. The group delay is 220 ns in both cases and the 3dB-bandwidth approximately 600 kHz. The resulting longitudinal impedances per cavity are $2.3 \text{ k}\Omega$ at 40 MHz and $5.6 \text{ k}\Omega$ at 80 MHz, with equivalent Q 's of 70 and 100, respectively. To further increase the amplifier stability margin (12 dB), the cavities are currently operated with a reduced loop gain of 40 dB.

8.2.5 Higher Order Mode Damping

While the beam impedance at the fundamental frequency is reduced electronically, potentially dangerous Higher Order Modes (HOMs) are passively damped. The strong capacitive loading of the cavities (low R/Q) has the positive side-effect that electric and magnetic energies are stored at separate locations inside the cavity volume, making the cavity behave more like a lumped-element circuit, pushing the frequencies of the first HOMs much higher. As a consequence, the first monopolar HOM of the 40 MHz cavity appears at 260 MHz, that of the 80 MHz cavities around 220 MHz. Also, the fundamental mode has virtually no electric field at the outer circumference of the cavity volume – electric couplers placed there thus do not couple to it, but they do couple to the HOMs.

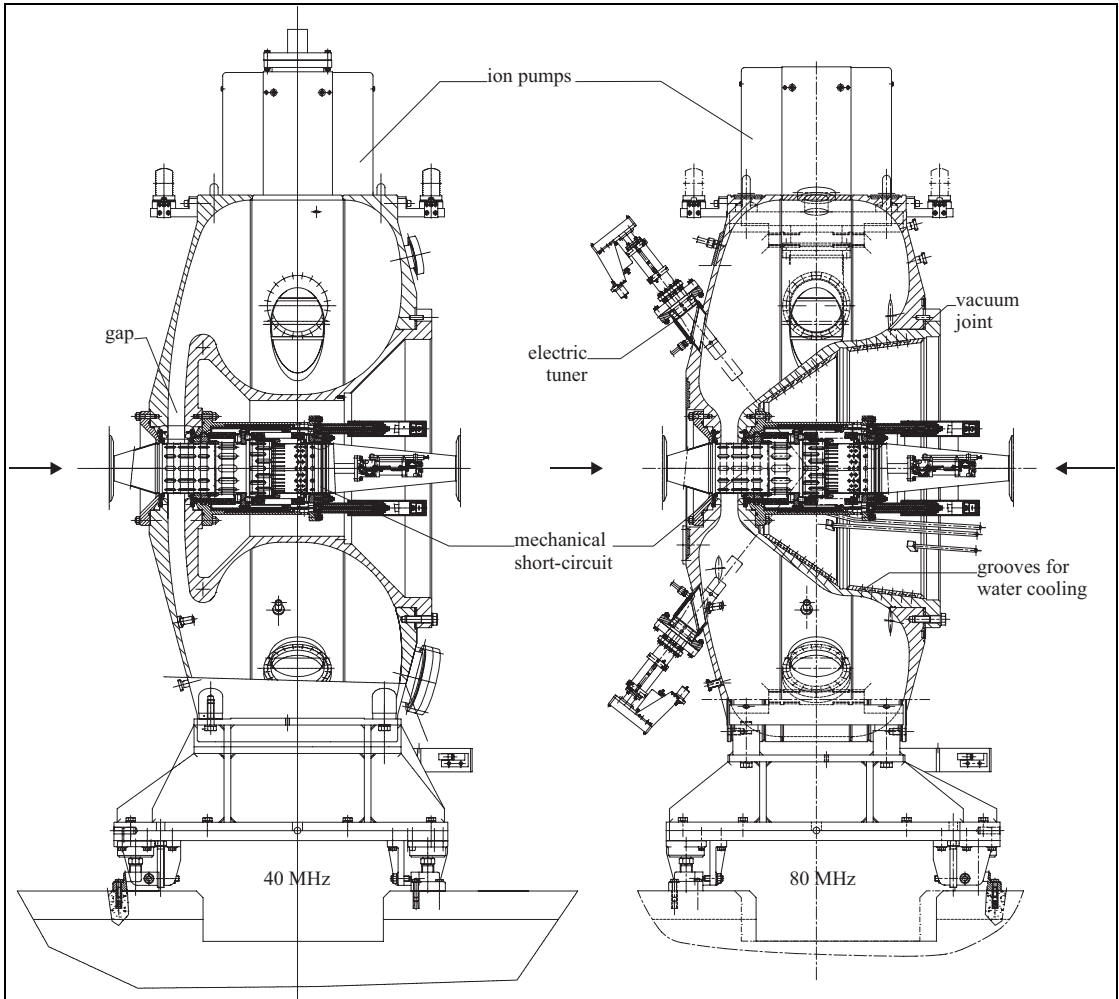


Figure 8.3: Longitudinal section of the 40 MHz (left) and 80 MHz cavities (right).

The HOM dampers now consist of short antennas, each of them optimised to couple to the electric field of an individual HOM. The actual dampers are $50\ \Omega$ loads outside of the cavity, connected to the antenna via feed-throughs. Four HOM dampers are used in each cavity. All HOM dampers were studied, optimised and built at TRIUMF. Most of the study and optimisation took place using a scale 1, copper lined wooden model of the cavity [10, 11]. For the 80 MHz cavity, the HOM dampers are water cooled.

8.2.6 Mechanical Short Circuit

The fast RF feedback reduces the cavity impedance seen by the beam significantly, but it requires the system to be switched on and running. When the system is switched off, the gap is closed by a pneumatically operated short-circuit.

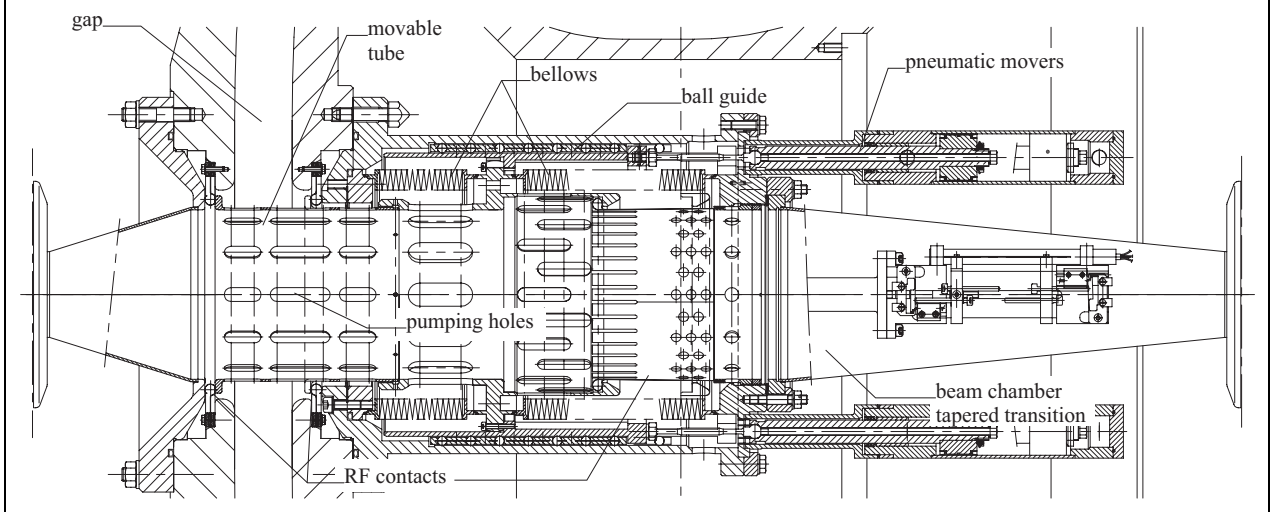


Figure 8.4: Construction of the mechanical short circuit (shown in its closed position).

The short-circuit consists of a metallic tube which can be moved like a piston across the gap (stroke 78 mm). The tube has the diameter of the vacuum chamber and is constrained by a cylindrical ball guide, situated outside of the vacuum. A number of holes in this tube allow efficient vacuum pumping. RF contacts assure well defined current paths in both open and closed position and two bellows assure vacuum tightness. The gap can be opened or closed in 0.6 s by two pneumatic arms and end switches serve as indicators and interlocks. The short-circuit system has been carefully tested (some 10^5 cycles in a specially constructed test set-up) and proven very reliable [12].

8.2.7 Amplifier

The design of the amplifier chain is influenced by several major constraints. The output power must be of the order of 350 kW for rapid cavity filling at high cavity voltage. A forward gain from the chain input to the cavity of about 90 dB is necessary so that at 40 dB loop gain the cavity loop pickup and the feedback summing amplifier can operate at low level (about 2 W). The additional phase shift round the loop for frequency excursions either side of the resonance frequency of the cavity (f_0) must not exceed $\pm 90^\circ$ ($\pm 180^\circ$ total) at the points where the loop gain is -12 dB (the gain margin). This imposes a loop group delay of 230 ns maximum.

These last two considerations of gain and delay imply a solid state pre-driver amplifier (65 dB gain), situated at 10 m distance from the cavity to reduce irradiation, followed by a low gain 40 kW driver amplifier for the final stage input. The group delay of these amplifiers is 35 ns and 100 ns respectively, leaving about 95 ns for the connecting cables and hybrid summing amplifier.

A TH681 tube operated at 22 kV High Voltage (HV) in grounded grid mode provides the final output power. The tube anode is connected to the cavity coupler via a short (about 60 cm) coaxial line transformer (see Fig. 8.5) and the cathode is matched by an *LC* network to the 50 Ω line from the 40 kW driver amplifier.

Strong side resonances exist due to transformation of the cavity impedance by line and coupler between anode and gap at frequencies near the cavity f_0 . The peaks and troughs of these resonances can provoke loop instability and strong frequency dependence of the anode to gap voltage step-up ratio respectively. Correct design of the line and coupler push these resonances away from and situate them symmetrically about, f_0 . The line is composed of several sections of different impedances such that the low voltage/high current (350 A) at the coupler window is transformed to 16 kV/25 A in the plane of the anode [12].

In the case of the 80 MHz amplifier, the higher frequency causes a voltage zero to occur just above the top of the TH681 tube. This provided a convenient point for the introduction of the 22 kV HV via a $\frac{1}{4}$ -wave isolator. From this point on toward the cavity the line impedance is kept at 18 Ω so that the voltage at the small coupler window is nominally less than 8 kV [13].

When the mechanical gap short-circuit is open during normal LHC operation, the amplifier chain operates at greatly differing power levels for quiescent beam induced voltage reduction, cavity filling or for lepton operation. The first of these three regimes requires low power and is quasi-continuous and maintenance of the final amplifier bias level of 22 kV at 3 A would be undesirable. For lepton operation where the pulse length is long (800 ms), both the final and the driver tube dissipation must be reduced to a minimum. The final and driver anode HV supplies are therefore modulated according to the regime of operation, the final HV supply rising to 22 kV at 3 A bias current only during the short high power pulse for LHC bunching, while it is kept at economic 15 kV, 1.5 A otherwise.

In the transient beam loading regime, the feedback is only required to reduce the induced gap voltage to the brink of the gap multipactor onset, when the induced signal falls into the lowest multipactor level and the amplifier does very little work. This is an unforeseen but very fortuitous side effect of low voltage gap MP.

8.2.8 40 MHz: Electric Coupling

The 40 MHz cavity has a mushroom shaped gap electrode (see Fig. 8.3), which makes capacitive coupling possible. A coupling antenna with an asymmetric profile extends from the ceramic window coupler port towards the gap electrode, the capacity being adjustable, via the asymmetry, by rotation in a range of approximately 2...5 pF [12]. This allows adjusting the voltage step-up ratio – it was used to test one of the cavities up to 470 kV at the gap. The resulting detuning can be compensated for by means of the coarse tuner described below. The ceramic coupling window is dimensioned to accept the final anode HV which is present on the coupling antenna to prevent any tendency to MP. During conditioning of the cavity gap (after venting), excessive MP may, however, occur and the electrons created can induce a heavy discharge of the HV to ground.

8.2.9 80 MHz: Magnetic Coupling

Although less convenient, a magnetic coupling loop was adopted for the 80 MHz cavity since the gap electrode is much smaller and a capacitive antenna would be excessively long. The self inductance of the

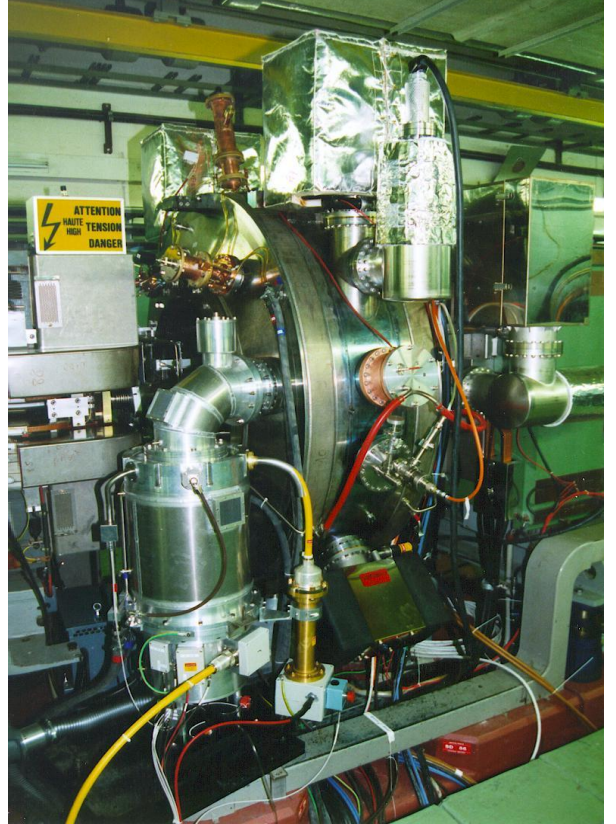


Figure 8.5: Installed 80 MHz cavity. The final amplifier can be seen in the foreground.

coupling loop strongly affects the resonances in the line to the final anode. This inductance was kept down to 140 nH by making the loop from a wide (6 cm) strip and by using the cavity wall for the loop return [13]. To prevent MP, the loop is DC isolated from the wall and kept at a potential of 1.2 kV; it is also water cooled for the long duty cycle lepton operation. The coupler step up ratio to the gap is 1:10 so that the equivalent coupler output is about 30 kV peak which further reduces to 8 kV at the ceramic window.

8.2.10 Tuner

Each cavity is equipped with two tuners, referred to as “coarse tuner” and “servo tuner”. The coarse tuners are manually adjusted in order to set the resonance frequency of the cavity to the centre of the tuning range of the servo tuner. This tuner compensates slow variations of temperature and atmospheric pressure, essentially during the high duty cycle lepton operation.

The tuners of the 40 MHz cavity consist of a large coupling loop, which is coupled via a feed-through to a variable capacitor for the servo tuner. For the coarse tuner, the loop is simply short-circuited – the tuning is obtained by the adjustment of the orientation of this loop in the magnetic field [14, 15].

The tuners of the 80 MHz cavity are capacitively coupled piston tuners. The coarse tuner and servo tuner are identical, but only the servo tuner is equipped with a motor drive [16]. The tuning ranges obtained are given in Tab. 8.3.

8.2.11 Parameters

Tab. 8.3 summarises some of the parameters obtained with the five realised cavities. All cavities are installed but nominal operation requires only one 40 MHz and two 80 MHz systems, the others are considered “spare”. It should be noted that some of the given numbers are just indications; the loaded Q e.g. depends subtly on amplifier bias current and DC anode voltage, the step up ratio depends slightly on the tuning, etc.

Table 8.3: Parameters of the installed systems.

	40 MHz systems [12]		80 MHz systems [13]		
Cavity, location in PS, Installation date	“Susan”, SS 78, 9/96	“Tjitske”, SS 77, 3/99	“Lydia”, SS 89, 1/98	“Barbara”, SS 88, 2/98	“Anne”, SS 13, 2/99
Nominal DC beam current	0.64 A, (cf. [17], p. 169)				
Beam current (assumed Gaussian, $\sigma = 1$ ns)	1.24 A		1.13 A		
Operating frequency:	40.055 MHz		80.11 MHz		
Measured Q_0 , Q_L :	18200, ~ 10000		22600, 11800		
Calculated R_S/Q_0 :	33 Ω		56 Ω		
Shunt impedance R_S , R :	600 kΩ, ~ 330 kΩ		1.26 MΩ, 660 kΩ		
Nominal gap voltage [kV]:	3...300		300		
Obtained gap voltage [kV]:	2...360		> 400		
Pulse length, duty cycle:	10 ms, 0.4 %		300 μs, < 0.1 % @ 400 kV (LHC) 800 ms, 25 % @ 210 kV (lepton option)		
Zero to full voltage rise time:	25 μs		15 μs		
Feedback loop gain:	43 dB		41 dB		
Feedback group delay:	220 ns		220 ns		
Feedback reduced R , Q :	2.3 kΩ, 70		5.6 kΩ, 100		
Voltage step-up gap/anode	21		24		
Servo tuning range [MHz]	39.96...40.18	39.95...40.11	79.82...80.18	79.77...80.14	79.86...80.22

8.2.12 Overall System Design

Fig. 8.6 shows a block diagram of the 40 MHz system. For simplification, the interlock system is omitted. The 80 MHz system is conceptually similar.

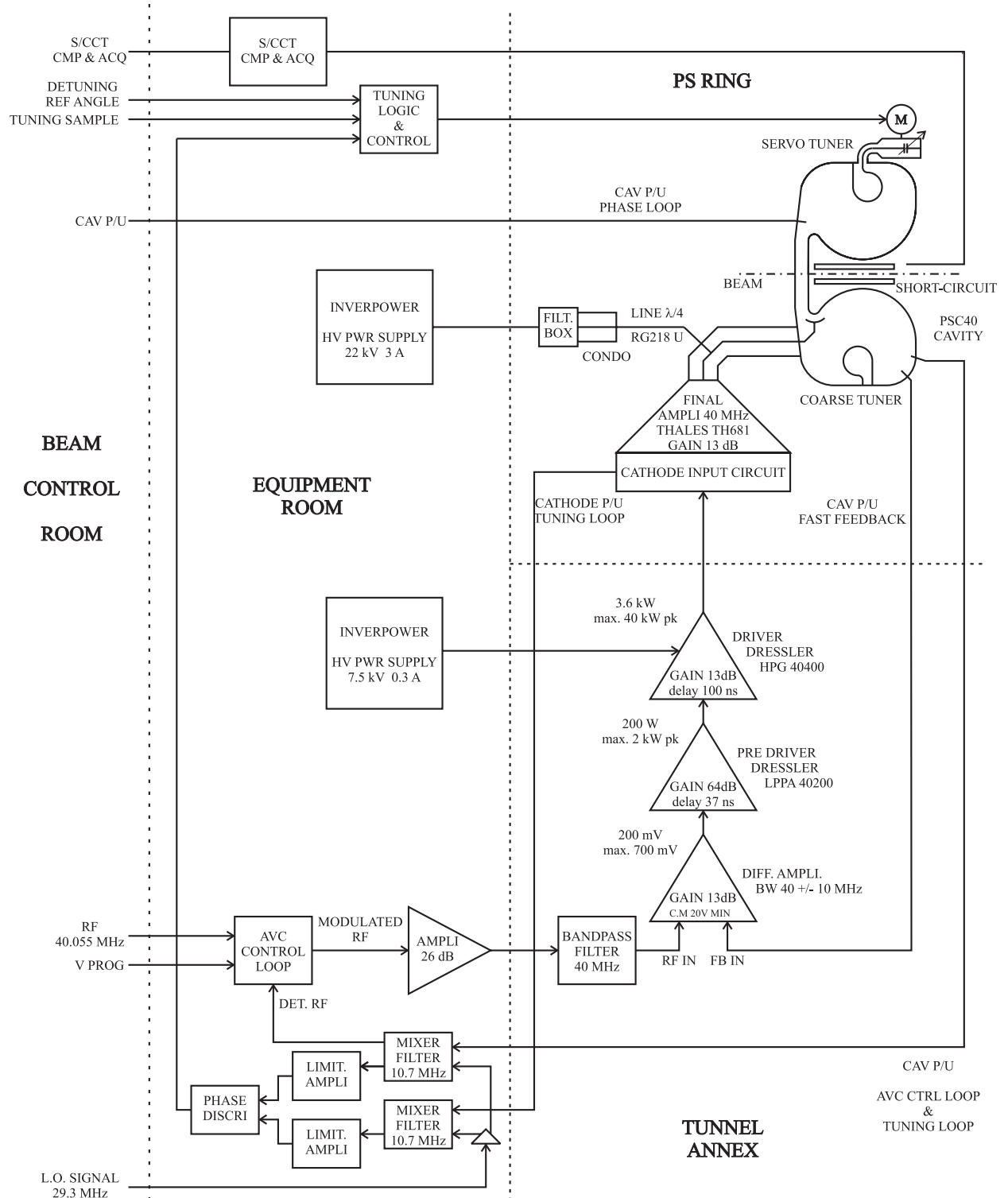


Figure 8.6: Simplified block diagram of the 40 MHz system. The final stage of the power amplifier is mounted directly onto the cavity. The driver amplifiers are located in the tunnel annex, situated approximately 10 m from the cavity.

REFERENCES

- [1] R. Garoby, *Status of the nominal proton beam for LHC in the PS*, Proceedings of the Workshop on LEP-SPS Performance, Chamonix, 1999.
- [2] M. Benedikt (Editor), *The PS complex as proton pre-injector for the LHC — design and implementation report*, CERN-2000-03, Geneva, 2000.
- [3] R. Garoby, *Multiple Splitting in the PS: Results and Plans*, CERN/PS 2001-004 (RF), Geneva, 2001.
- [4] R. Cappi, R. Garoby, S. Hancock, M. Martini, J.P. Riunaud, K. Schindl, H. Schönauer, *Beams in the PS complex during the LHC era*, CERN/PS 93-08 (DI), Geneva, 1993.
- [5] R. Garoby, *A Non-Adiabatic Procedure in the PS to Supply the Nominal Proton Bunches for the LHC into 200 MHz RF Buckets in SPS*; CERN PS/RF/Note 93-17, Geneva, 1993.
- [6] R. Garoby, *Requirements to the PS RF systems for filling the LHC with 25 ns spacing between bunches*, CERN PS/RF/Note 93-04, Geneva, 1993.
- [7] I. Enchevich, R.L. Poirier, *Perpendicularly Biased Ferrite Tuner for the CERN LHC cavity*; TRIUMF Design Note TRI-DN-97-28, Vancouver, 1997.
- [8] A.J. Hatch, *Suppression of Multipactor in Particle Accelerators*; NIM 41, 1966.
- [9] W.D. Kilpatrick, *Criterion for Vacuum Sparking Designed to Include Both rf and dc*; Review of Scientific Instruments 28, No. 10, 1957.
- [10] E. Jensen, R. Hohbach, A.K. Mitra, R.L. Poirier, *Higher-Order Mode Damping of the CERN PS 40 MHz Cavity*; Proc. EPAC '96, Sitges, 1996.
- [11] A.K. Mitra, S. Rose, *Higher-Order-Mode Damping of the CERN 80 MHz Cavity*; TRIUMF Design Note TRI-DN-97-8, Vancouver, 1997.
- [12] R. Garoby, D. Grier, E. Jensen, A. Mitra, R.L. Poirier, *The PS 40 MHz Bunching Cavity*; CERN/PS/97-039, Proc. PAC '97, Vancouver, 1997.
- [13] D. Grier, E. Jensen, R. Losito, A.K. Mitra, *The PS 80 MHz Cavities*; CERN/PS/98-021(RF), Proc. EPAC '98, Stockholm, 1998.
- [14] A.K. Mitra: *Servo Tuner for 40 MHz Cavity*, CERN PS/RF/Note 96-20, Geneva, 1996.
- [15] A.K. Mitra, R.L. Poirier, E. Jensen, *Coarse and Fine Tuners for the CERN PS 40 MHz Buncher Cavity*; Proc. PAC '97, Vancouver, 1997.
- [16] R. Losito, *Design report for the capacitive tuners of the 80 MHz cavity*, CERN PS/RF/Note 96-32, Geneva, 1996.
- [17] P. Lefèvre, T. Petterson (Editors), *The Large Hadron Collider, Conceptual Design*; CERN/AC/95-05(LHC), Geneva, 1995.

CHAPTER 9

TRANSVERSE EMITTANCE CONSERVATION AND MEASUREMENT

9.1 EMITTANCE CONSERVATION ISSUES

The conservation of the transverse emittance for the LHC beam throughout the injection chain is an important for reasons which are explained below. The performance of a collider is measured by the luminosity,

$$L = \frac{k_b N_b^2 f_{\text{rev}} \gamma}{4\pi \epsilon_n \beta},$$

which is proportional to the number of events per second and thus has to be maximised. This favours a large particle number per bunch N_b and a small normalised emittance ϵ_n . However, space charge effects at low energies work against this by limiting the beam brightness, N_b/ϵ_n , achievable. The strategy is therefore to produce the highest possible brightness beam at low energy and then to transport it through the injector chain by carefully avoiding any performance loss due to emittance blow-up. More detailed considerations can be found in Cha. 2.

The proton injection chain for the LHC consists of the Linac2, the PSB, the PS and the SPS. The 50 MeV beam coming from the linac is injected into the PSB using a multi-turn injection. At 1.4 GeV, four bunches of the four PSB rings are consecutively ejected towards the PS, filling 4/7 of the PS circumference. After injection of a second batch (two rings only) from the PSB, the beam is accelerated to 25 GeV in the PS and ejected towards the SPS. The beam intensities and emittance budgets along the injection chain for nominal and ultimate LHC beams are summarised in Tab. 9.1, no beam losses are taken into account.

Table 9.1: LHC nominal and ultimate proton beam intensities and emittances.

	Linac	PSB	PS	SPS
Nominal				
p/LHC bunch				
p/pulse	180 mA	$1.38 \times 10^{12}/\text{ring}$ (1 bunch/ring)	1.15×10^{11} 8.28×10^{12} (6 PSB bunches)	1.15×10^{11} 3.31×10^{13} (4 PS batches)
ϵ_n	1.0 μm	2.5 μm	3.0 μm	3.5 μm
Ultimate				
p/LHC bunch				
p/pulse	180 mA	$2.04 \times 10^{12}/\text{ring}$ (1 bunch/ring)	1.7×10^{11} 1.22×10^{13} (6 PSB bunches)	1.7×10^{11} 4.90×10^{13} (4 PS batches)
ϵ_n	1.0 μm	2.5 μm	3.0 μm	3.5 μm

The multi-turn injection into the PSB and strong space charge effects naturally lead to the largest emittance blow-up in the injection chain. Therefore special care has to be taken at injection to achieve a beam with the required high brightness (small emittance). This emittance should then be conserved throughout the injection chain. Therefore, besides the control of resonances and instabilities, the beam-transfers between PSB, PS and SPS are the major concerns. When transferring a beam between two machines, there are three main sources for rms emittance blow-up:

- injection mis-steering:
$$\frac{\Delta\epsilon}{\epsilon} = \frac{1}{2\epsilon} \left(\frac{\Delta x / \sqrt{\beta}}{\sqrt{\beta} \Delta x' + \alpha \Delta x / \sqrt{\beta}} \right)^2,$$
- betatron mismatch
$$\frac{\Delta\epsilon}{\epsilon} = \frac{1}{2} \frac{\beta}{\beta + \Delta\beta} \left(\frac{\Delta\beta / \beta}{\Delta\alpha + \alpha \Delta\beta / \beta} \right)^2,$$

- dispersion mismatch
$$\frac{\Delta\epsilon}{\epsilon} = \frac{\sigma_p^2}{2\epsilon} \left(\frac{\Delta D / \sqrt{\beta}}{\sqrt{\beta}\Delta D' + \alpha\Delta D / \sqrt{\beta}} \right)^2.$$

In the formulae above, α and β are the Twiss-functions in the matched case and $\Delta\alpha$ and $\Delta\beta$ are the deviations due to the mismatch, the same applies for the dispersion function D and D' ; $\sigma_p = (\Delta p/p)_{rms}$ is the standard deviation of the relative momentum spread. It should be noted that the emittance blow-up due to mis-steering and dispersion mismatch is inversely proportional to the initial emittance. Thus, these two error sources are particularly important for the LHC beam due to its small design emittance.

9.1.1 Transfer PSB to PS:

The expected maximum emittance blow-up between PSB ejection and PS ejection is 0.5 μm (Tab. 9.1). Assuming that 0.2 μm are assigned to effects during acceleration in the PS, the remaining 0.3 μm can be split into three equal parts for the blow-up sources mentioned above and one can quote typical values for maximum tolerable steering and matching errors between the two machines. The centre of the straight section 45 in the PS (location of the fast injection kicker) was chosen as reference point for the calculations¹. The Twiss-parameters are $\beta_x = 20.3 \text{ m}$, $\beta_z = 11.9 \text{ m}$, $\alpha_x = \alpha_z = 0$, $D_x = 3 \text{ m}$, $D'_x = 0$. It was assumed that the errors are only in position, beta-function and dispersion and are zero for the derivatives.

The maximum tolerable mis-steering or mis-matches are quoted in Tab. 9.2. Each effect alone accounts for an emittance increase in ϵ_n of 0.1 μm .

Table 9.2: Maximum tolerable steering/matching errors for the transfer PSB to PS.

PS-section 45 centre	horizontal	vertical
Beta-function	20.3 m	11.9 m
Dispersion	3.0 m	-
Injection mis-steering	$\Delta x = 0.9 \text{ mm}$	$\Delta z = 0.7 \text{ mm}$
Betatron mismatch	$\Delta\beta = 5.7 \text{ m}$	$\Delta\beta = 3.4 \text{ m}$
Dispersion mismatch	$\Delta D = 0.7 \text{ m}$	-

The optics presently in use for the transfer between PSB and PS is not well matched in terms of dispersion. Up to now, this fact was not too important but for the LHC beam, with a small transverse emittance and a large momentum spread ($\sigma_p = 1.25 \times 10^{-3}$), it becomes relevant. To improve in this area, modified optics [1, 2] which significantly reduce the dispersion mismatch (while preserving the betatron matching) was being tested and verified.

In the case of the PSB the fact that there are four rings which need to be recombined imposes additional difficulties. To minimise the injection oscillations in the PS it is required to individually correct the trajectories of the four bunches. The number of independent correction elements is in theory sufficient, but in practice it is not straightforward to equalise the trajectories from different rings to better than $\pm 1 \text{ mm}$. Furthermore, the reproducibility of the trajectories is not guaranteed and therefore an injection damper will be installed in the PS to provide bunch-by-bunch correction of these residual injection errors.

As far as betatron matching is concerned, the vertical dipoles in the recombination section create optical differences between the rings which cannot be corrected with the present hardware. The effect is small but if required it can be reduced by installing a correction quadrupole [3].

¹ It should be noted that for the calculation of the emittance blow-up due to mis-steering and dispersion mismatch the unnormalised emittances have to be used.

9.1.2 PS Injection Damper

A mis-steering of less than 1 mm at PS injection leads to a significant emittance increase of LHC-type beams (see Tab. 9.2). The four beams from the PSB, recombined to one and sent in two batches to the PS, undergo some unavoidable mis-steering because (i) small time-dependent variations of elements such as power converters or RF feedback loops lead to degrading beam orbits and (ii) the eight horizontal and vertical kicker magnets in the PSB-PS beam transport suffer from overshoot and flat-top ripple with frequencies of up to ~ 15 MHz (this latter effect cannot be corrected with steering dipoles). For these reasons, two injection oscillation dampers, one for each plane, are being built for the PS. They feature travelling-wave kicker magnets of 12.5Ω characteristic impedance with a bandwidth of ~ 20 MHz. One 3 kW power amplifier will drive each kicker, which would then be capable of reducing a 1.5 mm initial injection oscillation to less than 0.5 mm within 50 μ s (20 turns), to be compared to the 400 μ s filamentation time constant. Recent beam observations suggest that these systems would be quite suitable also to tackle transverse head-tail instabilities during the PS cycle, even at lower power (200 W available). As the prototype kickers and power amplifiers are not yet finalised and further machine experiments are required to fully understand all aspects of the instabilities, the parameters given here are preliminary.

New pickup electronics have been developed and a prototype was installed in 2003. The frequency range is 20 kHz to 40 MHz, enough to cover the requested bandwidth with some margin. It will also permit the damper to function over the full intensity range from 10^9 to 10^{13} protons per bunch, again somewhat exceeding the required range.

9.1.3 Transfer PS to SPS:

The beam optics of the TT2/TT10 transfer lines, linking PS and SPS has been reviewed and as a result the dispersion and the betatron matching was improved [4]. In addition to that, orthogonal tuning knobs to minimise the unavoidable residual mismatch were developed [5]. To minimise the blow-up due to injection mis-steering, the SPS damping system was re-engineered [6]. More details can be found in Chaps. 14 and 15.

9.2 BEAM DIAGNOSTIC UPGRADES IN VIEW OF LHC BEAMS

The high brightness LHC beams require close observation of possible emittance blow-up during acceleration in Linac2, PSB and PS and during transfers from one machine to the next. In view of these low-emittance beams, several diagnostics instruments have been substantially upgraded while a few new ones have been built in order to cope with new diagnostic requirements.

Two new Secondary Emission Monitor grids (SEM-grids) were installed in the PSB close to the injection septum and the SEM-grids in the PSB measurement line were upgraded. Eight new wire scanners for profile measurements in the 4 rings were installed in the PSB.

In the PS, the measurement targets have been upgraded and new electronics have been developed for their remote control. In addition, tests have been made for the development of a non-destructive profile measurement to measure beam profiles during the entire PS acceleration cycle. Unfortunately the results are high corrupted by background due to losses in the machine and further development in this direction has been abandoned.

9.2.1 Injection Matching Studies in the PS

In the PS ring, three SEM-grids are installed. In normal operation they are used to determine the emittance of the beam injected from the Booster. Very fast electronics has been built for one of these SEM-grids, allowing the measurement of beam profiles turn by turn (the revolution period at injection is 2.2 μ s for a 1.4 GeV beam). The electronics consists of fast amplifiers with a rise time of 100 ns and 40 MHz flash ADCs. With this modified SEM-grid the transverse matching between the four PSB rings and the PS was measured by recording the beam size oscillations during the first turns in the PS (Fig. 9.1). The beam was ejected after 30 turns in order to make sure that the SEM-grid did not overheat due to multiple beam passages.

The turn by turn profiles were fitted with a Gaussian and the evolution of the mean position as well as the profile width were calculated. From the position oscillations the dispersion parameters were extracted as well as the machine tune while the width oscillations were determined by betatron and dispersion mismatch [7]. These measurements can only be done during dedicated MDs because the presence of high intensity beams in the machine would destroy the detectors.

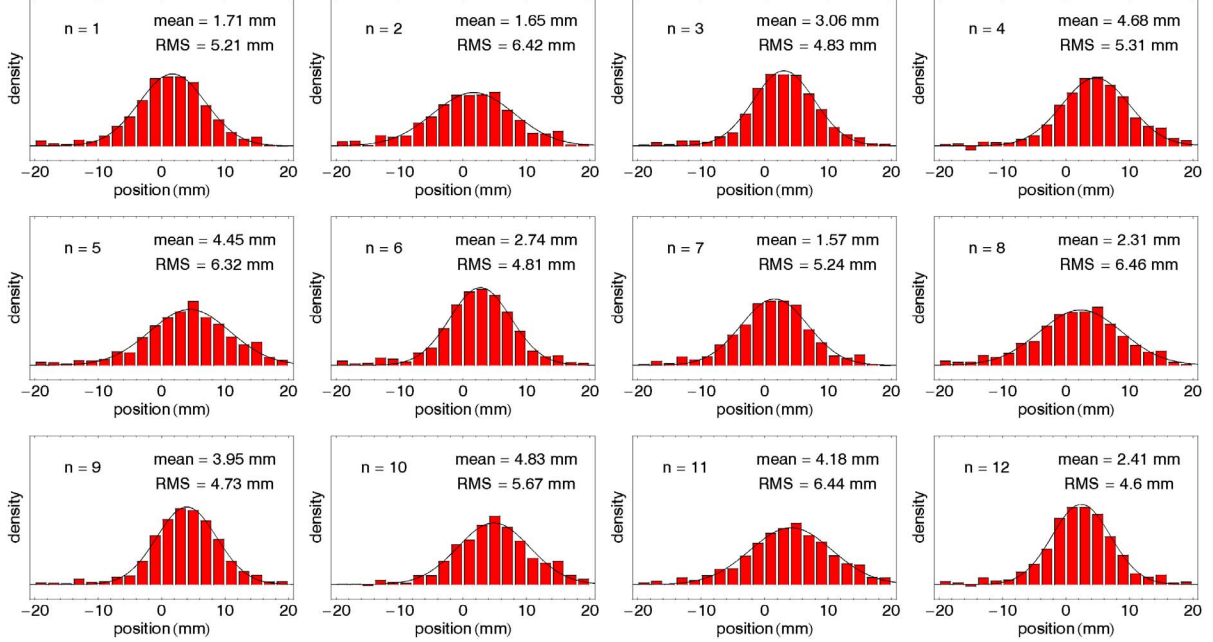


Figure 9.1: Turn by turn horizontal beam profiles measured at PS injection (first 12 turns).

9.2.2 The PSB Fast Wire Scanners

Since 1993, fast wire scanners are used in the PS to measure transverse beam profiles to very high precision and it was natural also to install these devices in the PSB in order to get consistent measurements in both machines. It was known that wire scanners could be used for 1 GeV proton beams, but their performance at lower energies, especially at 50 MeV injection energy, was doubtful. Before investing in ten new wire scanners (1 horizontal and 1 vertical for each of the 4 PSB rings + 2 spares) the spare PS wire scanner was mounted in ring 1 of the PSB for investigation. During machine studies in 1997/1998 its performance was tested and results compared to other already available measurements (BeamScope in the PSB, PSB measurement line and SEM-grids in TT2).

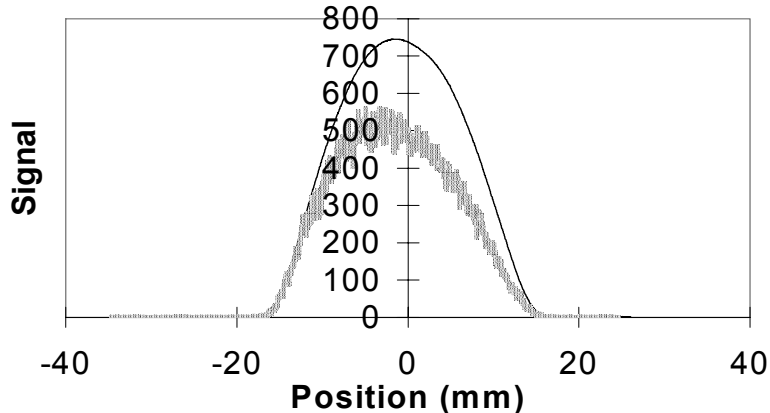


Figure 9.2: Profiles taken with photomultiplier (grey) and secondary emission at 50MeV.

The PS wire scanner uses a scintillator and photomultiplier system in order to detect secondary particles created by the interaction of the circulating beam with the passing wire. This method works fine down to proton energies of a few hundred MeV but fails at very low energies (below the pion creation threshold). In order to cover the full PSB energy range, measurement of the secondary emission current from the wire instead of detecting secondary particles on the scintillator (Fig. 9.2) was attempted.

Very clean profiles were obtained even at 50 MeV proton energy. Comparison between profiles taken with the two detection methods at higher energies showed no difference. Since the test measurements with the spare wire scanner yielded convincing results, the TRIUMF laboratory (Vancouver) has been contracted to build 10 such devices. For these new PSB wire scanners the control and readout electronics has seen a major overhaul and each scanner unit is now equipped with its own dedicated motor controller. These controllers consist of autonomous microprocessors with ADC and DAC for speed control thus taking away the burden of the very time critical movement control from the main VME processor. This processor is now used exclusively for the acquisition of wire position and profile signals from the photomultiplier and the secondary emission current from the wire. The application program for the PS wire scanners has been upgraded so that it is capable of driving the PS as well as the PSB version of the wire scanners.

9.2.3 The PSB Measurement Line

The PSB measurement was equipped with 3 SEM-grids per plane, to measure the emittance of the beam sent to the PS. Their mechanisms were more than 20 years old and needed replacement. It was decided that instead of replacing these mechanisms it would be better to have new, higher resolution grids installed permanently in the beam. The new grids consist of a series of wires instead of ribbons to minimise the interaction with the beam. The number of wires per plane has been increased to 32 and the wire distance decreased to 1 mm for the outer SEM-grids and 0.5 mm for the central one.

The analogue electronics chain was replaced and the digital electronics now uses VME ADCs instead of the old CAMAC scanning ADCs. The installation has been done during the 1999/2000 shutdown.

9.2.4 The PS Measurement Targets

In addition to the wire scanners, the measurement targets can be used in the PS to measure beam sizes. The target consists of a fork with 2 fingers whose distance can be adjusted. The fork flips into the beam and beam losses are observed on the DCBCT. The measurement targets, which can also be used for limiting the aperture, scraping the beam halo away, were only used manually up to now. In order to remotely control the devices, the motors adjusting the distance of the fork fingers had to be replaced. New electronics had to be developed giving remote access to internal parameters (fork finger distance, retention magnet, flip timing etc.). In addition, an application program controlling the devices, reading the beam loss from the DCBCT and displaying the results in a user-friendly way was developed.

9.3 OTHER BEAM DIAGNOSTICS

Not only the emittance and profile measurement devices, but many other beam measurement and diagnostics systems in the LHC pre-injector chain (Linac2, PSB rings and PS) underwent a close scrutiny to highlight the problems and to propose solutions for the essential elements of the LHC filling scheme. While the changes required in the linacs were minimal, close attention had to be paid to the existing systems in the PSB rings, PS and the beam transfer tunnel TT2. Many systems had to be improved and modified, essentially to cater for the new RF harmonics in both the PSB and the PS.

One of the limiting factors for high brightness beams are low order resonances. For this reason the resonance compensation scheme in the PSB has been revisited and resonance driving term measurements were carried out in 2002 using the existing PSB half-turn pickup. However, more precise results can be obtained from turn-by-turn beam position measurements in two consecutive PSB sections (separated by roughly 90° betatron phase advance). For this, two closed orbit pick-ups were modified and four new head amplifiers, with a bandwidth of up to 55 MHz, were implemented during the 2003/2003 shutdown. Extensive measurements with this system were carried out during the run 2003.

In 1993, the successful testing of the ideas behind the LHC filling scheme had shown that the existing PSB closed orbit measurement system was able to handle the new RF beam structures, though perhaps not perfectly. No major changes have been carried out in this system. It is however envisaged that the PSB closed orbit system will undergo a hardware upgrade in the LHC era to perfectly match the beam characteristics in the PSB.

A new tune measurement system [8, 9] based on the existing “*Q*-kickers” [10] for each of the four PSB rings, using synchronised beam excitation with a small-amplitude, one-turn kick and obtaining fast Fourier transform spectra using a DSP Board was developed. The kicker pulser length is gated to the varying revolution period (1670 ns at injection to 570 ns at extraction) and similarly, the ADC is synchronised to sample the signals at four times the revolution frequency. The system is fully integrated into the standard VME based control system. Tune measurements may be performed every 10 ms in both planes for each of the 4 rings through the full acceleration ramp (50 MeV – 1.4 GeV) in the nominal 1.2 s PSB cycle (Fig. 9.3). Measurements have shown that the amplitudes of the transverse oscillations, generated by a small-amplitude kick, are sufficiently small not to affect the beam emittance. Hence, tune measurements may be carried out all the time without affecting the beam. However, to improve the measurements near 1.4 GeV, the automatic control of the kicker amplitude is foreseen for implementation in the near future.

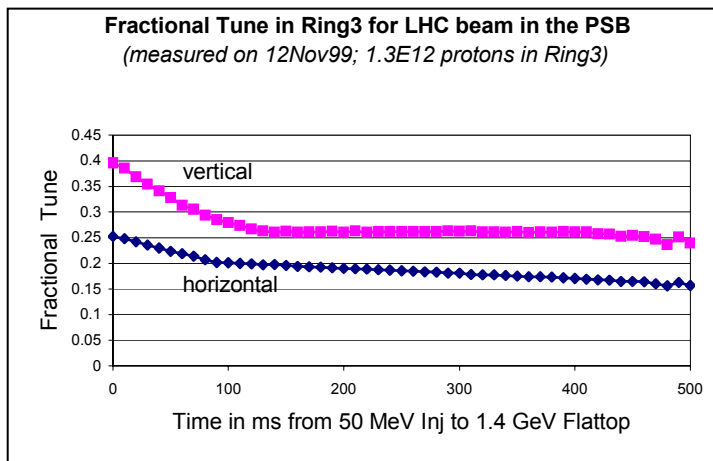


Figure 9.3: PSB tune measurement.

For the PSB to PS transfer channel, the digital system used for the position pickups needed minor changes to cater for the new RF structure of the beam.

In the PS ring, substantial work had to be carried out on the closed orbit and trajectory measurement system. The PS traditionally had a trajectory measurement system, based on the beam position acquisition over two consecutive turns, near injection as well as at any instant in the acceleration cycle. Given the new RF harmonics and gymnastics in the PS required for LHC operation, considerable hardware and software additions and modifications were necessary. This has led to continuity with the traditional trajectory measurements as well as the availability of additional capabilities, required for the double-batch injection, new beam structures and so on up to, but not including, measurements at the extraction of 72 bunches. The new trajectory and closed orbit system is fully integrated in the controls system and is spread over 3 networked VME crates [11-13]. New head electronics for the CODD pick-ups is being designed and a prototype is expected to be ready by early 2004. It should cover the full intensity range of beams in the PS.

Tests are being made using a “normaliser” capable of measuring the beam orbit during the full acceleration cycle. The results will be compared to the current closed orbit system. In the future this system may be made operational or a new combined trajectory and orbit system based on digital techniques will be designed and installed.

For the beam current transformers in the PS ring, the major implication has been the advent of double-batch filling from the PSB. However, most of the changes required are at the level of the timing and specific equipment (ADC channels, triggers and specific software) to provide additional measurement capabilities for this mode of operation. For example, the PS ring DCBCT required an extra facility to permit

measurement of the second batch. Similar changes are reflected in other systems like the one used in the PS for measuring beam current in each of the first six turns at injection for protons.

In the beam transfer line TT2 between PS and SPS, two new electrostatic wide-band pick-ups have been developed and installed to observe the particular characteristics of LHC type beams (72 bunches, 4 ns width, 25 ns separation). The pick-ups are judiciously spaced apart in sections 208 and 228 (to determine position and angle of each of the 72 bunches) and have electrodes based on an earlier design for a special 200 kHz - 300 MHz wide-band pick-up in section 98 of the PS ring. With new purpose built electronics the bandwidth of the pick-ups has been extended to a range of 6 kHz to 400 MHz. In addition these pickups were equipped with clearing coils in order to suppress the multiplication of secondary electrons (electron cloud effect). The coil current is controlled from the standard control system. The solenoid field reaches up to ~20 mT in the pick-up centre and no adverse effects were observed on the optics of the line. The signals from the electrodes as well as the sum signals are permanently connected to the analogue observation system and are routinely used for study purposes. The pick-ups also prove useful in observing other types of beams extracted from the PS to the TT2 transfer line, particularly the classical proton 5-turn extraction beam for the SPS. Further experience with this equipment has to be obtained before connecting it to the standard control system.

For beam current measurements in the TT2 transfer line, the LHC beam does not pose any particular problems. However, to supplement measurements from the existing fast beam current transformer TRA203, the lead ion transformers TRA372 and TRA379 have been modified to measure also proton beams. These transformers, built for the lead ion operation from 1994 onwards, measure the stripping efficiency and are installed just at the switching of the beam from the PS controlled TT2 beam line to the SPS controlled TT10 beam line. A new transformer, TRA386, has been installed upstream of the D3 beam dump at the end of TT2 to verify consistency of measurements under all operations. The fast BCT measurements are now completely uniform with automatic switching between the ranges of $\leq 4 \times 10^{10}$, $4 \times 10^{10} - 1 \times 10^{12}$, $1 \times 10^{12} - 4 \times 10^{13}$ electric charges and satisfying all known requirements for SPS and LHC needs.

REFERENCES

- [1] M. Martini, T. Risselada, K. Schindl, *Measurement of betatron and dispersion matching between Booster and PS*, CERN PS/AP Note 91-13, Geneva, 1991.
- [2] M. Benedikt et al., *Study of a new PSB-PS transfer line optics with improved dispersion matching by means of turn-by-turn beam profile acquisitions*, CERN PS/AE>Note 2001-003 (MD), Geneva, 2001.
- [3] M. Benedikt, A. Jansson, M. Sassowsky, *Proposal for a quadrupole correction magnet in the Booster recombination section*, PS/OP/Note 99-18, Geneva, 1999.
- [4] K. Hanke et al, *Measurement and optimisation of the PS-SPS transfer line optics*, Proc. of PAC '99, New York, 1999.
- [5] G. Arduini, K. Hanke, *Tuning knobs for the PS-SPS transfer line*, Proc. of PAC '99, New York, 1999.
- [6] W. Höfle, *Towards a transverse feedback system and damper for the SPS in the LHC era*, Particle Accelerators, Vol. 58, 1997.
- [7] M. Benedikt et al., *Injection matching studies using turn by turn beam profile measurements in the CERN PS*, 5th European Workshop on Beam Diagnostics and Instrumentation DIPAC, Grenoble, 2001.
- [8] A. Chapman-Hatchett, V. Chohan, E.T. D'Amico, *Tune Measurement for the CERN Proton Synchrotron Booster Rings using DSP in VME*, Proc. of PAC '99, New York, 1999.
- [9] M. Gasior, J.L. Gonzalez, *New Hardware of the tune measurement system for the Proton Synchrotron Booster Accelerator*, CERN PS/BD/Note 99-10, Geneva, 1999.
- [10] H. Koziol, *Q-measurement on the PS Booster*, CERN MPS/INT/BR 74-14, Geneva, 1974.
- [11] J.L. Gonzalez, *Specification for VME CODD Synchronisation*, CERN PS/BD/Note 98-05, Geneva, 1998.
- [12] T. Baglin, *High Sensitivity Amplifiers for PS Pick-ups*, CERN PS/BD/Note 98-06 (tech.), Geneva, 1998.
- [13] M. Ludwig, *The Synchronisation for the PS Closed Orbit Measurement System: Real time software development and implementation*, CERN PS/BD/Note 99-03(tech.), Geneva, 1999.

CHAPTER 10

PERFORMANCE OF THE PRE-INJECTOR COMPLEX

10.1 GENERAL ISSUES

10.1.1 Transfer Efficiency

Extensive machine experiments during the 2003 operation period have shown that, contrary to original expectations, significant beam losses occur in the LHC injector chain for nominal and ultimate LHC beams. Around 5% of the beam is lost in the PS-complex (starting from capture in the PSB to the TT2 transfer line) and between 10 and 15% is lost in the SPS, mainly at capture. These losses need to be compensated by an increase of the intensity from the pre-injector complex. Since it now seems reasonable to allow for some losses in the LHC as well, the number of protons for the “nominal” and “ultimate” LHC bunches in the PS and also the bunch intensities required from the PSB had to be redefined (see Sec. 2.3).

Since the transverse emittance budget is fixed, any increase in intensity also leads to an increase in beam brightness and thus to a larger space charge tune shift at injection into the PSB which is the limiting factor. The 25 ns bunch train is nearly a factor 3 more demanding on beam brightness in the PSB than the 75 ns train. This lies in the nature of the PS bunch splitting scheme where each PSB bunch is split in 12 LHC bunches for the 25 ns train but only in 4 LHC bunches for the 75 ns train.

For the 25 ns nominal beam an intensity increase of up to 20% is going to be acceptable. On the other hand, for the 25 ns ultimate beam, which is already only feasible in the PSB by using up some of the PS’s emittance budget, the required characteristics will become unattainable with present techniques and alternatives have to be considered (see Sec. 10.5).

For the 75 ns bunch trains no problems are anticipated for both nominal and ultimate LHC bunch intensities.

10.1.2 Beam Characteristics

With both 25 ns and 75 ns bunch spacing, the nominal characteristics specified for the LHC have been regularly obtained for the average bunch delivered to the SPS. However, characteristics (intensity, bunch length and transverse emittance) vary along the bunch train. Variations in transverse emittance are due to unequal emittances of the bunches from the four PSB rings, fluctuations in intensity can be caused by unequal intensities from the PSB and hardware imperfections in the PS, which also lead to variations in bunch length.

10.1.3 Uncaptured Beam and Parasitic Bunches

Typically around 1% of particles outside the bunches have been observed before ejection from the PS. They contribute to capture loss in the SPS and to the generation of parasitic bunches.

10.2 THE CASE OF 25ns BUNCH SPACING

At an intensity of 1.3×10^{11} protons per LHC bunch at PS ejection (nominal bunch intensity accounting for $\sim 10\%$ beam losses in the SPS), fluctuations inside the bunch train in intensity, bunch length and transverse emittances are within $\pm 10\%$, limited by the differences between PSB rings and hardware imperfections in the PS. Fig. 10.1 shows the normalised horizontal and vertical rms emittances measured with wire scanners all along the injector chain. The measurements in the PSB show: the horizontal emittances of the bunches in rings 2 and 4 and the vertical emittances of those in rings 1, 3 and 4; in the PS, they show: at injection all 6 bunches from two PSB batches (PS 1.4GeV) and just before ejection the 72 LHC bunches (PS 26GeV/c); in the SPS, they show: the 72 LHC bunches from one PS batch at injection

(SPS26GeV/c) and at top energy (SPS 450GeV). The emittance budget foresees $(\epsilon_{n,\text{hor}} + \epsilon_{n,\text{ver}}) \leq 5 \mu\text{m}$ at PSB ejection, $\epsilon_n \leq 3 \mu\text{m}$ for both planes at PS ejection and $\epsilon_n \leq 3.5 \mu\text{m}$ at SPS top energy.

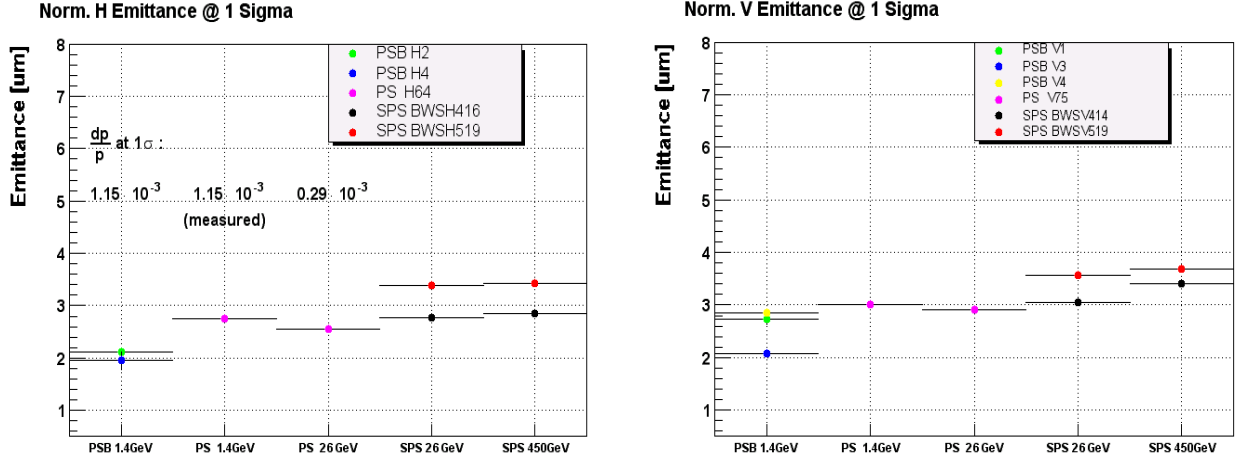


Figure 10.1: Normalised transverse rms emittances for the nominal 25 ns LHC beam along the injector chain (16.5×10^{11} protons per PSB bunch, 1.3×10^{11} protons per LHC bunch at PS ejection, 1.15×10^{11} protons per LHC bunch at SPS top energy).

At higher intensities, the PSB approaches its brightness limit and consequently the transverse emittances start to grow. In the PS, longitudinal coupled bunch oscillations increase the inter-bunch differences by creating different initial conditions for the bunches being split. To improve on this, a longitudinal damper is being prepared which will use the 10 MHz ferrite cavities that are still active during the first splitting at high energy.

10.3 THE CASE OF 75ns BUNCH SPACING

The performance specified for the nominal 75 ns spacing LHC beam has been obtained regularly for the average bunch delivered to the SPS. Bunch characteristics vary along the train. Even at nominal intensity, an asymmetry is observed which is attributed to the drift of the relative phase between harmonics 14 and 28 during the splitting process (see Fig. 10.2).

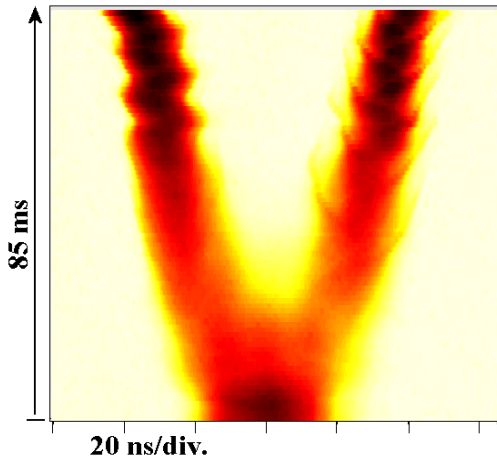


Figure 10.2: 75 ns bunch splitting at nominal intensity (1.15×10^{11} protons per LHC bunch, 25 GeV).

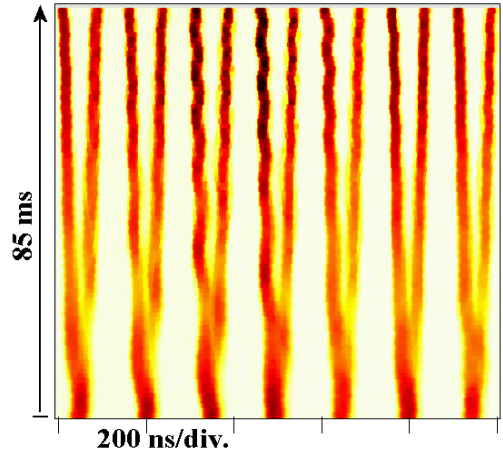


Figure 10.3: Incoherent bunch oscillations before and during 75 ns splitting (1.7×10^{11} protons per LHC bunch).

Because of this phenomenon, it has yet not been possible to equalise the 24 LHC bunches per PS batch simultaneously in intensity and longitudinal emittance.

In contrast to the 25 ns bunch spacing, the PSB operates well below its space charge limit and can therefore easily provide ultimate or even higher intensities within the emittance budget. However, at higher than nominal intensities coupled bunch oscillations appear in the PS, as in the case of the 25 ns bunch train and further increase the discrepancy between the final bunches (see Fig. 10.3). The same longitudinal damper will be employed as a cure.

10.4 PILOT BUNCH BEAMS

The LHC pilot beam consists of a single low-intensity bunch with 0.5×10^{10} protons and a normalised rms emittance of less than 1 μm in the LHC. The production of the pilot beam follows a different scheme than the one of the nominal LHC proton bunch train. Both the transverse and the longitudinal LHC bunch characteristics are already established in the PSB. After ejection from the PSB, the pilot bunch is passed on to the LHC by the downstream machines with the main concerns being to keep the bunch characteristics unchanged and to minimise longitudinal and transverse emittance blow-ups.

During 2002 extensive machine studies were made in the PSB to develop a strategy for pilot bunch production. The aim was to produce not only the low-intensity LHC pilot beam but also single LHC-type bunches with up to nominal intensity, $0.5 \times 10^{10} \leq N_b \leq 11.5 \times 10^{10}$ and with emittances variable between pilot and nominal emittance, $0.85 \mu\text{m} \leq \varepsilon_n \leq 2.5 \mu\text{m}$ at PSB ejection. The longitudinal emittance for all beam variants is kept constant at 0.3 eVs, slightly below the nominal one (0.35 eVs). This parameter space spans a factor 66 in beam brightness, N_b/ε_n .

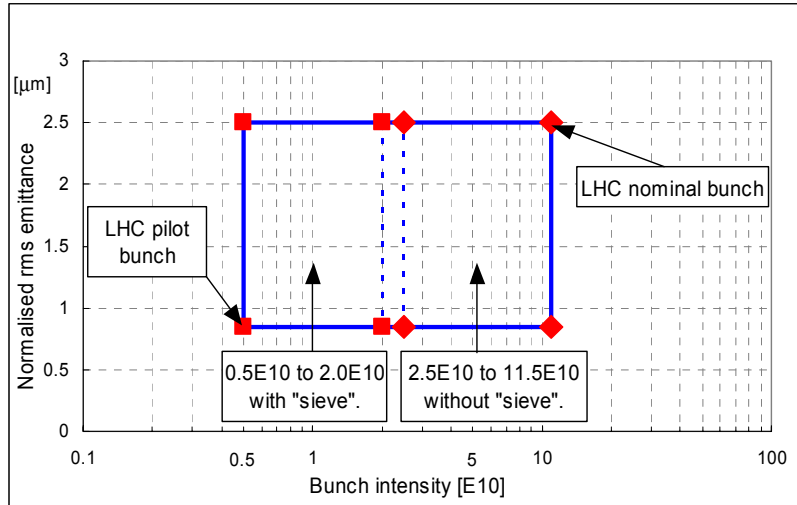


Figure 10.4: Range of PSB bunch characteristics obtained in 2002.

The main ingredients used to cover this large parameter space were:

- Insertion of the “sieve” in the linac transfer line to reduce the beam intensity (transverse density) by a factor 5.
- Controlled longitudinal blow-up (phase modulated RF on $h=10$) in the PSB to adjust the longitudinal density.
- Transverse shaving to set the transverse emittance.
- Longitudinal shaving (acceptance reduction during ramping) to set the longitudinal emittance.

By properly adjusting the procedures listed above, all the required types of bunches were obtained during 2002 in the PSB [1] as illustrated in Fig. 10.4. The low intensity bunches were obtained using the sieve in the linac to PSB transfer line. During 2003, significant effort was invested to study the acceleration of single bunch pilot-type beams in PS and SPS. Results are very satisfying as the bunch characteristics and especially the small transverse emittances were conserved up to SPS top energy for the pilot beam (0.5×10^{10} , 1 μm). No major difficulties were encountered during tests with a single nominal LHC bunch.

10.5 ULTIMATE BEAM

The level of unavoidable beam loss along the cascade of accelerators makes it impossible to attain the ultimate intensity per circulating bunch in the LHC with the standard schemes (see Sec. 2.3). Two different approaches are feasible to address this shortcoming:

- Increase the beam brightness in the PS, by means of RF gymnastics concentrating the beam in fewer bunches, in a fraction of the PS circumference, at an energy where space-charge is not a limitation. The resulting reduction of the number of bunches delivered per PS pulse will call for changing the LHC filling scheme, with an increase of filling time and a decrease of the filling factor.
- Increase the brightness of the beam in the PSB by injecting at a higher energy with a new linac (Linac4) replacing the 50 MeV Linac2, thus avoiding space charge limitations at injection.

10.5.1 Batch Compression in the PS

By slowly increasing the frequency of the RF holding the bunches, it is possible to reduce the fraction of the ring occupied with particles [2]. This is achieved by successively activating RF systems operating at increasing frequencies. A gap without particles is necessary in the initial beam. The following procedure can be sketched [3]:

- inject 7 (4+3) bunches from two PSB batches into the PS operating on harmonic 9
- accelerate this beam up to an intermediate energy where space charge is sufficiently reduced
- compress the 7 bunches into 7/14 of the PS circumference by adiabatically increasing from $h=9$ to 10, 11, 12, 13, 14
- accelerate the beam on harmonic 14 up to 25 GeV
- triple split the bunches using RF on $h=14, 28$ and 42 (similar process as used at 1.4 GeV for the 25 ns bunch train)
- double split the bunches changing the harmonic from 42 to 84 and rotate them before ejection, as in the present 25 ns bunch train scheme.

Finally, a train of 42 bunches spaced by 25 ns is sent to the SPS.

Because of space charge on the 1.2 s long PS flat porch at 1.4 GeV, the total intensity in the PS in that mode is limited to 1.1×10^{13} protons (1.6×10^{12} protons per PSB ring). Neglecting beam loss in the PS, the maximum intensity per bunch sent to the SPS is then 2.65×10^{11} protons. Ultimate intensity in the LHC will therefore be attained if transmission from PS to LHC is better than 64%.

10.5.2 New PSB Injector (Linac4)

Replacing the 50 MeV Linac2 by a 160 MeV Linac4, space charge is reduced by a factor two at injection energy in the PSB. Using the flexibility in painting possible with charge exchange injection, the brightness of the beam delivered by the PSB is expected to double and reach 3.6×10^{12} protons per ring within 2.5 μm rms in both transverse phase planes. With a single batch from the PSB, the following procedure can be applied [4]:

- inject 12 (4×3) bunches into the PS operating on harmonic 14¹
- accelerate the beam on harmonic 14 up to 25 GeV
- triple split the bunches using RF on $h=14, 28$ and 42 (similar process as used at 1.4 GeV for the 25 ns bunch train)
- double split bunches changing the harmonic from 42 to 84 and rotate them before ejection, as in the present 25 ns bunch train scheme.

Finally, a regular train of 72 bunches spaced by 25 ns is sent to the SPS.

¹ Each PSB ring delivers 3 bunches, obtained by triple splitting at 1.4 GeV with the existing RF system. $H=1$ RF voltage is applied before ejection to reduce the distance between bunches to a period on $h=14$ in the PS. The recombination kickers in the PSB to PS transfer line have to be modified for faster rise times.

Because of the very short time spent at 1.4 GeV, the increase by a factor 14/12 of the space charge induced tune spread in the PS is considered feasible. The total intensity in the PS is then 1.42×10^{13} protons. Neglecting beam loss in the PS, the maximum intensity per bunch sent to the SPS is then 1.97×10^{11} protons. Ultimate intensity in the LHC will be attained, with a single batch from the PSB, if transmission from PS to LHC is better than 86%.

If this transmission is not achieved, various batch compression schemes can be envisaged, necessitating the change of the LHC filling scheme, with an increase of the filling time and a decrease of the filling factor.

10.5.3 Comparison between Schemes

Both methods have to be studied in more detail. Their main features are summarised in Tab. 10.1. The new injector for the PSB is a more expensive but very attractive option which would ease operation and reduce the filling time of LHC, leaving more beam time from the PSB and PS available to other users. When combined with batch compression in the PS it has the potential of providing beams of much larger brightness which can be precious for further luminosity upgrades of the LHC.

Table 10.1: Comparison of methods to increase beam brightness.

	Batch compression	New PS injector
Implementation	Limited cost Fast (provided machine time and manpower are available)	Significant cost (~ 70 MCHF) Long (~ 3 years construction)
Exploitation	Complex, delicate & manpower intensive,	Simple & robust
Performance	Increased LHC filling time Reduced LHC filling factor Penalises other beam users	Reduced LHC filling time Usual LHC filling factor Beneficial to other users (more cycles available, with more protons per cycle)
Potential ^{*2}	Limited at $\sim 2.65 \times 10^{11}$ protons per bunch from the PS	Can go beyond 3×10^{11} protons per bunch from the PS when combined with a batch compression scheme

REFERENCES

- [1] M. Benedikt, *LHC pilot bunches from the CERN PS Booster*, Proc. of PAC 2003, Portland, 2003.
- [2] R. Garoby, *New RF exercises envisaged in the CERN-PS for the antiprotons production beam of the ACOL machine*, CERN-PS-85-36-RF, Geneva, 1985.
- [3] O. Bruning et al., *LHC Luminosity and Energy Upgrade: a Feasibility Study*; LHC Project Report 626, Chapter 11, CERN, Geneva, 2002.
- [4] F. Gerigk, M. Vretenar, *Design of a 120 MeV H- Linac for CERN High Intensity Applications*, CERN/PS 2002-069 (RF), Geneva, 2002.

² These are preliminary estimates that need to be refined. Upgraded instability damping systems for the PS will be necessary in both longitudinal and transverse phase planes to cope with that intensity.

CHAPTER 11

INTRODUCTION

The SPS will form the final link in the injector chain for the LHC, accelerating 26 GeV protons from the PS to 450 GeV before extraction via two specially built transfer lines connecting the SPS and the LHC ring tunnels. The first report detailing the upgrades needed for the SPS was published in 1993 [1]. This study was based on the use of superconducting magnets for the transfer lines. The report was later revised and incorporated into the LHC conceptual design report [2] once the decision to use room temperature magnets for the two transfer lines had been taken. A more detailed study was launched in 1996 and a comprehensive conceptual design report for the SPS as LHC injector was published in 1997 [3].

Since then, many changes have been made to the technical details of the SPS upgrade in preparation for the LHC. Many of these changes have come about as a result of changes, or additions, to the requirements. Most notably, major modifications have come about as a result of the following:

- The approval of the CNGS facility which will share the new SPS east extraction channel with the anti-clockwise LHC ring
- The final decision to shield impedance sources in the SPS and not to install a higher harmonic RF system in the SPS
- The decision to close the west experimental area, allowing a significant simplification to the west extraction channel
- Modifications to the bunch patterns and schemes for both protons and ions

In addition, an active machine development programme has been undertaken in the SPS to study the very bright beams required by the LHC. These studies have lead to considerable changes in both the technical details of the installed equipment and the operational procedures used to produce the LHC beam [4].

Chap.12 describes the LHC beam parameters and requirements in the SPS, together with the SPS cycles needed to produce the beam. As well as the nominal 25ns beam for LHC, other beams requested by the LHC are detailed: these include the pilot bunch, the 75ns beam and special schemes for early commissioning or TOTEM operation. The beam parameters in the SPS for the ultimate beam are also described.

One of the major challenges for the SPS is the conservation of the transverse emittance during the transfer through the SPS and its beam lines. Any transverse emittance growth in the SPS will directly affect the luminosity performance of the LHC. One of the major contributions to the emittance growth is the transfer and injection process. In order to stay within a very tight emittance growth budget, careful matching between the PS and SPS machines is required. Careful measurements are required to reach to required level of matching. In addition, the injection equipment in the SPS has been upgraded to pulse the kickers with a shorter rise time and substantially smaller ripple. The injection channel upgrades are described in Chap. 13. Any remaining injection errors will have to be damped by powerful transverse dampers, see Chap 14. The overall procedures for emittance preservation throughout the transfer, injection, acceleration and extraction processes are described in Chap. 15.

Some of the major hardware modifications and additions which are needed to transform the SPS into LHC injector are described in Chaps. 16-20. The existing 200 MHz travelling wave RF system is undergoing a major upgrade. This includes new power plant, circulators and cavity coupler modifications to cope with the increased beam loading. New low-level controls and synchronisation systems will also be put in place for the LHC beam. While the 400 MHz system described in [3] has been dropped, the 800 MHz RF system, already installed in the SPS ring, will play a vital role in stabilising the beam during acceleration. Considerable new hardware is required to make the 800 MHz system routinely operational.

The long straight section in LSS4 houses the new extraction channel and the first part of the transfer line TT40 towards both the LHC anti-clockwise ring (via TI 8) and CNGS (via TT41). This channel has been installed and commissioned successfully. The clockwise LHC ring will be filled from the existing west extraction via TI 2. The decision to definitively close the west experimental area of the SPS makes the LHC the only user of this channel and has allowed the layout in LSS6 to be simplified considerably. This channel will be modified during the coming long shutdown of the SPS in 2005.

The impedance reduction programme in the SPS has made a major contribution to the ability of the SPS to produce the LHC beam. Two major activities have taken place: Firstly the shielding of specific equipment, such as the magnetic septa, identified as an impedance source, secondly, the shielding of some 900 inter-magnet pumping ports has reduced significantly the resonant impedance in the machine and increased the stability of the LHC beam, even at the highest intensities. Some open questions remain, notably the impedance of the new extraction kickers installed in both LSS6 and LSS4.

The key to maintaining the very high quality beam demanded by the LHC in the SPS is the quality of the beam instrumentation. Many changes, additions and upgrades to the beam diagnostics have been made. This includes bunch-by-bunch measurements of intensity and position, additional transfer line monitors, matching measurement systems for the injection line and high quality, continuous emittance measurements throughout the acceleration cycle. Additional instrumentation has also been provided in the extraction channels. A set of scrapers will be needed to remove the tails of the particle distribution before transfer to the LHC. Finally the very bright LHC beam, compressed into 30% of the machine circumference has required an upgrade to the high energy internal beam dump. A completely new dump core has been designed and installed in the machine.

With many of the major upgrades already completed the SPS has demonstrated its ability to meet the stringent requirements of the LHC. Beam matching the requirements for LHC nominal operation has successfully been accelerated to 450 GeV. This is in spite of the discovery that the electron cloud effect is a major issue for the SPS [5]. Continued machine development to understand and cure the phenomena in the SPS has been accompanied by additional studies using the SPS as a test-bed for the LHC. Periods of beam conditioning are now routinely used to “scrub” the surface of the vacuum chambers, reduce the secondary electron yield and minimise the vacuum pressure rise. For the future, in addition to completing the hardware modifications, continued studies will be required to allow routine operation of the SPS as injector for LHC while still delivering high quality beams to the other SPS users in the periods when beam is not required by the LHC.

REFERENCES

- [1] E. Brouzet & K. Schindl, ‘*The LHC Proton Injector Chain*’, CERN/PS 93-39 (DI), CERN SL 93-37 (AP) LHC Note 256, 1993.
- [2] P. Lefevre & T. Petterson (ED.), ‘*The Large Hadron Collider, Conceptual Design*’, CERN/AC/95-05 (LHC), Geneva, 1995.
- [3] Collier P. et al., ‘*The SPS as LHC Injector, conceptual Design*’, CERN-SL-97-007-DI, Geneva, 1997.
- [4] Arduini G. et al., ‘*The LHC Proton Beam in the CERN SPS: An Update*’, LHC-Project Report 638, Proc. PAC 2003, Portland, OR, USA, 2003.
- [5] Jimenez J.M. et. al, ‘*Electron Cloud Studies and Analyses at SPS for LHC-Type Beams*’, Proc. PAC 2003, Portland, OR, USA, 2003.

CHAPTER 12

BEAM PARAMETERS AND REQUIREMENTS

12.1 CYCLE AND OPERATIONAL REQUIREMENTS

12.1.1 Standard LHC Filling Cycle

In the standard LHC filling cycle [1] between two and four PS batches are transferred from PS to the SPS at 26 GeV/c with an interval of 3.6 seconds between injections. After the injection of the last batch a ramp to 450 GeV/c is started. A ramp rate similar to that used for the p-pbar Collider is used (an average ramp rate of 78 GeV/sec), with the principal limitation from the RF power requirements at low energies. Once at 450 GeV/c the following actions take place during the flat-top, which is approximately 1 second long:

- The ramping of the extraction elements (magnetic septa and closed orbit bumpers) ready for extraction,
- The fine re-phasing of the SPS with respect to the LHC in order to inject into the LHC at the required azimuthal position,
- The compression of the bunch length by an RF voltage increase,
- Cleaning of the tails of the beam distribution down to $3-3.5\sigma$ by means of fast scrapers.
- The status and settings of various elements of the LHC, the transfer lines, the SPS and the extraction channel must be surveyed and checked before extraction is permitted.

Towards the end of the flat top the beam is extracted to one of the LHC rings, either via the west extraction zone to TI 2, or via the east extraction to TI 8. Once the beam has been extracted the machine is ramped back to the injection level for the next cycle. Fig. 12.1 shows the SPS supercycle required for a single injection into the LHC. Cycles having two, three or four PS batches will be required [2,3]. Injections occur at 0, 3.6, 7.2 and 10.8 s from the start of the supercycle, as 3.6 s is the cycle length for the LHC beam in the PS. A total of 24 such supercycles will be required to fill both rings of the LHC with beam. The length of any supercycle must be a multiple of the PS elementary cycle (1.2 s), which in this case is 21.6 s. The rms power consumption (for the machine dipoles and quadrupoles) is 19 MW. Using the above specifications, and neglecting the time required for changing from LHC Beam 1 to Beam 2, the LHC filling time will be about 9 minutes.

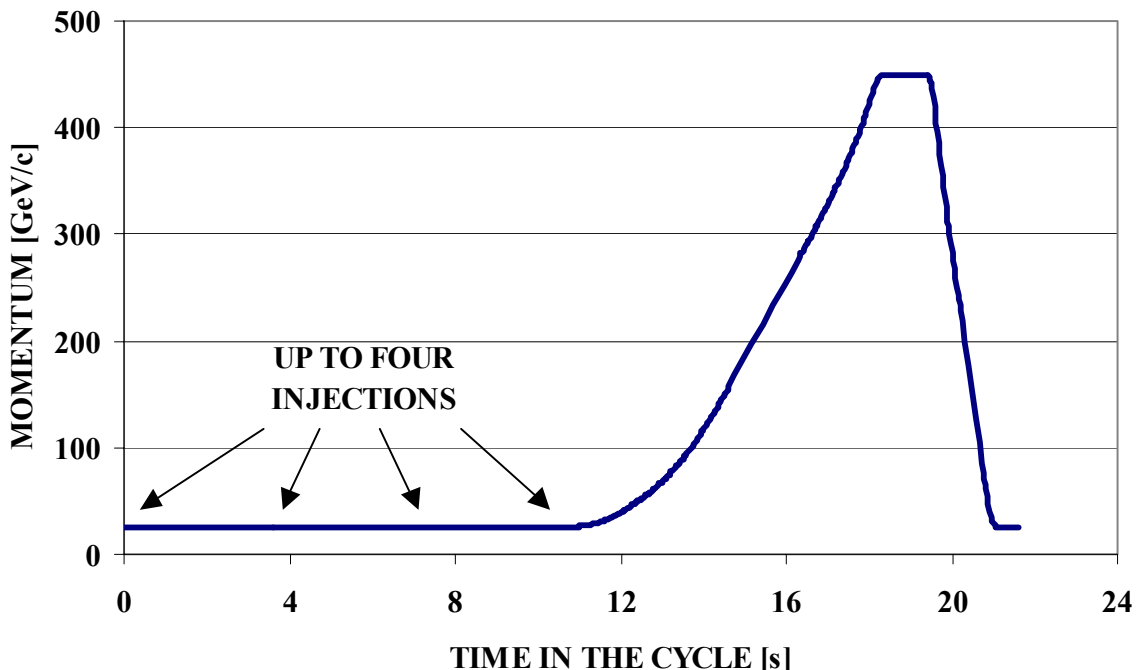


Figure 12.1: SPS supercycle for LHC filling.

Before starting the LHC filling process for each physics coast, one or more pilot bunches will be required [2,3,4]. The pilot bunch must be measurable by the beam observation systems of the LHC and its intensity must allow the complete loss of the beam at injection without quenching the LHC magnets, for this reason the pilot bunch is also called the safety beam. The safety beam will therefore consist of a single bunch, with an intensity of around 5×10^9 protons. The pilot bunch can be produced in the injector chain with the required intensity and emittance as well as with good parameter reproducibility [5]. This beam has been delivered for the TT40 extraction tests [6]. Its injection and acceleration in the SPS nevertheless requires specific settings for the machine. An alternative scheme would consist in injecting a more intense bunch in the SPS (e.g. a nominal LHC bunch) and reducing the intensity before extraction by scraping at 450 GeV/c. This would minimise the amount of tuning needed in the SPS in order to switch from pilot to nominal operation [7].

With the pilot intensity, the LHC beam instrumentation does not provide accurate enough measurements to guarantee a safe injection of the nominal beam into the LHC. For this reason, once the injection process and the LHC machine parameters have been roughly checked and adjusted with the safety beam, an intermediate beam consisting of 12 bunches (4 in the case of a 75 ns spacing beam) having nominal bunch parameters will be injected. These can be produced in the PS Complex by using a single Booster bunch instead of the usual 6 for the nominal beam. The intermediate beam can be used to fine tune the settings of the LHC machine. Once the LHC is ready, the nominal LHC beam will be injected, but only after having re-injected the pilot beam [2].

Recently it has been observed that dipole and quadrupole magnetic fields in the SPS injection plateau for the LHC filling cycle are not stable and trims in the functions driving the main dipoles and quadrupoles are required to compensate for their decay. The observations are consistent with a decay time constant of about 1 s for the main dipoles and around 0.5 s for the quadrupoles. This effect is very likely due to the decay of the eddy currents induced in the vacuum chambers during the ramp-down of the magnets [5]. Although a compensation for the field decay is applied, this is only approximate and the effect of the residual errors is not known. For this reason a longer supercycle might be required. This would allow for a longer pre-injection plateau in order to provide enough time for the eddy currents to decay. Investigations with beam are being performed during 2004 to try and disentangle the effects of the eddy currents and to provide operational solutions while minimising the total length of the SPS supercycle for the LHC.

Studies are also ongoing to reduce the PS Booster cycle length to 0.9 s or even to 0.6 s. This would allow a reduction of the PS LHC cycle and therefore of the injection plateau in the SPS with beneficial effects not only for the LHC filling time but, in particular, for the preservation of the emittance in the SPS.

12.1.2 Scrubbing

Operation of the SPS with the LHC beam during machine studies has shown that electron multipacting occurs in the SPS vacuum chamber as a result of the high bunch intensity, the short bunch spacing and the high Secondary Emission Yield (SEY) of the stainless steel vacuum chamber surface (see Sec. 15.6). Electron multipacting induces desorption of molecules from the vacuum chamber and dramatic pressure increases have been observed.

Experiments performed in the SPS in 2002 have shown that the SEY can be reduced by the electron bombardment induced by the beam. This conditioning, or scrubbing, effect reduced the SEY of a test surface from 2.1-2.3 (the as received surface) to about 1.5 during a 10-day period. During dedicated runs the machine is operated close to the vacuum interlock level, by acting on the number of PS batches injected and on the amount of time spent by the beam in each supercycle (adjustable by varying the timing of the beam dump in the supercycle). The initial SEY value is recovered as soon as a conditioned vacuum chamber is vented to air, although the re-conditioning is faster if the length of time that the chamber is at atmospheric pressure is kept short. As interventions on the vacuum system are inevitable during the annual accelerator shutdowns, ‘scrubbing’ runs lasting a few days will have to be scheduled in the SPS at the beginning of each year’s operation, before operation with LHC beams starts.

During the scrubbing run, the SPS is normally operated with a flat 26 GeV/c supercycle, having the possibility of injecting more batches. The length of the ‘scrubbing’ cycle is dictated mainly by the lifetime of the beam (which is poor at the beginning of the run) and the need to minimise the number of PS complex cycles devoted to this purpose and therefore the impact on other Physics programmes. An SPS supercycle length of 43.2 s has proved to be a reasonable compromise. The modification of the SEY is localised,

particularly in the main dipole magnets where the electron cloud is concentrated in stripes symmetrically placed with respect to the beam and parallel to the magnetic field lines. The separation of the stripes is proportional to the bunch intensity and inversely proportional to the bunch length. The location of the ‘scrubbed’ area also moves with the beam position and the bunch length. As a result it also varies during the acceleration. For this reason a ‘scrubbing’ period with acceleration to 450 GeV/c, on the cycle shown in Fig. 12.1, must follow the scrubbing run at 26 GeV/c.

The duration of a scrubbing run and/or the intensity of the beam injected in the SPS are presently limited by the beam-induced heating of the ferrites of the kickers installed in the machine. In particular the horizontal tune kicker (MKQH) and the extraction kickers (MKE) are affected, because of their relatively small vertical aperture [4]. Once the Curie temperature is reached in the ferrite, there is a reversible loss of the magnetic properties of the kicker. Even higher temperatures could result in mechanical damage to the ferrite blocks. The present understanding of the phenomenon indicates that the SPS can be operated at injection energy with two nominal intensity PS batches for a few days without interruption (assuming a beam duty factor close to 1). However, operation with the nominal LHC beam (4 PS batches) and with acceleration to 450 GeV/c is limited to less than 24 hours. These durations proved to be sufficient in order to reduce the SEY to acceptable values in the SPS and hence allow operation with the LHC beam. However, SPS kicker heating might be a limitation for the scrubbing of the LHC itself, if frequent injections are required [8]. Studies and experiments have been started to upgrade the kickers in order to eliminate, or at least reduce their heating.

12.1.3 Constraints on Cycle Composition and Controls Requirements

Although a significant reduction of the SEY is attained during the scrubbing runs, no complete suppression of the multipacting can be obtained in the arcs for the nominal LHC beam. When the SPS is operated with the LHC beam in parallel to fixed target physics, abnormal sparking of the electrostatic septa used for the slow-extraction and transverse instabilities affecting the fixed target beam have been observed, even after scrubbing. These effects come about as a result of the long time constant for the decay of the electron cloud. Operation with the nominal LHC beam in parallel with fixed target physics is therefore not planned at present.

Currently, during dedicated machine studies with the high intensity LHC beam, the high voltage on the cathodes of the electrostatic septa (ZS) is reduced to zero and the ZS ion traps are powered to help prevent electron multipacting. In addition, as a cautionary measure, the extraction girders are retracted. The fast vacuum valves in the extraction area are also blocked out in order to prevent intermittent closure that could damage the valves themselves. These fast valves are designed to protect the electrostatic septa from water inrush in the case of a mechanical failure of the coils of the magnetic septa. For this reason the cooling circuits of the magnetic septa are closed during operation with LHC beam.

All these actions, acceptable during machine study sessions prevent rapid supercycle changes between the LHC filling mode and conventional operation for fixed-target physics. The movement of the girders takes some minutes to complete, however, moving the girders can probably be avoided once the LHC beam is routinely in operation. On the other hand, applications to perform all the other actions in a rapid and deterministic sequence will have to be implemented.

The beams required by the LHC (pilot, intermediate and nominal) during a standard filling sequence will be accelerated using the same cycle but some retuning of the machine parameters (e.g. the betatron tunes) and of the settings of the beam observation and RF systems will be needed.

The LHC injectors will have to be able to switch between the different beams required for the LHC filling phase and between extractions to either one of the two LHC rings on a cycle-by-cycle basis [9]. In routine operation LHC filling will occur during SPS operation for fixed target physics, or during machine studies. Fixed-target physics periods are likely to include CNGS operation as well as slow extracted beams to the north experimental area. Rapid switching between LHC filling and other modes of operation is needed to maximise the efficiency for physics whilst guaranteeing equipment safety. The SPS control system must provide the tools for multicycling in terms of settings generation and maintenance, cycle timing, cycle management, interlock handling, hardware status and beam measurements.

12.2 BEAM PARAMETERS

The different beams required by the LHC cover a wide range of bunch and total beam intensities. In all cases the SPS will have to deliver beams to the LHC with the nominal longitudinal characteristics and the specified transverse emittances. In the case of the pilot beam the tolerance on the transverse emittance is looser, but the intermediate beam should be a good approximation to the nominal beam. The main parameters of the nominal and pilot LHC beams are listed in Tabs. 12.1 and 12.2, respectively. Realistic values of the SPS transmission efficiency have been taken into account based on the experience with the present machine set-up [5,8].

Table 12.1: Nominal LHC beam parameters

	Injection	Extraction
Proton momentum [GeV/c]	26	450
Number of bunches/PS batch	72	72
Number of PS batches/SPS batch	2-4	2-4
Number of particles per bunch [10^{11}]	1.3	1.15
Circulating beam current [A]	0.13-0.26	0.12-0.23
Bunch spacing [ns]	24.97	24.95
Bunch train spacing	224.7	224.6
Transverse normalised emittance (H/V) [$\mu\text{m}.\text{rad}$]	3.0/3.0	3.5/3.5
Longitudinal emittance [eV.s]	0.35	<0.8
Rms. bunch length [cm]	30	<15
Rms. energy spread [10^{-4}]	10.7	<2.8

Table 12.2: Pilot beam parameters

	Injection	Extraction
Proton momentum [GeV/c]	26	450
Number of bunches/PS batch	1	1
Number of PS batches/SPS batch	1	1
Number of particles per bunch [10^{11}]	0.055	0.05
Circulating beam current [A]	3.9×10^{-5}	3.5×10^{-5}
Bunch spacing [ns]	-	-
Bunch train spacing	-	-
Transverse normalised emittance (H/V) [$\mu\text{m rad}$]	0.9-3.0/0.9-3.0	1.0-3.5/1.0-3.5
Longitudinal emittance [eV s]	0.35	<0.8
Rms. bunch length [cm]	30	<15
Rms. energy spread [10^{-4}]	10.7	<2.8

Operation with the 25 ns beam will certainly start with bunch populations lower than the nominal one and the requested intensity will increase with the understanding of the machine and experiments. As the bunch population increases the brightness of the beam should be a constant to a rough approximation. However, experience shows that this is unrealistic at low intensities where additive sources of blow-up like injection errors and dispersion mismatch become the dominant source of emittance growth (see Chap. 15).

Beams with 75 ns spacing will be required during the early phases of LHC operation in order to minimise the problems associated with electron multipacting and keep the beam power in the LHC down. The basic parameters for this beam are listed in Tab. 12.3. In this table the baseline filling scheme is given [2,8]. This assumes the same PS batch spacing as for the 25 ns beam and provides some margin for the LHC injection

and beam dump kicker without any additional margin for the SPS injection kicker. An alternative filling scheme with increased PS batch spacing (from 224.7 to 274.6 ns) in the SPS could provide some margin for the rise-time of the SPS injection kicker, while only partially reducing the corresponding margin for the LHC kickers.

Table 12.3: Nominal parameters for the 75 ns LHC beam.

	Injection	Extraction
Proton momentum [GeV/c]	26	450
Number of bunches/PS batch	24	24
Number of PS batches/SPS batch	2-4	2-4
Number of particles per bunch [10^{11}]	1.3	1.15
Circulating beam current [A]	0.043-0.087	0.038-0.077
Bunch spacing [ns]	74.90	74.85
PS batch spacing	224.7	224.6
Transverse normalised emittance (H/V) [$\mu\text{m rad}$]	3.0/3.0	3.5/3.5
Longitudinal emittance [eV.s]	0.35	<0.8
Rms. bunch length [cm]	30	<15
Rms. energy spread [10^{-4}]	10.7	<2.8

One of the phases of the LHC commissioning will be the production of collisions with no crossing angle at the interaction points. This implies a large bunch spacing to avoid parasitic beam-beam encounters. The baseline filling scheme fulfilling these requirements consists of injecting 43 bunches into each ring of the LHC [2,3]. The corresponding filling scheme in the SPS, together with the requested beam parameters are listed in Tab. 12.4. This scheme will require the acceleration of a single bunch per PS cycle. The displacement of some bunches by 75ns with respect to their nominal position in the LHC might be needed to allow collisions in the LHCb experiment (values in parenthesis in Tab. 12.4).

Table 12.4: The ‘43-bunch’ beam in the SPS.

	Injection	Extraction
Proton momentum [GeV/c]	26	450
Number of bunches/PS batch	1	1
Number of PS batches/SPS batch	2-4	2-4
Number of particles per bunch [10^{11}]	1.2	1.15
Circulating beam current [A]	$1.66-3.32 \times 10^{-3}$	$1.6-3.2 \times 10^{-3}$
Bunch spacing [ns]	2022.57 (2097.48)	2020.95 (2095.8)
PS batch spacing	2022.57 (2097.48)	2020.95 (2095.8)
Transverse normalised emittance (H/V) [$\mu\text{m rad}$]	3.0/3.0	3.5/3.5
Longitudinal emittance [eV.s]	0.35	<0.8
Rms. bunch length [cm]	30	<15
Rms. energy spread [10^{-4}]	10.7	<2.8

An additional filling scheme with 156 bunches with 525 ns spacing has been conceived for the TOTEM experiment. This scheme will also be useful for commissioning and early operation [2,3]. The bunch spacing is still sufficiently large to allow operation of the LHC with zero crossing angles. This will require the acceleration of 4 equidistant bunches per PS cycle. The main parameters for this beam in the SPS are listed in Tab. 12.5. Some of the PS batches might be rotated by 75 ns in order to allow for collisions in the LHCb experiment (values in parenthesis in the Tab. 12.5).

Table 12.5: The 156-bunch beam for TOTEM Operation

	Injection	Extraction
Proton momentum [GeV/c]	26	450
Number of bunches/PS batch	4	4
Number of PS batches/SPS batch	2-4	2-4
Number of particles per bunch [10^{11}]	0.33	0.3
Circulating beam current [A]	$1.83\text{-}3.67 \times 10^{-3}$	$1.67\text{-}3.33 \times 10^{-3}$
Bunch spacing [ns]	524.37	523.95
PS batch spacing	524.37 (599.28)	523.95 (598.8)
Transverse normalised emittance (H/V) [$\mu\text{m rad}$]	0.8/0.8	0.9/0.9
Longitudinal emittance [eV s]	0.35	<0.8
Rms. bunch length [cm]	30	<15
Rms. energy spread [10^{-4}]	10.7	<2.8

Table 12.6 summarises the parameters of the ultimate LHC beam in the SPS. The ultimate beam has a 25ns structure, just like the nominal beam. However, the bunch intensity is increased while keeping the emittance constant until the point at which the assumed beam-beam limit is reached.

Table 12.6: Ultimate LHC beam parameters

	Injection	Extraction
Proton momentum [GeV/c]	26	450
Number of bunches/PS batch	72	72
Number of PS batches/SPS batch	2-4	2-4
Number of particles per bunch [10^{11}]	1.9	1.7
Circulating beam current [A]	0.19-0.39	0.17-0.34
Bunch spacing [ns]	24.97	24.95
PS batch spacing	224.7	224.6
Transverse normalised emittance (H/V) [$\mu\text{m.rad}$]	3.0/3.0	3.5/3.5
Longitudinal emittance [eV.s]	0.35	<0.8
Rms. bunch length [cm]	30	<15
Rms. energy spread [10^{-4}]	10.7	<2.8

REFERENCES

- [1] P. Collier, ed., ‘*The SPS as LHC Injector for LHC – Conceptual Design*’, CERN-SL-97-07-DI.
- [2] P. Collier, ‘*Baseline Proton Filling Schemes*’, Proceedings of the LHC Project Workshop – CHAMONIX XIII – Chamonix, January 19-23, 2004, J. Poole ed., CERN-AB-2004-014 ADM, p. 30-33.
- [3] R. Bailey, P. Collier, ‘*Standard Filling Schemes for Various LHC Operation Modes*’, LHC-Project Note 323, LHC-OP-ES-0003, EDMS No. 489439, 2004.
- [4] M. Benedikt, ‘*LHC Operational Beam Definitions*’, LHC-OP-ES-0002, EDMS No. 487892, 2004.
- [5] G. Arduini, ‘*LHC Beam in the SPS: Where do We Stand?*’, Proceedings of the LHC Project Workshop – CHAMONIX XIII – Chamonix, January 19-23, 2004, J. Poole ed., CERN-AB-2004-014-ADM, p. 34-43.
- [6] J. Uythoven, ‘*TT40 Experience and TI8 Beam Tests*’, Proceedings of the LHC Project Workshop – CHAMONIX XIII – Chamonix, January 19-23, 2004, J. Poole ed., CERN-AB-2004-014-ADM, p. 77-80.
- [7] G. Arduini, A. Verdier, ‘*Poor Mans Pilot and TOTEM bunches*’, AB-Note-2003-017 MD.

- [8] G. Arduini, J.-P. Delahaye, '*Outstanding Issues in the Injector Complex – Summary*', Proceedings of the LHC Project Workshop – CHAMONIX XIII – Chamonix, January 19-23, 2004, J. Poole ed., CERN-AB-2004-014-ADM, p. 1-8.
- [9] S. Baird, '*Routine Operation of the LHC*', Proceedings of the Workshop on LHC Performance – CHAMONIX XII – Chamonix, March 3-8, 2003, J. Poole, S. Dubourg, M. Truchet, eds., CERN-AB-2003-008 ADM, p. 282-284.

CHAPTER 13

THE SPS INJECTION CHANNEL

13.1 INTRODUCTION

The SPS injection channel was upgraded during the 2000-2001 machine shutdown. The injection kicker magnets (MKP) were partially replaced and the pulse forming networks were modified to fulfil the requirements of the LHC beams [1,2,3]. The layout in the BA1 surface building, which contains the MKP system power and control electronics, was modified in order to create space for additional kicker units.

With the addition of a kicker tank the kick centre of the injection kickers moved down stream. The small dipole installed after the kicker tanks had to be replaced by a stronger magnet to compensate for the slightly shorter lever arm. This dipole is used to steer the non-injected beam onto the injection dump.

13.2 SYSTEM PARAMETERS AND LAYOUT

The system parameters of the injection kicker system (MKP) are given in Tab.13.1. Originally the LHC ions required a rise time of less than 115ns. This very stringent requirement determined the system design, although after installation the LHC ion scheme was modified and the required rise time became comparable to the one needed for the LHC protons (smaller than 220 ns). The other requirement imposed at the design stage was on the kicker flat-top ripple, which for all LHC beams must be smaller than $\pm 0.5\%$. The new design required magnet modifications to reduce the rise time and PFN improvements to reduce the ripple.

The faster rise time was obtained by increasing the impedance of the system from 12.5Ω to 16.67Ω and by reducing the kicker magnet length from 22 cells to 17 cells. Adding additional magnets to the system compensated the reduced strength per magnet. The original MKP layout consisted of three magnet tanks with 4 magnets each. The new layout consists of two kicker tanks with 5 high impedance magnets each, one kicker tank with two high impedance magnets and one unmodified kicker tank with four low impedance magnets. A schematic of the system layout, which includes an optional Pulse Forming Line (PFL) for use with the LHC ion injection, is shown in Fig. 13.1. The PFL scheme was devised in order to meet the 115 ns rise time for LHC ions. As this is no longer requested by the LHC, the option of installing the PFL system has been shelved.

Table 13.1: The MKP kicker system requirements for various beams

Beam	Injection momentum GeV/c/q	Rise Time /ns	Flat Top / μ s	Fall Time / μ s	Ripple /%
LHC Protons	26	< 220	2.1	No Restriction	< ± 0.5
FT Protons	14	<1000	10.5	1.0	< ± 1.0
LHC Ions	17.1	<220	0.5	No Restriction	< ± 0.5
FT Ions	12.9	<1000	2.0	3.8	< $\pm 1/0$

13.3 MKP MAGNETS

The new MKP magnets have the following modifications with respect to the original magnets:

- To reduce the rise time of the magnets, the impedance was increased from 12.5Ω to 16.67Ω . This was done by reducing the surface area of the high voltage plates of the magnets.
- The number of cells was reduced from 22 to 17, in order to reduce the filling time of the magnet and hence reduce the rise time of the field.
- Damping resistors of 47Ω were added between the high voltage plates of each cell to damp the magnetic field oscillations.
- The gap between the magnet and the tank was screened to reduce the impedance seen by the beam.
- Capacitive pick-ups were installed on one magnet out of two to measure the magnetic field [4].
- On one magnet two temperature probes were installed on an earth plate to measure the beam induced heating. This temperature is rather close to temperatures of the outside of the ferrites.

- To avoid machining of beryllium, the new return conductors are made of titanium [5].

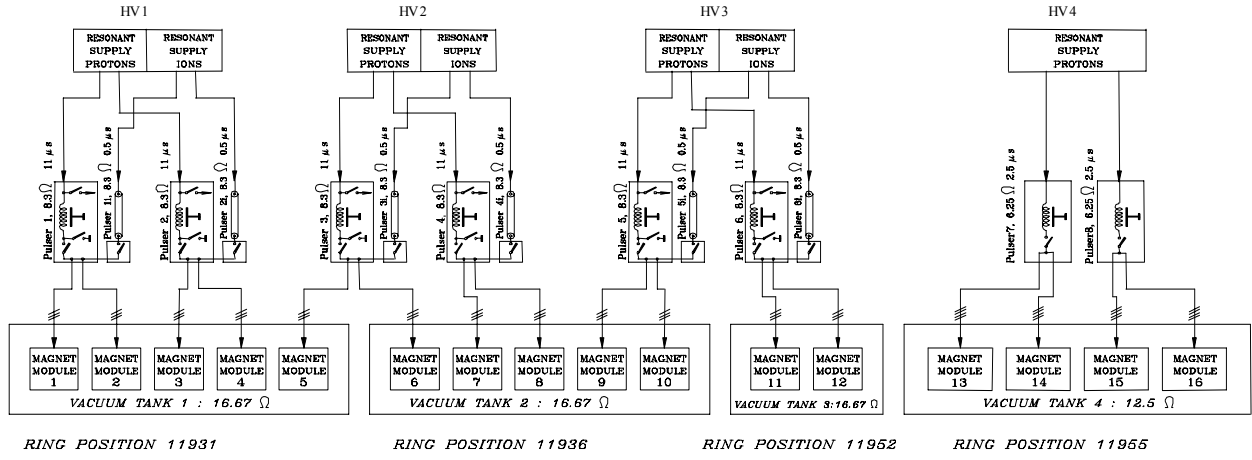


Figure 13.1: MKP system layout, which the option of the Pulse Forming Line (PFL) for the LHC ion injection.

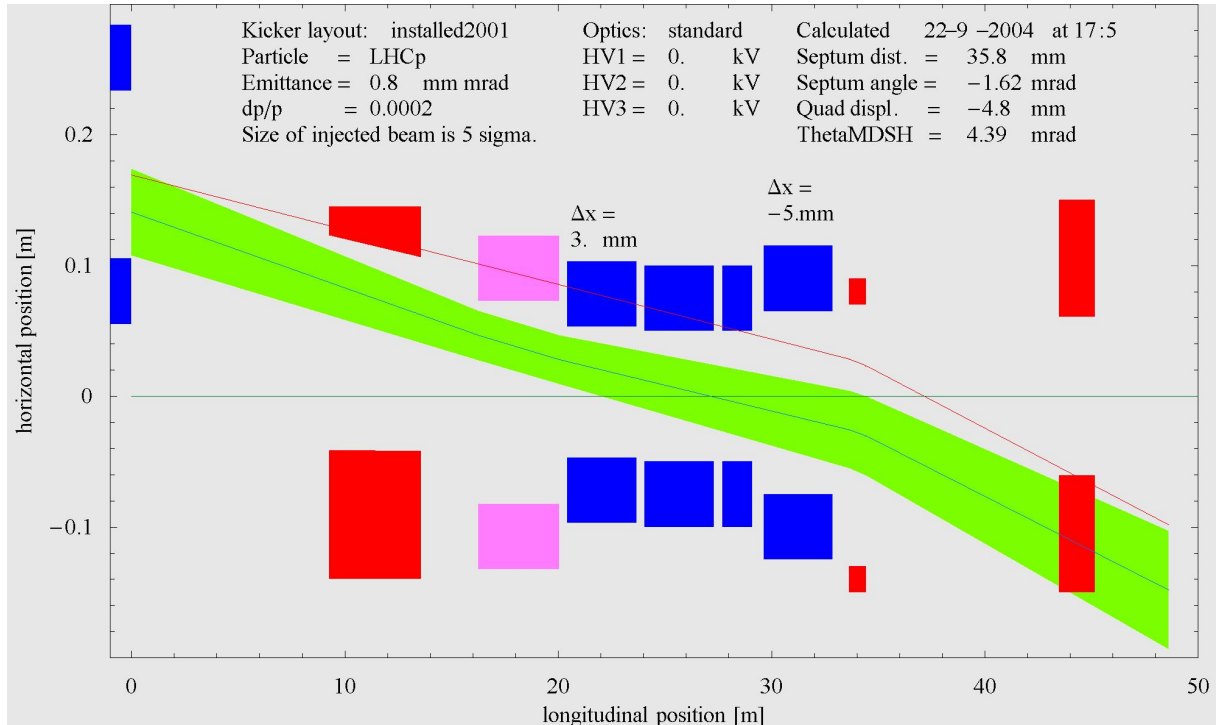


Figure 13.2: Horizontal apertures for the injected LHC beam.

The apertures of the 12 new S-type magnets are identical to the 8 magnets which were removed (full aperture $H \times V = 101 \text{ mm} \times 61 \text{ mm}$). The aperture of the 4 magnets which were not changed is larger in the horizontal plane, but smaller in the vertical ($141 \text{ mm} \times 54 \text{ mm}$). These apertures are sufficiently large, as illustrated in Fig 13.2. The 5σ beam is shown together with the horizontal displacements of the kicker tanks. All kicker tanks were installed with zero vertical displacement.

The integrated magnetic field of the non-modified L-magnets in the fourth tank is 32.9 mT.m/magnet for the LHC HV setting of 48.4 kV. For the same setting the modified S-Type magnets have an integrated dipole field of 17.4 mT.m/magnet. Fig. 13.3 shows the four MKP kicker tanks as installed in half cell 119 of LSS1. In the foreground the MDSH magnet, described in Sec. 13.5 can be seen.

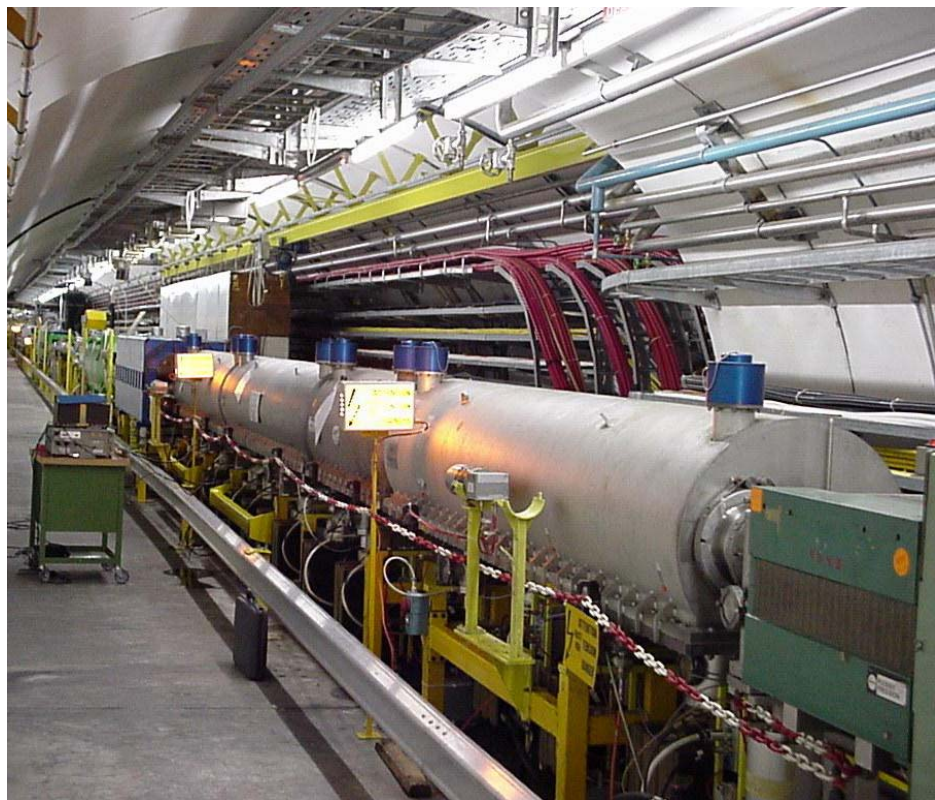


Figure 13.3: The MKP as installed in the tunnel.



Figure 13.4: Modified PFN tank for the S-Type MKP Kickers

13.4 MKP PULSE FORMING NETWORKS

The Pulse Forming Networks (PFN) at position 1 to 6 in Fig. 13.1 underwent the following modifications with respect to their original design:

- The impedance was increased from 6.25Ω to 8.33Ω to match two modified magnets in parallel.
- Continuous coils have replaced the small coils between each PFN cell in order to reduce the ripple of the magnetic field.
- Resistors of 50Ω were added between each PFN cell to reduce the field ripple.
- The components of the PFN front cells were adjusted to obtain the required pulse shape.

A modified PFN of this type is shown in Fig. 13.4.

13.5 MKP CONTROL SYSTEM

The MKP controls architecture has been totally renewed [6]. It consists of two essentially independent entities: one for the control of the equipment state (e.g. ON, OFF, STANDBY) and one for the control of the operational settings for the equipment (e.g. kick strength, kick delay, kick length). Typically, the equipment state control requires a response time in the order of 25 ms and is independent of the running machine cycle. This allows the use of industrial components, such as programmable logic controllers (PLC), to implement the required functionality. On the other hand, the MKP operational settings are tightly linked with the running machine cycle. Their control requires a software response time better than 1 ms and timing delays set with a resolution of 5 ns. For these reasons, a real-time operating system and dedicated hardware electronics modules must be used.

For safety reasons, all time critical actions, such as personal protection, are still performed directly at the hardware level with software only being involved for status acquisition.

The MKP state control is based on a SIEMENS S7-400 master PLC driving 4 different controllers through identical PROFIBUS-DP segments. These controllers are either connected as deported I/Os, or as decentralised I/Os when low-level intelligence is required. A fifth PROFIBUS-DP segment is implemented to interface the resources common to the four generators, such as the magnet temperature and vacuum monitoring systems. The PLC master is connected to the machine Ethernet TCP/IP network for communication with the application software layer.

The MKP settings control system consists of 13, G-64 crates connected through a MIL-1553 field bus to a LynxOS VME PowerPC. Synchronisation is provided to the machine timing system through a TG8 VME module. Each G-64 crate is composed of a set of either programmable modules, or passive signal conditioning modules. In order to limit the total number of modules, the same set of modules are used for each injection attached to a different running machine cycle. The operational functionality of the complete system is obtained through individual settings linked to each injection.

The management of the operational settings is based on a real time task implemented at the front-end level. Upon reception of an injection warning timing event, the TG8 module detects and decodes the event and interrupts a server thread that is in a blocking read state. Recognised interrupts make the thread reload the G-64 modules with voltage and timing parameters from a preloaded local table. This table is structured in terms of SPS cycle types and injection numbers and in each case contains the associated voltage and timing parameters.

Remote control of both systems is implemented through independent SPS2001 compliant device servers. For the settings control the device server runs on a LynxOS front-end computer, while for the state control the device server runs on a dedicated HP-UX workstation. In this scheme, the server processes are aware of the actual elementary SPS running cycle. Client programs can be automatically informed of data changes in servers through a data publish/subscribe mechanism. State management, setting and measurement contracts have been implemented through call-back routines at the server level. Expert actions have also been implemented in order to allow specialists access to an in-depth analysis of the complete system.

13.6 REPLACEMENT OF INJECTION DUMP MAGNET

A small dipole magnet just behind the kicker magnets is used to dump the injected beam on the centre of the target TBSJB when the kickers are switched off. The original magnet of the MDPH type was not strong enough to deflect the 26 GeV/c LHC beam on the target. The magnet and the corresponding power converter have been replaced. The new magnet is of the MDSH type which is sufficiently strong.

13.7 OPERATIONAL ISSUES

The HV settings of the different PFNs and the settings of the MDSH magnet to properly dump the beam with the injection kicker off for both the fixed target and the LHC beams are summarised in Tab. 13.2.

The timing of the system is critical for LHC operation as the rise time of the non-modified kicker magnets are well outside the 220 ns window. When the timing of the different PFNs is set, it is important to include in the analysis the filling time of the magnets (which is different for each of the different magnet types) and not just to consider the TMR signals [7]. A modification of the MKP PFNs number 7 and 8 is foreseen, which should reduce the magnetic field overshoot of the magnets in the unmodified tank and make the timing adjustment less critical.

Table 13.2: Reference settings of the MKP system for the different beams.

	HV generator 1 – 3	HV generator 4	MDSH setting
Fixed target, 14 GeV/c	49.2 kV	Off	2.08 mrad
LHC beam, 26 GeV/c	48.4 kV	48.4 kV	4.4 mrad

REFERENCES

- [1] L.Ducimetière, G.Schröder, J.Uythoven, E.Vossenberg, *Upgrading of the SPS injection kicker system for the LHC requirements*, EPAC'98, Stockholm, June 1998, also CERN SL-98-050 BT.
- [2] J.Uythoven, *The new SPS injection channel*, Proceedings of the workshop on LEP-SPS performance, Chamonix 1999, CERN-SL-99-007 DI.
- [3] J.Uythoven, J.Bonthond, L.Ducimetière, G.Schröder, E.Vossenberg, Q.Han, *The future of the SPS injection channel*, PAC'99, New York, 29 March – 2 April 1999, also CERN-SL-99-023 BT.
- [4] J.Uythoven, J.H.Dieperink, *High precision magnetic field measurements of fast pulsed magnets*, 12th international magnet measurement workshop, ESRF, Grenoble, France, 1 – 4 October 2001.
- [5] P.Knaus, J.Uythoven, *Transient thermal analysis of intense proton beam loss on a kicker magnet conductor plate*, EPAC2000, Vienna, 26 – 30 June 2000, also CERN-SL-2000-034 BT.
- [6] A.Antoine, E.Carlier, A.Marchand, H.Verhagen, *The new control system of the SPS injection kicker*, EPAC2002, Paris, 3 – 7 June 2002, also CERN-SL-2002-020 BT.
- [7] J.Uythoven, *Results of SPS MD 4/7/02*, Presentation in SPS Studies Working Group of 4 September 2002.

CHAPTER 14

THE SPS DAMPER

14.1 RE-ENGINEERING THE SPS DAMPER FOR THE LHC BEAM

The SPS transverse feedback system, also called the "transverse damper" combines three principal functions:

- damping of transverse injection errors
- feedback: curing transverse coupled bunch instabilities (dipole modes)
- excitation of transverse oscillations for beam measurements, see for example [7,15]

Since its inception in the late 1970's the SPS transverse feedback system [1] has undergone several major upgrades to cope with the increasing beam intensity and different beams [2,4,5]. In the framework of the project for the upgrade of the SPS as LHC injector [6,8,9,11], the transverse damper system has again been upgraded and re-engineered.

14.1.1 SPS Damper in 1996

In 1996 the SPS damper consisted of four electrostatic kickers, two per plane, with power amplifiers employing two tetrodes and installed directly under the kickers. All four kickers were installed in the dispersion suppressor left of LSS2 in a half period with missing MBA dipoles. The bandwidth of the system was about 6 MHz in feedback mode, with a 3 dB point at around 1.5 MHz and a maximum kick voltage of +/- 4 kV. With the fixed target beam at a bunch spacing of 5 ns, higher frequency coupled bunch dipole modes were cured by octupoles [4]. Digital signal processing was employed with a notch filter and a 1-turn delay, the hardware to perform the signal processing dating from the 1980's, and was clocked at 33 MHz [3].

14.1.2 Goals of the Upgrade for the LHC Beam

The aim of the upgrade, which was started in 1997, was to increase the total bandwidth of the feedback system to 20 MHz, half the LHC bunch frequency of 40 MHz. This was necessary in order to provide feedback for all possible coupled bunch dipole modes of the LHC beam with 25 ns bunch spacing. Moreover, the 3 dB bandwidth needed to be increased in order to achieve a rise-time compatible with the gap of eight missing bunches between the individual batches injected from the PS accelerator into the SPS. An increase of this 3 dB frequency from 1.5 MHz to 4.5 MHz was achieved by lowering the impedance (anode resistance) and rebuilding the power amplifiers with a more powerful tube giving a higher peak current. The higher current is needed in order to change the voltage on the kicker plates in the short time of 225 ns between the injected batches. As part of the upgrade all the electronics, the 100 W driver amplifiers and the power amplifiers were rebuilt, the infrastructure was upgraded, new power converters procured and software and controls re-engineered in a way that is compatible with the general SPS RF controls system. Fig. 14.1 shows the SPS tunnel with the horizontal damper H1, (BDH214.37). The kicker tank can be seen with the power amplifier installed below.

14.2 HARDWARE PARAMETERS AND ELEMENTS OF THE TRANSVERSE DAMPER

Fig. 14.2 shows a block diagram of the two vertical systems after the upgrade. The system V2 was moved in the shutdown 2000/2001 from the original position upstream of LSS2 to a new position downstream of LSS2. This position change was required in order to cure an instability that develops when too much feedback gain is applied at tunes close to the integer, or half integer (see Sec. 14.4). The horizontal systems H1 and H2 were left in place upstream of LSS2. Tab. 14.1 shows the optics parameters for the four systems. The global performance at 26 GeV/c (the injection momentum of the LHC beam) is given in Tab. 14.2. The horizontal systems use amplifiers with TH561 tetrodes, the vertical system uses RS2048 CJ tetrodes which have a lower performance. The requirements for the feedback system are summarised in Chap. 15. In the

following, the design and implementation of the individual building blocks of the damper system are described.



Figure 14.1: The SPS damper H1 (BDH214.37) with its power amplifier installed below the kicker tank.

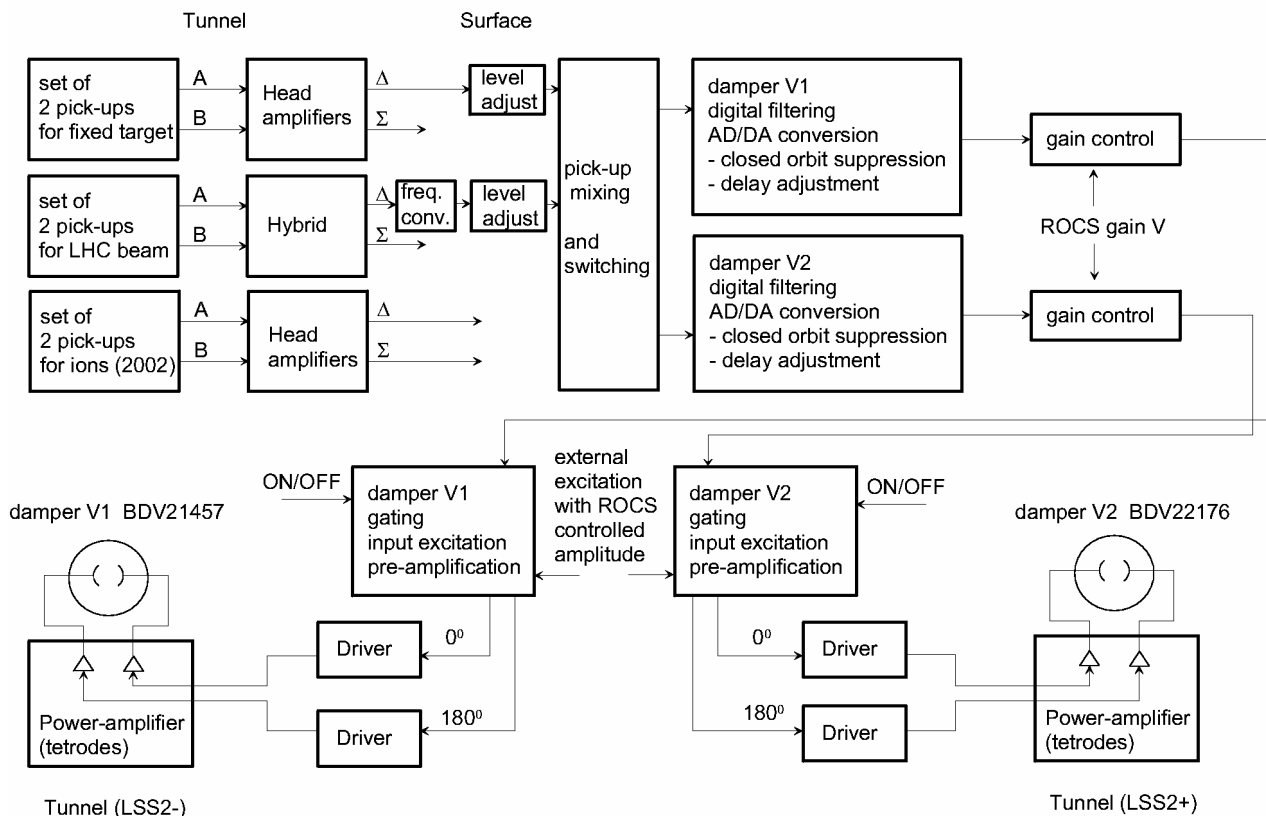


Figure 14.2: Block diagram of the two vertical damper systems V1 (BDV214.57) and V2 (BDV221.76).

Both the kickers and their associated power amplifiers are installed in the accelerator tunnel. The rest of the feedback system, including the 100 W driver amplifiers and all HV power converters, interlocks and control electronics is installed on the surface. The low-level part of the feedback system consists of front end signal processing for the pickup signals (different schemes and pickups are used for the large variety of beams). This is followed by a digital part working at a clock frequency of 80 MHz [16] and finally an amplification system. Feedback gain can be adjusted before and after the digital processing in order to make best use of the dynamic range available from the 12-bit ADC. A summing point is provided at the end of the low-level part which is used operationally in order to inject signals onto the damper. This facility is used principally for continuous tune measurements. In addition, use has been made of injected signals during machine development sessions for controlled beam blow-up. The damper signals are clipped and amplified before being sent to the power part of the equipment.

Table 14.1: Optics parameters and machine position of damper systems

System	Name in layout (position)	Beta function [m]
H1	BDH 214.37	77
H2	BDH 214.51	67
V1	BDV 214.55	39
V2	BDV 221.76	45

Table 14.2: Hardware performance of SPS damper systems:

Plane	number of systems	length mm	gap mm	voltage kV	kick strength μrad per system (at 26 GeV/c)
H	2	2396	142	2.9	1.9
V	2	1536	38	2.7	4.2

14.2.1 Kickers and Power Amplifiers

The electrostatic kickers represent a small capacitive load at low frequency to the power amplifiers. At higher frequencies, towards 20 MHz, a detailed analysis has to take into account the transmission line properties of the structure [10]. The connection to the power amplifier is made in the centre of the kicker. The vertical kicker has its $\lambda/4$ resonance frequency at about 100 MHz, while for the horizontal kicker the equivalent resonance is at 60 MHz. Both these are sufficiently far from the maximum operating frequency of 20 MHz to not pose any serious problems. The 3 dB roll-off frequency of 4.5 MHz is determined by the total capacitive loading and the anode resistance [10]. Between the low frequency and high frequency domains the RC roll-off introduces a phase lag of $\pi/2$. At the 3 dB frequency the phase lag is $\pi/4$. This phase lag is compensated by two second order all-pass filters in the low level part of the feedback loop. This introduces an additional frequency dependent phase shift, such that the total phase lag is linear with frequency up to 20 MHz. This linear phase shift corresponds to a constant group delay which can be absorbed into the overall 1-turn delay of the system. The total transfer function of power amplifier and compensating all-pass filters can be expressed as ($s=j\omega$):

$$F(s) = \frac{1}{1 + \tau \cdot s} \cdot \frac{s^2 - \frac{\omega_1}{Q_1} s + \omega_1^2}{s^2 + \frac{\omega_1}{Q_1} s + \omega_1^2} \cdot \frac{s^2 - \frac{\omega_2}{Q_2} s + \omega_2^2}{s^2 + \frac{\omega_2}{Q_2} s + \omega_2^2}$$

with $\tau = 35.4$ ns, $Q_1=1.840$, $Q_2=0.874$, $\omega_1/(2\pi) = 20.853$ MHz, and $\omega_2/(2\pi) = 11.511$ MHz.

In theory the phase of the overall transfer function deviates less than 2° from the linear case (= constant group delay) up to 25 MHz. In practice, with the analogue active filters used, a non linearity of better than 5°

has been achieved with a gain flatness of the all-pass part of ± 0.4 dB. In the future it is envisaged to improve the phase compensation further by incorporating it in the digital part of the feedback loop.

14.3 PERFORMANCE WITH LHC BEAM

14.3.1 Injection Damping

The performance of the injection damping is illustrated in Fig. 14.3. It shows the horizontal (upper trace) and the vertical damping (lower trace) for an LHC batch of nominal intensity. The damping time is approximately 0.5 ms. Operation at and beyond the electron cloud instability threshold requires careful monitoring and setting up of the damper.

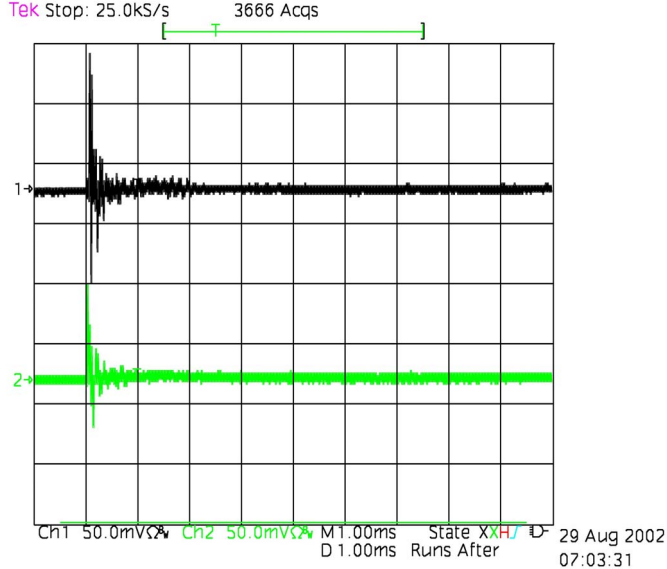


Figure 14.3: Horizontal (upper trace) and Vertical (lower trace) injection damping for the LHC type beam with 72 bunches at 10^{11} protons per bunch

14.3.2 Stability

Stability and damping for individual betatron lines can be checked at low frequency where the beam is stable without feedback, by inserting a network analyzer in the feedback path as shown in Fig. 14.4. The polar plots show a measurement of the open loop transfer function of beam and feedback system for the horizontal system H_1 and the vertical system V_1 . The measurement is usually done at different frequencies to verify and adjust feedback phase and the overall “one-turn” delay in the loop. The circles in the polar plot represent the combined open loop transfer function of beam $G(s)$ and feedback $H(s)$; orientation of $G(s)H(s)$ towards the negative half plane indicates stability of the closed loop transfer function (for betatron lines at 20 MHz in this example).

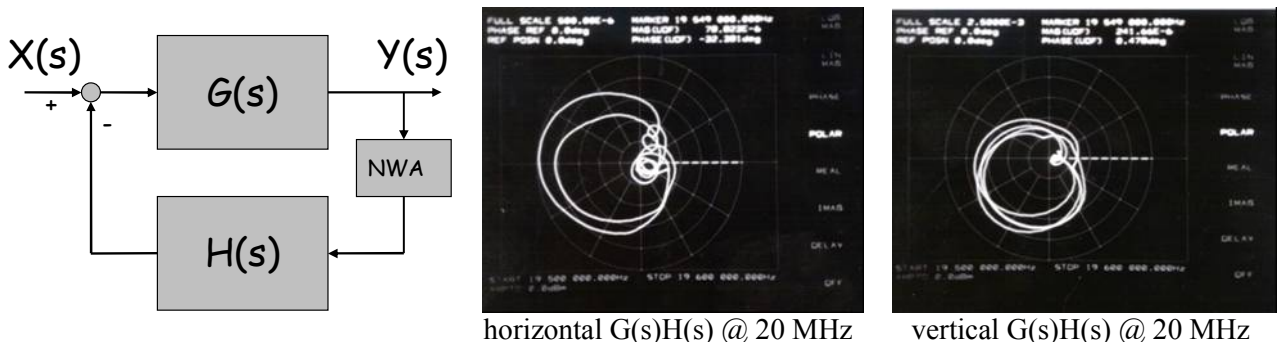


Figure 4: Results of beam transfer function measurement with feedback.

14.4 UNFORESEEN ELEMENTS DURING THE UPGRADE AND FUTURE EVOLUTION

14.4.1 The Electron Cloud Effect

The two principal consequences of the electron cloud effect and instability for the transverse damper systems and its upgrade were:

- The signals from the standard electrostatic pickups with high impedance electronics were disturbed and a new system with synchronous detection had to be put into place [12].
- There was an increase in the growth rates of horizontal coupled bunch instabilities and consequently the strength of the horizontal feedback systems may limit the damper performance with ultimate intensity.

The electron cloud effect and its cures are described in more detail in Chap. 15.6. In between the passage of two bunches, electrons, transversely accelerated by the electric fields of the passing bunches, will hit the chamber wall and the pick-up plates. Since the bunches are relatively short (<5 ns at injection, <2 ns at top energy) the beam spectrum extends to high frequencies, well beyond 200 MHz. The electrons of the electron cloud have a large energy spread and will hit the chamber wall during a time slot considerably longer than a bunch (>5 ns), but still shorter than the 25 ns bunch spacing. The spectrum of the electron cloud signal will therefore cut-off at a lower frequency than the true beam signal.

With the original wide band, high impedance pick-up electronics both the electron cloud signal from impinging electrons and the beam signal were measured. As a result of the high impedance loading of the pick-up, a quasi static signal persisted after the passage of a bunch and the electrons of the cloud. This signal seriously perturbed the feedback system to the extent that damping was impossible. The solution for the damper has been to move the processing to a higher multiple of the 40 MHz bunch frequency, allowing the pick-up to be matched to $50\ \Omega$. In this case, electrons hitting the pick-up are quickly removed and therefore no longer accumulate on the pick-up electrodes. The damper shares the four pickups (BPH 204.09, BPH 206.09, BPV 205.09 and BPV 207.05) with the SPS closed orbit system and a compatible solution had to be found. A frequency band at 120 MHz, i.e. three times the bunch frequency of 40 MHz, was chosen for the processing. This frequency is high enough in order not to be disturbed too much by the electron cloud effect. On the other hand, 120 MHz is reasonably close to the 200 MHz working frequency of the SPS orbit system.

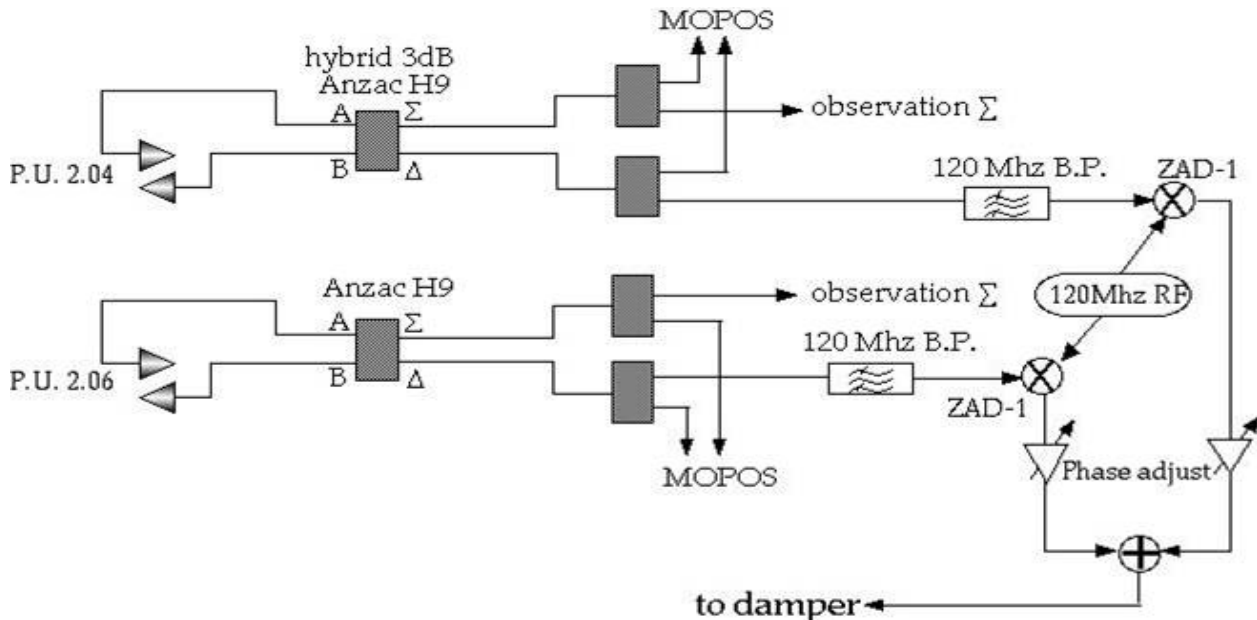


Figure 14.5: Principle of pick-up signal processing at 120 MHz (horizontal dampers). The betatron phase adjustment is done by combining the two orthogonal signals from pickups 2.04 and 2.06 with correct ratio and sign [13].

Pickups are matched to 50Ω by a wide band matching circuit, covering the range 40-240 MHz. The sum and difference signal are produced by hybrids. Fig. 14.5 shows the principle layout of the system that was used during the run during 2000 and with which the adverse effects of the electron cloud were overcome. Mixing was done with the 120 MHz frequency derived from the main 200 MHz RF frequency together with the revolution frequency. These reference signals are transmitted from the RF Faraday cage in BA3 to the damper installation in BA2, a distance of more than 1 km. Because of the distance, the phase of the 200 MHz signal shifts during acceleration. This effect is compensated by a phase shifter driven by the frequency program of the SPS.

Fig. 14.6 shows a pickup signal perturbed by the electron cloud (trace 2). This signal was produced using the high impedance electronics and base-band processing. For comparison an unperturbed signal (trace 4) is also shown. This was mixed down from 120 MHz. Both signals were taken with an LHC batch of 72 nominal intensity bunches [12].



Figure 14.6: Pickup signals: Trace 2 -perturbed by the electron cloud effect and Trace 4 - unperturbed.

The present solution does not completely suppress the effect of the electron cloud. Depending on the beam parameters this could become significant in the future, especially in the case of very short bunches and high intensities. If the energy spread of the electron cloud impinging on the pickup becomes smaller, the pulse generated in the pickup will be shorter and hence influence more the signal at the pickup processing frequency of 120 MHz. If this should become a problem in the future, it may be necessary to move the processing away from the 120 MHz sideband, to a higher multiple of 40 MHz. This is likely to be incompatible with the current sharing of the pick-ups between beam orbit observation and the transverse damper. Separate pick-ups would therefore be needed. This would require installation of dedicated pick-ups, which is not planned at present. An alternative is under investigation. This makes use of a Hilbert filter and a single pick-up (such as the existing couplers BPCR 214.34, and BPCR 214.35) for the phase adjustment. The Hilbert filter has already been tested successfully with beam [16,17]. In addition, the smaller diameter of the BPCR pick-ups would make it easier to apply an external magnetic solenoid field which can completely suppress the electron cloud effect.

14.4.2 Instability at Half Integer and Integer Tunes

With very high gains it can be shown that the feedback system becomes unstable when the tune approaches a half integer or integer value [14]. This occurred in the vertical plane where the standard tune in the SPS has been 26.58. The problem can be cured by installing the two damper systems at different betatron phases, the optimum being at orthogonal positions ($\pi/2$ phase shift in between the two systems). In practice after the relocation during the 2000-2001 shutdown there is a phase advance of about 60° between the two vertical systems. In the meantime the working point for the LHC beam has also changed which would have in any case cured the feedback instability. However, for fixed-target beam operation the original working point is still used and this justifies the modifications made.

14.4.3 Future Evolution and Use of the Damper within the Framework of the I-LHC Project

Currently there are no further upgrades needed for the operation of the SPS damper with the LHC proton beam. For operation with ions the use of the SPS damper is presently restricted to injection damping. Feedback along the ramp will not be provided. The present ion beams for fixed target physics do not require such a feedback. However, the intensity of the LHC ion beams to be accelerated in the SPS will approach the limit of the resistive wall instability threshold. The use of the SPS damper for ions along the ramp will require a modification of the digital signal processing in order to account for the large swing in frequency during acceleration. In addition, a re-design of the pickup electronics to optimise for the intensity per bunch and the bunch spacing might be necessary. These modifications may be implemented once studies have been made in the SPS with LHC ion beams.

The issue of the revolution frequency swing is illustrated in the following by comparing the situation for the proton LHC beam with the ion beam. The transverse feedback system as implemented is a “one turn delay” feedback: The signals acquired by the pickups are transmitted from the tunnel to the surface where they are delayed for “one turn” before being re-applied to the beam. If the pick-ups and kickers were installed at exactly the same location in the tunnel, the total delay required τ_i would equal the machine revolution time T , which in turn is a function of the revolution frequency and hence beam energy. In practice the total delay τ_1 is slightly different from T , as the pickups are not installed exactly at the place of the kickers. A large fraction of the electronic delay is realised in digital form, clocked at a frequency locked to the revolution frequency. This part correctly keeps track of the increasing velocity of the beam during acceleration. A smaller fraction of the delay comes from cable and electronic delay, which is fixed and does not change with beam energy. As a result there will be a small phase error in the feedback loop. If the feedback is perfectly adjusted at injection (26 GeV/c), the phase error at top energy (450 GeV/c) for the proton LHC beam amounts to between 17° and 18° at the highest frequency of the feedback system, i.e. 20 MHz [18]. This small phase error can be neglected. For the LHC ion beam the maximum feedback bandwidth must be 5 MHz (100 ns bunch spacing). Using the parameters of the present ion beam, together with the 5 MHz bandwidth leads to a large phase error, i.e. approximately 80°. Although the LHC ions will be injected at a higher energy than the present fixed-target ion beam, this effect needs to be taken into account. The phase error can be minimised by an appropriate choice of pickups (minimisation of fixed delay in cables). The residual phase errors will depend on the type of ions used and their injection energy. Analogue and digital methods exist to compensate for the phase error. These will be considered after 2006, should it be necessary.

REFERENCES

- [1] R. Bossart, L. Burnod, J. Gareyte, B. de Raad, V. Rossi, *The damper for the transverse instabilities of the SPS*, IEEE Trans. On Nucl. Sc., Vol. NS-26, No. 3, 3284-3286, 1979.
- [2] R. Bossart, J.-P. Moens, H. Rossi, *The new damper of the transverse instabilities of the SPS at high intensities*, CERN SPS/ABM/RB/Report 81-1, 1981.
- [3] R. Bossart, R. Louwense, J. Mourier, The digital notch filter of the damper, CERN SPS/ABM/Note/85-10, 1985.
- [4] R. Bossart, R. Louwense, J. Mourier, L. Vos, *Operation of the transverse feedback system at the CERN SPS*, CERN/SPS/87-10 (ABM), IEEE Particle Accelerator Conference, 763 (1987).
- [5] L. Vos, *Transverse Feedback System in the CERN SPS*, CERN SL-91-40 BI, CERN, Geneva, 1991.
- [6] L. Vos, *Damping of Coherent Oscillations*, CERN SL 96-66 (AP), 1996.
- [7] C. Boccard et.al., *Tune Measurements in the SPS as Multicycling Machine*, EPAC 1996 Sitges, pp. 1600-1603, Barcelona, 1996.
- [8] P. Collier (Ed.), *The SPS as Injector for LHC, Conceptual Design*, CERN-SL-97-007 DI, Geneva, 1997.
- [9] W. Hofle, *Towards a transverse feedback system and damper for the SPS in the LHC era*, Particle Accelerators, 1997, vol. 58, pp. 269-279.
- [10] W. Hofle, R. Louwense, *The deflectors of the SPS transverse damper - measurements and calculations*, SL-Note 97-45 (RF), CERN Geneva, 1997.
- [11] W. Hofle, *Transverse damping and fast instabilities*, CERN-SL-99-007 DI, pp. 86-91, CERN Geneva, 1999.

- [12] W. Hofle, *Observation of the Electron Cloud Effect on Pick-up Signals in the SPS*, CERN-SL-2000-007 DI, pp. 112-118, CERN Geneva, 2000.
- [13] W. Hofle, *Active feedback for curing the transverse resistive wall instability in the SPS*, CERN-SL-2000-007 DI, pp. 102-106, Geneva, 2000.
- [14] W. Hofle, *Progress with the SPS damper*, CERN-SL-2001-003 DI, pp. 317-319, CERN Geneva, 2001.
- [15] O. Berrig, W. Hofle, R. Jones, J. Koopman, J.-P. Koutchouk, H. Schmickler, F. Schmidt, *Excitation of large transverse beam oscillations without blow-up using the AC-dipole principle*, CERN-SL-2001-019 (BI), 2001.
- [16] V. Rossi, *Digital Signal Processing applications and Implementation for Accelerators - Digital Notch Filter with Programmable Delay and Betatron Phase Adjustment for the PS, SPS & LHC Transverse Dampers*, CERN-SL-2002-047 HRF, Geneva, 2002.
- [17] V. Vendramini, *Traitement du signal numérique pour le système de contre reaction transverse utilisant un seul pick-up avec application dans le SPS et dans le LHC*, SL-Note-2002-046 HRF, Geneva, 2002.
- [18] <http://cern.ch/proj-sps-damper>

CHAPTER 15

PRESERVATION OF THE TRANSVERSE EMITTANCE

15.1 INTRODUCTION

The brightness of the nominal LHC proton beam (i.e. the ratio between the bunch population and its emittance) is significantly higher than that of the other multi-bunch beams produced so far by the accelerators of the LHC injector chain. Only the bunches produced for the $p\bar{p}$ collider period had similar transverse and longitudinal brightness, however the total intensity of this beam was almost two orders of magnitude smaller than that of the nominal LHC beam. On the other hand, the beam for SPS fixed-target physics [1] has a total intensity comparable to the LHC ultimate beam, but its longitudinal and transverse brightness are far smaller. The LHC imposes a very tight transverse emittance blow-up budget: the SPS as LHC injector [2] has to deliver a beam with a normalised rms transverse emittance of at most 3.5 μm , while receiving a 3.0 μm beam from the PS.

Control of the transfer of the LHC beam from the PS to the SPS is critical for emittance preservation. The transfer is performed by fast extraction from the PS into the transfer line TT2-TT10 which connects the PS and SPS. The beam is then single-turn injected into the SPS. In the present filling scheme it is planned to have up to four injections per SPS cycle (see Chap. 12). In the SPS other potential sources of emittance growth come into play, including single-particle phenomena, such as resonances and transverse instabilities. When the SPS as LHC injector project [2] was launched the resistive wall instability was thought to be the main additional cause of transverse instabilities. However, during machine developments studies with the LHC beam in the SPS it became evident that coupling between the beam and the electron cloud it creates is in fact the dominant mechanism responsible for transverse instabilities. In this respect, the mechanisms and cures for emittance blow-up have had to be significantly reviewed.

15.2 THE TT2-TT10 TRANSFER LINE FROM PS TO SPS

The injection transfer line consists of two parts: the TT2 line (formerly used to transfer beam from the PS to the ISR) and the TT10 line, which branches off the TT2 line about 320 m downstream from the PS extraction. The TT2 line consists of a FODO lattice with a period length of about 18.5 m and a phase advance per cell of almost 30° in the horizontal plane and 50° in the vertical plane. The focussing and defocusing quadrupole families are independently powered. The FODO section is located downstream of a matching section, which consists of seven independently powered quadrupoles. An additional quadrupole, which is also independently powered, is installed just upstream of the switching dipoles to TT10. This quadrupole is downstream of the thin foil which is used to strip the ion beams for fixed target physics in the SPS experimental areas.

The TT10 line includes the switching magnets that bend the beam horizontally in the direction of the SPS (by 196 mrad) and the four vertical dipoles grouped in pairs of opposite strength. These dipole pairs are used to lower the beam by 32 m from TT2 down to the level of the SPS ring. The long distance transfer (about 800 m) consists of a FODO lattice, similar to that of the SPS machine. The FODO section has a period length of about 60.5 m and a phase advance per cell of almost 90° in the horizontal plane and 75° in the vertical plane. The matching between the lattices of TT2 and TT10 is made using a matching section located between the two FODO structures. This section consists of six independently powered quadrupoles (in addition to the single quadrupole at the end of TT2) and two independently powered interleaved doublets. The beta function and dispersion of the injection line are shown in Fig. 15.1.

15.3 STATIC INJECTION ERRORS

Detailed linear optical models exist for both the PS and SPS machines as well as for the injection transfer lines [3,4,5,6]. These models have been verified with beam based measurements and proved to reproduce the observations accurately [7,8,9]. The most difficult part of the model is the simulation of the optics as seen by the beam at extraction from the PS. Here the beam traverses a region where the fringe fields from the combined function main magnets are rather strong. For the LHC beam, this phenomenon is particularly

important, since at the extraction momentum of 26 GeV/c, the PS magnets are well into saturation and the fringe fields are strongest.

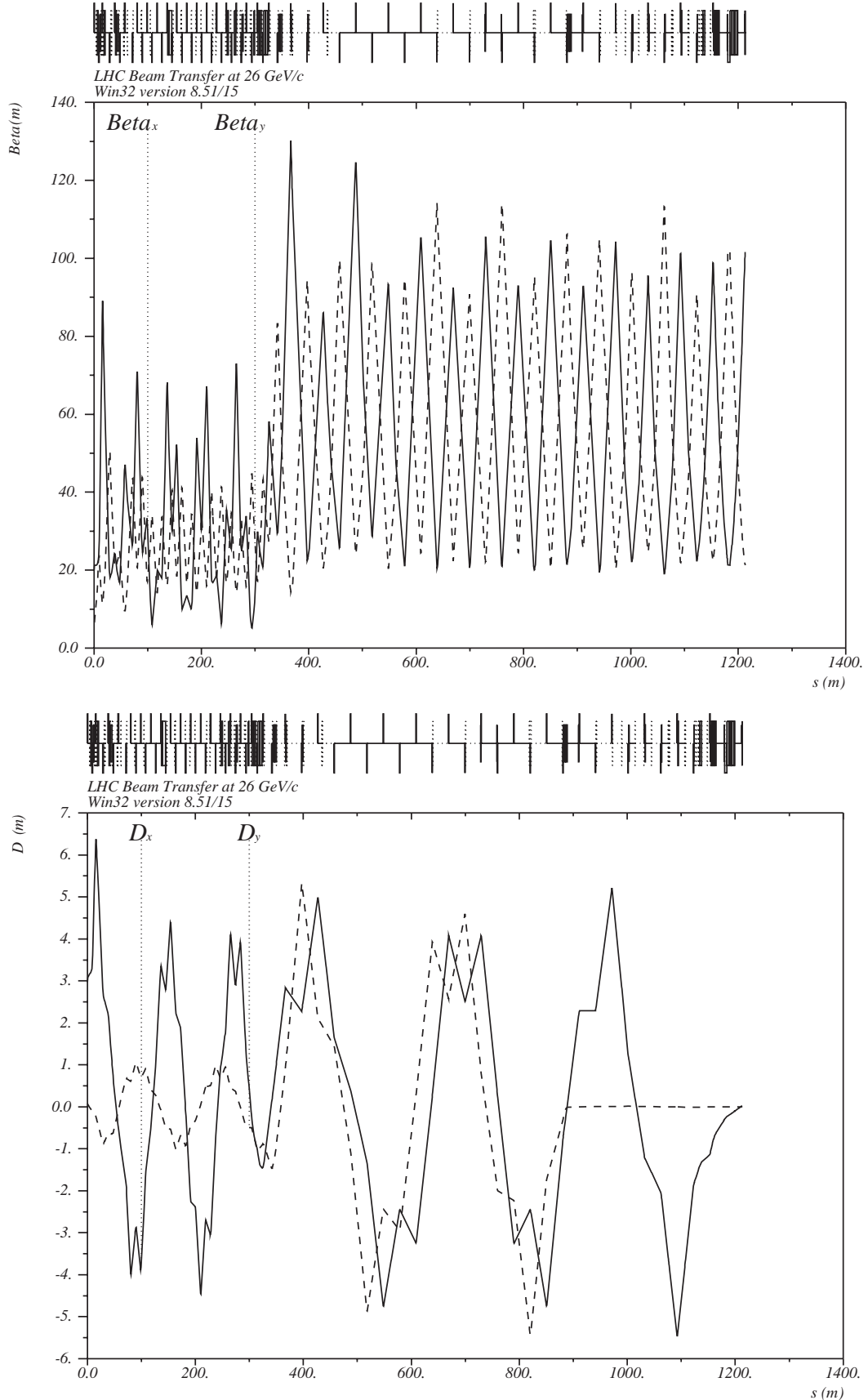


Figure 15.1: Beta (top) and dispersion (bottom) functions for the transfer line TT2-TT10.

Model calculations [10,11] of the PS magnet fringe fields which match the observations fairly well have been made, however, some uncertainties persist. Any uncertainties in the optical parameters of the extracted beam will propagate through the transfer line. In addition, other uncertainties coming from energy errors, together with magnet alignment and bending and quadrupole errors in the line must be taken into account. The combination of all error sources will lead to the following static errors on the beam:

- Injection errors
- Dispersion mismatch
- Betatron mismatch

Each of these errors, if not corrected, will provoke an increase in the transverse distribution of the beam because of filamentation. This occurs in all circular machines because of the presence of non-linear magnetic fields or electromagnetic phenomena, such as space-charge. The density of the core of the distribution is almost unaffected by these errors, but beam tails are created. The resulting dilution of the beam or the corresponding reduction of its brightness can be quantified by the so-called emittance blow-up after filamentation ($\Delta\epsilon_{af}$) [12], though this is a pessimistic representation of the loss in brightness. Each of the main error sources and its contribution to emittance blow-up is described below.

15.3.1 Injection Errors

Injection errors are the deviations in position and angle (Δx , $\Delta x'$) of the injected beam at the injection point with respect to the closed orbit of the machine at the same point. The emittance increase $\Delta\epsilon_{af}$ due to injection errors is given by:

$$\Delta\epsilon_{af} = \frac{\Delta X_n^2 + \Delta X'_n^2}{2}$$

where (ΔX_n , $\Delta X'_n$) are the normalised quantities corresponding to the above errors. The effects of injection errors are more severe for smaller values of the transverse emittance of the beam because of the additive nature of this source of emittance growth. These errors can be corrected down to the resolution of the observation system. For the SPS this resolution has a σ of 70 μm in the horizontal and 24 μm in the vertical plane [13]. Hence, correction at these levels implies a normalised emittance blow-up of:

$$\Delta\epsilon_{af,H(V)}^* = \beta\gamma \frac{\sigma_{H(V)}^2}{\beta_{H(V)}} \approx 1.4 \times 10^{-3} (1.6 \times 10^{-4}) \mu\text{m}$$

where $\beta_{H,V}$ (~ 100 m) are the horizontal and beta functions at the ring beam position monitors used for the correction of the injection oscillations and β and γ are the relativistic factors at injection. This contribution is completely negligible even for the beams with a very small normalised emittance ($\epsilon^* = 1 \mu\text{m}$).

15.3.2 Dispersion Mismatch

Dispersion mismatch at the injection point in the SPS is an additional source of emittance blow-up. This arises since off-momentum particles will be injected with a position and angle error with respect to the corresponding off-momentum closed orbit. They will then undergo betatron oscillations around that orbit in the SPS ring. While the injection error resulting from the average momentum offset can be corrected in a way similar to injection errors, the error experienced by each off-momentum particle cannot be corrected individually and will therefore result in a distortion of the beam distribution and in tails [12]. This phenomenon is particularly strong for the nominal LHC beam since it has a large momentum spread and small transverse emittance. For other types of LHC beam it can be even stronger, since some have a very small transverse emittance.

The emittance blow-up factor due to dispersion mismatch (ΔD , $\Delta D'$) is given by:

$$J_D = 1 + \frac{(\Delta D_n^2 + \Delta D'^2_n) \sigma_{\delta p/p_0}^2}{2\epsilon}$$

where $(\Delta D_n, \Delta D'_n)$ are the normalised dispersion and dispersion derivative errors at the injection point while $\sigma_{\delta p/p_0}$ and ϵ are the rms momentum spread and rms emittance of the beam, respectively.

The dispersion at the end of the transfer line depends on the value at the exit of the PS. The two matching sections can be used to match the actual dispersion to the required values at the injection point in the SPS.

The initial conditions for the dispersion and its derivative at extraction from the PS and the dispersion mismatch can be determined by measuring the dispersion in the transfer line and on the first turn in the SPS ring, which is here considered as a continuation of the transfer line. The measurement of the dispersion is performed by varying the momentum of the beam extracted from PS in steps and recording the transverse displacement at each available beam position monitor. The momentum offset Δp with respect to the reference momentum p_0 is calculated by measuring the change in radial position ΔR of the beam in the first turn and by applying the relation:

$$\frac{\Delta p}{p_0} = \frac{1}{\alpha_p} \frac{\Delta R}{R}$$

This procedure requires the knowledge of the radius R of the SPS machine and the momentum compaction factor α_p both have been measured quite precisely (see Tab. 15.2) [14,15]. A pencil beam (both in transverse and longitudinal emittance) must be used in order to avoid losses for large relative momentum offsets (a few 10-3) and to improve resolution. The typical parameters of such a beam are listed in Tab. 15.1.

Table 15.1: Parameters of the beam used for dispersion and dispersion mismatch measurements

Bunch intensity [10^{11} protons]	0.4
Number of bunches	1
Longitudinal emittance [eV.s]	0.16
Rms. momentum spread [10^{-3}]	0.2
Rms. bunch duration [ns]	2.5
Rms. normalised transverse emittance (H/V) [μm]	3 / 3

Additional beam position monitors have been added in the TT2 and TT10 lines. Previously, only secondary emission monitors were installed in TT2. In the TT10 line the additional monitors have been placed in such a way as to increase the overall accuracy of the measurement. The existing and newly installed monitors have been equipped with a low frequency acquisition system [16] in order to measure the long bunches of the beam. The method used takes advantage of the large number of beam position monitors in the SPS ring and provides an immediate picture of the mismatch with respect to the dispersion in the ring. Any deviation of the dispersion measured over the first turn from the SPS dispersion is an indication of a dispersion mismatch and potential emittance blow-up.

The measurement procedure is well suited for machine setup at the beginning of the run or in case of problems. The experience gained so far has shown that the precision of the measurement is better than 10 % in the initial values of the dispersion and its derivative [17,18]. This corresponds to a potential emittance blow-up factor of the order of 10% for the nominal LHC beam.

15.3.3 Betatron Mismatch

The mismatch between the beta functions at the end of the TT2-TT10 transfer line and those of the SPS machine at the injection point is an additional source of emittance blow-up. Once again a major source of difficulty is the uncertainty in the extraction conditions from the PS.

The corresponding blow-up factor after filamentation H is given by:

$$H = \frac{1}{2} \left[\frac{\beta_0}{\beta_m} + \frac{\beta_m}{\beta_0} + \left(\alpha_0 \sqrt{\frac{\beta_m}{\beta_0}} - \alpha_m \sqrt{\frac{\beta_0}{\beta_m}} \right)^2 \right]$$

In the above equation α_0 and β_0 are the expected Twiss parameters, while α_m and β_m are the measured ones. Unlike dipole injection errors and dispersion mismatch, the effect of a betatron mismatch on emittance is multiplicative. Hence the relative blow-up does not depend on the initial emittance. Betatron mismatch can be determined by measuring the beam size at three or more beam profile monitors per plane. This is valid if the momentum spread of the beam, the dispersion at the monitors and the transfer matrices between any pair of monitors are known ([17] and references therein). The emittance ϵ of the beam and the Twiss parameters α and β at any of the beam profile monitors can be derived from this measurement. The Twiss parameters can also be inferred at any other point in the line (and in particular at the PS extraction point) providing that the transfer matrix to that point is known.

The following secondary emission (SEM) monitors are installed in the transfer lines:

- Two SEM wire monitors (MSF257, MSF277) with a spacing of 0.5 mm,
- One SEM wire monitor (MSF267) with a spacing of 0.3mm,
- Three SEM grids with a pitch of 2.5 mm (MSG258, MSG268, MSG278) in TT2,
- Three SEM grids with a pitch of 2.5 mm (BSG102737, BSG102837, BSG102937) in TT10.

These monitors were normally used for the measurements of the profile of the fixed target beam however, the SEM grids do not have sufficient resolution to provide an accurate measurement of the emittance and hence the Twiss parameters, given the small beam size of the LHC beam. The pitch of the SEM grids coincides with the rms beam size and therefore only a few strips are intercepted by the beam. Furthermore, SEM monitors cannot be used with the LHC nominal beam because of the strong background signal induced on the grids by electron multipacting during the beam passage [19].

For these reasons five Optical Transition Radiation (OTR) screens have been installed in the injection line, one in TT2 and four in TT10. The OTR screens are imaged by CCD cameras and the optics collecting the transition radiation is of such a quality that resolutions of the order of 150 μm can be achieved [20]. Using the above monitors, the precision obtained in the Twiss parameters at the PS extraction point is of the order of 10% [17,18]. This corresponds to an emittance blow-up factor of a few percent for the nominal LHC beam.

15.3.4 Other Sources of Static Injection Errors

Any deviation of the beam momentum from the nominal value used to compute the settings of the magnetic elements of the line might also induce a non-negligible mismatch at injection [17]. The circumference of the SPS machine (corresponding to the length of the beam orbit going through the centre of all the ring beam position monitors) has been measured [14,15] and the injection momentum of the beam has been determined from the RF frequency at SPS injection. The corresponding values are listed in Tab. 15.2 for a perfect energy matching between PS and SPS.

Table 15.2: Beam momentum at injection for a perfect energy matching between PS and SPS.

SPS circumference [m]	6911.5542 ± 0.0094
RF frequency at injection [Hz]	200264560 ± 1
Harmonic number	4620
Beam momentum [GeV/c]	25.99 ± 0.03

Cross-plane coupling in the TT2-TT10 transfer line or in the PS machine at the extraction energy might be an additional source of emittance growth at injection in the SPS where coupling is corrected down to the 10^{-3} level using the closest tune approach. If coupling is present, non-vanishing XY cross terms appear in the

four-dimensional beam covariance matrix M_{4D} and the term ρ provides the expected blow-up factor after filamentation due to beam coupling.

$$\rho = \left(\frac{\det M_X \det M_Y}{\det M_{4D}} \right)^{1/4}$$

where M_X and M_Y are the two-dimensional sub-matrices in the horizontal and vertical planes [21].

Coupling in the injection line can also be generated by misalignments of dipole or quadrupole magnets in the form of tilts. The presence of coupling in the injection line can be measured by comparing the trajectories of a pencil beam (see Tab. 15.1) for different corrector excitations. Measurements have excluded the presence of significant localised sources of coupling in the injection line [21].

Once the presence of sources of coupling in the injection line is excluded, coupling at the extraction from the PS machine can be monitored using profile measurements made with the OTR screens in the injection line as these provide the two-dimensional beam distribution in space. This method is described in [21] and is an extension (including beam coupling) of that described in [22]. Each OTR monitor provides three constraints to the measurements (the correlations $\langle XX \rangle$, $\langle YY \rangle$ and $\langle XY \rangle$). The 15 independent elements of the 5×5 beam covariance matrix can be measured if at least 5 OTR screens are available. The number of fitting parameters and therefore the number of constraints reduces to 11 if no betatron-momentum correlation is assumed and if the dispersion is well known (from the measurement described in the Sect. 15.3.2). If the momentum spread of the beam is known the number of fitting parameters can be reduced to 14 and 10, respectively.

Using the precise knowledge of the dispersion in the transfer line the 11-parameter or 10-parameter fits have been applied to measurements made in the line. Though the available OTRs provide enough constraints, during the measurements more than one optics were loaded (typically three) in order to provide extra-redundancy for the fit [21]. An unmistakeable coupling term originating in the PS ring has been measured and indirectly confirmed by measurements performed in the PS ring at 26 GeV/c [23]. The expected mismatch due to measured coupling in the PS is of the order of a few percent. In the same way as for the estimated betatron and dispersion mismatch, this is a somewhat pessimistic estimate of the induced emittance growth.

The TT2-TT10 transfer line is equipped with three skew quadrupoles powered in series which are used for fixed-target operation. However, these are located in the TT10 matching section and their use for the LHC beam would reduce the number of free parameters available for betatron and dispersion matching to the SPS. Therefore it is preferable to correct the coupling in the PS ring itself.

Non-linear fields at extraction might result in a dependence of the initial conditions on the extraction trajectory and on the extraction energy. Presently there are no non-linear magnetic elements installed in the injection line to compensate for such non-linear phenomena.

15.3.5 Optical Parameters at Extraction from PS

During 2001 and 2002 a series of measurements was performed in order to precisely determine the initial conditions for the injection line. This measurement series included the dependence of the Twiss parameters and the dispersion together with its derivative on the momentum offset [24]. The results of these measurements are shown in Figs. 15.2 and 15.3. The corresponding blow-up factors have been estimated from the measurements and are shown in Fig. 15.4. The estimated blow-up factors are only marginally dependent on the estimated momentum offset in the interval $\pm 2 \times 10^{-3}$ that is relevant for the LHC beam assuming a parabolic momentum distribution.

The PS extraction point is defined to be the entrance of the quadrupole QFO105. The initial conditions at this point for the nominal momentum are listed in Tab. 15.3.

The estimated blow-up factor after filamentation is 40% in the horizontal plane and 5% in the vertical plane in the range of momenta $\pm 2 \times 10^{-3}$. As previously mentioned, this represents a pessimistic estimate of the core emittance growth.

Table 15.3: Measured initial conditions at the PS extraction point for the nominal momentum.

	Horizontal	Vertical
β [m]	22.8	6.77
α [1]	-2.18	0.419
D [m]	3.06	0.090
D'[1]	0.346	-0.029

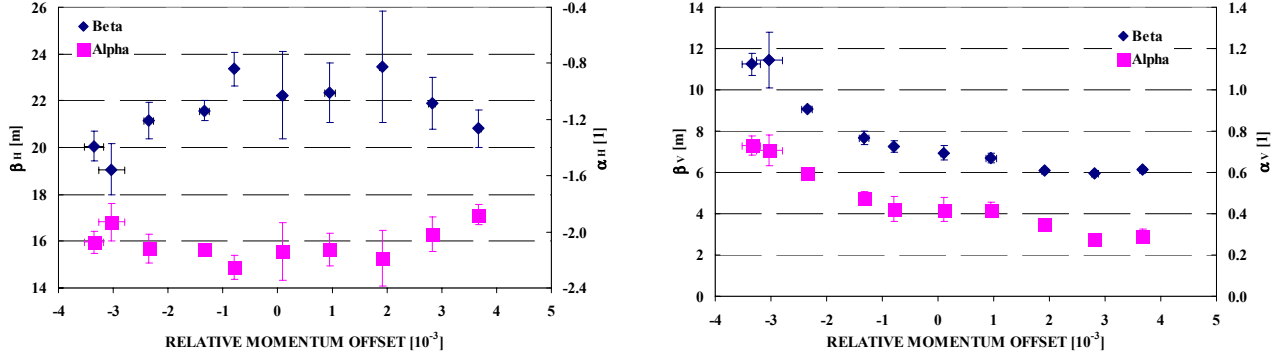


Figure 15.2: Horizontal (left) & vertical (right) β values at the PS extraction point vs. momentum offset.

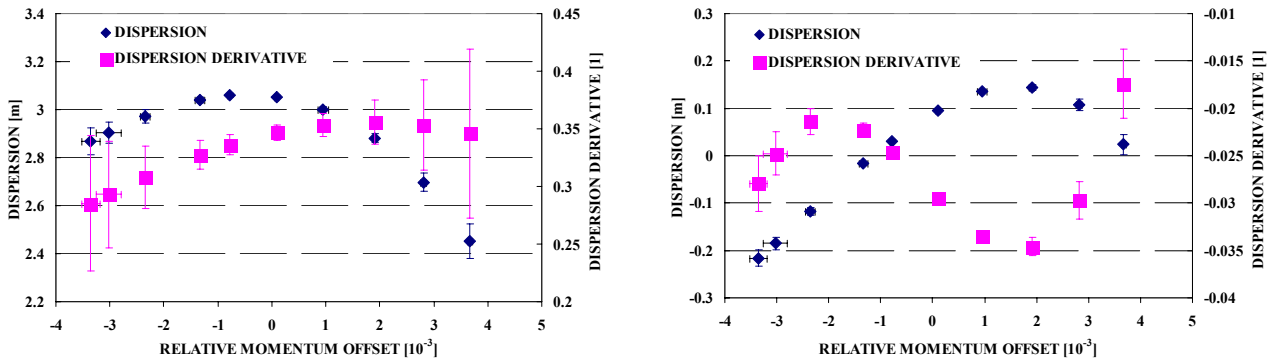


Figure 15.3. Horizontal (left) & vertical (right) D and D' at the PS extraction point vs. momentum offset.

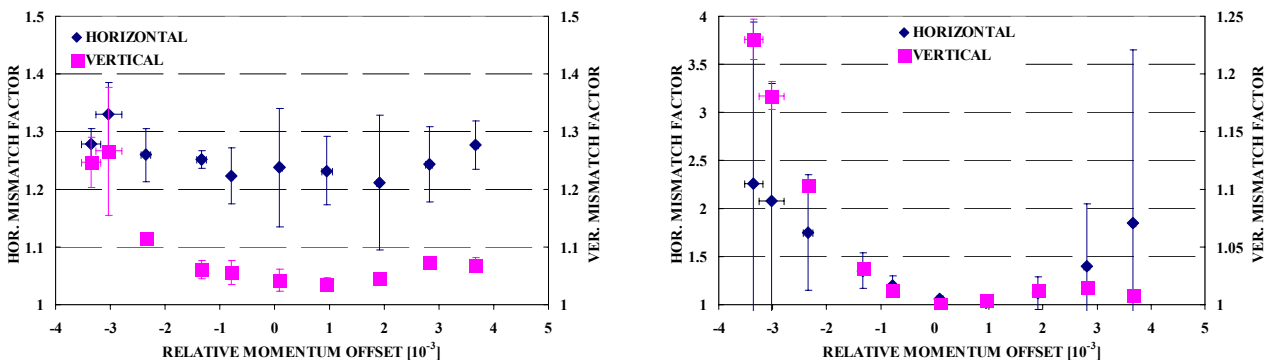


Figure 15.4: Betatron (left) and dispersion (right) mismatch factors after filamentation vs. momentum offset.

A new optics, taking into account these measurements and the new SPS working point has recently been computed in order to reduce the expected mismatch factors further, down to the 5% level ($\sim 0.15 \mu\text{m}$).

A set of wire scanners is installed in the PS and SPS rings to allow comparative emittance measurements. Measurements performed during 2002 in the PS and SPS confirmed that the blow-up factors derived above represent a pessimistic estimate of the core emittance blow-up. Fig. 15.5 shows the emittance of LHC bunch trains, consisting of 12 or 72 bunches, measured just before extraction in the PS and 10ms after injection in the SPS during 2002 [24]. It is interesting to note that the agreement between the PS and SPS values is particularly good for a bunch train consisting of 12 bunches, for which no significant source of blow-up is expected except injection errors. In Fig. 15.4 the error bars are the rms average of 10 consecutive measurements, except in the case of the measurement in the PS for a bunch population of 0.7×10^{11} protons. In this particular case only one measurement was performed.

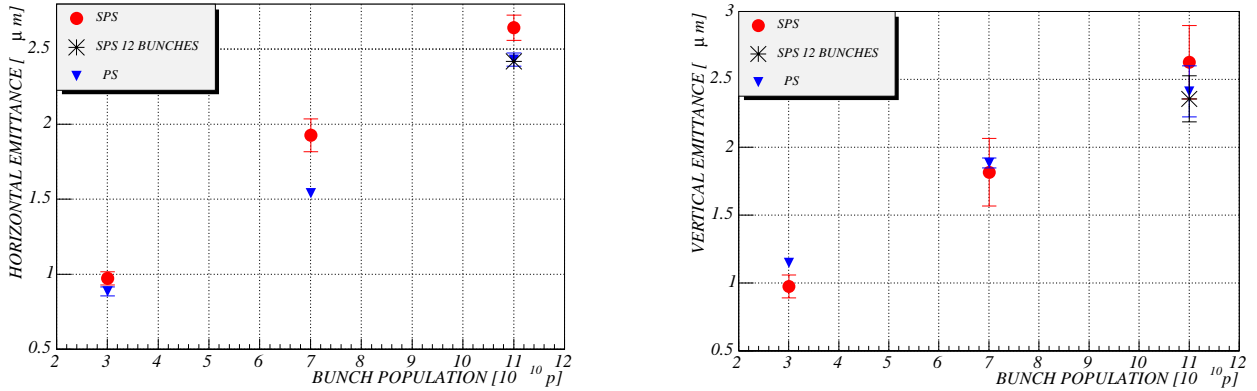


Figure 15.5: Horizontal (left) & vertical (right) emittance comparison for the LHC beam in the SPS and PS with different intensities and number of bunches.

15.3.6 Matching Correction Strategy During LHC Operation

The methods described above allow the measurement of the different static contributions to mismatch. With successive measurements and re-matching of the injection line it should be possible to control the blow-up at injection, after filamentation, to around 5% [17]. These measurements and corrections can only be performed at the beginning of each machine run or during dedicated machine tuning periods, since they demand beams with special characteristics (see Tab. 15.1) and the measurements themselves are time consuming. Further reduction of the mismatch may be obtained by a non-deterministic approach. This would consist of monitoring the beam profile oscillations after injection and minimising the oscillations by trial-and-error trimming of the transfer line matching quadrupoles. Special trim knobs (collections of quadrupole strength trims) can be calculated to give a specific variation of the Twiss or dispersion functions at injection.

The beam size at turn k , σ_k , at a given position in the SPS machine as a function of the betatron and dispersion mismatch is given by:

$$\sigma_k^2 = (\bar{D}\sigma_{\delta p/p_0})^2 + \bar{\beta}\varepsilon(H + J_D - 1) + \bar{\beta}\varepsilon \left[\sqrt{H^2 - 1} \cos[2k(2\pi Q) + \delta] + (J_D - 1) \cos[2k(2\pi Q) + 2\psi] \right] + 2\bar{D}\sigma_{\delta p/p_0} \sqrt{2\bar{\beta}\varepsilon(J_D - 1)} \cos[k(2\pi Q) + \psi]$$

$$\delta = \arctan \left[-\frac{\bar{\alpha}\beta_m - \alpha_m\bar{\beta}}{\beta_m - \bar{\beta}H} \right] \quad \psi = \arctan \left[-\frac{\Delta D_n}{\Delta D'_n} \right]$$

where \bar{D} , $\bar{\alpha}$ and $\bar{\beta}$ are the nominal dispersion and Twiss parameters at the position of the profile monitor and Q is the tune of the SPS machine.

Two matching monitors have been installed in the SPS in positions with and without horizontal dispersion (42194 and 51998) [25,26]. These are both OTR screens (12 μm Ti) with dedicated electronics and can be used to monitor beam size oscillations at injection. Two-dimensional beam profiles can be measured every

eight turns. Having data from positions with and without horizontal dispersion can be used to disentangle the contributions due to dispersion and betatron mismatch, which oscillate with different frequencies. This is not possible in the vertical plane due to the absence of dispersion. The mismatch measurement with the matching monitor is destructive. In fact, although thin, the Ti foils induce some direct blow-up due to multiple scattering and the beam must be aborted after a few tens of turns. For this reason harmonic analysis is difficult to apply.

The effectiveness of the process for reducing the injection mismatch below 5% will depend significantly on the orthogonality of the matching knobs. Studies have been devoted to the possibility of obtaining orthogonal knobs using the available set of quadrupoles and power converters in the injection line. These studies have shown that a complete set of tuning knobs for independent tuning of the Twiss and dispersion parameters cannot be obtained with the present transfer line optics [27,28]. A maximum of six optical matching knobs can be built for independent tuning of the parameters; D_H , D'_H , α_V , β_V , D_V , D'_V at the SPS injection point. Each tuning knob uses the same set of 10 quadrupoles and implies the installation of trim power converters (or trim quadrupoles) in proximity of the quadrupoles QID1011, QID1013, QID1019, QID1025 and QID1027. Numerical simulations confirm that the six knobs are orthogonal and exhibit negligible coupling over a tuning range corresponding to $\pm 5\%$ emittance growth. No satisfactory solution has been found for the parameters α_H and β_H , neither of which can be tuned over any practical range without affecting other parameters. This problem appears to be related to the absence of a dispersion-free region in the horizontal plane [28]. It seems reasonable to assume that 5% emittance growth should be allocated for mismatch at injection due to static errors.

On-line monitoring of the injection mismatch, at least during the pilot injections, could be guaranteed by OTR profile measurements in the injection line with limited emittance growth. With five OTR monitors available it is possible to measure the emittance, the Twiss and the dispersion parameters at one of the monitors if the momentum spread $\sigma_{\delta p/p_0}$ of the beam and the transfer matrices between any pair of monitors are known [22]. The momentum spread of the beam can also be measured with the multi-profile analysis method whenever six beam profile monitors are available. A redundancy in the number of beam profile measurements with respect to the number of unknowns is desirable in order to minimise the errors in the measurement [19].

Non-invasive monitoring of the emittance growth at injection can be performed by comparing the emittances measured with the wire scanners installed in the PS and SPS. In the SPS, wire scanners are installed in both non-dispersive and dispersive (in the horizontal plane) regions. This allows a measurement of the transverse emittance and the momentum spread of the beam after capture [24], however the measurement integrates over several turns and, in case of an observed blow-up, it does not provide any information about its origin.

Turn-by-turn non-destructive beam profile monitors are also under investigation. These include a quadrupolar pick-up [29] and an ionisation profile monitor with dedicated fast acquisition electronics [30].

15.4 STATIC ERRORS AFTER INJECTION

The main static sources of emittance growth after injection are related to multipole errors that could reduce the dynamic aperture of the machine. A model of the SPS machine including distributed allowed multipoles in the main dipoles and quadrupoles has been built and has been experimentally validated [9].

Two main ring sextupoles were displaced during the shutdown 2003-2004 in order to restore the original SPS layout and increase the dynamic aperture [31]. The layout has been modified in order to install the two low-beta insertions for collider operation and which is no longer necessary.

The high bunch intensity and the non-uniform distribution of the beam (both in the transverse and longitudinal plane) give rise to a tune spread coming from the direct space charge forces. This means that the beam occupies an area (tune footprint) instead of a point in the tune diagram. This phenomenon is particularly significant at injection. The horizontal and vertical tune spreads of the LHC beam in the SPS at injection are presented in Tab. 15.4 both for the nominal and ultimate intensities.

Table 15.4: Space-charge tune spread in the SPS at injection for the nominal and ultimate intensities.

	ΔQ_H	ΔQ_V
Nominal	-0.041	-0.054
Ultimate	-0.060	-0.079

The working point in the tune diagram must be chosen so as to avoid any overlap of the tune footprint with resonances and, in particular, systematic resonances. In the case of high-intensity machines there are additional considerations which enter into the choice of working point. For large machines, resistive wall is one of the main instabilities affecting the beam. The growth time of this instability depends on the tune of the machine because the real part of the resistive wall impedance depends on the frequency ω : $1/\omega^{1/2}$ (wall thickness \gg skin depth) or $1/\omega$ (wall thickness \sim skin depth). In both cases tunes just above the integer are favoured [32].

On the basis of these considerations the coherent tunes $Q_H = 26.185$ and $Q_V = 26.13$ have been chosen for the nominal LHC beam as compared to the tunes, $Q_H = 26.62$ and $Q_V = 26.58$, which are used for fixed-target operation.

Recent studies have shown that operation with high RF voltage at the injection flat-bottom might be required in order to minimize capture losses for the nominal LHC beam with 25 ns spacing. This implies a larger momentum spread and therefore a significant contribution to the vertical tune spread because of the large chromaticity required to fight the electron cloud instability (see Sect. 15.6.1). A new working point ($Q_H=26.12$ and $Q_V=26.185$) has been tested in order to avoid any overlap of the tune footprint with the vertical integer stop-band ($Q_V=26$). Very encouraging results have been obtained. The tune diagrams with the three above-mentioned working points and the systematic (thick lines) and non-systematic (thin lines) resonances from second to fifth order are presented in Fig. 15.6. The integer resonances are not shown.

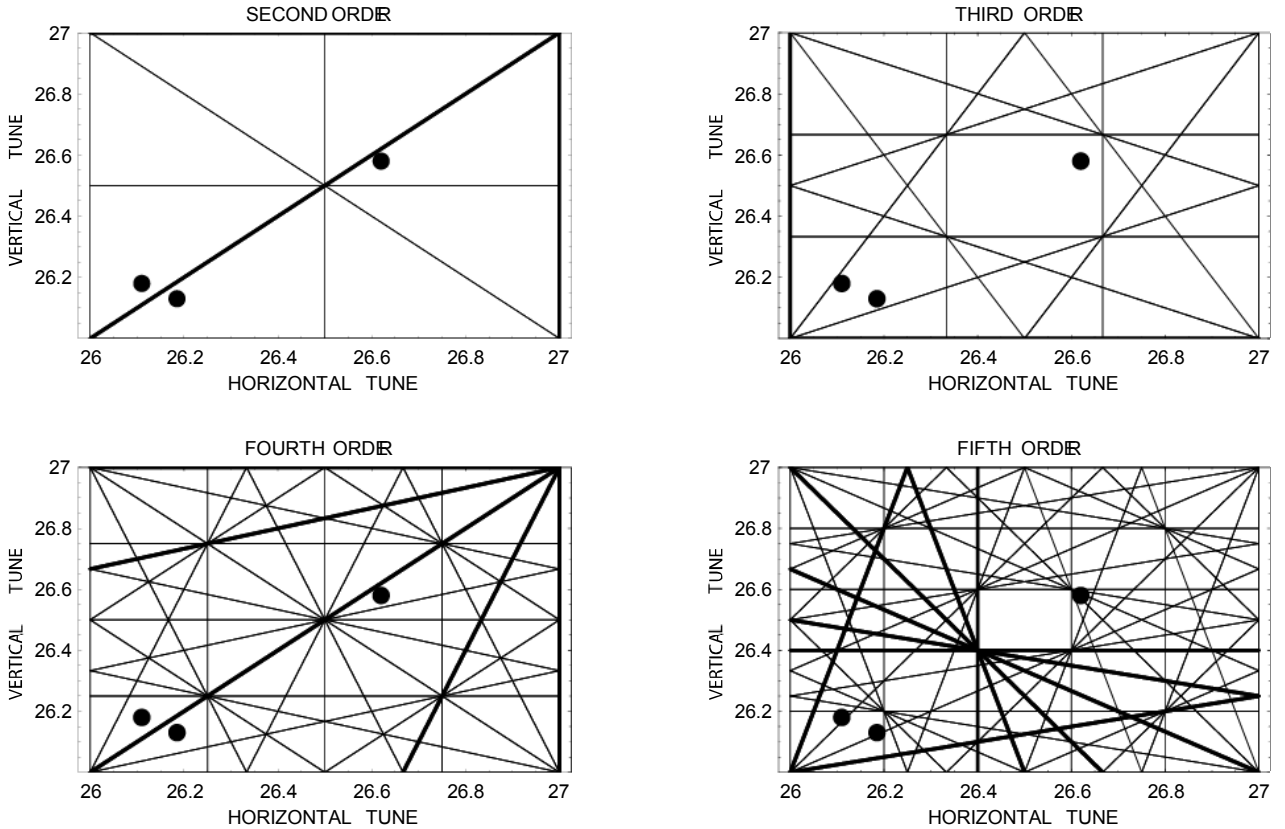


Figure 15.6: SPS working points with systematic and non-systematic second to the fifth order resonances

Table 15.5: Basic parameters of the SPS optics for the nominal LHC beam

	Horizontal plane	Vertical plane
Coherent tune	26.185	26.13
Maximum dispersion [m]	4.825	0.015
Maximum β [m]	107.12	107.73
Minimum β [m]	20.05	19.97
Gamma transition γ_{tr}		22.83
Momentum compaction α_p		1.919×10^{-3}

The basic parameters for the SPS optics used so far for the LHC beam are listed in Tab. 15.5. The Twiss parameters and dispersion functions for this optics at the injection point are listed in Tab. 15.6.

Table 15.6: Injection conditions of the SPS optics for the nominal LHC beam

	Horizontal plane	Vertical plane
β [m]	101.74	21.23
α [1]	-2.293	0.558
D [m]	0.033	0.005
D' [1]	0.009	0.0

15.5 DYNAMIC SOURCES OF EMITTANCE GROWTH

Dynamic sources of emittance growth include all sources of beam oscillations that cannot be predicted and therefore corrected in advance by adequate feed-forward mechanisms. These include:

- Injection errors varying from cycle-to-cycle
- Transverse instabilities.

A feedback system is installed in the SPS to control these perturbing effects. The specifications for such a feedback can be derived, based on the properties of the LHC beam. The additional criteria that the emittance blow-up during the injection process should not exceed 0.15 μm and the blow-up during the remainder of the SPS acceleration cycle should be less than 0.2 μm must also be met [2].

15.5.1 Injection Errors

The dynamic or varying part of the injection errors is due to [33,34]:

- Any ripple in the bending elements of the injection line, or of the PS extraction,
- Any ripple in the PS extraction kicker, or during the SPS injection kicker pulse flat-top,
- The finite rise-time of the PS extraction, or SPS injection kickers.

The emittance increase due to injection errors is caused by the decoherence of the injection oscillation resulting from the tune spread in the beam. Active damping reduces the emittance growth and the deflection strength required depends upon the expected error amplitude, while the extra gain (above the one that is needed for stability) depends upon the tune spread ΔQ . The expected emittance growth $\Delta\epsilon^*$ for a damper with gain G^1 is [33]:

$$\Delta\epsilon^* = \frac{\Delta\epsilon_0^*}{\left(1 + \frac{G}{2.5\Delta Q}\right)^2} \quad \text{where} \quad \Delta\epsilon_0^* = \beta\gamma \frac{\Delta X_n^2 + \Delta X'_n^2}{2}$$

here, $\Delta\epsilon_0^*$ is the emittance growth after filamentation in the absence of a transverse feedback.

Measurements performed in the SPS at 26 GeV/c seem to indicate that space charge plays a dominant role in the decoherence of a kicked beam [34]. In addition, non-linearities can also produce a tune spread and therefore decoherence; however, their contribution is negligible in the SPS. As a result the values of the space charge tune spread listed in Tab. 15.4 can be assumed when evaluating the required extra feedback gain at injection.

The present experience with the LHC beam indicates that residual injection errors due to the ripple of bending magnets in the TT2-TT10 line can induce peak-to-peak first turn trajectory distortions of less than ± 1 mm in both planes, after adjustment of the static errors. In the horizontal plane, the contribution of the ripple of the pulse flat-top of the PS and SPS extraction kickers must also be added. For the SPS injection

¹ The gain G is the ratio of the deflection at the output of the feedback to the position at the input, both in normalised units.

kicker a pulse flat-top ripple of $\pm 0.5\%$ and a kick rise-time of 220 ns have been assumed [33]. Similar normalised values have been taken for the PS extraction kicker [35]. Tab. 15.7 summarises the requirements (above the needs for stability) for the transverse feedback in order to keep the emittance growth due to dynamic injection errors below $\Delta\epsilon^* = 0.15 \mu\text{m}$.

Table 15.7: Transverse feedback requirements in order to keep the emittance growth due to dynamic injection errors below $0.15 \mu\text{m}$ for the nominal LHC beam.

	Horizontal plane	Vertical plane
$\Delta\epsilon^* [\mu\text{m}]$	0.15	0.15
$\Delta\epsilon_0^* - \text{bending magnets } [\mu\text{m}]$	0.28	0.28
$\Delta\epsilon_0^* - \text{SPS injection kicker } [\mu\text{m}]$	0.25	-
$\Delta\epsilon_0^* - \text{PS extraction kicker } [\mu\text{m}]$	0.25	-
$\Delta\epsilon_0^* - \text{total } [\mu\text{m}]$	0.78	0.28
ΔQ	0.041	0.054
Total gain	0.13	0.05

Non-nominal kicker rise-time and/or incorrect pulse synchronisation to the beam can result in bunch-to-bunch injection errors that might require a significant gain up to 20 MHz. For this reason, the aforementioned kicker rise time is mandatory for optimum performance.

15.5.2 Transverse Instabilities

Transverse instabilities are an additional source of emittance growth for the LHC beam. The high bunch intensity, the close spacing and high number of bunches are responsible for the occurrence of single- and coupled-bunch transverse instabilities. The most important ones are:

- Head-tail instability
- Resistive-wall instability
- Electron-cloud instability.

Head-tail instability

The head-tail instability is a single-bunch transverse instability driven by the SPS broadband impedance (see Chap. 17). It was already observed during $p\bar{p}$ operation where bunch intensities comparable to those of the LHC were injected in the SPS at the same injection energy. The most unstable mode is the $m = 0$ dipole mode. This can be stabilised by adjusting the chromaticity to be slightly positive (above transition). Recent observations and estimates seem to indicate that a fast head-tail instability might develop in the vertical plane for bunch populations close to the ultimate intensity and may require high values of the vertical chromaticity (ξ_v up to 1) to provide sufficient damping.

Resistive-wall instability

The resistive wall impedance drives coupled-bunch instabilities for high intensity beams. These can be observed with the fixed target beam (which almost completely fills the SPS ring) for total intensities above 2×10^{12} protons. For a uniformly filled machine the fundamental modes at 35 kHz (H) and 37.5 kHz (V) are unstable and the transverse feedback is needed to damp them. For a partially filled machine, higher frequency modes (up to 20 MHz) also become unstable although the dominant modes remain the low frequency ones, as shown in Fig. 15.7. The expected growth times for the nominal LHC beam are 40 and 18 turns in the horizontal and vertical planes, respectively. The latter growth times imply a feedback gain of 0.05 in the horizontal plane and 0.11 in the vertical plane [33].

Using octupole magnets to stabilise the LHC beam against the resistive wall instability would generate a tune spread of the order of 0.1 [35]. The octupole strength required is too large to be practical and would

require a higher gain of the feedback in order to keep the emittance growth due to injection errors within the above-mentioned budget.

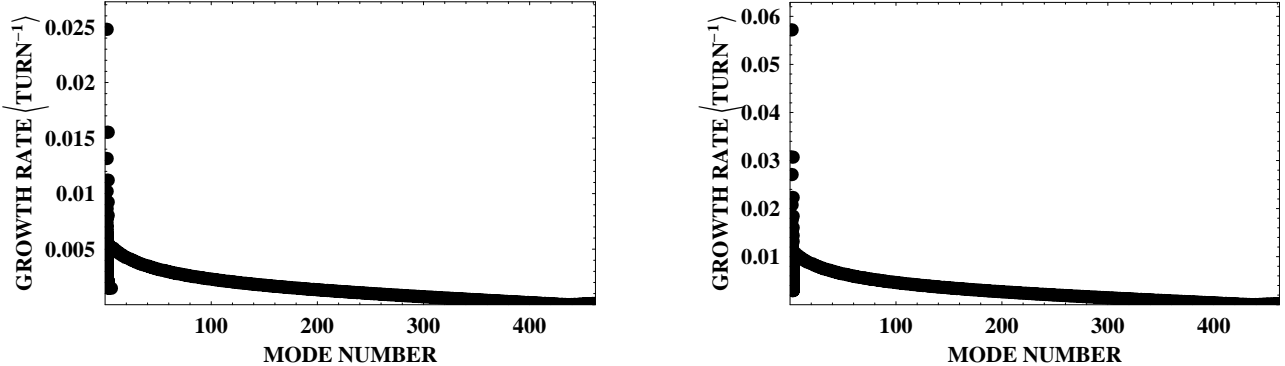


Figure 15.7: Growth rate of the resistive wall instability vs. mode number in the horizontal (left) and vertical (right) plane for the nominal LHC beam.

Electron-cloud instability

The electron cloud induced by the LHC beam in the SPS (see Sec. 15.6) is responsible for strong transverse instabilities. In the horizontal plane a coupled-bunch instability develops in about 40 turns at injection. In the vertical plane a single bunch TMCI-like instability (at about 700 MHz) occurs. In the vertical plane the transverse feedback cannot effectively damp the single bunch instability, since it is at such a high frequency. For the vertical plane high positive chromaticity values are presently the only known only cure capable of stabilising the beam. Unfortunately the high chromaticity leads to a decrease in the decoherence time and therefore imposes even tighter requirements on the feedback gain required to damp time varying injection errors. In the horizontal plane only low-order modes (up to few MHz) are excited and these can be damped by the transverse feedback. The gain required in the horizontal plane is 0.05.

15.5.3 Emittance Conservation During Injection Plateau and Acceleration

The feedback must remain active between consecutive injections during the whole injection plateau and then during the ramp, in order to fight coupled-bunch oscillations driven by the resistive wall and electron cloud instabilities. The beam will oscillate during the cycle up to the observation limit of the system. This limit is determined by the highest noise level in the feedback loop. This persistent oscillation will blow up, or heat, the beam emittance at a rate proportional to square of the tune spread and of the feedback position monitor resolution [33,36]. To meet the requirement of an emittance growth of less than 0.2 μm during the injection plateau and the ramp (i.e. for a total of 19.35 seconds), the average growth rate must be smaller than 0.01 $\mu\text{m}/\text{s}$. This is a pessimistic assumption since the tune spread decreases rapidly with energy in the case where space charge effects dominate.

15.5.4 Requirements for the Transverse Feedback

The requirements for the transverse feedback in terms of gain and normalised kick strength are summarised in Tab. 15.8. The maximum gain must be guaranteed over a bandwidth of a few MHz although the extension to 20 MHz, even with lower gain, allows the system to damp all the coupled-bunch modes for the LHC beam.

The requirements listed in Tab. 15.8 differ from those presented in [2] and take into account the recent experience gained with the LHC beam. In particular, they take into account the additional requirements imposed by the observation of the electron cloud instability in the SPS.

The dynamic range of the digital electronics of the observation part of the transverse feedback can be reduced at the expense of a reduced electronic acceptance. This would imply tighter constraints on the residual orbit distortion after correction and on the acceptable momentum offset.

Table 15.8: Requirements for the transverse feedback for the nominal LHC beam [33,36].

	Horizontal plane	Vertical plane
Gain to damp injection errors	0.13	0.05
Gain to damp resistive wall instability	0.05	0.11
Gain to damp electron cloud instability	0.05	-
Total gain	0.23	0.16
Normalised kick strength [$m^{1/2}$]	39×10^{-6}	16×10^{-6}
Resolution of the beam position monitor at $\beta = 100$ m [μm]	11	8
Least Significant Bit resolution [μm]	38	29
Electronic acceptance [mm]	± 19	± 15
Dynamic range [ADC bits]	10	10

15.6 ELECTRON CLOUD EFFECTS IN THE SPS

With the availability of the LHC beam from the pre-injectors in 1999, studies were started to determine the behaviour of the LHC beam in the SPS. From the first tests it became evident that electron multipacting was occurring in the SPS vacuum chambers in the presence of this beam [37]. Although this phenomenon was expected in the LHC because of the large number of photoelectrons produced by synchrotron radiation (10^3 photoelectrons/m per proton at 7 TeV), the SPS was thought to be immune since the number of seed electrons was expected to be much smaller, being mainly dominated by ionisation of the residual gas (10^7 electrons/m per proton) [38].

Electron multipacting in the SPS is the consequence of the high bunch intensity and the bunch spacing. The electrons accelerated by a bunch may gain enough energy to traverse the vacuum chamber before the next bunch passage and to extract secondary electrons from the chamber walls, in which case the following bunch in turn accelerates these secondary electrons. An exponential growth of the number of electrons occurs if the Secondary Electron Yield (SEY) of the vacuum chamber surface is larger than 1.0 at the energy of the impinging electrons. The energy gained by the electrons depends on the bunch population, bunch length, bunch spacing and on the chamber dimensions. These parameters determine the multipacting threshold. Multipacting is a single-pass phenomenon and has also been observed in transfer lines [19]. In this case, during the passage of the beam, an electron cloud builds-up along the batch until the space charge fields associated with the cloud itself on average cancel the beam field [39].

In the absence of beam the decay time of the electron-cloud might be larger than the beam gap or the revolution period or even last seconds [40]. Fig. 15.8 shows the build-up of the electron cloud along two consecutive batches with nominal spacing (225 ns), as measured with a dedicated electron cloud monitor. The electron cloud developed by the passage of the first batch does not disappear completely during the gap between two consecutive batches and the build-up of the electron cloud in the second batch is faster than in the first.

As a result of the electron bombardment, gas desorption occurs from the vacuum chamber walls and dramatic pressure increases (by more than a factor 100) are observed, mainly in the SPS arcs, preventing stable operation above the multipacting threshold.

The threshold for the onset of the beam-induced multipacting in the SPS has been measured for the LHC beam for 25, 50 and 75 ns bunch spacings. The results are presented in Tab. 15.9 and refer to the arcs. In each case, the data correspond to a single LHC bunch train at injection in the SPS and for an unconditioned surface.

Table 15.9: Threshold for the onset of the electron cloud in the SPS arcs for different bunch spacing for a single LHC bunch train at injection in the SPS.

Bunch Spacing [ns]	$N_{\text{bunch}} [10^{11}]$	# bunches/batch
25	0.3	72
50	0.6	36
75	1.2	24

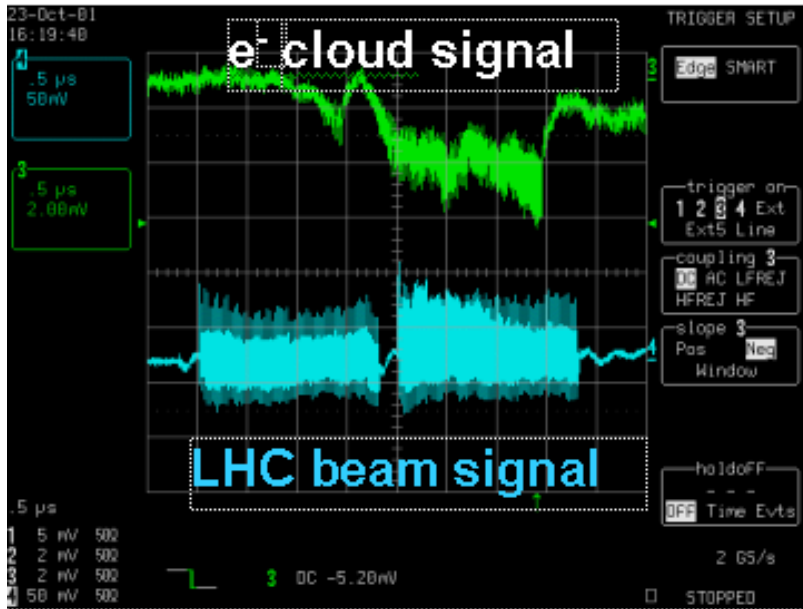


Figure 15.8: Electron cloud build-up along two LHC batches with nominal spacing [41]. The incident electron flux on the wall detected by a shielded pick-up is shown.

In the main dipole magnets (covering about 70 % of the SPS circumference) and above the threshold, the electron cloud surrounds the beam for bunch populations smaller than $0.5\text{--}0.6 \times 10^{11}$ protons; for larger values, electrons concentrate in two stripes positioned symmetrically with respect to the beam and parallel to the magnetic field lines. At the nominal bunch population or larger, a third stripe centred on the beam also appears [42].

The electron build-up is a strong limitation to the performance of beam instrumentation. A large distortion of the baseline of the signal provided by the high-impedance electrostatic pick-ups of the SPS transverse feedback has been observed [43] in the presence of the LHC beam and this required a modification of the observation part of the feedback, to replace the base-band processing which had been planned initially [2] (see Chap. 14).

Overwhelming noise on secondary emission and ionisation profile monitors in TT2-TT10 also prevents reliable emittance measurement of the nominal LHC beam in the injection line using SEM grids or SEM wires [19]. This leaves the OTR screens as the only reliable device for emittance measurement of the nominal LHC beam in the transfer line.

High voltage electrostatic devices like the electrostatic septa used for the slow extraction of the fixed-target beam to the North and West Areas are also affected by electron multipacting and operation with LHC beams is performed with low cathode voltage and powered ion traps in order to minimise the multipacting in the anodes (see Chap. 12).

15.6.1 The Electron Cloud Instability in the SPS and its Cures

Above the threshold for the onset of electron multipacting, transverse instabilities develop along the batch. These start from the tail and progress towards the head of the batch and result in strong emittance blow-up and even in beam losses. Fig. 15.9 shows the normalised rms emittance measured along a LHC bunch train consisting of 48 bunches a few tens of milliseconds after injection for a bunch population of $N_{\text{bunch}} = 0.8 \times 10^{11}$ p, higher than the threshold bunch population of $N_{\text{th}} = 0.2 \times 10^{11}$ p. The measurements were taken with the transverse feedback off and with low positive chromaticity ($\xi_H \sim \xi_V \sim +0.05$). The blow-up is particularly evident in the tail of the batch.

For a single batch with nominal bunch population all but the first ten to fifteen bunches are affected by the instability. The number of bunches affected decreases as the bunch intensity decreases. When more batches are injected with nominal batch spacing the instability affects a larger and larger number of bunches in

passing from the first to the last (fourth) batch. These observations are compatible with the measured build-up and decay of the electron cloud density along and between successive bunch trains, shown in Fig. 15.8 [41].

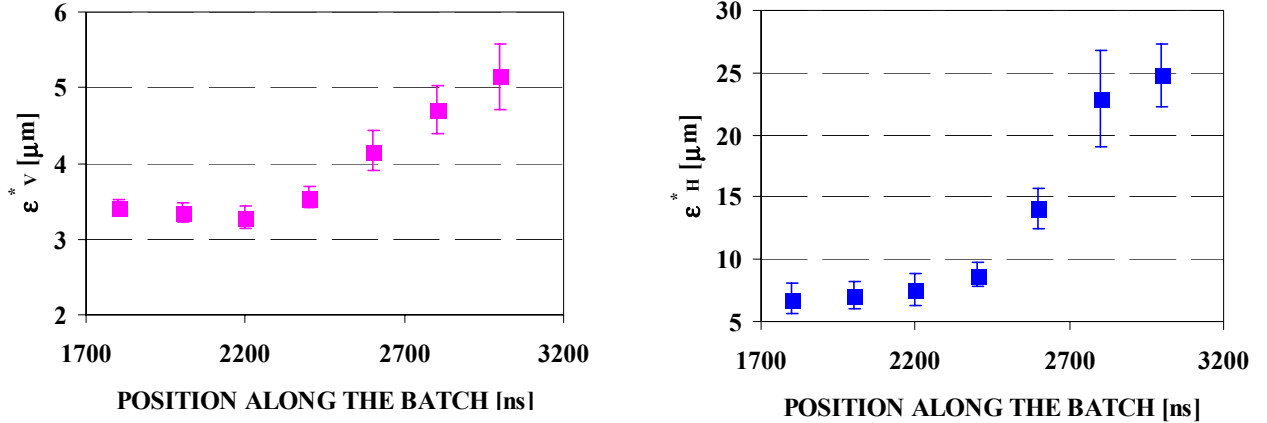


Figure 15.9: Horizontal (left) and vertical (right) rms emittance along the LHC bunch train a few tens of milliseconds after injection for $N_{\text{bunch}} > N_{\text{th}}$. The origin of the time scale is arbitrary.

The properties of the instability are significantly different in the horizontal and vertical planes. In the horizontal plane it manifests itself as coupled-bunch instability while in the vertical plane a single bunch Transverse Mode Coupling like instability occurs [44].

In the horizontal plane, low order coupled-bunch modes (up to few MHz) are the most unstable and can be damped by the transverse feedback. The rise time of the instability is of the order of 40 turns and is only weakly dependent on the bunch population. An additional gain of 0.05 must be allocated for damping the electron cloud instability in the horizontal plane (see Tab. 15.8). The rise time has been measured at different energies and it increases linearly with the momentum of the beam in the same way as for the resistive wall instability.

The vertical electron cloud instability is of a single bunch type: a measurement of the bunch-by-bunch position over several turns does not show any phase correlation among subsequent bunches. The instability mainly affects the tail of the batch and the rise time decreases with increasing bunch population (N_{bunch}). The maximum amplitude of oscillation is reached after about 600 turns for $N_{\text{bunch}} = 3 \times 10^{10}$ protons and in 300 turns for 5×10^{10} protons. A vertical motion inside the bunch at frequencies of about 700 MHz has been observed which may be associated with the electron oscillation frequency and possibly with additional external impedance. The single-bunch instability observed cannot be damped by the transverse feedback that can only detect and correct dipole modes. Running at high chromaticity (ξ_v up to 1.5) is the only cure found so far to fight the electron cloud instability in the vertical plane. Landau damping by octupoles requires impractical values of the detuning with amplitude. This cure has been tried but it resulted in significant blow-up and poor beam lifetime [45]. Another possible remedy for the vertical single bunch instability might be to use linear coupling [46].

15.6.2 Cures for the Electron Cloud Effects in the SPS

Though cures exist to fight the electron cloud transverse instabilities a remedy to minimise electron multipacting is mandatory in order to eliminate or minimise the electron cloud effects previously mentioned and in particular the dynamic pressure increase.

Solenoid fields [47] or clearing electrodes [48] can locally suppress electron multipacting but these solutions are not applicable for the SPS where multipacting occurs mainly in the main dipoles. Other methods consist of reducing the SEY of the vacuum chamber surface [49]. Methods include:

- Changing the surface composition by glow discharge treatments,
- Depositing TiN films, or Non Evaporable Getters such as TiZrV [50],
- Electron bombardment (or ‘scrubbing’).

The latter process has been thoroughly studied at CERN [51] and it has been recently observed in the SPS [52]. A reduction of the Secondary Electron Yield from 2.3 to 1.6 has been obtained after a few days of continuous dedicated running of the SPS with the nominal LHC beam at injection. A further reduction to around 1.5 has been achieved after several hours of running with the nominal LHC beam up to 450 GeV/c. The thresholds for the onset of the beam-induced multipacting have correspondingly increased from 0.3×10^{11} p/bunch to 1.0×10^{11} p/bunch in the arcs and from 0.5×10^{11} p/bunch to 1.3×10^{11} p/bunch in the straight sections. The dynamic pressure increase in the presence of LHC beams was reduced by a factor 10^4 in the same period. Some de-conditioning (i.e. an increase of the SEY) is observed if operation with the LHC beam is interrupted or the bunch intensity is reduced, though the initial SEY can be rapidly recovered if the initial beam conditions are re-established. Experience shows that the electron cloud activity cannot be fully suppressed and the final threshold intensities and SEY depend on the operational conditions of the machine.

For the above reason the measures to fight the electron cloud transverse instability mentioned above must be implemented to obtain nominal beam parameters.

REFERENCES

- [1] X. Altuna et al., *Acceleration of High Intensity Proton Beams in the SPS*, PAC 1999, New York, pp. 2617-2619 and CERN-SL-99-028-OP.
- [2] P. Collier, ed., *The SPS as LHC Injector for LHC – Conceptual Design*, CERN-SL-97-07-DI.
- [3] MAD model for the TT2-TT10 line.
- [4] G. Arduini, M. Giovannozzi, K. Hanke, J.-Y. Hemery, M. Martini, *MAD and Beam Optics Description of the TT2/TT10 Transfer Lines - Part I: Optics without Emittance Exchange Insertion*, CERN PS-Note-98-014 CA, CERN-SL-Note-98-040 OP.
- [5] MAD model for the PS ring.
- [6] MAD model for the SPS ring.
- [7] G. Arduini, M. Giovannozzi, K. Hanke, J.-Y. Hemery, *Study of the TT2/TT10 Transfer Line Optics via Transfer Matrix Measurement*, CERN-SL-Note-98-058 MD, CERN PS-Note-98-020 CA.
- [8] R. Cappi, M. Giovannozzi, M. Martini, E. Métral, G. Métral, R. Steerenberg, A.-S. Müller, *Optics Studies for the CERN Proton Synchrotron Machine: Linear and Non-linear Modelling using Beam Based Measurements*, CERN-AB-2003-017-ABP.
- [9] G. Arduini, F. Zimmermann, A. Faus-Golfe, N. Iida, R. Tomas, *2002 Non-linear Optics Measurements and Modelling for the SPS at 26 GeV*, CERN-AB-Note-2003-025 MD.
- [10] I. Kirsten, D. Manglunki, M. Martini, *Trajectory and optical parameters in a non-linear stray field*, CERN-PS-96-024.
- [11] D. Manglunki, M. Martini, *Beam Optics Modelling at CPS Extraction throughout a non-linear fringe field*, CERN-PS-97-015-CA.
- [12] G. Arduini, P. Raimondi, *Transverse emittance blow-up due to injection errors*, CERN-SL-Note-99-022-SLI.
- [13] J. Wenninger, *SPS Optics Measurements with Closed with Closed Orbits*, SL Seminar – 04/04/02.
- [14] G. Arduini, P. Collier, C. Niouille, L. Normann, *Measurement of the Circumference and of the Central Frequencies at 26 and 450 GeV in the SPS*, CERN-SL-MD Note 257.
- [15] G. Arduini, C. Arimatea, T. Bohl, P. Collier, K. Cornelis, J. Wenninger, *Energy Calibration of the SPS at 450 GeV/c with Proton and Lead Ion Beams*, CERN-AB-Note-2003-014 OP.
- [16] H. Schmickler, G. Vismara, *A logarithmic processor for Beam Position Measurements applied to a Transfer Line at CERN*, CERN-SL-2001-023-BI.
- [17] G. Arduini, *Mismatch Measurements*, CERN/SL-99-007 DI, p. 103-109.
- [18] K. Hanke, *Betatron Matching and Dispersion Matching*, CERN/SL-99-007 DI, p. 110-115.
- [19] R. Cappi, M. Giovannozzi, E. Métral, G. Métral, G. Rumolo, and F. Zimmermann, *Electron cloud build-up and related instability in the CERN Proton Synchrotron*, Phys. Rev. ST Accel. Beams 5 094401.
- [20] R. Jung, *Single Pass Optical Profile Monitoring*, CERN-AB-2003-064-BDI.
- [21] Y.-C. Chao, *New Results on TT2-TT10 Matching*, CERN-SL-2001-003 DI, p. 44-55.
- [22] G. Arduini, M. Giovannozzi, K. Hanke, D. Manglunki, M. Martini, *New Methods to Derive the Optical and Beam Parameters in Transport Channels*, Nucl. Instrum. Methods Phys. Res., A 459 (2001) 16-28.

- [23] C. Carli, G. Cyvoct, M. Giovannozzi, E. Métral, G. Métral, R. Steerenberg, *Emittance Exchange By Crossing A Coupling Resonance*, CERN-PS-2002-020-AE.
- [24] G. Arduini, Y.-C. Chao, M. Giovannozzi, D. Jacquet, J. Klem, D. Manglunki, M. Martini, G. Métral, F. Roncarolo, *Summary of the TT20/TT10 Transfer Line Studies in the Years 2001 and 2002*, CERN-AB-Note-2003-086 (ABP).
- [25] C. Bovet, J. Camas, R.-J. Colchester, G. Ferioli, J.-J. Gras, R. Jung, J.-M. Vouillot, *The OTR screen betatron matching monitor of the CERN SPS*, CERN-SL-99-050-BI.
- [26] C. Bovet, R. Jung, *A new Diagnostic for Betatron Phase Space matching at Injection into a circular Accelerator*, CERN-SL-96-034.
- [27] G. Arduini, K. Hanke, *Tuning Knobs for the PS-SPS Transfer Line*, CERN-SL-99-021-OP.
- [28] N. Iida, G. Arduini, F. Zimmermann, *Optics Matching Knobs for Injection from PS to SPS (TT2/TT10) Constructed by SAD Code*, CERN-SL-Note-2002-035 MD.
- [29] A. Jansson, *Non-Invasive Measurement of Emittance and Optical Parameters for High-Brightness Hadron Beams in a Synchrotron*, CERN-PS-2001-014-OP.
- [30] G. Ferioli, C. Fischer, J. Koopman, F. Roncarolo, *Beam Studies Made with the SPS Ionisation Profile Monitor*, CERN-AB-2003-066-BDI.
- [31] G. Arduini, A. Faus-Golfe, R. Tomas, *Study of the effect of restoring the original SPS lattice sextupoles configuration on single-particle stability*, CERN-AB-Note-2003-042 ABP.
- [32] J. Gareyte, *Observation and Correction of Instabilities in Circular Accelerators*, CERN-SL-91-09-AP.
- [33] L. Vos, *Mismatch, Damping and Emittance Growth*, CERN-SL-99-007 DI, p. 99-102.
- [34] L. Vos, *Transverse emittance blow-up from dipole errors in proton machines*, CERN-LHC-Project Report 193.
- [35] L. Vos, *Damping of coherent oscillations*, CERN-SL-96-66 (AP).
- [36] D. Boussard, *Evaluation of Transverse Emittance Growth from Damper Noise in the Collider*, SL-Note 92-79 (RFS) and LHC Note 218.
- [37] For a general overview on the measurements and simulations on the electron-cloud build-up and its effects see: *Proceedings of ECLOUD'02 – Mini-Workshop on Electron-Cloud Simulations for Proton and Positron Beams*, CERN-2002-001.
- [38] F. Zimmermann, *Electron-Cloud Simulations for SPS and LHC*, CERN-SL-2000-007-DI, p. 136-149
- [39] F. Zimmermann and G. Rumolo, *Two-Stream Problems in Accelerators*, CERN-SL-2001-057 (AP).
- [40] G. Arduini, *Electron Cloud and Ion Effects*, EPAC'02, Paris, and CERN SL-2002-056-OP.
- [41] J.-M. Jimenez, et al., *Electron Cloud with LHC-Type Beams in the SPS: A Review of Three Years of Measurements*, LHC Project Report 632 (2003).
- [42] J.-M. Jimenez, et al., *Electron Cloud Studies and Analyses at SPS for LHC-Type Beams*, PAC'03, Portland.
- [43] W. Höfle, *Observation of the Electron Cloud Effect on Pick-Up Signals in the SPS*, CERN-SL-2000-0007 DI, p. 112-118.
- [44] G. Arduini, K. Cornelis, W. Höfle, G. Rumolo, F. Zimmermann, *The Electron Cloud Instability of the LHC Beam in the CERN SPS*, PAC'03, Portland and CERN-LHC-Project-Report-637.
- [45] G. Arduini, *Observations on Transverse Instabilities*, CERN-SL-2001-003-DI, p. 125-134.
- [46] E. Métral, *Effect of Bunch Length, Chromaticity and Linear Coupling on the Transverse Mode-Coupling Instability due to the Electron Cloud*, CERN-2002-001, p. 211-218.
- [47] H. Fukuma, *Electron Cloud Effects at KEKB*, CERN-2002-001, p. 1-9.
- [48] R. Macek, *Possible Cures for Electron Cloud Problems*, CERN-2002-001, p. 259-268.
- [49] N. Hilleret et al., *Ingredients for the Understanding and the Simulation of Multipacting*, CERN-SL-2000-007 DI, p.130-135.
- [50] B. Henrist et al., *The secondary electron yield of TiZr and TiZrV non-evaporable getter thin film coatings*. Appl. Surf. Sci., 172(2001), p.95 and references therein.
- [51] N. Hilleret et al, *The Variation of the Secondary Electron Yield and of the Desorption Yield of Copper under Electron Bombardment: Origin and Impact on the Conditioning of LHC*, EPAC'02, Paris, p. 2553-2555.
- [52] J.-M. Jimenez et al., *Electron Cloud Studies and Beam Scrubbing Effect in the SPS*, LHC-Project-Report 634.

CHAPTER 16

RF SYSTEM AND LONGITUDINAL BEAM DYNAMICS

16.1 INTRODUCTION

The upgrade of the RF system in the SPS to allow acceleration of the proton beams for the LHC has involved many challenges both in understanding the longitudinal beam dynamics of the high-intensity beam in the SPS machine and in the development of the techniques and hardware required to control this beam. Before the upgrade began it was already known that these beams would suffer from both single- and coupled-bunch instabilities, leading to unacceptable emittance blow-up. In addition the high intensity bunches would induce very high beam-loading voltages in the cavities with all the inherent problems that this causes. The transfer to LHC with minimal loss also places stringent requirements on the bunch length and the bunch-to-bunch position error allowed at top energy.

The initial strategy for the upgrade was described in the conceptual design report published in 1997 [1]. It was proposed at that time that the machine impedance should be reduced by a campaign of RF shielding of elements with high R/Q and removal of non-essential equipment, to improve the power capability of the 200 MHz travelling-wave system, to introduce individual feedback and feed-forward systems for each cavity, to install a longitudinal feedback system, to use the existing 800 MHz system for controlled emittance increase, to provide a 400 MHz SC RF system to reduce the bunch length at top energy [2] and to raise the microwave instability threshold by reducing the transition energy [3]. In addition significant improvements to beam diagnostics were planned.

To test the option of using a 400 MHz SC cavity to reduce the bunch length, a prototype SC cavity was installed in LSS4 of the SPS [2]. By using the cavity off-tune it proved to be possible to reduce the bunch length simply by the beam-induced voltage. In practice some external power was still required to keep control over the cavity, but this was shown to be much less than that required by the normal approach of full RF feedback and an imposed voltage on-tune. Although the series of tests using this 400 MHz SC cavity indicated that the bunch length required could be achieved using the cavities in a semi-passive mode of operation, further analytic studies and simulations showed that a much better option for reducing beam loss at transfer to the LHC would be to install a 200 MHz capture system in the LHC itself. This became the base-line option. The maximum emittance that was assumed at 450 GeV at this time was 1 eVs.

Intensive machine studies accompanied the installation of the hardware upgrades and, as understanding increased, so these upgrades were modified. Towards the end of the programme, in 2002, the full nominal LHC beam was successfully accelerated in the SPS with an emittance at top energy of <0.7 eVs [4]. This is below the original specification and sufficiently low to envisage the “staging” of the 200 MHz capture system in the LHC. This installation of this system will be postponed until the need arises; for example if higher intensities lead to emittances greater than 1 eVs.

The impedance reduction programme, described in Chap. 17, was very successful, and reduced the single-bunch instabilities. The use of the 800 MHz systems for Landau damping, together with a small controlled emittance increase, cured the high-energy coupled-bunch instabilities and as a consequence a separate longitudinal feedback system became unnecessary. However, slow-growing low-mode number instabilities at 26 GeV required the addition of a longitudinal feedback using the main 200 MHz RF system itself.

The major modifications to the RF hardware systems in the SPS have therefore been:

- The upgrade of the power capabilities of the 200 MHz system
- A complete rebuild of the low-level servo-control electronics to improve the RF feedback and introduce RF feed-forward
- New low-noise phase and synchronisation loops
- New electronics for coarse and fine phasing of the bunch positions
- Longitudinal damping on the fundamental pass-band of the 200 MHz cavities
- An upgrade of the 800 MHz system including the low-level electronics
- Improved beam diagnostics

At the time of writing the hardware upgrades are being made progressively. They, and the major results from the machine studies, are described below.

16.2 BEAM DYNAMICS CONSIDERATIONS

16.2.1 Injection, Acceleration and Extraction Parameters

The main RF parameters, together with related machine parameters at injection and extraction in the SPS are given in Tab. 16.1. The transfer scheme for the proton bunches from PS to SPS uses the existing 200 MHz Travelling-Wave Cavity system (TWC) in the SPS and the new 40 and 80 MHz systems at 26 GeV in the PS. The injection working point has been chosen as a compromise amongst requirements from the bunch-to-bucket transfer, the beam loading in the SPS, the microwave instability limits in both machines and the possibilities offered by the new RF systems in the PS.

The bunch parameters chosen at transfer are a longitudinal emittance of 0.35 eVs and a bunch length of 4.2 ns. Shorter bunches would give more margin for injection errors and hence less risk of capture loss, but require the use of all three 80 MHz cavities in the PS and also give more beam loading in the SPS cavities due to the increased bunching factor. Capture loss mechanisms and beam-loading effects are described in more detail below. With this set of injected bunch parameters the most critical limitation for single-bunch intensity remained the microwave instability. Following the machine impedance reduction campaign (Chap. 17) the instability threshold for the microwave instability for the LHC bunch parameters was raised to levels well above nominal intensity. However the installation of the first set of LHC extraction kickers in 2003 reduced the threshold and this will be further reduced when the remaining four kickers are installed during 2005. Nonetheless, it is estimated that the threshold will remain comfortably above nominal intensity, but not necessarily above ultimate intensity. As a consequence, possibilities for shielding these kickers are being studied.

The matched voltage at injection is 750 kV, but a capture voltage of \sim 2 MV is used. The higher voltage reduces the effect of beam loading, provides more stability against low-frequency coupled bunch instabilities at 26 GeV and produces an emittance blow-up that helps stabilise the beam against coupled-bunch instabilities later in the cycle. After filamentation at 26 GeV the emittance is \sim 0.4 eVs.

Table 16.1 RF and related beam parameters at SPS injection and extraction

	Unit	At Injection, 26 GeV	At Extraction, 450 GeV
Bunch area (2σ)	eVs	0.35	0.7
Bunch length (4σ)	ns	4.2	1.8
Energy spread (4σ)	10^{-3}	3.6	1.16
Intensity per bunch (Nominal)	10^{11} p	1.3	1.15
Number of bunches/batch		72	72
Number of batches		3 or 4	3 or 4
Intensity/beam	10^{+13} p	2.8 or 3.7	2.5 or 3.3
Bunch spacing	ns	25	25
Frequency accelerating system	MHz	200.2644	200.3944
Voltage accelerating system	kV	2000	7000
Frequency Landau system	MHz	801.0576	801.5776
Voltage Landau system	kV	0 (200)	700
Bucket area (2σ)	eVs	0.68	3
Bucket height, $\delta E/E$	$\pm 10^{-3}$	4.1	1.1
Synchrotron frequency	Hz	257	238
Peak current (@ 200 MHz) in batch	A	1.08	1.42
pk-pk phase modulation along batch	ps	-	± 250

The parameters at extraction are given by the need to minimise capture losses at injection in the LHC. For injection errors of 50 MeV in energy and ± 250 ps in phase it is estimated that a bunch of emittance of 0.7 eVs and length below 2 ns can be captured by the LHC 400 MHz system alone with losses below 1% [5]. The losses would be 2% for an emittance of 1 eVs and essentially zero for 0.6 eVs. The phase error has contributions from the beam loading in the 200 MHz wideband TWC, which varies along the batch, together with the static error coming from the imperfect synchronisation between the two machines. The energy error comes from the decay of the persistent dipole currents in the LHC, after compensation by programming the closed-orbit dipoles. The variation in the SPS magnetic field at 450 GeV is about an order of magnitude lower.

Up to about 300 GeV, the 200 MHz voltage is adjusted for an emittance of 0.5 eVs (95% of full bucket). Later the voltage is raised to provide room for preventive blow-up. On the flat top the voltage is raised to maximum voltage in order to minimise the bunch length at extraction, which takes place after synchronisation onto the LHC reference. The 800 MHz system is used for Landau damping during acceleration and on the flat top. The 800 MHz system voltage is normally set to 1/10 of the main accelerating system voltage and bunch-shortening mode is used. The Landau system can also be used at injection if required.

16.2.2 Single Bunch Instabilities

Single bunch instabilities, in this case mainly the microwave instability, have been cured for the nominal beam by the reduction in high-frequency machine impedance following the shielding of the pumping ports and other elements. The effect of the microwave instability was most evident from the turbulent behaviour of bunches observed along the flat bottom at 26 GeV, which lead to a significant emittance increase. In general, it is difficult to disentangle effects coming from noise in the RF system itself from effects caused by the microwave instability. A campaign of noise reduction in the hardware, in particular that associated with the phase loop components, while successful in reducing the observed noise did not improve the blow-up situation significantly. It was only after the impedance reduction campaign that the turbulent effects completely disappeared and the emittance remained constant – indeed it became necessary to have a small amount of controlled emittance blow-up in order to keep the beam stable at high energy (see below).

16.2.3 Transverse Mode Coupling Instability (TMCI) and Beam Break-up.

Although the TMCI was the main limitation on single-bunch intensity for the lepton beam in the SPS it has not yet been observed with protons. Simulation programmes can explain the observed lepton thresholds, but give values for proton threshold intensities below those actually in operation, the most critical energy being at injection [6]. Indeed in $p\bar{p}$ operation, bunches with an intensity higher than 1.5×10^{11} were routinely accelerated with no transverse blow-up, albeit at a higher longitudinal emittance of ~ 0.6 eVs. The impedance reduction programme has reduced the transverse impedance from a value of $Z_t = 23 \text{ M}\Omega/\text{m}$ to $14 \text{ M}\Omega/\text{m}$ (2002) and TMCI instabilities are not seen on the nominal LHC beam. It is not clear at the moment at which intensity the TMCI will be observed.

16.2.4 Coupled-bunch Instabilities

When the intensity becomes high, either locally, or on average, the bunches are potentially unstable. Coupled-bunch instabilities at intensities as low as 2×10^{12} per batch (2.8×10^{10} per bunch) have been observed during acceleration at energies around 280 GeV. To control these instabilities a number of steps have been taken. The first has been to lower the machine impedance as much as possible, in particular the impedance sources from medium and high Q resonators. This has been achieved by removing unnecessary equipment, such as the RF cavities for lepton acceleration and shielding other elements. It has also proved necessary to introduce RF feedback and feed-forward. This is not only needed to reduce the phase variation inside the batch by lowering the induced beam-loading voltage, but also to increase instability thresholds for coupled-bunch modes falling inside the bandwidth of the 200 MHz TWC and to prevent possible system instability due to coupling between the different beam-control loops. Finally, dedicated coupled-bunch

feedback using the 200 MHz cavities has been introduced to combat slow growing, low-mode number instabilities at 26 GeV.

The 800 MHz Landau system has been used to combat coupled-bunch instabilities. Studies have shown that the most efficient way of using these cavities is in bunch-shortening mode [7]. This is mainly due to the much easier operation in this mode during acceleration. In bunch-lengthening mode the precision required on the phase setting between the two RF voltages in bunch is much higher at $\sim 1^\circ$ which must be maintained under strong beam-loading conditions. Errors of $\sim 15^\circ$ remove any gain in beam stability. In both modes it is also important not to create areas inside the bunch where the synchrotron frequency remains constant. These areas have no inherent stability. To do this in practice, the ratio of the main RF voltage to the 800 MHz voltage is kept around 10:1.

Even with the increased synchrotron frequency spread from the 800 MHz system, it is still necessary to introduce some emittance blow-up during acceleration. An increase in emittance from ~ 0.5 eVs to ~ 0.6 eVs is needed to maintain stability at high voltages on the flat top. Various methods of doing this have been tried including resonant excitation using the 800 MHz system. The most effective has proved to be a modulation of the RF phase at 200 MHz using band-limited noise centred on the synchrotron frequency. The latter is programmed according to the acceleration parameters and produces the required 10% increase in bunch length with no losses [8].

Fig. 16.1 shows a typical voltage programme through the cycle and the associated bunch length calculated for a given emittance. Fig. 16.2 shows the increase in threshold impedance achieved by adding the 800 MHz system.

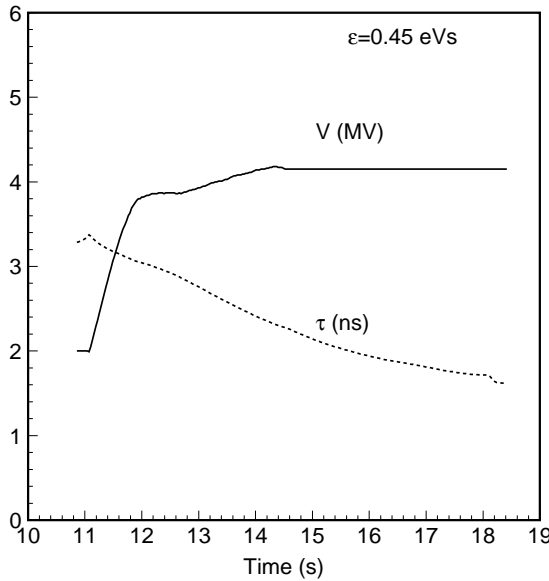


Figure 16.1: Typical voltage programme and resulting bunch length through the cycle (without the final increase for transfer to the LHC).

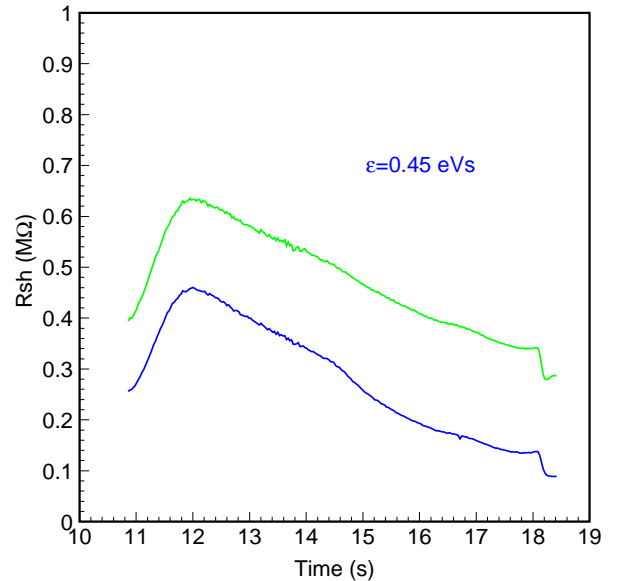
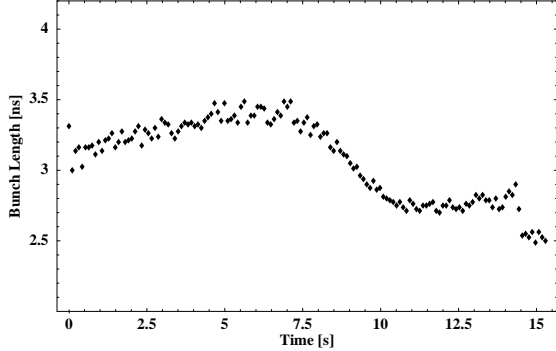


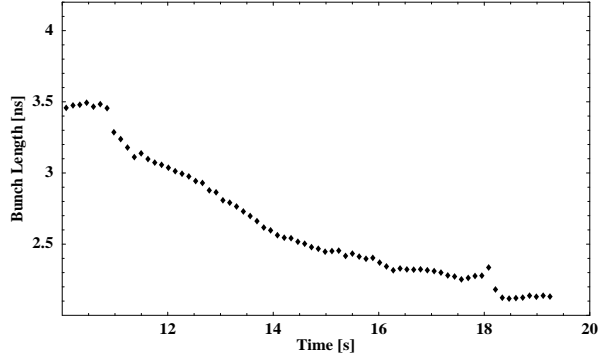
Figure 16.2: Threshold impedance through the cycle with (upper), and without (lower) 800 MHz, for the voltage programme from Fig. 16.1

In Fig. 16.3 the measured bunch length for the nominal intensity through the cycle is given before and after the impedance reduction campaign. The voltage programme is the same as that shown in Fig. 16.1. Measurements made before show the bunch length increasing continuously from 3 ns to 3.5 ns due to turbulence along the 26 GeV plateau. In this case the final bunch length is ~ 2.5 ns at high energy.

The situation after the upgrade shows the bunch length decreasing to 2.1 ns at top energy. Measurements made in 2003 showed that the beam has become slightly more unstable, although still controllable with the 800 MHz Landau damping system and small controlled blow-up. This is thought to be due to the first set of LHC extraction kickers, which were installed in the machine during the 2002-2003 shutdown.



In 2001. The acceleration ramp starts at 7.26s



In 2003. The acceleration ramp starts at 10.86s

Figure 16.3: Measured bunch length through the cycle before and after the upgrade

16.2.5 Beam Loading Effects

The travelling-wave structures used for acceleration in the SPS [10] are characterised by a filling time of the order of ~600 ns. Constant power applied to the cavity causes the voltage to rise linearly, while that induced by the beam rises parabolically as the batch enters the cavity. At constant RF power, beam loading makes the bunches which pass during the first 600 ns see different voltages. Because the injected bunches are equi-spaced and the equilibrium bunch spacing in the SPS must have some phase modulation along the batch, there will be emittance growth from filamentation. To minimise this, a feed-forward system must be used in addition to the one-turn feedback system. The resulting phase errors at 26 GeV with 2 MV RF are then limited to $\sim \pm 10^\circ$ at 200 MHz ($\sim \pm 140$ ps).

In order to minimise the bunch-to-bunch phase modulation at extraction to the LHC the above-mentioned loops must be used together with an increase to the maximum voltage. For an RF voltage of 7 MV the resultant phase modulation is estimated to be $\sim \pm 11^\circ$ at 400 MHz ($\sim \pm 75$ ps). Strong beam loading can also cause some instability by coupling the RF loops: another reason for having efficient feed-forward and feedback.

Although the beam current component at 800 MHz is lower than that at 200 MHz, beam loading in the 800 MHz cavities must also be compensated. It was found impossible to accurately control the relative phase between the two systems when the induced voltage in one of the two 800 MHz cavities, unused and idling, was not taken into account.

16.2.6 Capture Losses

Capture losses are caused by particles from the injected bunch falling outside the receiving bucket. This can occur because of injection errors in phase and energy, or a mismatch between the shape of the bunch in phase space and that of the bucket. This can be exacerbated by transients in the RF feedback and feed-forward systems at the moment of injection. These transients may be caused by the intense beam which modulates the RF voltage in phase and amplitude for a few machine turns. In addition, errors can be different for different bunches along the batch. This may be due, for example, to the variation in beam loading on the scale of the revolution period. Recent studies have shown that in the SPS a significant modification to the bucket shape can come from the RF system reacting to the energy lost by the particles in the different impedances remaining in the ring by creating accelerating buckets. Even a small stable phase angle (~ 1 to 2°) can make significant changes to the bucket shape and in particular, reduce the bucket length by about 10%. The result is increased capture loss. An interesting side effect is that all lost particles eventually lose energy and move in one direction relative to the captured beam. At present, the capture losses are around $\sim 5\%$ at nominal intensity.

16.2.7 Machine Impedance

Out of the six RF systems present in the SPS in 1998, only two are left in the ring. These are the 200 MHz and 800 MHz travelling wave (TW) systems. A third system, the 100 MHz RF system, previously used for long bunch capture in lepton and $p\bar{p}$ operation, may be re-installed for the LHC ion beam.

The campaign of impedance reduction in the SPS has eliminated the single-bunch microwave instability which led to uncontrolled emittance blow-up for intensities up to the nominal for LHC. However longitudinal coupled-bunch instabilities are observed even for very low batch intensities and are cured by using the Landau system during acceleration in conjunction with preventive emittance blow-up. Measurements show that the threshold of this instability does not have a strong dependence on total intensity (proportional to the number of batches) and is defined more by the batch intensity. This suggests that the source of the impedance has a relatively low Q. A search for the impedance responsible for this instability has not given conclusive results so far; however there is some indication that the HOM of the TW 200 MHz RF system at 629 MHz ($R_{sh} = 0.4 \text{ M}\Omega$, $Q = 500$) could be a source.

The impedance reduction programme has been extremely important for the SPS to reach nominal LHC beam intensities and parameters. It is essential that the impedance should not be allowed to increase in the future.

16.3 HARDWARE MODIFICATIONS

16.3.1 Travelling-wave (200 MHz) System Upgrades

Nominal LHC filling requires high local intensities in the SPS and the even higher intensities expected for the “ultimate” beams imply increased power requirements for the main 200 MHz travelling-wave system. The compensation of direct beam-loading and transient effects dominates the power budget. However, the length of travelling-wave cavities is an additional parameter that plays a role. This can be optimised as a function of the bunch and machine parameters at a given beam intensity. A constraint on the length can come from the use of counter-phasing to produce low voltages; a common technique in accelerators. The problem here is that counter phasing in the presence of beam loading can lead to either much higher or much lower power in a given cavity. This can be very important for power couplers where multipactoring effects can lead to forbidden power ranges.

Estimations [11] showed that the peak power capability of the 200 MHz systems should be raised to $\sim 1.3 \text{ MW}$ from $\sim 750 \text{ kW}$. This power is not required continuously, but rather with a duty factor of $\sim 40 \%$. As a result, the only major power element that required an upgrade was the high power coupler. The coaxial transmission lines are capable of transporting 750 kW continuously with no breakdown up to a peak power of 1.5 MW . The power amplifiers required minor modifications in order to provide the 1.3 MW pulsed power levels requested. Changing the couplers also allowed an attempt to be made to remove the low-power multipactoring regions and hence the need for counter-phasing.

The optimum cavity length for the ultimate beam intensity turns out to be four sections, while for nominal intensities it is between four and five sections. The travelling-wave structures have the peculiarity that the forward transfer function, amplifier-to-cavity voltage, has zeros at frequencies where the beam can induce voltage in the cavity. Since the length of the cavity determines these “zero” frequencies it is advantageous to have cavities of different lengths in order to use one to compensate the other. Consequently it has been decided that the present length of the cavities; two four-section ones and two five-section ones, should be kept until intensities above nominal have been attained.

Power coupler and cavities

The original couplers were designed for operation with a maximum continuous power of 350 kW , but had already been pushed to reach 750 kW both in pulsed and continuous mode. However it was clear that at these levels they were already at risk of breakage and could not go further. The new high intensity demands pushed the requirements to $\sim 1.3 \text{ MW}$ pulsed and 750 kW CW. In addition, the old couplers had troublesome multi-pacting regions below 100 kW that implied the use of counter-phasing techniques to obtain low voltages.

The old couplers were based on a design using two windows, each containing a cylindrical ceramic piece to provide the vacuum-air interface. The new coupler, which again contains two windows in parallel, has a window designed around a more solid circular ceramic disc. Tests with the new windows on a test cavity after conditioning gave 800 kW pulsed ($10\text{ }\mu\text{s}/23\text{ }\mu\text{s}$) into a matched load. This level was maintained over many hours with no problems. The couplers themselves have been tested at a level of 400 kW CW for each window. This level corresponds to a total of 1.6 MW pulsed and 800 kW CW for the complete coupler. The new design has also removed the troublesome low-power multipactoring zones which were present in the old design. Fig. 16.4 shows the new couplers as installed on a 200 MHz TWC in the SPS tunnel.

New conditioning loops have been installed together with the new coupler. These regulate the power according to the vacuum pressure in the coupler and operate in the beam-out time of the SPS cycles. This system keeps the couplers in excellent condition and allows the use of any power level during operation with beam.



Figure 16.4: The new power couplers installed on the cavity.

During the replacement of the power couplers, other necessary improvements were carried out including the re-alignment of the cavities. Cavity 2 was re-aligned in during the 2000/2001 shutdown. In this case, due to lack of time, the cavity sections were not separated. This lead to large measured errors in positioning and the alignment of this cavity will be repeated in 2005. Cavity 1 was re-aligned in 2001/2002, cavity 3 in 2002/2003 and cavity 4 in 2003/2004. Other improvements included the matching of the input and output sections of the power lines, the suppression of the 1 MW switches for reversing the power flow in the cavities, and the upgrading of the water-cooled RF loads on the cavities to accept 550 kW each (there are two for each cavity).

Amplifiers

The amplifiers have undergone, or are undergoing, several modifications to improve their performance and adapt them to the high-power pulsed operation required for LHC beams in the SPS. Filtering components, high-voltage capacitors and inductances, have been upgraded in both the amplifiers and the HT power supplies. These upgrades are designed to allow the amplifier to withstand the modulation at the revolution frequency which comes from the beam-loading in the cavities from the partially filled ring.

One major problem has been the linearity of the high-power amplifier system. This limits the impedance reduction obtained with the RF loops. To improve this, circulators will be introduced to improve matching between the 10 kW pre-driver and the 125 kW driver in the Siemens power amplifier system. In addition, in

the Philips power amplifier chain will be replaced by a single 1 kW tube amplifier, to improve cross-modulation performance the low-power 125 W and 600 W transistorised amplifiers. In the long term it is planned to replace the 125 kW drivers in the Siemens chain by a 60 kW amplifier. This new amplifier will be based on an amplifier used for the 200 MHz lepton standing-wave cavities. This should improve reliability in the high-power pulsing environment, but will also free four 125 kW amplifiers to act as spares for the final amplifiers.

16.3.2 Cavity Controller

For the SPS as LHC injector upgrade, new and upgraded cavity control elements have been added to the traditional cavity amplitude and phase control circuits in order to actively reduce the impedance of the RF cavities as seen by the beam. These systems help maintain control of the beam by minimising the induced transient voltages in the cavity caused by the strong beam-loading. The new elements include an upgraded RF 1-turn feedback system and a new RF feed-forward system, both of which are applied to each cavity separately. The RF feedback measures the cavity voltage and tries to keep this equal to the reference voltage by inserting correction signals via the power amplifiers. The RF feed-forward measures the beam current, estimates the corresponding beam-loading, and then also corrects for this via the power amplifiers.

The RF 1-turn feedback

The 1-turn feedback loop provides gain in narrow bands around the revolution frequency harmonics and a total loop delay equal to one machine turn [13]. Travelling-wave cavities have the peculiarity that the forward cavity response has transmission zeros associated with a 180° phase shift. This would make a simple proportional feedback unstable at moderate loop gain and therefore must be corrected.

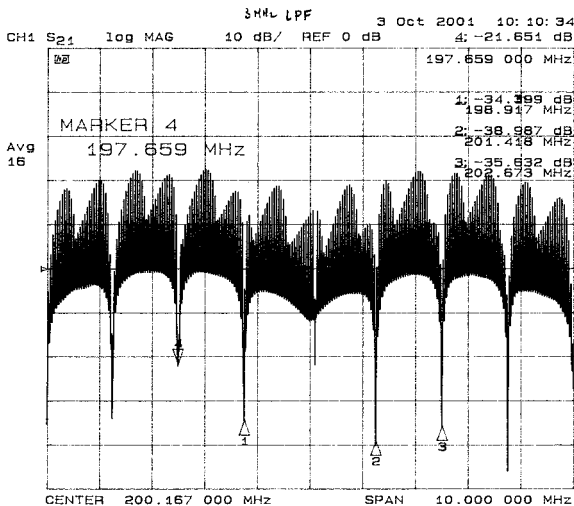


Figure 16.5: Filter response for a five-section cavity.

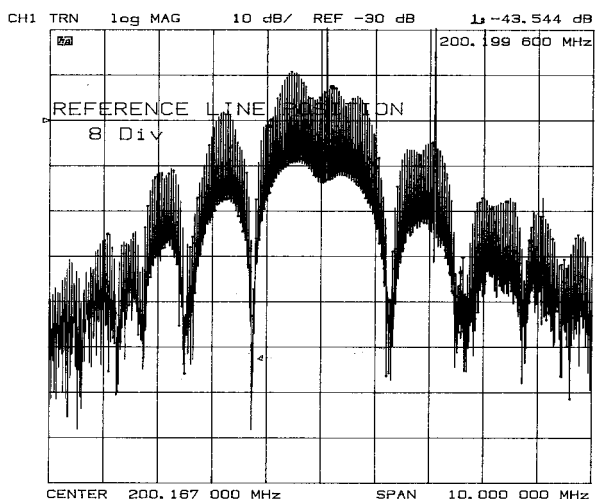


Figure 16.6: Overall loop response for the filter, Philips amplifier and five-section Cavity.

The first version, installed and tested in 2001, worked well at 26 GeV but with a reduced stability margin at 14 GeV where the cavities are required to operate for the fixed-target beam. In addition, the stability was reduced for the LHC beam at the extraction energy of 450 GeV. This stability reduction arose from the fact that while the revolution frequency harmonics, $n \times F_{\text{rev}}$, change with beam energy, the cavity zeros are fixed in frequency. To take account of these effects a more sophisticated version, using two heterodyned systems in series, was installed in 2002, with good results. The cavity signal is down-converted from 200 MHz to an intermediate frequency at ~ 10 MHz (IF). The first system uses a local oscillator frequency linked to the RF frequency F_{rf} creating a response that follows F_{rf} during the ramp. It has two filters working at the IF: a comb filter with resonances at multiples of F_{rev} incorporating a 1-turn delay and a notch filter at the exact RF frequency to prevent competition between the 1-turn RF feedback loop and the slow amplitude loop. Both filters were implemented in Infinite Impulse Response (IIR) form. The second system uses a fixed frequency linked to the cavity central frequency as local oscillator. A digital post-filter, in Finite Impulse Response (FIR) form, introduces an additional 180° phase shift at each cavity zero in order to maintain loop stability.

In addition, the gain is boosted as the frequency moves away from the cavity central frequency in order to compensate the decreasing forward cavity response.

Fig. 16.5 shows the overall amplitude response of the filter for a five-section cavity at $F_{rf} = 200.265$ MHz. The F_{rev} comb and the notch at F_{rf} can clearly be seen. The modulation of the F_{rev} lines is an artefact which comes from limitations on the resolution of the measurement. The F_{rev} lines move during acceleration as F_{rf} increases. The zeros of the cavity are indicated by the markers 1 to 4 in Fig 16.5. These remain unchanged during acceleration. The gain increases away from the centre frequency in a band of ± 3 MHz, then reduces for stability reasons.

Fig. 16.6 shows the overall open loop amplitude response with the five-section cavity together with the Philips amplifiers. It can be seen that the filter zeros superpose on the cavity zeros. This is essential to keep the sign of the overall response positive.

The 1-turn feedback gives a final performance of 18-20 dB reduction in impedance at the cavity centre frequency (~ 200.2 MHz) and ~ 6 dB reductions on the second lobe of the cavity response. In this case the corresponding frequencies are at ~ 197.9 MHz and ~ 202.6 MHz for cavities 1 and 2 and ~ 198.3 MHz and ~ 202.1 MHz for cavities 3 and 4. This performance remains constant over the whole 14-450 GeV energy range.

RF feed-forward

This system measures the beam current, filters it and provides a correction signal with correct amplitude, phase and delay to the power amplifier in order to cancel the beam induced voltage in the cavity [13]. The compensation of the imaginary part of beam-loading impedance cannot be complete since the cavity response presents transmission zeros at some frequencies where the beam-induced voltage is non-zero.

By the end of 2000 all four cavities were equipped with a feed-forward system. The beam current signal at 200 MHz from the pick-up is treated in a digital filter chain to reproduce the beam-loading voltage expected in each cavity and the inverse of this is injected back into the cavity. In practice, the pick-up signal is mixed down with F_{rf} to provide I/Q base band signals [14,15]. Two identical chains process these signals before they are mixed back up to 200 MHz, each chain comprising a digital filter consisting of two branches in parallel. A real-valued transfer function (even-symmetric FIR) synthesises the real part of the beam-loading impedance exactly and an imaginary-valued transfer function (odd-symmetric FIR) approximates the imaginary part [14]. After the filter, an I/Q modulator is used produce the RF correction signal.

The systems provide ~ 14 dB impedance reduction at the exact RF frequency at injection energy. Due to the imperfect phase tracking during the ramp this drops to ~ 10 dB at top energy (450 GeV). The bandwidth is limited to ~ 1 MHz due to the uncorrected amplifier response.

Fig. 16.7 shows the I and Q components of the cavity voltage at injection taken from the I/Q demodulator on cavity 1 with nominal LHC beam (1.1×10^{11} protons/bunch, 72 bunches). The first turn has the uncorrected beam-induced voltage whereas the second turn is corrected. Fig. 16.7 was taken just after careful adjustment and is significantly better than the typical performances mentioned above.

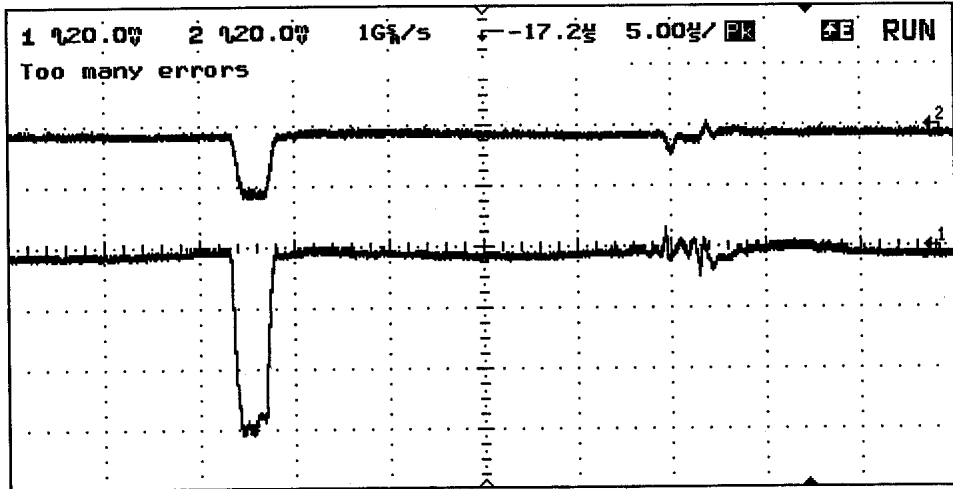


Figure 16.7: I and Q components of the cavity voltage at injection with nominal beam.

Phase along the batch

Apart from improving the threshold for coupled-bunch instability, the feedback and feed-forward systems also equalise the spacing between bunches for transfer into the LHC buckets. Fig. 16.8 shows the phase along the four batches with nominal beam at 450 GeV. The RF voltages in this case were: 7 MV at 200 MHz and 700 kV at 800 MHz used in bunch-shortening mode. The distance between the two horizontal markers corresponds to 165 ps.

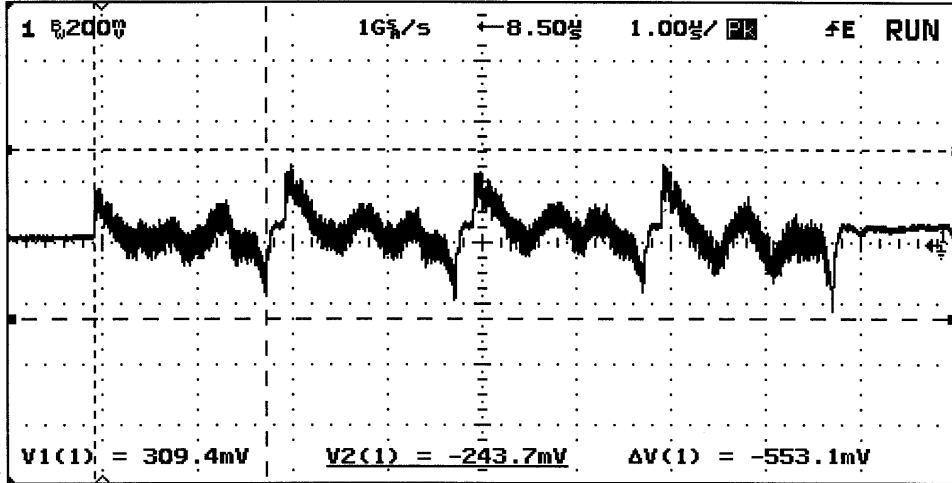


Figure 16.8: Relative phase along four batches for nominal beam at 450 GeV.

16.3.3 Beam Control System

Low-level loops

The different loops [16,17] that make up the beam control system are shown in Fig. 16.9. The phase discriminator compares the beam phase with the total accelerating voltage of all four cavities. The loop itself samples the phase of the first batch by averaging over approximately 10 bunches. This is a very strong loop with a time constant of 2-3 revolution periods and is used to damp synchrotron oscillations. A limiting amplifier in series with the phase pick-up increases the dynamic range so that low intensity pilot beams are also correctly treated.

In the new beam control system there is no radial loop; experience from $p\bar{p}$ operation showed that it is difficult to make a loop of this type sufficiently noise free. Instead, a synchronisation loop is used whereby the phase of the primary VCO is phase-locked to the frequency program. The loop works at 40 MHz rather than at 200 MHz in order to reduce the dynamic range required. By programming the phase advance network time constant as a function of the synchrotron frequency it is also possible to use this loop for acceleration. This avoids requiring a frequency loop which would have had a varying phase relationship with the frequency program. As a result, it is possible to anticipate the position of the bunches with respect to the LHC reference and therefore minimise re-phasing times before extraction to LHC. More details on this aspect are given below.

The frequency program uses a digital signal processor (DSP) to compute the frequency from the magnetic field and the required radial position. It provides the input values to the direct digital synthesiser (DDS). A careful choice of DDS is required to maximise the spurious free dynamic range and thus minimise noise in the system.

The coarse frequency program, which drives the VCO as a function of B field and reduces the dynamic range needed in other loops had to be redesigned to reduce noise. The new version is based around 16-bit technology.

Machine synchronisation – injection and extraction

The techniques used for synchronisation at injection and extraction [16,17] are the same as was used for the CPS-SPS-LEP bunch-into-bucket transfer, with one major addition. This is a mechanism to minimise the time spent re-phasing at top energy. The LHC sends two reference signals to the SPS for synchronisation at

450 GeV; the fiducial frequency ($f_c = 1/27 f_{rev}^{SPS} = 1/7 LHC f_{rev}^{LHC}$) which defines the position in LHC where the batch should be injected and the LHC 400 MHz RF reference, for fine synchronisation. Similarly, the SPS sends two signals to the PS with the same purposes; the revolution frequency and the 200 MHz SPS RF reference.

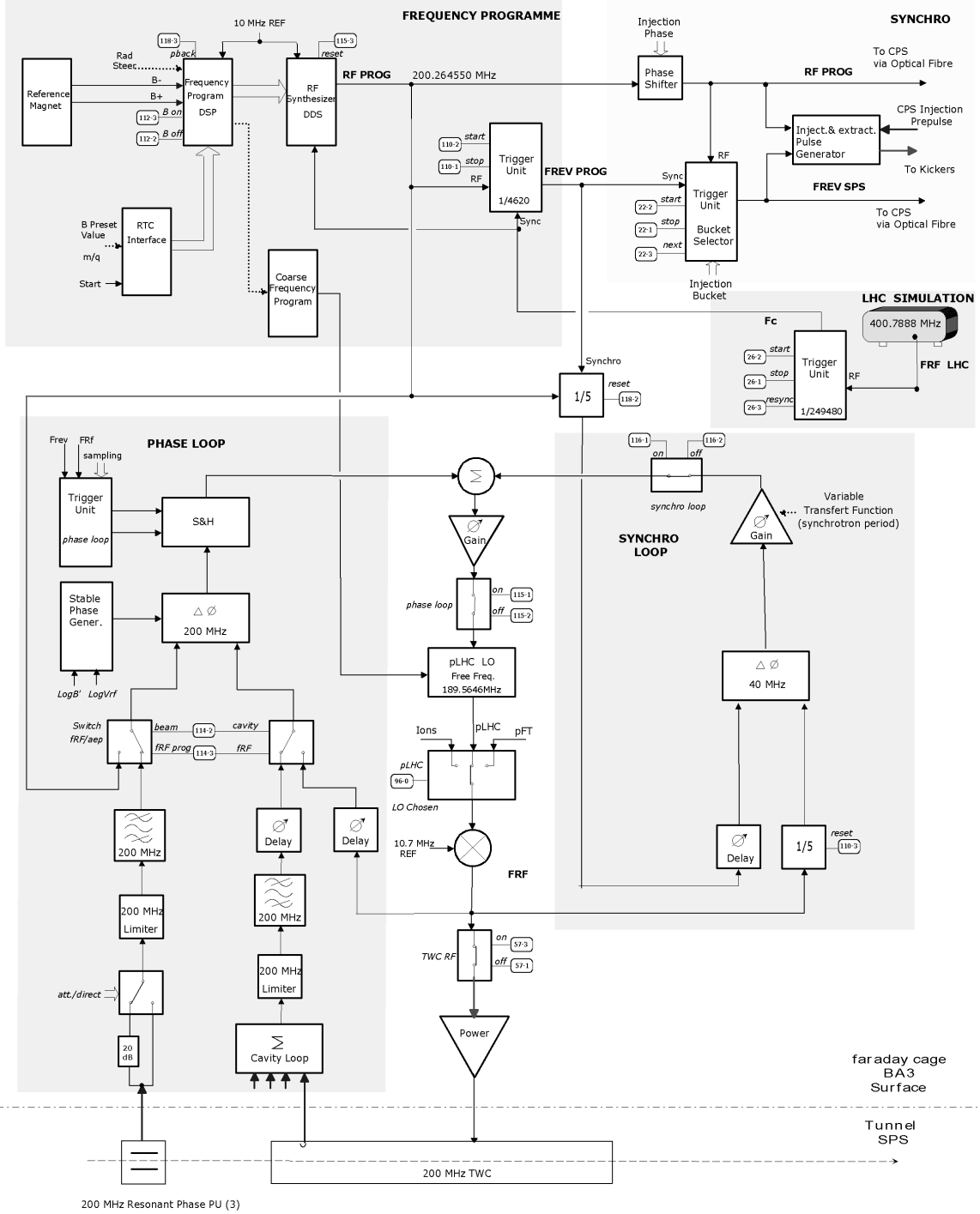


Figure 16.9: The Beam Control System.

To minimise the re-phasing at extraction, the movement of the batches with respect to the LHC reference during acceleration is estimated. The batches can then be injected into a pre-defined place in the SPS to arrive correctly placed at 450 GeV. This is possible because a synchronisation loop rather than a radial or frequency loop is used. The RF frequency changes during acceleration, but exactly follows a frequency programme initially derived from the B-field. However, the latter is not exactly reproducible from cycle to cycle and the integrated phase change over the cycle may be large. To cope with this there is a two-step

procedure. For a few calibration cycles without injection into the LHC the B field drives the frequency program and the resulting frequency function is recorded. For filling the LHC the frequency program is driven by the recorded-frequency function, ignoring the B field. A further complication is that the magnetic ramp is driven from the master timing generator (MTG) which is unrelated to the fiducial frequency. It is necessary to measure the difference in time between the two trains and pre-adjust the phase of the frequency program before injection from the PS. All these features have been implemented in the Frequency Program DSP using the Frequency Shift Keying (FSK) function of the DDS. The resultant phase jitter cycle to cycle measured at 450 GeV is below 25 ns.

The final stages in the SPS-LHC synchronisation involve a small re-phasing in frequency by ramping the frequency from the SPS frequency at 450 GeV to the LHC injection frequency, together with a re-phasing in phase. This is achieved in two stages. Firstly the coarse phase error (25 ns max) is measured using a time-to-digital converter and corrected by a small frequency bump. Secondly a fine correction is made using a phase discriminator comparing the SPS RF (or the beam) to the LHC RF in order to define the precise frequency bump. The time needed to complete re-phasing is at most 50 ms.

Longitudinal damping

For batch intensities above 3.6×10^{12} (i.e. 5×10^{10} protons/bunch) a dipole-mode coupled-bunch instability with a dominant mode below 1 MHz has been observed on the injection plateau at 26 GeV. Although slow-growing it led to unacceptable longitudinal emittance growth along the flat bottom. To damp this instability a longitudinal feedback system was introduced using the main RF cavities TWC1 and TWC3 as kickers.

The 200 MHz band-pass filtered signal from a beam monitor is mixed with the RF frequency to give a measurement of the phase of each bunch. This signal is then digitised at the bunch frequency, 40 MHz. The signal is treated by an IIR digital filter having a response with zeros at the revolution frequency lines to reject the stable phase offset and resonances at the synchrotron sidebands to provide the $\sim 90^\circ$ phase shift desired for damping. A low-pass (3 MHz) FIR filter together with a DAC, a variable gain amplifier and an output mixer complete the chain. The RF kick produced is added in quadrature to the main RF to provide phase modulation.

The gain is adjusted during acceleration for optimum damping. The instability at 26 GeV is damped up to the maximum intensities so far injected, $\sim 1.0 \times 10^{13}$ /batch. The gain is boosted by a factor 3 for 30 ms during each injection except the first. This is to damp injection oscillations and hence reduce emittance increase from filamentation.

Fig. 16.10 shows the phase error of the second batch from injection onwards for nominal intensity and an intentional $\sim 30^\circ$ error. Left plot: no damping, right: with the damper on.

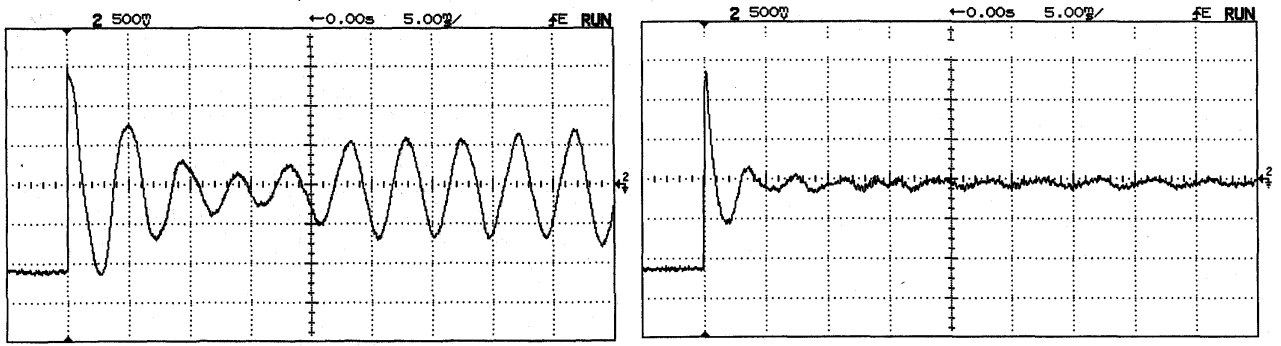


Figure 16.10: Phase error observed at injection of the second batch, left: damping off, right: damping on.

16.3.4 Travelling-wave (800 MHz) System Upgrades

Two 800 MHz travelling-wave cavities are installed in the SPS, each powered by a 200 kW power amplifier consisting of four klystrons in parallel. The 800 MHz system is used to stabilise the beam by increasing the synchrotron frequency spread within the bunch. It can also be used to produce controlled emittance increase by resonant bunch excitation. With 200 kW per cavity available it has been possible to

stabilise the nominal beam using around 10% of the voltage used at 200 MHz. This has been achieved using just one cavity, the other remaining un-powered.

The klystron design for this system is very old and only a few spare components are available. A study of the power requirements for the LHC beam in the SPS and the other beams that will be accelerated in the future has shown that by using both cavities, the total power per cavity required in the future will be \sim 100 kW. As a consequence, the system can be re-configured with only two klystrons per cavity. This effectively doubles the number of spares and hence increases the system lifetime by several years.

Long-term solutions remain to be finalised. Two options are under study; one based on the new IOT tube for which little experience exists, the other involving the re-construction of the existing klystrons in industry. In addition, for reliable operation of the amplifiers, the main transformers and the thyristor regulators of the high voltage DC power converters have to be replaced. The precise choice of components for the power converters will depend upon the final choice of either IOT or klystron.

The beam-control part of the 800 MHz system consists mainly of standard amplitude and phase control loops to provide an RF voltage locked to the 200 MHz voltage seen by the beam. The beam-induced voltage in both cavities must be taken into account even if only one cavity is used and the beam-control is designed accordingly. However, the beam-loading compensation is only partial and may have to be improved. This might finally lead to the use of a 1-turn delay feedback system similar to that used for the 200 MHz travelling-wave cavities.

16.3.5 Diagnostics and Beam Quality Control

Before the LHC beam is extracted from the SPS it must be verified that it is safe to do so and no harm can come to downstream machine elements. In addition it is planned to check that the beam is of sufficient quality to meet the needs of the LHC. There are therefore two priority levels of extraction interlock. Level 1 control is essentially to protect the LHC machine against equipment damage. Level 2 should avoid extraction of any beam outside a given specification which, although not harmful to the LHC equipment, would unnecessarily stress LHC machine elements or degrade the LHC luminosity. These issues are still under study but some remarks can be made.

Level 1 control: Before the LHC beam is extracted from the SPS successful synchronisation between the SPS and LHC must be verified. This can be done by measuring the azimuthal position of the SPS batch, consisting of up to four PS batches, with respect to the LHC reference. The aim here is to avoid the injection of an SPS batch on top of a batch already circulating in LHC, or injecting an SPS batch into the abort gap. A longitudinal pick-up is necessary to obtain a beam-derived pulse indicating the position of the beginning of the SPS batch.

Level 2 control: checks will be made on individual bunch phase, bunch length and longitudinal emittance for the RF system. If these parameters are outside specifications the beam will not be fully captured in LHC, stressing the momentum collimation system and leading possibly to the creation of ghost bunches when the voltage is raised for acceleration. Ghost bunches may also be generated in the SPS. A way to detect these in the SPS and to avoid their extraction to LHC is desirable and under study.

It is probably sufficient to make one measurement of these parameters in the last few milliseconds before extraction and to take a decision in the remaining time whether or not to extract the beam. Several measurements could be made along the cycle while the beam is in the SPS or especially at the flat top to monitor the stability of individual bunches.

Unequal bunch populations can also lead to problems in the LHC including reduced luminosity. The monitoring of the individual bunch intensities will be done using a 40 MHz BCT [18].

The hardware for Level 2 in the RF system will consist of a longitudinal pick-up. This will be used to obtain bunch profiles for digital analysis, for single-bunch phase detection and for bunch-length determination. Un-captured beam and ghost bunches outside the batch could also be detected by using a high dynamic range spectrum analyser.

16.4 OPERATIONAL RESULTS

In 2002, following the scrubbing run, the injected intensity of the LHC beam reached nominal values for the first time [4]. At the end of the operation year in 2002 stable LHC beam with better than nominal longitudinal parameters was obtained on the 450 GeV flat top.

These beam parameters were:

- Four batches with intensity 1.15×10^{11} /bunch (total intensity 3.3×10^{13} protons)
- Bunch length (4σ) = 1.6 ns
- Longitudinal Emittance (2σ) = 0.6 eVs
- Maximum bunch-to-bunch phase modulation = ± 80 ps.

This excellent result is due in large part to the SPS impedance reduction program, the RF hardware upgrades and the additional beam stabilising methods described above – including the use of the 800 MHz system and controlled emittance blow-up. In 2003 with increased intensity available from the pre-injectors higher than nominal intensity, 1.2×10^{11} /bunch was obtained at top energy.

REFERENCES

- [1] *The SPS as injector for LHC – conceptual design*, editor P. Collier, CERN-SL-97-07 DI, March 1997.
- [2] T. Bohl, D. Boussard, T. Linnecar, V. Rodel, *A Superconducting RF Cavity for Bunch Compression of the High Intensity SPS Proton Beam at Transfer to LHC*, EPAC 96, Sitges, Spain.
- [3] T. Bohl, M. Lamont, T. Linnecar, W. Scandale, E. Shaposhnikova, *Measurement of the Effect on Single Bunch Stability of Changing Transition Energy in the CERN SPS*, EPAC '98, Stockholm, Sweden.
- [4] P. Baudrenghien, T. Bohl, T. Linnecar, E. Shaposhnikova, J. Tückmantel, *Nominal longitudinal parameters for LHC beam at 450 GeV in the SPS*, SL-Note-2002-045 MD, Dec 2002.
- [5] J. Tückmantel, *Realistic simulation of LHC with a RF system*, Proc. LHC workshop, CHAMONIX XI, CERN-SL-2001-003 DI.
- [6] T. Linnecar, E. Shaposhnikova, *Requirements for beam parameters in the SPS when used as LHC injector*, CERN SL Note / 94-87 RF.
- [7] T. Bohl, T. Linnecar, E. Shaposhnikova, J. Tückmantel, *Study of Different Operating Modes of the 4th RF Harmonic Landau damping System in the CERN SPS*, EPAC '98 Stockholm, Sweden..
- [8] T. Bohl, T. Linnecar, E. Shaposhnikova, J. Tückmantel, *Controlled Longitudinal Emittance Blow-up in the SPS as Injector and LHC test-Bed*. AB-Note-03-084 MD.
- [9] P. Baudrenghien, T. Bohl, T. Linnecar, E. Shaposhnikova, J. Tückmantel, U. Wehrle, *RF Studies of LHC Beam in the SPS*, AB-Note-2003-071 MD.
- [10] G. Dome, *The SPS Acceleration System Travelling-wave Drift-Tube Structure for the CERN SPS*, CERN-SPS/ARF/77-11.
- [11] T. Bohl, *The 200 MHz Travelling-wave Cavities in the SPS*, Proc. Chamonix X, CERN-SL-2000-007 DI, Jan 2000.
- [12] M. Bazan, H. Haebel, H.P. Kindermann, *Numerical Optimisation of the 1.2 MW Coupler for the SPS as LHC Injector*, SL- Note-97-75 RF.
- [13] D. Boussard, *Control of Cavities with High Beam Loading*, IEEE Transactions on Nuclear Science, Vol. ns-32, No. 5, Oct 1985.
- [14] P. Baudrenghien, G. Lambert, *Reducing the Impedance of the Travelling-wave Cavities, Feed-forward and one turn delay feed-back*, Chamonix X, pp 94-101, Jan 17-21, 2000, CERN-SL-2000-007 DI.
- [15] P Baudrenghien, G. Lambert, *Control of strong beam loading, Results with beam*, Chamonix XI, pp. 63-72, Jan 15-19, 2001, CERN-SL-2001-003 DI.
- [16] P. Baudrenghien, T. Linnecar, D. Stellfeld, U. Wehrle, *SPS Beams for LHC: RF Beam Control to Minimize Re-phasing in the SPS*, EPAC 98.
- [17] P. Baudrenghien, *Beam Control for Protons and Ions*, Proceedings of the IXth Chamonix workshop, Jan 25-29, 1999, CERN-SL-99-007 DI.
- [18] SPS as LHC Injector Committee minutes, SLI 2003-04-04.

CHAPTER 17

MACHINE IMPEDANCE ISSUES

17.1 INTRODUCTION

17.1.1 Longitudinal Impedance and the Microwave Instability

The longitudinal single bunch (microwave) instability has been observed in the SPS in practically all operation modes: with leptons and protons, below and above transition energy, with RF on and RF off [1,2]. Although in many cases not harmful, this instability became an important issue for the high intensity and high quality beams required for LHC [3]. Before the nominal LHC beam was available in the SPS, estimations based on measurements of microwave instability threshold showed that the LHC bunch would be unstable at injection in the SPS well below the nominal intensity, 1.15×10^{11} p/bunch.

The microwave instability was identified by an uncontrolled longitudinal emittance blow-up accompanied by high frequency (microwave) signals. Measurements with long bunches injected with RF off allowed the dominant resonant impedances with high R/Q to be seen as peaks in the unstable beam spectra [4], as illustrated in Fig. 17.1. The spectra of Fig. 17.1 were taken at 26 GeV with the RF switched off and a bunch intensity $N = 6.0 \times 10^{10}$, a longitudinal emittance $\epsilon = 0.22$ eVs and a bunch length $\tau = 25$ ns.

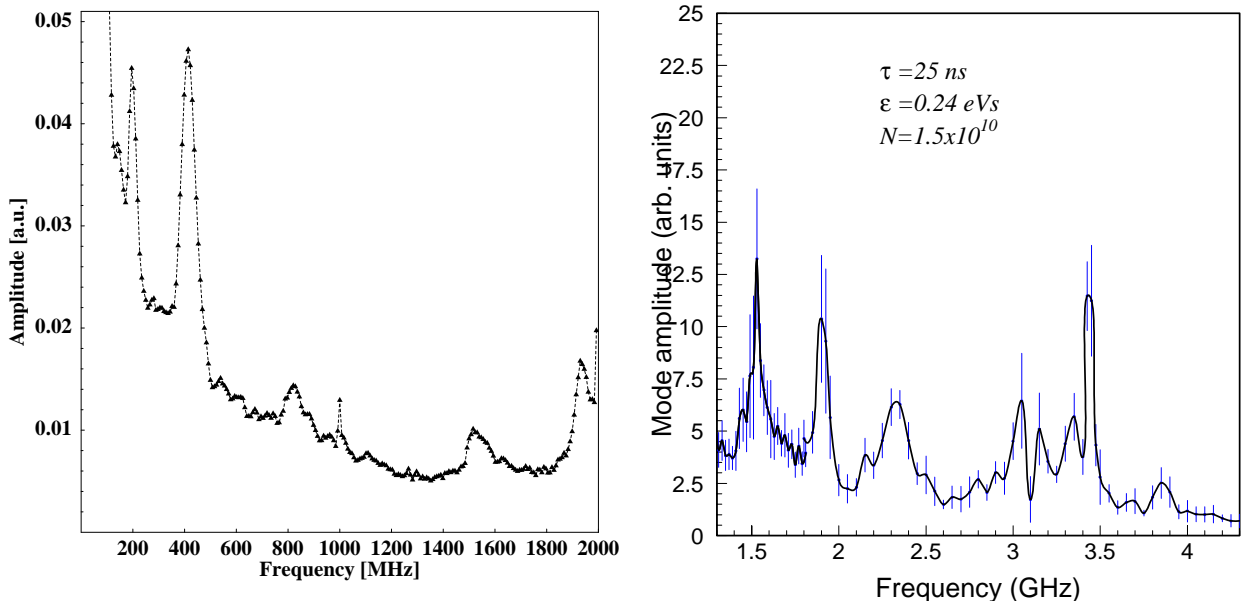


Figure 17.1: Left: unstable bunch spectra up to 2 GHz (1999), Right: Spectra at high frequencies (1996).

Most of the peaks with frequencies in the range 100–800 MHz were identified with impedances of the five different RF systems installed in the machine at that time (SW 100 MHz, TW and SW 200 MHz, SC 352 MHz and TW 800 MHz). High frequency peaks at 1.5, 1.9, 2.4... GHz were due to resonances in the ~1000 vacuum pumping ports, which are cavity like objects distributed all around the ring [5]. These had a total R/Q in the range 25–45 kΩ and Q~50 [6].

The peak at 400 MHz with very high relative amplitude in Fig. 17.1 was first attributed to the impedance of the 16 tanks of the MSE and MST septa. Calculations using a simplified model of the MSE and MST septa did not give significant impedance. However, bench measurements showed a clear peak at the frequencies of interest. These cavity like objects were shielded during 1998-2000 [7] (see below) and the SC 400 MHz RF cavity was removed from the ring in 1998. However, even after these changes, the instability was still present, albeit with slightly increased threshold [8].

Given their transverse dimensions the electrostatic septa, ZS, were possible alternative candidates for the 400 MHz peak. The 10 ZS tanks would have been very difficult to shield. Fortunately, the ZS were

CHAPTER 17

MACHINE IMPEDANCE ISSUES

17.1 INTRODUCTION

17.1.1 Longitudinal Impedance and the Microwave Instability

The longitudinal single bunch (microwave) instability has been observed in the SPS in practically all operation modes: with leptons and protons, below and above transition energy, with RF on and RF off [1,2]. Although in many cases not harmful, this instability became an important issue for the high intensity and high quality beams required for LHC [3]. Before the nominal LHC beam was available in the SPS, estimations based on measurements of microwave instability threshold showed that the LHC bunch would be unstable at injection in the SPS well below the nominal intensity, 1.15×10^{11} p/bunch.

The microwave instability was identified by an uncontrolled longitudinal emittance blow-up accompanied by high frequency (microwave) signals. Measurements with long bunches injected with RF off allowed the dominant resonant impedances with high R/Q to be seen as peaks in the unstable beam spectra [4], as illustrated in Fig. 17.1. The spectra of Fig. 17.1 were taken at 26 GeV with the RF switched off and a bunch intensity $N = 6.0 \times 10^{10}$, a longitudinal emittance $\epsilon = 0.22$ eVs and a bunch length $\tau = 25$ ns.

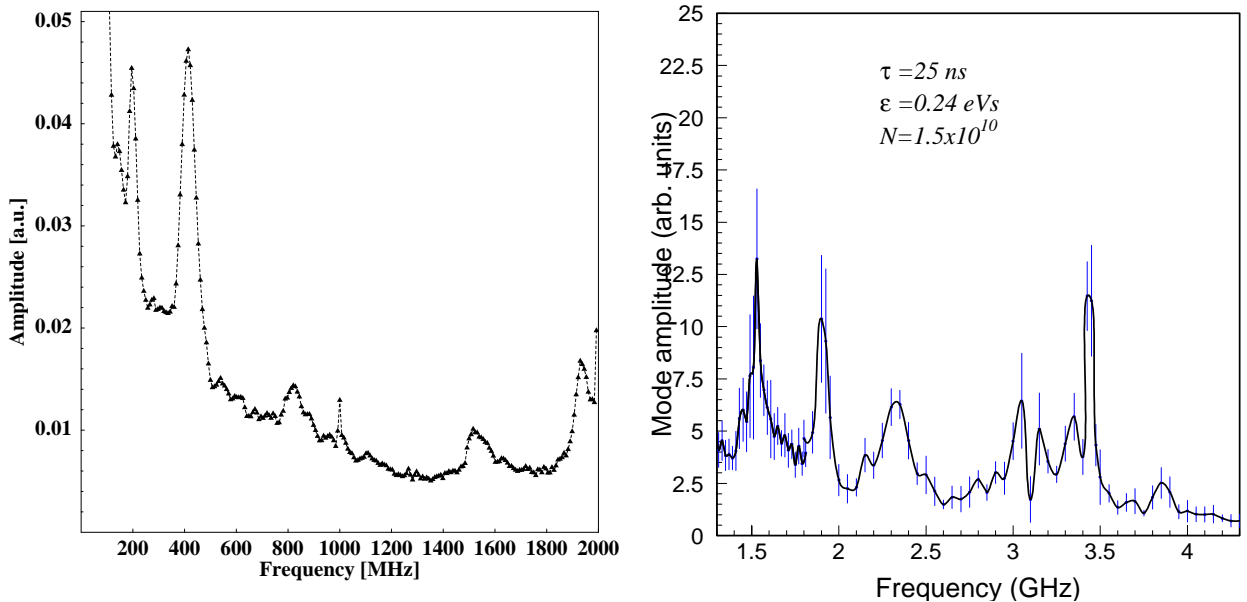


Figure 17.1: Left: unstable bunch spectra up to 2 GHz (1999), Right: Spectra at high frequencies (1996).

Most of the peaks with frequencies in the range 100–800 MHz were identified with impedances of the five different RF systems installed in the machine at that time (SW 100 MHz, TW and SW 200 MHz, SC 352 MHz and TW 800 MHz). High frequency peaks at 1.5, 1.9, 2.4... GHz were due to resonances in the ~1000 vacuum pumping ports, which are cavity like objects distributed all around the ring [5]. These had a total R/Q in the range 25–45 kΩ and Q~50 [6].

The peak at 400 MHz with very high relative amplitude in Fig. 17.1 was first attributed to the impedance of the 16 tanks of the MSE and MST septa. Calculations using a simplified model of the MSE and MST septa did not give significant impedance. However, bench measurements showed a clear peak at the frequencies of interest. These cavity like objects were shielded during 1998-2000 [7] (see below) and the SC 400 MHz RF cavity was removed from the ring in 1998. However, even after these changes, the instability was still present, albeit with slightly increased threshold [8].

Given their transverse dimensions the electrostatic septa, ZS, were possible alternative candidates for the 400 MHz peak. The 10 ZS tanks would have been very difficult to shield. Fortunately, the ZS were

subsequently eliminated as the source of the instability following bench measurements which showed the tanks had insignificant impedance at 400 MHz. On the other hand, laboratory measurements done on the MKE kickers [9] showed that the impedance of these objects at 400 MHz could be responsible for the instability. Most of these kickers were removed from the ring during the 2000/2001 shutdown and none of them were left in the ring in 2002. During the 2002/2003 shutdown 5 kickers were re-installed in the SPS (for one of the extraction channels to the LHC) but this time having been screened.

During 1998, measurements using a fixed target beam with a total intensity close to that of the nominal LHC beam, but 10 times smaller bunch intensity, showed a longitudinal emittance blow-up by a factor 10 during acceleration (0.2 eVs \rightarrow 2.0 eVs). Later, continuous emittance blow-up of the LHC beam was observed on the flat bottom (at 26 GeV) for bunch intensities above 3×10^{10} [10]. Measurements with 42 LHC bunches of 8×10^{10} p/bunch at 450 GeV with the 800 MHz RF system on (stabilising the beam against coupled-bunch modes) showed an emittance blow-up up from 0.35 eVs to around 1eVs [11].

Different solutions to avoid or cope with this uncontrolled emittance blow-up due to the microwave instability were studied [3,8,12]:

- Installation of extra quadrupoles to decrease the transition energy in the SPS,
- reduction of the impedance of the instability sources,
- installation of a 200 MHz RF capture system in the LHC.

Measurements on the flat bottom confirmed the improved bunch stability with lower transition energy [13]. However, the most attractive cure was the removal or shielding of the elements concerned. In addition it was decided to install a 200 MHz RF system in the LHC.

To be able to follow-up the impedance reduction program and to see the consequences for the beam, different types of reference measurements were started. For the longitudinal plane, the results are presented in Sec. 17.6.1.

17.1.2 Transverse Impedance and the Resulting Tune Shifts

The electromagnetic fields associated with a moving bunch produce wake fields in the surrounding vacuum chamber which act back on the bunch and affect the transverse beam stability.

The strength of the interaction of the beam with its environment can be characterised by the (machine or coupling) impedance. Here the transverse (horizontal or vertical) impedance which affects only the transverse motion is discussed. The transverse impedance can formally be obtained as Fourier transform of the transverse wake functions. It causes a transverse deflection and does not affect the longitudinal motion or particle energies.

Table 17.1: Relevant SPS Parameters

Variable	Symbol	Value
Momentum	P	26 GeV/c
Revolution Frequency	T_0	43347.3 Hz
Betatron Tunes	$Q_{x,y}$	~ 26.2
Synchrotron Tune (at 3MV)	Q_s	6.9×10^{-3}
Momentum Compaction	α_c	1.92×10^{-3}
Phase Slip Factor	η	0.618×10^{-3}
Bunch Population	N	1.2×10^{11}
Rms. Bunch Length	σ_t	~ 0.5 ns

The effect on the bunch centroid is a complex frequency shift of:

$$\Delta\omega_\beta = \frac{Nec}{4\sqrt{\pi}\omega_\beta(E/e)T_0\sigma_t} i(Z_\perp)_{eff} \quad (17.1)$$

where N is the number of particles in the bunch, E its energy, T_0 the revolution frequency, $\sigma_t = \sigma_z/c$ the bunch length and $\omega_\beta = 2\pi Qf_{rev}$ the betatron frequency [14]. Eq. 17.1 applies to both horizontal and vertical motion. The dependence on $1/E$ implies that the largest tune shifts are expected at the lowest energies and that the transverse stability will be most critical at the injection energy, which is 26 GeV for LHC beams in the SPS.

Tab. 17.1 lists the relevant SPS parameters. $(Z_\perp)_{eff}$ is the effective transverse impedance. For a round chamber this is the impedance convoluted with a weight function, h , representing the longitudinal bunch shape:

$$(Z_\perp)_{eff}(\omega_\xi) = \int_{-\infty}^{+\infty} Z_\perp^\perp(\omega) h_m(\omega - \omega_\xi) d\omega \quad (17.2)$$

For the 0-mode coherent bunch oscillation and Gaussian bunches the weight function is:

$$h_0(\omega) = \frac{\sigma_t}{\sqrt{\pi}} e^{-(\omega/\sigma_t)^2}$$

This is a Gaussian in ω with an rms. width of $1/(\sqrt{2}\sigma_t)$ or, equivalently, a Gaussian in frequency $f = \omega/(2\pi)$ of width $\sigma_f = 1/(2\pi\sqrt{2}\sigma_t)$. For $\sigma_t = 0.5$ ns, the rms. width in frequency is 225 MHz and the weight has dropped to 5% at $f = 0.275/\sigma_t = 551$ MHz. The Gaussian weight function in Eq. 17.2 is centred at ω_ξ which depends on the chromaticity:

$$\xi = Q'/Q = \frac{\Delta Q}{Q} / \frac{\Delta p}{p}$$

Together with the phase slip factor, η , according to:

$$\omega_\xi = \xi \frac{\omega_\beta}{\eta} \quad (17.3)$$

For the SPS at 26 GeV, $f_\xi = \omega_\xi/(2\pi) = 2.08$ GHz.

The SPS has a rather flat vacuum chamber with V/H ratios from 1/3 to 1/4 in the bending sections. This asymmetry enhances the tune shift in the vertical plane [15]. The SPS as LHC injector operates above transition ($\eta > 0$). It can be assumed that the transverse SPS impedance can be approximated by a transverse broad band ($Q = 1$) impedance of the form:

$$Z_\perp = \frac{\omega_r}{\omega} \frac{R_\perp}{1 + iQ \left(\frac{\omega}{\omega_r} - \frac{\omega_r}{\omega} \right)} \quad (17.4)$$

with the resonant frequency, $\omega_r = 2\pi f_r$, where $f_r = 1.3$ MHz in this case.

For positive chromaticity, a positive real part of the transverse impedance results in a positive imaginary tune shift; implying exponential decay of coherent centroid motion, that is damping. The (positive) imaginary part of the transverse impedance results in a real (negative) tune shift. Small coherent tune shifts can, at least to first order, be compensated by an increased machine tune (increased quadrupole strength). Large tune shifts, of the order of, or larger than, the synchrotron tune Q_s can cause fast beam break-up or transverse mode coupling instabilities.

17.2 THE PUMPING PORT SHIELDING PROGRAMME

The possibility that the pumping port/bellows assemblies of the SPS vacuum system contributed to the longitudinal microwave instabilities, was first expressed in 1997 [16] and the conceptual design report of the

SPS as LHC injector proposed a scheme for ‘smoothing’ these cavities [3]. Further studies with LHC beams identified several contributory sources to the instability [17], but also confirming the pumping ports (PPS) as a major factor. Obsolete lepton related components (RF SWC cavities etc.) were removed in the impedance improvement project but it became evident that the equipment that could not be removed needed to be shielded in some way. Programmes were launched to shield the extraction septa and kicker tanks (Secs. 17.3 and 17.4) and, since they could not be removed, a parallel campaign to shield the approximately 1000 PPS around the SPS was made.

17.2.1 Machine layout

The basic SPS machine comprises 216 main quadrupole magnets alternately focussing and defocusing, in a classic FODO lattice, with a half cell length of 32 m. The space between the quadrupoles is occupied by 4 main bending magnets and a short straight section, as shown in Fig 17.2, where:

- QF = Quadrupole Focussing in the horizontal plane,
- QD = Quadrupole Defocusing ie focussing in the vertical plane,
- MBA = Dipole with large horizontal aperture,
- MBB = Dipole with large vertical aperture,
- SSS = Short Straight Section girder supporting BPM and correctors, together with, various multipole magnetic correction elements at different locations around the SPS.

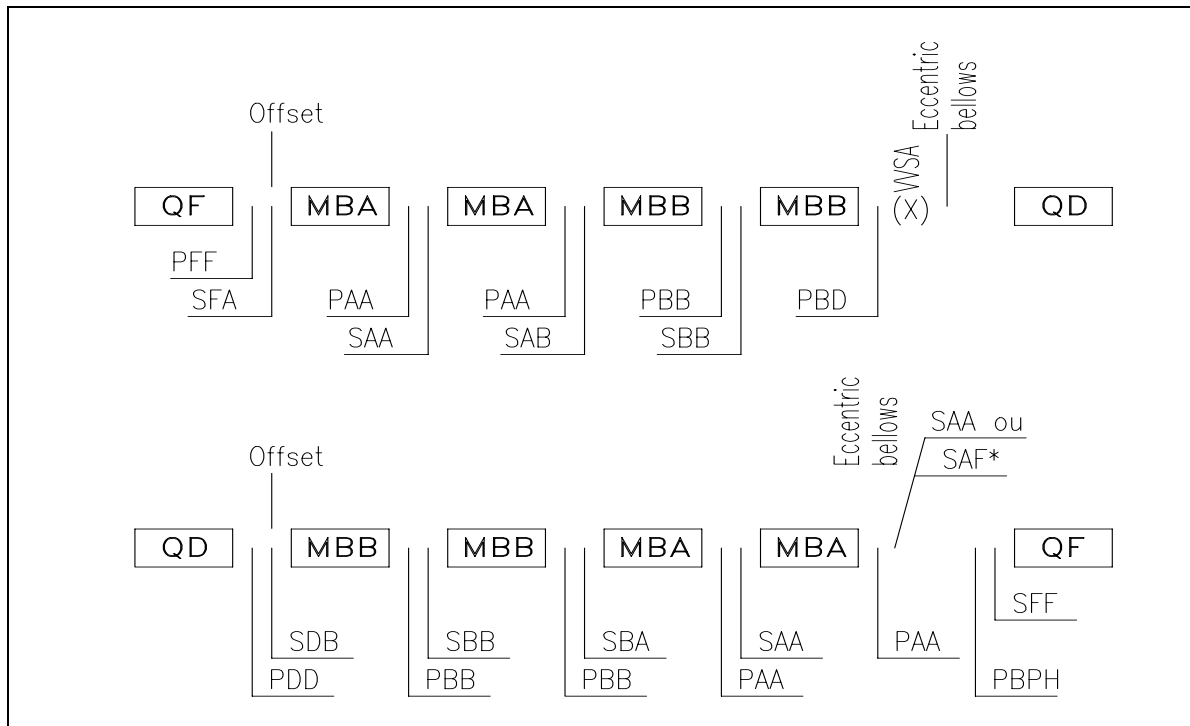


Figure 17.2: Two SPS half periods showing the types of PPS installed

The SPS takes the form of six arcs. The numbering system for each sextant starts in mid arc and follows the direction of the (proton) beam. At the centre of each sextant the main bends are missing from 4 half-periods creating 6 long straight sections (LSS) and allowing room for special equipment for injection, extraction and acceleration.

The magnetic gap of each type of magnet has been optimised. As a result, the physical aperture of the machine changes frequently around the 6.9 km circumference. In the curved sections, which constitute over 90% of the SPS, the dipoles are placed very closely together longitudinally. Between adjacent magnets there is an inter-magnet gap of some 30 cm, most of which is encumbered by the two sets of magnet coils, see Fig 17.3.

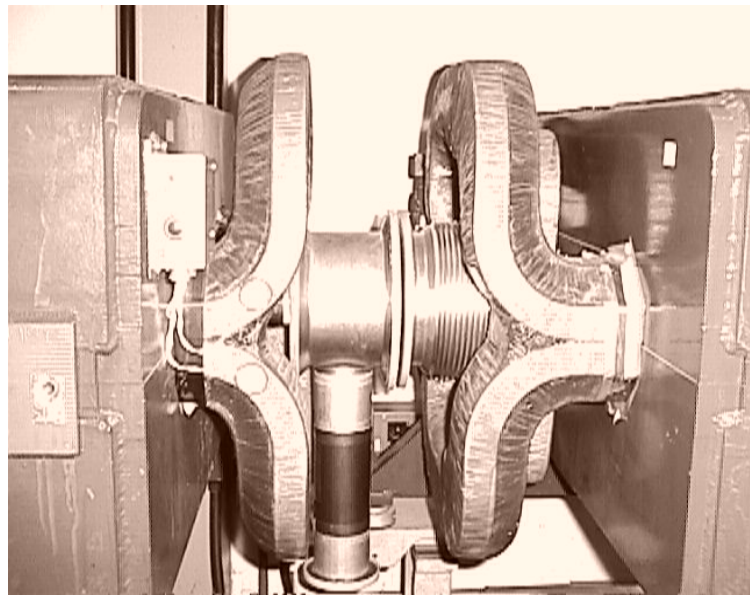


Figure 17.3: Gap between 2 main SPS dipoles

17.2.2 The SPS Vacuum System

Given that the SPS aperture varies as a function of the magnetic elements, the profile of the stainless steel vacuum chamber, which constitutes most of the circumference, also changes. There are six main chamber types in the SPS which are illustrated in Fig. 17.4. In addition to the standard chambers shown a few other specialised chambers are installed in the machine; specifically wide aperture chambers in the injection and extraction regions.

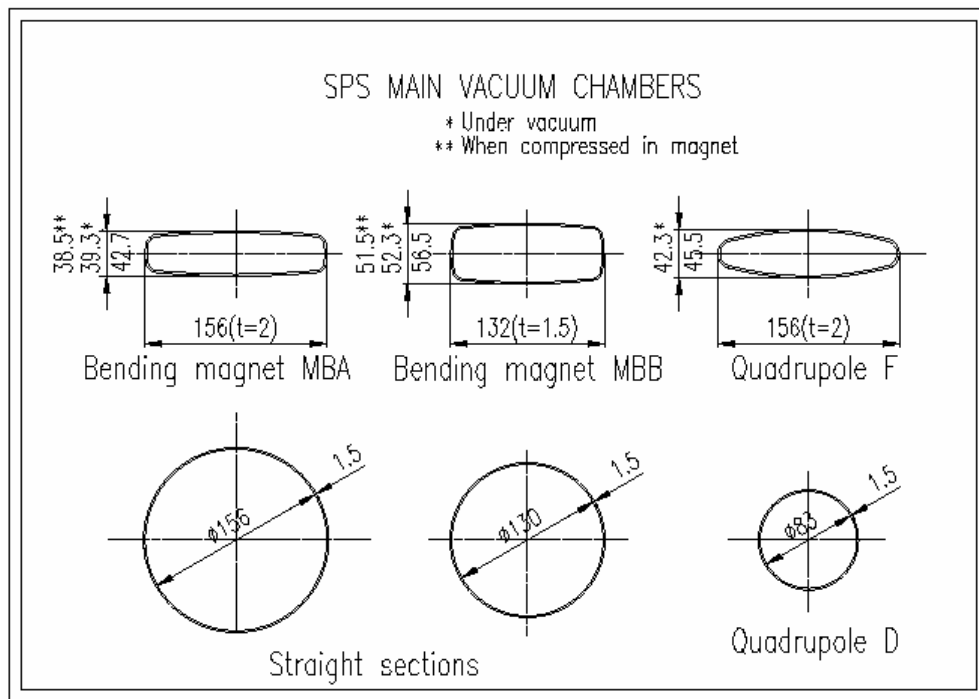


Figure 17.4: Vacuum chamber profiles of Main Magnets and Drift Chambers

Throughout the major part of its circumference, the vacuum chamber of the SPS is clamped between the poles of the main magnets. Each magnet is therefore equipped with a chamber whose profile is specific. In order to standardise components in the repetitive parts of the SPS, flexible bellows and vacuum pumping

ports, are made a standard (156 mm) diameter to accommodate all of the profiles in Fig 17.4, only the form of the pressed adaptor end plate is profile specific. For all chamber profiles other than the 156 mm diameter drift chamber, a cavity is formed where the bellows and pumping port of the adjacent magnet are clamped together. Any solution for smoothing across the PPS cavities had to allow for both magnet removal and the changes in the vacuum chamber section profile where necessary. A retractable centre contact solution was adopted to permit magnet removal and vacuum joint fitting, together with a series of transition pieces to smooth the change of profile across the cavity.

17.2.3 PPS Design Criteria and Constraints

To a large extent the RF requirement to fully shield the cavity from the beam is in contradiction with the necessity to pump an adequate vacuum inside the shield. Measurements in the vacuum laboratory showed that the shields needed to be perforated in order to improve the conductance. Vacuum experts calculated the requisite surface area of the openings and the RF team suggested the shape and positioning of the holes. Examples of various PPS were fitted in the SPS in specially installed cavities, equipped with RF probes (see Fig. 17.5) and the design modified until acceptable results were obtained. The best RF results were obtained while maintaining an acceptable vacuum conductance by grouping round holes on the sides of the shields. Oval holes or slots were found to be less satisfactory.

Those cavities across which the chamber profile changed were equipped with transition cones in order to smooth the change of section. The transition was systematically installed on the bellows sub assembly half of the cavity since the spring mechanism on the pumping port side required that the top and bottom surfaces of the shield be parallel (see Fig. 17.6). Stainless steel (type AISI 304L) was chosen for shield construction for its good out-gassing properties and its compatibility with the existing vacuum system.

Since the vacuum chambers are clamped between the poles of the main dipoles, the theoretical sectional profile of the chamber is somewhat deformed. Early design iterations relied upon shields cut from standard pieces of vacuum chamber. However, since their profile was uncompressed, they aligned poorly with the deformed chambers of the magnets. Consequently shields were produced in industry with sections corresponding to the compressed profiles of the chambers in the magnets.

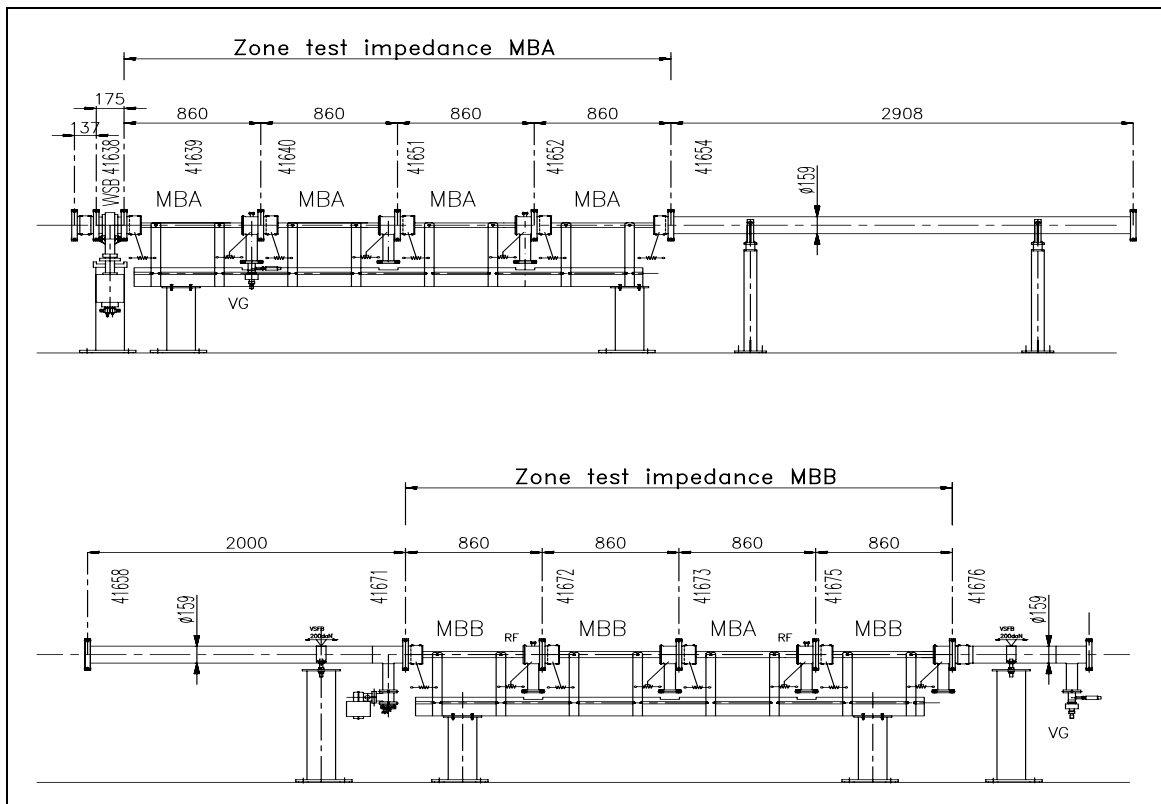


Figure 17.5: The PPS test-bed installed in LSS4

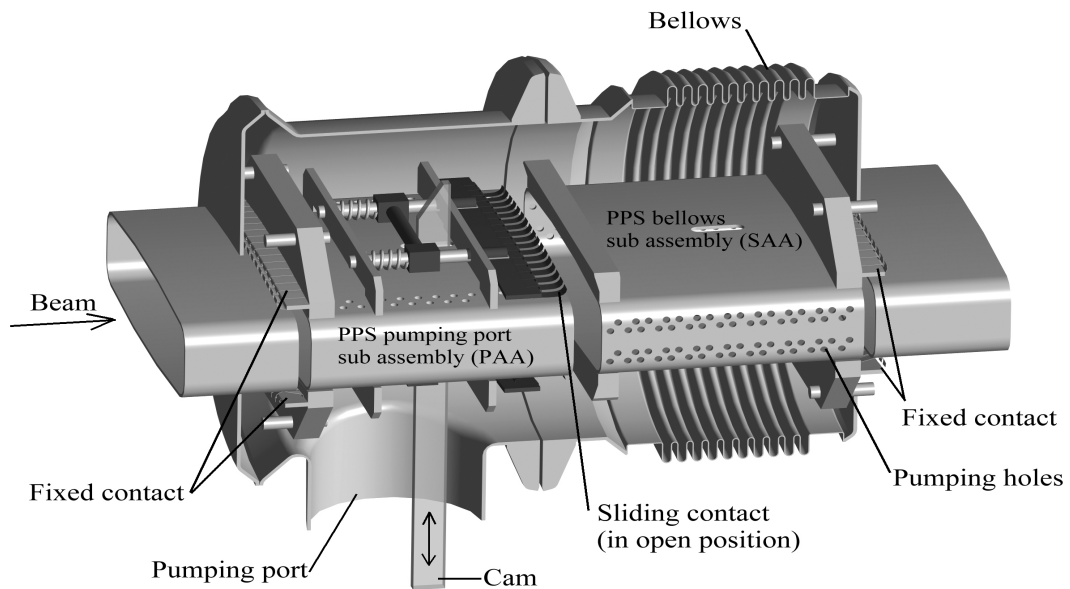


Figure 17.6: Cutaway view of PPS shielding between 2 MBA dipoles.

Laboratory tests proved that a good electric contact was absolutely necessary across the gap between the half shields as well as between the shields and the magnet chambers. A sliding mechanism was therefore necessary between the half shields to allow magnet installation and removal as well as vacuum joint fitting between the flanges. A spring mechanism which allowed the contacts to be retracted by means of a cam introduced via the pumping port was adopted (Fig. 17.6). The cam remained in place maintaining the contact open during installation, after which it was removed and the compressed spring closed, bridging the gap. The contacts between shields and magnet chambers were made fixed. The contact fingers are sprung in order to allow for any accumulation of errors in form and positioning of the shield halves and also to accommodate the 4.2 mrad angular offset between main dipoles that is necessary in an arc formed of straight magnets. A good deal of flexibility was also necessary for the fixed contacts since the joint between the magnet chamber and the end plate of the bellows and pumping port is hand welded and consequently rather rough. No standard finger contacts were found to fulfil the PPS requirements; a design based upon a commercially available clip-on contact strip was therefore produced at CERN and manufactured in industry. CuBe was chosen as contact material being the industry standard giving both a good electrical contact together with good spring characteristics. The clip-on feature allowed for fast fitting together with acceptable out-gassing performance. The two spring contact types are shown in Figs. 17.7 and 17.8

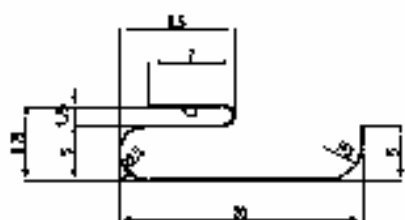


Figure 17.7: Central Sliding CuBe Contact

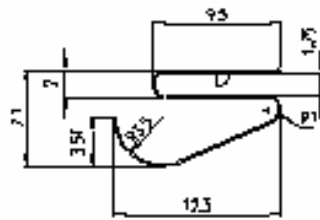


Figure 17.8: Fixed end CuBe contact

17.2.4 Shield Types

Each PPS assembly comprises 1 subassembly called ‘pot’ located in the pumping port, together with a ‘bellows’ subassembly fixed inside the flexible bellows half of the cavity (Fig.17.6). The breakdown of the types of shield subassembly that were necessary to cover all the various situations encountered around the SPS is shown in Tab 17.2. Those codes beginning with ‘P’ refer to subassemblies located in ‘pots’ and those beginning with ‘S’ to a ‘bellows’ subassembly. Since ‘B’ is widely used elsewhere in the code system, ‘S’ for soufflet was chosen for the sake of clarity. Code letters ‘A’ & ‘B’ refer to the dipole chamber type (MBA & MBB respectively), while ‘F’ & ‘D’ correspond respectively to QF and QD profiles.

Each shield code is therefore composed of 3 letters which indicate location (P or S), upstream profile, followed by downstream profile taken in the proton beam direction. Thus in Fig. 17.5 above, the subassemblies PAA and SAA are shown since the MBA profile is unchanged across the cavity. Had the downstream magnet been an MBB for example, shields PAA & SAB would have been shown.

A survey of the real PPS cavity lengths taken in-situ around the whole SPS circumference showed that the maximum possible translation of the central contact was not sufficient to cover the range of lengths. Shields were therefore produced in Short, Normal and Long lengths. Since the length of the ‘pot’ half of the cavity is obviously fixed, length variations could only be accommodated on the bellows side. Tab. 17.2 shows the various shield types necessary to cover the different chamber sections, transitions between sections and three lengths of each bellows shield. Types 29 and 30 were special cases designed to marry to the aperture of a vacuum sector valve rather than a standard chamber profile.

17.2.5 Installation

The inherent difficulty of access to the PPS cavity is clearly shown in Fig. 17.3. By removing the first and third dipoles in each half period, together with the elements of the SSS where necessary, access was gained to either end of the removed element as well as the corresponding ends of the neighbouring elements. It can be seen from Tab. 17.2 that a total of over 1000 cavities were shielded, requiring the removal and replacement of around 470 magnetic elements including 370 main dipoles each weighing 17 tonnes. Certain special vacuum chambers with non-standard sections were left unshielded during the main installation period and subsequent beam measurements showed that the SPS impedance was sufficiently improved for these high-cost instances to remain unshielded (see Sec. 17.6).

Teams comprising members of the magnet, vacuum, transport and survey groups carried out the installation process with help from radiation protection and main-ring installation personnel.

Prior to removing a main dipole, the vacuum sector was vented to atmospheric pressure, the cooling water system drained and the length of each PPS cavity measured to determine whether a Short, Normal or Long model shield was to be fitted. Following this, the vacuum system was disconnected and the coil connectors un-brazed from the bus-bars. The magnet was then removed and, while safely supported by the special hydraulic machine, its PPS were fitted at either end together with the PPS of the accessible cavities of the adjacent magnets. After fitting the shields, the cams were inserted via the pumping ports to retract the moving centre contacts, the dipole was carefully replaced in its original position then realigned, reconnected, re-brazed. Finally, the cams were removed to close the central CuBe contacts, leaving only vacuum leak-detection to complete the process. In total around 370 main dipoles were treated in this way together with about one hundred auxiliary magnetic elements involving slightly different methods. Thus the whole of the SPS vacuum system was at open to air at some time during the process and the whole machine was re-aligned.

Around 20% of the SPS was equipped with PPS during the 1999/2000 shutdown. Although no measurable impedance improvement was observed (or expected) during the 2000 run, at least the PPS proved not to cause any aperture restriction. Installation of the remaining 80% of the machine (except the few special cases) was carried out after the end of LEP operation (end 2000). The shields could not be made compatible with the synchrotron radiation masks installed to protect the SPS elements during operation with leptons [18]. For the early installation a series of modified SR masks were fitted and the types of PPS to be shielded were restricted in order to remain compatible with LEP operation in 2000. For the remaining installation the SR masks were systematically removed from the machine.

Table 17.2: Table of shield types with reference codes, drawing numbers and quantities.

Item Nr.	PPS Type	Model	Model number	Size	PPS sub/assembly		TAG	Total manufactured	Total installed
					Drawing Nr. SPSVSRFS				
1	Pot	MBA	1		0080.1	PAA	391	384	
2	Pot	MBB	2		0083.1	PBB	307	288	
3	Pot	QF	3		0108.1	PFF	100	96	
4	Pot	QD	4		0131.1	PDD	110	96	
5	Pot	MBB-QD	5		0146.1	PBD	105	96	
6	Bellows	BHP-QF	6		0150.1	SFF	120	108	
7	Bellows	MBA	7	Short	0081.1	SAA-S	22		
8	Bellows	MBA		Normal		SAA-N	188	205	
9	Bellows	MBA		Long		SAA-L	26		
10	Bellows	MBA-MBB	8	Short	0082.1	SAB-S	22		
11	Bellows	MBA-MBB		Normal		SAB-N	106	96	
12	Bellows	MBA-MBB		Long		SAB-L	22		
13	Bellows	MBA-QF	9	Short	0124.1	SAF-S	5		
14	Bellows	MBA-QF		Normal		SAF-N	80	70	
15	Bellows	MBA-QF		Long		SAF-L	5		
16	Bellows	MBB	10	Short	0084.1	SBB-S	22		
17	Bellows	MBB		Normal		SBB-N	191	192	
18	Bellows	MBB		Long		SBB-L	21		
19	Bellows	MBB-MBA	11	Short	0085.1	SBA-S	22		
20	Bellows	MBB-MBA		Normal		SBA-N	101	96	
21	Bellows	MBB-MBA		Long		SBA-L	23		
22	Bellows	QF-MBA	12	Short	0115.1	SFA-S	15		
23	Bellows	QF-MBA		Normal		SFA-N	85	96	
24	Bellows	QF-MBA		Long		SFA-L	15		
25	Bellows	QD-MBB	13	Short	0138.1	SDB-S	20		
26	Bellows	QD-MBB		Normal		SDB-N	85	96	
27	Bellows	QD-MBB		Long		SDB-L	20		
28	Pot	BPH	14		0166.2	PBPH	120	108	
29	Bellows	VVSA-1	15		0171.3 (VAT)	SVVSA-1	20	14	
30	Bellows	VVSA-2	16		0171.3 (CETEC)	SVVSA-2	10	5	
TOTAL							→	2379	2046

17.3 THE SEPTUM SHIELDING PROGRAMME

17.3.1 Introduction

The extraction septa MST and MSE were identified as an important source of transverse impedance, at about 400 MHz [19]. A programme to shield the large vacuum tank volume from the circulating beam was therefore undertaken.

17.3.2 Design and Installation

The RF shielding of the extraction septum magnets used a simple semi-cylindrical perforated steel sheet, formed to a radius of 135 mm, to match the aperture of the entrance and exit flanges on the MSE vacuum vessel [20]. The electrical contact at the extremities is made by means of sprung bronze-beryllium multi-contacts, so that the image currents induced by the beam can flow in a continuous path through the device. The shield proper is fixed to the septum support girder in the tank, with sufficient play in the mechanical mountings to allow for thermal expansion during the bakeout.

The RF shields have been fitted to all 21 of the MST and MSE magnets installed in the SPS and to all spare and newly-constructed magnets. One magnet was equipped with a screen which was fitted with Pt100 temperature gauges – during the first year of operation the temperatures were monitored, with maximum increases seen of the order of 10° for the highest intensities and shortest bunch lengths. Impedance measurements made in the SPS after the septum shielding program showed that the strong resonance line at 400 MHz has been largely suppressed [21].

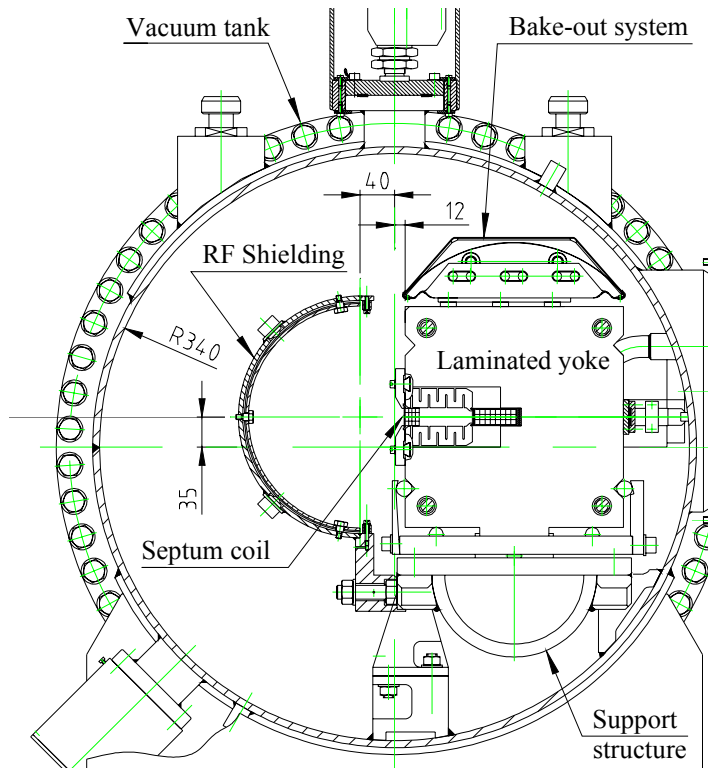


Figure 17.9: Cross-section of the MSE septum, showing the RF screen.

17.4 THE KICKER TANK SHIELDING

17.4.1 Introduction

The impedance of the SPS kicker magnets is partly due to the ferrites and partly due to the cavities between the magnets and the vacuum tank. Sec. 17.7 treats the impedance of the ferrites and the resulting beam induced heating. This section treats the impedance due to the gaps between magnets and vacuum tanks.

For the newly installed kicker tanks these gaps have been shielded. The shielding provides a by-pass for the image currents between the kicker module and the vacuum tank and subsequently lowers the coupling impedance in the longitudinal and transverse planes.

17.4.2 Design and Installation

The injection kickers MKP

The SPS injection kicker magnet system (MKP) consists of a total of 16 magnets housed in four vacuum tanks (see Chap. 13). The first three tanks, with in total 12 magnets, are equipped with RF shielding. For these tanks the entrance and exit gap between the tank and the magnet and the gaps between magnets has been shielded by transition pieces so that the beam does not see the resonant cavities. Fig. 17.10 shows the places where shielding has been applied for a kicker tank with 5 magnets (first two tanks).

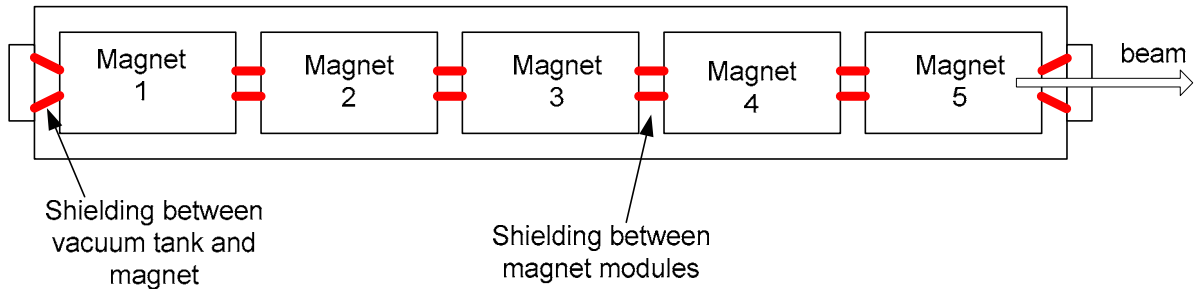


Figure 17.10: Schematic view of a modified injection kicker tank, indicating the places where shielding has been applied.

A single transition piece has been installed at the entrance and exit of the kicker tank between the circular beam opening of the vacuum tank and the rectangular opening of the kicker aperture,. Between the magnets the rectangular aperture has been shielded with four separate plates. The plates and the magnet support structure are connected by RF multi-contacts. Fig. 17.11 shows the shielding for the MKP magnets.

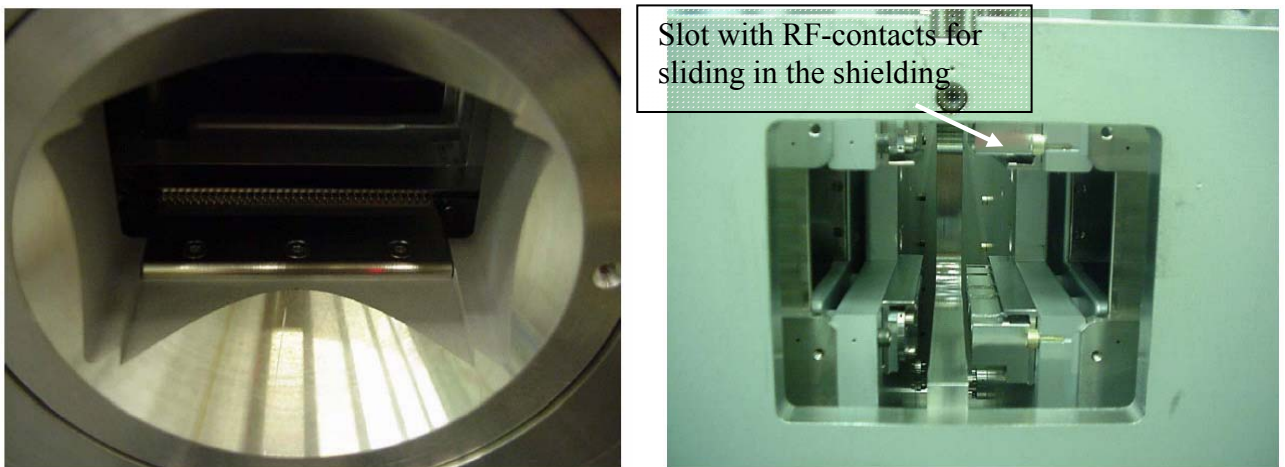


Figure 17.11: Shielding of the gap at the entrance of the MKP tank, transition from circular to rectangular aperture (left). The gap to be shielded in-between two magnets (right) with the slots equipped with RF-contacts in which the screening plates can be installed visible at the top and bottom of the gap.

The Extraction kickers MKE

The extraction kickers, MKE, are housed in individual vacuum tanks and shielding of the gaps between magnet and vacuum tank has been installed in the five new kickers in LSS4 and will be applied to the four kickers to be installed in LSS6. The transition pieces are basically identical to the ones used for the injection kickers, MKP, described above. Coaxial wire measurements of the longitudinal beam coupling impedance of

the MKE modules with and without shielding have been made [22], but the interpretation of the measurements is very delicate. Bunch spectra measurements indicate the benefit of the installed shielding, see Sec. 17.6.

17.5 REMOVAL OF OBSOLETE EQUIPMENT AND VACUUM CHAMBER STANDARDISATION

The SPS layout included a legacy of equipment dating from the $p\bar{p}$ era, including the low- β insertions and the anti-proton injection kicker tanks (MKA). These elements were duly removed and the layout rationalised to meet the machine's new role. The harmonic correctors were also removed at this time. Once LEP operation finished at the end of 2000, it was possible to remove all equipment associated with leptons including: the 100MHz and 200MHz standing wave RF cavities, 352MHz superconducting cavities and the injection and extraction elements.

On the short straight sections of the machine the normal procedure for installing drift chambers was to use standard 156 mm circular chambers. On many SSS this meant that the chamber section changed several times. This was particularly true in the case of SSS associated with QF quadrupoles. A typical example with just a lattice sextupole magnet on the girder might have the following chamber transitions:

- MBA-QF Between the last dipole and the lattice sextupole
- QF-156mm Between sextupole and drift chamber
- 156mm- MBA Between drift chamber and orbit corrector/BPM package
- MBA-QF Between orbit corrector/BPM and QF quadrupole.

In this case the drift chamber produces a long cavity which can not easily be shielded. Fig. 17.12 shows an SSS of this type. The large aperture drift chamber can clearly be seen to the right of the lattice sextupole. This drift chamber cavity would contribute directly to the overall impedance. The solution in this case is to replace the 156 mm standard chamber by a more appropriate section, either QF, or MBA. The associated pumping ports are then shielded using the standard elements described in Sec. 17.2. A systematic check of all SSS in the machine was undertaken and, where appropriate, changes were made to the drift chambers to minimise the cavities generated by vacuum chamber section changes.



Figure 17.12: Typical SSS before smoothing the chamber cross-sections.

The replacement of the wide aperture 156 mm chambers by smaller sections does not impact on the aperture of the machine, as long as the smaller section vacuum chamber is well aligned to its neighbours. As short straight section girders are normally assembled and aligned on the surface before installation in the machine, this was not considered to be a major problem. In addition, measurements made since the change of policy have not shown any reduction in the aperture of the machine.

17.6 MEASUREMENTS OF THE EFFECT OF THE IMPEDANCE REDUCTION PROGRAMME WITH BEAM

17.6.1 Longitudinal Results and Measurements with Beam

The results of the SPS impedance reduction in the longitudinal plane can be seen both from the reference measurements done in 1999 (before impedance reduction) and in 2001 (after) [23] and also from the parameters obtained for LHC beam at 450 GeV over the last few years [24].

The different sets of reference measurements were done at 26 GeV using single bunches with similar longitudinal parameters. While the results with RF on (bunch lengthening and quadrupole frequency shift with intensity) demonstrate the global effect of the impedance reduction on bunch stability, measurements of bunch spectra with RF off allow the detailed changes at particular frequencies to be seen.

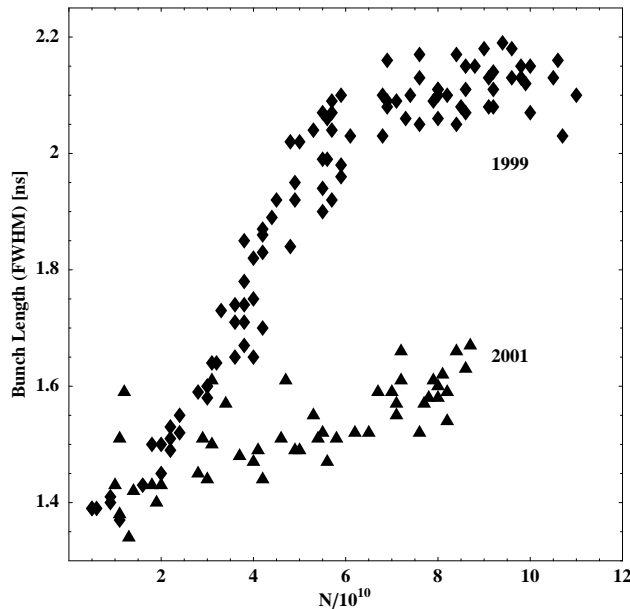


Figure 17.13: The bunch length measured 600 ms after injection as a function of bunch intensity in 1999 and 2001. Data taken at 26 GeV, $\epsilon=0.15$ eVs, $V=900$ kV.

Bunch Lengthening

The bunch length increases with intensity; firstly due to potential well distortion (defined by the low frequency inductive part of the impedance, $\text{Im } Z/n$) and then, above some threshold intensity, also because of emittance blow-up caused by the microwave instability.

In Fig. 17.13 measurements made in 1999 and 2001 of the bunch length (full width half maximum) at 600 ms after injection at 26 GeV is shown as a function of intensity. The difference in the slope is around a factor 7. Clearly in 1999 the microwave instability threshold was at or below 3×10^{10} p/bunch. In 2001 the smooth increase with intensity due to potential well distortion can clearly be observed. Particle simulations [25] showed that it was principally the impedance of the vacuum ports which was responsible for the uncontrolled emittance blow-up observed before 2001. The shielding of these elements [26] has practically eliminated the microwave instability.

Simple scaling from the 2001 data, which were obtained for a bunch emittance of 0.15 eVs, shows that a single LHC bunch at 26 GeV should be stable at least up to the ultimate intensity (1.7×10^{11} p/bunch).

Quadrupole frequency shift

The linear shift of quadrupole frequency, f_2 , with intensity, N, can be described as:

$$f_2(N) = f_2(0) + bN \times 10^{-10} \quad (17.5)$$

where $f_2(0)$ is the quadrupole frequency at zero intensity and the coefficient b is proportional to the low frequency inductive impedance $\text{Im } Z/n$.

The results from measurements of the quadrupole frequency in 1999, 2001 and 2003 (after the installation of the 5 MKE kickers) are presented in Fig. 17.14. The 900 kV capture voltage was chosen in 1999 to match to the bunch at the highest intensities in order to prevent particle losses. Unavoidably this voltage was too high for matching at low intensities and led to quadrupole oscillations immediately after injection. The quadrupole frequency was measured from oscillations of the peak detected signal at different bunch intensities.

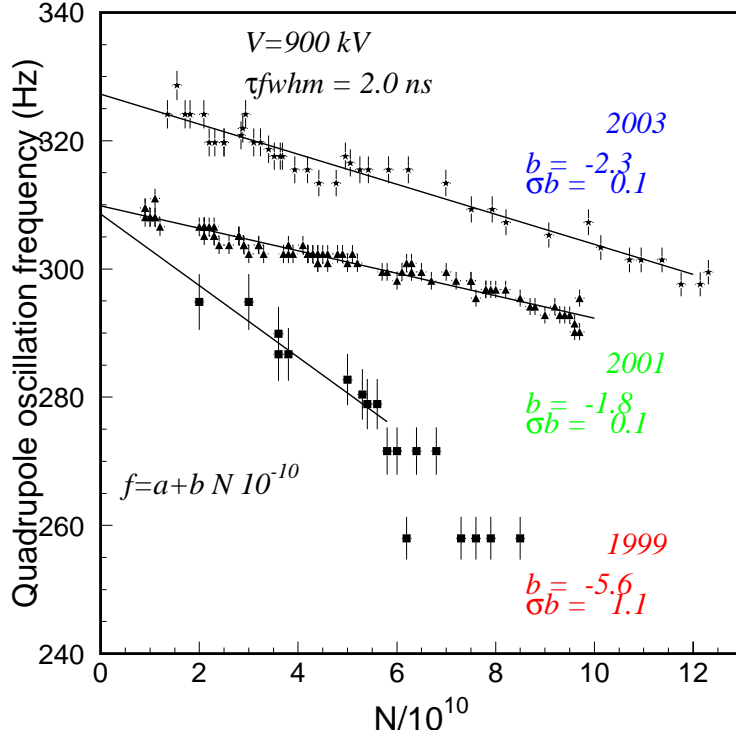


Figure 17.14: Quadrupole oscillation frequency as a function of bunch intensity in 1999, 2001 and 2003. The longitudinal emittance (measured in the PS at the lowest intensities) was 0.15 eVs.

Table 17.3: Low frequency inductive part, Z/n , of the different elements in 1999 and reduction in 2001.

Element	No.	$\text{Im } Z/n [\text{Ohm}]$
TW200-F Cavities	4	4.9
TW200-HOM	4	0.25
TW-800F Cavities	2	0.35
Lepton RF Cavities	28	1.7
Pumping Ports	900	3.0
MKE + MKP Kickers	6	2.0
MSE + MST Septa	8	0.1
Bellows	900	0.1
Total Reduction		6.8

A factor 2.5 reduction in the slope, proportional to $\text{Im } Z/n$, was measured on average (for different bunch lengths) in 2001 [23]. However, in 2003 one can see an increase of the slope by 30% which can be attributed to the re-installation in the ring of 5 the MKE kickers. These kickers are equipped with transition pieces which electrically connect the beam pipe in the ferrite to the tank itself and damp the cavity modes in the tank (see the spectrum measurements below), but have not changed the impedance at low frequencies (below 300 MHz) [27].

The results of the measurements are close to what one could expect from the impedance budget for $\text{Im } Z/n$ in 1999, 2001 and 2003. Contributions from the different machine elements are shown in Tab. 17.3 [5,6,28]. All items were in the ring in 1999, only the top three in 2001 and for 2003 one should add the contribution from the MKE kickers (5 modules). In 2001 the expected reduction in $\text{Im } Z/n$ from the impedance budget is 6.8Ω (from 12.4Ω to 5.6Ω). The contribution from space charge at 26 GeV is around -1Ω . This corresponds to a reduction factor of 2.5.

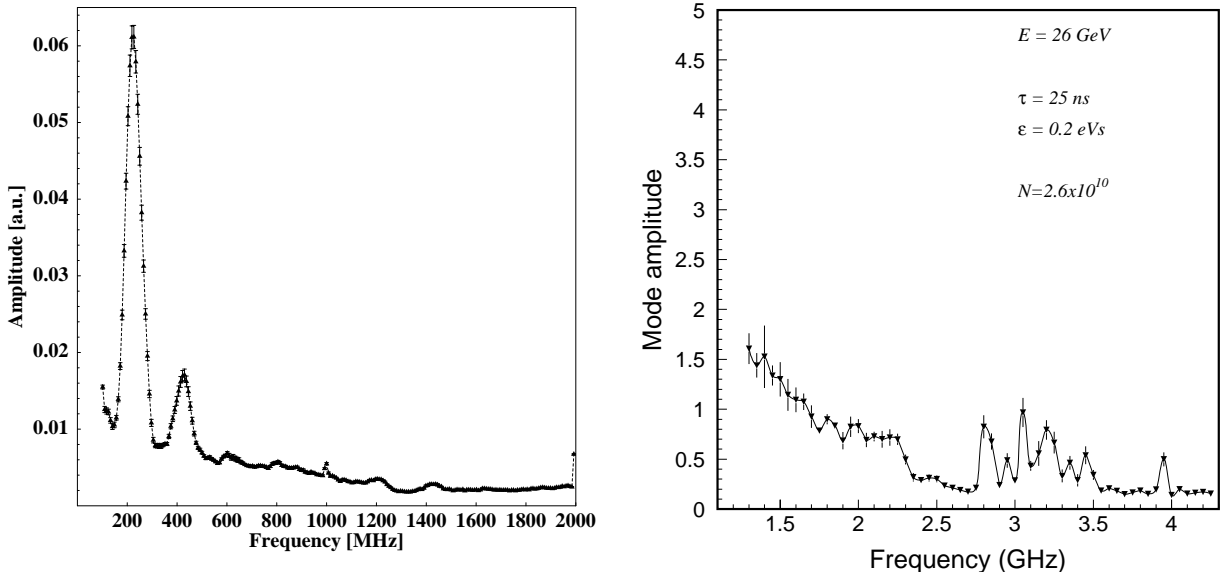


Figure 17.15: Left: Unstable bunch spectra up to 2 GHz, bunch intensity $N=6\times10^{10}$, $\epsilon=0.22$ eVs, bunch length $\tau=25$ ns [23]. Right: Spectra at high frequencies. Measurements made during 2001 at 26 GeV with RF off.

Spectrum measurements

Reference measurements of the spectrum of long bunches with RF off were started in 1999 to monitor changes of impedance at particular frequencies of interest. Comparison between the measurements done in 1999 (Fig. 17.15, left) and 2001 (Fig. 17.15, right) shows that for the same bunch and machine parameters (26 GeV , $N = 6.0 \times 10^{10}$, $\epsilon = 0.22 \text{ eVs}$, $\tau = 25 \text{ ns}$) the amplitude of the 400 MHz signal after the removal and shielding of the MKE and MKP kickers is much less. The remaining signal is the second harmonic of the 200 MHz component which appears due to the impedance of the 200 MHz TW RF system. Measurements done in 2003 (after re-installation of the MKE kickers) with the same bunch parameters are similar to the results of 2001.

In comparing Fig. 17.15 with Fig 17.1 it can be seen that the signals at 1.5, 1.9 and 2.4 GHz coming from the impedance of the pumping ports are no longer visible in the measurements of 2001. However the signals above 2.8 GHz have not changed. During machine studies (MDs) in 2002 these signals were proved to be due to pick-up resonances excited by the stable bunch and not due to an unstable line density modulation. It should be noted that the pick-up cut-off frequency for propagating waveguide modes is 2.8 GHz.

Other consequences of the impedance reduction

Another result of the impedance reduction is the significant increase of bunch intensity which can cross transition energy. In MDs in 2002 transition crossing without losses was possible with at least $7 \times 10^{10} \text{ p/bunch}$ instead of $2 \times 10^{10} \text{ p/bunch}$ as in the past.

An important consequence already observed with the LHC beam in 2001 was the absence of continuous emittance blow-up, leading to losses on the flat bottom that had been seen before [10]. After the scrubbing run done at the beginning of operation in 2002, the injected intensity of the LHC beam could be increased beyond nominal intensities. Even for significantly higher bunch and beam intensities an emittance blow-up much smaller than in 2000 [11] was measured on the flat top in 2002 [29], so that even some controlled emittance blow-up is introduced to fight against coupled bunch instabilities [24].

17.6.2 Transverse Results and Measurements with Beam

Fig. 17.16 shows a comparison of the observed tune shifts with intensity in the vertical plane, measured on single bunches in the year 2000 before [30] and in 2001 after the major part of the hardware changes [31]. The beam conditions were very similar in both cases.

The observed tune shifts with current in the horizontal plane are much smaller, as illustrated in Fig. 17.17. Tab. 17.4 summarises the results on the imaginary part of the effective horizontal and vertical impedances, as calculated from Eq. 17.1 for several series of measurements in the years 2000 and 2001. The errors quoted were obtained from the spread of results within one year. Details are given in [32,33].

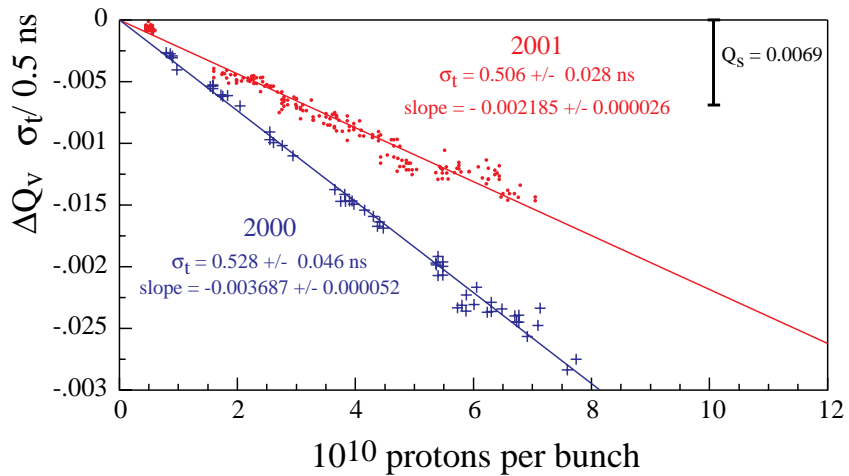


Figure 17.16: Comparison of measured coherent tune shifts (normalised to bunch length) with intensity in the vertical plane in the years 2000 (before) and 2001 (after) the major part of the impedance reduction campaign.

Table 17.4: $\text{Im } Z_{\perp}$ from the coherent tune shift with intensity.

Year	$\text{Im } Z_x \text{ M}\Omega/\text{m}$	$\text{Im } Z_y \text{ M}\Omega/\text{m}$
2000	-0.9 ± 1.8	26 ± 3
2001	-0.35 ± 0.53	18.4 ± 0.5

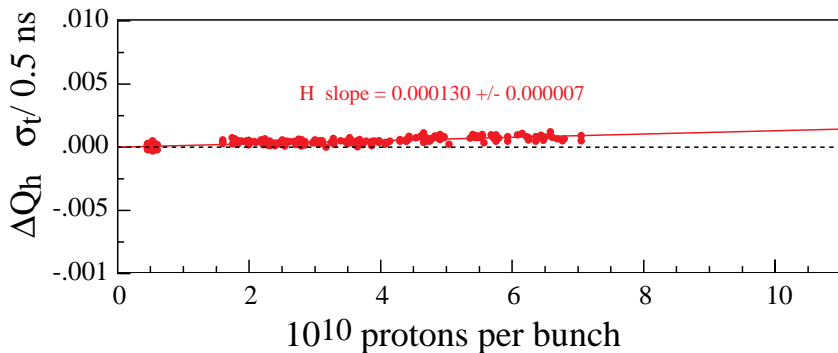


Figure 17.17: Coherent tune shift (normalised to bunch length) vs. intensity in the horizontal plane recorded in 2001.

A significant transverse impedance reduction, of the order of 40% was observed between the years 2000 and 2001. Measurements in the year 2003 indicated an increase in the transverse impedance compared to the year 2001, resulting in a partial cancellation of the impedance reduction achieved previously. This may be attributed to the installation of kickers needed for the extraction towards the LHC.

A very fast single bunch transverse beam instability has in fact been observed in the SPS at injection energy for nominal LHC injection intensities and reduced longitudinal emittances [34,35]. A further effort to reduce the transverse SPS impedance may be needed to guarantee the stability in the SPS of ultimate LHC intensities.

17.7 BEAM INDUCED HEATING

17.7.6 Kickers

Introduction

The real part of the longitudinal impedance of the ferrites installed in the SPS kickers can lead to significant beam induced heating of the magnets. Fig. 17.18 shows the temperature variation during the SPS scrubbing runs in 2004 measured on the MKE extraction kickers, installed in LSS4. The temperatures are measured on the ceramic spacers which touch the ferrites. If a part of the ferrite itself reaches temperatures above the Curie temperature, around 125°C, it loses its magnetic properties and the magnetic field strength will be reduced. Structural damage to the kicker magnets cannot be excluded for temperatures above 150°C. For a measured temperature of about 80°C it is expected that the part of the ferrite close to the beam reaches the Curie temperature. Presently the beam in the SPS is aborted if the measured MKE temperature reaches 90°C.

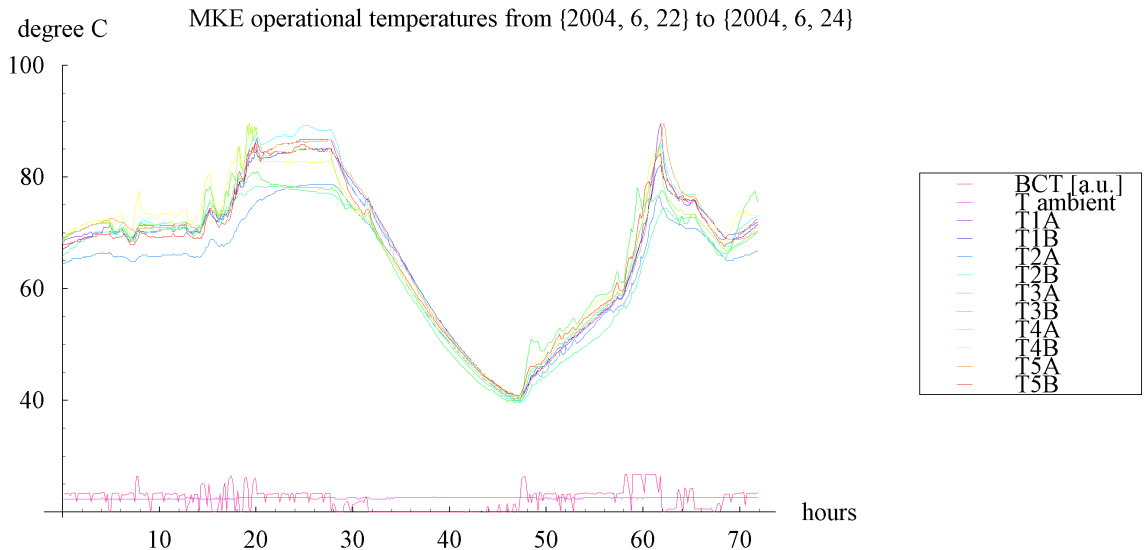


Figure 17.18: Measured MKE temperatures on the ceramic spacers during the 2004 scrubbing run.

Impedance of the MKE kicker magnet

The longitudinal coupling impedance of the ferrites of the different SPS kicker magnets can be calculated as a function of the frequency with the model as presented in [36], taking into account the metal conductors in the horizontal plane. The ferrites used are of the low conductivity NiZn family (type 8C11). In the model the initial relative permeability $\mu_r=460$, $\epsilon_{r,i}=12$ and a maximum frequency for ferri-magnetic losses of 9.8 GHz are used.

The calculated impedance for the MKE magnet has been compared with wire measurements using the log formula for impedance evaluation [37], see Fig. 17.19. It shows a good agreement, although the characteristic impedance of the wire (about 200Ω) is much lower than the distributed impedance of the magnet to be measured (up to $4 k\Omega$).

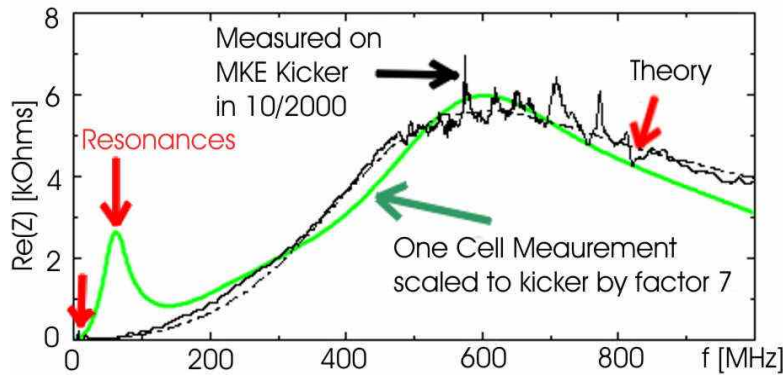


Figure 17.19: Single MKE kicker cell impedance measurements compared to the measurement of a complete 7 cell magnet and calculations [38].

Machine measurements: Spectra

To calculate the power deposition in the magnet the impedance needs to be multiplied with the bunch spectrum and by assuming a Gaussian bunch spectrum, the deposited power can be calculated. For acceleration of a nominal LHC beam in the SPS, the power deposition calculated is about 700 W/m in the MKE magnets, assuming a bunch length (1σ) of 0.5 ns, 4 batches of 72 nominal LHC bunches of 1.1×10^{11} protons each and a duty factor of 0.5. The duty factor is an important parameter, as the bunch length will shorten during acceleration generally, whilst the simple calculation is made for a constant bunch length. The bunch length and its distribution are therefore critical and often unknown variables.

It is preferable to use measured bunch spectral amplitudes to calculate the deposited power instead of assuming a Gaussian, or any other kind of distribution. The power spectra at the harmonics of the bunch spacing frequency of 40 MHz up to 1 GHz have been measured throughout the cycle during SPS operation with an LHC beam. These spectra can then be multiplied with the impedance of the magnets as given in Fig. 17.19. The resulting power as a function of time in the SPS cycle is shown in Fig. 17.20 for 2003 and 2004 data. The 2003 curve shows the spikes caused by the four injections into the SPS. After the fourth injection the power increases due to the shortening of the bunch length during acceleration. The calculated average power deposited during the 21.6 s cycle is 467 W/m for the MKE magnets (measured for 4×72 bunches, 1.2×10^{11} protons per bunch). The 2004 curve shows a longer super cycle with two injections and no acceleration and an average power of 243 W/m.

Fig. 17.20 also shows the measured spectral amplitudes for the different frequencies together with a Gaussian distribution before acceleration (2003 data). It clearly shows that a Gaussian distribution is not a realistic representation. The 0.5 ns bunch length used in the calculations for the LHC beam presented above, leads to higher estimated powers than deduced from the measured bunch spectra, although the impedance is high between 400 MHz and 1 GHz.

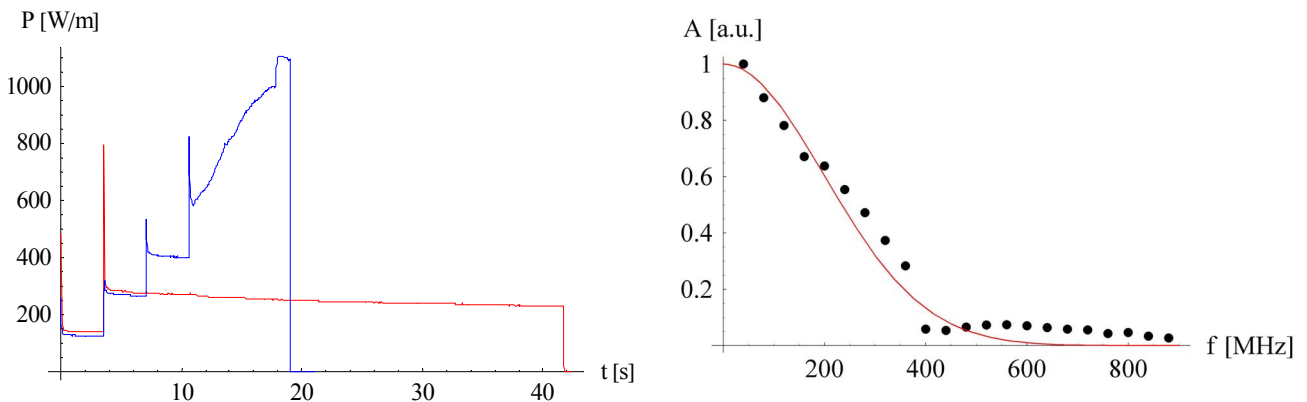


Figure 17.20: Deposited power in an MKE magnet, calculated from measured spectral amplitudes during an SPS cycle (left) and the comparison of measured spectral amplitudes at $t=4$ s into the cycle (dots) and a Gaussian bunch distribution with $\sigma = 0.8$ ns (right).

Cooling of the MKE kickers

Calculations and laboratory measurements have shown that it would be impossible to operate the MKE magnets with nominal CNGS and LHC beams over longer periods without additional cooling, as the ferrites would reach the Curie temperature. For this reason the newly installed MKE kicker magnets are equipped with water-cooled aluminium nitride plates which are in good thermal contact with the ferrites, see Fig. 17.21. Temperature probes are positioned on the outside of the ferrites. A finite element model of the magnet including its cooling system has been made to optimise the design and estimate its performance [39].

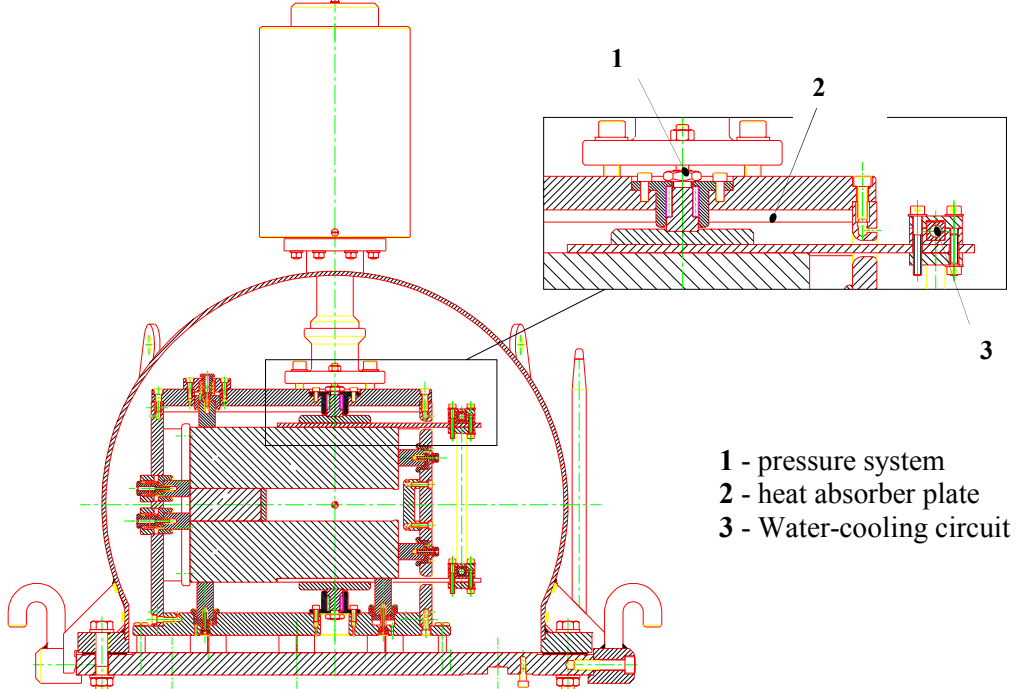


Figure 17.21: The MKE water-cooling system with aluminium nitride plates for the heat transfer between the ferrites and water-cooling tubes.

After heating of the MKE magnets with beam in the SPS, the kick strength of a magnet was evaluated by measuring the amplitude of the beam position oscillation induced by a single kick for different ferrite temperatures. The results are shown in Fig. 17.22. The horizontal axis is the temperature measured on the MKE magnet, which is not the highest temperature inside the ferrite. For the MKE magnet it can be seen that from a measured temperature of about 80°C upwards the kick strength is reduced, indicating that the core of the ferrite has reached the Curie temperature.

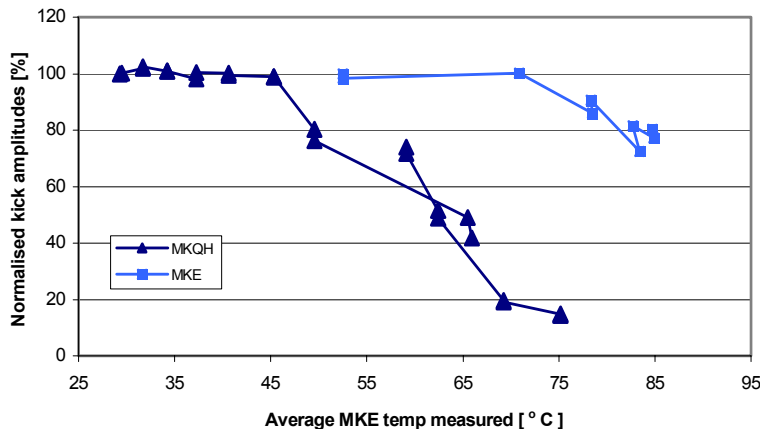


Figure 17.22: MKE and MKQH kick strength measured by the beam for different measured MKE kick temperatures.

Fig. 17.22 also shows measurements for the MKQH magnet, the horizontal Q kicker in the SPS. It is basically identical to the MKE magnet but not equipped with water-cooling. The kick strength of this magnet is reduced for temperatures above about 45°C measured at the MKE temperature probe. This indicates that the cooling system allows more than twice the power to be deposited in the magnet before the Curie temperature is reached.

Operational scenarios for MKE

The calculated power deposition of 243 W/m during the 2004 scrubbing run quoted above led to a measured equilibrium temperature of the ferrites of about 80°C (Fig. 17.18). From kick measurements it is also known that at this temperature the core of the ferrite reaches the Curie temperature and the kicker is no longer operational. Using this calibration of equilibrium temperature versus deposited power, scenarios can be made for SPS operation with alternating LHC and CNGS beams [40,41]. Generally, the operation of the SPS with nominal LHC beams would lead to an equilibrium temperature well above the Curie temperature, while for the operation with nominal CNGS beams, the expected equilibrium temperature will be below the Curie temperature. As the filling of the LHC is expected to be relatively short compared to CNGS operation, the maximum operational temperature is expected to be below the Curie temperature. A possible operational scenario is illustrated in Fig 17.23. Here alternating LHC filling and CNGS operation is assumed. Two hours of LHC filling with nominal beam, with an expected equilibrium temperature of 163°C, is alternated with nominal CNGS operation for 10 hours, with an equilibrium temperature of 78°C. In this case the expected maximum ferrite temperature reached is around 105°C. Presently it is only during the scrubbing runs that the maximum temperature of the MKE kickers allowed poses an operational limit to the SPS. For CNGS and LHC beams above nominal intensities, the MKE temperatures could possibly limit operation as well.

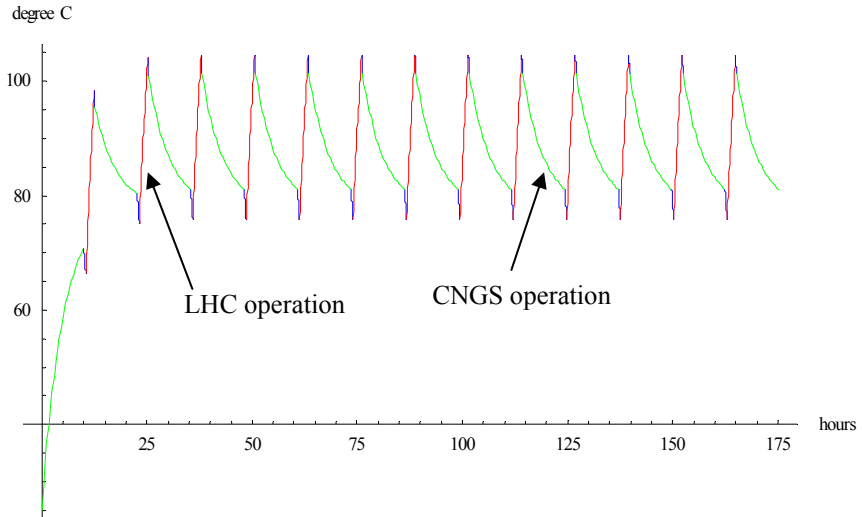


Figure 17.23: Maximum MKE ferrite temperatures for an SPS operational scenario, alternating LHC filling and CNGS operation.

Other SPS kicker magnets

The impedance of the MKE and MKQA kicker magnets is larger than any of the other ferrite loaded kicker magnets in the SPS, due to their ratio of horizontal and vertical apertures. Tab. 17.5 gives an overview of the expected power deposition of a nominal LHC beam for a theoretical 0.5 ns ($1\ \sigma$) Gaussian beam and assuming a duty factor of 0.5, calculated with the method as described in [36]. The modified injection kicker magnets, MKP-S, have two temperature probes and indicate far lower temperatures than the ones measured for the MKE modules. This agrees with the expected deposited power as mentioned in the table. The MKP-L module is presently not equipped with temperature probes. The value quoted for the MKQH magnet is without the recently installed resistive layer coated ceramic inserts [42]. With these inserts the longitudinal impedance is significantly reduced and no kick strength reduction was observed with MKE temperatures measured up to 90°C.

Table 17.5: Deposited power for a 4×72 LHC type bunches (bunch intensity 1.1×10^{11}), a Gaussian bunch length of 0.5 ns and an overall duty cycle of 0.5. The MKQH value is without the newly installed shielding.

Magnet Type	Full H-aperture [mm]	Full V-Aperture [mm]	Power [W/m]
MKE-L	147.7	35	700
MKE-S	135	32	664
MKP-S	100	61	79
MKP-L	140	54	278
MKQH	135	34	598
MKQV	102	56	101
MKDV I	75	56	37
MKDV II	83	56	52
MKDH	No ferrites		

REFERENCES

- [1] D. Boussard, G. Dome, T. Linnecar & A. Millich, “*Longitudinal phenomena in the CERN SPS*”, IEEE Trans. on Nucl. Scie., NS-24 (3), p. 1399, 1977.
- [2] L. Evans & J. Gareyte, Performance limitations of the CERN SPS collider, CERN SPS/85-15 (DI-MST), 1985.
- [3] “*The SPS as Injector for LHC: Conceptual Design*”, Ed. P. Collier, CERN-SL-97-07 DI, 1997.
- [4] T. Bohl, T. Linnecar & E. Shaposhnikova, “*Measuring the resonance structure of accelerator impedance with single bunches*”, Phys. Rev. Lett., v. 78, p. 3109, 1997.
- [5] T. Linnecar & E. Shaposhnikova, “*Resonant impedances in the SPS*”, CERN SL-Note 96-49 RF, 1996.
- [6] W. Hofle, “*Calculations of longitudinal modes in the SPS inter-magnet pumping ports*”, CERN SL-Note 96-40 RF, 1996.
- [7] Shielding design was done by F. Caspers and A. Rizzo.
- [8] E. Shaposhnikova, “*The 400 MHz instability - where are we?*”, Proceedings of the LHC Performance Workshop, Chamonix XI, p. 78, CERN-SL-2001-003 DI, 2001.
- [9] F. Caspers, C. Gonzalez, M. D'yachkov, E. Shaposhnikova & H. Tsutsui, “*Impedance measurement of the SPS MKE kicker by means of the coaxial wire method*”, CERN PS/RF/Note 2000-004, 2000.
- [10] T. Linnecar, “*Progress with LHC beams in the SPS seen from the Faraday Cage*”, Proceedings of the LHC Performance Workshop, Chamonix XI, p. 58, CERN-SL-2001-003 DI, 2001.
- [11] T. Bohl, “*LHC type beams in the SPS. Bunch length and longitudinal emittance*”, Proceedings of the LHC Performance Workshop, Chamonix XI, p. 73, CERN-SL-2001-003 DI, 2001.
- [12] D. Boussard, E. Chiaveri, H. P. Kindermann, T. Linnecar, S. Marque & J. Tuckmantel, “*Design considerations for the LHC 200 MHz RF system*”, LHC Project Report 368, 2000.
- [13] T. Bohl, M. Lamont, T. Linnecar, W. Scandale & E. Shaposhnikova, “*Measurement of the effect on single bunch stability of changing transition energy in the CERN SPS*”, Proceedings of the 1998 European Particle Accelerator Conference, Stockholm, Sweden, EPAC 1998.
- [14] F. Sacherer, “*Single-beam collective phenomena, transverse, bunched beams*”, Proceedings of the 1976 Erice school on accelerators, M.H. Blewett (Ed.), CERN yellow report 77-13, (1977) p.198 ff.
- [15] J. Gareyte, “*Impedances: Measurements and Calculations for Non-symmetric Structures*”, Proceedings of the 2002 European Particle Accelerator Conference, Paris, France, EPAC 2002 and CERN-SL-2002-028.
- [16] E. Shaposhnikova, “*Signatures of the Microwave Instability*”, CERN-SL-99-008 HRF.
- [17] E. Shaposhnikova, “*Present Knowledge of the Longitudinal SPS Impedance*”, CERN/SL-2000-007 DI.
- [18] B. de Raad, “*Shielding the SPS Against Synchrotron Radiation*”, CERN SL/90-119 (DI), 1990.
- [19] M. Albert et al., Resonance Driving Terms experiment in the SPS at 26GeV in 2001, SL-Note-2001-035-MD, CERN, 2001.
- [20] R. Guinand, Supply of 20 large cylindrical ultra-high vacuum tanks in stainless steel for the SPS extraction system, CERN EDMS 113654, 2000.

- [21] E.Shaposhnikova, T.Bohl, ‘*Results from the impedance reduction in the CERN SPS*’, Proc. 20th ICFA Advanced Beam Dynamics Workshop on High Intensity and High Brightness Hadron Beams ICFA-HB2002, Batavia, pp 62-64, 2002.
- [22] F.Caspers, A.Mostacci, H. Tsutsui, *Impedance Evaluation of the SPS MKE Kicker with Transition Pieces between the Tank and Kicker Module*, CERN-SL-2000-071 (AP), October 2000.
- [23] T. Bohl, T. Linnecar & E. Shaposhnikova, “Impedance reduction in the CERN SPS as seen from longitudinal beam measurements”, Proceedings of the 2002 European Particle Accelerator Conference, Paris, France, EPAC 2002.
- [24] “RF system and longitudinal beam dynamics”, chapter 16 of this Report.
- [25] T. Linnecar & E. Shaposhnikova, “Microwave instability and impedance measurements in the CERN SPS”, Part. Acc., 1997, v. 58, p. 241.
- [26] P. Collier, M. Ainoux, R. Guinand, J. M. Jemenez, A. Rizzo, A. Spinks & K. Weiss, “Reducing the SPS impedance”, Proceedings of the 2002 European Particle Accelerator Conference, Paris, France, EPAC 2002.
- [27] F. Caspers, A. Mostacci & H. Tsutsui, “*Impedance evaluation of the SPS MKE kicker with transition pieces between tank and kicker module*”, CERN SL-2000-071 (AP), 2000.
- [28] L. Vos, “*Computer calculation of the longitudinal impedance of cylindrically symmetric structures and its application to the SPS*”, CERN SPS/86-21 MS, 1986.
- [29] P. Baudrenghien, T. Bohl, T. Linnecar, E. Shaposhnikova & J. Tuckmantel, “*Nominal longitudinal parameters for the LHC beam in the CERN SPS*”, Proceedings of the Particle Accelerator Conference, Portland, Oregon, USA, PAC 2003.
- [30] G. Arduini et al., ‘*Measurements of the SPS transverse impedance in 2000*’, Prepared for IEEE Particle Accelerator Conference (PAC 2001), Chicago, Illinois, 18-22 Jun 2001.
- [31] H. Burkhardt, G. Rumolo & F. Zimmermann, “*Coherent beam oscillations and transverse impedance in the SPS*”, Proceedings of the 2002 European Particle Accelerator Conference, Paris, France, EPAC 2002 and CERN-SL-2002-030.
- [32] G. Arduini, H. Burkhardt, F. Zimmermann & M. Zorzano, “*Measurements of the SPS single bunch coherent tune shifts and head-tail growth rates in the Year 2000*”, CERN, SL-Note-2001-002 MD.
- [33] H. Burkhardt, G. Rumolo & F. Zimmermann, “*Measurements of SPS Single-Bunch Coherent Tune Shifts and Head-Tail Growth Rates in the Year 2001*”, CERN, SL Note 2001-043 (MD), 7-12-2001.
- [34] G. Arduini, H. Burkhardt & E. Métral, “*Observation of a fast single bunch instability on protons in the SPS*”, CERN AB-Note-2003-093 (MD), Dec. 2003.
- [35] H. Burkhardt, G. Arduini, E. Benedetto, E. Métral & G. Rumolo, “*Observation of a Fast Single-Bunch Transverse Instability on Protons in the SPS*”, Proceedings of the 2004 European Particle Accelerator Conference, Lucerne, Switzerland, EPAC 2004.
- [36] H. Tsutsui, *Some Simplified Models of Ferrite Kicker Magnet for Calculation of Longitudinal Coupling Impedance*, CERN-SL-2000-004 AP.
- [37] A.W. Chao, *Handbook of Accelerator Physics and Engineering*, World Scientific Publishing, 1999, p. 570.
- [38] F. Caspers, *SPS Kicker Impedance Measurement and Simulation*, CERN-SL-2000-007 DI, January 2000.
- [39] M. Timmins, A. Bertarelli, J. Uythoven, E.H. Gaxiola, *SPS Extraction Kicker Magnet Cooling Design*, CERN AB-Note-2004-05-BT, January 2004.
- [40] J. Uythoven, minutes of APC meeting 3 October 2003.
- [41] J. Uythoven, minutes of APC meeting 17 September 2004.
- [42] F. Caspers, E. Gaxiola, T. Kroyer, M. Timmins, J. Uythoven, “*A Retrofit Technique for Kicker Beam-Coupling Impedance Reduction*”, proceedings EPAC 2004, Luzern, also CERN-AB-2004-048; Geneva.

CHAPTER 18

EXTRACTION TOWARDS THE LHC

18.1 INTRODUCTION

Two fast extraction systems are required in the SPS to deflect the 450 GeV proton and ion beams into the transfer lines and then to the LHC. This chapter describes the requirements, the equipment used, the modifications to the existing systems and the performance aspects of the extraction channels.

The proton and lead ion beams for the anti-clockwise ring (beam 2) of the LHC will be extracted using a new system built in LSS4 and transferred to LHC Point 8 via the transfer line TT40-TI8. The same extraction channel will be used to transfer protons to a neutrino target for the proposed long baseline Neutrino to Gran Sasso (CNGS) project.

For the clockwise LHC ring (beam 1), the existing extraction channel in LSS6 will be modified, for beam transfer to the LHC point 2 via the transfer line TT60-TI 2. The existing resonant extraction system will be upgraded for fast extraction only.

18.2 REQUIREMENTS

Conventional fast extraction will be used in both LSS4 and LSS6 with horizontal closed orbit bump, fast kicker and magnetic septum. Vertical closed orbit bumpers will also be used for precise vertical beam positioning at high energy. For LSS4, additional requirements are imposed by CNGS, including the need for a sequence of two fast extractions. The general requirements that must be satisfied are:

- A large enough aperture for injected, bumped and circulating beam
- Loss-free fast extraction of the entire 8 μ s long LHC type beam
- Compatible with FT beams for CNGS and resonant extraction in LSS2

18.2.1 LSS4

In the long straight section LSS4 of the SPS a new conventional fast extraction [1,2,3] has been installed using horizontal closed orbit bumpers, extraction kickers and conventional DC electromagnetic septum magnets (MSE) located just after the quadrupole QFA418. The beam is moved close to the MSE using a horizontal closed orbit bump and is then kicked horizontally across the septum, with the kicker field rising during a gap in the circulating beam. The extraction septum then deflects the beam out of the SPS vacuum chamber and into the transfer line TT40, with the required position and angle. The extraction channel in LSS4 requires the installation of five kickers MKE, eight bumper magnets, three enlarged quadrupoles (QDA417, QFA418 and QDA419), an absorber TPSG (dummy septum) and six extraction septum magnets, for which the existing design of the 17 mm thick MSE septum is used. The extraction has been designed for two different proton beams, LHC and CNGS. The Pb⁸²⁺ beam for LHC is considered as having the same transverse dimensions as the proton beam and as such is not considered explicitly.

18.2.2 LSS6

The extraction channel in LSS6 has been in use for many years for the resonant extraction of beams towards experiments in the west area. After the closure of this area at the end of 2004, the extraction system will be upgraded for LHC [4] with removal of the electrostatic ZS septa, modification of the girder for the existing DC septa, addition of extraction kickers and other modifications concerning the replacement of a machine quadrupole, a new scheme for the extraction bumpers, new instrumentation and interlocks. The extraction uses the existing MST and MSE septum magnets, located before and after the quadrupole QFA618. The beam is moved close to the MST septum using a horizontal closed orbit bump and is then kicked horizontally across the septum, with the kicker field rising during a gap in the circulating beam. The extraction septum then deflects the beam out of the SPS vacuum chamber and into the transfer line TT60, with the required position and angle. The upgrade of the extraction channel in LSS6 requires the installation of four kickers MKE, bumpers, the removal of one enlarged quadrupole (QFA416), an absorber TPSG

(dummy septum) and the modification of the bumper magnet system. The new fast extraction channel in LSS6 will be used only for small emittance LHC beams.

18.3 EXTRACTION EQUIPMENT SYSTEMS

The modification or construction of several equipment systems is necessary for the extraction channels. These are listed in the following sections.

18.3.1 Horizontal Bumper Systems

For each extraction, four horizontal bumper magnets will be used at locations near QFx14, x16, x20 and x22, to allow an adequate closed orbit bump at the entrance of the septum. The largest horizontal bump that could be envisaged in operation is about 60 mm at the entrance to the MSE septum (determined by the 90 mm good field limit in QFA418, the septum thickness and the required clearances). With this size bump there is about 25% strength remaining for horizontal orbit correction up to about ± 20 mm at QFAX18. All power supplies are 400 A, 700 V as specified in [5]. The rather unfavourable position of HB2 with β_x of around 50 m is a consequence of the location of the extraction kickers in this half-cell which, because of their limited strength, have to be located as close as possible to QFx16.

18.3.2 Vertical Bumper System

Vertical bumper magnets installed at locations near QDx13, x15, x21 and x23 will allow a vertical orbit correction of ± 15 mm at QD419. A vertical correction of ± 8 mm is possible at the septum in half-cell 418. All power supplies are 80 A, 200 V [5]. The obvious location at x17 is not possible, since an enlarged bumper magnet aperture would here be necessary, requiring a new design.

18.3.3 Kickers

For LHC and CNGS the existing MKE kickers are upgraded and/or renewed [6,7] to meet the specifications, as shown in Tab. 18.1. For LSS4, the extraction towards CNGS needs two extractions per SPS-cycle, requiring a rise time / fall time of less than 1.1 μ s and a flat-top of 10 μ s. For LHC there is only have one extraction per SPS-cycle, requiring a flat top length of 8 μ s. In LSS6 the rise-time can be much longer since this extraction channel is only for LHC extraction. The MKE kicker system is a characteristically terminated travelling wave system, powered by a resonant charging circuit consisting of two parallel 2 kV 50Hz AC. power supplies. These charge two capacitor banks, which feed a 60 kV step-up transformer via (safety) thyristors. The resonant charging circuit is connected to the pulse forming networks (PFNs) via a capacitor, diode and resistor auxiliary circuit permitting switch-off and over-voltage limitation. Extraction is triggered by a pre-pulse to the resonant charging supply, charging the PFNs to the required voltage. After this the “main” thyratron switches are triggered, discharging the PFNs into the magnets and terminating magnet resistors (TMR). For LSS4, the fall time requirements mean that five “clipper” switches are used to cut the magnetic field and dump the remaining PFN energy into the diode-stack and Terminating Dump Resistor (TDR). For CNGS the second extraction starts with recharging the PFN with the second capacitor bank.

The usual thyratron (gas discharge) “dump” switches are replaced by semiconductor power diodes to reduce long term costs and improve lifetime and reliability. In LSS4, if a switch “missing” (switch doesn’t close when triggered) or “erratic” (switch closes without being triggered) occurs, all clipper switches are triggered to protect the septa [2].

To meet the rise/fall time specification, several changes to the existing MKE design have been made, including modification/adjustment of the PFN front cells, sorting of PFN capacitor/coil section values and magnet and TMR wave impedance matching. In addition, two capacitive pick-ups are installed per magnet enabling measurement of the “kick” when installed in the SPS machine [8]. These diagnostics give a detailed picture of the “kick” field rise, fall and pulse length (flattop) times including the magnet filling time and the overshoot. The extraction kicker system will be equipped with PT100 temperature probes to provide an interlock for the loss of ferrite permeability above the Curie temperature.

For the proposed LHC and CNGS beam-operating conditions, the SPS extraction kickers will be exposed to a large beam induced thermal power. The ferrites will be heated due to the high frequency polarisation (power losses) of the magnetic dipole moments. Above the Curie-temperature the spontaneous magnetisation disappears and the material becomes paramagnetic. To cope with the ferrite heat dissipation cooling measures are implemented and the magnets are equipped with water-cooled AlN cooling plates on the top and bottom of the ferrites [8]. More details are given in Chap. 17. Fig. 18.1 shows a cross section of the MKE magnet with the cooling plates.

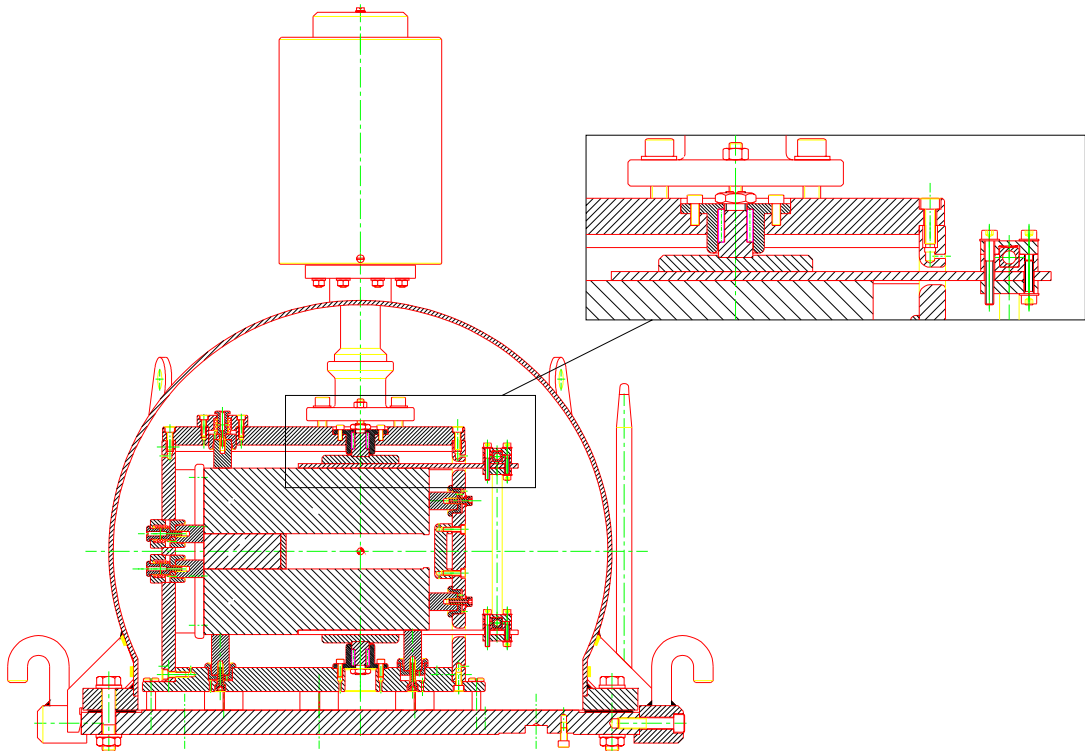


Figure 18.1: Cross-section of the MKE kicker magnet, with the cooling system detail enlarged.

18.3.4 Absorber or Dummy Septum

To protect the first extraction element from the impact of a mis-steered beam, an absorber TPSG (dummy septum) will be installed just upstream of the first MST or MSE. This element will serve to dilute the beam to a safe level in the event of an accidental mis-steering. Direct impact of a small fraction (approximately 2×10^{12} protons or 5%) of the extracted beam intensity could damage or destroy one or more septum magnet coils. A comprehensive interlock system is required to survey the beam positions, beam losses, bumper and septum currents, kicker charging voltages, etc. However, operator error can never be excluded and several other modes of failure are also possible. Therefore, a physical protection element, the TPSG, has been placed immediately upstream of the first septum coil to reduce the particle flux on the coil to a safe level, such that the temperature in the copper does not exceed 100°C. In addition, the instantaneous temperature rise in the cooling water should not exceed 10°C.

For LSS4 the 2.9 m TPSG4 absorber [9] is a composite shield made up from 2.1 meter of graphite and 0.8 meter of aluminium alloy, installed in a 2.9 meter long solid stainless steel core of 250 mm x 300 mm cross-section similar to the MSE laminated yoke. The absorber element consists of 10 units of 210mm long isostatic pressed graphite bars (density 1.77 g/cm³) with a cross-section of 19.25 mm x 30 mm and 1 unit of 800 mm long DIN AlMgSi0.5 type aluminium alloy bar (density 2.7g/cm³) having the identical cross-section as the graphite parts. Simulations of the conditions to which the absorber will be subjected have shown the maximum temperatures remain safely below the melting point. However, the maximum equivalent stresses may slightly exceed the elastic limit in the aluminium section of the diluter and a new design will be needed,

based on the absorber for LSS6. It should also be noted that beam losses on the absorber and MSE septa will generate high radiation levels for which sufficient shielding must be provided [10].

For LSS6, the TPSG6 will use graphite to dilute, followed by titanium and Inconel to absorb the energy [4]. To keep the absorber relatively easy to handle, it will be constructed as a set of 2 consecutive absorbing blades, each within its own vacuum envelope. The total longitudinal length between flanges of this assembly will be limited to 4 m. The absorbing elements will be edge cooled with a copper tube connected to the demineralised water circuit available on the MST girder. This cooling circuit will limit the temperature rise caused by beam losses during normal operation, as well as remove the energy deposited in the absorbing elements after a beam sweep or impact.

Table 18.1: MKE kicker parameters.

Parameter	Unit	MKE-L	MKE-S
Number of magnets (LSS4)		3	2
Number of magnets (LSS6)		2	2
Vertical gap	Mm	35	32
Horizontal gap	Mm	148	135
Nominal voltage	kV	52	52
Nominal field	T	0.0702	0.0772
Magnetic length	Mm	2174	2174
$\int B \cdot dl$ max	Tm	0.1525	0.1678
Kick at 450 GeV/c	Mrad	0.1017	0.1118
Kick / kV at 450 GeV/v	μ rads / kV	1.956	2.151
2-98% rise time (LSS4)	μ s	1.1	1.1
2-98% rise time (LSS6)	μ s	5.0	5.0
98%-2% fall time (LSS4)	μ s	1.1	1.1
98-2% fall time (LSS6)	μ s	5.0	5.0
Flat-top duration (LHC)	μ s	7.9	7.9
Flat-top duration (CNGS)	μ s	10.5	10.5
Flat-top ripple (LHC)	%	\pm 0.5	\pm 0.5
Flat-top ripple (CNGS)	%	\pm 1.0	\pm 1.0

18.3.5 Septum Magnets

The magnetic septum must deflect the beam by about 12 mrad and must also give the required 265 mm offset and 10 mrad exit angle at the extraction point. The extraction uses six of the DC septa, MSE [11,12] already installed in the extraction channels in LSS2 and LSS6. This approach has the advantage of using proven equipment and also keeping the number of sub-systems to be maintained to a minimum. The performance of the equipment is well known and the construction straightforward. The main parameters of the MSE magnets are given below in Tab. 18.2. The six MSE magnets are mounted on a single rigid girder, pre-aligned to follow the trajectory of the extracted beam and optimise the aperture available [13]. A cross-section of the system configuration in extraction channel LSS4 is shown in Fig. 18.2.

The magnets, pumping modules (MP) and TPSG diluter are mounted on a 23 m long rigid support girder using adjustable support feet, allowing horizontal and vertical alignment. The support girder is assembled from seven elements connected together by intermediate joining plates. Each standard girder element is 3.3 m long and consists of a welded structure made of 260×180×10 mm MSH profiles. To allow vertical alignment, each element is equipped with 4 adjustable jacks, which stand on low-friction ball bearings. The complete girder is motorised in order to retract the septum and optimise the local SPS aperture during

machine setting up. This retracted position is achieved by a girder movement of 35 mm upstream and -10 mm downstream, with a precision and reproducibility of ± 0.1 mm using two independent motors.

The magnets positions on the girder are pre-aligned to the trajectory of the extracted beam in order to give it a maximum aperture. The longitudinal position of the two motors has been carefully chosen and confirmed by ANSYS calculations to minimise the flexion of the girder, which will occur due to the friction of the ball bearings, mechanical resistance of the water-cooled cables and tension of the vacuum bellows at the quadrupoles.

Table 18.2: MST and MSE Septum magnet parameters

Parameter	Unit	MST	MSE
Septum thickness	mm	4.2	17.25
Gap height	mm	20	20
Maximum field	T	0.471	1.508
Kick at 450 GeV/c	mrad	0.702	2.249
Magnetic length	m	2.247	2.237
$\int B \cdot dl$ max	Tm	1.0583	3.373
Peak current	A	7,500	24,000
$\int B \cdot dl / I$	Tm/A	$1.41 \cdot 10^{-4}$	$1.41 \cdot 10^{-4}$
Magnet spacing (centre)	mm	3,234	3,234

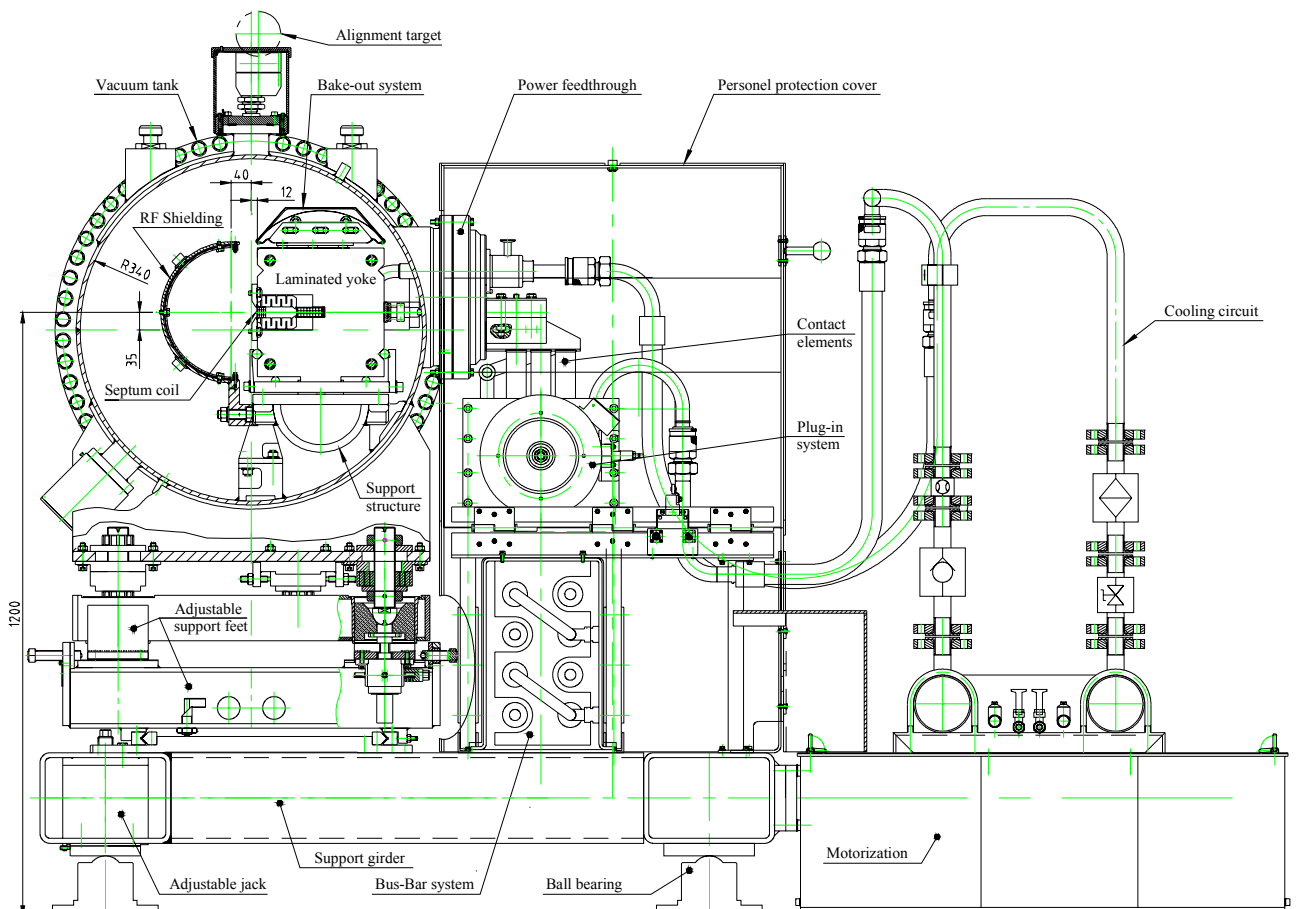


Figure 18.2: Cross section of MSE extraction septum showing vacuum tank, alignment girder, hydraulic and electrical connections.

18.3.6 Beam Instrumentation

The extraction channels are equipped with screens on the septum girder at the beginning of the first and end of the last septum magnets. Beam loss monitors are installed along the extraction channel, at the extraction element locations. For the circulating beam, large aperture BPCE couplers are installed on the quadrupoles in the extraction region, to accurately measure the bumped beam position [14]. The linearity and stability of the system should allow interlocking of the bumped beam position to within 0.5 mm. More details of the instrumentation are given in Chap. 19.

18.3.7 Main Ring Magnets

In LSS4 the main machine quadrupoles QD417, QF418 and QD419 with good field regions extending to 70 mm have been replaced by enlarged quadrupoles. QFA418 must have an enlarged aperture (90 mm good field region) to accommodate large beam excursions and QDA419 will be an enlarged quadrupole with a coil window through which the extracted beam passes. The field in this window is quadrupolar (F-quad), with a gradient of -0.16 of the main gap and an axis displaced by 0.3009 m [15]. In LSS6 the enlarged quadrupoles exist already in these locations; the QFA616 must be replaced by a normal QF in order to optimise the downstream kicker position.

18.3.8 Radiation Protection

In LSS4 some modifications are necessary to improve the radiation shielding between ECX4 and ECA4. The existing access chicane has been modified to increase the safety factor in the case of beam loss in the extraction and precautions in ECX4 taken concerning access during operation [16]. Beam loss monitors should help minimise losses during extraction and activation monitors are also planned.

18.4 TRAJECTORIES

The trajectories were calculated using MAD and the optimum extraction angle and position obtained. The constraints imposed were a flat orbit outside the extraction bump, a horizontal extraction bump of the required amplitude at the septum and that the maximum beam excursion in QFA418 should not exceed 89 mm (good field region of the quadrupole). The required element strengths are shown in Tab 18.3. The extraction uses a ‘slow’ (of the order of a hundred ms rise time) closed orbit bump to move the circulating beam near to the septum at extraction energy. During this time the field of the septum is also ramped up. At the correct timing the extraction kicker MKE is powered and the beam deflected into the gap of the septum.

The layouts of the extraction channels have been optimised with the present equipment parameters, to maximise the aperture available for the injected, circulating and extracted beams. Fig. 18.3 and Fig. 18.4 show the horizontal trajectories through the LSS4 and LSS6 extraction for the LHC beam at injection, at maximum bump amplitude and during extraction. A $\pm 3\sigma$ beam envelope is plotted.

Table 18.3: Nominal strengths of extraction elements (mrad).

Element	LSS4 LHC	LSS4 CNGS	LSS6 LHC
HB1	-0.002	-0.001	0.000
HB2	0.565	0.5004	0.438
HB3	0.383	0.339	0.320
HB4	0.162	0.144	0.090
MKE-S	0.100	0.110	0.102
MKE-L	0.110	0.121	0.112
MST	-	-	0.535
MSE	2.078	2.083	1.827

In the vertical plane the contributions to the error in the beam position through the septum magnet come from the alignment of the machine quadrupoles and the quality of the closed orbit. At present in the SPS in fixed-target operation the total rms of the closed orbit in the vertical plane is of the order of 2.5 mm. Since the vertical bumper system will be used to adjust the orbit to compensate for long-term drifts, the somewhat pessimistic assumption is made that the maximum vertical orbit error at the septum is $O_y = \pm 2$ mm.

In the horizontal plane the septum position can be adjusted, to reduce the orbit error contribution. The assumption is made that at injection $O_x = \pm 4$ mm and at high energy $O_x = \pm 1$ mm. Taking the contributions from the pulsed horizontal bending elements, the bumpers and kickers, these two systems together add another ± 0.4 mm error. The maximum horizontal orbit error is then $O_x = \pm 1.4$ mm at extraction.

There are several sources of mechanical imprecision or instability which contribute to the overall mechanical tolerance to be assumed for the calculation of the beam aperture. For the MSE system these are estimated as follows:

- Single MSE magnet septum mechanical precision (± 0.5 mm)
- Tolerance between MSP assembly in vacuum tank and external alignment socket (± 0.1 mm)
- Initial alignment of magnets on girder (± 0.1 mm)
- Short- and long-term stability of the SPS tunnel floor in LSS4 (± 0.3 mm)

Adding these figure gives a maximum possible mechanical error in both horizontal and vertical planes of $M_y = M_x = \pm 1.0$ mm.

18.5.2 Vertical Aperture at Extraction

The extracted beam must pass within the gap of the septum magnet, which is kept as small as possible to minimise the current required to produce a given field. Assuming zero local vertical dispersion and a vertical aperture of A_y , the aperture N available in numbers of beam sigma is given by:

$$N_y = (A_y / 2 - O_y - M_y) / (K_\beta (\beta \epsilon_y)^{1/2})$$

The aperture available in the vertical plane at extraction is shown in Fig. 18.5 and Fig 18.6, for LSS4 and LSS6 respectively.

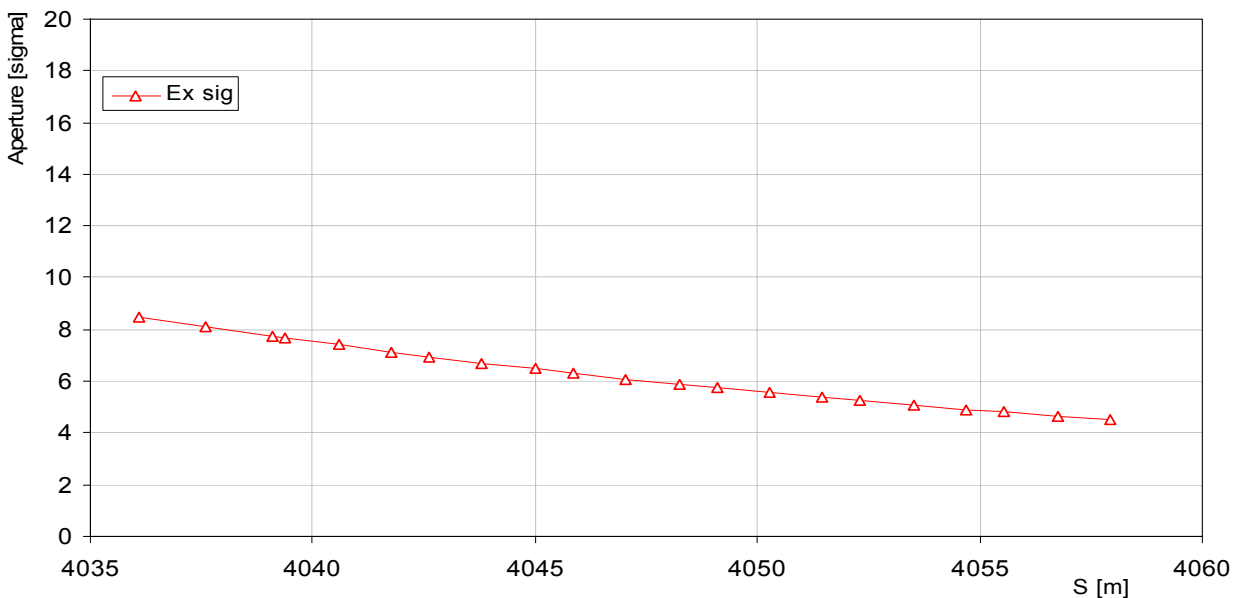


Figure 18.5: Vertical aperture for extracted beam (CNGS emittance) in the extraction elements in LSS4.

18.5.3 Horizontal Aperture for Bumped Beam

The bumped beam must pass close to the first septum (and the absorber element). With non-zero local dispersion D_x and a momentum spread $\delta p/p$ and a physical spacing A_{xb} between beam axis and outer (circulating beam side) septum edge, the available aperture in sigma is given by:

$$N_{xb} = (A_{xb} - O_y - M_y) / (K_\beta (\beta \epsilon_x + |D_x \delta p/p|^2)^{1/2})$$

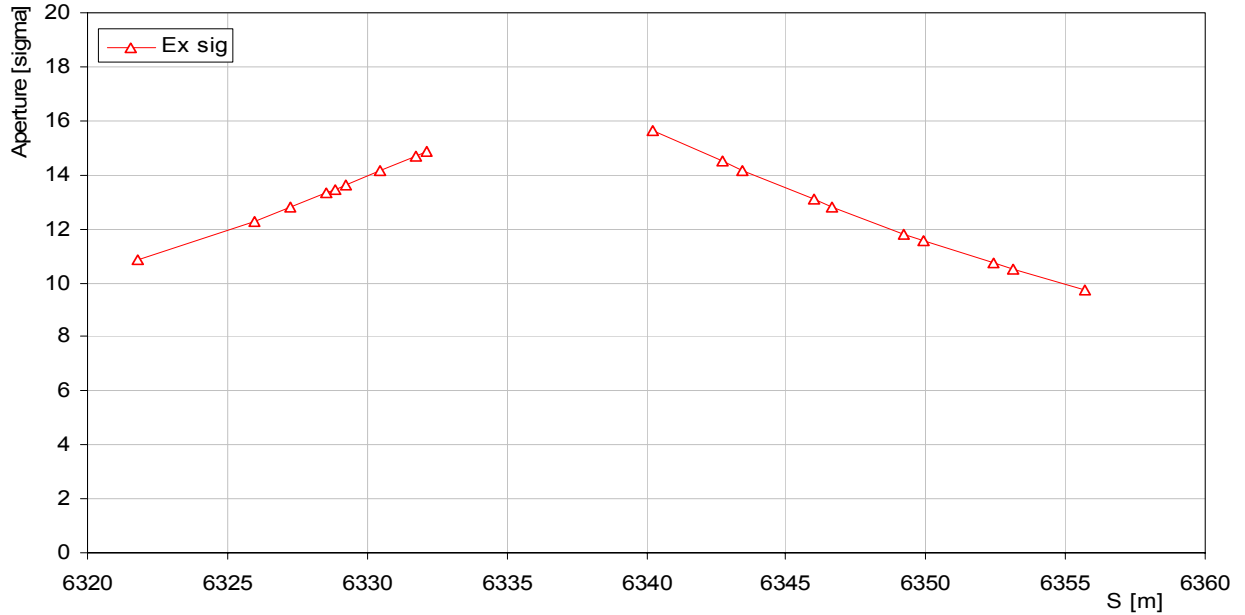


Figure 18.6: Vertical aperture for extracted beam (LHC emittance) in the extraction elements in LSS6.

18.5.4 Horizontal Aperture at Extraction

The extracted beam must also pass as close to the first septum (and the absorber element) as possible, to maximise the aperture available for the circulating beam. With a physical spacing A_{xe} between beam axis and outer (extracted beam side) septum edge, the available aperture in sigma is given by:

$$N_{xe} = (A_{xe} - O_y - M_y) / (K_\beta (\beta \epsilon_x + |D_x \delta p/p|^2)^{1/2})$$

18.5.5 Horizontal Aperture at Injection

While the strength of the extraction kicker and the beam size at the septum define aperture at extraction (above), the transverse septum position and the beam size at the septum define the aperture at injection. The septum is positioned as far outside as possible; this is however limited by the maximum particle excursion allowed in the enlarged quadrupole QFA418. Taking a limit of 89 mm for this excursion and placing the centre of the beam about 5σ inside this limit, the limiting position of the septum is at A_{xi} . The available injection aperture is given by

$$N_{xi} = (A_{xi} - O_y - M_y) / (K_\beta (\beta \epsilon_x + |D_x \delta p/p|^2)^{1/2})$$

here, ϵ_x is the emittance at injection energy. The FT beam is here the limiting case. Note that these figures could be improved, if necessary, by the application of a negative injection bump at the septum, for example a bump of -10 mm would give about an extra 1.4 sigma for the aperture at injection.

The aperture available in the horizontal plane at injection, bump and extracted is shown in Fig. 18.7 and Fig. 18.8, for LSS4 and LSS6 respectively. Note that the injected beam shown is the FT one, where the emittance is much larger.

18.6 EFFECTS OF MST AND MSE STRAY FIELD

The stray field from the MST and MSE septum magnets has been measured [17] and simulations made, with measurements performed in the SPS to determine the extent of the effect on the beam. The stray field is not expected to degrade the circulating beam emittance.

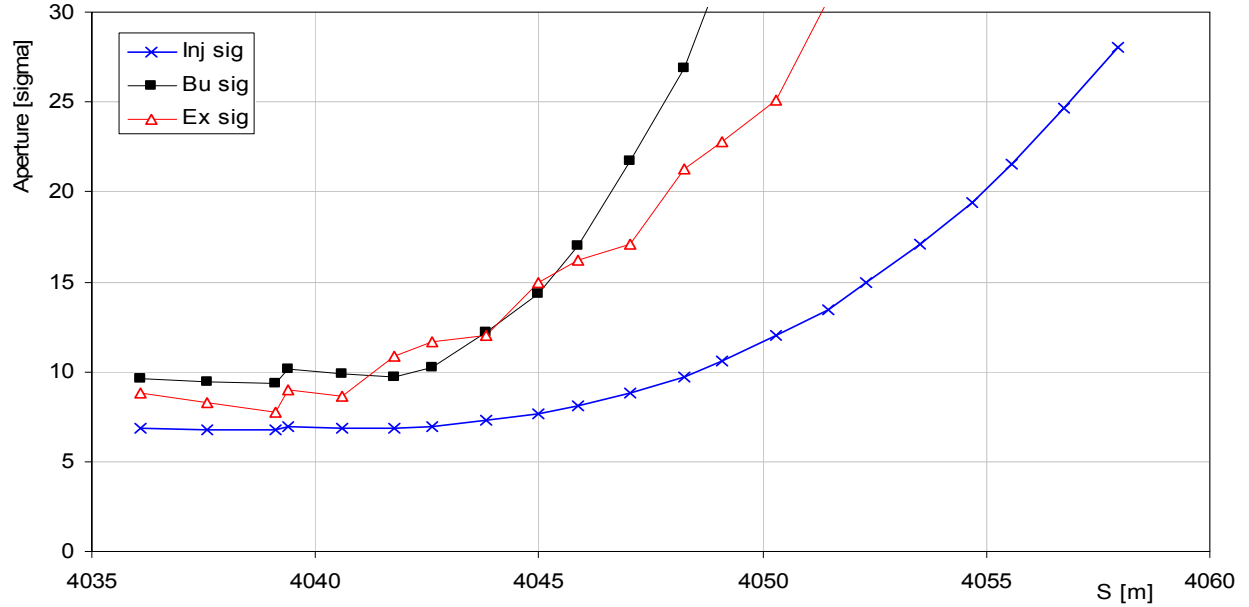


Figure 18.7: Aperture available at extraction elements in LSS4

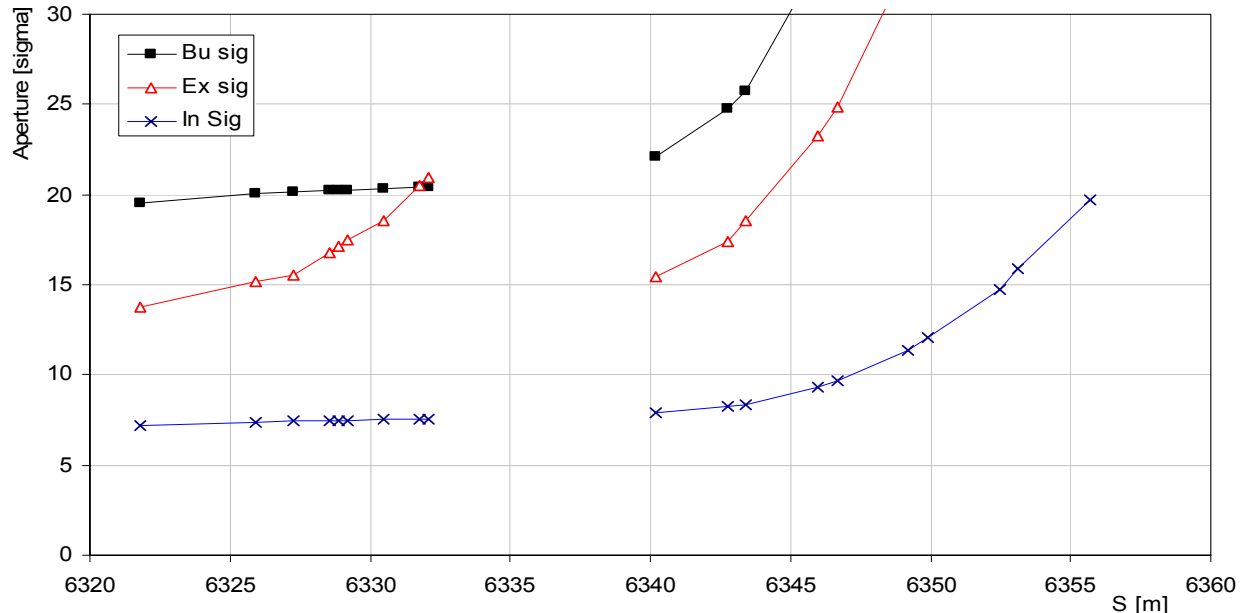


Figure 18.8: Aperture available at extraction elements in LSS6

18.7 STABILITY AND FIELD ERRORS

The stability of the extraction has been treated in detail in [18]. With the specified tolerances, the random contribution (rms variation) from the SPS orbit and the extraction system is expected to be $\pm 0.16 \sigma_x$ and $\pm 0.11 \sigma_y$, with a further $\pm 0.22 \sigma_x$ systematic variation due to the kicker waveform. These are included in the total delivery imprecision figures discussed in Chap. 22.

18.8 INTERLOCKING AND MACHINE PROTECTION

Active surveillance and interlocks are required to minimise the risk of equipment damage following a failure. The protection of the extraction equipment and the downstream transfer lines will depend heavily on a fail-safe interlock (or veto) system, which surveys critical equipment and beam parameters. Just prior to extraction (ideally around 1 ms before the kicker is triggered) the system should verify the bumper currents, the septum current, the charging of the kicker supply, the girder position, the horizontal orbit and the beam emittance. If any of these are not within the predefined tolerances then the extraction must be inhibited and the beam should be dumped. Full details can be found in [19].

Some failures cannot be covered by a surveillance system, notably extraction kicker faults such as erratics or missing triggers. In this case the TPSG element must safely intercept the beam and prevent damage to the extraction equipment, in particular the MSE septum. The correct set-up of the extraction channel in this respect, together with the surveillance and interlocking of the bumped beam position and the MSE girder position is essential.

REFERENCES

- [1] P. Collier et al., ‘*The SPS as Injector for LHC: conceptual design*’, CERN SL 97-07 (DI), 1997.
- [2] B. Goddard et al., ‘*The new Extraction Channel for LHC and CNGS*’, EPAC’00, Vienna, 2000, CERN SL 2000-036 (BT), 2000.
- [3] B. Goddard, ‘*Fast extraction*’, IXth Chamonix Workshop on SPS and LEP Performance, 1999, CERN-SL-99-007 DI, pp.126-130, 1999.
- [4] J. Borburgh et al., ‘*The Design of the New Fast Extraction Channel for the LHC*’, EPAC’04, Lucerne 2004. CERN-LHC-Project-Report-752, CERN, 2004.
- [5] B. Goddard, ‘*New power supplies for LSS4 extraction bumpers*’, Memorandum to A. Beuret and M. Royer, 9 April 1998.
- [6] E. Gaxiola et al., ‘*Upgrade of the SPS Extraction Kickers for LHC And CNGS Operation*’, CERN SL 2002-042 (BT), 2002.
- [7] E. Gaxiola et al., ‘*Upgrade and Tests of the SPS Fast Extraction Kicker System for LHC and CNGS*’, EPAC’04, Lucerne 2004, CERN-AB-2004-037; CERN, 2004.
- [8] J. Uythoven et al., ‘*Beam Induced Heating of the SPS Fast Pulsed Magnets*’, EPAC00 Lucerne, July 2004.
- [9] B. Goddard et al., ‘*Transient Thermo-Mechanical Analysis of the TPSG4 Beam Diluter*’, CERN-SL-2002-060-ECT; Geneva : CERN, 19 Dec 2002.
- [10] H. Vincke, ‘*Radiation levels in ECA4 caused by beam losses in the septum magnet to be installed in ECX4*’, CERN-TIS-2002-025-RP-TN, 2002.
- [11] J. Dupin, ‘*Extraction Septum Magnets for the SPS*’, CERN/SPS/ABT/EX/JD/ph/81-42, 1981.
- [12] W. Weterings et al., ‘*The MSE Septum Magnet System of the New Fast Extraction Channel of the SPS at CERN*’, MT-18 Magnet Technology Conference, Morioka, 2003, CERN-AB-2003-089-BT; CERN, 17 Oct 2003.
- [13] B. Balhan et al., ‘*Alignment and girder position of the MSE septa in the LSS4 extraction channel*’, CERN SL-Note 2002-014 BT, 2002.
- [14] N. Catalan-Lasheras et al., ‘*Calibration of BPCE.41801 and SPS extraction bump in LSS4*’, CERN AB Note 2003-046, 2003.
- [15] B. Goddard and M. Gyr, ‘*The SICOPEX program version V.0: theory and user’s guide*’, CERN-SL-98-055 BT, 1998.
- [16] G. Stevenson, ‘*Radiation protection considerations in LSS4*’, Minutes 5th meeting of SLI Committee,

- [17] R.Chritin, '*Mesures magnetiques d'un aimant dipole de type MSE*', SL-Note-99-053-MS.- Geneva : CERN, 11 Nov 1999.
- [18] B.Goddard, Expected delivery precision of the injected LHC beam, CERN/LHC Project note 337, 2004.
- [19] R.Giachino et al., '*Architecture of the SPS beam and extraction interlock systems*', CERN-AB-2003-010-OP; CERN, May 2003

CHAPTER 19

BEAM INSTRUMENTATION

19.1 TT2/TT10 INSTRUMENTATION

19.1.1 Beam Position Measurement

The beam is transferred from the PS to the SPS via the combined TT2/TT10 transfer line (see Chap. 15). Each of these lines is equipped with beam position monitors (BPM) of which 6 are located in TT2 and 14 in TT10. Each BPM is mounted orthogonally and consists of four, 60 cm long, straight strip-line electrodes. The vertical and horizontal position of the beam centroid is obtained from each BPM.

The acquisition system is based on logarithmic amplifier electronics [1], where the position is obtained directly as the LOG (electrode A) – LOG (electrode B). This method has the advantage that only one coaxial cable is required to transmit the position data to the surface buildings. In order to minimise the cable lengths the system is split in two; with the acquisition system for the first ten BPM's in the PS Y-Building (Building 269) and the system for the second ten in the SPS at BA1. Each one of these acquisition chassis is auto-triggered by the first pick-up it contains.

The signal from each pick-up can be switched to supply one of two logarithmic amplifier chains, one working at 200 MHz for full LHC batches and SPS fixed-target proton beams, the other one working at 22 MHz for single bunches and SPS fixed-target heavy ion beams.

Calibration of the complete system is performed by injecting signals at 0 dB and ± 6 dB through the upstream ports of opposing strip-lines, allowing the offset and gain of the system to be determined for each set of acquisition electronics.

For a centred beam the linearity is $\pm 100 \mu\text{m}$ over 70 dB, with a resolution of $20 \mu\text{m}$ for a batch measurement and $50 \mu\text{m}$ for a single bunch.

19.1.2 Intensity Measurements

The PS to SPS transfer lines are equipped with two identical fast beam current transformers for transfer efficiency measurements, one located at the beginning of TT2 and the other near the end of TT10 [2]. For LHC proton and ion bunches the dynamic range of the transformer covers intensities from 3×10^8 to 5×10^{11} charges per bunch, with a bandwidth covering the range from 200 Hz – 500 MHz and a very low droop of less than 0.2 % per μs . This low droop means that no baseline restitution is required during the passage of the LHC batch. The acquisition electronics is based on a 40 MHz integrator chip developed by the Laboratoire de Physique Corpusculaire (Clermont-Ferrand) for use in the LHCb Pre-shower Detector [3]. This allows bunch by bunch intensity measurements for LHC type beams. The integrated charge is digitised using a 12-bit ADC and treated and stored using the digital acquisition board (DAB) developed for the LHC beam position system (see Vol. 1, Sect. 13.1). Synchronisation of the acquisition with each bunch is obtained using the SPS beam synchronous timing as provided by the TTC system (Sect. 19.2).

Calibration of the system is performed by injecting a stable current, corresponding to 2×10^{10} charges in 25 ns, into a calibration winding around each transformer. A single shot bunch-by-bunch intensity measurement is predicted to have a resolution of $\sim 5 \times 10^8$ charges and an accuracy of $\sim 2 \times 10^9$ charges.

19.1.3 Beam Profile Monitors

The measurement of the beam profile at several locations in the transfer line is needed in order to determine the transverse beam size of the injected beams at each location and hence compute their emittance. Five standard SPS BTV tanks are installed along the injection line TT2/TT10. Another 12 screen monitors are also available for simple beam observation purposes in case of problems with the BPMs.

The BTV mechanisms are equipped with two different types of screen material [7]:

- Luminescent screens made of 1 mm thick chromium doped alumina (AL_2O_3 [Cr]).
- Optical Transition Radiation [OTR] screens made of a 12 μm thick foil of titanium.

The alumina screens are normally used for low intensity beams and the OTR screens for high intensity ones. The light produced by the screen is extracted through a window and focused on an image intensifier optically coupled to a standard CCD camera.

A set of neutral density optical attenuators controls the quantity of light transmitted to the camera as a means of coping with the large dynamic range to be covered. In terms of intensity the dynamic range goes from 5×10^9 protons to around 2×10^{13} protons per injection.

The TV signal is connected to TV monitors that allow the observation of the beam in real time in the Control Room. In addition, the signal is passed to a VME acquisition board that digitises the TV frame with a resolution of 300 x 400 pixels. The digitisation is made with 8-bit precision. The data from the acquisition is used to generate horizontal and vertical projections for a single frame that corresponds to a single pass of the beam. A 2-Dimensional surface representation is also available. Depending on the choice of the fixed optics in front of the CCD camera, the spatial resolution can range from 150 to 300 $\mu\text{m}/\text{pixel}$.

One of the TT10 screens is equipped with a 32 channel multi-anode photomultiplier making it possible to measure the profiles of the individual bunches of a PS batch at 40 MHz [9]. The multi-anode photomultiplier is mounted on a rotating table enabling the system to acquire the beam projection along the desired axis.

19.2 SPS INSTRUMENTATION

19.2.1 Beam Position Measurement

For LHC type beams the first turn and orbit are measured in the SPS using the standard SPS orbit system (MOPOS) [4]. Most of the 216 pick-ups used are electrostatic “shoebox” monitors, measuring either in the horizontal (at high β_H) or vertical (at high β_V) plane. The signals from these high impedance pick-ups are matched to 50Ω at 200 MHz before passing through a passive hybrid to produce a sum and difference signal. The acquisition system is based around a 200 MHz homodyne receiver, the output of which is filtered, sampled and digitised to give a sum and difference signal from which the position can be calculated. Gain switching (in 10 dB steps up to 90 dB) is required to cover the large dynamic range needed for all types of SPS beams, with each gain requiring its own calibration factors. The system is equipped with enough memory to store the orbit for all turns during a given SPS elementary cycle. This enables multi-turn (normally 1000 turn) measurements to be performed with specific monitors, or for all beam position monitors, at any time within the cycle.

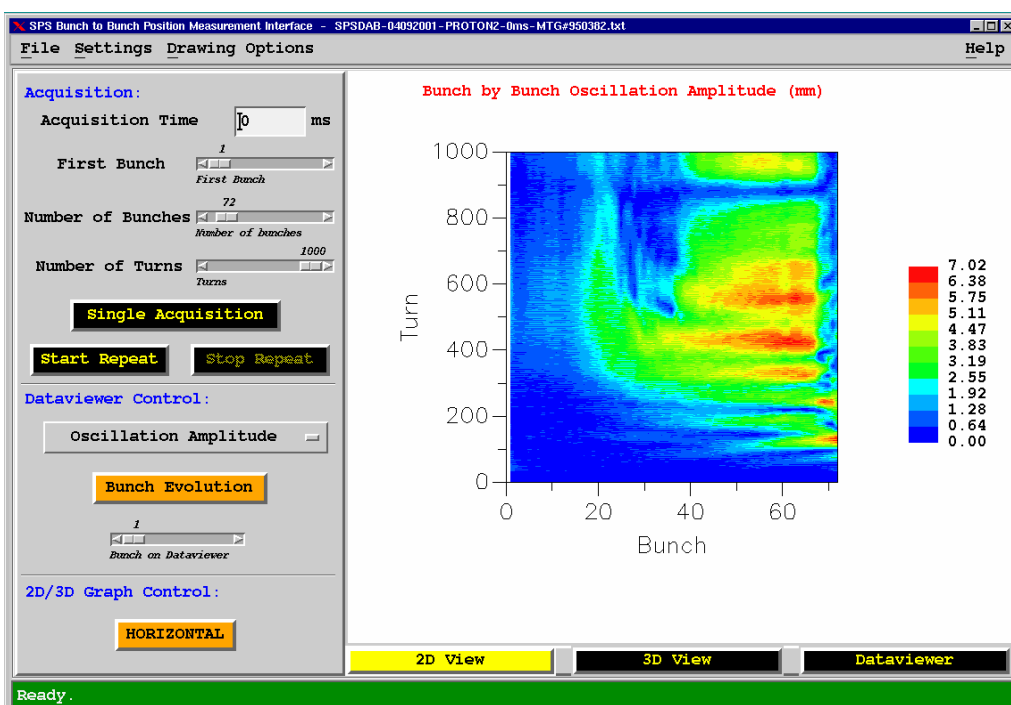


Figure 19.1 Study of the electron cloud instability in the SPS using the 40MHz bunch by bunch position measurement system.

Three large aperture strip-line coupler pick-ups (BPCE) form part of the SPS to LHC extraction interlock on each LHC extraction channel, in LSS4 and LSS6. The acquisition of these pick-ups is performed using the standard MOPOS system, with an additional algorithm incorporated to correct for the non-linearity of the pick-up at large amplitudes. These pick-ups are read out 50 ms before the extraction and are used to ensure that the extraction bump is within the limits set for the acceptance of the septum magnet.

In addition to the global orbit acquisition, the SPS is equipped with a single BPM located in LSS4. This BPM is fitted with LEP-type button electrodes and the LHC orbit acquisition electronics. This allows the measurement of bunch by bunch position over thousands of turns at any time in the cycle for any beam spaced by multiples of 25 ns. Such a pick-up has proved very useful for instability studies and in particular to understand the behavior of the LHC batch or batches under the influence of an electron cloud. Fig. 19.1 shows a typical result from such a study for a 72 bunch LHC batch at injection in the SPS. The first bunches are seen to be stable, while bunches towards the tail of the batch develop large oscillation amplitudes as a result of instabilities provoked by the electron cloud.

19.2.2 Beam Loss Monitors

The SPS beam-loss monitoring (BLM) system is used to localise beam losses during the injection, acceleration and extraction processes. Nearly 300 ionisation chambers are installed around the SPS ring. The currents generated by the chambers are treated by the BLM acquisition system which consists of 10 VME chassis which are installed in various surface buildings around the machine.

The ionisation chambers are parallel plate type monitors filled with nitrogen at atmospheric pressure. Each monitor has a volume of one liter. The electrical drift field strength is set to 1600 V/cm. An integrator integrates the ionisation chamber current during the whole SPS elementary cycle. Every 20 ms, a 12 bit ADC samples the integrator output and the digital value is stored in the memory of a VME acquisition module.

The acquisitions are triggered using SPS timing events pre-programmed in the SPS elementary cycle. The beam-loss server returns data either in raw ADC counts, or calibrated in units of mGy. A fixed-display is provided for the machine operators. This display can show the integral dose of each Beam Loss monitor or the evolution of losses for a single Beam Loss monitor throughout an elementary cycle.

The dynamic range of the LHC beams, from pilot to four batches at nominal intensity is around 10^4 . Assuming that the losses scale linearly with the total intensity, several gain stages are needed on the acquisition board to cover this large dynamic range with a 12 bit ADC.

A signal to the beam dump is generated when the loss rate exceeds a given preset threshold [8].

19.2.3 Intensity Measurement

The SPS is equipped three DC beam current transformers (BCT). Two are for high intensity beams and one for low intensities. The low intensity BCT, located in Point 4 (BCT414), covers the range from 2 μ A to 50 mA. This corresponds to the range 3×10^8 charges up to 7×10^{12} charges in 23 μ s. This BCT is therefore used for measuring single bunches and the heavy ion fixed-target beam. Two identical high intensity BCTs are located in Point 1 (BCT116) and Point 3 (BCT318). The measuring range of these BCTs is between 20 μ A and 1100 mA. The corresponding beam intensities are 3×10^9 charges and 1.6×10^{14} charges in 23 μ s. Two such BCTs are provided for redundancy reasons as the signals are also used by the beam dump system for its energy tracking. A direct analogue output from each of the three BCTs is sent to the accelerator control room for use on the teletext server showing the SPS status pages.

Point 3 in the SPS is also equipped with a fast beam current transformer identical to those installed in TT2 and TT10 (see Sect. 19.1). For LHC type beams this monitor is capable of bunch-by-bunch measurements at rates of up to 100 Hz throughout the SPS cycle. The measurements are triggered by the SPS beam synchronous timing. Such measurements allow the visualisation of bunch-by-bunch intensity variations at injection and extraction, but also give the relative loss from each bunch throughout the acceleration process.

Passive beam current transformers are also installed in points 4 and 6 and provide analogue signals which are used to time-in the extraction systems of TI8 and TI2 respectively.

19.2.4 Tune and Chromaticity Measurement

The dedicated SPS tune measurement system uses a single kick technique followed by FFT analysis to determine the horizontal and vertical betatron tunes of the machine. Each plane is equipped with four “Q-kicker” modules of varying strength, allowing kicks of up to 2 mm at 450 GeV. It is also possible to apply a chirp excitation to the beam via the transverse damper, with which it is possible to follow the tune evolution along the cycle in 50 ms intervals. Chromaticity is measured by changing the RF frequency on successive cycles and measuring the corresponding tune change. The beam oscillation information is retrieved from both strip-line couplers and electrostatic pick-ups, depending on the mode of operation.

The tune acquisition system consists of a CPU module (PowerPC based), a main timing receiver module (TG8), a timing module providing ADC sampling clocks and up to 12 Beam Oscillation System sampler modules (BOSC) [5]. Each of the BOSC modules can be used to acquire two individual signals with 16 bit ADCs over up to 10^6 consecutive SPS turns. Typically the two signals are the delta and sum signals from a specific beam position pickup. Three different beam types can be treated:

1. A single bunch. As the module used to generate the ADC sampling clock has a jitter of more than 10 nsec, an auto-trigger (a peak and hold mechanism that finds the peak of the sum signal) is used to sample the data for sum and delta channels.
2. Low intensity batched beams, typically heavy ions. The input signals are filtered at 4 times the revolution frequency and sampled using the standard sample and hold mode. Specially designed low-noise amplifiers allow a correct acquisition even if the total intensity is down to a few 10^9 charges.
3. High intensity batched beams. Here the front-end electronics is based on high frequency FET amplifiers inside the SPS tunnel that have the advantage of not needing a 200 MHz structure to work. This system can therefore also be used when setting-up the SPS resonant slow extraction.

The first two modes above can cover a dynamic range of 10^3 or 60 dB using external gain stages. The low-level software is completely driven by the MTG timing events. The generic warning event which arrives 500 msec before the beam is injected is used to program the gains and delays needed for the next cycle. The generic beam-in event, which arrives at turn zero of the injected beam, is used to reset the ADC samplers and to start the acquisition from that turn onwards. The generic beam-out event, which arrives at the end of the elementary cycle, is used for book-keeping on the completed cycle and to trigger the reading of raw-data from the low-level crate.

19.2.5 Head-Tail Monitor

The head-tail monitor was originally installed to study a new technique for the measurement of the chromaticity, via head-tail phase shifts [6]. It has now also become a standard instrument for providing transverse, bunch-by-bunch, wide band signals. These are used to study a variety of instability issues in particular for LHC type beams. The system consists of a 60 cm long strip-line coupler, followed by a 2 MHz- 2 GHz passive hybrid and a fast digital sampling oscilloscope (2 Giga-samples/s). The acquisition is gated around a region of interest, which may be a single bunch, a full batch or a complete turn and is re-triggered on this region for up to 350 consecutive turns. The resulting data is retrieved via a GPIB link for analysis and display by a high level graphical user interface.

19.2.6 Beam Synchronous Timing

The beam synchronous timing (BST) is required for much of the specific LHC beam instrumentation in the SPS. This is distributed via a fibre-optic network, using the Timing, Trigger and Control (TTC) system designed for the LHC detectors. The TTC infrastructure allows the 40 MHz bunch clock, a 23 μ s turn clock and arbitrary control data to be recuperated at each beam instrumentation station by a BST receiver card. A full description of the receiver card is given in Vol. 1 Sect. 13.9.

19.2.7 Beam Profiles Measurement Instruments

Wire Scanners

Wire scanners are the main instruments for the transverse beam emittance determination in the SPS. Two different scanner types are distinguished by the wire transport mechanisms used. The linear transportation mechanisms reach a speed of 1 m/s and are therefore limited to a maximum proton intensity of 5×10^{12} . The rotational wire mechanism based scanners reach a speed of 6 m/s and the beam heating limit is well above the nominal LHC proton intensity of 3×10^{13} . In either case the accuracy of the profile measurement is limited by the systematic errors. The lowest relative systematic error (below $\Delta\sigma/\sigma = 2\%$) is reached by the linear wire transportation system. Because of the more fragile and indirect wire position measurement system, the rotational wire scanners reach a relative systematic error of $\Delta\sigma/\sigma = 6\%$ [10]. The errors are estimated by comparing the different systems with each other under various operational conditions. In the SPS, a total of 6 linear and 6 rotational based wire systems are installed.

In the operation periods of 2002 and 2003 it was noted that the scanner tank, acting as a cavity, stored RF power which strongly heated the wires. This led to an acceptable combination of bunch length and intensity limit. If exceeded the heating often resulted in destruction of the wire. This limitation has been eliminated by introducing RF power absorber material on the inner walls of the scanner tanks. The build up of electromagnetic fields is reduced by two orders of magnitudes for some modes as seen in Figure 19.2.

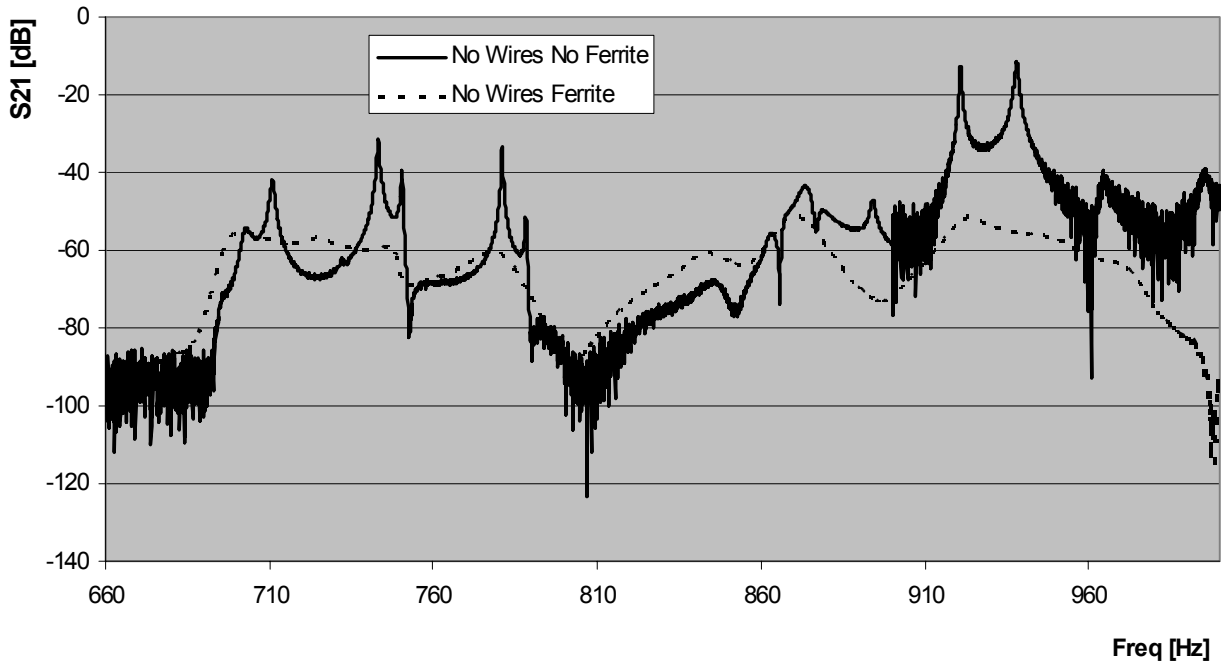


Figure 19.2: Electrical field strength spectrum inside a SPS rotational wire scanner tank with and without damping material on the walls of the tank.

Synchrotron Light Monitor

A synchrotron light monitor from the $p\bar{p}$ era [16] has been rejuvenated and installed in LSS5. It has given interesting results above 320 GeV. More work will be done to make the monitor useful at lower energies and to approach the accuracy of the LEP monitors which have provided emittance values with a precision better than 5% under comparable conditions [17].

Gas Monitors

Ionisation Profile Monitors [IPM] exploit the signal provided by the ionisation of the vacuum rest gas during the beam passage. Monitors are presently installed in LSS44 and LSS5 of the SPS. A first monitor

was provided by DESY and inserted in the increased gap of a correction dipole magnet. This was done with a view to improve the resolution by channelling the primary electrons along magnetic field lines. After acceleration of the primary electrons onto a Multi Channel Plate (MCP) for multiplication, the electrons impinge on a fast phosphor screen; the image of which is acquired by a CCD camera. This experimental monitor was installed in sector 4 of the SPS and provided good results. In particular, it gave the possibility to acquire transverse profiles with rms values below 700 μm with a good resolution (better than 50 μm) and to use the monitor in a turn by turn mode. This mode was particularly useful to perform injection matching studies [11,12].

Based on the results from the experimental monitor, a new prototype was built and installed in LSS5 of the SPS during 2002. With a more compact design the monitor is built such that it meets the criteria for incorporation into the LHC itself [13].

During the commissioning of the monitor it was discovered that electron cloud effects in the chambers of the monitor perturbed the measurements. To reduce this the various detector components located inside the SPS vacuum chamber were coated with NEG. The NEG coating is known to reduce electron multi-pacting by a reduction in the secondary electron yield of the vacuum chamber surface. The result was very good and tests resumed in 2003 with this prototype. Profiles of beams ranging from an LHC pilot bunch (5×10^9 protons) up to 4 PS batches of nominal bunches (3.5×10^{13} protons) could be measured and tracked throughout complete SPS acceleration cycles. Fig. 19.3 shows some profiles measured with this instrument. The profile of a pilot bunch accelerated to 450 GeV, measured under normal SPS vacuum pressure (2×10^{-8} hPa) is presented.

These results qualify ionisation monitors for transverse profile measurements in the SPS and in the LHC; at least for beam sizes larger than 700 μm . These instruments can also be used in turn by turn mode for injection studies.

Cross-calibrations carried out between wire scanners and the Ionisation Profile Monitors lead normally to an agreement of 3% to 5% [14]. However, for LHC type beams, the necessary dynamic range in the SPS, from one batch at 26 GeV to 4 batches at 450 GeV, cannot be covered properly with a single gain setting of the IPM. Saturation effects can generate discrepancies between the two devices of up to 20% on the measured beam rms values [12]. To solve this problem the implementation on the IPM of a variable gain control during the cycle is under study.

Gas monitors based on the luminescence of N₂ were also tested in the SPS [15]. In order to get enough signal from gas luminescence, the N₂ pressure needs to be increased locally up to 5×10^{-7} hPa. This possibility has been incorporated into the previously mentioned IPM prototype [13]. Hence, if the local N₂ pressure is increased, while transverse profiles in the vertical plane are measured by extracting the signal from ionisation, another independent optics channel provides simultaneously the profiles in the horizontal plane by looking at the signal from luminescence. Promising results were obtained in 2003 and are illustrated in Fig. 19.3.

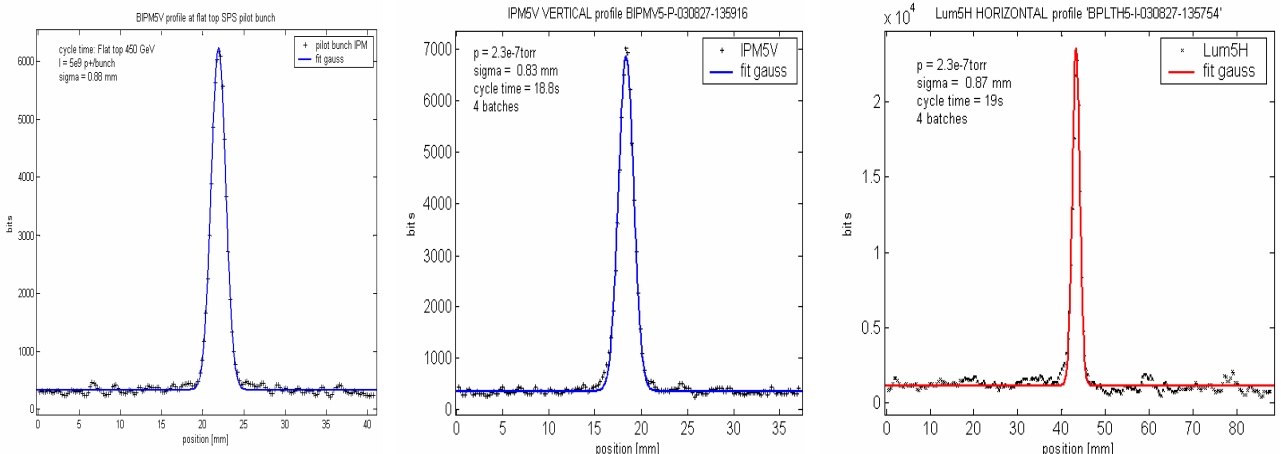


Figure 19.3: Profile measured with the SPS Gas Monitor Prototype installed in sector 5: Vertical profile (ionisation signal) of a pilot bunch (5×10^9 p) at 450 GeV, $P = 2 \times 10^{-8}$ hPa (left); Vertical profile (ionisation signal) of an LHC beam (3.5×10^{13} p) at 450 GeV, $P = 2 \times 10^{-7}$ hPa (centre); Corresponding horizontal profile (luminescence signal) of the same LHC beam as in centre (right).

19.2.8 Injection Matching Monitoring

Matching the transfer line to the machine is vital to preserve the emittance of the beam transmitted to the LHC. A new type of monitor [18] has been tested to perform the betatron and dispersion matching at injection. It is based on the measurement of the beam profile variations over a limited number of turns immediately after injection. The monitor uses a $12\text{ }\mu\text{m}$ titanium screen generating optical transition radiation (OTR) which is observed using a CCD camera operating in a dedicated fast acquisition mode. In order to avoid damaging the screen the beam is dumped after the desired number of turns. This method only requires the knowledge of the non-integer part of the tune, which can be measured very precisely with the Q-meter, or even with the matching monitor itself.

The matching monitor can provide a measurement of the mismatch to better than 1% in each plane. Two monitors are installed in the SPS: one in LSS4 in a low Dispersion region, the other in LSS5 in a region with Dispersion. Preliminary tests have been performed and were encouraging [19], see Fig. 19.4.

Another possibility for transfer line matching is to use the IPM monitor (Sect. 19.2.7) in a turn by turn mode at injection. Preliminary tests have been made and the results look encouraging [12]. The IPM monitor is, *a priori*, less sensitive than the screen monitor. However, it has the advantage of being non-destructive and non-intercepting and can be used to provide permanent monitoring. If the sensitivity argument turns out to be an important issue, it can be used to measure relative changes between screen re-matching procedures.

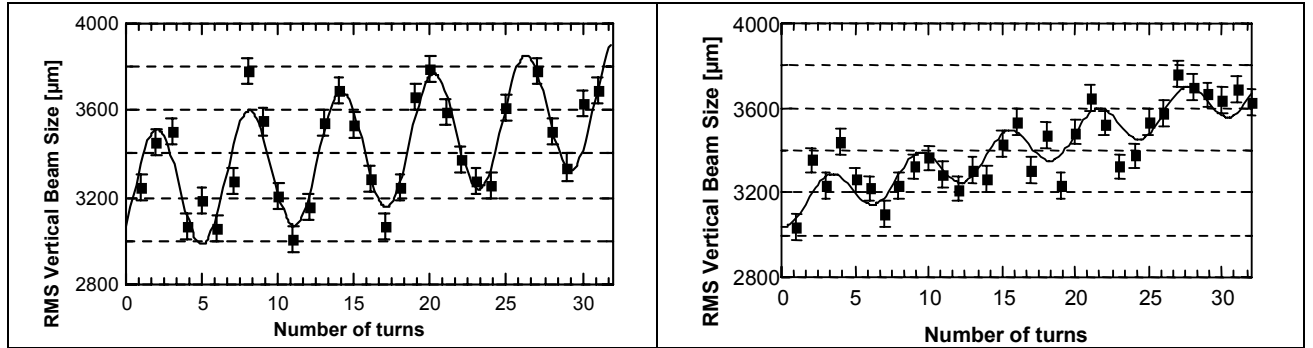


Figure 19.4: Beam size evolutions measured with the LSS4 screen monitor before and after matching [19]

19.2.9 Scrapers

The SPS beam emittance must be controlled just before extraction to the LHC. In particular, low density tails, if present, must be removed using fast scraping targets. Horizontal and vertical scrapers, originally installed in the ISR, are installed in sector 5 of the SPS to test this concept. The scrapers are associated with two sets of four collimator blocks, two horizontal and two vertical ones, which originate from LEP. The primary set is at a phase advance of 90° with respect to the scraper and the secondary set is at a phase advance of 90° with respect to the primaries. This scheme was implemented to make sure that losses induced by the scraping process can be concentrated at the scraping location, hence keeping the rest of the machine clean. This has been confirmed by tests performed at 26 GeV and 450 GeV [20]. In Fig. 19.5, it is clearly shown that during scraping the loss pattern around the SPS is not changed outside the scraper and collimator area, demonstrating the efficiency of the collimation scheme. The 3 loss peaks generated by the scraper, primary and secondary collimators are discernible when scraping.

Recent studies for protection of the LHC during the injection process have revealed the need for skew scraping in the SPS. A third scraper will therefore be installed with the other two. The exact physical angle of this scraper will be determined once the final location is known. The present location for the scraper is not optimum since the dispersion is non zero. The scraping is therefore not purely transverse, some momentum scraping also occurs. A new set of locations for the complete scraper system are presently under study. The new location for the fast scraper itself needs to have a low dispersion and space at 90° and 180° downstream for the collimator sets. Ideally the new location should not be in a clean region of the machine, since the regular use of the scraper for the LHC beams will generate significant local radiation during heavy scraping.

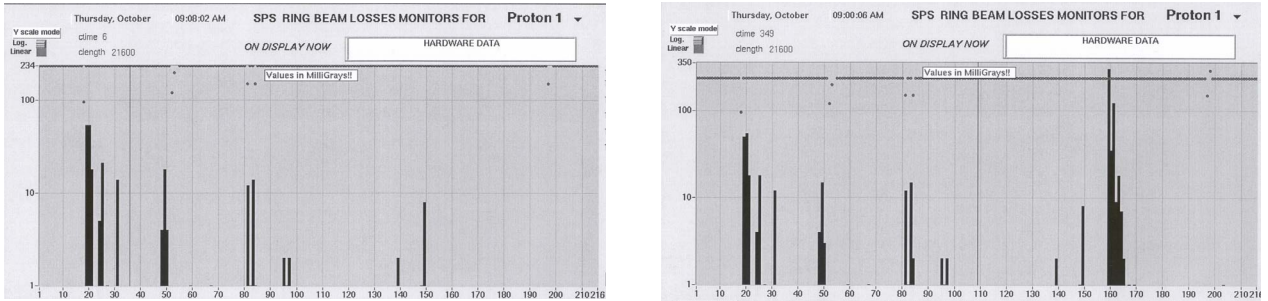


Figure 19.5: Beam losses with (left) and without (right) scraping in LSS5. Outside the scraper region there is nearly no change in the loss pattern around the ring.

19.3 EXTRACTIONS

19.3.1 BTVEs

Six new TV screens will be installed in the two fast SPS extractions, LSS4 and LSS6, in order to visualise the transverse beam spot. Two monitors are located upstream and downstream the MSE septum in LSS4 and four monitors at the entrance and exit of both the MST and the MSE septa in LSS6.

Because of the severe space constraints at these locations, TV monitors with a special geometry had to be developed and incorporated into the septum vacuum pumping modules. Each monitor is equipped with a phosphorescent alumina plate for use at low intensity and with a 12 µm titanium foil providing optical transition radiation at nominal currents. Both are approximately 20×60 mm rectangular screens, tilted by 45 degrees with respect to the beam axis and moved IN and OUT via a linear displacement controlled by stepping motors. The signal processing is the same as for the TV screens of the injection line, TT10 (Sect 19.1). The first two monitors, installed in LSS4, were successfully tested during the September 2003 test of this fast extraction.

REFERENCES

- [1] H. Schmickler, G. Vismara, “A logarithmic processor for Beam Position Measurements applied to a Transfer Line at CERN”, CERN-SL-2001-023-BI, presented at DIPAC 2001, Grenoble, France, May 2001.
- [2] H. Jakob et al, “A 40 MHz Bunch by Bunch Intensity Measurement for the CERN SPS and LHC”, CERN-AB-2003-056-BDI, presented at DIPAC 2003, Mainz, Germany, May 2003.
- [3] G. Bohner et al, “Very Front-end Electronics for the LHCb pre-shower”, LHCb-2000-047, CERN, 2000.
- [4] C. Boccard et al, “Performance of the new SPS beam position orbit system (MOPOS)”, CERN-SL-99-048-BI, presented at DIPAC’99, Chester, UK, May 1999.
- [5] H. Jakob et al., “SPS Tune Measurements”, DESY Report M-95-07, presented at DIPAC’95, Travemunde, Germany, 1995.
- [6] S. Fartoukh, R. Jones, “Determination of Chromaticity by the Measurement of Head-Tail Phase Shifts Simulations, Results from the SPS and a Robustness Study for the LHC”, CERN-LHC-Project-Report-602.
- [7] R. Jung et al., “Single Pass Optical Profile Monitoring”, CERN-AB-2003-064 BDI, June 2003, presented at DIPAC 2003, Mainz, Germany, May 2003.
- [8] G. Ferioli et al., “Protection and Diagnostic Systems for High Intensity Beams”, CERN-SL-2000-032-BI.
- [9] G. Ferioli et al. “Beam profile measurements at 40MHz in the PS to SPS transfer channel”, CERN SL-99-043 BI, August 1999, presented at DIPAC 99, Chester, UK< May 1999.
- [10] F. Roncarolo, et al., “Accuracy determination of the SPS wire scanner monitors”.
- [11] G. Ferioli et al., “Sensitivity Studies with the SPS Rest Gas Profile Monitor”, Proc. of DIPAC2001, 13-15 May, 2001, ESRF, Grenoble, France and CERN-SL-2001-026 BI.

- [12] G. Ferioli et al., “*Beam Studies Made with the SPS Ionization Profile Monitor*”, Proc. of DIPAC2003, 5-7 May, 2003, Mainz, Germany and CERN-AB-2003-066 BDI.
- [13] C. Fischer et al., “*Design and Test of a New Rest Gas Ionisation Profile Monitor Installed in the SPS as a Prototype for the LHC*”, Proc. Beam Instrumentation Workshop 2004, Knoxville, Tennessee, 3-6 May 2004.
- [14] C. Fischer & J. Koopman, “*Measurements made in the SPS with a Rest Gas Profile Monitor by Collecting Electrons*”, Proc. of Beam Instrumentation Workshop 2000, Cambridge, Massachusetts, 8-11 May 2000.
- [15] G. Burtin et al., “*The Luminescence Profile Monitor of the CERN SPS*”, Proc. of EPAC200, 26-30 June, 2000, Vienna, Austria and CERN-SL-2000-031 BI.
- [16] R. Bossart et al., “*Observation of visible synchrotron radiation emitted by a high energy proton beam at the edger of a magnetic field*”, NIM, 164, pp 375-380, 1979.
- [17] P. Castro et al., “*Cross-calibration of emittance measuring instruments in LEP*”, SL MD Note 202, February 1996.
- [18] C. Bovet, R. Jung: “*A new diagnostic for betatron phase space matching at injection into a circular accelerator*”, LHC Project Report 3, May 1996, Proc. of EPAC’96, Sitges, 1996.
- [19] C. Bovet et al., “*The OTR screen betatron matching monitor of the CERN SPS*”, CERN SL-99-050 BI, August 1999, presented at DIPAC 99, Chester, May 1999.
- [20] C. Fischer, J.J. Gras, R. Jung, “*Scraping and Collimation Tests in the SPS*”, AB-Note-2004-037 MD, April 2004.

CHAPTER 20

THE INTERNAL BEAM DUMPING SYSTEM

20.1 SYSTEM DESCRIPTION

There are three main ways in which the SPS internal beam dump will act:

- Firstly, the internal beam dumping system is automatically triggered at the end of each SPS beam cycle in order to remove any remaining beam from the machine after the last extraction and before the magnets begin to ramp down ready for the next beam cycle.
- Secondly, the internal beam dumping system is automatically fired in case of emergency conditions or interlocks generated by other equipment. Poor beam quality or abnormal beam losses can also provoke an emergency beam dump.
- Finally, the beam dump may be deliberately activated at a specific time in the running SPS beam cycle for reasons which include machine tuning and special machine development tests.

The system consists of a pair of kicker magnets which are used to deflect the circulating beam onto an absorber built around the vacuum chamber. Two absorber blocks are installed: one (TIDH – Target, Internal Dump, Horizontal deflection) is optimised to dump the beam at energies up to 30 GeV, while the other (TIDV– Target, Internal Dump, Vertical deflection) is used at energies above 100 GeV. The beam cannot be cleanly dumped in the energy range 30-100 GeV. In order to reduce the maximum energy density deposited on the TIDV, the beam is kicked vertically downwards and swept in a horizontal sine-like pattern to provide beam dilution.

20.2 RATIONALE FOR A DESIGN UPGRADE

The original configuration of the TIDV remained practically unchanged over more than twenty years of operation in spite of a substantial increase in the beam intensities routinely accelerated in the SPS. The original SPS design [1] was for 1×10^{13} protons per cycle with initial maximum beam energy of 300 GeV. Intensities of almost five times this have been routinely accelerated to 450 GeV.

The total intensity of the nominal LHC beam in the SPS is not as high as the fixed-target beam used during operation for the west area neutrino facility and foreseen for CNGS operation. The nominal LHC beam has a total intensity of 3.3×10^{13} protons. However, while the fixed-target beam fills 10/11th of the SPS circumference, the LHC beam fills just 1/3rd. The peak intensity therefore reaches twice the fixed target case. The situation for the ultimate LHC beam in the SPS is even worse. The ultimate LHC beam in the SPS has a total intensity of 4.9×10^{13} protons compressed into 34% of the circumference. A fixed target beam having the equivalent peak intensity would require a total intensity of $\sim 1.3 \times 10^{14}$ protons. The sweeping system for the internal beam dump was designed to spread the energy from a beam which essentially filled the circumference of the SPS. Compressing the beam into a smaller section of the circumference reduces the efficiency of the sine-like sweep pattern.

The core of the original TIDV consisted of a water-cooled, slotted block of Al₆Cu aluminium-alloy, forged and heat-treated for maximum strength. The block was centred in a water-cooled, Cu/Cr/1Zr copper alloy cylinder, forged and heat-treated. The copper was machined and electron beam welded from two half cylinders and formed an integral part of the SPS Vacuum Chamber with passage for both injected and circulating protons. The core assembly was mounted within two water-cooled, cast iron shielding blocks.

Energy deposition induced by particle cascades produces local heating and thermal stresses in the absorber. Simulations [2] showed that the ultimate LHC beam in the SPS would cause an unacceptable temperature rise in the original aluminium core. For this reason the TIDV was redesigned [3] to accept a proton beam of LHC injection energy and intensity. For the new design a more balanced distribution of energy deposition [4] is achieved within the core. Simpler in conception, the new core consists of a number of 2μm-Ti-coated graphite blocks [5], pressed into the lower half of a welded, standard industrial OFE,

copper cylinder. Immediately downstream of the graphite are common aluminium-alloy blocks, followed by a length of copper, and a rearguard of tungsten. As a precautionary measure, thin 100 μm -thick titanium foils are affixed to the graphite blocks, to prevent possible migration of graphite particles within the vacuum chamber. The copper is water-cooled. The cast iron shielding is unchanged, as is the sweep pattern of the dumped beam. Graphite (about 90 kg) is used in this instance within the SPS vacuum chamber, for the first time. Cross-sections of the core of the TIDV are shown in Fig. 20.1, while Fig 20.2 includes a longitudinal cut through the core showing the different absorber materials: carbon, aluminium, copper and tungsten.

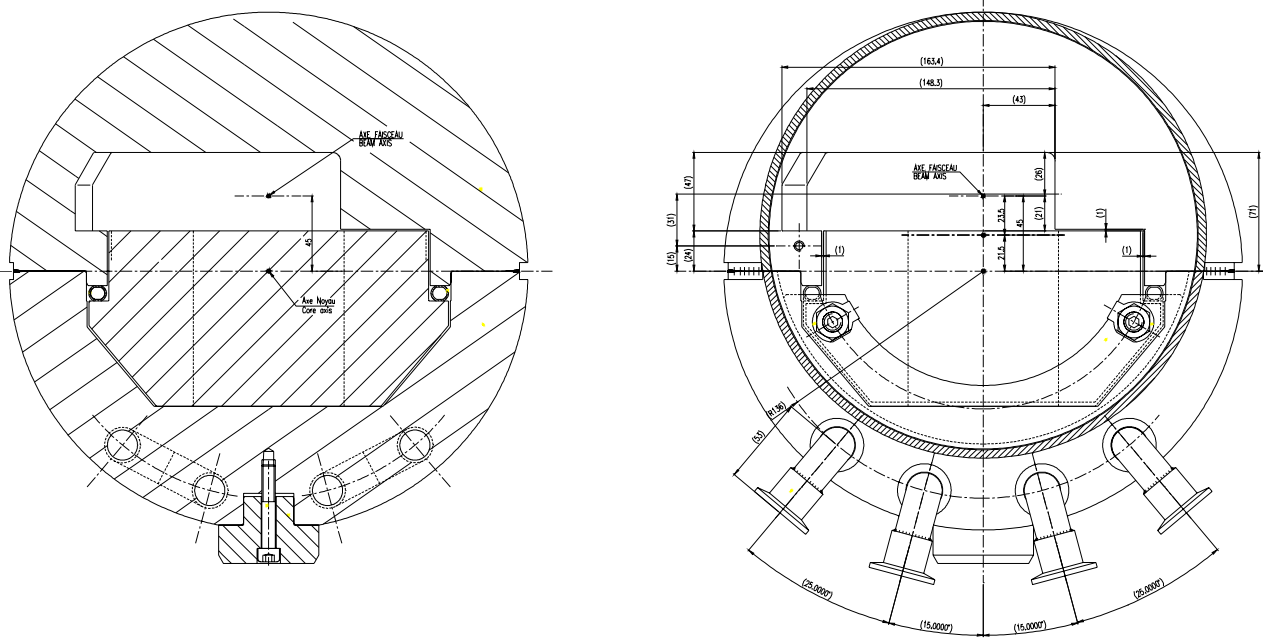


Figure 20.1: Cross-section and front-view of the TIDV core

20.3 ASSEMBLY AND TESTING

Prior to the selection of a type of graphite with optimum mechanical, thermal, and vacuum properties, several varieties were tested for the bake-out and degassing behaviour [6]. The most suitable graphite was considered to be the type 2020 PT.

The core components were assembled in a clean room with all due precaution and the copper half-cylinders were clamped rigidly to acquire the necessary constraint for good thermal contact as well as for precise weld preparation. The clamped assembly was dispatched to a contractor for electron beam welding of the copper cylinders and vacuum end-flasks.

Upon recuperation by CERN, the core was out-gassed at 150 °C for 24 hours using a pressurised hot water system and vacuum tested. Out-gassing and vacuum figures proved to be perfectly acceptable, with respect to SPS standard requirements [7]. The core was then assembled within the cast-iron shielding blocks. A further out-gassing period was then undertaken with the pressurised hot water circulating system.

20.4 INSTALLATION AND COMMISSIONING

The first TIDVG beam dump was installed in the LSS1 during the shut down of November 1999. In January of the year 2000, the dump was brought to its position in the tunnel, connected to the vacuum system, and subjected to about 60 hours of pumping and out-gassing tests. By the end of March and prior to machine start up, a pressure of 1.5×10^{-8} mbar was measured in the proximity.

Systematic dumping tests began with low beam intensities, increasing over a couple of weeks to reach $\sim 9 \times 10^{12}$ protons per cycle at 450 GeV. The effects of this repetitive dumping were reflected by a steady increase in vacuum pressure to nearly 10^{-6} mbar (Fig. 20.3), followed by steady recovery with beam off.

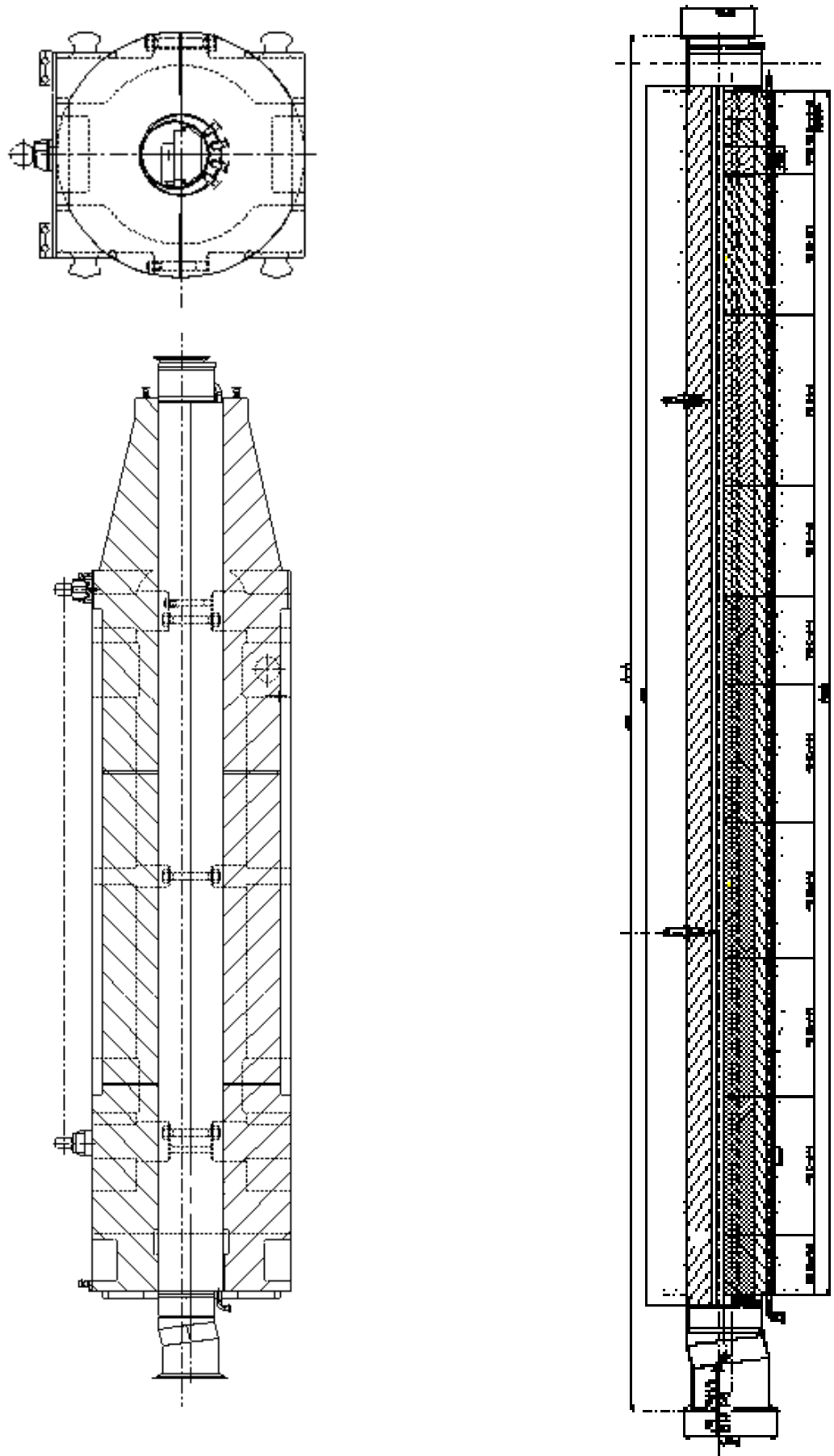


Figure 20.2: Schematic views of the TIDV absorber with a longitudinal cross-section of the absorber core.

Testing continued with a series of ten successive dumps of 2.5×10^{13} protons during the period while the machine set up the required intensities for fixed-target operation [8]. During this test the copper surface temperature rose to about 60°C and the local vacuum pressure to 9.2×10^{-6} mbar. In effect, the core was being baked-out and de-gassed as a result of the high temperatures generated by the deposited beam and vacuum recovery became more marked with successive dumping.

After about 4 weeks of operation the normal SPS physics run was underway, with occasional beam dump triggers under normal operational conditions. With the beam off, the vacuum pressure was recorded at 9.8×10^{-9} mbar. After five months of continuous operation, the pressure profile with beam off indicated an all time record for any TIDV, of 2.8×10^{-9} mbar (see Fig. 20.4). The pressure increases to around 1×10^{-8} mbar under normal operation conditions, with an intensity of about 3×10^{12} protons dumped at 450 GeV (Fig.20.5).

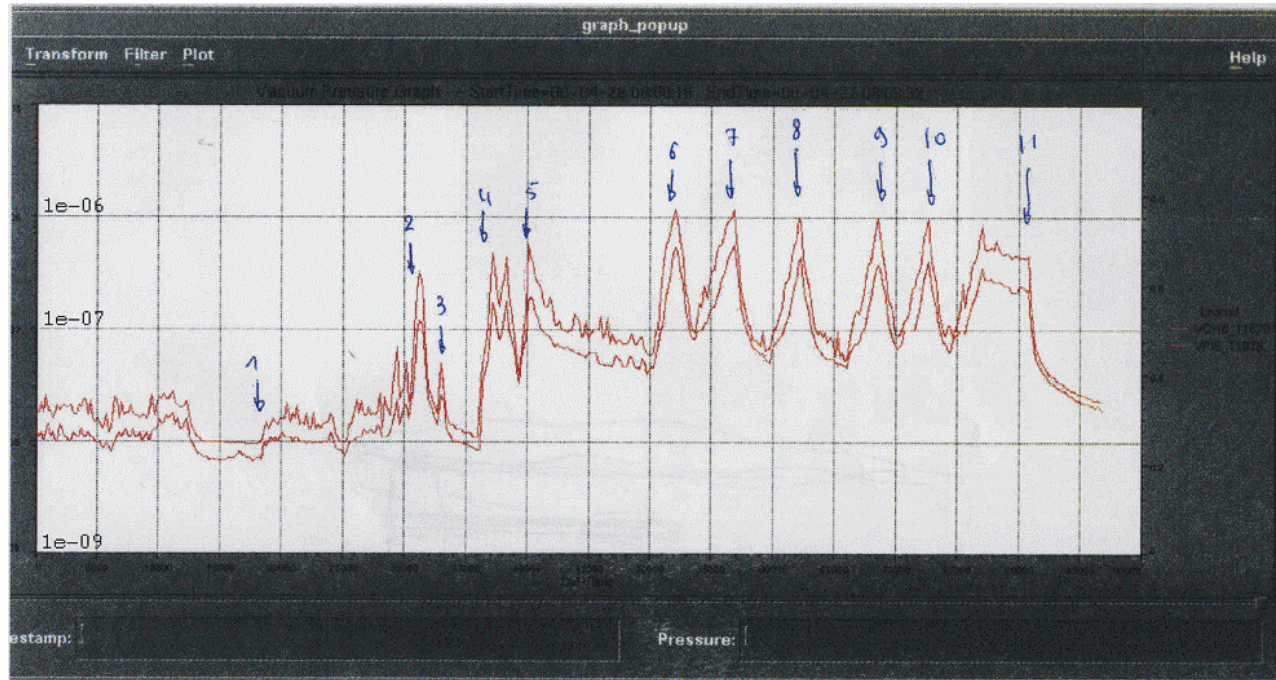


Figure 20.3: Systematic dumping of 9×10^{12} protons at 450 GeV on 27th of April 2000

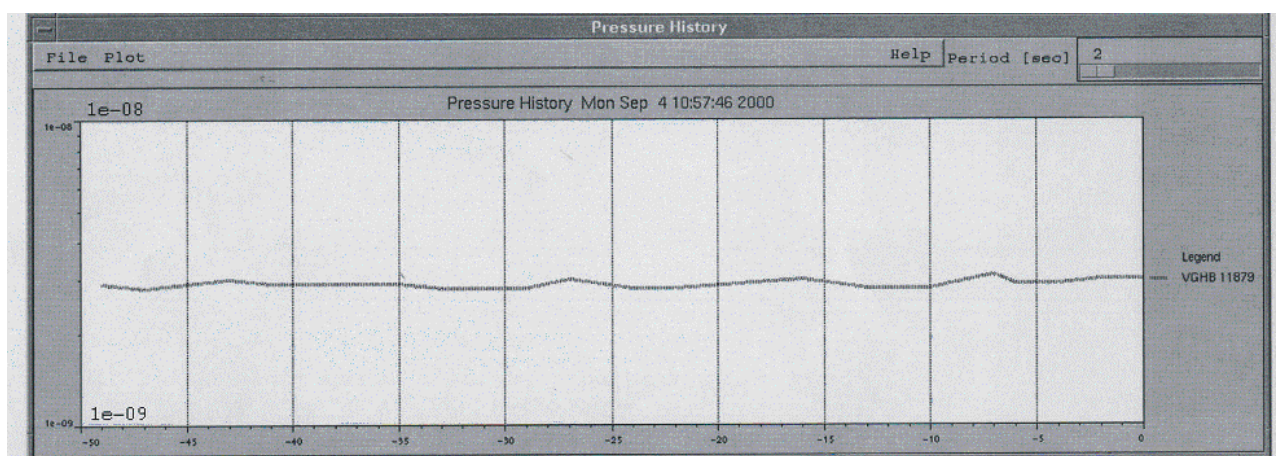


Figure 20.4: Vacuum pressure with beam off after five months of continuous operation

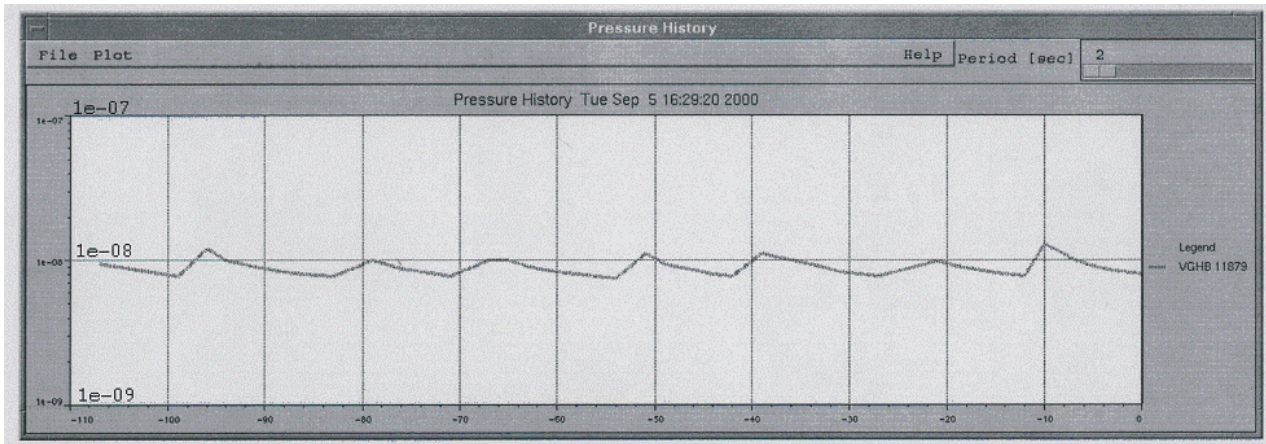


Figure 20.5: Normal vacuum conditions ($\sim 3 \times 10^{12}$ protons at 450 GeV) after five months of continuous operation

REFERENCES

- [1] The SPS Conceptual Design Report, “*The 300 GeV Programme*”, CERN/1050, 1972.
- [2] S.Péraire, “Décharge sur le dump interne TIDV du SPS de faisceaux destines au LHC”, CERN SL/Note 96-15 (BT/TA), Feb 1996.
- [3] SL drawing SPS 8034 41 0065 0.
- [4] J.M. Zazula & M. Ross, “*Transient Temperature Distributions Effected by Dumping the SPS Beam (LHC Injection Regime)*”. CERN SL/Note 95-91 (BT/TA).
- [5] S. Calatroni, H Neupert & W. Vollenberg, “*Production of Titanium coatings on Graphite Blocks*”, CERN EST SM Dec 1999.
- [6] R. Cornali & J. M. Jimenez, “*Measure du Taux de Degazage de Divers Types de Graphites*”, LHC-VAC/RC Vacuum Technical Note 99-08 Juillet 1999.
- [7] G. Mathis & K. Weiss, “*Test Beam Dump SPS n°2, après réparation des quatre angles chez Techmeta*”, 23-11-1999.
- [8] M. Ross, “*The Millenium Dump: TIDV Commissioning –April 2000*”, SL-Note-2000-050-BT, 2000.

CHAPTER 21

INTRODUCTION

21.1 SITUATION

Two new transfer lines, TI 2 and TI 8, with a combined length of 5.6 km are being built to transport protons at 450 GeV/c and ions from the SPS to the LHC. The geographical layout of these lines is shown in Fig. 21.1. Also shown are some of the main geometrical parameters. An overview of these lines including the LHC injection systems has been given in [1,2].

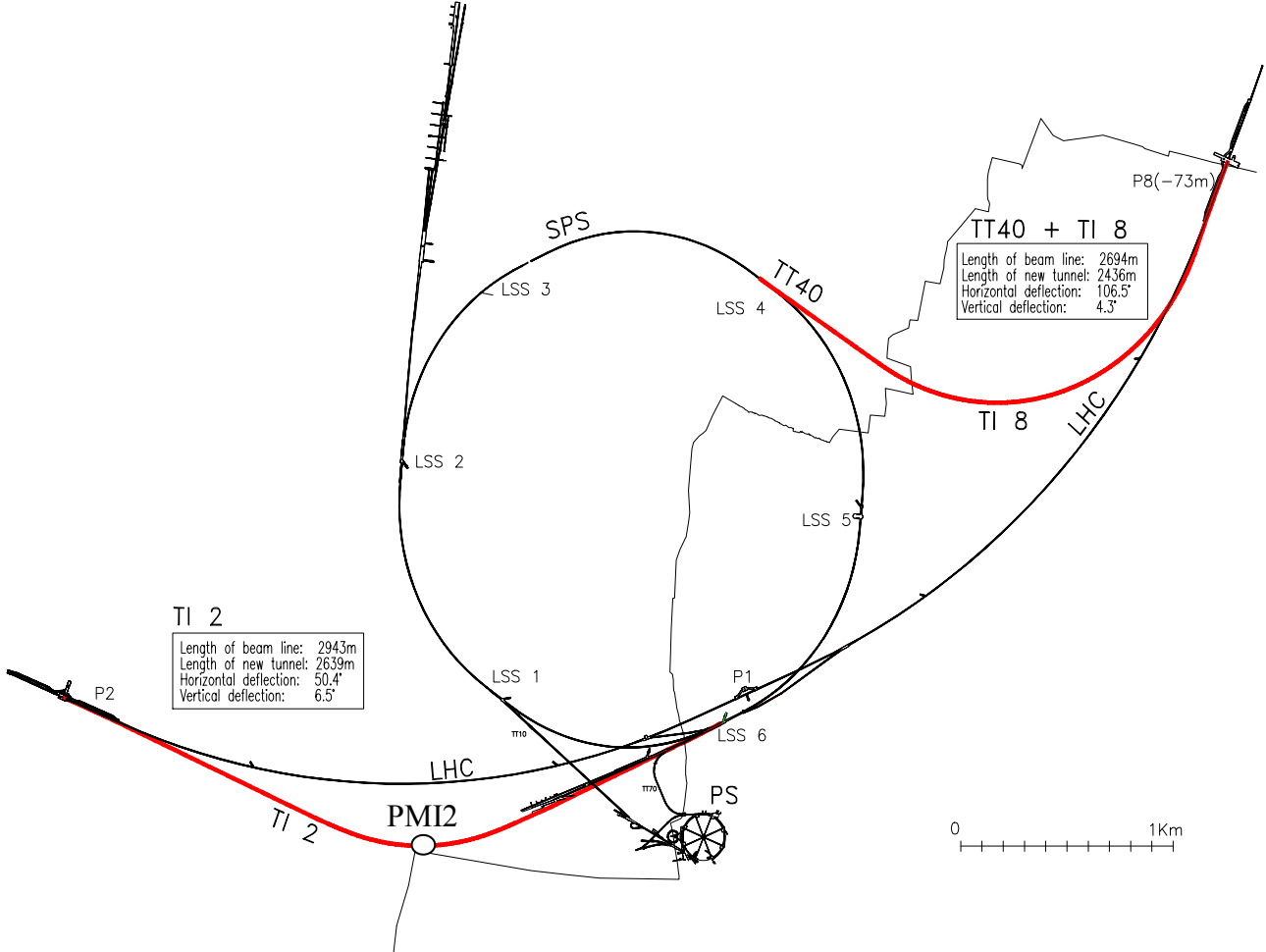


Figure 21.1: Overall layout of TI 2 and TI 8

The TI 2 line branches off from the existing SPS transfer line, TT60, in the switchyard, TCC6. The switchyard is some 250 m downstream of the LSS6 extraction point (see Chap. 18). TI 8 transports the beam over about 2.9 km to the injection point into LHC Ring 1, about 150 m left of IP2. The present slow resonant extraction in LSS6 will be converted into a fast extraction [3] after the closing of the SPS West Area at the end of 2004.

The beam to be sent down TI 8 leaves the SPS through the new fast extraction in LSS4, which was commissioned in 2003 [4] and arrives after about 2.7 km some 160 m right of IP8 for injection into Ring 2 (this IP is displaced away from the injection point by 11.22 m). The first 100 m of this new beam line is in common with the primary proton line to the CNGS facility [5]. Following the normal SPS nomenclature, this section of beam-line is called TT40.

A detailed description of the LHC injection systems is given in Chap. 16 of Vol. I, while the SPS extraction channels for the LHC are described in Chap. 18 of the present report.

The vertical profiles of the two tunnels are given in Fig. 21.2 and Fig. 21.3. Also shown is a line showing the approximate transition level between the limestone rock (below) and the glacial moraine (above). TI 8 drops some 70 m to bridge the altitude difference between the SPS and the LHC in that area. It is built completely in solid limestone rock. In order to stay entirely in the rock TI 2 has to pass below an underground river. In spite of the fact that the start and end point are at approximately the same altitude, additional vertical deflection is required to move the tunnel below the river, before raising it to the level of the LHC. More civil engineering related details are contained in Chap. 2 of Vol. II.

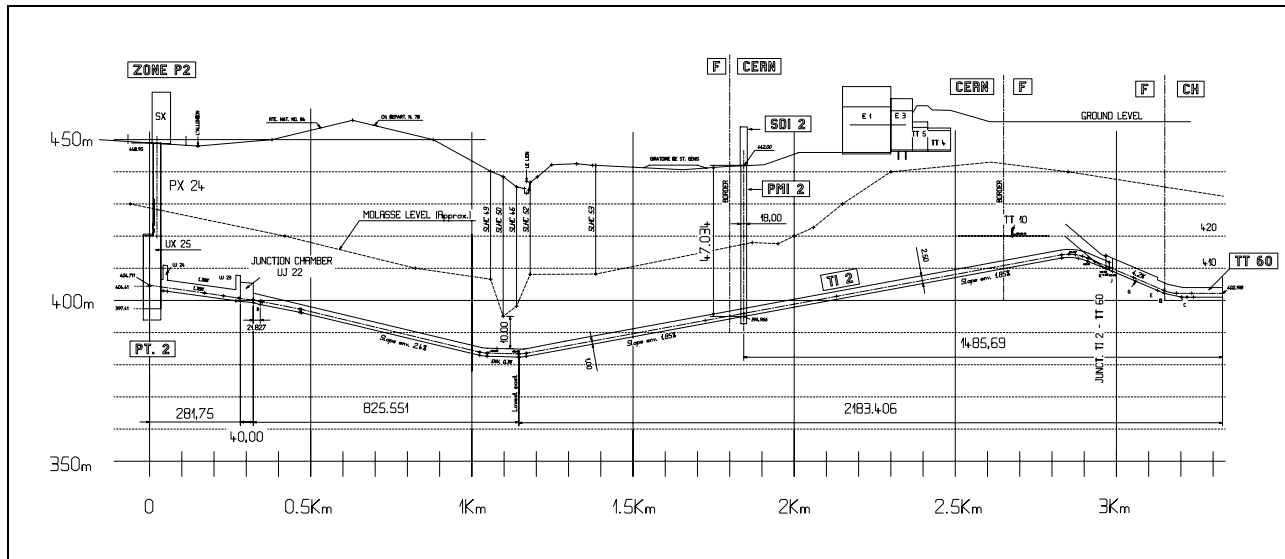


Figure 21.2: Vertical Profile of TI 2.

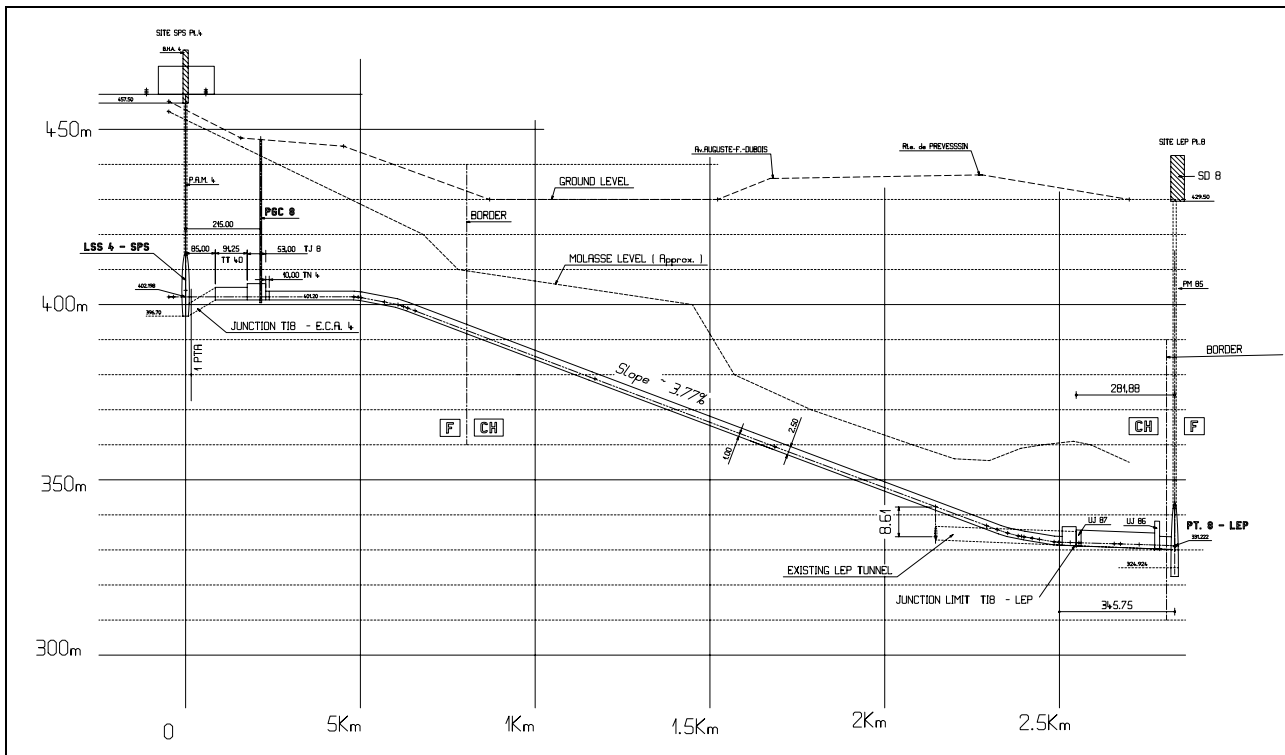


Figure 21.3: Vertical Profile of TI 8.

21.2 OVERALL DESIGN CONSIDERATIONS

A number of different variants to transfer beam from SPS to LHC have been considered during the design phase, including polarity reversal of the SPS to fill both LHC rings and the use of superconducting magnets. Since the lines will only be used during a fraction of the time (the possible filling schemes are described in

Chap.12 of this Volume) considerations of overall economy have finally led to the adoption of the present scheme based on room temperature magnets. The layout chosen also has the advantage that it leaves the LHC high-luminosity insertion in IR1 unaffected.

To reduce cost, the transfer line tunnels have a diameter of just 3 metres. Many components have been recuperated from closed down installations and existing infrastructure is used as much as possible. Classical magnets of compact design are used for the main dipole and quadrupole series. These were built by the Budker Institute for Nuclear Physics at Novosibirsk, in the framework of the contribution of the Russian Federation to the LHC.

A careful control of the trajectory and the preservation of the very small emittance during transfer and injection are of key importance. The main design goals in terms of beam performance and optics were to meet the LHC orbit with high precision and reproducibility (including all errors to better than $\pm 1.5\sigma$), to achieve a perfect optical match and to remain sufficiently flexible to accommodate future changes in both the SPS and the LHC optics.

21.3 STATUS AND PLANNING

Civil engineering and general services installation is finished for both tunnels. During the summer of 2004 the beam line in TI 8 will be installed [6]. Beam commissioning of the entire TI 8 line (with the exception of the LHC injection) is scheduled for October 2004 [7]. Line installation in the upstream part of TI 2, up to a point 200 m away from the access shaft PMI2 (indicated in Fig. 21.1 and Fig. 21.2), is foreseen to start towards the end of 2004.

The downstream part of the TI 2 tunnel will be used to transport LHC cryomagnets into the machine. For this reason the beam line will not be installed until the transport of the LHC components is complete [8].

REFERENCES

- [1] A.Hilaire, V.Mertens, E.Weisse, “*Beam Transfer to and Injection into LHC*”, Proc. EPAC’1998, Stockholm, 1998 and CERN/LHC Project Report 208.
- [2] V.Mertens, “*Transfer and Injection*”, Proc. SPS & LEP Performance Workshop, Chamonix X, 2000.
- [3] J.Borburgh et al., “*The Design of the New SPS LSS6 Fast Extraction Channel for the LHC*”, Proceedings of the 2004 European Particle Accelerator Conference, Lucerne, Switzerland, EPAC 2004.
- [4] B.Goddard et al., “*Beam commissioning of the SPS LSS4 Extraction and the TT40 Transfer Line*”, Proceedings of the 2004 European Particle Accelerator Conference, Lucerne, Switzerland, EPAC 2004.
- [5] K.Elsener (ed.), “*The CERN Neutrino Beam to Gran Sasso (NGS): Conceptual Technical Design*”, CERN 98-02 (1998).
- [6] A.Spinks, “*TI 8 Installation and Hardware Commissioning*”, Proc. LHC Performance Workshop Chamonix XIII, 2004.
- [7] J.Uythoven, “*TT40 Experience and TI 8 Beam Tests*”, Proc. LHC Performance Workshop, Chamonix XIII, 2004.
- [8] V.Mertens, “*Getting TI 2 Operational*”, Proc. LHC Performance Workshop Chamonix XIII, 2004.

CHAPTER 22

TRANSFER LINE OPTICS AND LAYOUT

22.1 INTRODUCTION

This chapter describes the layout and optics design of TI 2 and TI 8 [1], the trajectory correction scheme [2] and the required performance. Careful control of the trajectory and the preservation of the very small emittance during transfer and injection are of key importance, because of the very limited mechanical aperture of the line magnets [3], the high intensity and energy in the beam, the limited numbers of correctors and pick-ups and the tight tolerances on the beam parameters at injection into the LHC [4].

Details of the magnets, powering, vacuum civil engineering and other services (water, ventilation and transport) are covered elsewhere in the LHC design report.

22.1.1 Design Goals

The transfer lines must allow the beams to be injected onto the LHC orbit with high precision and reproducibility [5] while ensuring an adequate optical match and remaining sufficiently flexible to accommodate any future machine optics changes. The machine protection elements in the lines should prevent the transfer of beams which could cause damage to the LHC, either by generating interlocks, or by passive protection. The main performance specifications for the lines are given in Tab. 22.1.

Table 22.1: Main performance specification for the transfer lines (tolerance values).

Parameter	Unit	Value
Beam emittance from SPS (1 σ normalised)	μm	3.5
Beam energy	GeV	450
Maximum beam intensity	p^+	$4.9 \times 10^{+13}$
Beam energy spread (1 σ)	$\Delta p/p$	0.0015
Energy acceptance	$\Delta p/p$	± 0.003
Injection precision in LHC	σ	± 1.5
Tuning range for SPS optical parameters at extraction point (β, α)	%	± 20
Tuning range for LHC optical parameters at injection point (β, α)	%	± 20
Transverse emittance growth from all mismatch effects	$\varepsilon/\varepsilon_0$	1.05
Transverse oscillation amplitude transmitted into the LHC for failure cases	σ	± 7.5
Aperture	σ	± 6.0

22.2 GEOMETRICAL LAYOUT

The geometrical layout of the lines is dictated by:

- The choice of SPS points 4 and 6 for the location of the fast extraction systems
- The choice of LHC points 8 and 2 for the corresponding injection systems
- By the relative geometries of the two machines
- The magnetic rigidity of the beam extracted from the SPS
- The strength of the main bending dipoles in the lines.

For LHC Ring 1, the beam is extracted from SPS LSS6 [6] and transferred to LHC Point 2 by the existing TT60 transfer line and TI 2. For Ring 2 the beam is extracted in SPS LSS4 [7] and transferred via TT40 and TI 8. The total horizontal and vertical deflections and offsets of the combined TT60-TI 2 and TT40-TI 8 lines are given in Tab. 22.2. The horizontal and vertical sections of the lines are shown in Fig. 22.1

The SPS is aligned in the plane normal to the local gravity vector at the centre of the SPS accelerator. The plane of the SPS is therefore tilted with respect to the CERN Coordinate system (CCS) by 0.24 mrad. Note

that this angle is also the maximum of the slope ϕ to be found in the SPS ring. For geological reasons associated with the civil engineering of the tunnel, the plane of the LHC machine was built at a fairly large angle of 1.4% (14 mrad) to the CCS. The geometrical matching of the lines must therefore respect the alignment differences between the two machines, as summarised in Tab. 22.2. In this table the extraction point of the SPS is defined as the exit plane of the quadrupole QDA4(6)19 coil window and that the injection point of the LHC is defined as the entrance of the first injection septum MSI. The XYZ coordinates in Tab. 22.2 are given in the CERN coordinate system, where Y represents the altitude.

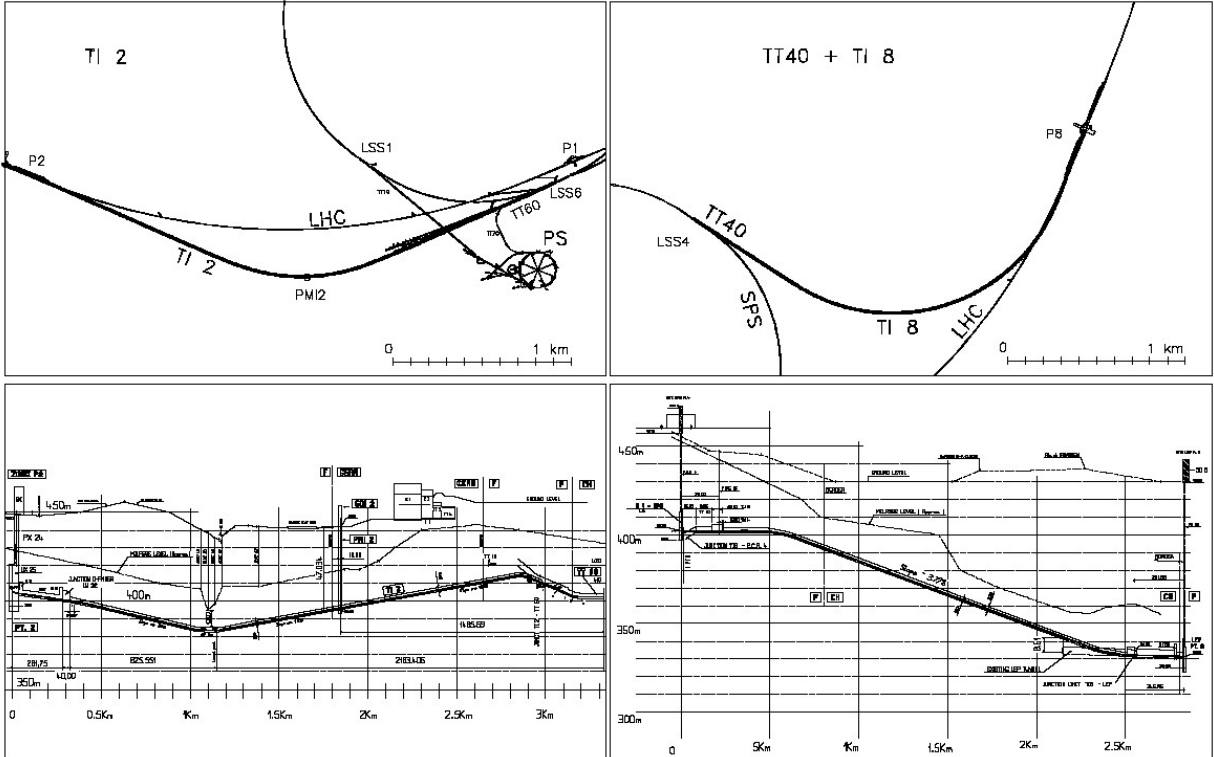


Figure 22.1: Horizontal and vertical sections of TI 2 and TI 8.

Table 22.2: Main geometrical parameters of TI 2 and TI 8.

Parameter	Unit	TI 2	TI 8
Length	m	3116.732	2627.501
Vertical height difference	m	1.124	70.875
Horizontal bending angle	degree	48.22	103.04
Vertical bending angle	degree	6.5	4.3
Maximum vertical slope	degree	4.3	3.8
SPS extraction point location:	m	-2083.528	-2314.717
	m	2402.179	2401.752
	m	2586.131	4456.102
LHC injection point location:	m	817.045	-4391.382
	m	2401.056	2330.877
	m	2615.609	4807.174

22.3 OPTICS

Both lines use a FODO lattice with 90° phase advance per cell and a half-cell length of 30.3 m. The structure is similar to the SPS with each half-cell containing four dipoles, as shown in Fig. 22.2. Short straight sections with space for instrumentation and dipole corrector magnets follow each quadrupole, as illustrated in Fig. 22.3. The main optical parameters and requirements are summarised in Tab. 22.3.

The main horizontal arc in TI 2 has been designed as an achromat. Space reasons dictated a different solution for TI 8. Beam optics calculations to second order show negligible effects which do not require higher-order corrections. The optics functions for TI 2 and TI 8 are shown in Fig. 22.4 and 22.5 respectively

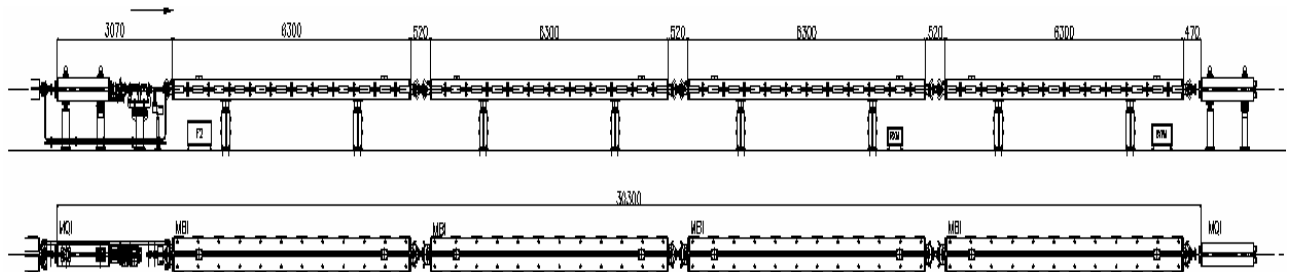


Figure 22.2: Half-cell layout (MBI version).

Table 22.3: Summary of main optics parameters for the transfer lines.

Parameter	Unit	TI 2	TI 8
β_x max	m	308.5	240.8
β_y max	m	289.5	274.6
β_x max (arc section)	m	101.2	101.2
β_y max (arc section)	m	101.1	101.1
$ D_x $ max	m	3.82	3.88
$ D_y $ max	m	3.97	1.34
D_x rms	m	1.42	1.78
D_y rms	m	0.55	0.20
μ_x total	2π	12.07	10.54
μ_y total	2π	12.24	10.32
Half-cell length	m	30.3	30.3
Number of half-cells		95	85

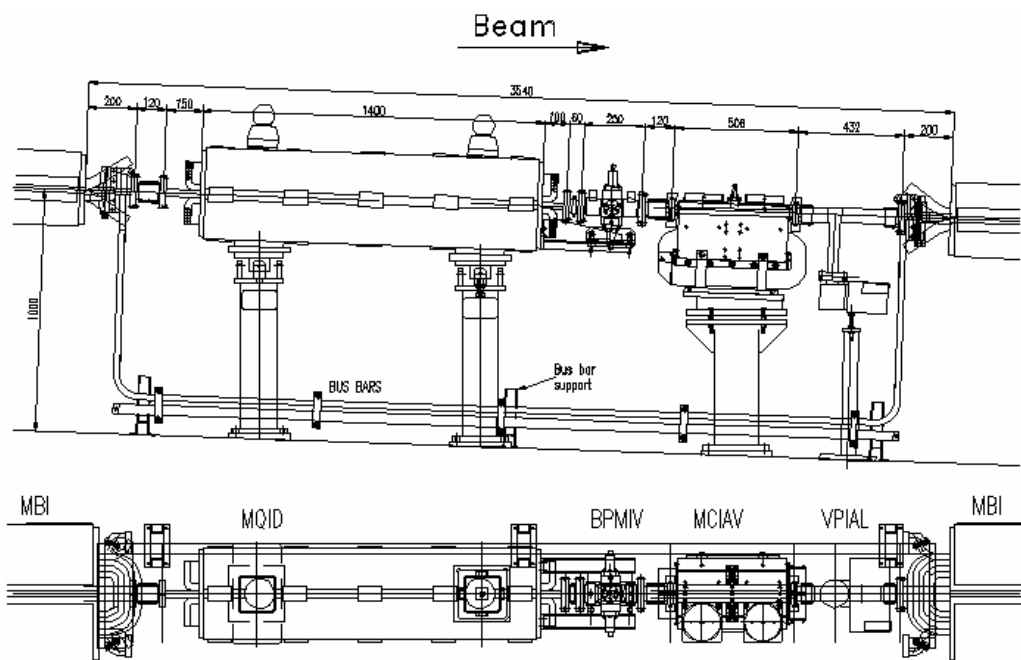


Figure 22.3: Short-straight section layout, showing vertical BPM and corrector.

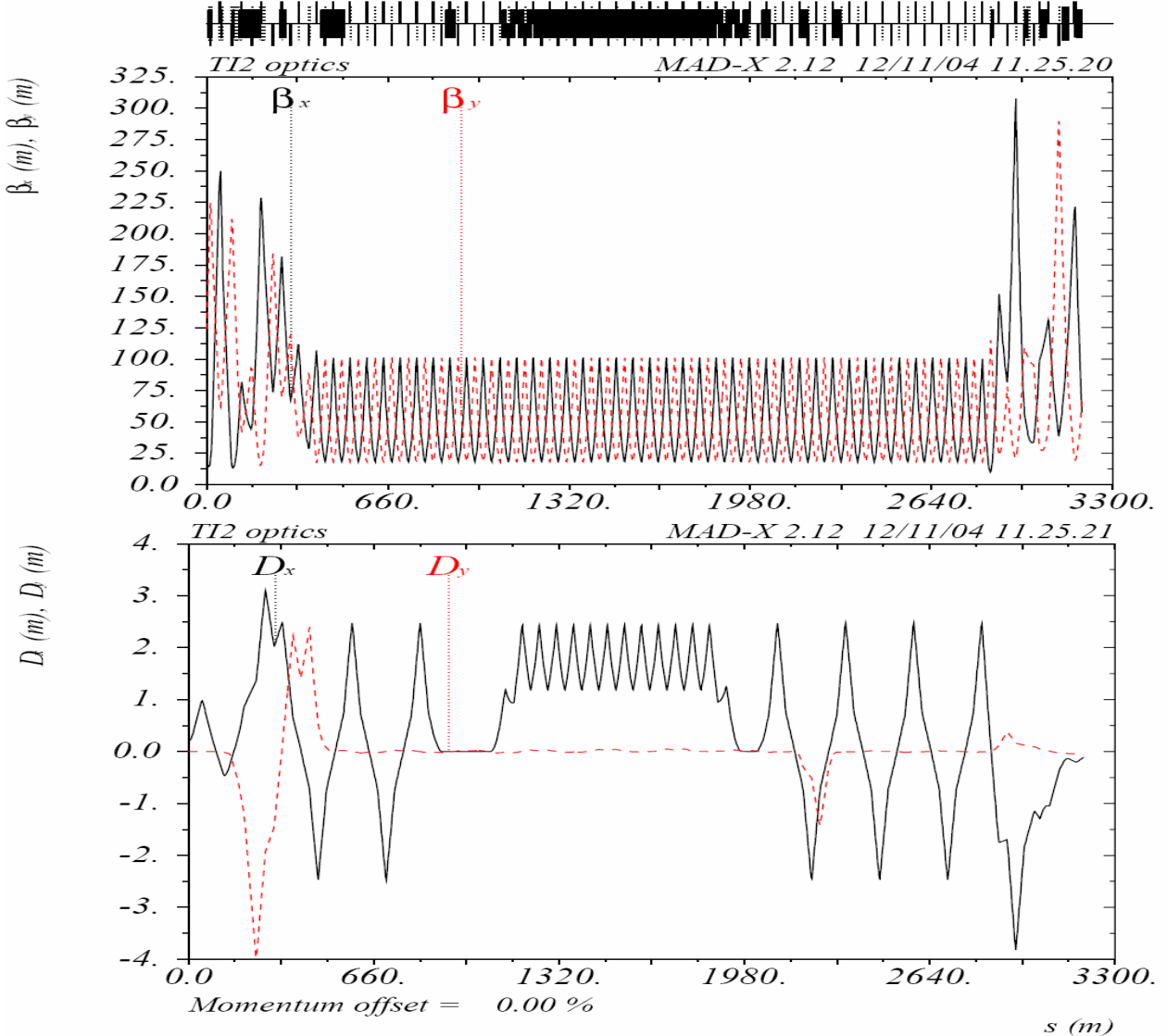


Figure 22.4: TI 2 optics functions.

22.3.1 Optics Design Features and Constraints

The arcs of the transfer lines are matched to the SPS and the LHC by means of sets of dedicated quadrupole magnets on either end of the lines. The six arc constraints in TI 8 are matched to the SPS with seven matching quadrupoles (four quadrupoles in TT40 and three in TI 8). In the case of TI 2 the transfer line arc is matched to the SPS using six quadrupoles in TI 2 (there are also six matching quadrupoles in the existing TT60 line). On the LHC ends, both lines are equipped with 10 matching quadrupoles.

With the present layout the dispersion matching in both planes on the LHC side is difficult and limits the tunability of the lines. This arises from a combination of several issues: the maximum gradient of 57 T/m for the matching quadrupoles, the aperture constraint of $\geq 6\sigma$ in the arc and the aperture bottleneck towards the end of the lines. The additional constraints imposed by the phase advance relations between the transfer line collimators (TCDI) limit the flexibility further. To guarantee sufficient protection, the phase advance conditions between the TCDI must be constrained to within a few degrees of their nominal values. The TCDI system is based on 3-phase collimation (3 collimators per plane with 60° between two subsequent collimators, or $60^\circ + n \times 180^\circ$ in case of space problems) and is installed to protect the MSI septum and the LHC cold aperture. The TCDI are located as close as possible to the MSI and the LHC and hence are located in the LHC end matching section. Any changes of the LHC optics at the injection points affect the phase advances in the matching sections, resulting in a trade-off between mismatch to the LHC and protection level

of the TCDI. The optics versions of both lines need to be matched to the LHC optics (presently version v6.5) with the constraints of the layout and powering, to guarantee enough line aperture and the optimum phase advance conditions between the TCDI collimators.

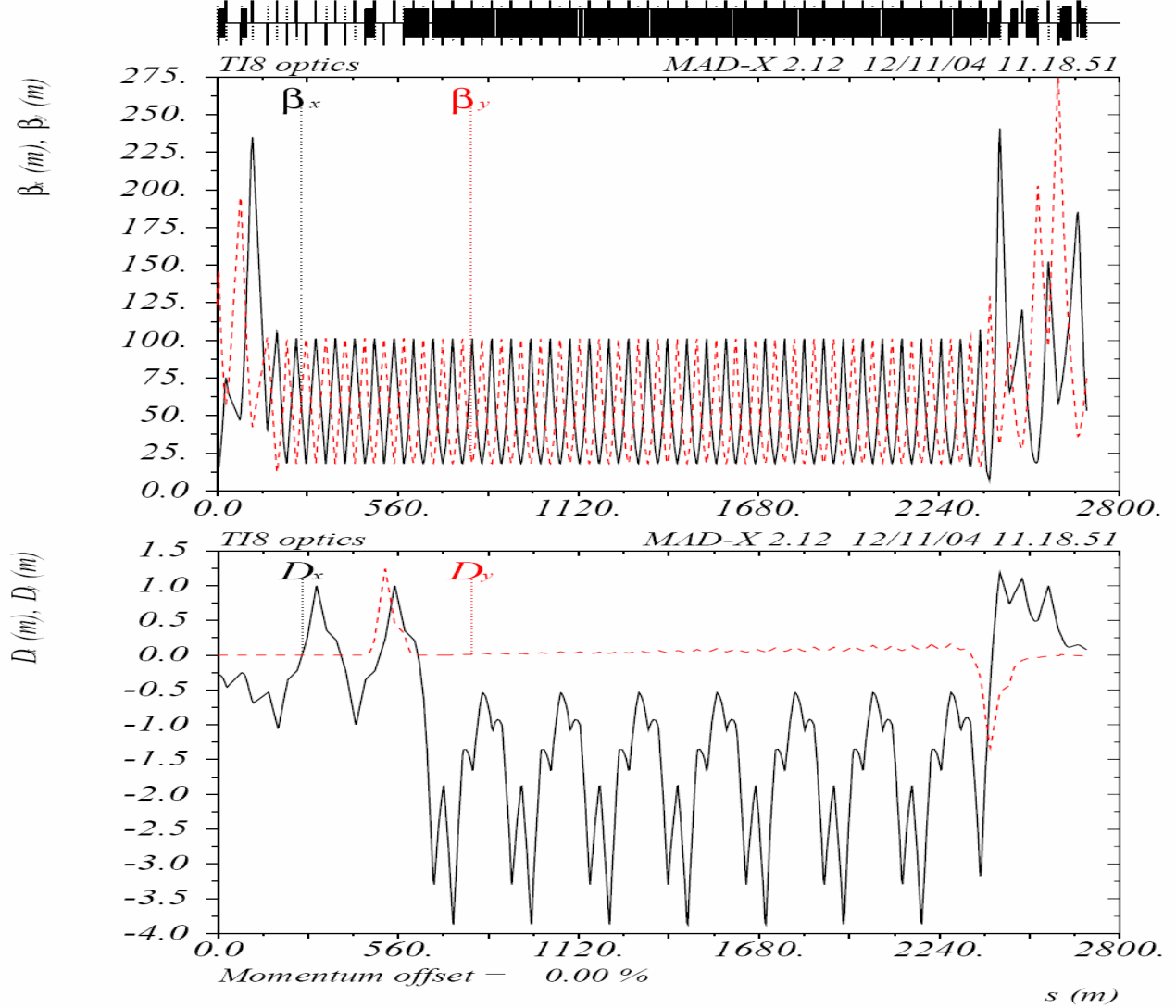


Figure 22.5: TI 8 optics functions.

22.3.2 Mismatch and Errors

The tight emittance budget for transfer and injection into the LHC places stringent requirements on the various mismatch factors which can occur [8]. Mismatch leading to emittance growth can arise from several sources. The total contribution of all of the above effects must be less than the emittance growth budget of 1.07, which presents a difficult challenge. For the effects identified below, this means that each contribution must be below about the 1-2 % level.

Steering error

In the LHC the steering errors are normally dealt with by the damper system and the emittance blow-up will be a function of the injection errors, the damper strength and the filamentation time. For the transfer lines the maximum injection error is specified as $e_{\text{inj}} \leq 1.5 \sigma$. The residual blow-up after the action of the feedback depends on the filamentation and damping times [9]. For the specified filamentation and damping times of 68 ms and 5 ms respectively [10], the maximum 1.5σ injection error gives an emittance increase of about 0.5 %.

Betatron mismatch

The beam will be optically mismatched [11] when the α and β of the injected beam do not match those of the LHC. This may be due to optical errors in the line, or a mismatch at the SPS extraction point. To respect the emittance budget of about 2% increase, the mismatch parameter λ (defined as the ratio of the largest semi-axes of the mismatched and matched ellipses) must be less than 1.10.

Dispersion mismatch

The dispersion can also be mismatched at the injection point, leading to emittance growth [12]. For an energy spread of about 10^{-3} , the maximum tolerable dispersion mismatch is very small, at about 0.05 m and 0.002 rad, for ΔD and $\Delta D'$ respectively.

Energy error

An energy error between the machines can also lead to an emittance growth. For a nominal dispersion of about 0.1 m, a (relatively pessimistic) energy error of 5×10^{-4} gives an emittance growth of about 0.3 %.

Geometrical mismatch

There can also be a geometrical mismatch at injection with a tilt between the beam XZ plane delivered by the transfer lines and that of the LHC. The expected emittance increase is about 1.3 % given the design tilt mismatch of 52 mrad between TI 8 and the LHC [13].

Coupling

Coupling between the planes in the transfer line can also lead to an emittance growth at injection. For the LHC transfer lines the coupling, \mathbf{k} , is expected to be less than 5 %. The emittance growth from this source will therefore be below 0.1 %.

Summary

The expected maximum levels of each contribution are given in Tab. 22.4 together with the limits placed on the various optical parameters. The total expected emittance increase is of the order of 6%, which is just inside the specified emittance budget.

Table 22.4: Summary of emittance increase contributions and associated limits on optical parameters.

Effect	Parameter	Unit	Limit	expected ϵ/ϵ_0
Steering error	τ_{DC} / τ_d (damping ratio)	-	≥ 14	1.005
	ϵ_{inj}	σ	≤ 1.5	
Betatron mismatch	λ (mismatch factor)	-	≤ 1.1	1.020
Dispersion mismatch	ΔD (dispersion error)	m	≤ 0.05	1.020
	$\Delta D'$ (dispersion prime error)	rad	≤ 0.002	
Energy error	$\Delta p/p$	-	$\leq 5 \cdot 10^{-4}$	1.003
Geometrical mismatch	θ (tilt mismatch)	rad	≤ 0.052	1.013
Coupling	\mathbf{k} (coupling factor)	-	≤ 0.05	1.001
Total				1.063

22.3.2 Energy Acceptance

The energy acceptance of the line is a function of the aperture, the optics and the corrected trajectory. The specified acceptance in $\Delta p/p$ is ± 0.003 . For TI 8 the acceptance has been checked by simulating the transmission of a beam as a function of the energy offset, using the full aperture model and the various errors, for 1000 corrected trajectories simulated with all errors. The simulated distribution of transmissions is shown in Fig. 22.6. Defining the acceptance as the 99% transmission limit, the simulation gives an energy acceptance for TI 8 of around ± 0.003 .

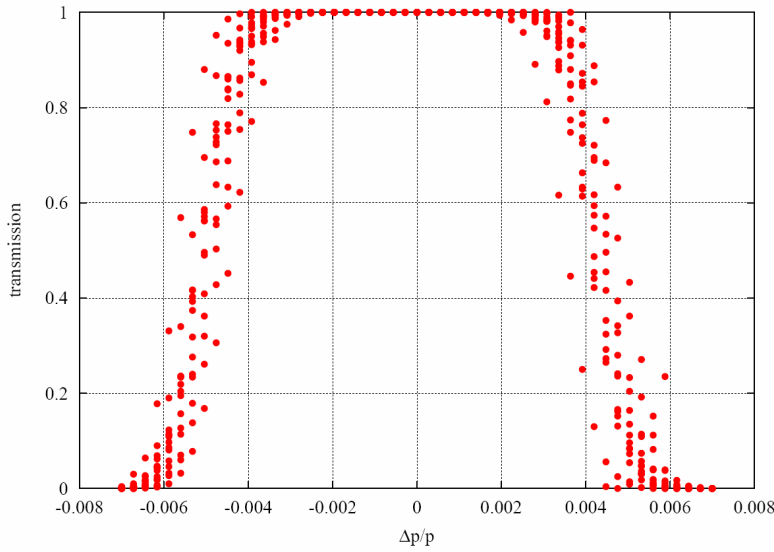


Figure 22.6. Simulated transmission as a function of beam energy offset, for TI 8 with all errors.

22.3.3 Beam tilt accumulation

A horizontal bending dipole aligned with an inclination (slope) angle ϕ with respect to the reference coordinate system introduces a small tilt (roll) angle ψ into the beam. For small angles ψ is proportional to the product of the magnet bending angle α and the slope ϕ . For most transfer lines this effect can be neglected, but for long lines with many horizontal bending magnets on relatively steep vertical slopes relative to the reference frame, a non-negligible tilt angle ψ can accumulate between the local beam plane and the reference alignment system. This can result in a mismatch at injection with subsequent emittance blow-up. In addition other undesirable effects, such as non-orthogonal trajectory measurement and correction can become important. A detailed description of this effect is given in [14].

In TI 8, this effect is significant. The roll angle ψ accumulates along the line, reaching 65 mrad at the LHC injection point. This is much larger than the 13 mrad local tilt of the LHC machine. With no additional measures, the (x,y) plane of the beam would therefore have an inclination of about 52 mrad to that of the beam in the LHC.

There are two separate issues which have to be considered:

Firstly, the accumulation of ψ along the transfer line due to the combination of vertical and horizontal bends. This does not depend very much on whether the line is designed so that the dipole magnets are aligned with zero tilt or with the local beam tilt. However, the quadrupoles, correctors and pickups will be aligned with respect to the local beam tilt to ensure that the system stays orthogonal to simplify the trajectory correction and to avoid coupling between the planes. For TI 8 this means an alignment of up to 3.7° with respect to the vertical of the local CERN reference system.

Secondly, the effect of the mismatch in ψ between the end of the transfer line and the LHC. For the TI 8 injection point this effect is about 52 mrad. Correction can only be accomplished by rotating the plane of the beam with a system of skew quadrupoles at the end of each line. However, the emittance increase expected from this effect is small, below 2 % [12]. A potentially more important effect is the repopulation of the transverse tails of the beam, which are removed above about 3.5σ in the SPS. Analysis has shown that the coupling between the planes induced by the tilt can populate the beam tail significantly [14], with amplitude growths of around 20%. An effective remedy is to remove particles in the tails which have simultaneous large horizontal and vertical amplitudes by means of a tilted X-Y scraper in the SPS [15]. In this case, skew correction of the tilt plane is not required, since the amplitude growth is less than 10%.

22.4 TRAJECTORY CORRECTION

Following in-depth study [2,16] a correction scheme is used in which two out of every four adjacent cells in each plane are equipped with correctors. Full correction is performed at the beginning and the end of each line. TI 2 uses 55 correctors, while TI 8 requires 43, in addition there are 55 and 46 beam position monitors in the two lines, respectively. The placement of these is designed to keep the maximum trajectory excursion amplitude to below 4.5 mm. Fig. 22.7 shows the distribution of expected maximum trajectory excursions for TI 8.

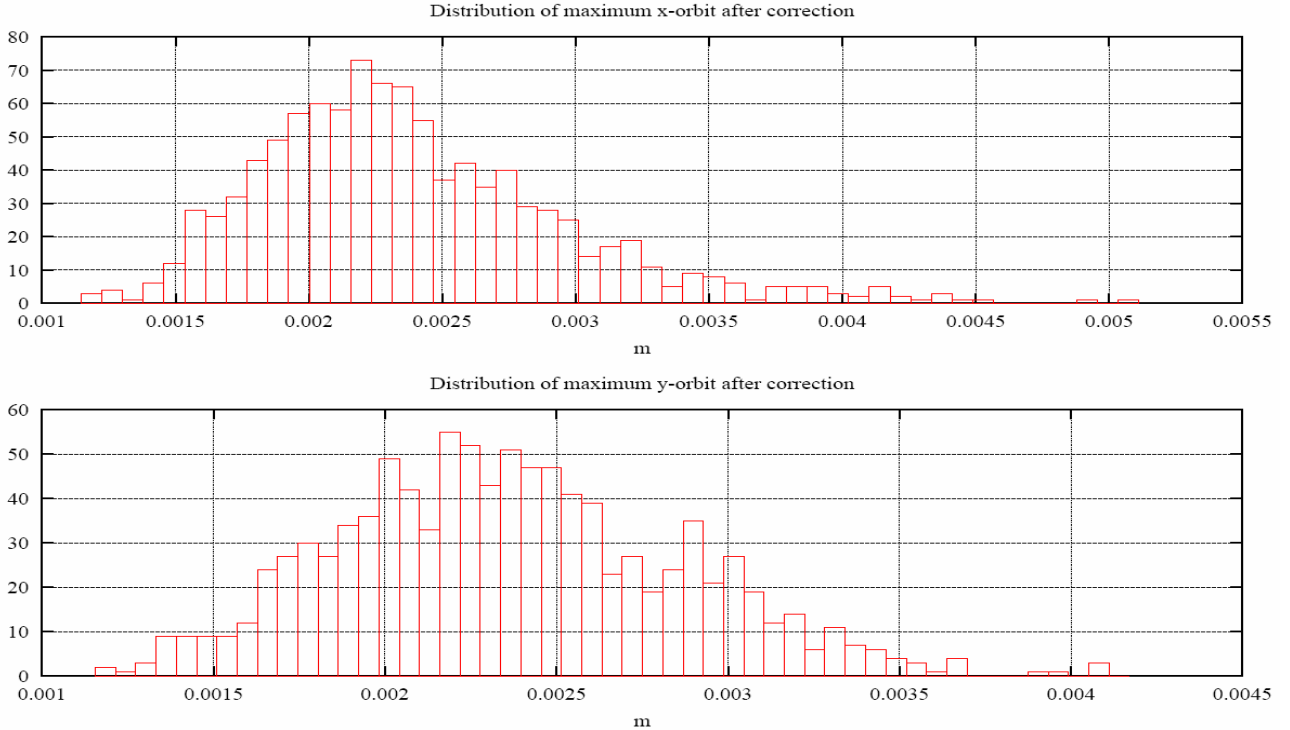


Figure 22.7: Distribution of maximum amplitudes for TI 8, based on 1000 trajectory corrections simulated with all errors.

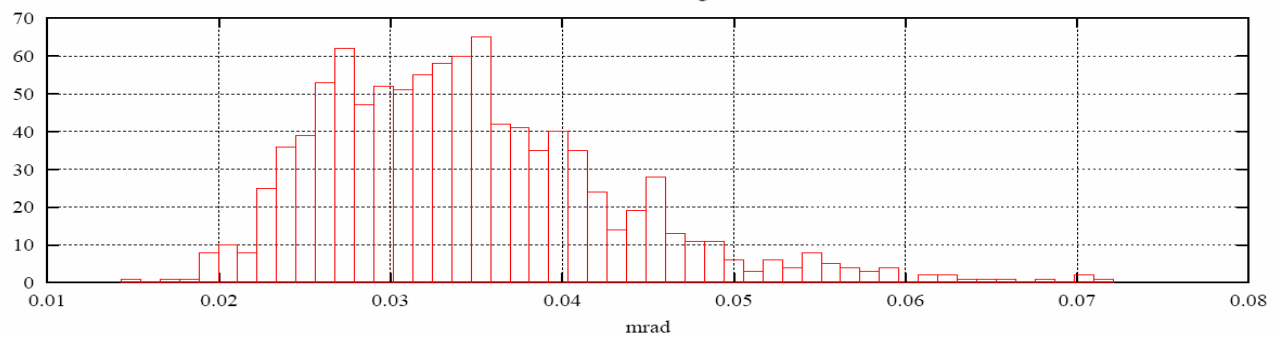
The study shows that the correctors, including dipole groups, can correct orbit excursion caused by error distributions up to 3σ . Exceptions are found in the correctors in both planes responsible for compensating injection errors, assumed to be Gaussian-distributed with rms equal to 0.5 mm in position and 50 μ rad in angle. This deficit in corrector range becomes less severe and eventually vanishes, as the injection error magnitudes are reduced. Fig. 22.8 shows the distribution of expected maximum corrector strengths for TI 8.

For 1-to-1 steering, a missing monitor can lead to a singular steering configuration. This in turn can result in an excessive correction if not handled correctly. In such cases disabling one corrector resolves the problem. In the over-constrained case of the steering in the periodic sections, the configurations are generally less susceptible to excessive corrections as a result of missing monitors.

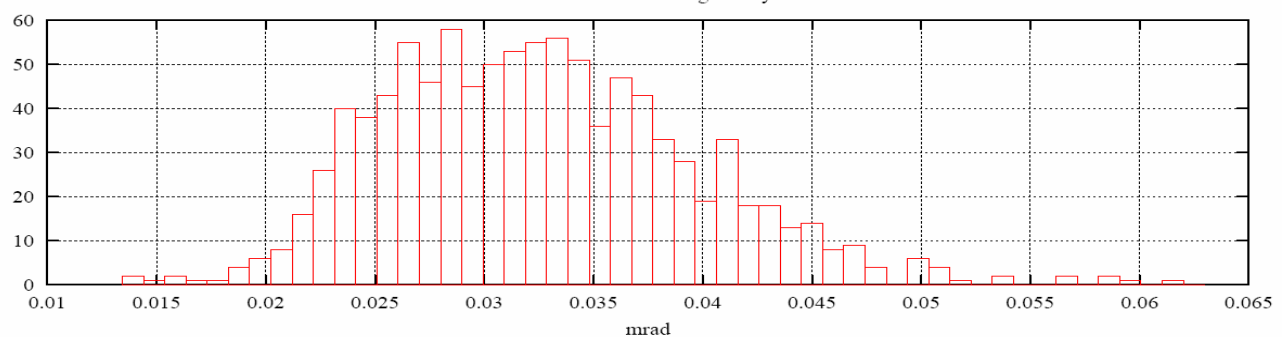
The limited correcting power for fighting injection errors causes some sensitivity of the trajectory error to the correction process at the beginning of the TI 2 and TI 8 lines. Large peaks are associated with corrector scaling errors, all caused by the same correctors responsible for fixing injection errors. This sensitivity can only be fixed by orbit control upstream of the injection point.

The difficulties which might arise with monitor anomalies illustrate the importance of an intelligent trajectory correction algorithm. The best way to deal with a missing monitor is not always to disable individual correctors, but to disable singular combinations of correctors, achievable only through the use of an intelligent real-time algorithm.

Distribution of maximum strength for x-correction



Distribution of maximum strength for y-correction



from the random effects in various elements is about 0.35σ horizontally and 0.30σ vertically. For these effects the whole beam will be injected at the specified amplitude, since the period of the power converter ripple (\sim milliseconds) is much longer than the batch length ($\sim 10 \mu\text{s}$). A further systematic offset of about $\pm 0.25 \sigma$ horizontally and $\pm 0.35 \sigma$ vertically has to be added for the kicker waveform. The variation along the kicker pulse will reproducibly sweep the bunches in each batch over this range. The bunches are not uniformly distributed within this range and the resulting oscillations have implications for the performance of the damper. This is especially true in the vertical plane as a result of the high frequency components present in the early part of the MKI pulse. Taking a 99% (3 σ) confidence limit for the random effects, the overall precision is then 1.25σ in both H and V for LHC beams 1 and 2. This is within the specification of 1.5σ . The distribution of the bunches in the vertical plane will have implications for the setting-up of the injection into the LHC, since normally one would try to inject the average bunch position onto the LHC orbit. If this is done with the bunch distribution from the MKI, the actual range of offsets coming from the MKI waveform will be $+0.2$ to -0.5σ . The random effect in the vertical plane is dominated by the precision of the SPS orbit and any drifts in the transfer line. In the horizontal plane the contributions from the orbit, drift and main magnet families are of a similar order of magnitude.

22.6 APERTURE

The transferred beams must stay within the available aperture. The strongest aperture constraint comes from the main dipoles of the transfer line, the MBI, with their full gap height of only 25 mm. This aperture results in a maximum tolerable vertical trajectory excursion, near the defocusing quadrupoles, of ± 4.5 mm.

The aperture N in number of sigma available to the beam is derived using:

$$N = ([A/2 - E_{\max}(\beta/\beta_{\max})^{1/2} - K_\beta D \Delta p/p]/K_\beta)/\sigma$$

here, A is the full physical aperture remaining after mechanical and alignment tolerances and sagitta are taken into account. $K_\beta = 1.1$ is the optical mismatch parameter, β_{\max} the maximum beta function in the regular arc, E_{\max} the maximum allowed orbit excursion, $\sigma = (\beta \epsilon)^{1/2}$ the betatron beam size and $\Delta p/p = 0.0015$ the momentum spread.

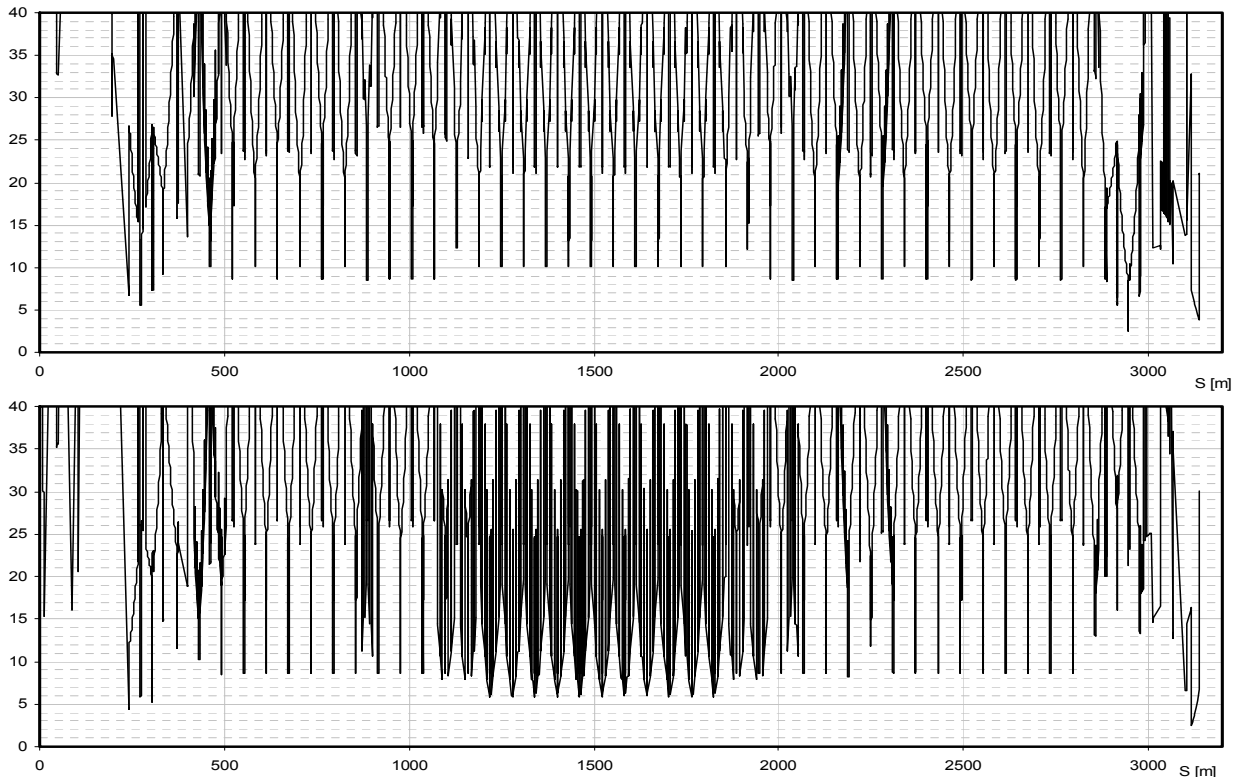


Figure 22.9: Horizontal (top) and vertical beam aperture (σ) for TI 2.

Figs. 22.9 and 22.10 show the aperture N calculated for the horizontal and vertical planes of the two lines, using the full physical aperture model. Fig. 22.11 shows the distribution of apertures expected at the six worst aperture bottlenecks in TI 8. This was based on the result of 1000 corrected trajectories simulated with all errors.

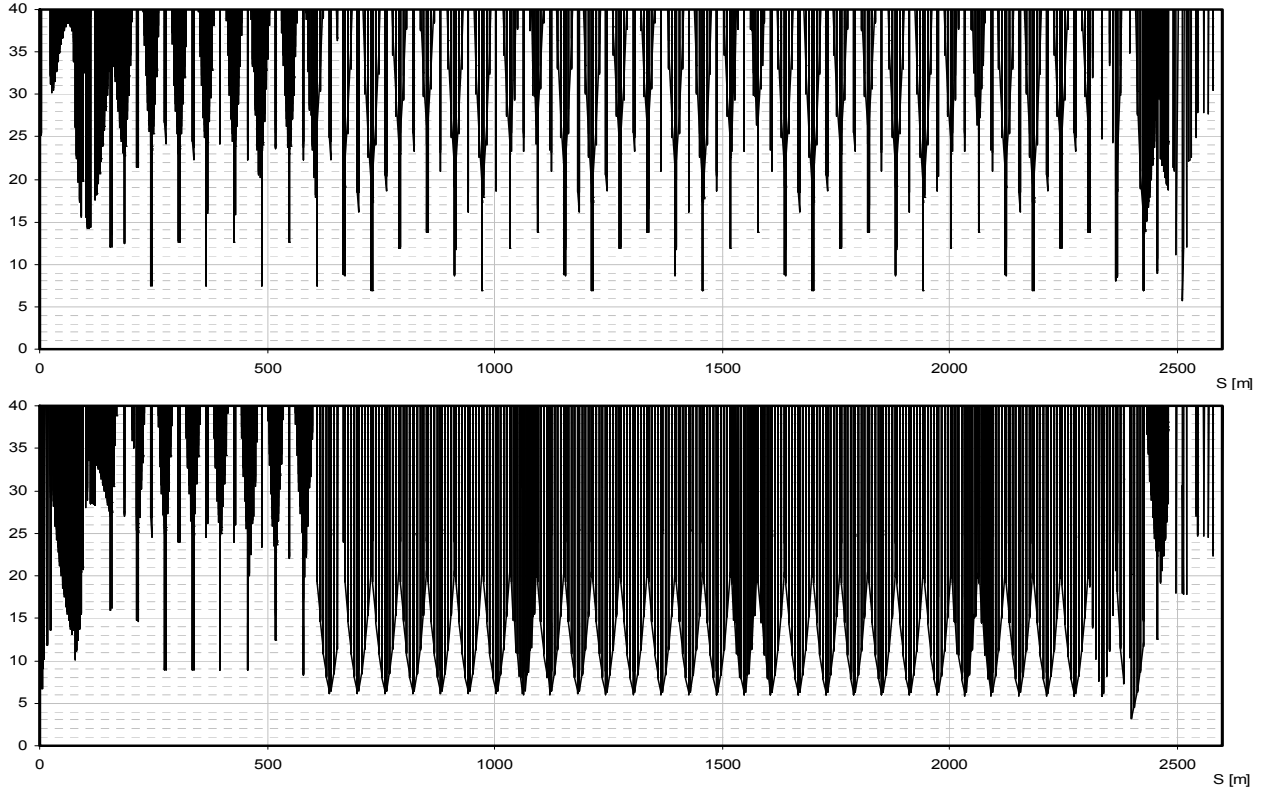


Figure 22.10: Horizontal (top) and vertical beam aperture (s) for TI 8.

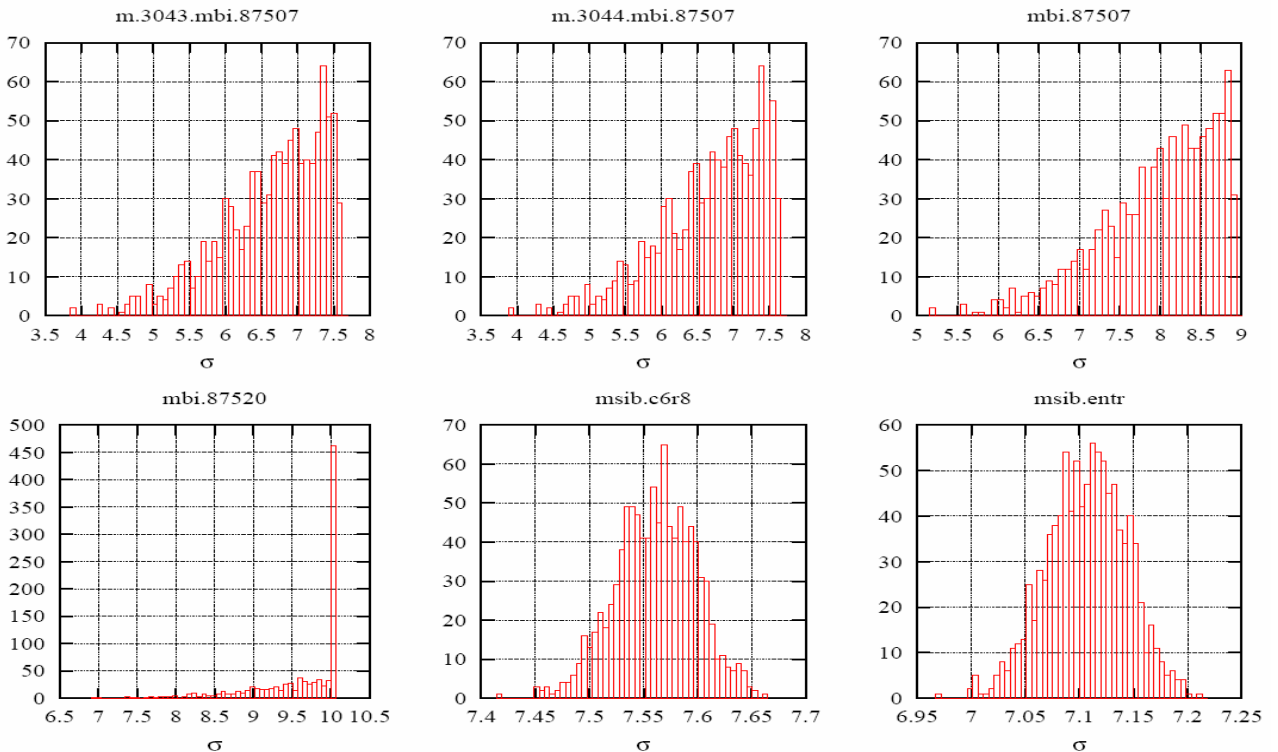


Figure 22.11: Aperture bottlenecks in TI 8. Histograms show the simulated aperture remaining for the beam for 1000 corrected trajectories, after all errors are included.

22.7 INTERLOCKS AND SURVEILLANCE

The beam parameters mean that the bunches must stay within the available aperture to avoid severe damage to components. For some of the power supplies this corresponds to an error of just 10^{-3} , which is assumed to be the interlock level for the power supply current surveillance. The power supplies must be surveyed until the last few milliseconds before extraction, to minimise the risk of a trip and a disastrous reduction in the current.

The interlocking of the SPS extractions and LHC injections are intimately linked to the transfer line interlocks and must ensure that out-of-tolerance beams cannot be extracted, transferred or injected. The use of passive protection devices is already widespread, with the TPSG in the extraction channel, the TCDI collimators in the transfer line and the TDI, TCDD and TCLI collimators in the injection regions of the LHC.

REFERENCES

- [1] A. Hilaire et al., “*Beam Transfer to and Injection into LHC*”, EPAC’98, Stockholm, June 1998 and CERN/LHC Project Report 208.
- [2] A. Hilaire et al., “*Trajectory Correction of the LHC Injection Transfer Lines TI 2 and TI 8*”, CERN/LHC Project Report 122.
- [3] A.Hilaire et al., “*The Magnet System of the LHC Injection Transfer Lines TI 2 and TI 8*”, LHC-Project-Note-128; CERN, 1998.
- [4] O. Brüning, J. B. Jeanneret, “*Optics Constraints Imposed by the Injection in IP2 and IP8*”, CERN/LHC Project Note 141 (1998).
- [5] B.Goddard, “*Expected delivery precision of the injected LHC beam*”, CERN/LHC Project note 337, 2004.
- [6] J.Borburgh et al., “*The Design of the New Fast Extraction Channel for the LHC*”, EPAC’04, Lucerne 2004. CERN-LHC-Project-Report-752, CERN, 2004.
- [7] B. Goddard et al., “*The new Extraction Channel for LHC and CNGS*”, EPAC’00, Vienna, 2000, CERN SL 2000-036 (BT), 2000.
- [8] B.Goddard, V.Kain, “*Expected emittance growth from errors at injection into the LHC*”, to be presented at PAC’05, Tennessee 2005.
- [8] L.Vos, “*Transverse emittance blow-up from dipole errors in proton machines*”, LHC-Project-Report-193, CERN, 1998.
- [9] W.Hofle et al., “*Transverse damping system for the future CERN LHC*”, PAC 2001.
- [10] P.M.Hanney and E.Keil, “*How does betatron mismatching affect beam size and density?*”, CERN-ISR-TH/69-32, 1969.
- [11] G.Arduini, P.Raimondi, “*Transverse emittance blow-up due to injection errors*”, SL-Note-99-022-SLI, CERN, 1999.
- [12] T.Risselada, “*Evaluation of the emittance blow-up at injection due to beam tilt in the LHC injection lines*”, CERN Beam Physics Note 76, 2004.
- [13] B.Goddard et al., “*Geometrical alignment and associated beam optics issues of transfer lines with horizontal and vertical deflection*”, LHC-Project-Report-719; CERN, 2004.
- [14] V.Kain, *Notes of the LHC Injection Working Group Meeting held on meeting held on 28 July 2004*
- [15] H.Burkhardt, R.Schmidt, “*Intensity and Luminosity after Beam Scraping*”, CERN-AB-2004-032-ABP; CERN, 2004.
- [16] Y.Chao & V.Mertens, “*Analysis and Optimisation of Orbit Correction Configurations Using Generalised Response Matrices and its Application to the LHC Injection Transfer Lines TI 2 and TI 8*”, LHC-Project-Report-470; CERN, 2001.

CHAPTER 23

GENERAL SERVICES

23.1 WATER COOLING

23.1.1 Demineralised Water Systems

The demineralised distribution system in TI 2 and TI 8 is mainly used for cooling the magnets coils and the water cooled cables installed in the tunnels [1,3]. Additional cooling must also be provided for the beam stoppers, or TED, in each line.

Primary water is supplied from the LHC cooling towers (SF2 and SF8) and acts as the heat sink for the demineralised water. The primary water is cooled down by these cooling towers and then is pumped to the underground cooling stations. These cooling stations are located in the technical caverns, UW25 and UW85. The demineralised water is cooled by the primary water loop via a set of heat exchangers. Once cooled, the demineralised water is sent to respective injection tunnel via supply and return pipelines in a secondary closed cooling circuit. This circuit is equipped with all the necessary control and regulating devices.

The main parameters characterising the secondary demineralised water system are as follows:

Inlet design temperature	27°C (tolerance $\pm 1^{\circ}\text{C}$)
Set point	26°C
Design pressure (p)	16 bar
Δp available	6 bar
Conductivity	<0.5 $\mu\text{S}/\text{cm}$
ΔT inlet / outlet	15 K

The water cooled cables are supplied from the same pipeline as the magnets.

23.1.2 Mechanical Characteristics

The pipes used in the construction of the secondary circuits, together with all other pieces that come in contact with the water, are made of stainless steel. Compensators are installed in the supply and return pipelines in order to guarantee the appropriate contraction in case of a cool down without creating unacceptable stress on the pipes and supports. The dimensioning of the pipeline allows a margin of 15 % for any future power increase.

23.1.3 Cooling power requirements

The cooling power requirements have been defined by the users and are grouped in Tab. 23.1. These requirements served as the baseline for the hydraulic calculation of the circuits.

Table 23.1: Cooling power per injection tunnel

Circuit	Cooling Power (kW)
TI 2 (not including downstream TED)	1702
TI 2 TED (UJ22 side)	215
Water cooled cables	166
TOTAL TI 2	2083
TI 8 (not including downstream TED)	2967
TI 2 TED (UJ82 side)	215
Water cooled cables	136
TOTAL TI 8*	3318

* Some of the water cooled cables for the TI 8 tunnel are supplied from the cooling station in building BA4 of the SPS.

23.2 TUNNEL VENTILATION

The LHC main tunnel is divided in eight independent volumes, called “sectors” which are treated separately [3]. Two air handling units provide an air supply at each even point of a sector and two extraction units extract the air at the odd point of the corresponding sector. See Fig. 23.1 and Fig. 23.2.

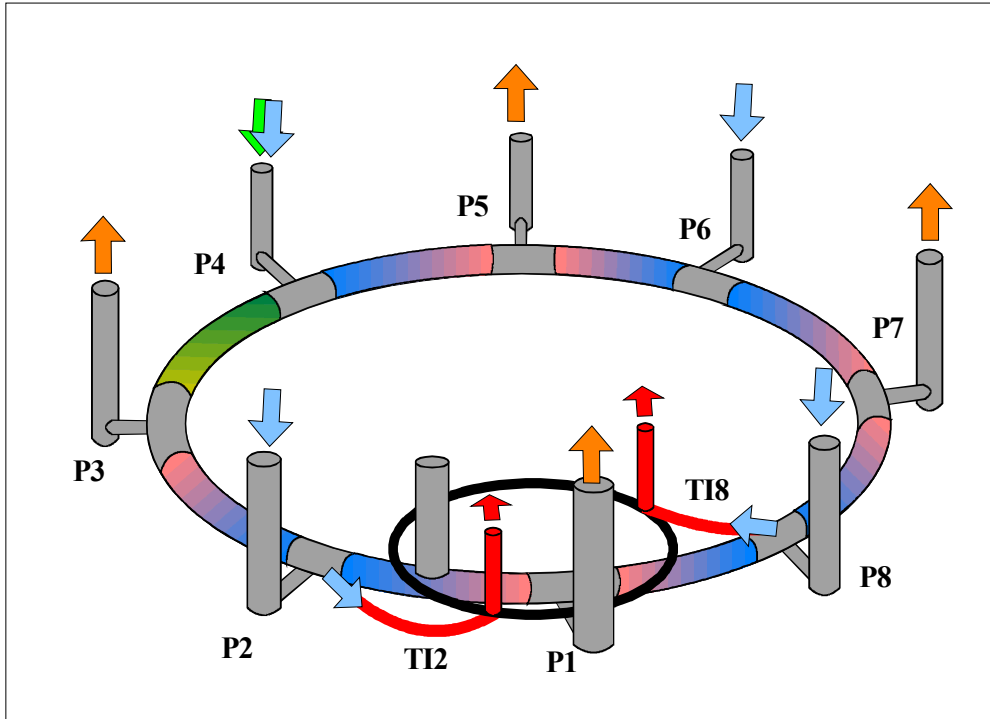


Figure 23.1: Schematic layout of the air-flows in the LHC tunnel.

The TI 2 and TI 8 injection tunnels will be in operation only during the period when beam transfer from the SPS to the LHC is taking place. The magnetic elements of the lines are pulsed following the SP supercycle for LHC filling.

A fraction of the air flow available in sectors 1-2 and 1-8 is deviated to the respective injection tunnel via dedicated extraction units. For TI 2 an extraction plant is located in SUI2 at the upstream end of the tunnel. This plant consists of two extraction units, one for normal extraction (with filters) and a second for emergency and cold smoke extraction. The same principle applies for TI 8, where the extraction plant is located in building SUI8.

In the design of the air handling installations, one of the most important aspects is the heat load which the air system must handle. This head load is the residual from many sources which cannot be evacuated in any other way. However, the air handling system must also provide many other functions including:

- Supply fresh air for people during access into the transfer tunnels
- Provide heating and ventilation during access and operation
- Provide the means to de-stratify the air and maintain a suitable temperature at the surface of the equipment
- Prevent condensation by dehumidification
- Permit cold smoke extraction (temperature < 100°C)
- Purge the air of the tunnel before access
- Filter the exhaust air
- Supply sound attenuation of the exhaust air

In each injection tunnel, the ventilation system will run in one of four operating modes, as shown in Tab. 23.2. In addition, Tab. 23.3 and Tab. 23.4 show the heat dissipation in the air in the injection tunnels and the resulting tunnel conditions.

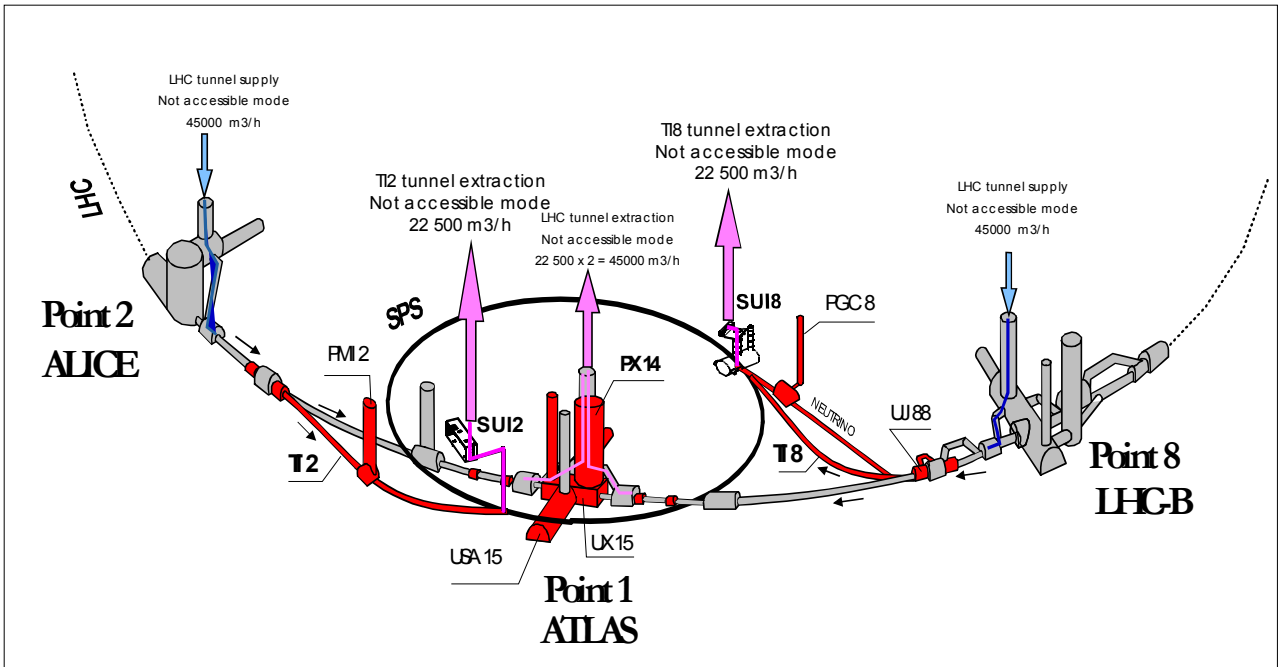


Figure 23.2: Schematic layout of the air-flows in the TI 2 and TI 8 injection tunnels.

Table 23.2: Air flow rate in each injection tunnel for different modes of operation

Injection Tunnel	Reduced consumption mode [m ³ /h]	Accessible mode [m ³ /h]	Not Accessible mode [m ³ /h]	Emergency mode [m ³ /h]
TI 2	7 500	9 000	22 500	45 000
TI 8	7 500	9 000	22 500	45 000

Table 23.3: Sources of heat dissipation into the air of the injection tunnels

Injection Tunnel	Cables [kW]	Water pipes [kW]	MBI (Dipoles) [kW]	MQI (Quads) [kW]	B340 (Dipoles) [kW]	B280 (Dipoles) [kW]	BI and Lighting [kW]	Total [kW]
TI2	200	20	127	20	35	0	11	413
TI8	190	20	267	20	13	5	11	526

Table 23.4: Injection tunnels conditions

Air supplied at the entrance:	Exhaust air:
Dry bulb temperature: $20 \pm 2^\circ\text{C}$ Dew point: $\leq 11^\circ\text{C}$	Dry bulb temperature: $> 45^\circ\text{C}$ Dew point: $\leq 12^\circ\text{C}$

It should be noted that calculations suggest that the available air flow will not cover the heat dissipation shown in Tab. 23.3, for continuous operation. To allow this, additional local water cooled systems would have to be installed. The operating period of the injection will therefore be limited as the temperature in the tunnel will slowly rise to reach the maximum acceptable temperature for the installed equipment.

23.3 ELECTRICAL DISTRIBUTION

Electrical power for the transfer tunnels is distributed from both the LHC side and the SPS side [1,2]. For the injection tunnel TI 2, buildings LHC SR2, SPS BA6 and SPS BA7 are used to house the power converters and the medium and low voltage (MV/LV) switchboards. Galleries and ducts facilitate cabling between power transformers and converters. For TI 8, buildings LHC SR8 and SPS BA4 are used.

In each case the main dipole chain, consisting of MBI magnets, will be powered by water-cooled cables whilst rest of the magnets will be powered by conventional copper and aluminium cables.

23.3.1 Recuperation

In cases where the LEP installation met current safety and technical standards and when it was financially justifiable, infrastructure and equipment has been recuperated from LEP for re-use in the LHC transfer line installations.

23.3.2 Configuration

The main focus of the study of the electrical general services for the TI 2 and TI 8 was on the large voltage drops in cables as a result of the long lengths of the injection tunnels. In the past when LEP was built, alcoves were made at 1450 meter intervals of the 27 km ring to house transformers and switchboards. From these locations, electrical power was distributed for the general services. This avoided the voltage drops coming from very long cable lengths.

The cabling lengths of TI 2 and TI 8 are considerably longer: each is approximately 3 km. There is no provision for alcoves in either line. For TI 2, the ideal location of the transformer is at the top of the PMI2 shaft, outside the SMI2 building. This is approximately at the centre of the TI 2 tunnel length. For TI 8, it has been decided to install a power transformer and a switchboard in the TJ8 cavern at the SPS end of the tunnel and one in TE80 at the LHC side. Larger cable sizes have had to be used in order to keep voltage drops on cables to acceptable levels.

For TI 8, in order to make space for the new cables, disused power and control cables from the false floor of BA4, from the PAP4 shaft, from the ECA4 barracks and from the ECX4 lower cavern have been removed. A transformer pit and the connecting galleries behind BA4 have been constructed and the BA4 floor prepared to receive the steel flooring for the power converters. During the SPS shut-down 2002-2003, BB4, PAP4, ECA4 barracks, ECA4 cavern, TA40 access tunnel and TT40 machine gallery were equipped with most of the cable trays to carry machine and electrical general services cabling into TI 8. During 2004 the final cabling campaigns have been made to prepare for commissioning of the installed elements.

For TI 2 the old power and control cables in the false floor of BA7 have been removed to make way for the new cables. In addition, the floor of BA7 has been prepared to receive the steel flooring for the power converters. The cabling campaign for TI 8 began during the 2003-2004 shutdown.

23.3.3 Power Balance

The main dipole circuit is the major constituent of the power load for the injection tunnels. An analysis has been made in order to compare the reserve power capacity on the existing SPS pulsed power network, against the new load that will be added by the transfer lines TI 2 and TI 8 on the SPS side. This pulsed power network already passes through each of the BA buildings. The associated compensators for the 18 kV SPS pulsed loop are the main compensator at Prevessin (BEQ1) together with an auxiliary compensator at BB3.

The total load for TI 2, fed from BA6 & BA7, is 16.15 MVA whilst the total load for TI 8 is fed from BA4 and amounts to 30 MVA. For TI 2 the combination of BEQ1 and the auxiliary compensator BB3 is sufficient for the additional load. However, for TI 8, adding the load to the existing SPS pulsed loop would overload the loop. As a result it has been necessary to run an additional 18 kV pulsed link from the BE substation at Prevessin to BA4 for TI8. The associated compensator for the new 18 kV link is the new Static Var Compensator (BEQ2), installed on the Prevessin site.

A redistribution of the pulsed load for the SPS pulsed loop has been carefully studied and is being implemented.

On the LHC side the power situation is much simpler since there is ample power available on the network on both sites. The total load for point 2 will be 7.4 MVA (for TI 2). At this point there are two 38 MVA transformers connected in parallel. At point 8 of the LHC, TI 8 will require 5.8 MVA. A single transformer with a rating of 38 MVA is installed at this point. The existing LHC compensators have sufficient power ratings of 50 Mvar (Point 2) and 25 Mvar (Point 8).

23.3.4 Cable Dimensioning, Voltage Drop and Heat Dissipation

For each magnet circuit the voltage drop has been calculated and a cable size chosen in such a way as to not to exceed the permitted voltage drop. During the process of determining cable sizes, consideration was also given to the available space on cable trays, heat dissipation to air by the power cables and the cost. Corrector cables were carefully selected to keep the voltage drop to an acceptable level and may not necessarily have a uniform cross section for each corrector circuit.

23.4 POWER RAIL

In addition to eventually carrying the one of the beams from the SPS to LHC, the tunnel TI 2 will be used as the main route for the installation of all LHC cryogenic and the majority of warm magnets. The largest objects, the main LHC dipoles on their train weigh up to 40 tonnes. As a result powerful underground transport vehicles have been purchased. Since internal combustion engines are forbidden in the underground areas of the LHC for safety reasons, the transport vehicles are equipped with electric motors. The rated power of these motors is 380V/100A.

All existing LEP tunnels are equipped with the old monorail which has sliding contact power conductors with a rated power of 100A. These can easily be reused for the LHC transport vehicle power feed.

Because of the length of TI 2 and TI 8, battery power cannot be used for transport in these tunnels. Batteries having sufficient stored power would have a weight of up to 2 tonnes. Such batteries, moving in such a restricted tunnel would constitute a major safety hazard (acid emissions etc...). As a result it was decided to install a power feed rail in both the TI 2 and TI 8 injection tunnels. This rail is equivalent to LHC main tunnel rail, but has reduced dimensions because of the smaller space available.

At the time of writing, the installation of 6876 m of power rail has been completed and the tests are in progress.

23.5 MONITORING

The monitoring and operation of the general services for the transfer lines forms part of the general monitoring done for CERN and the LHC [3]. It concerns the following systems: electrical distribution, cooling and ventilation, access safety systems as well as the evacuation system.

The operation and monitoring of the general services will be based on both a 24 hour, 365 days shift service provided by the Technical Control Room (TCR) and on specialised equipment groups for each of the technical domains.

Dedicated computing support provides a technical infrastructure monitoring system (TIM) to the TCR. The TIM integrates and homogenises the domain specific monitoring and control systems deployed by the equipment groups.

Once the equipment is installed, faults and breakdowns will be immediately visible in the TCR, from where an impact and cause analysis is carried out. Procedures are established to ensure reliable situation assessment and fast, well directed repair interventions.

REFERENCES

- [1] S. Akhtar, J. Kühnl-Kinel, “*ST/EL and ST/CV services for TI 2 & TI 8 LHC Injection Tunnels*”, ST-Note-2002-019, 5th ST Workshop, Echenevex, France, 28-30 January 2002.
- [2] S. Akhtar, “*Powering the Transfer Lines TI 2 and TI 8*”, ST-Note-2001-019, 4th ST Workshop Chamonix, France, 30 January - 2 February 2001.
- [3] LHC Design Report - Volume II (LHC Infrastructure and General Services), 2003

CHAPTER 24

TRANSFER LINE MAGNETS

24.1 INTRODUCTION

With an overall line length of 5.6 km and an overall deflection of 152° the magnet system of the LHC injection transfer lines TI 2 and TI 8 comprises almost 700 magnets, corresponding to almost the equivalent magnetic length of the SPS. Economy considerations led to the decision to use classical warm main dipoles and quadrupoles of compact design. The main dipoles, quadrupoles and the new correction magnets are supplied in the framework of the contribution of the Russian Federation to the LHC. Apart from three special dipoles all remaining magnets required for the new lines have been recuperated from closed down installations. These came mainly from the SPS-LEP transfer lines TI 18 and TI 12, together with the anticlockwise injection tunnel into the SPS from the PS, TT70. The main parameters of the magnets and the required quantities are described in this chapter.

24.2 MAIN Dipoles, MBI

Since no set of dipole magnets existed to allow the required 152° total deflection in the available space, new main bending magnets had to be designed and constructed. Initial plans to use superconducting dipoles and quadrupoles were abandoned after analysis of the overall cost. On one hand a lot of cryogenic support equipment would have been needed for the two transfer lines and on the other hand, TI 2 and TI 8 will only be powered for relatively short periods during injection [1] and therefore keeping the electricity consumption rather low. The penalty of using classical magnets is that the limited strength has lead to substantially longer transfer tunnels. The final choice was therefore a solution using classical magnets having a length of 6.3 m and a field of 1.81 T [2]. Their cross section is given in Fig. 24.1.

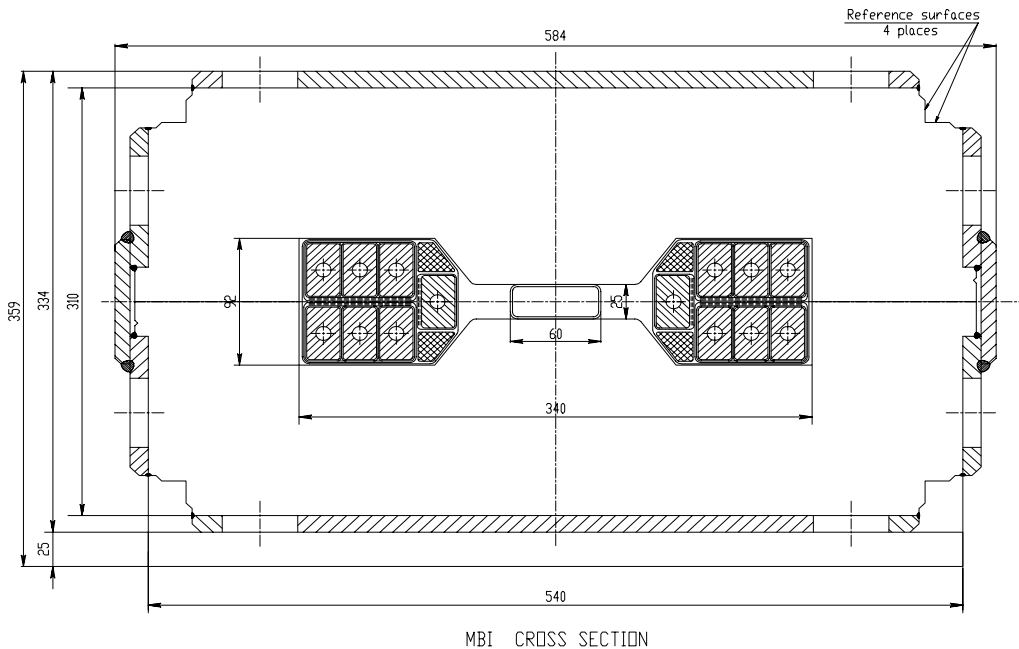


Figure 24.1: MBI cross section

Since the main dipoles in the transfer lines account for the bulk of the required electrical power, a careful optimisation of the parameters was required to minimise the power consumption and arrive at an economic solution. The main parameters of these magnets are summarised in Tab. 24.1.

Table 24.1: MBI main parameters

	Value	Units
General		
Gap Height	25	mm
Nominal Field	1.81	T
Dimensions		
Overall Length	6.7	m
Core Length	6.3	m
Overall Width	584	mm
Overall Height	367	mm
Coil		
Resistance (at 20°C)	1.935	mΩ
Inductance	2	mH
Excitation		
Nominal Current	5340	A
Rms. Current	2314	A
Dissipated Power	11	kW
Cooling per Half Coil		
Pressure Drop	2	Bar
Water Flow	7	l/min
Temperature Rise	11	°C
Weight		
Coils (copper)	735	kg
Core	7900	kg

The coil parameters were chosen so as to allow to re-use the (relatively high-current) main LEP power supplies. All 112 main dipoles in TI 2 will be powered as a series from one power converter unit. The 236 magnets of TI 8 will use two power supplies [3]. To limit costs the upper and lower half coils feature a half-integer number of windings. All upper half coils are directly connected in series constituting the go conductor. The return conductor is formed from the lower half coils which are also connected in series. This design avoids the need for a separate return line, or bus bar system, along the dipoles.

To limit costs further, a gap height of just 25 mm was chosen. This forms the strongest aperture constraint in both lines. With the vacuum chambers installed the resulting physical full vertical aperture for the beam is 20.4 mm [4]. A rather elaborate correction scheme is therefore needed to keep the beam within this aperture.

The MBI magnets have been constructed at the Budker Institute of Nuclear Physics (BINP) in Novosibirsk in the framework of the Cooperation Agreement between CERN and the Russian Federation concerning Russia's participation in the LHC project. All 360 MBI magnets, including 12 spare magnets and 13 spare coils, have been delivered to CERN and are ready for installation.

24.3 MAIN QUADRUPOLES, MQI

As for the MBI magnets a classical solution was chosen for the 178 lattice and matching quadrupoles needed to equip TI 2 and TI 8. With a core length of 1.4 m these magnets have a nominal gradient of 53.6 T/m [5] at a nominal current of 530 A. Their inscribed diameter is 32 mm. A cross section can be found in Fig. 24.2. Their main parameters are summarised in Tab. 24.2.

All focusing and defocusing lattice quadrupoles of TI 2 will be powered in series by three power supplies recuperated from LEP. Two supplies are employed in TI 8 since MQIF and MQID magnets will use different settings for optics reasons. Matching elements will use a number of individual power supplies which have also been recuperated from LEP [3].

Like the MBI, the MQI quadrupoles are being constructed by BINP. All 184 MQI magnets, including 6 spare magnets and 12 spare coils, have been delivered to CERN and are ready for installation.

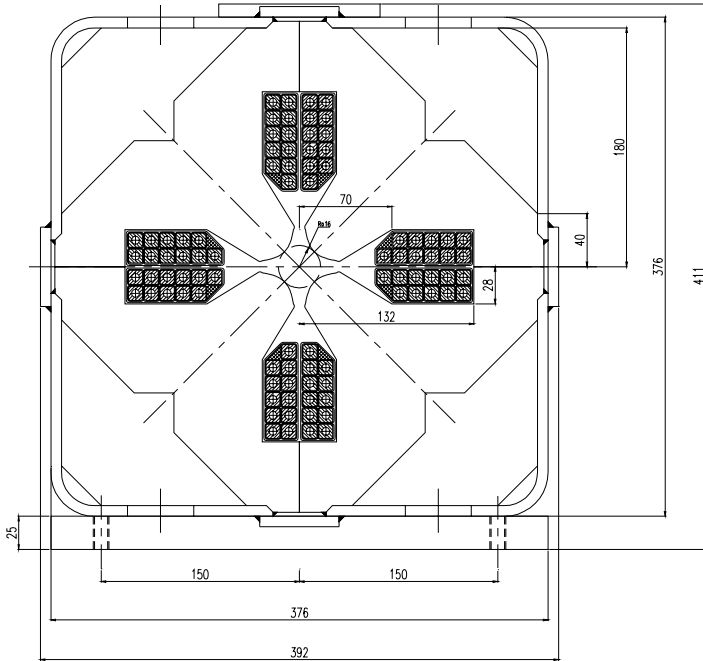


Figure 24.2: MQI cross section

Table 24.2: MQI main parameters

	Value	Units
General		
Radius of inscribed circle	16	mm
Nominal Gradient	53.6	T/m
Dimensions		
Core Length	1.4	m
Overall Width	392	mm
Overall Height	411	mm
Coil		
Resistance (at 20°C)	36	mΩ
Inductance	13	mH
Excitation		
Nominal Current	530	A
Weight		
Total Weight	1070	kg

24.4 OTHER MAGNETS

Almost all other dipoles have been recuperated from installations which were no longer used after LEP operation had come to an end. These came mainly from the electron injection line into SPS, TT70, and the electron and positron injection lines into LEP, TI12 and TI18. In total the recovery, refurbishment and re-use of 56 B340 magnets, 11 B280 and 2 MBB magnets was necessary. The cross section of the B340 magnets is shown in Fig. 24.2 and their main parameters in Tab. 24.3. The corresponding cross section and parameters for the B280 magnets are given in Fig 24.4 and Tab. 24.4 respectively. The MBB magnets are one of the two SPS main magnet types. Their characteristics can be found in [7].

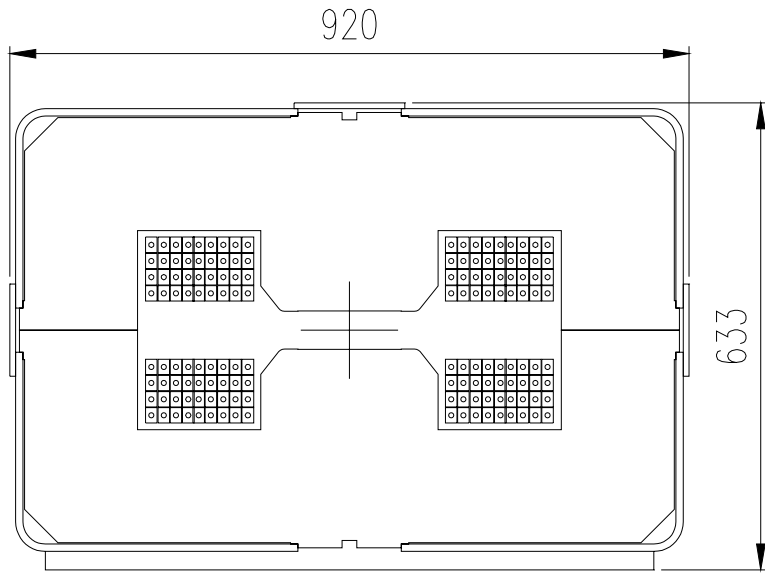


Figure 24.3: B340 cross section.

Table 24.3: B340 main parameters

	Value	Units
General		
Gap Height	52	mm
Nominal Field	1.6	T
Dimensions		
Core Length	3.412	m
Overall Width	920	mm
Overall Height	633	mm
Coil		
Resistance (at 20°C)	37.6	mΩ
Inductance	120	mH
Excitation		
Nominal Current	1000	A
Rms. Current	433	A
Dissipated Power	7	kW
Cooling per Half Coil		
Pressure Drop	6	Bar
Water Flow	36	l/min
Temperature Rise	15	°C
Weight		
Coils (copper)	1360	kg
Core	11900	kg

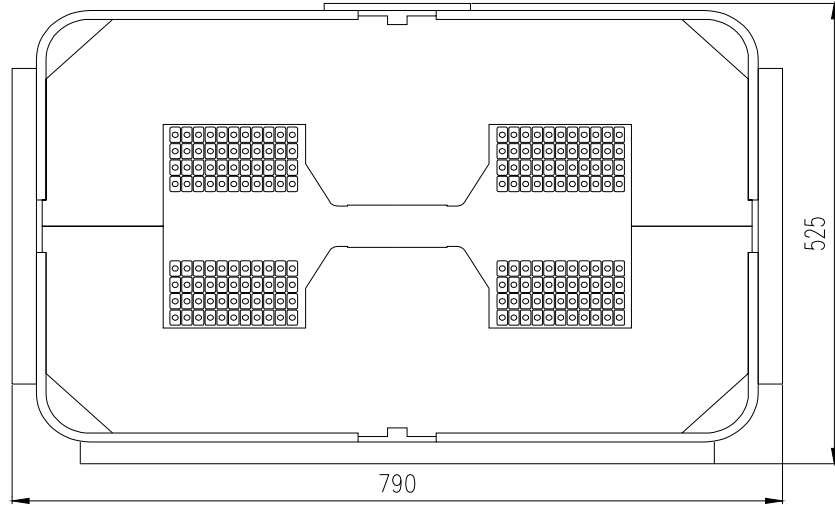


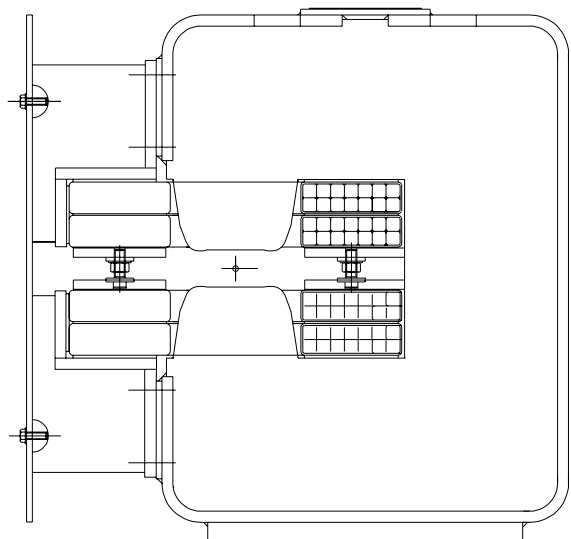
Figure 24.4: B280 cross section

Table 24.4: B280 main parameters

	Value	Units
General		
Gap Height	48	mm
Nominal Field	1.7	T
Dimensions		
Core Length	2.8	m
Overall Width	790	mm
Overall Height	525	mm
Coil		
Resistance (at 20°C)	66.3	$\text{m}\Omega$
Inductance	103	mH
Excitation		
Nominal Current	822	A
Rms. Current	356	A
Dissipated Power	8.5	kW
Cooling per Half Coil		
Pressure Drop	6	Bar
Water Flow	25.6	l/min
Temperature Rise	30	$^{\circ}\text{C}$
Weight		
Coils (copper)	805	kg
Core	6000	kg

In addition to the recuperated dipoles mentioned above three special C-type dipoles (denominated MBHC) have been built. These were needed in the extraction channel towards TI 8 near LSS4 (at this point the line is called TT 40). The cross section of these magnets is given in Fig. 24.5 and their main parameters in Tab. 24.5.

Two QTR and one QTL type quadrupoles have been re-used in the TT 40 part of TI 8 due to the larger aperture requirements of the CERN Neutrino to Gran Sasso (CNGS) line TT41. Details of these can also be found in [7].



corrector magnets. A total of 91 MCIA correctors are needed to equip the two transfer lines and have once again been constructed at BNIP. In order to minimise the costs and spares the design of the horizontal and vertical correctors was chosen to be identical [6]: the positioning of the magnet on the supports defines the type of deflection. The Cross-section of an MCIA (in the orientation as a horizontal corrector, MCIAH) is shown in Fig. 24.6. The main parameters of the MCIA are given in Tab. 24.6.

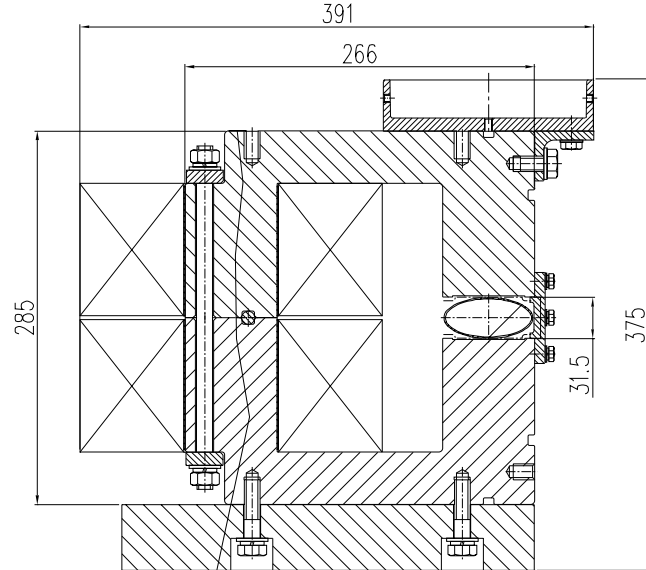


Figure 24.6: MCIAH cross section

Table 24.6: MCIAH main parameters

	Value	Units
General		
Gap Height	32.5	mm
Nominal Field	0.27	T
Dimensions		
Overall Length	0.615	m
Core Length	0.45	M
Overall Width	400	mm
Overall Height	375	mm
Coil		
Resistance (at 20°C)	10	mΩ
Inductance	10.5	mH
Excitation		
Nominal Current	3.5	A
Dissipated Power	0.17	kW
Cooling		
Natural Convection		
Weight		
Total weight	300	kg

Two SPS type correctors (MDS) are installed in TT40 and TI 8 where the need for high correction strength coincides with the need for a larger aperture than that provided by the MCIA correctors. It has been verified that higher-order multipole correctors are not needed to operate TI 2 and TI 8 correctly.

24.6 SUMMARY AND CONCLUSION

The total quantities of each type of magnet needed for each of the two LHC transfer lines is given in Tab. 24.7. Spares are not included. The magnet system of the LHC injection transfer lines is of considerable volume. A maximum of magnets and power supplies have been recuperated from then closed-down installations. Newly built magnets feature a cost-optimised design. For the bulk of the new magnets construction has been completed.

Magnet Type	Required Quantities		Sum
	TI 2	TT 40 + TI 8	
MBI	112	236	348
MBB	2		2
B280	6	5	11
B340	33	23	56
BHC		3	3
<i>Sum Dipoles</i>	153	267	420
MCIAH	22	22	44
MCIAV	26	21	47
MDS		2	2
<i>Sum Correctors</i>	48	45	93
MQI	95	83	178
QTR		2	2
QTL		1	1
<i>Sum Quadrupoles</i>	95	86	181
Total	296	398	694

REFERENCES

- [1] The LHC Study Group, “*The Large Hadron Collider Conceptual Design*”, CERN/AC/95-05 (LHC) (1995).
- [2] G. Kouba et al., “*The bending magnets for the LHC injection transfer lines*”, Proceedings of the 17th Int. Conf. On Magnet Technology, MT17, Geneva, Switzerland, September 2001.
- [3] P. Burla, CERN, private communication.
- [4] A. Hilaire, V. Mertens & E. Weisse, “*Trajectory Correction of the LHC Injection Transfer Lines TI 2 and TI 8*”, LHC Project Report 122 (1997).
- [5] K.M. Schirm et al., “*The quadrupole magnets for the LHC injection transfer lines*”, Proceedings of the 16th Int. Conf. On Magnet Technology, MT16, Ponte Vedra Beach, Florida, USA, September 1999.
- [6] Definitive Technical Specification for the MCIA resistive correction dipole magnets for the TI 2 and TI 8 beam transfer lines, CERN AT-MEL, April 2003.
- [7] SPS Conceptual Design Report, “*The 300 GeV Programme*”, CERN/1050, 1972.

CHAPTER 25

TRANSFER LINE POWERING

25.1 INTRODUCTION

The magnets that guide and focus the beams during their transfer from the SPS to the LHC will be powered by 144 new power converters. These range in power from 250 W to 9.7 MW. Several power converter technologies and topologies will be used, based not only on the circuit electrical characteristics and the required performance, but also on the topology of the re-used power converters. To reduce the global cost, it was decided:

- To maximise the re-use of the available equipment retrieved from LEP and SPS.
This equipment will be refurbished and adapted to ensure compatibility with the SPS system as the transfer lines will be part of the SPS machine from an operation point of view. Consequently, the SPS remote control system (MUGEF) and the SPS interlock system will be used.
- To minimise the length of the cables.
The power converters will be installed at the both ends of each tunnel.
- To install the power converters in existing surface buildings.
For TI 2, the power converters will be installed in BA7 and SR2; for TI 8, the power converters will be installed in BA4 and SR8.

Nevertheless in some cases, it is necessary to buy new power converters. Because of the different equipment origins, all equipment will undergo a standardisation process in order to facilitate operation and maintenance of the power converters.

25.2 GENERAL RUNNING

All large power converters will operate in a pulsed mode for economical reasons (electrical power and thermal design). The small power converters for the correctors will run in DC as their losses are negligible.

For the transfer lines, the only important operating characteristic is the flat top current, with the global cycle similar to that used for the SPS. However, the transfer line cycle has been optimised to reduce the rms current value that in turn reduces the overall electrical consumption. Thus the rms current value of the proposed reference cycle (see below) is 0.36 I nominal whereas the rms current value in the magnets is about 0.45 I nominal due to the current decay in the free-wheel diodes.

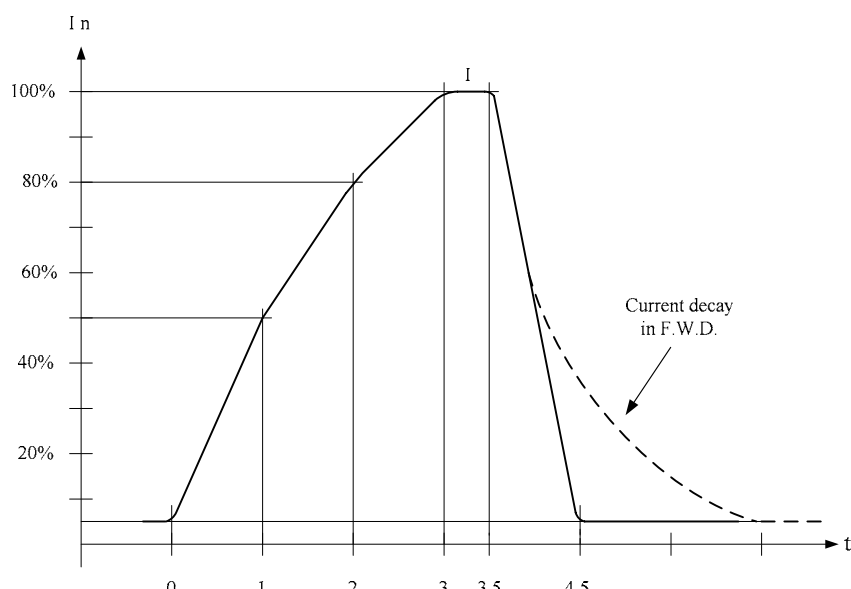


Figure 25.1: Proposed transfer line cycle

25.3 POWER CONVERTER REFURBISHMENT

All re-used power converters will be refurbished before re-installation to assure a good reliability. Refurbishment principally involves:

- Changing the main circuit breaker
- Installing a new electronics crate (identical to the SPS electronics crate)
- Installing new DCCTs (Direct Current Current Transformers)
- Re-cabling the control part to be compatible with the new electronics.

25.4 OVERVIEW OF TI 2

The power converters for both the extraction system of the west area and the TT60 line of TI 2 have been retained. However to prolong their useful life, each converter has been refurbished and reinstalled. The additional power converters required for TI 2 are installed in the BA7 (SPS) and SR2 (LHC) surface buildings. The list of power converters with their main characteristics is given in Tab. 25.1.

Table 25.1: TI 2 power converters

TI 2													
Converter name	Magnet Type	Number of Magnets in Series	Inom [A]	I max DCCT [A]	Cable total length (estimated) m	Cable section mm ²	Reproducibility 24h ± ppm of I max	Reproducibility 1/2h ± ppm of I max	P.C. Loc.	Converter type	Origin	Source	Umax Conv. [V]
MBI 2213M	MBI	112	5150	5400	4000	1500	50	20	SR2	RA3/A	LEP	18000	1800
MQIF 2580M	MQI	26	490	600	5880	630	100	40	SR2	RA1/S	LEP	18000	1300
MQIF 2840M	MQI	13	490	600	2500	630	100	40	SR2	RB9/H	LEP	400	350
MQID 2850M	MQI	40	490	600	5996	630	100	40	SR2	RA1/S	LEP	18000	1300
MBB 2015M	MBB	2	3690	4400	620	1920	100	40	BA7	R21	SPS	18000	160
MBIBH 2931M	B280	6	725	800	1272	1000	50	20	SR2	N10	New	400	450
MBIAV 2063M	B340	17	925	1000	814	480	50	20	BA7	RA1/MG	LEP	18000	1300
MBIAV 2685M	B340	12	900	1000	3034	1260	100	40	SR2	RA1/S	LEP	18000	1300
MBIAV 2911M	B340	4	565	800	1616	630	100	40	SR2	RB9/O	LEP	400	350
MQID 2010	MQI	1	370	500	760	240	100	40	BA7	RB4	LEP	400	105
MQIF 2020	MQI	1	290	400	696	240	100	40	BA7	RB15	LEP	400	100
MQID 2030	MQI	1	270	400	636	240	100	40	BA7	RB15	LEP	400	100
MQIF 2040	MQI	1	330	500	576	240	100	40	BA7	RB4	LEP	400	105
MQID 2050	MQI	1	460	600	484	240	100	40	BA7	RB8	LEP	400	210
MQIF 2060	MQI	1	470	600	544	240	100	40	BA7	RB6	LEP	400	200
MQIF 2860	MQI	1	500	600	1658	500	100	40	SR2	RB6	LEP	400	200
MQID 2870	MQI	1	510	600	1598	500	100	40	SR2	RB6	LEP	400	200
MQIF 2880	MQI	1	410	600	1538	500	100	40	SR2	RB6	LEP	400	200
MQID 2890	MQI	1	460	600	1478	500	100	40	SR2	RB6	LEP	400	200
MQIF 2900	MQI	1	390	600	1416	500	100	40	SR2	RB6	LEP	400	200
MQID 2910	MQI	1	220	400	1356	500	100	40	SR2	RB15	LEP	400	100
MQIF 2920	MQI	1	320	500	1270	500	100	40	SR2	RB4	LEP	400	105
MQIF 2930	MQI	1	380	500	1246	500	100	40	SR2	RB4	LEP	400	105
MQIF 2940	MQI	1	150	300	1146	500	100	40	SR2	RB2	LEP	400	200
MQID 2950	MQI	1	280	500	1076	500	100	40	SR2	RB4	LEP	400	105

25.5 OVERVIEW OF TI 8

For TI 8 a new extraction system has been installed at point 4 of the SPS. This involves 9 additional power converters, four for vertical bumpers, four for horizontal bumpers and one for the MSE magnets. These converters are part of the SPS machine and are described in Chap. 18. The additional power converters for TI 8 are installed in the BA4 (SPS) and SR8 (LHC) surface buildings. The list of power converters together with their main characteristics is given in Tab 25.2.

Table 25.2: TI 8 power converters

TI 8													
Converter name	Magnet Type	Number of Magnets in Series	Inom [A]	I max DCCT [A]	Cable total length (estimated) m	Cable section mm ²	Reproducibility 24h \pm ppm of I max	Reproducibility 1/2h \pm ppm of I max	P.C. Loc.	Converter type	Origin	Source	Umax Conv. [V]
TT 40													
MBHC 4001M	BHC	3	900	1000	652	750	100	40	BA4	RB13	LEP	400	300
MDSV 4002	MDS	1	0	400	714	240	100	40	BA4	N08	New	400	125
MBHA 4003M	B340	4	1000	1100	761	800	100	40	BA4	RA2	LEP	18000	550
QTMD 4001	MQI	1	470	500	606	240	100	40	BA4	RB6	LEP	400	200
QTRF 4002	QTR	1	100	400	652	240	100	40	BA4	RB10	LEP	400	250
QTRD 4003	QTR	1	70	300	714	185	100	40	BA4	RB2	LEP	400	200
QTLF 4004	QTL	1	250	400	782	185	100	40	BA4	RB10	LEP	400	250
TI 8													
MBI 8160M	MBI	236	5250	5400	2000	1500	50	20	BA4	2xRA3/T	LEP	2x18kV	3600
MQIF 8700M	MQI	34	500	600	5508	630	100	40	SR8	RA1/MG	LEP	18000	1300
MQID 8710M	MQI	34	500	600	5700	630	100	40	SR8	RA1/MG	LEP	18000	1300
MCICH 8040	MDS	1	240	400	1094	185	100	40	BA4	RB10	LEP	400	250
MBIAH 8788M	B340	7	900	1000	1210	1260	100	40	SR8	N11	New	18000	600
MBIAV 8110M	B340	12	800	1000	1883	400	100	40	BA4	RA1/MG	LEP	18000	1300
MBIBV 8774M	B280	5	730	800	1325	1260	100	40	SR8	RB9/H	LEP	400	350
MQID 8010	MQI	1	400	500	892	240	100	40	BA4	RB6	LEP	400	200
MQIF 8020	MQI	1	410	500	952	240	100	40	BA4	RB6	LEP	400	200
MQID 8030	MQI	1	600	600	1012	240	100	40	BA4	RB6	LEP	400	200
MQIF 8720	MQI	1	500	600	1614	500	100	40	SR8	RB6	LEP	400	200
MQID 8730	MQI	1	600	600	1554	500	100	40	SR8	RB6	LEP	400	200
MQIF 8740M	MQI	2	300	400	1490	500	100	40	SR8	RB15	LEP	400	100
MQID 8750	MQI	1	490	600	1434	500	100	40	SR8	RB6	LEP	400	200
MQIF 8760	MQI	1	500	600	1374	500	100	40	SR8	RB6	LEP	400	200
MQID 8770	MQI	1	360	500	1314	500	100	40	SR8	RB4	LEP	400	105
MQIF 8780	MQI	1	320	500	1254	500	100	40	SR8	RB4	LEP	400	105
MQID 8790	MQI	1	290	400	1126	500	100	40	SR8	RB15	LEP	400	100
MQIF 8800	MQI	1	360	500	1066	500	100	40	SR8	RB4	LEP	400	105
MQID 8810	MQI	1	290	400	1006	500	100	40	SR8	RB15	LEP	400	100

25.6 GENERAL PERFORMANCE

The cycle to cycle reproducibility, given in the Tab. 25.1 and Tab. 25.2, is defined as the maximum deviation of the average value of the flat top current, I , over a period of half an hour. The precision is expressed in ppm of I_{\max} . The environmental conditions are assumed to not change and are defined in [1].

The cycle to cycle reproducibility for 24 h is defined as the maximum deviation of the average value of the flat top current over a period of one day, taking into consideration the full range of permissible changes of operating and environmental conditions. The precision is again expressed in ppm of I_{\max} .

In all cases a constant current ripple contribution from the converter itself is added to the drifts described above. The current ripple is dependant on the converter voltage ripple (given in each topology description – see below) and also on the magnet characteristics. The current ripple can be derived from the following transfer function:

- $I_{\text{ripple}}/U_{\text{ripple}} = 1/(R * (1 + jL\omega/R))$
- With R and L resistance and inductance of the load (cables + magnets).

25.7 POWER CONVERTER TOPOLOGIES

25.7.1 Six-pulse Power Converters

The main characteristics of the 6-pulse power converters are:

- Working range: I min 5% of I_{\max} , I_{\max} 100% of DCCT range,
- Voltage ripple of V_{\max} : 2×10^{-3} at 50 Hz; 1×10^{-2} at 300 Hz,
- Typical small-signal current loop bandwidth: 10 Hz.

In order to handle the magnet current ramp-down under the worst fault condition, e.g. a power cut, the converters are equipped with a free-wheel diode. The 6-pulse power converters are made of one thyristor full bridge or two thyristor half bridges.

Full bridge topology

This topology concerns the RB2, RB10 and RB15 types. The complete converter is composed of a circuit breaker, a 50 Hz transformer, a thyristor bridge and passive filter assembled in one cubicle. The complete converter is air-cooled. A schematic circuit diagram is shown in Fig 25.2.

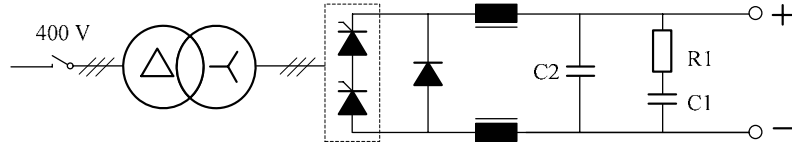


Figure 25.2: A full-bridge thyristor converter 6 P topology

Two half bridges topology

This topology concerns the R21 type. The complete converter is composed of a circuit breaker, together with a 50 Hz transformer which has two secondary windings that are phase shifted by 180°. Two half thyristor bridges and a passive filter make up the remainder of the active elements which are all installed in one cubicle. The complete converter is air-cooled.

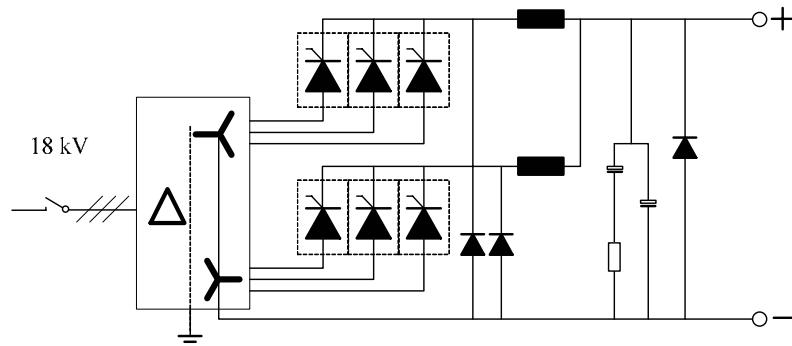


Fig. 25.3: A Two half-bridge thyristor converter, 6 P topology

25.7.2 Twelve-pulse Power Converters

The main characteristics of this type of converter are:

- Working range: I min 5% of I max, I max 100% of DCCT range,
- Voltage ripple of V max: 2×10^{-3} at 50 Hz; 5×10^{-3} at 600 Hz,
- Typical small-signal current loop bandwidth: 10 Hz.

In order to handle the magnet current ramp-down under the worst fault condition, e.g. power cut, the converters are equipped with free-wheel diodes. The 12-pulse power converters are made of series, parallel or series-parallel combinations of full bridge thyristors.

12-pulse parallel power converter

This topology concerns the N10, N11, RB4, RB6, RB8, RB9, RB13 and RA2 converter types. The complete converter is composed of a circuit breaker together with two sub-converters phase-shifted by 30° and connected in parallel, resulting in a 12 pulse configuration. The complete converter is air-cooled. A schematic circuit diagram is shown in Fig 25.4.

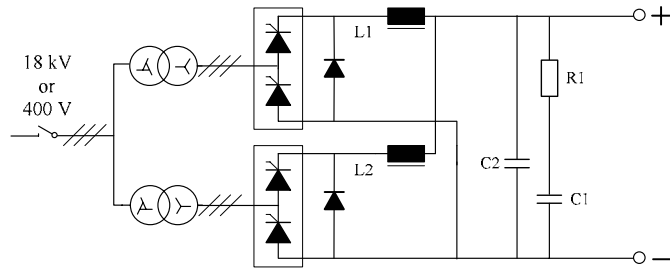


Figure 25.4: A 12-pulse parallel power converter

12-pulse series power converter

This topology concerns the RA3 types. The complete converter is composed of a circuit breaker and two sub-convertisers phase-shifted by 30° and connected in series, resulting in a 12 pulse configuration. The thyristor bridges and the chokes of the passive filter are water-cooled.

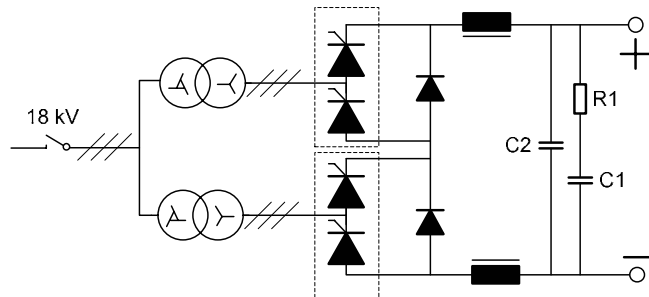


Figure 25.5: A 12-pulse series power converter

12-pulse series-parallel power converter

This topology concerns the RA1 types. The complete converter is composed of a circuit breaker and two series sub-convertisers phase-shifted by 30° and connected in parallel, resulting in a 12 pulse configuration. The complete converter is air-cooled.

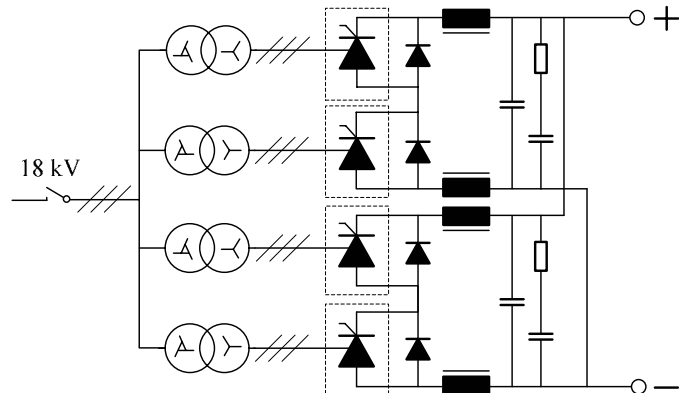


Figure 25.6: A 12-pulse series-parallel power converter

25.7.3 Bipolar Power Converters with Mechanical Polarity Changer

These bipolar power converters are made with 6-pulse or 12-pulse power converter which has a mechanical switch added at the output. The polarity can only be changed at zero current and does not occur during normal machine operation. Power converters using this topology are denoted by an “S” at the end of their type name.

25.7.4 Four-quadrant (4Q) Switch-mode Converter

This topology concerns the NO8 type. The MDSV 400293 magnet requires a 4-quadrant power converter, capable of regulating zero current. The main characteristics are:

- Voltage ripple of V max: 1×10^{-3} at 16 kHz,
- Typical small-signal current loop bandwidth: 10 Hz.

This 4-quadrant power converter is composed of: a main circuit breaker, a step-down transformer, a diode rectifier bridge, a DC passive filter, a brake chopper to dissipate the magnet energy in case of converter fault, a chopper bridge unit, a high frequency filter and a crowbar. Fig 25.7 shows the circuit.

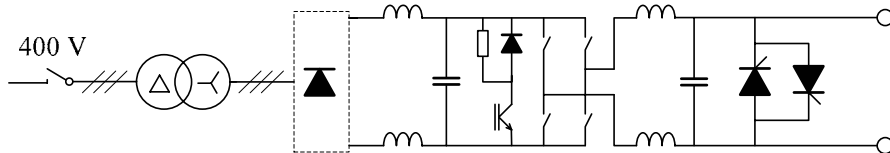


Figure 25.7: A 4-quadrant switch mode converter

25.7.5 Power Converters for the MCIAV and MCIAH Correctors

Ninety one NX type power converters (± 70 V, ± 3.5 A) are needed to feed the MCIAV and MCIAH corrector magnets. These are 4-quadrant power converters with zero current regulation and are identical to the existing SPS units. More details can be found in [2].

25.8 DISTINCTIVE FEATURES OF THE TI 8 MBI POWER CONVERTERS

The TI 8 MBI magnets will be fed by two series connected power converters 1800V/5400A, installed in BA4. These two power converters will run in Master/Slave mode. Only the Master will be seen by the control room. The slave converter will be fully controlled by the Master. For economic reasons, these two converters will also feed the MBG magnet chain of CNGS. A diagram of the general arrangement is given in Fig. 25.8.

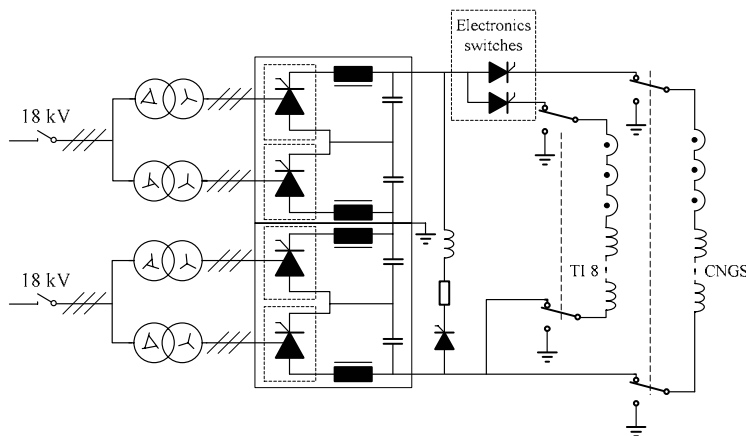


Figure 25.8: TI 8 MBI Power converter arrangement

Two mechanical switches per magnet chain permit an earth connection for safe intervention even while the converter is operating on the alternative chain. The mechanical switches are operated in four modes:

- 1) TI 8 without CNGS
- 2) CNGS without TI 8
- 3) TI 8 and CNGS
- 4) Neither TI 8 nor CNGS.

When functioning in mode 3 “TI 8 and CNGS”, all mechanical switches are in position to permit both magnet chains to be powered. In this case, the thyristor switches in series with each magnet chain can control which magnet chain is enabled on a cycle-by-cycle basis.

Two additional DCCTs (one in each circuit) are available for an independent interlock circuit that will prevent beam extraction if the magnet chains do not have the correct current.

Operation of this circuit requires a two-quadrant converter to assure the same current ramp rate independent of the TI 8 or CNGS system. In this way the current in the circuit is guaranteed to reach zero, permitting the turn off of the electronic thyristor switch before turning on the thyristor switch of the alternative circuit. Under normal operation, the magnet current is ramped down under closed loop regulation. In case of a power converter fault, the magnet current will decay with a natural time constant through the free-wheel thyristor.

25.9 POWER CONSUMPTION AND LOSSES

The additional power consumption and losses due to the transfer line power converters in the buildings BA7, SR2, BA4 and SR8 are indicated in the table 25.3.

Table 25.3: Additional power consumption and losses due to the transfer lines

Building	Flat Top Real power	Flat top Apparent power	Water flow	Water losses	Air losses
BA7	1.1 MW	2.9 MVA	0	0	48 kW
SR2	11.8 MW	17.5 MVA	4 m ³ /h	80 kW	108 kW
BA4	18.6 MW	28.6 MVA	8 m ³ /h	200 kW	84 kW
SR8	1.7 MW	4.0 MVA	0	0	90 kW

25.10 CONTROLLING THE POWER SUPPLIES FOR TI 2 & TI 8

25.10.1 Control Equipment for the Transfer Line Power Supplies

The control of the transfer lines TI 2, TI 8 and TT40 will be made to be the same as the rest of the SPS. For this Mugef systems will be used. Mugef ROCS corresponds to a standard hardware and software, ROCS indicating the last important upgrade of this system in 1998 (based on VME, LYNXOS and many standardised modules). A MUGEF crate is capable of controlling up to 64 power supplies, with each Mugef being connected directly to the Ethernet and to the SPS Timing networks. Additionally, there are two special lines, "Remote Reset" and "Remote Terminal". A standard Mugef crate consists of:

CPU:	PowerPC603
System managing:	SAC = System Arbiter Controller
Non volatile memory:	MEM206
Timing:	TG8
Commands & status:	Statophone 1.0
Analog measurement:	MPV915
Function generator:	New Wave 3.1.

Specific cards or modules needed for the SPS main power supplies, the control of RF cavities and for the Transfer Lines, are added to this standard crate.

25.10.2 Specificities of the Mugef for the Transfer Lines TI 2 & TI 8

Fast Extraction Interlock

The addition of a fast extraction interlock function to the standard Mugef system requires the addition of a special hardware device. This will provide basic local diagnostics as well as the connection to the central Interlock crate in each building.

Very high precision Power Supplies

For the five most demanding precision power supplies, the standard Mugef crates are equipped with a different function generator card. On these cards, the general 16 bit DAC is replaced by a special 18 bit DAC that ensures 16 bit monotonicity over the full bipolar range in addition to improving other parameters.

25.10.3 Fast Extraction Interlock System (FEI)

In order to avoid damaging the vacuum chamber of the transfer lines when a power supply fails, a measurement of the current of all the power supplies concerned must be taken immediately before each extraction. If the current of one or more units is outside a preset tolerance, the extraction must be prevented. In order to be able to optimise the measurement speed compared to the expected error rate, it is possible to set the following parameters separately for each power supply:

- 1) The nominal value of the current at the time of extraction. To increase the reliability of the system, a second ‘Extraction Current Reference’ (in addition to the regulation current reference) is sent and compared with the measured value. If the measured value exceeds the accepted tolerance on the reference value, the fast extraction interlock is activated.
- 2) The tolerance of the permitted current without interlocking the system.
- 3) The sample number "N" for the measurement which defines the degree of measurement filtering. The precision (and thus the reliability) of measurement increases with "N".

How the F.E.I. works

Each Mugef crate has a centralised fast measurement system of all the currents. The functionality for the fast extraction interlock is created by the addition of some hardware and software enhancements to this measuring system.

The Mugef system measures the all of the power converter output currents each millisecond. For a full Mugef crate this means that 64 Power supplies × 2 channels = 128 measurements are made per millisecond. Just before extraction, the following sequence is carried out:

- The extraction system sends an extraction request signal (event) to all Mugefs,
- Each Mugef sets the “fast interlock” process to maximum priority. This process consists of building an average of “N” samples of the measured current for each measurement and comparing it with the instantaneous nominal value,
- For each power supply, the Mugef processor extracts the “out of tolerance” bit, and memorises it.
- The logical “OR” of all the “out of tolerance” bits controls the “extraction permitted” output of the Mugef crate.

As operation of the Transfer Lines shares some vacuum chambers with the CNGS, it is envisaged to implement a Fast Extraction Interlock that is localised to the relevant vacuum zone. This will be performed by means of programmable masks that will group subsets of the Mugef crate into several interlock signals dedicated to a particular zone.

REFERENCES

- [1] J.P. Burnet, “*Technical Specification for the Renovation of a Series of Thyristor power Converters with rating from 5 kW to 10 MW*”, IT/2353A/SL, December 1997.
- [2] A. Dupaquier, “*Technical Specification for D.C. Power Converters rated ±3.5 A, ±70 V*”, IT-2114/SL, November 1992.

CHAPTER 26

BEAM INSTRUMENTATION

26.1 INTRODUCTION

The transfer line beam position monitors (BPMI) allow steering of the beam throughout the length of the line and up to the entrance of the septum magnets. Fast BCT (beam current transformer) coils and acquisition electronics are required to acquire the intensity of individual LHC bunches. Standard SPS type beam-loss monitors (BLMI) will be used to localise the losses linked to the beam transfer. BTVI (beam television) screens using either the standard luminescence screen or optical transition radiation effect (OTR) screens will be provided to allow the transverse beam sizes to be determined and offer complementary position information during the setting up and steering. All of the installed instruments are designed to cope with the full variety of LHC beams planned. All the systems have been developed to fulfil the functional specifications described in [1].

26.2 POSITION MEASUREMENT

The SPS to LHC transfer line trajectory measurement system consists of 53 monitors in TI 2 and 47 monitors in TI 8, connected to acquisition electronics capable of 40 MHz bunch by bunch measurements.

26.2.1 Beam Position Monitors

There are 2 types of beam position monitors (BPMs) in the SPS to LHC transfer lines: 34 mm diameter button electrode monitors (BPMI) and 110 mm strip-line monitors (BPK). The vast majority of the pick-ups are of the button electrode type (48 in TI 2 and 43 in TI 8), for which the buttons have been recuperated from the LEP machine (see Fig. 26.1(a)). Although the majority of the pick-ups will be used to measure a single plane, four buttons have been mounted on each BPM body to allow for a future upgrade of the system to dual plane measurements. The pick-up body has a diameter of 60 mm and is located on the downstream side of the quadrupole (see Fig. 26.1(b)). The mounting and alignment of the body and support will be performed before magnet installation in the tunnel.

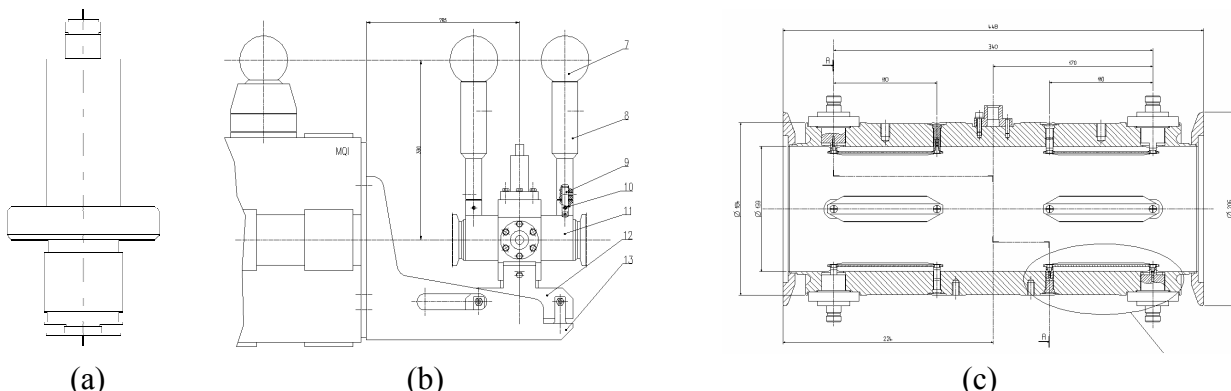


Figure 26.1: (a) LEP button electrode; (b) BPMI body and support mounted on the downstream side of the quadrupole; (c) BPK strip-line monitor

The BPK strip-line monitors are dual purpose monitors developed for the first 4 pick-ups in TI 8 (TT40), which are capable of measuring both the LHC and CNGS beams. For reasons of aperture, the first five pick-ups in TI 2 (TT60) will also be of this type. Since the LHC acquisition electronics cannot measure beams with a 200 MHz structure, a double pick-up is required to avoid having to split the signal at the source. The BPK is therefore a dual strip-line monitor (see Fig. 21.1(c)), each strip-line having a length of 110 mm and short circuited at the downstream end for the LHC electronic output and the upstream end for the CNGS electronic output. The diameter of the body is 133 mm, while the inter-electrode diameter is 116.7 mm.

26.2.2 BPMI Acquisition System

The trajectory acquisition system is identical to that of the LHC orbit and trajectory acquisition system which is fully described in Vol. I, Sect. 13.12 of the design report. In most cases the front-end chassis will be located near the quadrupoles containing the pick-up. The exceptions are the pick-ups near the injection and extraction points, where concerns over the radiation level in these areas has led to a regrouping of the front-end electronics about 150m away from the extraction or injection point. For TI 2 (including TT60) the VME acquisition electronics will be located in BA70, while for TI 8 (including TT40) the VME acquisition electronics will be located in HCA442. As for the LHC system, connection between the front-end and the VME electronics is via a fibre-optic link, while the control of the front-end crate (sensitivity setting, calibration, power supply status etc) is via a 31 kbit/s WorldFIP link. The system is expected to function within specifications between 2×10^9 and 2×10^{11} charges per bunch. A detailed breakdown of the expected performance is given in Vol. I, Sect. 13.13. Three pick-ups in each transfer line will be equipped with acquisition in both planes in order to allow an additional intensity measurement to be performed at these locations (with a precision of around 5-10%). The front-end intensity card will be installed in the same front-end chassis as the position electronics and has been constructed to use the same fibre-optic link and digital acquisition electronics.

26.3 INTENSITY MEASUREMENT

Both TI 2 (TT60) and TI 8 (TT40) will be equipped with two beam current monitors, one located at the start and one at the end of each line. The acquisition crates will be located in BA60 (TT60), UA23 (TI 2), HCA442 (TT40) and UA87 (TI 8). Both the beam current transformers and the acquisition electronics used are identical to those installed in the PS to SPS transfer lines and the fast transformer in the SPS ring.

26.3.1 Beam Current Transformers

The fast beam current transformers (FBCTs) will integrate the charge of each LHC bunch spaced by a multiple of 25nsec. Because of the single-pass nature of the beam in the transfer line, good performance is obtained without applying the DC restoration technique necessary for circulating beams.

26.3.1 BCT Acquisition Electronics

Two multiplexed 20MHz integrators are used and the result of integration is digitised and stored in the memory of the DAB acquisition card. SPS extraction pre-pulses and the 40 MHz bunch clock transmitted via the SPS Beam Synchronous Timing (BST) system are used to trigger the acquisition systems.

The measurement precision for the pilot beam of 5×10^9 protons in a single bunch is expected to be around 5 %. In the worst case a 10 % error should be envisaged, whilst for the nominal LHC beam the error will be below 1 %. The transformer cores will use low droop, radiation hard materials. The specified droop for the cores is below 2 %/ μ s and the sensitivity should be approximately 1.25 V/A.

26.4 BEAM-LOSS MEASUREMENT

Beam-loss monitors are placed at strategic locations in the SPS to LHC transfer lines, notably where the risk of having losses are the highest.

26.4.1 BLMI monitors

The SPS type beam-loss monitors (BLMI) are used to identify the location of beam losses during the extraction process. About 60 ionisation chambers will be installed in the SPS to LHC transfer lines. The ionisation chambers are parallel plate type monitors and are filled with nitrogen at atmospheric pressure. Each monitor has a volume of one litre. The electrical drift field strength is set to 1600 V/cm.

26.4.2 BLMI Acquisition System

The currents generated by the chambers are treated by the BLMI acquisition system. This consists of a total of 4 VME chassis in for TI 2 and TI 8, which are installed in surface and underground areas. An integrator integrates the ionisation chamber current during the extraction process. The integrator output is then sampled by a 12-bit ADC and the digital output value stored in memory. The whole read-out chain is implemented in a dedicated VME module. The acquisitions are triggered by SPS timing events pre-programmed in the corresponding LHC or CNGS cycle. The beam-loss server can return the data either in raw ADC units, or calibrated in units of mGy. If the losses scale linearly with the total intensity, then dynamic range in losses stemming from the LHC beams reaches a factor of 10^4 between a single pilot bunch and four batches of ultimate intensity. To cover this large dynamic range with the 12 bit ADC, several gain stages are used on the acquisition card. Each VME crate is capable of treating up to 40 beam-loss monitors and is placed such as to minimise the cable lengths.

26.4.3 Beam-loss Interlocks

The beam loss monitors in the transfer lines and in the injection region form part of the SPS extraction interlock system [3]. Whenever the measured rates exceed a given preset threshold, the extraction from the SPS is inhibited for the following cycles. A machine operator has the possibility to reset this interlock in order to perform tests and, if required, improve the steering of the line or of the extraction channel. An automatic reset mechanism may be applied to prevent unnecessary machine downtime in case of a spurious problem, as is already done in the SPS ring.

26.5 BEAM-PROFILE MEASUREMENT

The SPS to LHC transfer line profile measurement system consists of a total of 16 BTV tanks in each of the two transfer lines. The CCD cameras, each connected to acquisition electronics are capable of doing a single 3-D measurement per injection into the LHC. As the passage of the beam through the screens will create a certain amount of emittance blow-up, they will not be left in the beam path, but rather be inserted on demand during studies on the transfer line optics.

26.5.1 BTVI Mechanism

The BTV monitors will be distributed along each of the transfer lines, including the injection point into the LHC. The latter monitors are described in more detail in Vol. I, Sect. 16.5 of the LHC design report. Each monitor will be equipped with a phosphorescent alumina screen which is designed for use mainly with the low intensity pilot beam and with a $12\text{ }\mu\text{m}$ thick titanium foil providing optical transition radiation at nominal currents. The first three monitors, located before the beam dump in TT40 and TT60 are of standard mechanical type as used in all other SPS lines [4]. For the others, new designs have been developed or are under development. The following nine monitors, named BTVI, will be installed on the 60 mm vacuum chamber of the transfer line. As for the SPS standard screens, their mechanism is based on a rotating displacement to set the screens IN and OUT of the aperture, actuated by a DC motor. However their design is more compact in order to fit their environment and to get the necessary precision [4]. In Fig. 26.2(a) 3-D drawing of a BTVI assembly is shown. By a 90° rotation, either of the screens can be set IN or OUT of the vacuum chamber aperture. The BTVI monitors, produced at JINR (Dubna) in Russia, will also be used to equip the TT41 CNGS line.

For completion, the last four TV monitors in the lines, called BTVSI, will be installed at each injection insertion, downstream of each septa and at each end of the injection kickers and upstream the TDI absorber. These last monitors will therefore be installed on the circulating beam vacuum chamber. Because of the proximity of the adjacent ring, space constraints are more severe in this case. Moreover, it is required to ensure the vacuum chamber smoothness to reduce the machine impedance when the screens are removed and the beam circulates. Therefore a completely different mechanical design is under study for these monitors, based on a linear displacement, however, they will still be activated using the same DC control as the BTVI.

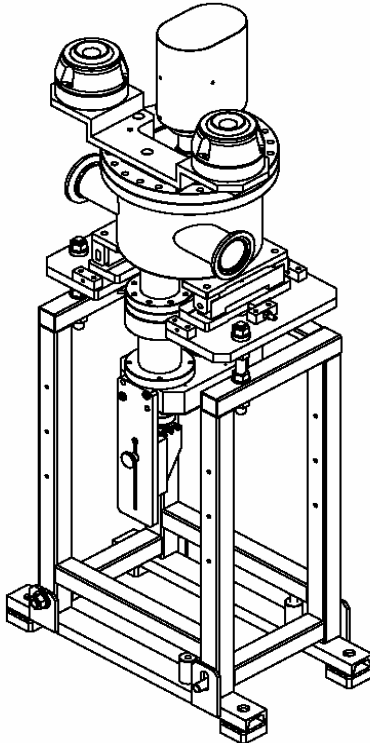


Figure 26.2: Mechanical design of a complete BTVI assembly installed in TI 2 and TI 8

26.5.1 BTVI Acquisition system

The acquisition of the beam profile data is based on high-resolution CCD cameras. These are linked to a newly developed BTV acquisition card that allows the acquisition of a two-dimensional image with a digitisation resolution of 300x400 pixels. The screen position, as well as filters and an external lamp, can be controlled from the same VME module. All monitors will provide two-dimensional information as well as the projections into horizontal and vertical profiles.

26.5.2 Reproducibility on Position and Size Measurements

Measurements on a BTVI tank [5] have shown that the reproducibility on the measurement of the beam size and the centre-of-mass for a spot size equivalent to that of the LHC beam is very good. The beam position (centre-of-mass) acquired over 10 consecutive screen movements changes by around 100 μm peak-to-peak and the beam size is determined to within 1 %. These figures are well within the specifications. Even better results are expected with the newly designed BTVI tank, notably if special care is taken during the alignment of the BTVI screens.

26.5.3 BTI Acceptance

The BTV screens with a 65 mm diameter will entirely cover the vacuum chamber aperture. The profile monitor optics and readout will allow either large area coverage, at the expense of a loss in accuracy or small area coverage optimised for optics and emittance measurements. During the first commissioning of the lines, the profile monitors will be tuned to cover the largest possible fraction of the aperture.

26.5.4 BTVI Interlocks

The position of the intercepting transverse profile monitors will be surveyed by the SPS software interlock system. Depending on the operation mode of the LHC, the software interlock system should prevent beam

extraction when the profile monitors would intercept the beam. This is to avoid undesired emittance blow-up of the beam. This interlock can, however, be bypassed for machine experiments and during verifications of the transfer line optics. There are also ideas to incorporate a low-level software interlock on the movements of the BTV mechanisms in case the circulating intensity transmitted by the SPS BST system is above a certain threshold. This is because the alumina screens will be damaged by passage of the very dense high intensity LHC beam.

REFERENCES

- [1] J.Wenninger et al, “Instrumentation for the TI 2 and TI 8 Transfer Lines”, EDMS Document LHC-B-ES-0004.
- [2] G.Ferioli et al., “Protection and Diagnostic Systems for High Intensity Beams”, CERN-SL-2000-032-BI.
- [3] R. Giachino et. al., “Architecture of the SPS Beam and Extraction Interlock Systems”, CERN-AB-2003-010-OP.
- [4] R. Jung et al., “Single Pass Optical Profile Monitoring” DIPAC 2003
- [5] Minutes of the 25th BI LHC/CNGS Technical Board.

CHAPTER 27

TRANSFER LINE DUMPS, SAFETY STOPPERS AND COLLIMATORS

27.1 EXTERNAL BEAM DUMPS (TED)

Three new external beam dumps (TED) will be installed in TI2 and TI8. These beam obstacles are the natural evolution of the existing SPS ones, placed in TT20 and TT60 [1]. The TED will be located in TT40, at the end of the TI8 tunnel and at the TI2 exit. The existing TT60 dump will act as the upstream TED for TI2.

The TED are required to intercept the high energy beam extracted from the SPS. This is concentrated in very short pulses (in the range 7.8 μ s to 10.5 μ s) at high intensities. In the extreme case the TT40 TED has to withstand the impact of the CNGS beam with up to 7×10^{13} protons every 6 seconds at 400 GeV. The dumps should withstand these conditions for several hours, for example during extraction setting up, without alteration of the properties of the core.

The new transfer tunnels are rather small and pose significant space and transport difficulties for large, heavy items such as the TED. In spite of this, an effort was made to keep the new TED for the LHC compatible with the present SPS ones. This has the advantage of equipment standardisation and allowed the saving of one complete assembly by sharing a spare TED between the SPS and the LHC. However, the dimensions and material composition of the absorber core have been improved in order to cope with the LHC beam parameters.

A schematic view of the TED geometry is presented in Fig. 27.1. The outer cast iron shielding is identical to the present SPS one with two 4300×960×480 mm yokes each weighing 9.5 tons and providing handling and positioning facilities. Cooling is provided by four independent circuits using Ø16 mm diameter tubing. The shielding fully encloses a polycrystalline graphite core (type R7500 by SGL), which is split into twenty cylinders Ø80 mm, 145 mm long. These cylinders are thermally shrink-fitted at about 200°C into five aluminium tubes (EN AW 6082-T6) Ø80/160 mm, 600 mm long, which are connected lengthwise. In addition, a downstream solid cylinder of same length and same alloy is added. The six elements are assembled by means of elastic pins, and by four press fitted [3] stainless steel tubes Ø14/16 mm, which are twin-linked to form two independent water-cooling circuits. The compete 160 kg assembly is fitted into a copper tube made of four CuOFE elements Ø160/310 mm, 900 mm or 940 mm long and of a downstream solid cylinder, 790 mm long. Elastic pins and press fitted tubes keep these five elements together, which are also cooled by two independent water circuits. This assembly method avoids expensive electron beam welding of the special (and fairly brittle) copper alloy. A Ø58 mm insert, 250 mm long, made of high-strength (UNS C17200) Cu-Be alloy, is shrink fitted by liquid nitrogen in the upstream part of the solid copper cylinder.

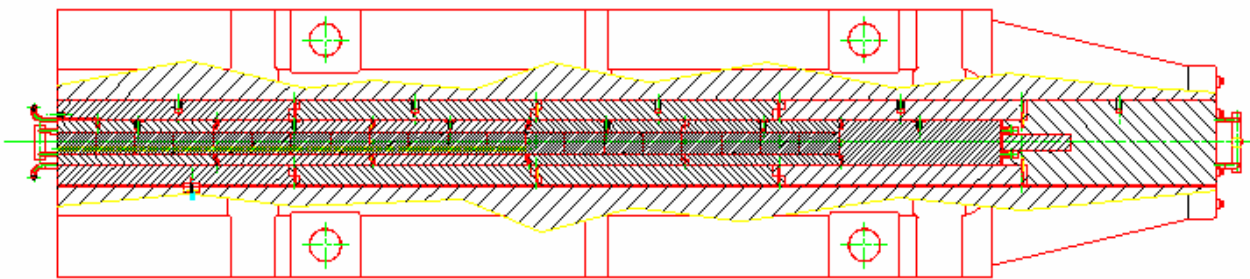


Fig. 27.1: TED schematic side view. The beam direction is from left to right.

The copper part of the dump core weighs about 2.4 tonnes and the complete TED therefore weighs about 21.6 tonnes. The eight independent water cooling circuits are fed by a collector located at the downstream end of the external shielding. This provides a heat transfer coefficient of 0.8 Wcm⁻² per °C to each circuit, with a maximum water speed of 2 m/s. In practice, each TED requires a total flow rate of about 18 m³/h.

Since the core itself has no structural function, steady state temperatures around 200 °C can safely be accepted in the aluminium and 300 °C in the copper. Because of the small size of the beam spot, the maximum attained energy density in the graphite is quite high, while lower temperatures are reached in the aluminium and copper. At the ultimate LHC beam intensity, the adiabatic maximum temperature increases are: 800°C in graphite, 130 °C in aluminium and 165 °C in copper. Temperatures drop rapidly away from the beam axis, with very high thermal gradients. The ensuing thermal stresses are below those allowed [4] for standard fine-grain graphite and aluminium alloys, while in copper and iron they are not. For copper, a more resistant alloy was therefore selected. As it would be too expensive to replace the whole of the copper part, a 25 cm short cylinder Ø5.8 cm, made of special Cu alloy, was thermally shrink fitted into the upstream part of the standard copper block, where equivalent stresses remain <70 MPa.

Only 1.5 % of the beam energy is estimated to escape from the TED. The graphite core absorbs 21.9 % of the beam energy, while the aluminium, copper and iron sections absorb 20.5 %, 36.1 % and 13.1 % respectively. The maximum allowed beam intensity for safe operation is given as a function of the pulse duration in Fig. 27.2. This graph is extended to show the slow extraction pulses as presently aborted on the SPS dumps.

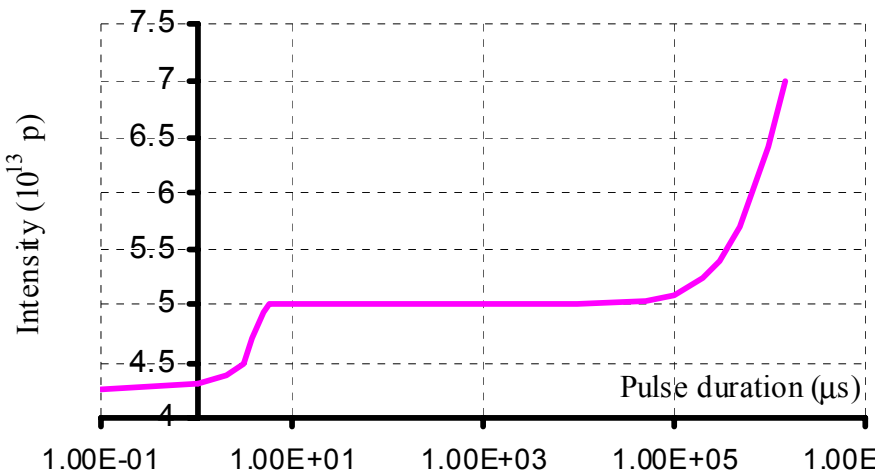


Figure 27.2: Maximum allowed intensity of a 450 GeV proton beam of radial size 0.58 mm, dumped every 16.8 s on a TED.

27.2 EXTERNAL SAFETY BEAM STOPPER (TBSE)

One safety beam stopper (TBSE) will be installed in the TI 8 beamline, immediately after the switch magnets and just before the entrance to the TI 8 tunnel. A second TBSE is planned for the entry of the TT41 neutrino tunnel [2] as a safety protection for the CNGS facility. It will be identical to the LHC one. The closure of the SPS west experimental area means that TT60 now serves only TI 2 with beam. As a result, the TED in TT60 can also act as a safety stopper for TI 2. Like the TED, the TBSE beam obstacles are the natural evolution of the existing SPS ones, placed in TT20 and in TT60 [1].

The stopper, which is dedicated to personal safety, is only supposed to absorb the occasional (ideally never) pulse of beam. This would be a single shot of 450 GeV protons concentrated in a very short pulse (in the range 7.8 μs to 10.5 μs). Once again the extreme case would have an intensity of up to 7×10^{13} protons. The TBSE design adopts the same structure as the TED core, with the copper part substituted by iron for cost and technical reasons. A schematic side view of the TBSE is presented in Fig. 27.3. It is much simpler than the TED since it has neither external shielding, nor cooling circuit. The inner graphite/aluminium core is made in the same way as the TED one, the aluminium elements only being assembled by elastic pins. The outer steel (C45 W) core is made of two pinned elements: an Ø120/240 mm tube, 3620 mm long, nesting a downstream solid cylinder, 500 mm long. The complete TBSE core weighs about 1.2 tons.

The TBSE has less stringent requirements than the TED. Since it is expected to receive only single beam aborts, only adiabatic temperatures have to be taken into account, and no cooling is needed. Since copper and iron have very close density, atomic number and specific heats, the above considerations also apply to the

TBSE. The peak of energy deposition in iron is very close to the front, where the maximum temperature increase is about 130 °C; only 15 °C is found on the side. The lack of a massive cast iron shield results in a poor lateral containment. In this case 20 % of the beam energy escapes the TBSE. The aluminium and iron sections absorb 16.7 % and 36.3 % of the beam energy respectively.

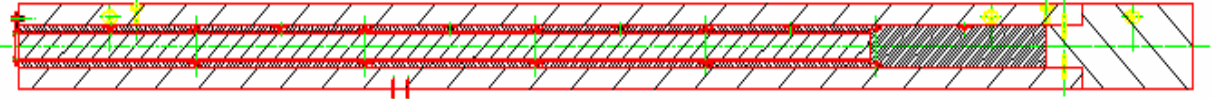


Figure 27.2: TBSE schematic side view. The beam direction is from left to right.

27.3 THE TRANSFER LINE COLLIMATION SYSTEM (TCDI)

The TI 2 and TI 8 transfer lines will be pulsed, with a close surveillance of power supply currents and beam parameters. Nevertheless, failure modes exist which could result in uncontrolled beam loss and serious damage to either the transfer line or the LHC equipment. To protect the equipment in the LHC injection regions and the LHC machine, a set of transfer line collimators (TCDI) will be installed.

Detailed studies and analyses [6,7] of the requirements for LHC protection have demonstrated that movable collimators are required in the transfer lines for protection in case of mis-steered beams. These will protect the LHC machine elements, including the small aperture MSI magnets, from damage. The aperture in the LHC arc at injection is just 7.5σ . The collimation requirements for the transfer lines have had to be adjusted accordingly. The nominal injected LHC intensity is about 20 times above destruction level and several orders of magnitude above the quench level of the cold magnets. Prior to injection into the LHC, scraping at about 3.5σ will be performed in the SPS, just before extraction. The transfer through the lines TI 2 and 8 and the injection into the LHC will be adjusted using pilot intensities, below the quench level and well below any damage level. Failures resulting in major beam loss at injection, for example by trips or wrong strengths of correctors in the pulsed transfer lines, cannot be completely excluded but are expected to be rare.

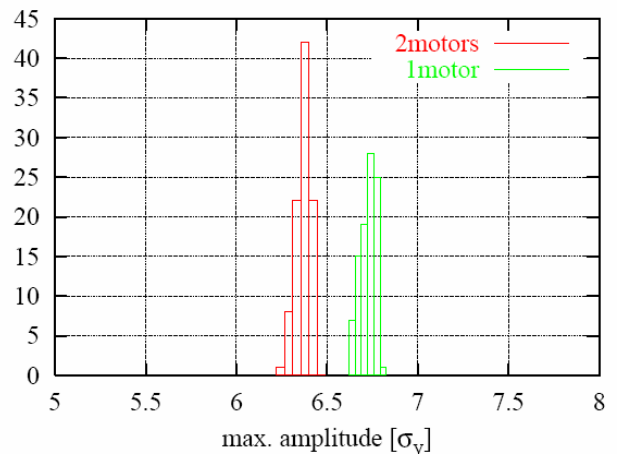
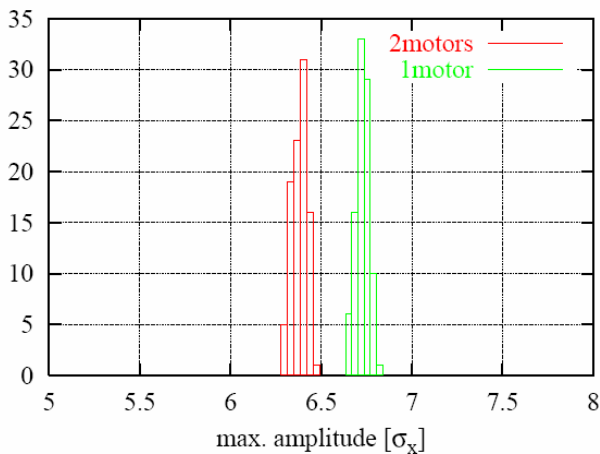


Figure 27.3: Distribution of maximum particle amplitude transmitted into the LHC for the 0-60-120 degree TCDI system, for horizontal and vertical planes.

The main function of the TCDI collimators is to dilute the beam sufficiently to avoid any destruction in such cases. The TCDI system will protect the LHC to 6.4σ in each plane, with a total of 7 collimators per line. Momentum collimation will be performed in the first available space with high dispersion, and requires only one collimator. Betatron collimation will protect the tight MSI septum aperture, the injection region and the LHC cold aperture against bending errors upstream, and will therefore be placed towards the end of the line. A total of 6 collimators are necessary to achieve the required protection, using a phase coverage of 0-

60-120 or equivalent. For optics flexibility it is clearly an advantage to have a solution using 0-60-120, instead of the alternative 0-45-90-135, which has an extra phase advance constraint. For integration purposes the situation is also easier.

The protection level has been simulated by tracking beams through the collimators installed at ideal locations in TI 8. This tracking was performed with optical errors (beta-beating) included from the SPS and from sources in the line. The 0-60-120 solution provides an adequate protection, with maximum transmission below 6.4σ , for a nominal (i.e. guaranteed minimum) aperture of 4.5σ at each collimator. The results are shown in Fig. 27.3. The chosen solution uses TCDI equipped with 2 motors per jaw. The tracking results for the case when a single motor per jaw is used are also presented. For TI 8, the 0-60-120 option is easier to fit physically in the line, with the natural matching solution having very convenient locations for all devices, except the H120 collimator. However, the location for the alternative H300 is available. For TI 2 the natural positions are at 240 and 300 degrees in both planes, to avoid difficult matching and integration. The provisional locations for the TCDI collimators in TI 2 and TI 8 are given in Tabs. 27.1 and 27.2 respectively.

Table 22.6: Provisional TCDI collimator locations for the transfer line TI 2.

Name [m]	s [m]	$\Delta\mu$ to TCDI _{MSI} [°]
TCDIMOM	403.1	-
TCDIH300	2818.0	300
TCDIH240	2852.0	60
TCDIHMSI	3108.8	0
TCDIV300	2844.0	300
TCDIV240	2893.0	60
TCDIVMSI	3110.8	0

Table 22.7: Provisional TCDI collimator locations for the transfer line TI 8.

Name [m]	s [m]	$\Delta\mu$ to TCDI _{MSI} [°]
TCDIMOM	668.8	-
TCDIH300	2385.5	300
TCDIH060	2547.0	60
TCDIHMSI	2622.1	0
TCDIV120	2441.5	120
TCDIV060	2498.3	59
TCDIVMSI	2620.1	0

To protect local elements from damage arising from particles scattered from the TCDI jaw secondary TCDIM shields are required downstream of the TCDI collimators. With the exception of the last TCDIM these will be low-technology, low-cost objects around the beam pipe. The last element immediately upstream of the MSI must withstand higher temperatures than the others. Fig. 22.13 shows the temperature rise simulated in magnets downstream of a TCDI collimator and TCDIM mask, for a full LHC ultimate beam impact. A detailed functional specification and a preliminary design of the TCDI collimators with 1.2 m long graphite jaws (similar to the secondary LHC collimators) followed by a 50 cm long iron shielding outside the beam pipe can be found in [8].

A detailed functional specification and a preliminary design of the TCDI collimators with 1.2 m long graphite jaws (similar to the secondary LHC collimators) followed by a 50 cm long iron shielding outside the beam pipe can be found in [5].

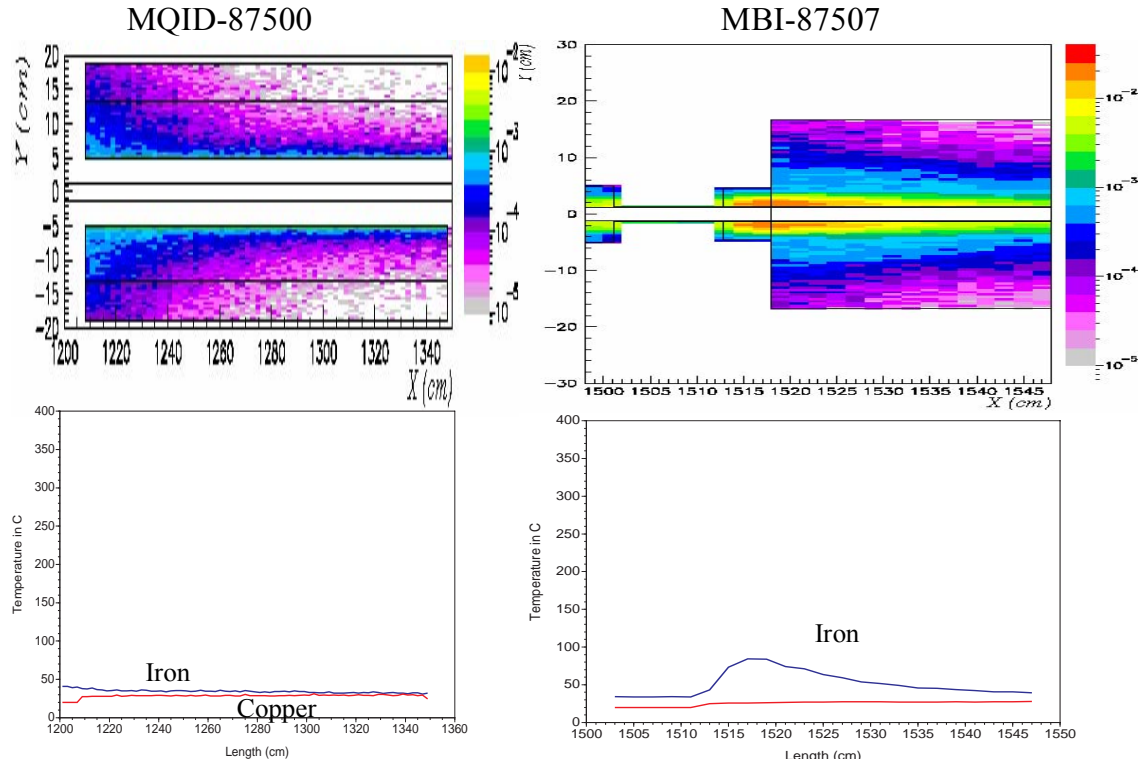


Figure 22.13: Energy deposition maps and maximum temperature rise profiles in MQID87500 and MBI87507, for full LHC ultimate beam impact on the graphite jaw of an upstream TCDI collimator.

REFERENCES

- [1] A. Ijspeert, P. Sievers, “*Proposal for a New External SPS Beam Dump*”, CERN/SPS/ABT/Int. 82-2 (1982).
- [2] E. Cennini et al., “*SPS Safety Chain Modification for the LHC Transfer Lines and the Long Baseline Neutrino Facility*”, SL-Note 99-010 SLI (1999).
- [3] P. Gerdil, A. Ijspeert, “*Cooling of absorber blocks by means of press fitted water tubes*” CERN/SPS/ABT/Int. 82-3, Prévessin – October 1982.
- [4] S. Péaire, P. Sala, “*Beam Dumps and Beam Stoppers for LHC and CNGS Transfer Lines*” CERN-LHC-Project-Report-465, Geneva, 7 Feb 2001.
- [5] H. Burkhardt, B. Goddard, V. Kain, W. Weterings, “*TCDI transfer line and LHC injection protection collimators*”, LHC-TCDI-ES-0001, Geneva, 7 Feb 2001.
- [6] H. Burkhardt et al., “*Protection Devices in the Transfer Lines to the LHC*”, PAC’03, Portland, LHC-Project-Report-641; CERN, 2003.
- [7] H. Burkhardt et al., “*Collimation in the Transfer Lines to the LHC*”, EPAC’04, Lucerne, LHC-Project-Report-768; CERN, 2004.
- [8] H. Burkhardt et al., “*Function and concept of TCDI transfer line collimators*”, LHC-TCDI-ES-0001-00-10, (EDMS 433291), 2003.

CHAPTER 28

VACUUM SYSTEM FOR LHC TRANSFER LINES TI 2 AND TI 8

28.1 INTRODUCTION

The Vacuum Group is responsible for the design, manufacture and installation of all the vacuum components of the transfer lines in collaboration with the Beams Transfer Group. The main components are the drift-space and magnet vacuum chambers, bellows, pumping ports, supports and vacuum instrumentation. The work, including the installation of the components in the tunnels has been carried out in collaboration with the Budker Institute of Nuclear Physics in Novosibirsk (BINP, Russia).

The requirements and layout of the vacuum system and the calculations of the pressure profile expected over two standard half-cells (~ 60.6 m) are presented below.

28.2 VACUUM REQUIREMENTS AND BASIC PRINCIPLE

The dynamic pressure, i.e. the pressure in presence of beam, in the LHC transfer lines is equal to the static pressure because there is only a single beam passage and as a result of the low beam losses expected. Therefore, the design pressure has been fixed to optimise the lifetime of the pumps.

About 50 ion pumps in each transfer line will be used to achieve a high vacuum ($<10^{-5}$ Pa), a value which is low enough not to deteriorate the lifetime of ion pumps. These pumps have been chosen mainly for their high reliability, simplicity, cleanliness and because their currents give indications on the local pressure. They also provide reliable interlocks for the sector valves in case of pressure rises. The roughing of the vacuum system down to 10^{-3} Pa before switching on the ion pumps is done with mobile turbomolecular pumping stations.

28.3 LAYOUT AND PRESSURE PROFILE

Each transfer line has about 96 half-cells, composed of one quadrupole magnet, a beam position monitor, a dipole corrector, a pumping port and 4 dipoles.

The vacuum sectors are about 450 metres in length and start immediately after the beam separation in the TT60 or TT40 transfer lines. They end immediately after the beam dumps (TED) in the downstream part of the transfer lines, about 50 meters upstream the injection into the LHC main ring. Each vacuum sector has three roughing valves for the connection of both the mobile pumping stations and leak detectors and one combined Pirani and Cold Cathode gauge (Type BALZERS FullRange).

The ion pumps, with an effective pumping speed of 20 l/s, are installed every half-cell at the bottom of the pumping ports. For cost reasons, only half of them (one in two is skipped) have been connected to a power supply. The pumps which are not powered will serve as spares.

Fig. 28.1 shows the pressure profile expected over two half-cells (60.6 m) with an ion pump powered every two half-cells and assuming an outgassing rate of 4×10^{-7} Pa.m/s (4×10^{-10} mbar.l/s.cm²) after 24 hours of pumping. This outgassing is derived from the outgassing measurements made on the first batch of dipole chambers received at CERN.

The outgassing, which is mainly composed of water (unbaked system), will decrease with a slope of t^l where t is the time in hours. An average pressure of 3×10^{-4} Pa will be achieved after about one week of pumping, assuming the previous pumping sequence.

The measurements obtained during the installation of the TI8 transfer lines showed a faster decrease of the pressure. A pressure in the low 10^{-5} Pa has been achieved after about 2 weeks of pumping.

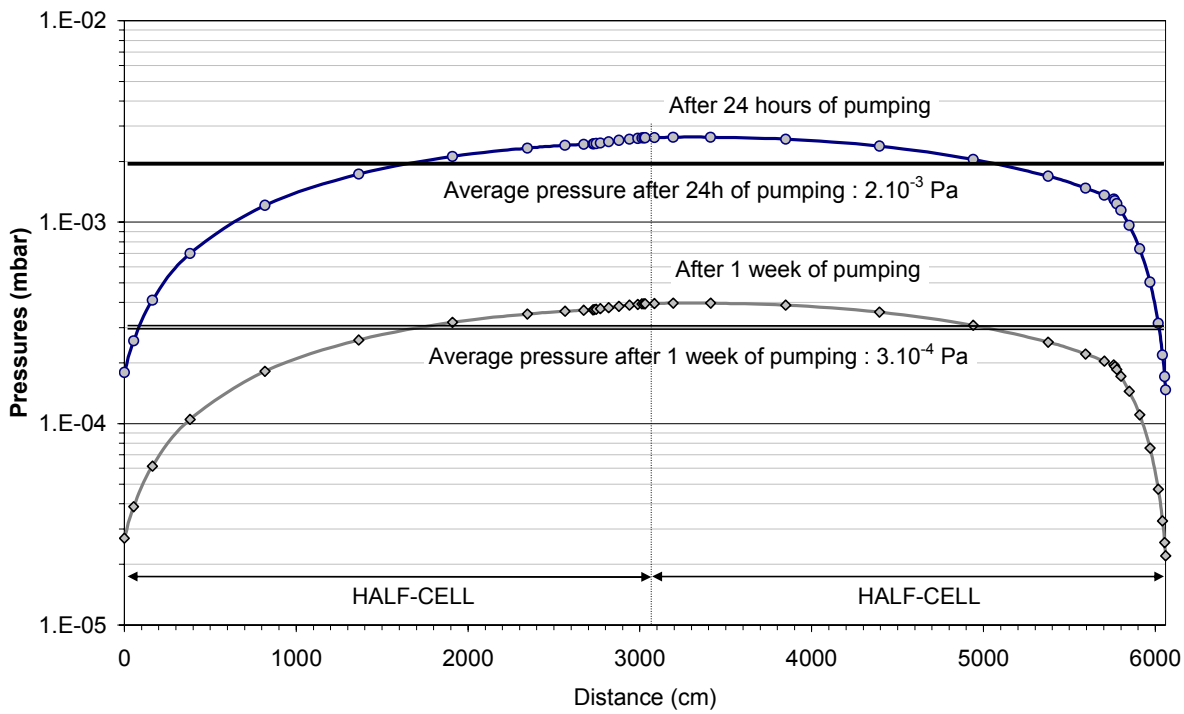


Figure 28.1: Pressure profile expected over two half-cells (60.6 m) with an ion pump powered every two half-cells and assuming an outgassing rate of 4×10^{-7} Pa.m/s (4×10^{-10} mbar.l/s.cm 2) after 24 hours of pumping.

28.4 VACUUM COMPONENTS AND VACUUM CONTROL SYSTEM

About 830 bellows, 690 chambers for magnets (dipoles, quadrupoles and correctors), 350 drift-space chambers and 180 pumping ports compose the vacuum system of the two LHC injection transfer lines. These two thousand pieces will be interconnected using 2000 coupling connections with chain clamps and aluminium gaskets.

28.4.1 Magnet Vacuum Chambers

The beams circulate in stainless steel vacuum chambers with a low magnetic permeability. The vacuum chamber section varies depending on the position along the beam line.

About half of the quadrupole magnets have a circular aperture, the other have an elliptical chamber which can be oriented horizontally or vertically. Fig. 28.2 shows the different types of apertures used for the transfer lines.

The dipole and dipole corrector magnets have elliptical or nearly rectangular chambers. To maximise the beam aperture, the dipole vacuum chambers are installed in the magnets and compressed while welding the two half yokes together.

28.4.2 Drift-space Chambers and Interconnections

To simplify the alignment of the straight sections, the drift-space chambers are circular pipes with an inner diameter of 60 mm (Fig. 28.2), much larger than the beam aperture required.

All chambers, bellows, pumping ports and all other equipment of the beam lines are interconnected using quick-disconnect conical flanges (KF63), chain clamps and aluminium gaskets.

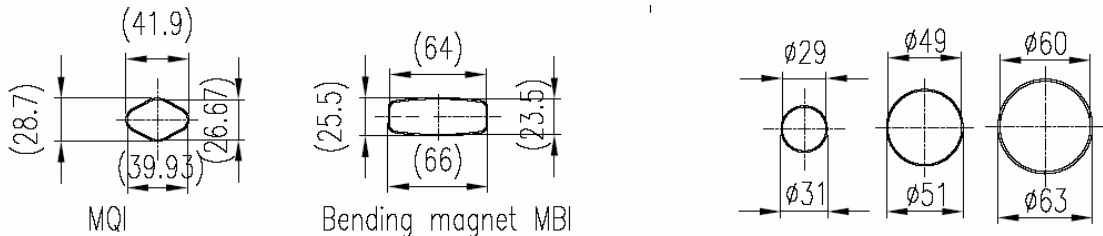


Figure 28.2: Section of the vacuum chambers in the SPS and LHC Transfer lines. In the transfer lines, the quadrupoles are called MQI, the dipoles MBI.

28.4.3 Vacuum Control and Pressure Monitoring

All the sector valves, ion pumps and gauges will be controlled using the Vacuum PVSS interface which is used for the PS and SPS machines. This application, which is being upgraded for the LHC, allows pressure monitoring and data storage. All actions requested like closing/opening of sector valves, switching ON or OFF of ion pumps are recorded for post mortem analysis. The pressures measured by the gauges and ion pumps are recorded once per minute and this gives indication of the status of the vacuum system, allows small leaks to be identified from trends and will be used for post mortem analysis if a huge leak induces a stoppage of all ion pumps. Figs. 28.3 and 28.4 show the main page of the Vacuum PVSS application and the synoptic and sectorisation of the LHC injection transfer lines, respectively.

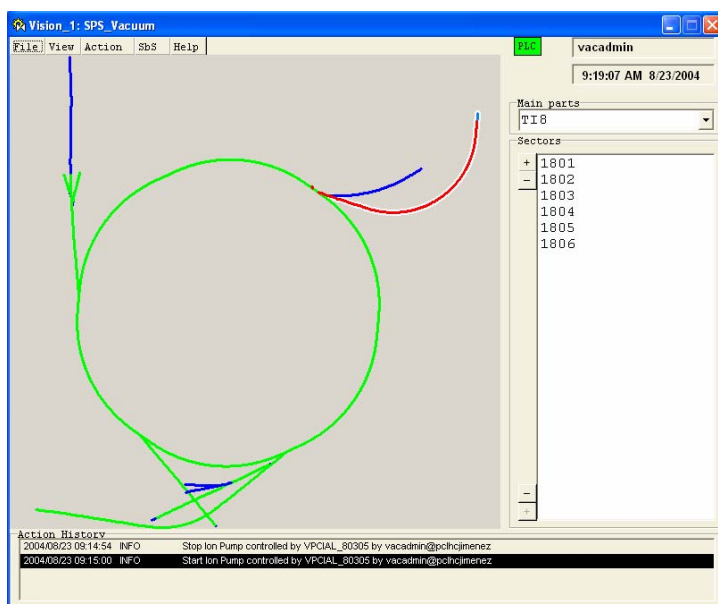


Figure 28.3: Main page of the Vacuum PVSS application which allows the access to the control interfaces for the SPS and LHC injection transfer lines.

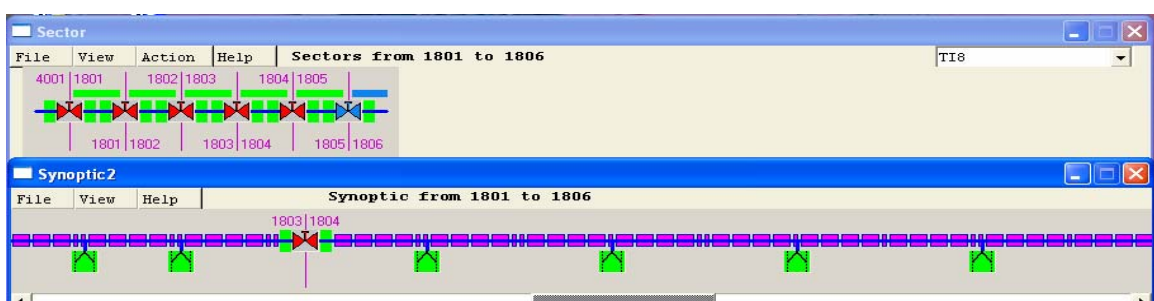


Figure 28.4: Vacuum sectorisation and mechanical synoptic of the LHC injection transfer line.

CHAPTER 29

ACCESS AND SAFETY

29.1 ACCESS SYSTEMS

The SPS access system and interlock chains have been extended to incorporate the SPS to LHC transfer lines. Only the parts of the transfer lines which are physically located inside the LHC tunnel are incorporated in the LHC access system (see Vol. 2, Chap. 5). In the medium term it is planned to migrate the access control system for the SPS and transfer lines to a system similar to LHC.

The controlled areas of the SPS and transfer lines are split into access zones bounded by interlocked doors or gates. The system operates on the buffer-zone principle i.e. there is always a “dead zone” between the danger area where beam could be present and an occupied zone; in this buffer zone there must be no beam and no personnel.

For each access zone of the transfer lines, a pair of safety chains covers the beam and access requirements. These act on both up- and down-stream access zones in order to propagate interlocks upstream to prevent beam injection and allow access downstream of the buffer zone. In each case an access chain (ACS) is paired with a beam interlock chain (MIS).

The state of each chain depends upon a set of safety elements, beam elements for the MIS chain and access system status for the ACS chain. Access in a delimited zone can only be granted if the associated MIS chain is in the correct state to prevent beam. Likewise, machine interlocks can be lifted and beam put through a zone only when the corresponding ACS safety chain is in the appropriate state. The pairing of a MIS and an ACS chain is made in such a way that only one of them is allowed to be active, determined by the position of a key on the access console. This key cannot make the chain active unless all conditions (interlocks etc.) attached to that chain are fulfilled.

It is a requirement that two independent elements are interlocked to stop the beam. Each of these elements should be sufficient by itself to stop the beam entering the downstream area. In practice, three elements are used.

Access conditions will be the same as those described in Vol. 2, Chap. 3 for access from the LHC areas. Until the SPS access and control system is migrated to the LHC system, the requirements for users entering areas under SPS control will be the same as those for other SPS areas.

29.2 SAFETY SYSTEMS

The safety hazards in the transfer lines are rather similar to those in the LHC but with the notable absence of cryogenics. The main concerns are:

- Ionising radiation
- Isolation of workers underground in a long and extended tunnel system
- Limitation to the number of evacuation paths in case of an accident and confinement of volumes underground
- Presence of combustible materials
- Work in the presence of magnetic fields
- Electrical risks

The safety systems for protection of personnel are therefore very similar to those described in Vol. 2, Chap. 3.

29.3 TI 2 ACCESS AND SAFETY

The layout of TI 2 in Fig. 29.1 shows the main elements of the safety systems and the location of the gates which enclose the zones. TI 2 is split between SPS and LHC zones which are separated by the inter-zone gate. Access to the downstream end requires that there is no beam in the LHC.

29.3.1 Important Safety Elements

The three elements which are interlocked for access to the upstream part of TI 2 are the extraction septa, the movable beam stop and the dipole magnet in TT60. These elements are located upstream of the zones depicted in Fig. 29.1. For access in the downstream part of TI 2, the three elements are a dipole pair (MBB201), the movable beam stop (TBSE) and the dipole chain (MBIAV206).

Table 29.1: Safety elements in TI 2

Zone	Description	Safety Elements (EIS)
Upstream TI 2	SPS and TI 2	MSE6183, TED6103, MBB6104
LHC and Downstream TI 2	LHC and downstream TI 2	MBB201, TBSE, MBIAV206

Table 29.2: Beam status requirements for access into TI 2 zones

Zone	TI 2	LHC
SPS TCC6 and Upstream TI 2	OFF	
LHC and Downstream TI 2	OFF	OFF

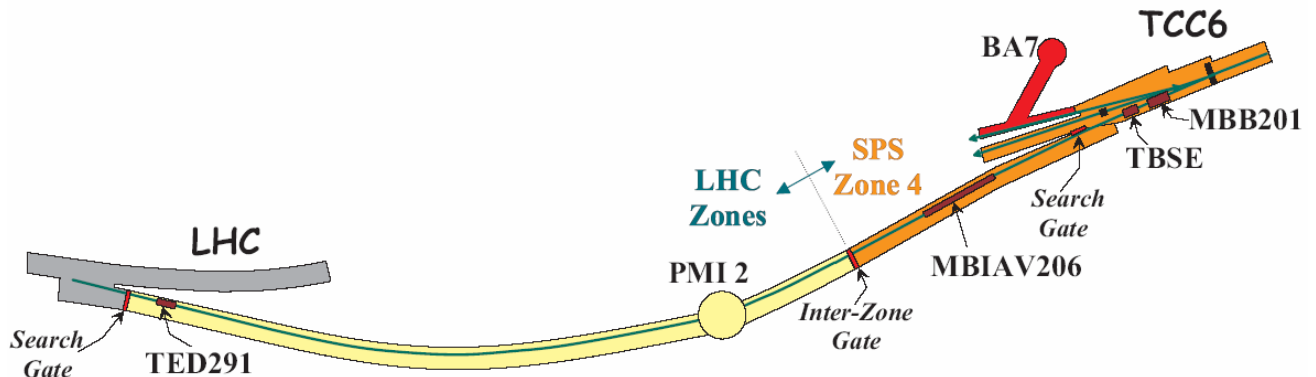


Figure 29.1: Schematic layout of TI 2 showing the essential access elements

29.3.2 Access Points

Access into the upper part of TI 2 and TCC6 is usually done through access points located in BA6 or BA7. These access points are part of the SPS access system.

Access into the lower part of TI 2 should normally be done through Site 2 of the LHC and therefore via LHC access points.

There is no personnel access possible via the PMI2 shaft which is reserved for equipment.

29.4 TI 8 ACCESS AND SAFETY

Fig. 29.2 gives the layout of TI 8 and the CNGS lines and indicates the main safety elements and interlock chains associated with the transfer lines.

29.4.1 Important Safety Elements

The interlocked elements for access to the various zones in TI 8 are summarised in Tab. 29.3. The table also includes the elements in the transfer line which are required for access in the downstream area which is the LHC tunnel. The corresponding beam status values are given in Tab. 29.4. A description of the interlock elements is given in Tab. 29.5.

MACHINE INTERLOCK SAFETY CHAINS

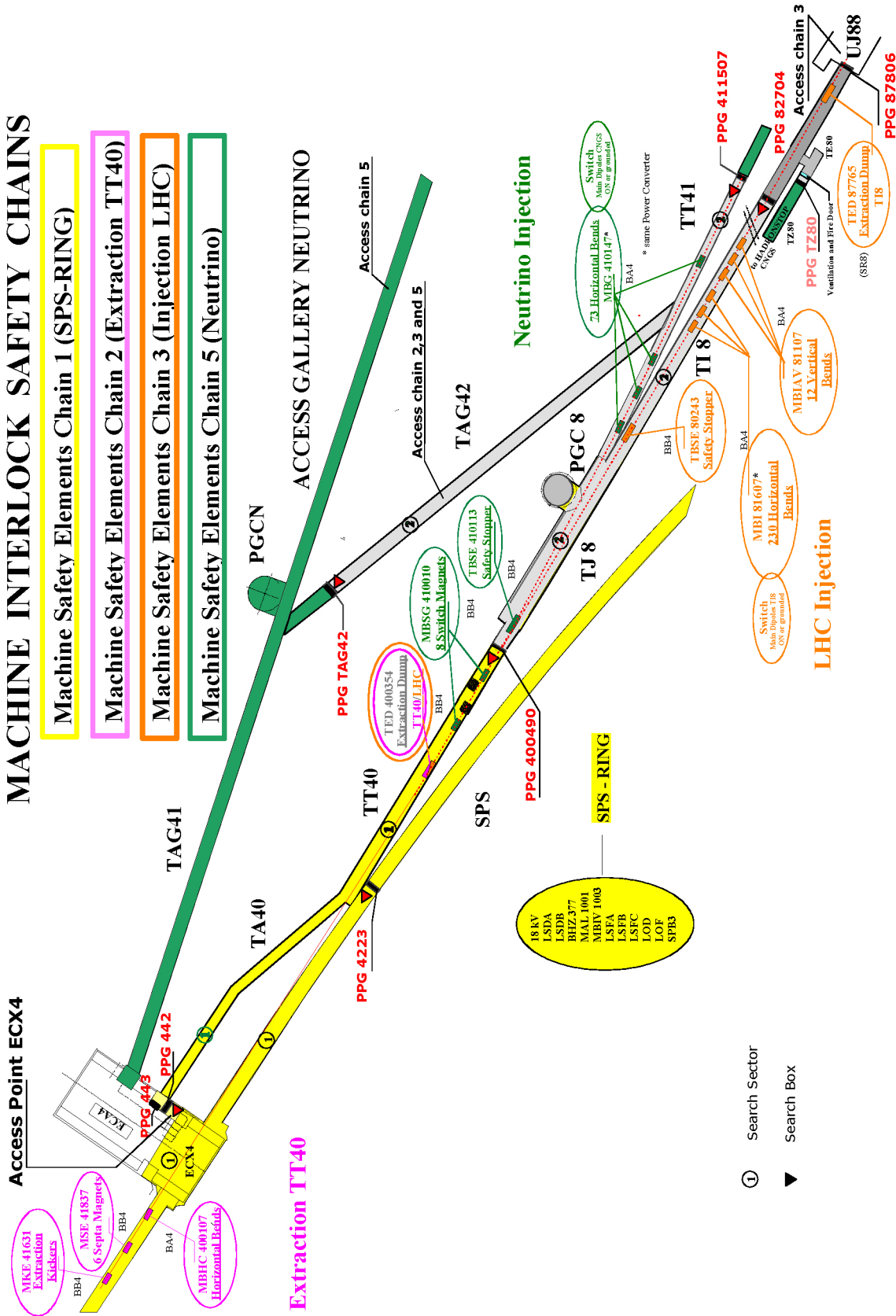


Figure 29.2: Schematic layout of TI 8 and the zones associated with the CNGS beams showing the essential access and safety elements.

The use of TT41 and TI 8 for beam are mutually exclusive and the horizontal bends in the two lines are powered from a single power converter which is switched between them. When one line is operating, the magnets in the other line are earthed.

Table 29.3: Summary of safety elements for the access zones in TI 8 and CNGS transfer line and LHC

Description	Safety Elements (EIS)
SPS and TT40	SPS OFF (chain 1)
TJ8, upstream TI 8 and upstream TN 4	MKE/MSE, MBHC4001, TED4003
Downstream TI 8	TED4003, MBIAV, TBSEL, MBI, TED8776, LHC OFF
AGN, CNGS Target cave and Downstream TN 4	MBS400, TBSEN, MBNE
End stop cavern	TED4003, MBS400, MBNE, MBIAV815, MBI, LHC OFF
LHC tunnel	MBIAV815, MBI, TBSEL, TED877

Table 29.4: Beam status requirements for access into TI 8 zones

Description	SPS	TT40	TJ8	TI 8	TN4	LHC
SPS and TT40	OFF	OFF	OFF	OFF	OFF	
TJ8, upstream TI 8 and upstream TN 4		OFF	OFF	OFF	OFF	
Downstream TI 8				OFF		OFF
AGN, CNGS Target cave and Downstream TN 4					OFF	
End stop cavern			OFF	OFF	OFF	OFF

Table 29.5: Safety elements for TI 8

MKE/MSE	East extraction kickers and magnetic septa.
BHC4001	3 Dipoles situated within the SPS tunnel for the extracted beam to TT40.
TED4003	Full-beam stopper situated within TT40 and upstream of the switch magnets.
MBS400	Neutrino switch magnet chain.
TBSEL	Safety stopper at the beginning of TI 8.
TBSEN	Safety stopper at the beginning of TN4.
MBIAV815	Chain of vertical bends towards the beginning of TI 8.
MBI	Main chain of horizontal bends in TI 8.
MBNE	Main chain of horizontal bends in TN4.
TED877	Full-beam stopper situated at the downstream end of TI 8.

29.4.2 Access Points

Access into the upstream areas (SPS, TT40, TJ8, upstream TI 8 etc.) is normally done through an access point located in ECA4 and part of the SPS access system.

Access into the upstream part of the CNGS installation (covering Access Gallery Neutrino, AGN, and TN4) is done through a separate access point located in ECA4.

Access into the downstream part of TI 8 and the downstream part of the CNGS installation is normally done through Site 8 of the LHC and therefore via LHC access points. The end stop cavern is classified as a confined space and will require a special access procedure.

There is no personnel access possible via the PGC8 shaft which is reserved for equipment. The PGCN shaft has been condemned and will not be used either for personnel or for equipment access.

CHAPTER 30

INTEGRATION AND INSTALLATION

30.1 INTEGRATION ISSUES

30.1.1 Introduction

In order to minimise civil engineering costs, the cross-section of the TI 2 and TI 8 transfer line tunnels has been kept to a minimum. Because of the very limited space available for both equipment and transport, a detailed integration study has been made for the transfer lines. This included the beamline equipment as well as the associated power and control cabling, tubing for water cooling, the transport power rail and general services such as leaky feeder cables, lights and safety elements. Furthermore, a new special purpose transport system had to be developed for installation of the accelerator components in order to meet the very stringent limitations on the space available in the transfer line tunnels. The integration of TI 2 was particularly complicated because the tunnel downstream from PMI 2 will also be used for the transport of cryomagnets to the LHC main ring. Initial installation of the LHC machine will be done without any beamline components being installed in this region. However, the integration of the final installation has taken into account the fact that the passage of cryomagnet transport convoys is still possible once the complete transfer line has been installed.

30.1.2 Integration of TI 8

All the integration and installation issues of TI 8 have been studied in detail. Apart from some optimisation of the cable tray positions around the MBIAV magnets, no major problems were found to incorporate all the required services. Around these MBIAV magnets, which are considerably larger than all the other beamline components, extra space for the magnet and the installation equipment had to be created. A typical TI 8 cross section is given in Fig. 30.1 and more detailed cross sections can be found on drawing LHCLSI_0006.

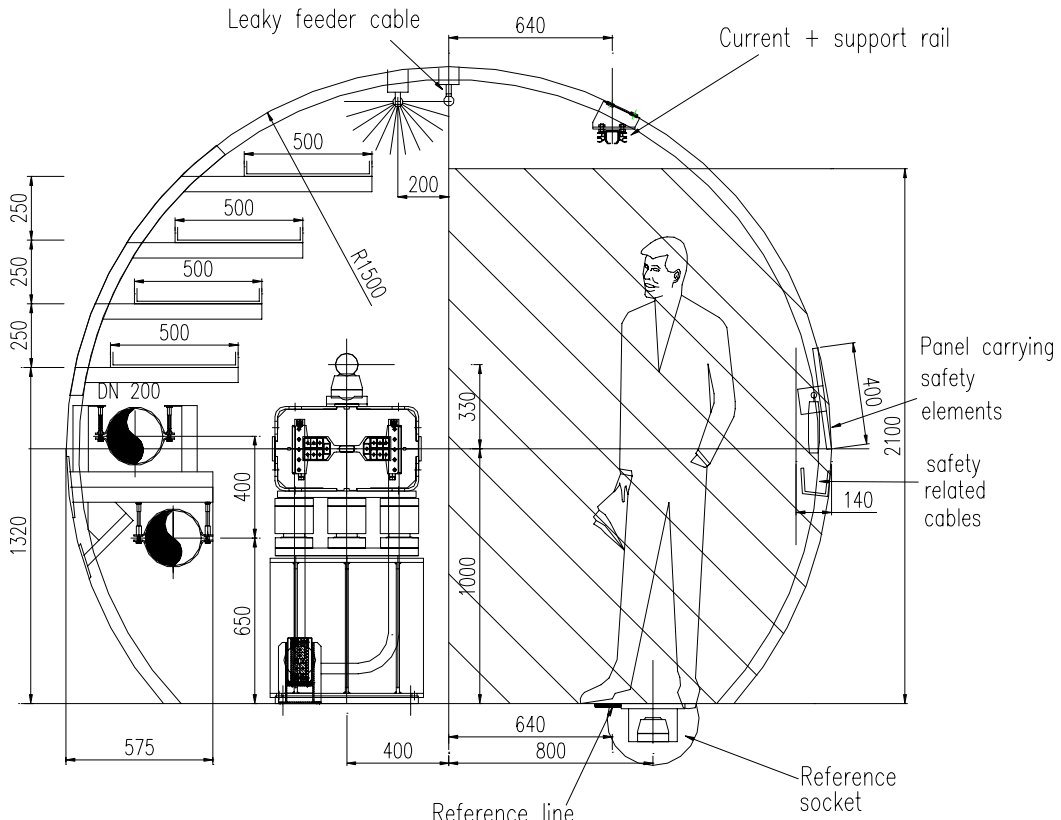


Figure 30.1: A typical TI 8 cross section, the hatched surface indicating the reserved space for transport.

The TED beam stoppers, which are movable for operational reasons, are other large objects in the transfer line tunnels. The stroke of the movement has been increased such that the complete object can be moved further towards the tunnel wall during installation in order to avoid interference with the transport equipment.

As a result of the complexity of the interference between the transfer line and the LHC tunnel, the complete integration studies of the downstream part of the tunnel, between TED87765 and MKIMA5R8 were done by using 3-D techniques. The study included the UJ88, RH87 and RA87 parts of the LHC tunnel and all equipment and services were successfully integrated. The only outstanding integration issue concerns the TCDI collimators, where the mechanical design still has to be finalised. Nevertheless, preliminary studies have shown that sufficient space is available for these objects, although the design of the TCDI for the protection of the MSI will need to take into account the close proximity of the beam pipe of the second ring of the LHC.

30.1.3 Integration of TI 2

The integration and installation issues of the TI 2 transfer line upstream of PMI 2 are comparable to those of TI 8. On the other hand the part downstream from PMI 2 was more complicated, since this section of the tunnel will be used for the transport of cryomagnets to the LHC main ring. Although the initial installation campaign will be done before any injection line magnets are installed, the integration studies needed to take into account the required space in case a cryodipole needs to be replaced once all equipment is installed. For the standard cross section, a solution has been found and a TI 2 cross section downstream of PMI 2 is given in Fig. 30.2, showing the most critical situation around a MBIAV magnet. More detailed cross sections can be found on drawing LHLSI_0007.

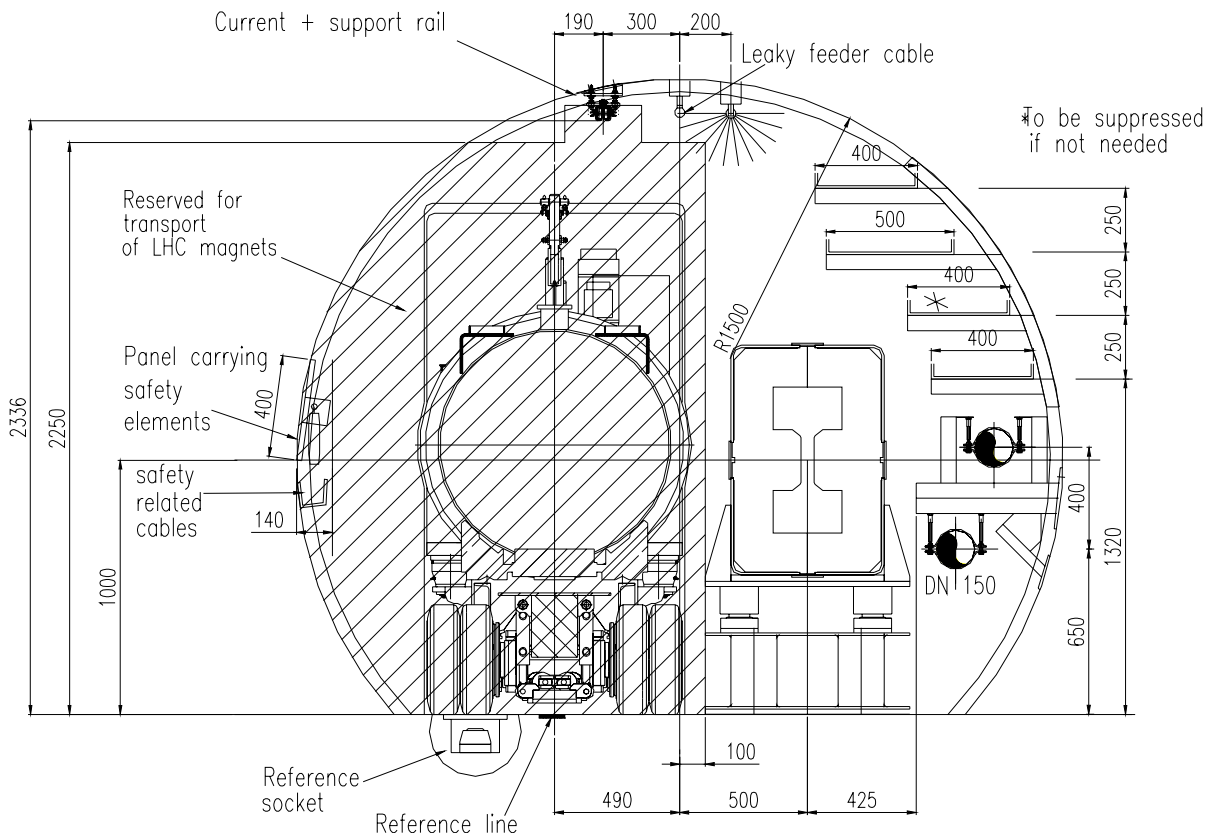


Figure 30.2: A typical TI 2 cross-section between PMI 2 and UJ22, in this case around an MBIAV.

As for TI 8, the complete integration studies of the downstream part of the tunnel, between TED29133 and MKID5L2B1 were done by using 3-D techniques. The study included the UJ22, RH23 and RA23 parts of the LHC tunnel with the area where the TI 2 tunnel joins UJ22 being particularly complicated since the

cryomagnet transport follows the axis of the transfer line beam pipe which moves very close to the TI 2 tunnel wall at the exit. The integration studies showed that insufficient space was available for all services and in particular the cable trays in this region. For this reason the power cabling now enters the TI 2 tunnel by means of 2 special purpose Ø250 mm holes which have been drilled between the LHC and TI 2 tunnels about 4 meters upstream of TED29133. The same remarks concerning the integration of the TCDI collimators into TI 2 apply as for TI 8. Furthermore, the optimum position of the 90° horizontal TCDI is 6 m downstream of TED29133, this being the same space limited area where the TI 2 tunnel joins UJ22 as mentioned above, which may strongly influence the design and maximum size of the TCDI vacuum vessel.

30.2 TRANSPORT AND INSTALLATION SYSTEM

30.2.1 Passage of cryomagnets in TI 2

A downstream part of the TI 2 tunnel will be used for the transport of the approximately 1700 cryomagnets that are to be installed in the LHC main ring. This region includes the PMI 2 shaft and the downstream tunnel right to UJ22, where the TI 2 tunnel joins the LHC main ring. In addition, the first 200m of tunnel upstream of PMI 2 will be used for parking vehicles waiting for cryomagnets to be lowered down the PMI 2 shaft.

Because of the limited TI 2 cross section, the beamline components in the downstream part of TI 2 will not be installed until the cryomagnet installation transport activities have been completed. A typical TI 2 cross section downstream of PMI 2 before installation of accelerator components is given in Fig. 30.3. Also the distance between the beam line and the centre of the tunnel downstream of PMI 2 has been increased to 500 mm, as compared to 400 mm in the rest of TI 2 and TI 8 (see Fig. 30.1). This action was taken in order to allow more room for the cryomagnet vehicle passage once the injection line magnets have been installed. After beamline installation, the passage of cryomagnet transport convoys will still be possible, but with small clearances and the recovery of a vehicle in the event of breakdown will therefore be more difficult and time consuming.

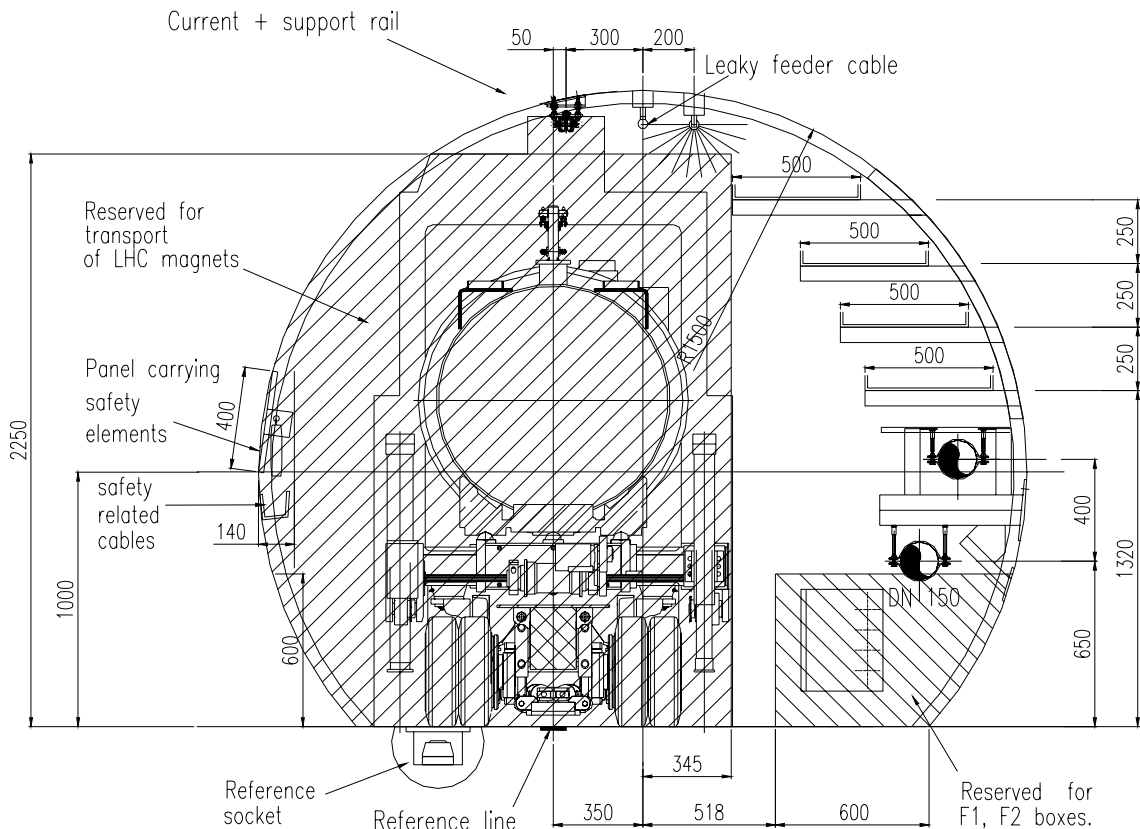


Figure 30.3: A typical TI 2 cross-section, between PMI 2 and UJ22 before installing the beamline

The electrical power needed for the cryomagnet transport vehicle will be provided by a sliding conductor rail mounted along the upper surface of the tunnel. The same type of power rail will be fitted throughout the length of the TI 2 and TI 8 tunnels to also provide power for the special vehicles used for the transport of transfer line components. The power supply trolleys running on the power rails are suitable for both cryomagnet and injection line transport vehicles. An automatic guidance system has been implemented, which is also identical for both types of vehicle, in order to allow reasonably fast passage in the restricted space available. The path to be followed by this system is defined by a highly reflective line on a black background painted on the floor along the transport passage in TI 2 and TI 8.

During installation, space will be necessary at the base of the PMI 2 shaft for the facilities and equipment to be used by the transport operators. After completion of the installation, the base of the PMI 2 shaft will be closed with concrete shielding blocks, forming a wall and roof over the injection line. If a cryomagnet needs to be replaced this shielding will be removed using the crane of the SMI 2 building.

The LHC design report, Vol. II, Chap. 12 gives a more detailed description of the cryomagnet transport vehicles and their operation [1].

30.2.2 Transport System for Transfer Line Components

A new transport system for the installation of the beamline components has been conceived to meet the very stringent space requirements in the LHC transfer line tunnels. A modular system of very compact electrical tractors, so-called buggies, was chosen. These motorised carrier vehicles can turn 90° on the spot in order to displace and position a load laterally and are equipped with a set of air cushions for lifting and lowering of the weight. In this way magnets or other accelerator components can be placed directly onto their supports in the beamline.

The relative compactness of the load carrying buggies was achieved by displacing the cubicles for powering and controlling the motors onto a common auxiliary vehicle, which is linked via cables to the buggies. The vehicles can be powered from the power rails via buffer batteries, which provide autonomy of about 3 km, as well as absorb electrical power produced during downhill transport. Cabins at front and rear of the auxiliary vehicle seat two transport staff and house the touch screens for programming and monitoring the automatic guidance system of the convoy. The cabins are also equipped with a steering wheel and brake pedals for direct control by the driver and manual driving and positioning of the vehicles can also be done via a handheld, wireless control unit.

The Buggy-modules

The original and quite unusual concept of the buggies, specified in detail in [2] and [3], consists of a combination of three wheels turning individually under a load carrying chassis with a longitudinally nodding saddle structure. A three dimensional view of the buggies is given in Fig. 30.4.

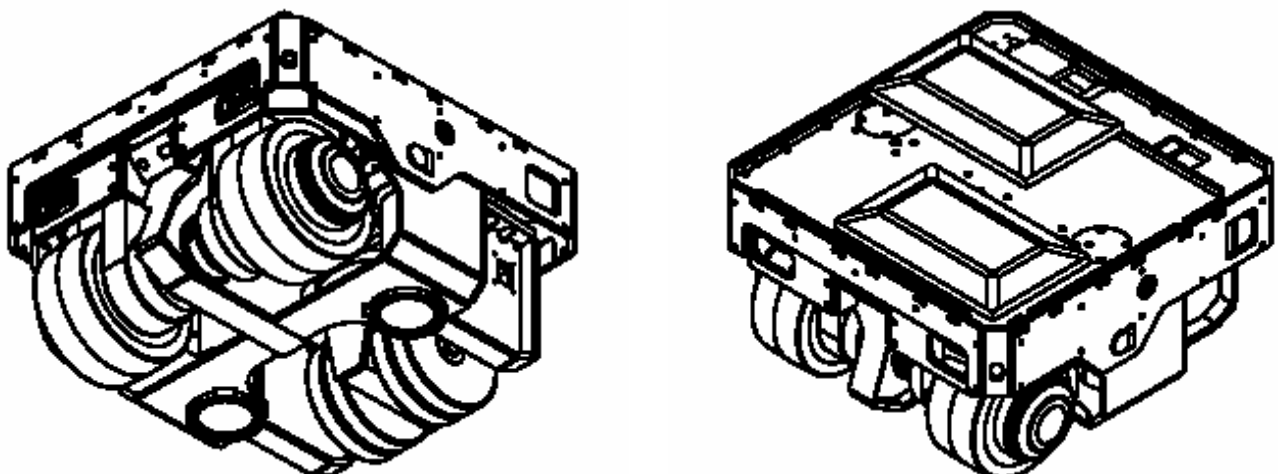


Figure 30.4: Three dimensional, bottom and top view of the buggies.

The positions of the motorised wheels are individually calculated and controlled by a central computer and each module has a load carrying capacity of 9 tonnes. This robust design has the possibility to combine up to 8 of these load carrying modules into one convoy. The mobility of the buggies is based on one castor wheel, built up from four slices, together with two motorised wheels, each equipped with a 3.4 kW in-wheel motor. Each of the wheels can be turned 130° by individually controlled steering motors. The motorised wheels are equipped with disc brakes and a 25.9:1 planetary reduction gear, which allows the vehicle to climb slopes up to 8 %.

A maximum load of 9 tonnes can be placed on the saddle-like structure, distributing the weight equally onto the wheels and allowing the chassis underneath to follow changes in slope. Each Buggy-module is 960 mm long, 940 mm wide and 540 mm high. Two rectangular air cushions placed on top of the saddle structure allow the load to be lifted by about 60 mm.

Optical guidance is done via a camera, equipped with 16 laser diodes, which is mounted onto the front of the chassis and is centred between the steered wheels. A convoy travelling at its maximum speed of about 4 km/h can be guided within a precision of +/-10 mm. Figs. 30.1, 30.2 and 30.3 show the position of the overhead current and support rail which is used for powering the vehicles and the reference line on the floor for the automatic guidance system.

Typical applications, girders and adapters

The Buggy modules will work in sets of two, linked mechanically on one side by a girder in order to have a well defined steering geometry. The girders are situated on the passage side of the tunnel to allow the convoy to enter under the beamline without interfering with the magnet supports, as shown in Fig. 30.5. This is also the optimum arrangement to channel cables and supply hoses between the auxiliary vehicle and the Buggies. In addition, this configuration gives a maximum freedom for tilt between the modules, to compensate for imperfections in the tunnel floor.

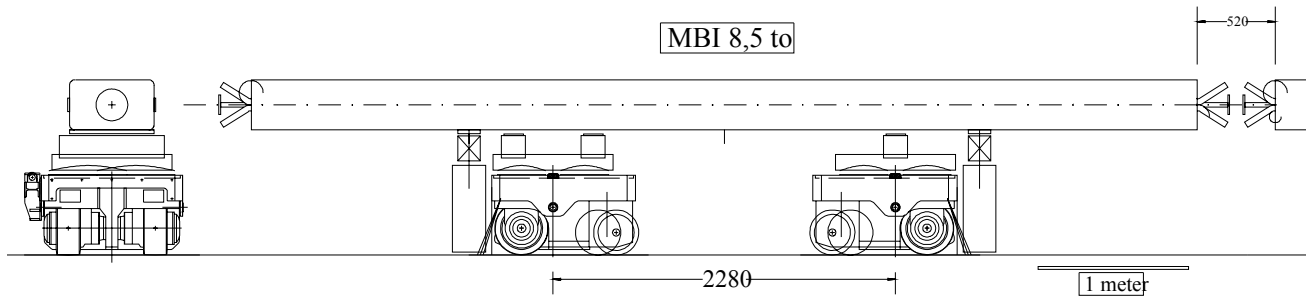


Figure 30.5: Typical application of the transport system in the transfer lines, showing an MBI installation.

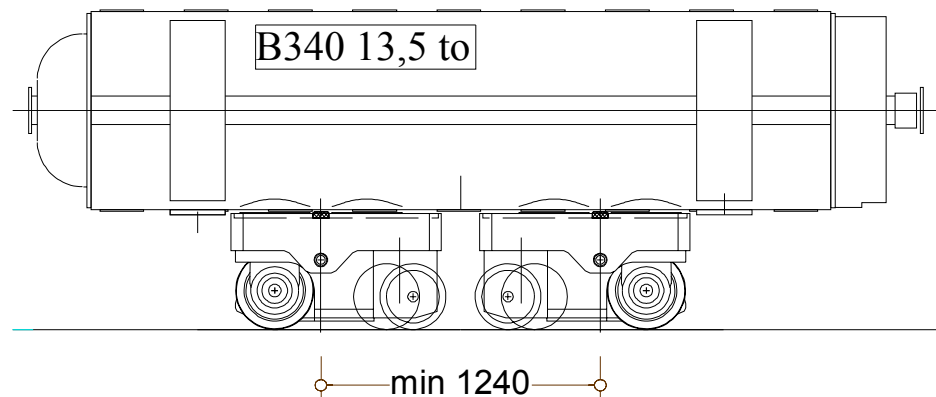
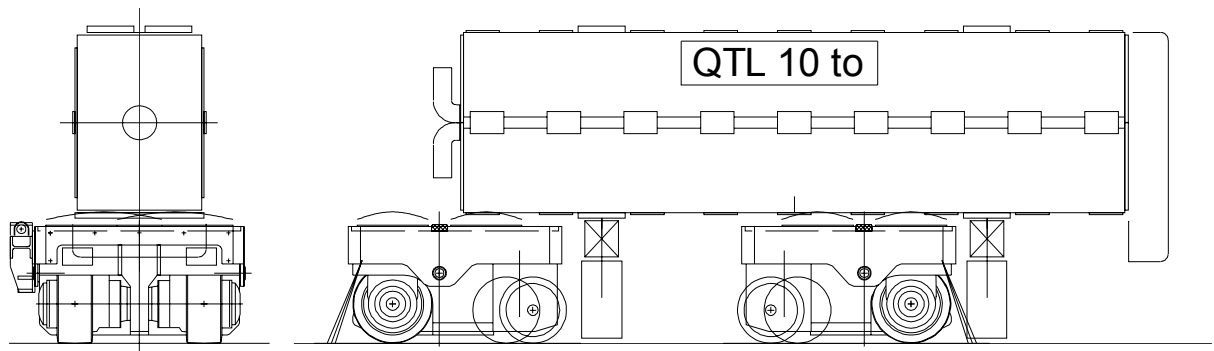


Figure 30.6: MBIAV transport in the transfer lines

The girder structures, which typically add 120 mm to the width of a convoy, are based on reinforced I-profiles and allow the distance between two Buggies to be changed in steps of 40mm within the range of 1240 mm to 3160 mm. Typical applications of the transport system for the transfer line components are shown in Figs. 30.5, 30.6 and 30.7.



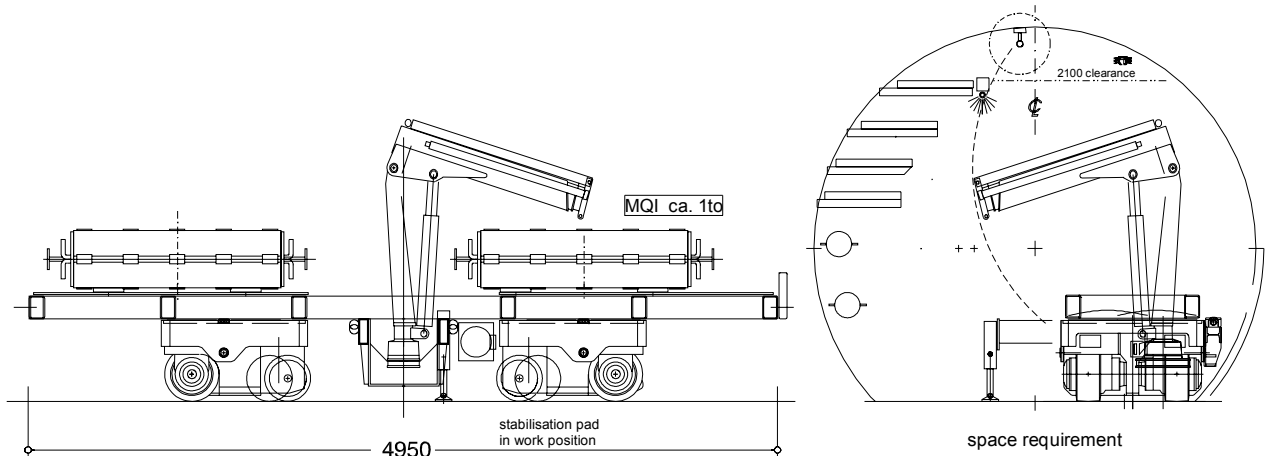


Figure 30.9: Installation of an MQI quadrupole using the special purpose crane girder.

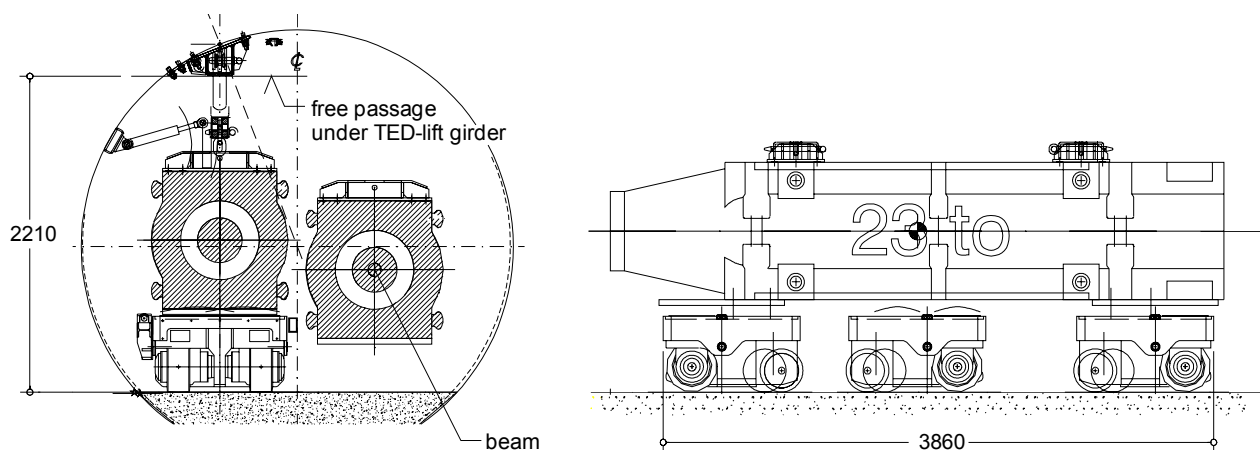


Figure 30.10: TED lifting device and transport configuration.

REFERENCES

- [1] R. Saban, “*Logistics and Installation*”, LHC Design Report, volume II - LHC Infrastructure and General Services, Chap. 12.
- [2] G. Kouba, “*Supply of Induction Guided Bogies for Magnet Installation in TI2 and TI8*”, CERN SL, IT-2949-SL-LHC, 2001-02-22, EDMS 306286.
- [3] G. Kouba, “*Supply of optically guided Buggies*”, Revision of IT-2949-SL-LHC.

CHAPTER 31

COMMISSIONING

31.1 INTRODUCTION

The installation of the TI 8 transfer line was finished at the end of July 2004. It was followed by a hardware commissioning period of 12 weeks and a cold checkout period of two weeks. The commissioning with beam took place during two 48-hour periods during two weekends at the end of October and the beginning of November 2004. The tests have taken place at the time of writing and the details and results of the different test periods together with their conclusions are described below.

The TI 8 commissioning followed the commissioning of the extraction in LSS4/TT40 in 2003. The early commissioning of TI 8 in 2004 has the advantage of disentangling issues related to injection (sector test planned for 2006) from those concerning TI 8. It also served as an important test-bed for beam instrumentation and the control system. All equipment to the downstream beam absorber (TED) was commissioned with beam. The remaining part of TI 8, downstream of the TED, will be commissioned together with the injection elements in LHC point 8 during the sector test. At this time the commissioning of the transfer line collimators will be done, since these were not installed at the time of the 2004 beam tests.

TI 2 can only be completely tested after the transport of LHC magnets through the lower part of the transfer line and installation of the lower part of the line has been completed. As a result, hardware commissioning of the complete line is currently planned for the beginning of 2007 and beam commissioning will take place just before the commissioning of the injection in LHC point 2. However, hardware commissioning of the upstream part of TI 2 in the middle of 2005 is possible.

31.2 HARDWARE COMMISSIONING OF TI 8

The aim of the hardware commissioning period was to check all equipment in the transfer line without beam. It took place between 26 July and 11 October 2004. The main tasks performed during this period were the following:

- The running of all power converters up to their maximum specified currents. If necessary, adjustments were made to stabilise their currents.
- Generation of conditions for air flow and other checks of the ventilation system.
- Verification of the magnet temperature interlock system.
- Verification of the magnet polarities – corrections were made where necessary.
- Vacuum tests: verification of remote information from the ion pumps, gauges; remote opening and closing of the valves (one magnet was replaced where the vacuum chamber had a leak).
- Calibration of the water cooling system of the magnets – adjustment of the valves controlling the water flow.
- Tests of the control system (on the SPS fixed target super cycle).
- Test of the Beam Interlock Controller.
- Test of the beam diagnostic devices (beam position monitors, beam loss monitors, screens and BCT).

In the same period, the alignment of the magnets was verified and some adjustments in the horizontal plane were made to a few magnets that were found to have significant alignment errors. Some of the water hoses for the magnets only became available for installation during the hardware commissioning period and had to be installed then. All tests were concluded with positive results in the time allocated.

31.3 COLD CHECKOUT OF TI 8

After the hardware commissioning period, two weeks were used for cold checkout (12 to 25 October 2004). During the cold checkout period the complete system was operated from the Prévessin Control Room (PCR) by the Operations Group together in collaboration with the people responsible for the beam commissioning. The following tests were performed:

- Cycling of all magnets together on the fixed target cycle. The corrector magnets were run at their maximum current without cycling. All control was made using the controls applications from the control room.
- Temperatures of the different types of magnets (coil and yoke) and tunnel air temperatures were monitored.
 - The tunnel air temperature interlock which inhibits extraction and then switches off the main power converters was set at 35°C. The interlock temperature was never reached. Fig. 31.1 shows the temperatures measured during the cold checkout period during operation with a 16.8 s cycle.
 - The coil temperature was measured on the main dipole MBI 81620. It indicates that when all TI 8 magnets were powered at their nominal currents, the air temperatures in the vicinity of that magnet reached an equilibrium temperature about 3°C higher than when the magnets were not powered.
 - The temperature measured in the concrete of the tunnel wall continued to rise very slowly by a small amount during the test period. From the measurements it can be concluded that it will be possible to run the LHC transfer lines continuously for many days before tunnel temperatures limit operation.
- Tests of the Beam Interlock Control system and its interface with the other operational systems.
- Tests of the access control system and their related safety elements (TED and TBSE) in collaboration with the Departmental Safety Officer.
- Checks of the correct functioning of and communication with all beam instrumentation.
- Checks of the logging and retrieval of all signals (magnet currents, beam diagnostics, temperatures).
- Checks of the ‘remote oscilloscope system’ (OASIS) used for diagnosis and setting up of the extraction kicker MKE.
- Checks of the correct function of all control applications software including the fixed displays.
- Checks of the radiation monitoring displays.
- Checks of the vacuum displays.

All tests during the cold checkout period were performed successfully.

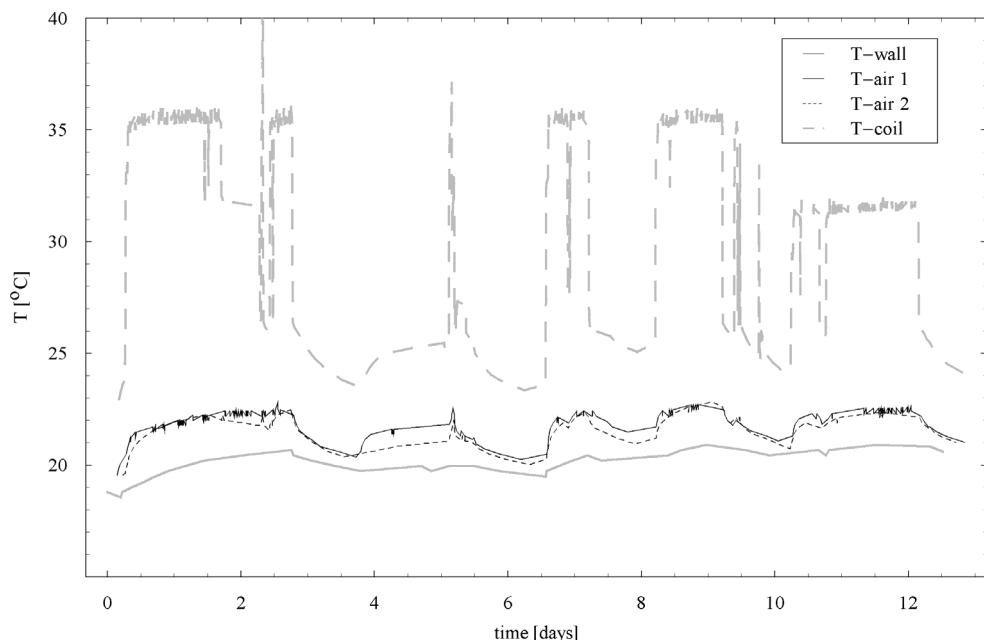


Figure 31.1: Temperatures measured in the TI 8 tunnel during the cold checkout period using a 16.8 s cycle.

31.4 BEAM COMMISSIONING OF TI 8

The commissioning with beam took place over two weekends, 23-25 October and 6-8 November 2004. The SPS extraction was set-up first, with beam being sent to the TT40 beam absorber (TED). The energy of TI 8 was set to 449.2 GeV/c following an energy calibration of the SPS [1,2]. After moving the TT40 TED and the TI 8 beam stopper (TBSE) out, the beam travelled the additional 2.5 km to the absorber block at the end of the TI 8 tunnel without any steering. The picture of the first beam arriving on the luminescent screen just in front of the TED at the end of TI 8 is shown in Fig. 31.2.

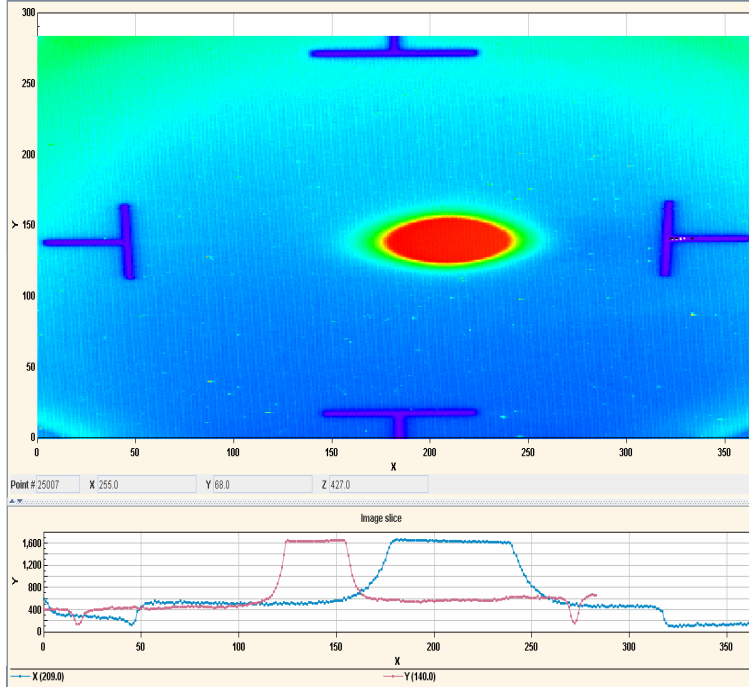


Figure 31.2: Image of the first beam on the downstream TI 8 beam absorber.

Subsequently the beam diagnostics were tested and calibrated with beam. The response of each beam position pick-up was measured by individually powering orbit correctors in both planes. This measurement, together with a detailed measurement of the dispersion, showed a small difference in the optics with respect to the design values. This was later traced to two quadrupoles at the beginning of the transfer line, QTRF4002 and QTLF4004, which had an incorrect maximum current setting in the database and this resulted in a 20% error in their current setting. This was corrected for the subsequent weekend of beam tests. During this second weekend many of the beam tests were repeated with the corrected optics. The overall programme included:

- Optics measurements using different corrector settings and measuring the trajectory response.
- Measurement of the dispersion functions in the transfer line by changing the beam energy of the SPS with the RF frequency.
- Measurement of the energy acceptance of the line. This was also performed by changing the RF frequency in the SPS. The results are shown in Fig. 31.3.
- Measurement of the physical aperture of the line by making trajectory oscillations with different phases and measuring the transmission.
- The Twiss parameters were measured by combining the OTR screen data.
- Parasitic beam stability measurements throughout the beam tests.
 - The average value of the beam stability for the different beam position monitors was found to be around 100 μm RMS [4]. This corresponds to about 1/8 of the 1σ nominal beam size.
- Parasitic beam coupling measurement throughout the beam tests. The coupling between the two planes was found to be around 2 % [4].
- No significant effect of the magnet's temperature on the trajectory was measured
- Multi-bunch commissioning of the beam instrumentation.

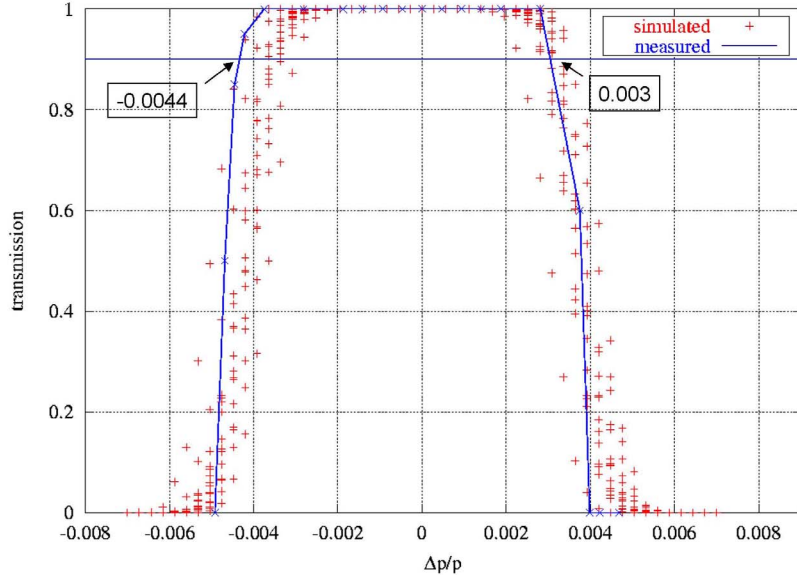


Figure 31.3: Measured TI 8 energy acceptance compared with tracking results for which realistic operational conditions were considered [3].

The beam period in the second weekend was also used to test the transfer line collimator alignment procedure with beam. The jaws of the collimator installed just in front of the TT40 TED were moved and the effect on the beam transmission was measured by the beam current transformer (BCT) installed in the lower part of the transfer line.

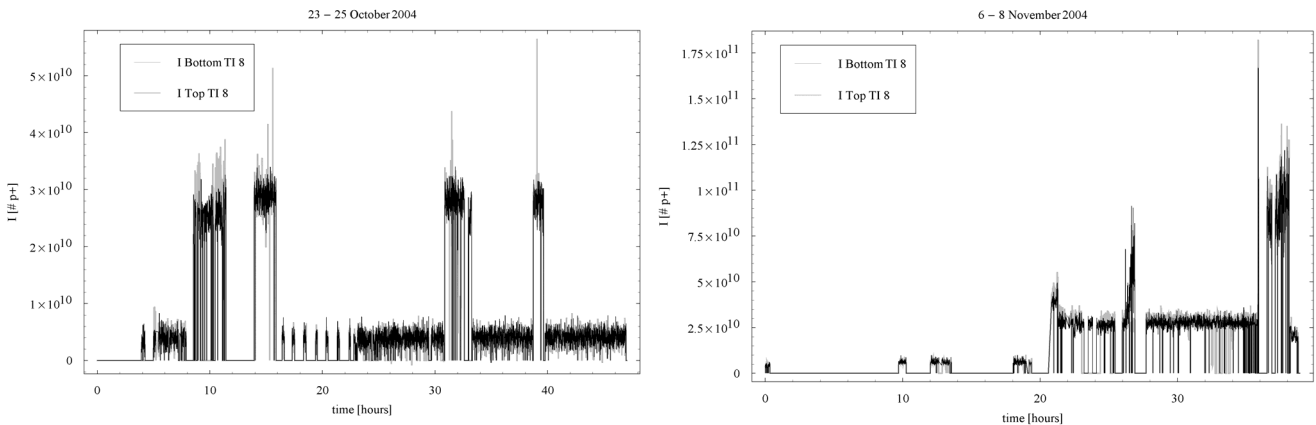


Figure 31.4: Beam intensities measured in the upper part and the lower part of TI 8 during the two test periods.

For most of the first test period single pilot bunches with an intensity around 5×10^9 protons were used. To improve the resolution of the beam position monitors and the screens, higher single bunch intensities of around 3×10^{10} protons were used for some periods. During a limited period towards the end of the second test, the beam position monitor behaviour was tested with multiple bunches. The beam intensities over the two test periods are plotted in Fig. 31.4.

During the first test period the total beam intensity dumped on the beam absorber at the end of the line was around 3.5×10^{13} protons. During the second test period this was around 5.1×10^{13} protons. The predicted intensity was in the range of $5-15 \times 10^{13}$ protons for both periods. During the tests the experimental pit at LHC Point 8 (including several 100's of metres to either side) was closed for all access. Additional shielding was installed just downstream of the TED at the end of TI 8 and outside of the TI 8 tunnel (see Fig. 31.5). The radiation levels in the LHC tunnel were measured two hours after the beam was stopped. The levels were found to be highest at the wall in R88, immediately adjacent to the beam absorber block (see Fig. 31.5).

After the first test the measured value at this position was $1.5 \mu\text{Sv/h}$; after the second test this was higher, $7 \mu\text{Sv/h}$ and local shielding was put up for several days in order to allow general access in this area. This higher measured dose was caused by the higher intensity multi-bunch operation towards the end of the test period and was in good agreement with calculations. General access, without the need to carry a film badge or personal dosimeter, was given for the LHC pit and the LHC tunnel only a few hours after both beam tests finished.

It was found very useful to have two periods for beam tests, separated by at least two weeks. This gave sufficient time to analyse the data of the first beam tests and to perform repairs for minor faults found during the first test period.

The general performance of the transfer line was according to the design criteria, with high beam stability and optics parameters very close to the design values. The beam diagnostics were tested and proved to be sufficiently performant to identify small errors in the settings.

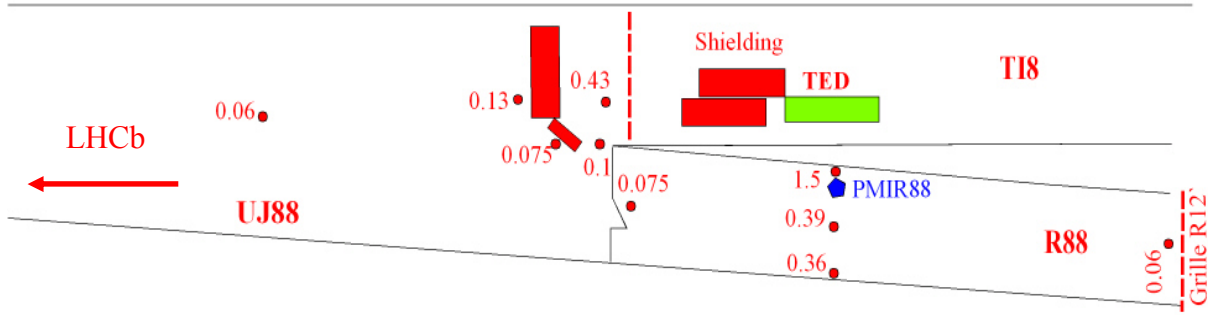


Figure 31.5: Measured activity at the end of the TI 8 transfer line, two hours after the beams were stopped [5]. Values are given in $\mu\text{Sv/h}$.

REFERENCES

- [1] J.Wenninger, “*SPS Momentum Calibration and Stability in 2003*”, AB-Note-2003-091 OP.
- [2] G.Arduini et al., “*Energy Calibration of the SPS at 450 GeV/c with Proton and Lead Ion Beams*”, AB-Note-2003-014 OP.
- [3] V.Kain, to be published.
- [4] J.Wenninger, to be published.
- [5] N.Conan and H.Vincke, private communication.

CHAPTER 32

INTRODUCTION

The LHC physics programme is mainly based on proton-proton collisions. In addition, shorter running periods, typically one month per year, with heavy-ion (lead) collisions are included in the programme [1, 2]. While lighter ions are considered as well, the baseline scheme deals with Pb ions, because they are the most difficult to produce and most rewarding in terms of physics results. Therefore this report almost exclusively deals with Pb ions.

At present, a fixed-target ion experimental physics programme is still in full swing at the SPS. Naively, one would assume that this fixed-target acceleration scheme (Linac3 - PS Booster - PS - SPS, [3]) may be well adapted to fill the LHC. It corresponds to the proton injector chain, but of course with Ion Linac3 replacing Proton Linac2. The problem is that, contrary to the protons, the required LHC Pb ion phase-space density cannot be achieved via the PS Booster, the fixed-target Pb beam falling short by a factor of ~ 30 in terms of beam brightness and ~ 1000 in terms of luminosity in the LHC. This factor 30 can be gained in essentially two ways: first, by an ion source with an instantaneous current 30 times higher than the one generated by the present ECR (Electron Cyclotron Resonance) source; second, by phase space cooling.

An initiative to develop an extremely high-intensity, short-pulse ion source based on a high power CO₂ laser, the “Laser Ion Source” study at CERN [4], has been discontinued recently, because the few results obtained so far, though interesting, are still far from satisfying the stringent beam requirements called for by the LHC. Another type of source, pioneered by BNL for RHIC, the Electron Beam Ion Source (EBIS), has enjoyed spectacular progress in recent years, but would still need a lengthy upgrading programme to meet LHC specifications, too risky for the start-up of LHC with Pb ions, scheduled for April 2008.

CERN has a long-standing experience in phase-space cooling. In particular, electron cooling, ideally suited for fast cooling of highly-charged ions at low (\sim MeV/n range) energies, was pioneered in LEAR (Low Energy Antiproton Ring, mothballed in 1997) and is a key ingredient of the so successful AD (Antiproton Decelerator). These are the reasons why CERN’s baseline scheme to produce Pb ions for the LHC is based on LEIR (Low Energy Ion Ring), the LEAR machine after upgrading. In this scheme, initially proposed in 1993 [5], several long (~ 200 μ s), low-intensity pulses from Linac3 (albeit improved by a factor two after source upgrading) are transformed into short (~ 200 ns), high-intensity, small-emittance bunches by accumulation and cooling in LEIR, before being accelerated and sent to the PS. In this latter machine, two such bunches are transformed, on flat porches during acceleration, to four bunchlet pairs by extremely elaborate RF gymnastics. The distance between pairs is 100 ns, the LHC bunch spacing. Eight to thirteen such PS pulses are accumulated during an SPS injection plateau and then accelerated in the SPS; before extraction to the LHC, the bunchlet pairs are recombined to nominal LHC bunches.

A series of tests with Pb ions on LEAR in 1997 has successfully demonstrated the feasibility of the accumulation/cooling scheme, with a missing factor of ~ 3 compared to LEIR requirements [6]. The upgrading programme from LEAR to LEIR ($\sim 3/4$ of the project resources), with adaptation work also in Linac3, the PS and SPS machines (together $\sim 1/4$), is aimed at improvements which make up for the missing factor.

In the following chapters, the proposed upgrading programme [7, 8], called “Ions for LHC” (I-LHC) project, is presented, with particular emphasis on matching the natural performance limitations of the injector chain to the LHC baseline Pb ion beam request. Accompanying the beam along the injector chain, beam dynamics aspects are discussed and the ensuing hardware upgrading programme is presented. An important aspect to keep in mind is the short delay imposed by a rather late decision on the ion injector chain. Therefore, the scheme presented here has not undergone a full optimisation process. However, there is confidence that the parameters chosen are not far from the best possible ones.

Even after upgrading, the ion injector chain will be subject to basic limitations whose impact on the performance is not always easy to predict. Some of these limitations are rather hard-edged and well defined, others will only be known after commissioning of the accelerators concerned, including the LHC. In order to enable some learning process with reduced risks, an Early Lead Ion Scheme has been devised. While keeping to the nominal bunch population (7×10^7 Pb ions at collision), the number of ion bunches is cut down to 60 (compared to 600 for the nominal baseline scheme) and the luminosity to 5×10^{25} (instead of the baseline luminosity of 10^{27} cm⁻²s⁻¹). Not only do the users accept this low initial luminosity which still

enables early discoveries, but also the task for the injector chain is substantially easier, with malfunctions having less dramatic consequences in the LHC rings.

REFERENCES

- [1] The LHC Study Group, *Large Hadron Collider, The Accelerator Project*, CERN/AC/93-03 (LHC), 1993.
- [2] The LHC Study Group, P. Lefèvre and T. Petterson (Editors), *The Large Hadron Collider, Conceptual Study*, CERN/AC/95-05 (LHC), 1995.
- [3] D. Warner (Editor), *CERN Heavy Ion Facility Design Report*, CERN 93-01, April 1993
- [4] C.E. Hill, D. Küchler, H. Kugler, R. Scrivens, *Options for Upgrading of the CERN Pre-Injector Ion Source*, Proc. XXIst Lin. Acc. Conf., Kyongju, Korea, August 2002, CERN/PS/2002-67 (PP).
- [5] P. Lefèvre, D. Möhl, *A Low Energy Accumulation Ring of Ions for LHC (A Feasibility Study)*, CERN/PS 93-62(DI), LHC Note 259, 1993.
- [6] J. Bosser, C. Carli, M. Chanel, C. Hill, A. Lombardi, R. Maccaferri, S. Maury, D. Möhl, G. Molinari, S. Rossi, E. Tanke, G. Tranquille, M. Vretenar, *Experimental Investigation of Electron Cooling and Stacking of Lead Ions in a Low Energy Accumulation Ring*, CERN/PS 99-033(DI) and Particle Accelerators, Vol. 63, p. 171-210, 1999.
- [7] M. Chanel, *LEIR, the Low Energy Ion Ring at CERN*, EPAC2002, Paris, June 2002.
- [8] K. Schindl, *LHC Request and Overview*, Session “Preparation with Pb Ions”, Proc. Workshop on LHC Performance Chamonix XII (edited by J. Poole), March, 2003, p.66.

CHAPTER 33

ION BEAM REQUEST AND OVERVIEW

33.1 LHC BASELINE BEAM REQUEST

The main LHC client requesting high-luminosity running with Pb ions is ALICE, but more recently CMS and ATLAS have also expressed their interest. Pb-Pb collisions are the priority for the first 2-3 years of ion operation. Next on their programme are proton-lead collisions for 1-2 years, followed by lighter ion colliding beams about five years after ion start-up [1]. Clearly there is time left to deal with the lighter ions at a later stage, once one has learned about the issues of Pb ions in the LHC.

The principal LHC Lead ion beam parameters required to attain the design luminosity per experiment, $L = 10^{27} \text{ cm}^{-2} \text{ s}^{-1}$, are given in Tab. 33.1.

Table 33.1: Lead nominal (baseline) parameters in LHC at collision

Parameter	Unit	Value	Comments
energy/nucleon	TeV/n	2.76	
initial luminosity L_0	$\text{cm}^{-2} \text{ s}^{-1}$	10^{27}	
number of bunches/bunch harmonic		592/891	
bunch spacing	ns	100	
β^*	m	0.5	about same as p
crossing angle	μrad	80	
number of Pb ions/bunch		7×10^7	
transverse emittance (norm., rms)	μm	1.5	same physical emittance as p for same B_p
rms beam radius at IP	μm	16	same as p
longitudinal emittance/charge	eVs/charge	2.5	
rms bunch length	cm	7.5	
L half-life (2/3 experiments)	h	4.6/3.1	

The LHC baseline parameters for lead ions strike a balance between high luminosity and several fundamental limitations [2, 3].

33.1.1 Limitations in LHC

Electromagnetic interactions limit luminosity

Colliding ions changing their charge/mass ratio: during a store, peripheral collisions between $^{208}\text{Pb}^{82+}$ ions may lead to the loss of a neutron ($\rightarrow ^{207}\text{Pb}^{82+}$ by electromagnetic dissociation) or to capturing an electron after pair production ($\rightarrow ^{208}\text{Pb}^{81+}$, cross section ~ 280 barns). Both processes give rise to a change in momentum/charge. While the ions losing a neutron are intercepted by the collimators, the ones having captured an electron (momentum/charge changed by $> 1\%$) are likely to be lost in a superconducting dipole of the dispersion suppressor. A magnet quench may then occur at a luminosity of as low as $4 \times 10^{26} \text{ cm}^{-2} \text{ s}^{-1}$, potentially limiting the LHC Pb design performance (see Vol. 1, Chap. 21). However, there are some safety factors in hand.

Marginal sensitivity of position monitors

The nominal LHC ion bunch intensity in collisions, 7×10^7 Pb ions/bunch ($\sim 6 \times 10^9$ charges/bunch) is still visible on the beam position monitors (BPM). During the store, this bunch population may decrease below their initial sensitivity of 4×10^9 charges/bunch; a recent upgrade of the electronics has set this limit to $\sim 2 \times 10^9$ charges/bunch [4] and provides somewhat more margin.

Luminosity lifetime

During a store, the luminosity is deteriorated mainly by particle losses due to ion-ion collisions, with a somewhat weaker contribution due to transverse emittance growth caused by Intra-Beam Scattering (IBS).

This lifetime is roughly inversely proportional to the number of high-luminosity experiments and as low as 3 hours with 3 of them.

Transverse emittance same as protons

The ions have to be accommodated into the LHC dynamic aperture, in much the same way as the protons, thus the ion *physical* emittance is designed to match the one for protons at any given magnetic rigidity (for example at LHC injection and collision energies).

Each LHC ring will be filled with almost 600 Pb ion bunches. Contrary to proton-proton collisions, the ion experiments are rather relaxed in terms of bunch-to-bunch intensity variations because the ion event rate is much lower than the bunch repetition frequency; however, limitations in the ion injector chain define a tolerance of about $\pm 20\%$.

33.2 INJECTOR CHAIN: OVERVIEW, LIMITATIONS

The LHC injector chains for protons and Pb ions are identical except for the first two accelerators: proton Linac2 is replaced by heavy ion Linac3 and the PSB by LEIR. For lead ions, the intensity/emittance ratio achievable via the PSB falls short of LHC specifications by a factor ~ 30 , hence the proposal to use phase space cooling to make up for this factor. The ion injector chain is pivoting on LEIR, the (mothballed) LEAR after substantial upgrading, with a new powerful electron cooling system as key ingredient. The device enables accumulation of 4-5 pulses from Linac 3 to obtain an adequate intensity (10^9 Pb ions) and beam cooling in all three phase planes so as to squeeze these ions into very small emittances ($\epsilon_{rms}^* \sim 0.7 \mu\text{m}$).

The parameters of the lead ion injector chain are restrained by several basic limitations.

33.2.1 Limitations in the Injector Chain

Linac3 ion intensity

Linac3 is expected to deliver up to $50 \mu\text{A}$ Pb⁵⁴⁺ (after stripping); this requires upgrading of the source [5]. Only with 70-turn injection into LEIR (with high efficiency through stacking in all three phase planes) can the nominal intensity per Linac pulse be attained. An RF cavity in the Linac3-LEIR line ramps the beam energy during the $200 \mu\text{s}$ pulse to enable stacking in the longitudinal phase plane.

Space charge in LEIR, PS, SPS

Space charge at injection field in LEIR, PS, SPS, leads to a spread in betatron tunes (space charge detuning ΔQ) and straddling of resonances, followed by emittance blow-up and eventually particle loss. Assuming a Gaussian distribution in all three phase planes, the vertical space charge tune shift (spread) of the central particle is

$$\Delta Q_y(0,0) = \frac{Z^2}{A} \frac{r_p N_b R}{\sqrt{2\pi} \beta \gamma^2 \epsilon_{y,n} \sigma_l} \left\langle \frac{1}{(1 + (a(s)/b(s)))} \right\rangle \quad (33.1)$$

where Z, A are the ions' charge state and the mass number, respectively; N_b the number of ions per bunch; R the machine circumference/ (2π) ; β and γ relativistic factors; $\epsilon_{y,n}$ is the normalised vertical rms emittance; σ_l the rms bunch length (bunch assumed Gaussian); $a(s)$ and $b(s)$ are horizontal and vertical beam sizes along the circumference.

Tune spread ΔQ

ΔQ is a tune spread rather than a shift because (i) the transverse Gaussian distribution renders the individual particle tune strongly dependent on its respective betatron amplitude; (ii) the synchrotron motion moves the particles periodically towards the head and tail of the bunches (lower density, smaller ΔQ), passing through the high density centre (large ΔQ); note that the “central” (in 6D phase space) particle features the largest value. Space charge is strongly decreasing with increasing beam energy but – somewhat surprisingly – is still critical in the SPS where the bunches are very short ($\sim 1 \text{ ns rms}$). The LEIR minimum ejection energy is dictated by the maximum tolerable ΔQ in PS of ~ 0.20 , corresponding to a magnetic rigidity of about 4.2 Tm for Pb, while the PS has to accelerate the beam to maximum magnetic rigidity (86.7 Tm) to cope with the SPS space charge limit.

RF systems

While the large-band (frequency swing ~ 10) LEIR RF system is a new development, the PS and SPS will use existing RF systems to save resources and avoid adding to their respective impedance budgets. In particular, the hardware installed in the PS for protons to generate 4 ns bunches will be employed for ions as well. The choice of the ion bunch spacing of 100 ns in the LHC has been driven, among other aspects, by this type of consideration, but its generation requires elaborate RF gymnastics in the PS.

Vacuum: dynamic pressure and ion losses

The ions charge state may change due to interaction with the rest gas (LEIR, PS) or by electrons captured when ions interact with the cooling beam (LEIR). These ions are lost instantly and will in turn desorb molecules from the vacuum pipe surface, thus further increasing the pressure. In order to guarantee a beam life-time of ~ 30 s as required for accumulation in LEIR, the dynamic pressure has to be in the 10^{-12} mbar range, necessitating bake-out, beam scrubbing, loss localisation and possibly installation of getters in high-loss zones [6]. The higher LEIR-PS transfer energy helps reducing these losses in the PS as charge exchange cross sections are lower.

33.2.2 Injector chain overview

The LHC injector chain for ions is sketched in Fig. 33.1, including the principal ingredients of the upgrading programme [7, 8, 9] and its key parameters are compiled in Tab. 33.2.

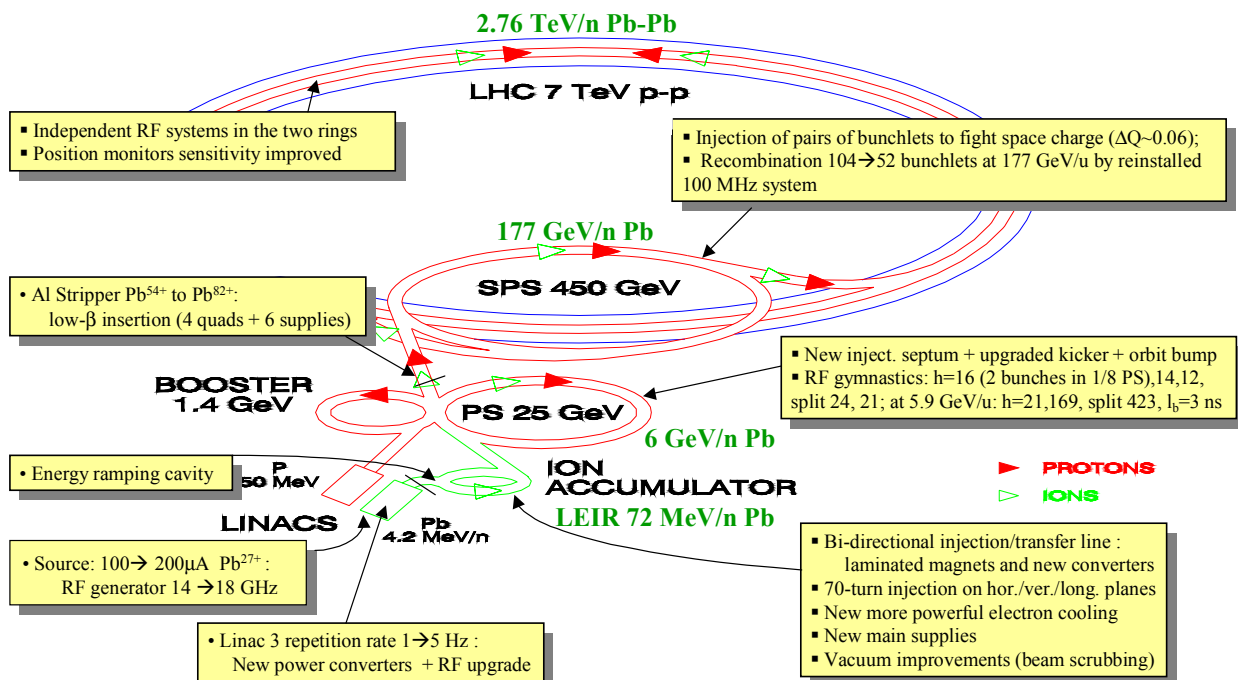


Figure 33.1: Overview of the LHC ion injector chain

Stripping

There are two stripping stages: one is a thin C foil at the Linac3 output, generating several adjacent charge states, amongst them Pb^{54+} produced with $\sim 16\%$ efficiency; the other one, an Al foil in the PS-SPS line, generates a fully-stripped Pb^{82+} beam. For the latter, the tight transverse emittance budget requires the implementation of a “low- β -insertion” at the foil to minimise emittance blow-up due to Coulomb scattering.

Table 33.2: LHC ion injector chain: key parameters for Pb ions at extraction energies

	Linac 3	LEIR	PS	SPS
Output energy	4.2 MeV/n	72.2 MeV/n	5.9 GeV/n	176.4 GeV/n
^{208}Pb charge state	27+/54+ ¹	54+	54+/82+ ¹	82+
output $B\beta$ [Tm]	2.28/1.14 ¹	4.80	86.7/57.1 ¹	1500
number of batches to fill following machine	4-5	1	13,12,8	12
bunches per ring		2 (1/8 PS)	4 or 4x2 ²	52,48,32
ions per pulse ³	1.15×10^9	9×10^8	4.8×10^8	$<4.7 \times 10^9$
ions per LHC bunch	1.15×10^9	2.25×10^8	1.2×10^8	9×10^7
bunch spacing [ns]		350	100 or 95/5 ²	100
$\epsilon_{\text{rms}}^* (= (\beta\gamma)_{\text{rel}} \sigma^2 / \beta_{\text{twiss}}) [\mu\text{m}]$	0.25	0.7	1.0	1.2
ϵ_{long} [eVs/n]		0.05	0.05/0.025 ²	0.24 ⁴
ϵ_{long} per LHC bunch [eVs/n]		0.025	0.05	0.24
4σ bunch length [ns]		200	3.9	1.65
2σ rel. momentum spread ² ($\Delta p/p$) _{2σ}	0.4×10^{-3}	1.2×10^{-3}	6.5×10^{-4}	5.8×10^{-4}
repetition time [s]	0.2-0.4	3.6	3.6	54
space-charge ΔQ at injection		0.07 ⁵	0.17	0.082/0.041 ²

¹stripper stages between Linac 3 and LEIR and between PS and SPS; parameters before/after stripping

²with splitting into four pairs of bunchlets at PS extraction to ease space charge in the SPS

³Linac3 pulse: 50 μA x 200 μs of Pb^{54+} after stripping at 4.2 MeV/n

⁴In SPS and LHC convention for Pb^{82+} : 1 eVs/n ≈ 2.5 eVs/charge

⁵After RF capture in LEIR

Bunchlets

Optionally, the 4 PS bunches are split into 4 pairs of bunchlets, each featuring $\frac{1}{2}$ of the nominal population, reducing the space-charge tune spread in the SPS to ~ 0.05 . The four bunchlet pairs are recombined to four bunches before extraction from the SPS. This splitting is not part of the baseline programme, because the space-charge limit of the SPS is not very well established and a subject of further studies [10].

Nominal Ion Bunch Pattern in the LHC

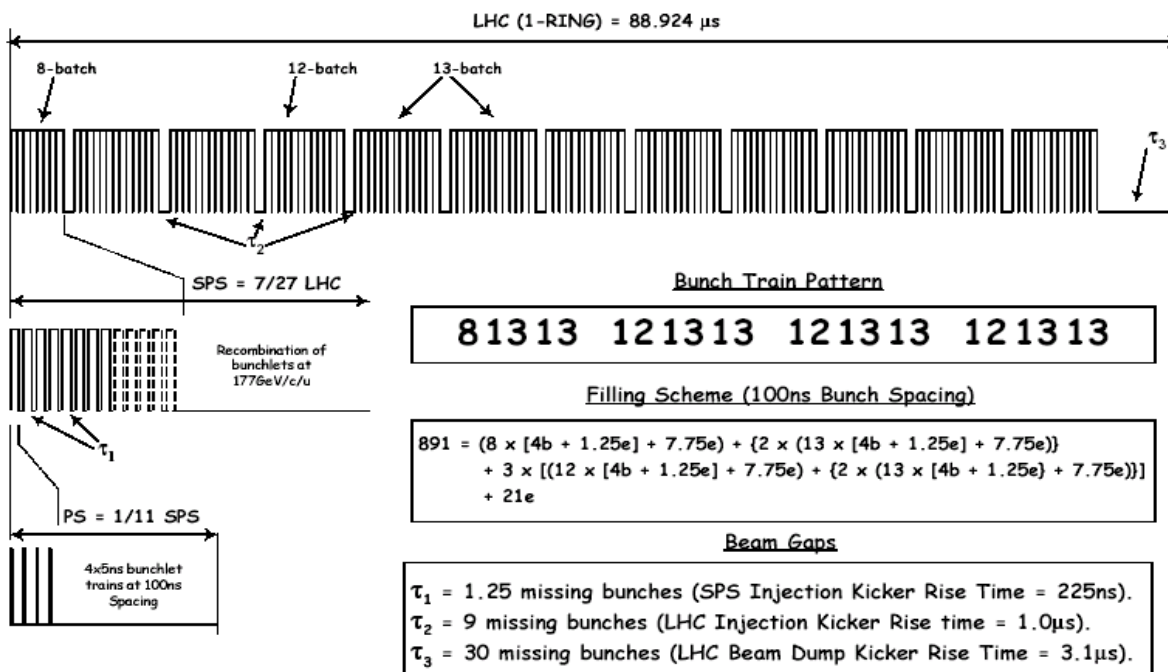


Figure 33.2: Lead ion bunch pattern for baseline filling scheme in PS, SPS and LHC.

Efficiency, emittance budget

The overall efficiency of the scheme (from Linac3 output after stripping to LHC store) is $\sim 6\%$. The emittance budget (physical emittances) in the chain is as tight as the one for protons. This implies that beam instrumentation and dampers have to do their job equally well at the much lower ion intensities, which is a big challenge. By contrast, the SPS and LHC machines require large longitudinal emittances to lower the IBS growth rates. Therefore the longitudinal emittance budget is much more generous, to the point where controlled blow-up has to be used in these machines.

Filling the LHC, bunch pattern

The LHC filling time with Pb ions will be about 10 minutes/ring. The baseline Pb ion bunch pattern in PS, SPS and LHC machines is sketched in Fig. 33.2.

33.3 EARLY LEAD ION OPERATION SCHEME

The base-line (nominal) Pb ion injectors scheme will still be subject to basic limitations, some of them hard-edged and well defined, others only known after running-in of the accelerators concerned, including the LHC. In order to minimise the risk of these limitations jeopardising performance or even destroying LHC equipment in the initial ion-ion phase, an “early” lead operation scheme was proposed and adopted at the 2003 Chamonix Workshop [11]. First, this scheme is much easier to implement within the tight time schedule and second, it enables early studies on limiting phenomena in the ion chain without potentially disastrous consequences, in particular quenches in the LHC. Thirdly, even the much lower luminosity (\sim factor 20) would enable the experiments to fully exploit the early discovery potential of Pb-Pb collisions in the LHC. This factor ~ 20 in luminosity ($L_0 = 5 \times 10^{25} \text{ cm}^2 \text{ s}^{-1}$) is due to a reduction of the number of bunches by a factor 10 (~ 60 instead of ~ 600 per LHC ring) and by increasing β^* by a factor 2 (0.5 to 1 m). However, the number of ions per LHC bunch is the same as in the base-line scheme, 7×10^7 Pb ions/bunch.

Table 33.3: Rationale behind the early lead scheme

Limitation of Baseline (Nominal) Lead Scheme	Change in Early Lead Scheme	Comments
Accumulation of 4 Linac pulses in LEIR yielding 9×10^8 ions per LEIR cycle	1 Linac pulse is sufficient to produce 2.5×10^8 ions/LEIR pulse	No accumulation in LEIR; LEIR/PS cycle 2.4 instead of 3.6 sec
Very elaborate RF gymnastics in the PS with complicated beam control	PS accelerates just one bunch on $h=16$. No splitting into bunchlet pairs.	Beam control very much easier, with larger chances for swift commissioning
SPS injection plateau 42 s long because up to 13 PS batches accumulated	SPS injection plateau 7 s with only 3 or 4 PS batches accumulated	Less losses caused by IBS and RF noise on SPS injection plateau
Injection of bunchlet pairs in the SPS so as to halve its space charge ΔQ to 0.05	No splitting in the PS, further simplifying RF gymnastics	SPS space charge ΔQ of ~ 0.1 acceptable on shortened injection plateau?
Recombination of bunchlet pairs in SPS before extracting to the LHC	Not required (hopefully)	Re-installation of existing 100 MHz system in the SPS postponed
LHC BPM sensitivity $> 2 \times 10^7$ Pb ions/bunch	Intensity 7×10^7 p/bunch as in nominal (baseline) scheme	BPM's do their job with the early scheme as well
LHC quench limit due to ECPP [†] at $L < 10^{27} \text{ cm}^{-2} \text{ s}^{-1}$	With $L_0 = 5 \times 10^{25} \text{ cm}^2 \text{ s}^{-1}$, studies without risk possible	ECPP proportional to luminosity, thus early scheme far from quench limit.
Luminosity lifetime short	Much longer with lower L_0	
Bunch spacing 100ns	Bunch spacing $\sim 1.35 \mu\text{s}$	Kicker rise times not an issue

[†]Electron Capture after Pair Production: possible cause for magnet quenches, potentially limiting L_0

The reasons why this early Pb ion scheme is easier to implement and the limiting phenomena which can be studied without risks are presented in Tab. 33.3. The early Pb ion scheme with its most salient features is depicted in Fig 33.3. In short, this scheme aims at a simplified setting-up of the injector chain while

postponing the commissioning of the baseline (nominal) scheme in order to (i) alleviate the risk of material damage; (ii) remove the tight constraints on the running-in schedule; (iii) provide an opportunity to study limiting phenomena under less pressure.

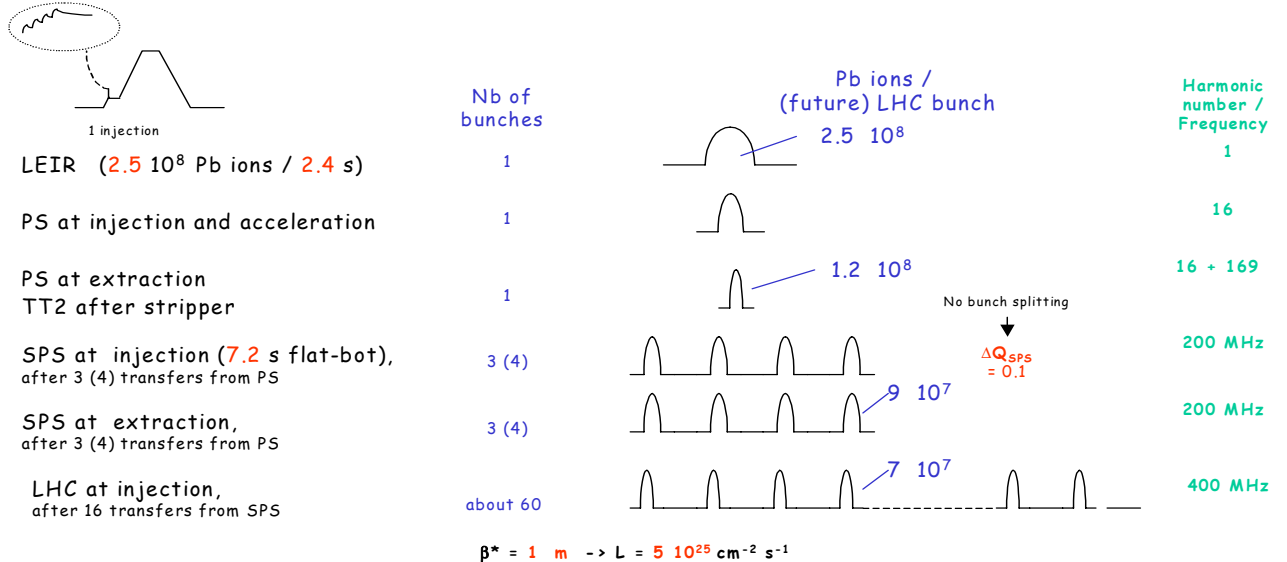


Figure 33.3: Early Pb ion operation scheme, basic features

33.4 INJECTOR CHAIN, OTHER VARIANTS

The upgrading of LEIR is a major endeavour and the resources for its exploitation are not negligible, therefore schemes to provide the LHC with ions via the PSB but without LEIR (no phase space compression) were explored: (i) Pb ions from an ECR source; (ii) Pb ions from a Laser Ion Source (LIS); (iii) Oxygen ions from an ECR source. Research into LIS has been discontinued recently as results obtained so far, though interesting, are far from satisfying the stringent LHC requirements. The two other schemes were assessed (Tab. 33.4) based on past experience with the oxygen and lead fixed-target programmes as well as some dedicated beam tests in the PSB [12].

Table 33.4: Estimated LHC performance with Pb or O via the PSB, without LEIR

Scenario	charges /bunch in LHC	ions/bunch in LHC	$L_0 [\text{cm}^{-2} \text{s}^{-1}]$	comments
Pb ⁸²⁺ , via PSB (upgraded ECR)	2.4×10^8 (BPM “blind”)	2.9×10^6	1.7×10^{24} (ALICE “blind”)	$L_0 > 10^{25}$ required by ALICE
O ⁸⁺ via PSB ¹ (upgraded ECR)	6.1×10^9	7.6×10^8	1.2×10^{29}	OK but ALICE not interested
Pb ⁸²⁺ , via LEIR	5.7×10^9	7×10^7	10^{27}	for reference

¹During an oxygen run, no protons can be sent to the PSB in pulse sharing mode, unless the Linac2 to PSB line undergoes a major upgrade.

Whereas the Pb scenario with the PSB is well below useful LHC performance, the oxygen scheme would be adequate, but the physics with these light ions does not appear attractive. However, the option should be kept in mind as a fallback solution. Fig. 33.4 sketches the LHC performance with the “baseline” and “early” Pb schemes, as well as the two scenarios via the PSB (Pb, O) in an intensity/luminosity diagram; major limiting effects are shown as well. The small working area in terms of intensity/bunch is highlighted.

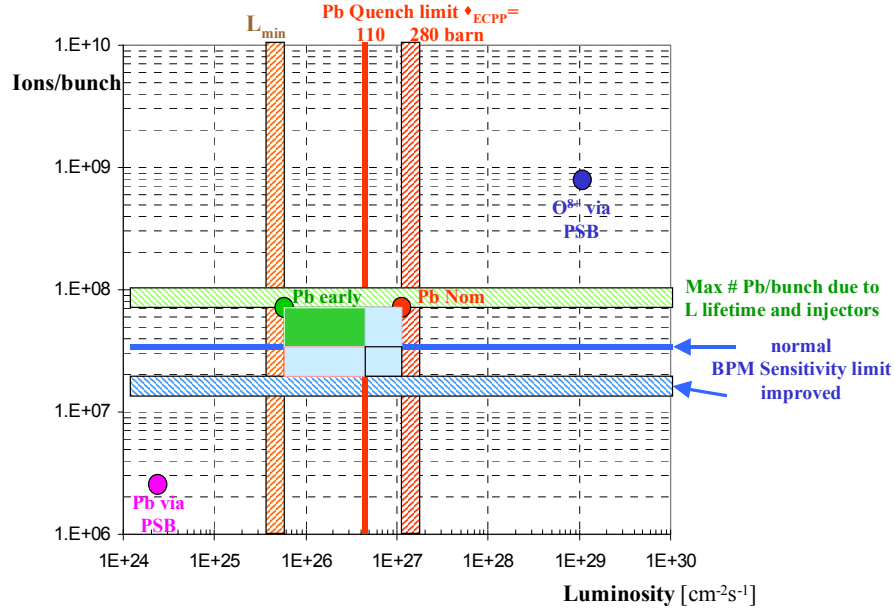


Figure 33.4: LHC performance with injector scenarios based on LEIR (Early and Nominal = Baseline) or the PS Booster (ECR source performance improved).

33.5 FUTURE OPTION: LIGHTER IONS

The LHC ion physics programme is based on Pb ions for the first three to four years of operation. Therefore the “baseline” project to prepare the LHC ion injectors is exclusively dealing with lead ions. However, after this period, physicists envisage studying Pb-p collisions, for which two independent RF systems are being built for the LHC rings. A few years later, collisions between lighter ions (favoured are mainly Ar and to a lesser extent Kr, In, O, see Table 33.5) will be requested in order to vary the energy density obtained in collisions and thus to improve understanding of the quark-gluon plasma [1].

Table 33.5: Typical lighter ions envisaged for the future LHC programme

Element	A	charge state Z in SPS, LHC (fully stripped)	charge state in LEIR, PS	initial luminosity L_0 probably limited by
In	115	49	37	space charge PS, SPS or LHC quench limit
Kr	84	36	29	space charge PS
Ar	40	18	16	space charge PS
O	16	8	8	space charge PS

In earlier proposals, lighter ions were considered as part of the base-line scheme and treated in much detail accordingly [2, 13]. This paradigm has now changed and the lighter ions are considered as an improvement programme. Several of the limitations will be much better known once the LHC works with lead ions and five years should be sufficient to upgrade and optimise the ion injector for Ar, Kr, In and O, in the light of these findings. Each of the ions will require a separate, unique mode of operation and possibly hardware changes, as most of the parameters and limitations strongly depend on the ion chosen.

To get an idea about what performance one can expect with lighter ions, one starts with a very simple (and pessimistic) assumption: with the ions fully stripped, the number of charges per bunch at collision is invariant. For example, with the same charge per bunch, there would be ten times more O^{8+} than Pb^{82+} ions per bunch and 100 times higher luminosity. In fact, the luminosity for lighter ions will be much better than in this model (one or two orders of magnitude) for the following reasons:

- The cross section for nuclear effects during collisions is much lower for lighter ions, so ECPP will probably not limit LHC performance for ions lighter than In.
- Intra-Beam Scattering may be a stumbling block on the SPS and LHC injection plateaus as well as during LHC collisions. The effect scales with $(Z^2/A)^2$, so lighter ions suffer less.
- Space charge: the figures for the tune spread ΔQ (Eq. 33.1) anticipated for Pb (Table 33.2) are seriously limiting the performance in LEIR, PS, SPS. Here the factor Z^2/A also helps for lighter ions.

- The ECR source tends to favour lighter ions in the sense that more charges are produced. Future tests with the upgraded ECR source will provide actual figures.
- Stripping efficiencies between Linac3 and LEIR are better for lighter ions.
- With a lower electron capture cross section for a given energy, lighter ions will suffer much less from losses due to interactions with the rest gas in LEIR and PS.
- The only effect favouring heavy ions is the synchrotron radiation damping time which scales as A^4/Z^5 (A is the mass and Z the charge of the ion) for a given magnetic rigidity (see Vol. 1, Chap. 21); synchrotron radiation damping is fastest for lead.

In general, the hardware upgrades of the ion injector chain have been designed without any other ion than Pb in mind. As an exception to this rule, two important parameters have sneaked into the baseline project in view of performance with lighter ions:

- PS injection energy: the lead extraction energy of LEIR has been set to 72 MeV/n (magnetic rigidity 4.8 Tm). At this energy, the space charge tune spread ΔQ of the nominal Pb beam at PS injection is 0.17 (Tab. 2.1), somewhat smaller than the estimated PS limit of about 0.20 - 0.25, thus 55 MeV/n (4.2 Tm) would have been sufficient for Pb. The energy of 72 MeV/n coincides with the lower frequency limit of the PS cavities with $h=16$, corresponding to two bunches ($h=2$) from LEIR. Moreover, it provides some margin for the Pb beam. Note that the higher magnetic rigidity will reduce space charge in the PS for lighter ions which is their overall performance bottleneck as suggested in Tab. 33.5.
- RF cavities with large frequency range: acceleration in LEIR requires a frequency range of about 0.7 to 2.8 MHz for Pb^{54+} , whereas the required range extends to 4.7 MHz for light ions ($Z/A \leq 0.5$). The new cavities, equipped with a novel core material, will not be tunable but broad-band (0.4 – 4.7 MHz) thus enabling light ions to be accelerated in LEIR to a magnetic rigidity of 4.8 Tm, as the lead ions. A further asset of this choice is the possibility of superposing several RF signals into the same cavity.

REFERENCES

- [1] J. Schukraft, *ALICE Ion Physics Programme*, presented at the LHCC Workshop on Ion Physics at the LHC, CERN, June 2002, <http://doc.cern.ch/age?a021004>
- [2] D. Brandt, *Review of the LHC Ion Programme*, LHC Project Report 450, Dec. 2000.
- [3] John M. Jowett, *Ions in the LHC Ring*, Proc. Chamonix XII Workshop on LHC Performance (edited by J. Poole), March 2003, p. 84.
- [4] R. Jones, Private Communication.
- [5] C.E. Hill, D. Küchler, R. Scrivens, M. Vretenar, *ECR Ion Source and Linac3 – Present Status and Future Work*, Proc. Chamonix XII Workshop on LHC Performance, March 2003, p. 70.
- [6] E. Mahner et al., *Molecular Desorption of Stainless Steel Vacuum Chambers Irradiated with 4.2 MeV/u Lead Ions*, Physical review Special Topics – Accelerators and Beams, Vol. 6, 013201 (2003), January 2003.
- [7] M. Chanel, *LEIR and its Transfer Lines*, Proc. Chamonix XII Workshop on LHC Performance, March 2003, p. 73.
- [8] M. Martini, *Status of what has been done and what has to be done on PS and Transfer Lines*, Proc. Chamonix XII Workshop on LHC Performance, March 2003, p. 76.
- [9] D. Manglunki, *Status of what has been done and what has to be done on SPS*, Proc. Chamonix XII Workshop on LHC Performance, March 2003, p. 81
- [10] H. Burkhardt, J. Gareyte, G. Rumolo, L. Vos, J. Wenninger, F. Zimmermann, *Investigation of Space Charge effects in the SPS*, Proc. 2003 PAC Portland, Oregon, May 2003.
- [11] C. Carli, J.P. Riunaud, *Summary of Session “Preparation with Pb Ions, from Source to Collisions”*, Proc. Chamonix XII Workshop on LHC Performance, March 2003, p. 9.
- [12] Experiments on PSB performed by M. Chanel.
- [13] M. Chanel, *Ion Accumulation for LHC*, Workshop on Beam Cooling and Related Topics, Bad Honnef, Germany, May 2001.

CHAPTER 34

SOURCE AND LINAC3

Linac3 (Lead Linac, [1]) (Fig. 34.1) will serve as a pre-injector of lead ions for LHC. However, some modifications and improvements are required which are presented in this chapter.

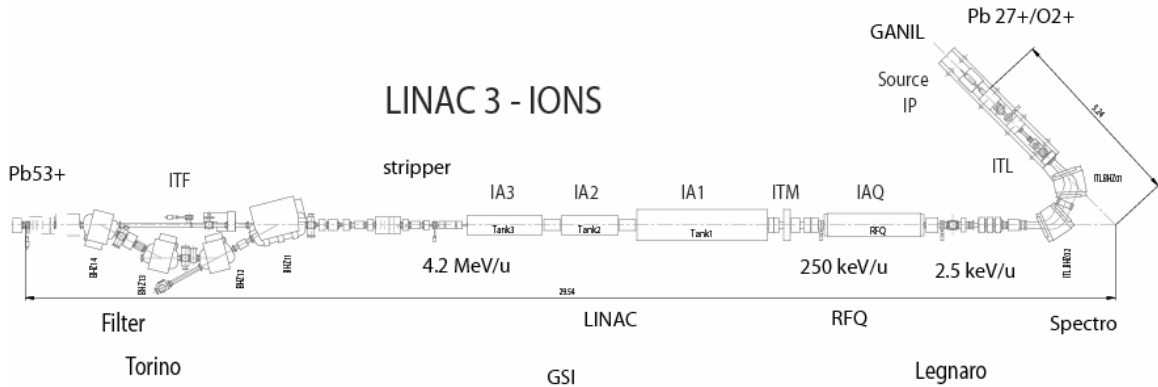


Figure 34.1: Layout of the Lead Linac

34.1 SOURCE UPGRADE (14 – 18 GHz, 100 to 200 μ A)

The mainstay for the production of light and heavy multi-charged ions since the inception of the CERN ion programme in 1986 has been the Electron Cyclotron Resonance Ion Source (ECRIS) [2]. These sources were used, initially, to produce oxygen and sulphur ions and were developed to produce high currents of medium charge state heavy ions (e.g. Pb^{27+}) in a pulsed afterglow mode of operation. For practical reasons, ions are extracted from the source at about 2.5 keV/u (20 kV for Pb^{27+}).

The performance of the 14.5 GHz ECR4 ECRIS running in afterglow mode was sufficient for the SPS fixed target programme for Lead ions but falls considerably short of that required for LHC. However, stacking the ions from Linac3 in the LEIR machine is a possible solution. Tests in 1997 with a source current of 100 e μ A and with Linac3 running at 2.5 Hz showed that 25% of the required intensity for LHC would be attained without modifications [3,4,5]. Raising the repetition rate of Linac3 to 5 Hz would reduce the gap and, apart from a few components, the Linac3 can work at this higher rate.

Any further gain must come from the ion source and the Linac3 transmission. Operation in recent years has concentrated on maintaining long-term stability of the beam sent to the next accelerator in the chain (PSB). This stability was gained at the cost of ultimate performance of the ion source. It is felt that an increase of 10-15 % could be achieved in the Linac3 output by optimising the source performance, but at the cost of overall stability and the requirement of regular adjustment. Equally, a search should be carried out to find acceptance bottlenecks in the present Linac3 chain, which could be reduced by minor corrections to the optics.

Linac3 was designed to accelerate Pb^{25+} but has always accelerated Pb^{27+} due to the risks of excessive X-ray emission from the accelerating cavities. Nowadays, after the long conditioning experienced by the cavities, this will be less of a problem. Acceleration of the same electrical current of Pb^{25+} would result in a gain of 4-5 % in the number of particles after stripping.

The theory of ECR plasmas predicts that the attainable plasma density (and hence the maximum extractable current) scales as the resonance (microwave) frequency squared. Recent tests in the framework of a European collaboration [4] have confirmed the effect up to 28 GHz [2]. As the resonance magnetic field scales only with frequency, the present ECR4 could operate at up to 18 GHz instead of presently 14.5 GHz with only minor modifications and possibly exchanging a mirror coil power supply. Naturally a new microwave power source would be needed. From the frequency scaling, this should give a potential gain of 1.5 in ion intensity. With these measures it should be possible to push the current to the desired 200 e μ A

(Tab. 34.1). A question mark exists over the strength of the hexapole. However, in afterglow mode, the source seems to run with reduced confinement as compared to a CW source, a weaker than optimum hexapole may be an advantage. In any case, upgrading the field in this permanent magnet device would be quite problematic.

Another improvement possibility lies in the fact that the ion source gives a distribution of charge states with a peak around Pb^{26+} . The present analysis spectrometer after the ion source is highly selective for one charge state. Acceleration of more than one charge state in the Linac3 is feasible with lower transmission away from the central charge state. If three charge states around Pb^{26+} could be injected into the Linac3, there could be potential for doubling the beam intensity. A charge state of the plasma gas, O^{2+} , would also be accelerated but would be lost after the stripper. Stripper lifetime could be affected by the increased intensity and repetition rate. The higher intensity of O^{2+} could give rise to emittance blow up problems at low energy due to space charge. Additionally, another potential source of emittance blow up is the mismatch experienced by adjacent charge states with the linac adjusted to an optimum charge state.

The frequency scaling suggests another solution, that of doubling the microwave frequency to 28 GHz, which would result in a factor four in intensity. Currently, development of this type of source is the subject of a European collaboration [6] one of whose objectives is to produce 1 emA of Pb^{27+} . Unfortunately, such a high current, with its attendant adjacent charge states together with ions from the plasma gas would be very difficult to extract and transport at present extraction energies. Hence, an increase in extraction energy by a factor of about three will be needed. This would then require a new (and longer) RFQ and probably a major upgrading of the present Low Energy Beam transport. The costs of these modifications together with the (high) cost of a 28 GHz source system make this option rather expensive. The performance and reliability of these super sources remains to be demonstrated.

Table 34.1: ECR Parameters for $^{208}\text{Pb}^{27+}$

Resonance Frequency	18.	GHz
Resonance Field	0.65	Tesla
Extraction Energy	2.5	keV/u
Extraction voltage	20.	kV
Extracted current	~ 200	μA
Typical pulse length	200	μs
Pb ions / 200 μs pulse	$9 \cdot 10^9$	
ϵ^* rms	0.07	μm

34.2 LINAC REPETITION RATE TO 5 Hz

The Linac3 quarter-wave buncher cavity at 250 keV/u showed some problems at high duty cycle during the 2.5 Hz tests in 1997. The temperature increase in its long inner tube, caused too large a frequency shift which could not be compensated by the tuner. In order to be able to run at 5 Hz, water-cooling of the inner tube will be implemented. A special water-cooling plate has been prepared and tests at 5 Hz are planned, once the connection to the Linac3 cooling circuit has been completed.

The other Linac3 cavities do not present particular problems at 5 Hz. The IH structures and the debuncher were originally designed at GSI for duty cycles an order of magnitude higher, while the RFQ was designed for 10 Hz.

The majority of the magnets in Linac 3 are DC magnets and are thus compatible with 10 Hz operation. The small number of pulsed quadrupoles have been shown to be capable of supporting an rms current at least equivalent to 10 Hz operation either unmodified or with the addition of forced air cooling. Their power supplies were just capable of operating at 2.5 Hz and will be replaced. New power supplies will be needed for the pulsed steering dipoles.

34.3 ENERGY RAMPING CAVITY

During the 1997 tests, a momentum ramping of $\pm 0.4\%$ of the Linac3 beam was obtained by a 10% modulation of the voltage in the IH Tank3. It will now be provided by a dedicated RF cavity, placed as close as possible to the output of Tank3. This solution will decouple the Linac3 setting from the ramping,

simplifying the setting-up of the machine and the operation of the ramping hardware. Moreover, a larger momentum variation could be provided without affecting the beam energy distribution or, for extreme variations, the charge state distribution and hence the beam current.

In order to provide the ramping with minimum voltage and no increase of the energy spread, a 101 MHz cavity has to be placed immediately after the stripper in the ITF line. Space for the new cavity can be found by removing a diagnostics box just after the stripper. This box was only used during commissioning and its removal will not affect the operation of the linac. The space is sufficient for a 4-gap spiral loaded resonator similar to the one used as debuncher at the end of the ITF line, a design that provides high shunt impedance and simple construction and tuning. The required energy variation will be achieved by modulating the cavity phase around the zero-crossing phase. In spite of the higher voltage required, this approach is preferred to amplitude modulation because of the simpler circuitry and a lower risk of multipactoring in the cavity.

Simulations of beam transport for different energies indicate that the ramping cavity can provide the required momentum variation with virtually no increase in the energy spread. The phase of the debunching cavity positioned 11 m downstream of the ramping cavity will need to be modulated too to compensate for the different time of flight.

The ramping cavity (Tab. 34.2) will be built by IAP-Frankfurt, who built the debunching cavity, with a tuner developed and built at CERN. The RF amplifier will be solid-state delivering a maximum of 4 kW at 1% duty cycle. A phase modulator placed in front of the low level RF electronics will allow variation of the cavity phase according to a profile generated with an external GFA.

Table 34.2: Main parameter of the ramping cavity

Operating frequency	101.28 MHz
Max. Momentum variation	$\pm 1\%$
Nominal effective voltage	250 kV
Duty cycle (max.)	0.5 %
Total length	700 mm
Max. Diameter	250 mm
Min. ramping time	50 μ s (for 1% momentum variation)

34.4 SHIELDING

Three radiation sources have to be taken into account: neutrons, x-rays from the source and x-rays from the Linac3. Some dedicated radiation measurements around the source and the Linac3 were performed in 2002.

At present there is no detectable neutron production from ion interaction with the Linac3 structure. This is consistent with the expected dose equivalent rate calculation using [7] with the present beam parameters and assuming that about 5% of beam is lost between 250 keV/u and 4.2 MeV/u. Assuming that the losses remain the same with the possible maximum increase in beam intensity of a factor of 50 (given by a factor of 10 from the new very bright ion sources like a 28 GHz ECRIS times a factor of 5 in the Linac3 repetition rate), the prediction of a neutron dose equivalent rate of around 1 μ Sv/h is perfectly acceptable in a controlled area. However, about 2/3 of the beam at 4.2 MeV/u is stopped in the dump, so locally the neutron dose rate might reach 10 μ Sv/h. A local shielding around the dump may be envisaged if the measurements with beam show higher values.

The improvement of the present 100 e μ A current to 200 e μ A or higher with a future ECR source means an increase of the plasma electron density by a factor of two or more, that is, an increase by the same factor in X-ray emission, i.e. X-ray dose rate. Therefore some more shielding will most likely be required at the source. For an effective energy of about 600 keV as given in [7], a reduction of the radiation by a factor of three can be achieved with about 1 cm of lead or less than 10 cm of concrete.

The X-ray emission induced by stray electrons in the Linac3 structure is proportional to the Linac3 repetition rate. An increase of a factor of five in the X-ray dose rate is therefore expected. Some extra shielding will be required along the Linac3. For an effective energy of these X-rays of about 200 keV as estimated in [8], a reduction of a factor of five in the dose rate can be achieved with about 2 mm of lead or less than 10 cm of concrete.

Extra shielding will have to be defined after measurements on the source and Linac3 under real operating conditions.

34.5 CONTROLS

The control system presently implemented in the Linac3 needs to be extended to integrate the modifications of the Linac3 in view of LEIR operation. Two types of extension are required: a new VME front-end computer with the appropriate modules to drive the new hardware (the amplifier of the energy ramping cavity) and new front-end software to handle the controls and acquisitions of the Linac3 running at 0.833 Hz to 5 Hz rates. Like the controls for LEIR, industrial components based upon PLCs (Programmable Logic Controller) will be used, wherever suitable, in complement to standard VME components.

REFERENCES

- [1] D.J. Warner (Editor), *CERN Heavy-Ion Facility Design Report*, CERN 93-01, April 1993
- [2] R. Geller, Electron Cyclotron Resonance Ion Sources and ECR Plasmas, IOP Publishing, Bristol, 1996.
- [3] S. Baird et al., *Recent Lead Ions Tests in LEAR for the LHC*, Nuclear Instruments and Methods in Physics Research A 391 (1997) 17-23.
- [4] J. Bosser, et al., *Results on Lead Accumulation in LEAR for the LHC*, CERN/PS 98-033(CA) and Proc. of EPAC98, June 22-26, 1998, Stockholm, p. 253.
- [5] J. Bosser, et al.; *Experimental Investigation of Electron Cooling and Stacking of Lead Ions in a Low Energy Accumulation Ring*, CERN/PS 99-033(DI) and Particle Accelerators, Vol. 63, p. 171-210.
- [6] European Community Contract HPRI-CT-1999-50014.
- [7] D. Hitz, et al., *Results and Interpretation of High Frequency Experiments at 28 GHz in ECR Ion Sources*, Future Prospects, Proc. 9th Int. Conf. Ion Sources, Oakland, September 2001, Rev. Sci. INST. , 73, 509 (2002)
- [8] A.H. Sullivan, *Radiation expected from the lead linac to be constructed at CERN*, Report TIS-RP/IR/92-15 and PS/HI Note 92-06 (1992).

CHAPTER 35

LEIR

35.1 OVERVIEW

Central to the LHC ion injector chain is the upgraded LEIR ring [1, 2]. Its role is to transform a series (4-5) of long (~ 200 μ s), low-intensity ion pulses from Linac3 into high-density, short (~ 200 ns) bunches by accumulation and phase space cooling. Electron cooling has been chosen because of its fast (<0.4 s) cooling times at 4.2 MeV/u which are unequalled by other techniques.

Each Pb^{54+} linac pulse is injected by stacking 70 turns into the 6-D phase space [3, 4]. An inclined septum magnet enables appropriate filling of the two transverse phase planes, while longitudinal filling is ensured by ramping the mean energy along the pulse. In this way, the 70 turns are injected with $\sim 70\%$ efficiency. The electron cooler strongly reduces the phase space volume of the injected beam, slightly decelerates the beam and adds it to the stack sitting at a slightly lower energy. Once four to five Linac3 pulses are accumulated and cooled, electron cooling is stopped. This is followed by adiabatic capture and acceleration of two bunches to 72 MeV/u. The sequence of events is sketched in Fig. 35.1 showing a LEIR cycle of 3.6 s length.

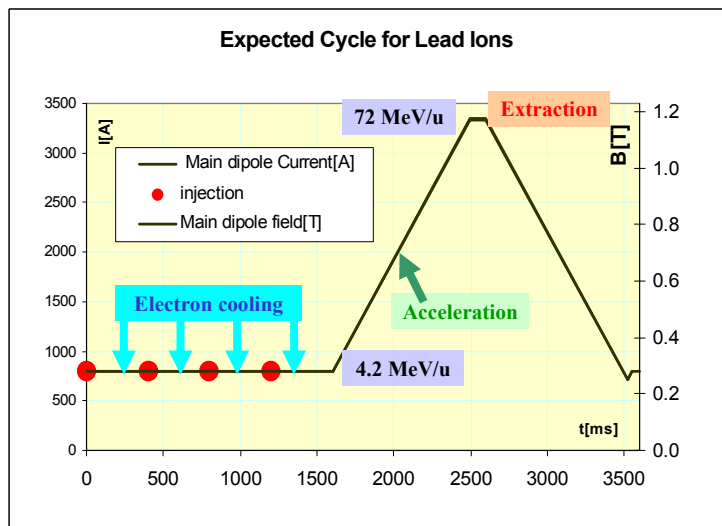


Figure 35.1: LEIR cycle for Lead ions, with four pulses from Linac3 every 0.4 s.

In the nominal (baseline) scheme, two bunches of $4.5 \cdot 10^8$ ions each (total $9 \cdot 10^8$ per LEIR pulse) are produced and transferred every 3.6 seconds to the PS. The design of this scheme is based on the 1997 test run with Lead ions in LEAR [5, 6] where convincing results were obtained (Fig. 35.2). This test essentially confirmed the validity of the proposed accumulation and cooling scheme in LEIR, despite a missing factor of ~ 3 in terms of intensity reached after four linac pulses. The reasons for this missing factor are now well understood and the lessons learnt during the tests were invaluable to define the most salient features of the LEIR upgrading programme:

- (i) increase the Linac3 current by a factor 1.5 and possibly 2,
- (ii) multi-turn injection with stacking in the vertical phase space as well,
- (iii) shortening of electron cooling down time from 400 to 200 ms by increasing the electron current (made possible with the new gun),
- (iv) improve dynamic vacuum by a factor ~ 5 to obtain a dynamic pressure in the 10^{-12} Torr range.

Accumulation of 4-5 Linac3 pulses with a useful efficiency is only feasible with a beam lifetime large compared to the 1.6 s accumulation/cooling time. The lifetime is dominated by (i) charge exchange due to interactions with the rest gas (Pb^{54+} captures or loses an electron) yielding a lifetime of ~ 30 s with the stringent UHV measures proposed; (ii) capturing of an electron from the cooler beam. The lifetime due to the latter effect for a cooler current of 300 mA and a hollow electron beam is expected to be in the range

between 15 s and 30 s. With both loss rates taken together, the overall beam lifetime is then expected to be in the range between 10 s and 15 s.

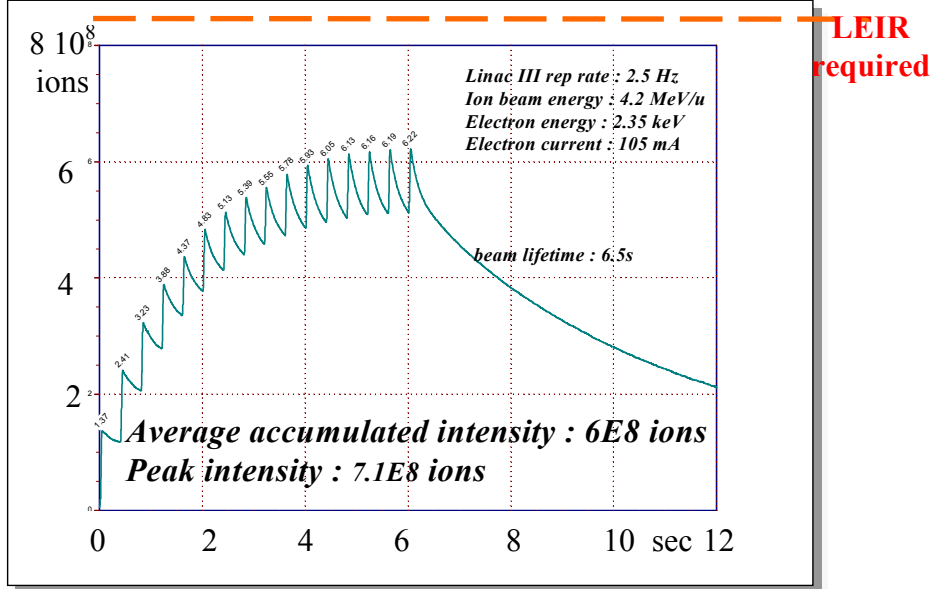


Figure 35.2: Accumulation and cooling of Pb ions during the 1997 feasibility test in LEAR. The dotted line corresponds to the LEIR output requirement for the LHC baseline Pb ion performance.

The layout of the upgraded LEIR ring is depicted in Fig. 35.3. The beam circulates anti-clockwise (contrary to LEAR). Straight Section (SS) 10 (injection) features non-zero dispersion (as does SS 30), whereas SS 20 (electron cooling) and SS 40 (extraction) require zero dispersion, resulting in a proposal for a lattice with two-fold symmetry. While the LEAR bending magnets stay in their respective locations, the quadrupoles in LEIR will be re-arranged into four doublets and four triplets.

In the upper left corner of Fig. 35.3, the beam coming from Linac 3 (at 4.2 MeV/u) and the one extracted towards the PS (72 MeV/u) enter a common line (~60 m) where they travel in opposite directions and at very different (factor ~4) magnetic rigidities. The naïve way to tackle this issue is to change the magnetic strength and polarity of all elements between LEIR injection and extraction, see Fig. 35.1. While this is unavoidable for some bending magnets, clever optics settings for both directions without changing quadrupole polarities have been found, leading to significant savings on power converters.

35.2 LAYOUT AND BEAM DYNAMICS

35.2.1 Basic Layout

The position and the basic shape (“square” with four bending sections, each one deflecting the beam by 90° and four straight sections, each one with a total length of about 12.8 m) of the LEIR machine, shown in Fig. 35.3, is fixed by the fact that the existing LEAR bending blocks will be reused at their current position. The fourfold periodicity (resulting in identical lattice parameter in the four straight sections) of the former LEAR machine cannot be kept, since injection and cooling necessitate rather different lattice parameters in the relevant straight sections. The solution is to adopt a quasi-twofold periodicity (apart from the perturbation due to the solenoid of the cooler) and to install injection and cooling in adjacent straight sections ER.SS10 and ER.SS20. In addition, one quadrupole will be added per quarter of the machine in the cooling section and opposite to it, in order to allow suitable optics of the machine. Hence, focusing will be provided by triplets in the cooling section ER.SS20 and the opposite section ER.SS40 and doublets in the injection section ER.SS10 and opposite to it in ER.SS30. Extraction will take place in the section ER.SS40 opposite the electron cooler, since this leads to a simple geometry of the injection and extraction lines and the beam is small due to the vanishing dispersion and this in turn renders the extraction simpler (smaller kick required by the extraction kicker). In order to avoid synchro-betatron resonances, the two RF cavities will be installed in section ER.SS40, where the dispersion vanishes. The new magnetic alloy loaded cavities need very little

space, so acceleration equipment and extraction septum can be installed in the same section. The extraction kicker will be installed in section ER.SS30 as far downstream as possible. In the LEIR machine, the beam will rotate counter-clockwise (contrary to LEAR), because this renders the optics design of the transfer lines slightly easier without introducing significant drawbacks. All these considerations lead to the basic layout shown in Fig. 35.3. Further systems (correction dipoles and sextupoles, beam diagnostics devices, damper ...) are distributed at suitable locations around the ring.

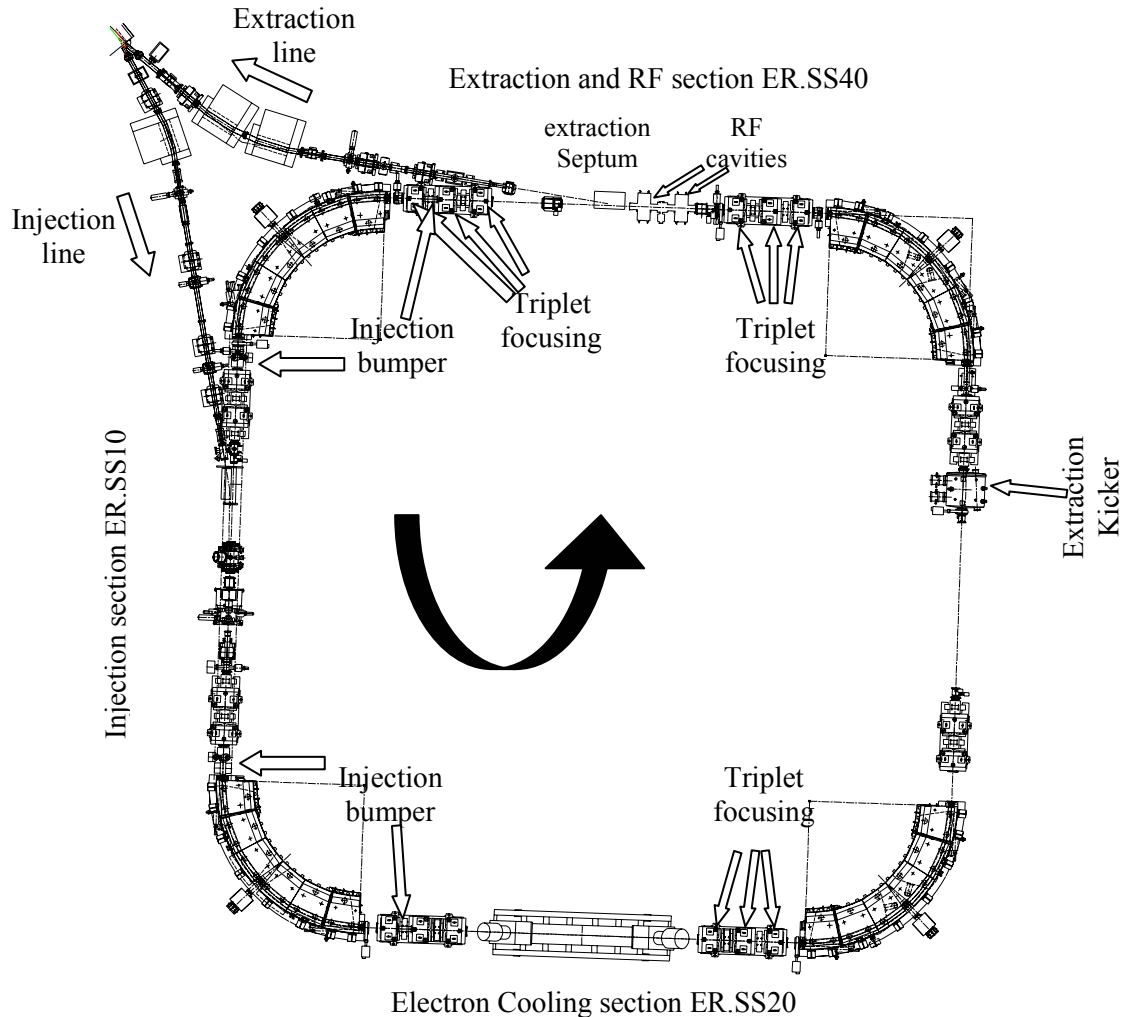


Figure 35.3: Basic Layout of the LEIR Machine

35.2.2 Lattice

Constraints

The main constraints to be fulfilled by the lattice are :

- **Injection section :**
The special multi-turn injection envisaged for LEIR requires a relatively large normalised dispersion, $D/\beta_x^{1/2}$, at the location of the injection septum. On the other hand, in order to maintain good momentum acceptance, the dispersion should not be too large. Thus, a small horizontal betatron function and a not too large dispersion are desired. Note that the horizontal betatron function obtained with the given geometry and other constraints are a compromise and are not as small as desired.
- **Electron Cooler :**
During cooling down time measurements, betatron functions around 5 m and a finite dispersion

were found to enhance cooling rates. Thus, the lattices presented here have been tuned to $\beta_H = \beta_V = 5$ m, but in order to simplify operation with energy ramping during injection, zero dispersion $D = 0$ m has been chosen. However, setting a small (negative) dispersion is possible if required.

- Acceptances :

The acceptances have to simultaneously accommodate the stack already in the machine and the injected beam. While the required horizontal acceptance can be easily obtained due to the large horizontal apertures, it is less obvious to obtain lattices with sufficient vertical acceptance of say 40 μ m.

- Working Point :

The multi-turn injection with simultaneous stacking in 3 phase spaces puts additional constraints on the working point, on top of the usual requirements to stay clear of dangerous resonances in order to avoid losses and beam blow-up. In particular, the working point must not be located too close to a coupling resonance to allow the injection of long linac pulses with good efficiencies.

Coupling due to the Cooler and its Compensation

A solenoidal field is necessary in order to focus the electron beam of the cooler, however, this affects the ion beam as well and introducing coupling. Different schemes to compensate this coupling have been envisaged. Compensation by skew-quadrupoles is, in principle, possible if the field of the solenoid is not too strong. In the case of the LEIR, the locations available to install skew quadrupoles are not at very suitable betatron phases for efficient coupling correction. Hence, very strong skew quadrupolar components, comparable to that of the normal quadrupoles would be necessary which in turn lead to large perturbations of the lattice functions all over the ring. In addition, due to the non-negligible effect of the skew quadrupoles on the lattice properties outside the electron cooler region, perfect compensation is not possible for strong solenoidal field (in particular for lighter ions due to their higher charge over mass ratio). For that reason, compensation with solenoids was chosen. In addition two (out of four available in total) trim power supplies are used, each one connected to two quadrupoles, in order to reduce the effect of the cooler and the compensation solenoids on the betatron functions outside the straight section SS20.

For the time being, a precise field map of the cooler to be installed in LEIR is not yet available. The electron cooler has been modelled as a solenoid with a length $L = 4.30$ m and with azimuthal symmetry. The coupling is compensated by two compensation solenoids with a length of 0.40 m on either side of the cooler installed at a distance of 3.15 m from the centre of the straight section. If skew quadrupolar fields are present in the region around the toroids (see Sec. 35.6), the residual coupling can be compensated efficiently by also using the skew-quadrupoles ER.QSK21 and ER.QSK22.

Proposed Lattice

The working points for different variants of the LEIR lattice are plotted in the resonance diagram shown in Fig. 35.4. The arrows point from the zero intensity working point to the point with the largest direct space charge tune shift expected for Pb ion operation, i.e. immediately after bunching. The nominal working point $Q_H = 1.82$, $Q_V = 2.72$ stems from an optimisation of the injection efficiency. However, it is close to several 4th order difference resonances and the third order $3Q_V = 8$ resonance. If the small transverse emittances required cannot be reached, one may be forced to shift another working point. The higher working point plotted in Fig. 35.4 is not compatible (too close to the coupling resonance) with high injection efficiencies, but may be useful for bunching and acceleration after accumulation. The lower working point plotted in Fig. 35.4 is compatible with high injection efficiencies, but may be too close to the half-integer $Q_V = 2.5$. With such a working point, the machine is sensitive to focusing errors (resulting in strong beta-beating) and after bunching, some ions might even cross the resonance resulting in significant blow-up. However, one might end up with a scheme where accumulation takes place with this lower working point plotted in Fig. 35.4 and then move closer to the coupling diagonal and away from the half-integer resonance for bunching and acceleration. Note that, for operation with lighter ions, larger direct space charge tune spreads are expected and the choice of a suitable working point becomes more delicate.

Lattice functions along the accelerator are shown in Fig. 35.5 to Fig. 35.7. The three plots correspond to the three potential working points mentioned above. One notes that small shifts of the working point of the

order of about 0.10 result in significant changes of the lattice functions around the ring. This clearly demonstrates that the margin for shifting the working point is rather limited. Some parameters of possible low energy lattices of LEIR are given in Tab. 35.1.

Table 35.1: Some basic parameters of the three reference LEIR lattices. The figures apply to the low energy lattice with a solenoidal electron cooler field of 1000 G and for Pb^{54+} ions.

Working point : Q_H	1.82	1.64	1.85
Q_V	2.72	2.57	2.82
Strength in m^{-1} ER.QDN11, 12, 31 and 32	-0.5786	-0.5515	-0.5897
Strength in m^{-1} ER.QFN11, 12, 31 and 32	0.4584	0.4482	0.4625
Strength in m^{-1} ER.QFN21, 22, 41 and 42	0.1219	0.0696	0.1393
Strength in m^{-1} (without trim) ER.QDN21, 22, 41 and 42	-0.6553	-0.5828	-0.6830
Strength in m^{-1} (without trim) ER.QFN23, 24, 43 and 44	0.3675	0.3013	0.3841
Additional strength in m^{-1} (due to trim) ER.QDN21 and ER.QDN22	0.0037	0.0101	0.0061
Additional strength in m^{-1} (due to trim) ER.QFN23 and ER.QFN24	0.0235	0.0160	0.0188
Horizontal betatron function (in m) At the centre of the injection section	4.29	2.96	4.62
Vertical betatron function (in m) at the centre of the injection section	3.87	5.85	2.94
Dispersion in the injection section (in m)	10.30	10.13	10.37

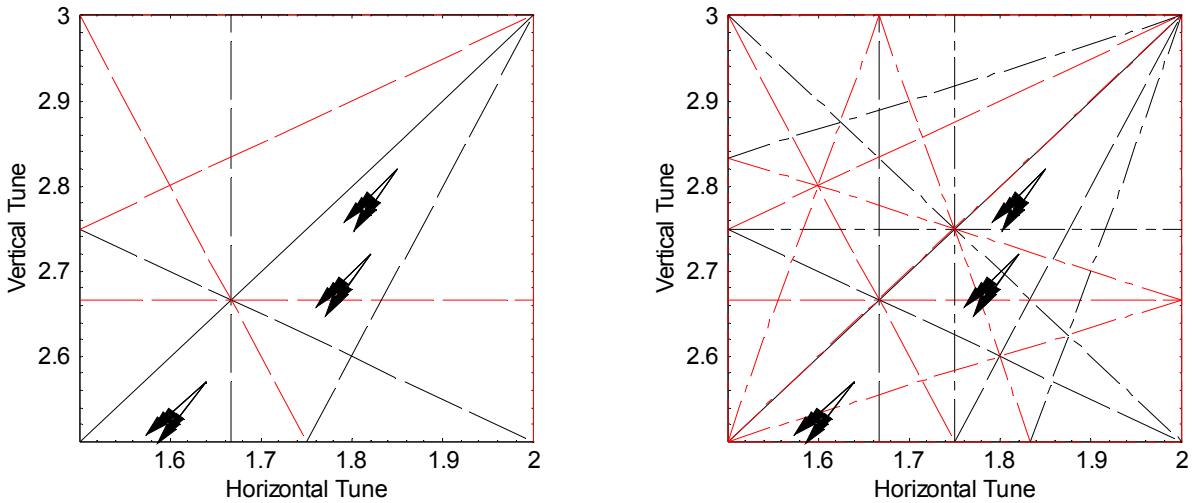


Figure 35.4: Potential LEIR working points in resonance diagrams up to order 3 (left) and 4 (right). The arrows point from the zero intensity working point to the working point with the largest direct space charge tune shift, just after bunching at the centre of the bunch. A bunching factor of $B_f = 0.38$, relative RMS momentum spreads of $1 \cdot 10^{-3}$, $2 \cdot 10^{-3}$ and $4 \cdot 10^{-3}$ and transverse Gaussian distributions with normalised emittances $\epsilon_H^* = \epsilon_V^* = 0.7 \mu\text{m}$ and $\epsilon_H^* = 1.0 \mu\text{m}$, $\epsilon_V^* = 0.5 \mu\text{m}$ have been assumed. The space charge tune shifts have been computed for a simplified lattice without coupling.

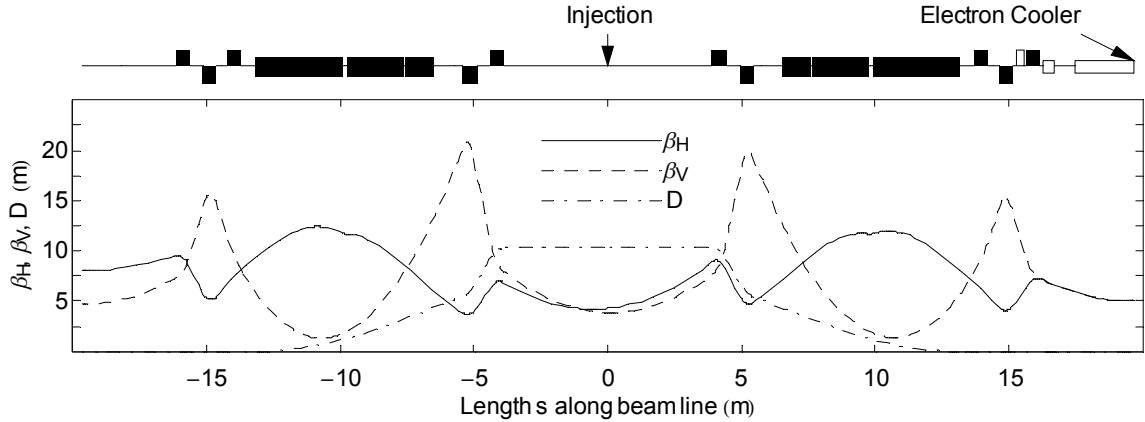


Figure 35.5: Lattice functions along the reference orbit for one half of the LEIR machine tuned to the nominal working point (Q_H, Q_V)=(1.82, 2.72).

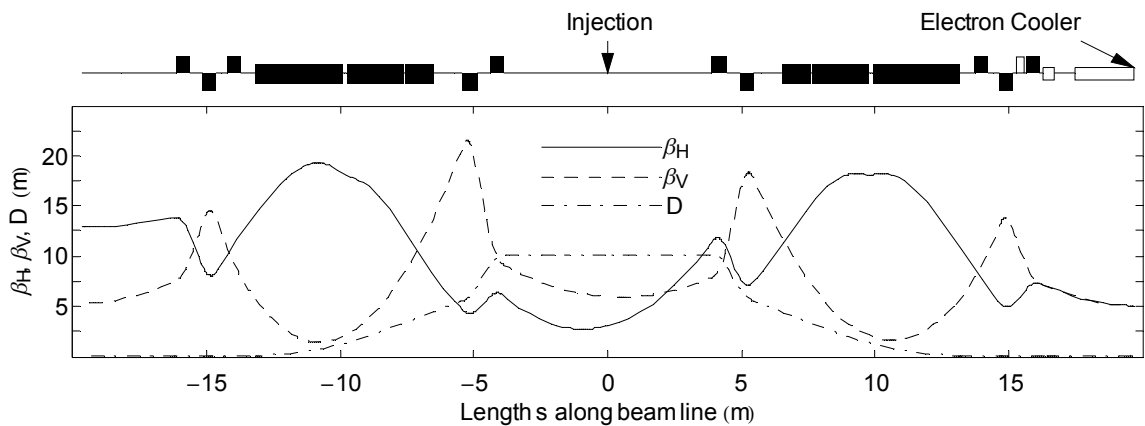


Figure 35.6: Lattice functions along the reference orbit for one half of the LEIR machine tuned to the lower working point (Q_H, Q_V)=(1.64, 2.57).

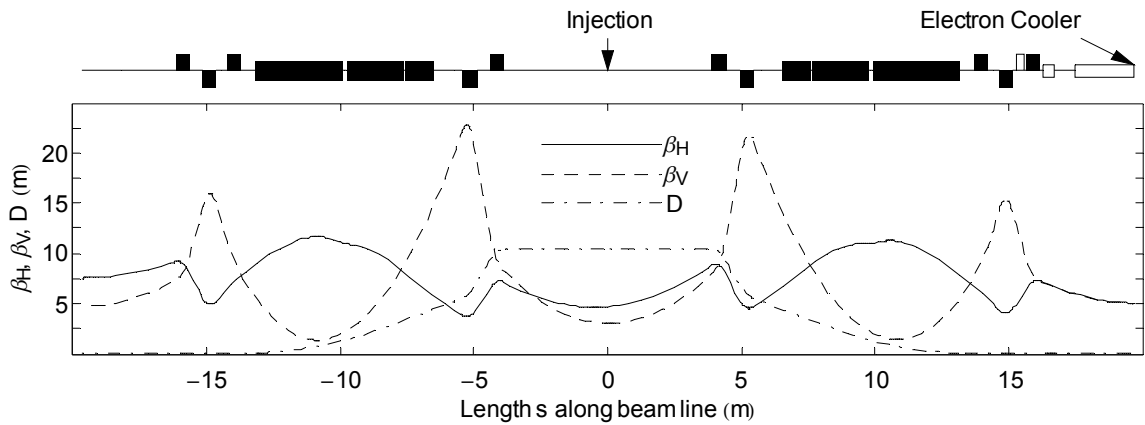


Figure 35.7: Lattice functions along the reference orbit for one half of the LEIR machine tuned to the higher working point (Q_H, Q_V)=(1.85, 2.82).

35.2.3 Intensity Dependant Effects

Space Charge tune shift

Incoherent space charge tune shifts of about $\Delta Q = -0.07$ are expected after bunching for a nominal Pb^{54+} beam. This tune shift leads to a tune spread, since on the one hand, the ions in the centre of the bunch “see” this maximum tune shift and on the other hand, ions in the tails are not affected. This tune spread restricts the choice of a suitable working point, since the whole area in a resonance diagram covered by the beam must be accommodated in a region free from dangerous low order resonances as already mentioned in Sec. 35.2.2.

Intra beam scattering

Intra Beam Scattering (IBS) growth times are short for high charge states, low beam energies and high densities. In fact, IBS will probably be the main phenomenon leading to blow-up acting against the electron cooling. Thus, the emittances which can be achieved during electron cooling are determined by the equilibrium between blow-up dominated by IBS and the damping due to the cooling force. Due to the strong longitudinal “cooling force” experienced by an ion of the circulating beam, the momentum spread of the beam is expected to be very small (extrapolating from observations in LEAR one expects RMS values of about $\sigma_p/p = 0.2 \cdot 10^{-3}$) immediately after cooling. Thus, right after switching off the cooler and before or at the start of the bunching, large longitudinal IBS growth rates are expected. However, with increasing longitudinal emittance, the growth rate will decrease quickly and the beam will finally end up in a quasi equilibrium situation (with constant ratio between the emittances in the three phase spaces) with slow growth due to IBS in all three phase spaces.

IBS growth rate computations for the lattice envisaged for LEIR are not available. Longitudinal IBS growth rates with the LEAR lattice and for beam emittances expected after accumulation and bunching have been computed ranging from a fraction of a second for the small momentum spread beam to a few seconds for the larger momentum spread after bunching [7]. For sufficiently large (but within the nominal longitudinal emittance) momentum spreads, IBS growth times large compared to the time needed for bunching and acceleration have been found. Although the IBS growth rates with the LEIR will be somewhat different from the ones computed using the LEAR lattice, this phenomenon is not expected to compromise the proper functioning of the machine.

Transverse Instabilities

During the accumulation tests in 1997, no signs of transverse instabilities have been observed with the 70 MHz bandwidth active damper switched on and with about half the intensity needed for nominal Pb operation of LEIR. The damper of LEIR (re-using the old strip-line pick-up and kicker, but with new electronics) will have a larger bandwidth of 100 MHz (see Sec. 35.7.3). Thus, for Pb operation of LEIR, no limitations due to transverse instabilities are expected.

However, if transverse instabilities turn out to compromise performance (unlikely for Pb operation, but to be expected with lighter ions) efficient cures which can be implemented easily, exist:

- Increase of the momentum spread by periodically modulating the cathode voltage of the electron cooler to increase Landau damping. This leads to a periodic change of the energy of the cooling electrons and, in turn, to a larger momentum spread of the ions. This method has been applied successfully in LEAR [8] and CELSIUS [9]
- Use of the stochastic cooling equipment, initially installed for LEAR and still available, with a lower gain as damper working up to some 500 MHz. This method has been successfully applied in the past to damp transverse instabilities of cooled proton and antiproton beams in LEAR.

Longitudinal Instabilities

A significant contribution to the longitudinal coupling impedance seen by the beam which had not been present in the LEAR machine, stems from the new magnetic alloy cavities, when they are not short-circuited (see Sec. 35.7). In fact, in this case the real part of the longitudinal coupling impedance Z_n/n increases from about 100Ω to 400Ω for $n = 1$. In addition, at the low accumulation energy, the direct space charge impedance is large and contributes an imaginary part in the order of 8000Ω to Z_n/n . Thus, for the most

critical case for $n = 1$, $Z_n/n = (400 - 8000 i)\Omega$. A stability diagram is shown for various distributions in Fig. 35.8. The quantity :

$$U + i V = (Z_n/n) (N Q^2 e) / (T_{rev} \beta^2 \gamma (E_0/e) \eta 2\pi (\sigma_p/p)^2)$$

with T_{rev} the revolution time, N the number of ions, Q the charge state, β and γ the relativistic factors, E_0 the rest energy of the whole ion and η the momentum slip factor, must remain inside the boundaries plotted for different distributions. The two stars on the figure denote this quantity for momentum spreads of (a) $\sigma_p/p = 0.2 \cdot 10^{-3}$ and (b) $\sigma_p/p = 1.0 \cdot 10^{-3}$. One notes that for the small momentum spread expected after electron cooling and for distributions with short tails, the beam would not be stable, mainly due to the lack of tails in the distribution. For a Gaussian, the quantity $U + i V$ is well inside the stability boundary. For comparison, a dotted circle corresponding to the Keil-Schnell criterion with the additional (pessimistic) approximation that the full width of half maximum of the momentum spread is $(\Delta p/p)_{FWHM} \sim 2 (\sigma_p/p)$ is shown.

In conclusion, the nominal coasting Pb ion beam at the end of accumulation is expected to be close to the limit of stability. However, when the beam reaches this limit, the Schottky noise is acting back on the beam via the impedance. This leads to longitudinal heating of the beam, creating stabilising tails [10]. Thus, no problems due to longitudinal instabilities are expected for LEIR operation. Longitudinal instabilities could also be cured by heating the beam (e.g. by periodic jumps of the voltage of the electron cooler voltage, see above) to increase Landau damping.

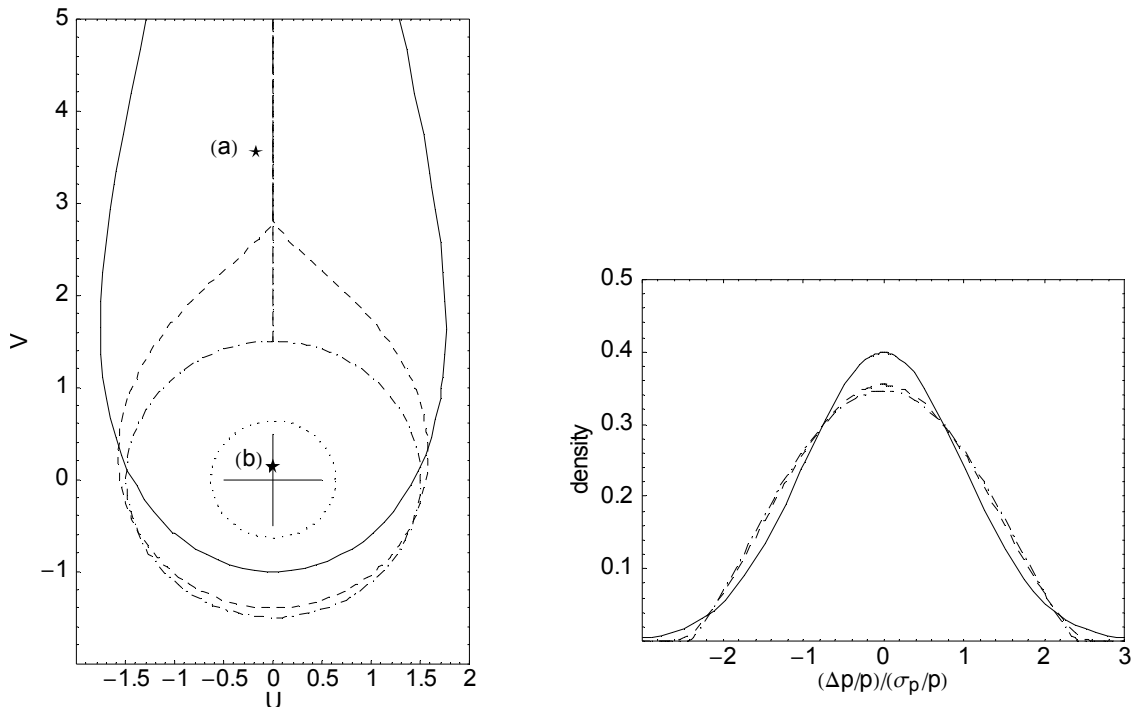


Figure 35.8: Longitudinal stability diagram (left image) with normalised impedances for momentum spreads of (a) $\sigma_p/p = 0.2 \cdot 10^{-3}$ and (b) $\sigma_p/p = 1.0 \cdot 10^{-3}$. The stability boundaries for a Gaussian distribution (solid line), a parabolic squared distribution (dashed line) and an elliptic to the third power (dot-dashed line) are shown. These distributions are shown in the right image.

35.3 INJECTION AND EXTRACTION

35.3.1 Multi-turn Injection with Simultaneous Stacking in Momentum and in Horizontal and Vertical Phase Space

Multi-turn injection with simultaneous stacking in momentum and in both transverse phase spaces is one of the key ingredients for high stacking rates in LEIR :

- This method allows the injection of a $200 \mu\text{s}$ long linac pulse (corresponding to about 70 revolutions in LEIR) with good efficiency (of about 70 % according to simulations) while keeping the stack in the machine.
- The transverse emittances of the injected beam will be relatively small (e.g. $\epsilon_H = 60 \mu\text{m}$ and $\epsilon_V = 40 \mu\text{m}$), but the momentum spread will be large. In fact, the newly injected beam will “sit above” the stack in terms of momentum and then be decelerated and merged with the stack. Such an arrangement is suitable for fast electron cooling, because the longitudinal cooling forces experienced by an ion of the circulating beam in the cooler, are typically larger than the transverse ones.

This special multi-turn injection is a straightforward extension of simultaneous stacking in horizontal phase space and momentum, a method [3, 4] successfully demonstrated in the framework of the accumulation test [5] in LEIR. For LEIR, stacking in the vertical phase space will take place as well in order to further increase the length of the Linac pulse that can be injected with good efficiency. A key ingredient for multi-turn injections with stacking in momentum and in transverse phase space is a lattice with a relatively large normalised dispersion at the location of the injection septum.

The method is sketched in Fig. 35.9, showing horizontal positions during the injection as a function of time. A closed orbit bump is generated and decreases linearly with time during the injection as in the case of conventional multi-turn injection in horizontal phase space. In addition the energy of the beam delivered by the linac is ramped, i.e. the energy increases during the linac pulse. This energy ramp is adjusted in such a manner that the momentum dependant orbit $b + D \times (\Delta p/p)_R$, corresponding to the momentum $(\Delta p/p)_R$ of the ions coming from the Linac, is kept constant during the whole injection process. Since the beam is injected at the same position wrt its momentum dependant orbit, the beam is injected with the same betatron amplitude all along the process. After the first revolutions, the beam stays well inside the septum due to the betatron oscillations. Since the beam oscillates in both phase spaces, it misses the septum for a large number of turns, if the working point is chosen in an appropriate manner. Cross sections of the beam at the exit of the injection section are plotted in Fig. 35.10 at various stages during the injection process. A more detailed description of multi-turn injection with stacking in horizontal phase space and momentum is given in references [3, 4]

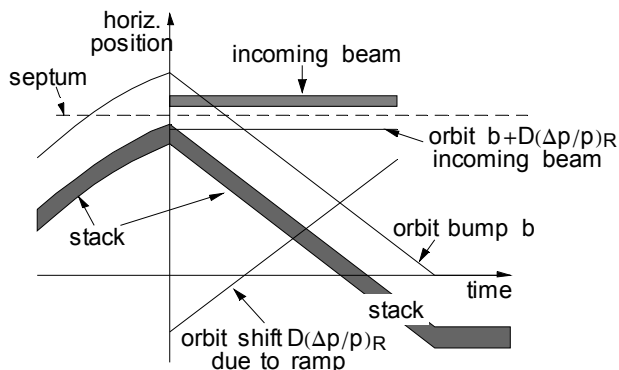


Figure 35.9: Horizontal positions during multi-turn injection into LEIR. $(\Delta p/p)_R$ denotes the relative momentum ramp which changes linearly during a linac pulse. The bump collapses within $210 \mu\text{s}$ from its maximum of about 43.5 mm down to zero. The momentum ramp extends from $-0.4 \cdot 10^{-3}$ at the beginning of the injection to $3.6 \cdot 10^{-3}$ at the end of the injection some $200 \mu\text{s}$ later.

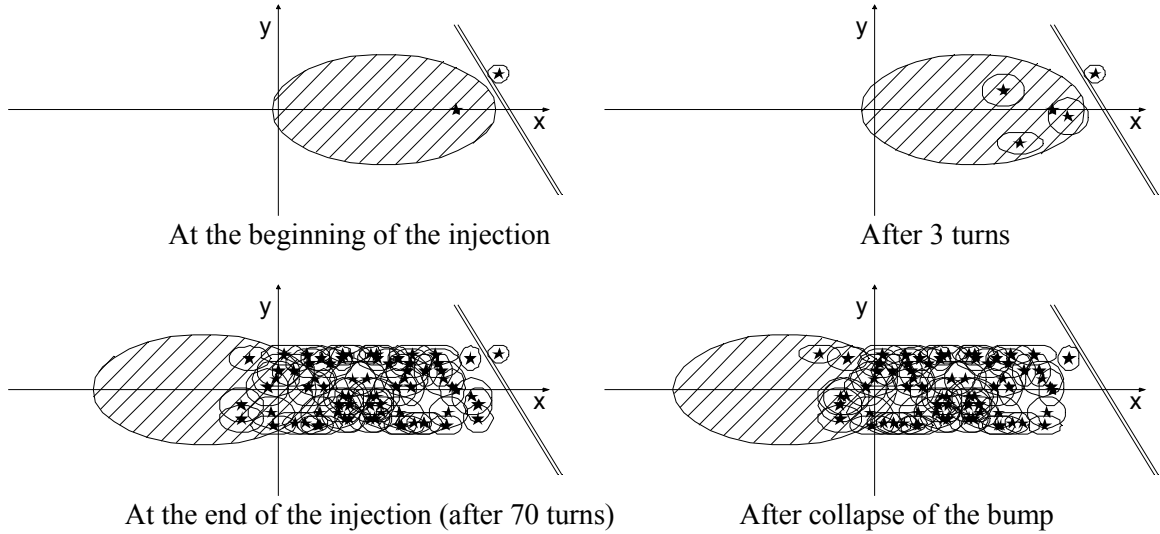


Figure 35.10: Cross sections of the beams at the location of the injection septum during multi-turn injection with stacking in all three phase spaces. At the beginning the bump is at its maximum and shifts the stack (represented by the hatched area) close to the septum. The arriving beam is represented by the ellipse at the outer side of the septum.

In order to achieve good injection efficiencies, a small effective thickness of the injection septum is mandatory. The solution adopted for LEIR is to combine first a magnetic septum ER.SMH11 providing a large deflection of some 175 mrad and installed sufficiently far upstream in order not to reduce the available aperture, followed further downstream by a very thin (effective thickness a few tenth of a mm) inclined electrostatic septum ER.SEH10.

35.3.2 Extraction

The ion beam will be extracted from LEIR by conventional fast extraction. During the last milliseconds before the actual extraction, the beam is moved close to the extraction septum ER.SMH40 by an orbit bump. A fast kicker magnet deflects the beam to the outer side of the septum.

Practical complications arise because the betatron phase advance between the kicker magnet and the septum is not optimal and due to the limited strength of the dipoles generating the bump. There is not enough space and phase advance to install both the extraction kicker and the septum in the same straight section SS40. Thus, the kicker had to be placed in section ER.SS30 as close as possible to the second triplet, i.e. at the closest possible location upstream from the extraction septum. The phase advance between the kicker and the extraction septum is more than the optimal $\pi/2$. In order to achieve a zero slope of the trajectory of the extracted beam, a bump with a positive slope at the location of the septum is necessary as shown in Fig. 35.11. Also sketched is the space needed by the beam versus available apertures at various stages along the extraction process. One concludes that there is no serious aperture bottleneck at extraction. Nominal deflection angles necessary during the extraction process are given in Tab. 35.2. Note that the deflection angles of some dipoles are relatively close to their respective maximum and, thus, this might slightly complicate the orbit correction.

Table 35.2: LEIR extraction elements. The orbit bump is created using five corrector dipoles. The kicker ER.KFH40 deflects the beam to the outer side of the septum ER.SMH40.

Element	Deflection (mrad)	Strength (Gm)
ER.DWH32	3.04	146.2
ER.DHN41	1.56	74.7
ER.DHN42	-4.13	-198.3
ER.DWH41	-0.1	-4.8
ER.DWH42	4.78	229.2
ER.KFH32	6.43	308.7
ER.SMH40	130	6240

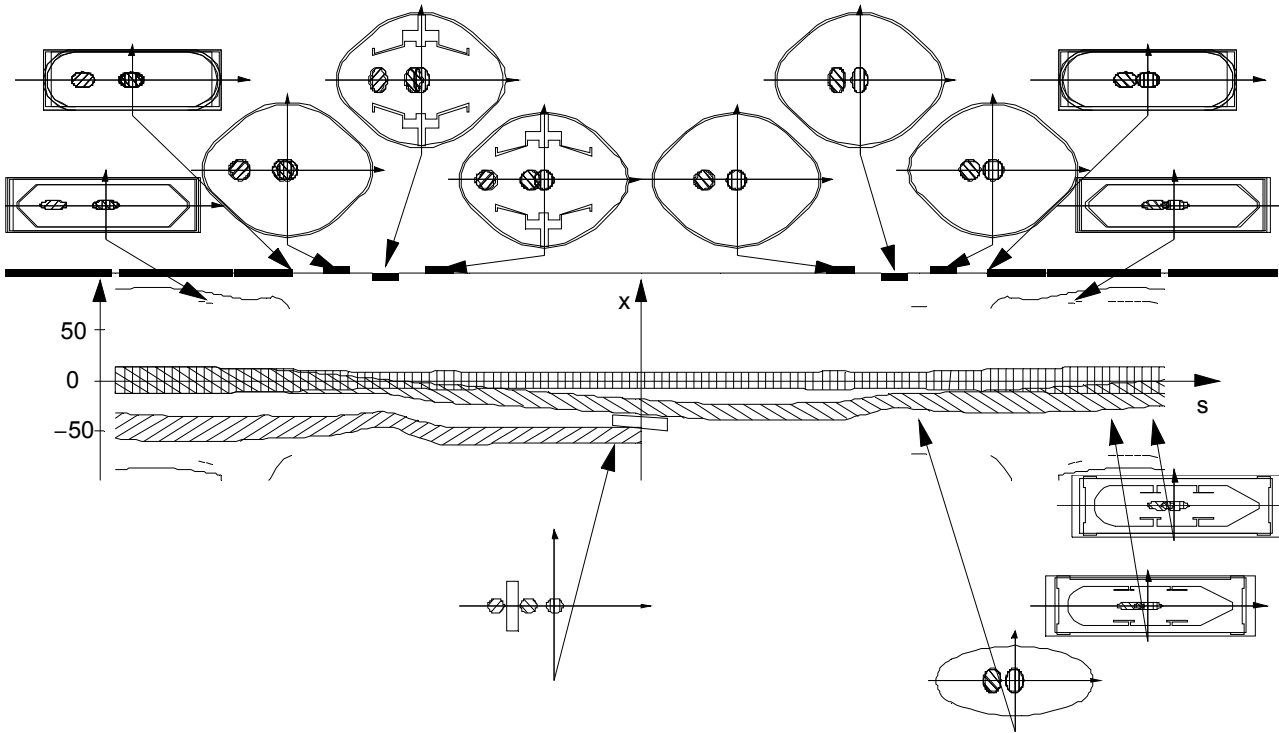


Figure 35.11: Beam cross sections during the LEIR extraction process and available apertures in the extraction section. The drawing in the centre shows a top view, with the beam travelling from left to right and, thus, the x-axis pointing towards the inside of the LEIR ring. The horizontal axis of the plots showing beam cross sections points towards the inside of the LEIR ring as well.

35.4 INJECTION/EXTRACTION SEPTA

The design for both injection septa is based on a beam rigidity of 1.1375 T.m, corresponding to an energy of 4.2 MeV/nucleon for Pb^{54+} ions.

35.4.1 Magnetic Injection Septum, ER.SMH11

The first septum, called ER.SMH11, is installed close to the end of the injection line from Linac 3. It is a dc 10-turn magnet with a stainless steel vacuum chamber in the magnet gap. The magnet is displaced vertically by approximately 30 mm and mounted on a slope to allow for the combined horizontal vertical injection scheme. The magnet can be opened and removed to allow the vacuum chamber to be baked out or to provide access to the magnet coil for maintenance. The technical specification is shown in Tab. 35.3 and a cross section in Fig. 35.12. The magnet is recovered unchanged from the old LEAR machine. However, a new mechanical support and vacuum chamber will be built and a new mounting of this vacuum chamber to the magnet will be developed. The power supply for this septum is described in Sec. 35.8.

Table 35.3: Technical specification of the magnetic injection septum ER.SMH11

Deflection angle	175	mrad
Integrated magnetic field ($\int B \cdot dl$)	0.199	T.m
Gap field	0.241	T
Gap height	55	mm
Gap width between conductors	156.6	mm
Magnet length (physical)	900	mm
Magnetic equivalent length	825	mm
Septum conductor thickness	7.7	mm
Number of conductor turns	10	
Current (dc)	1055	A
Downward pitch angle	14.5	mrad
Magnet inductance	315	μ H
Magnet resistance	11.5	$m\Omega$
Demineralised water cooling requirement	< 40	l/min.

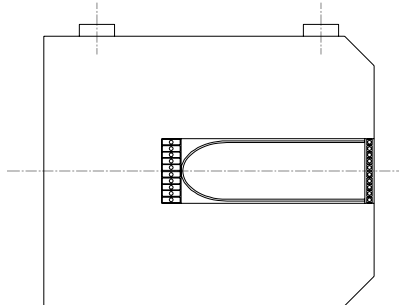


Figure 35.12: ER.SMH11 cross-section

35.4.2 Electrostatic Injection Septum, ER.SEH10

The second septum necessary for injection into LEIR will be an electrostatic septum, called ER.SEH10. This septum is installed in the LEIR ring itself. The septum foil is tilted by 30 degrees to cope with the combined horizontal vertical injection scheme. The design of this new septum is based on the one of the LEAR electrostatic septum. The internal surface under vacuum and the pumping configuration are optimised to cope with the stringent vacuum requirements. A vacuum in the low 10^{-12} mbar range is expected. The technical specification is shown in Tab. 35.4 and a cross section in Fig. 35.13. Both cathode and septum foil have a radial and angular displacement system. The cathode is made of titanium, while molybdenum is used for the septum ribbon. The entire vacuum tank will be bakeable up to 300° C.

Table 35.4: Technical specifications of the electrostatic injection septum ER.SEH10

Gap between electrodes nominal (min., max.)	40 (30, 50)	mm
Nominal cathode inclination (min., max.)	6 (0, 10)	mrad
Nominal voltage (max.)	51 (90)	kV
Horizontal deflection at nominal voltage	25	mrad
Total deflection provided by septum	28.9	mrad
Nominal electric field	1.121	MV/m
Septum foil and cathode inclination	30°	
Septum foil thickness (molybdenum)	0.1	mm
Septum foil length	0.768	m
Cathode length	0.720	m
Good field region ($h \times w$)	40×30	mm \times mm
Tank length	0.914	m

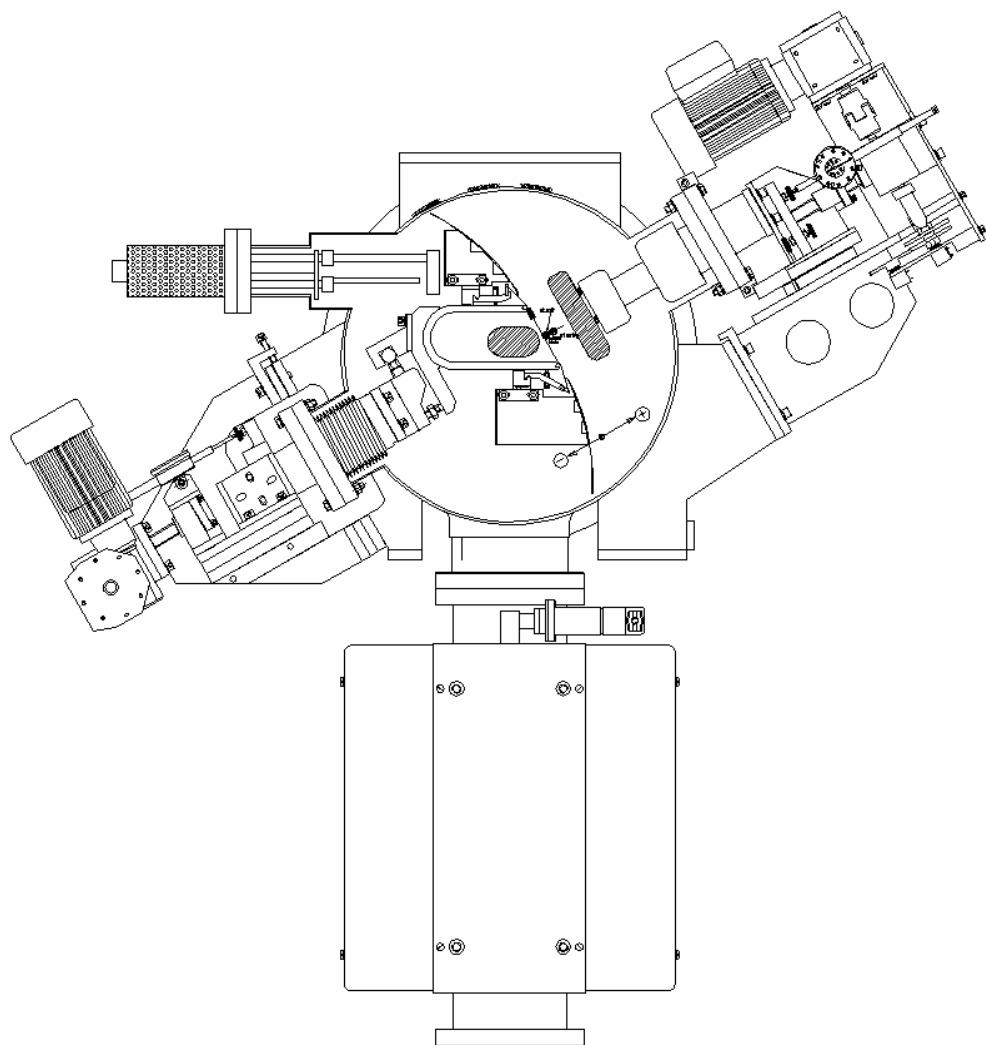


Figure 35.13: SEH10 cross-section

The power for this electrostatic septum is supplied by power supplies recovered from LEP 2 ZL electrostatic separators. Two power supplies, delivering a maximum of 200 kV at 15 mA, are connected to a high voltage switch, so one power supply is used for operation, while the second is installed as an operational spare. All these components are connected with standard 160 kV LEP cable. The high voltage switch is linked to the septum via a high voltage damping resistor. These components are installed in the LEIR ring close to the septum.

35.4.3 Magnetic Extraction Septum, ER.SMH40

The design for the extraction septum is based on a beam rigidity of 4.8 T.m, corresponding to an energy of 72 MeV/nucleon for Pb^{54+} ions. Septum ER.SMH40 is installed at the very beginning of the LEIR extraction line. It is a pulsed single turn magnet with a thin-wall stainless steel vacuum chamber in the magnet gap. A new concept will be developed to allow a pulsed magnet to work outside vacuum and provide the required field in the stainless steel vacuum chamber. The vacuum chamber, with a circular cross section, is curved to follow the beam trajectory. The magnet can be opened and removed to allow the vacuum chamber to be baked out at 300°C or to provide access to the magnet coil for maintenance. The technical specification is shown in Tab. 35.5 and cross section and longitudinal views are shown in Fig. 35.14. The power Converter for this septum is described in Sec. 35.8.

Table 35.5: Technical specification of the magnetic extraction septum ER.SMH40

Deflection angle	138	mrad
Integrated magnetic field ($\int B \cdot dl$)	0.662	T.m
Gap field	0.779	T
Gap height	50	mm
Gap width between conductors	120	mm
Magnet length	920	mm
Magnetic equivalent length	850	mm
Septum conductor thickness	4 – 20	mm
Effective septum thickness as seen by the beam (conductor, screen, vacuum chamber walls)	10	mm
Number of conductor turns	1	
$\emptyset_{\text{inside}}$ magnet vacuum chamber	44	mm
Magnet vacuum chamber wall thickness	< 1.5	mm
Radius of curvature of magnet vac. chamber	6.16	m
Peak current	30.4	kA
Half sine pulse width	> 5	ms
Flat top duration	> 400	μ s
Magnet inductance	2.7	μ H
Magnet resistance	0.15	$m\Omega$

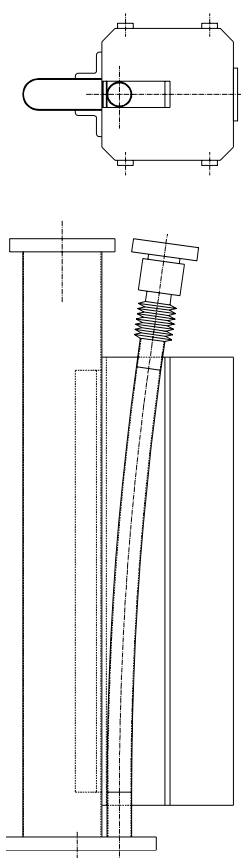


Figure 35.14: Cross-section of ER.SMH40 with vacuum chamber

35.5 INJECTION/EXTRACTION KICKERS AND BUMPERS

35.5.1 Injection Bumpers

The characteristics of the multi-turn injection system require a symmetrical arrangement of four fast dipole magnets (ER.DFH42, ER.DFH11, ER.DFH12 and ER.DFH21) centred on the injection septa.

These fast dipoles magnets (bumpers) comprise a three-piece ferrite C-core and a four turn conductor moulded together and enclosed in an aluminium box. Two such C-pieces are mounted face to face to form a window frame magnet. This type of construction permits easy mounting and dismounting of the assembly to allow the vacuum chamber to be baked out. A cross-sectional drawing of the magnet is shown in Fig. 35.15. The two back-leg windings are connected electrically in series. The magnetic circuit is split on the vertical centreline, so that the longitudinal coupling impedance is minimised. The split is aluminium filled, thus presenting an efficient eddy current shield for the field induced by the beam.

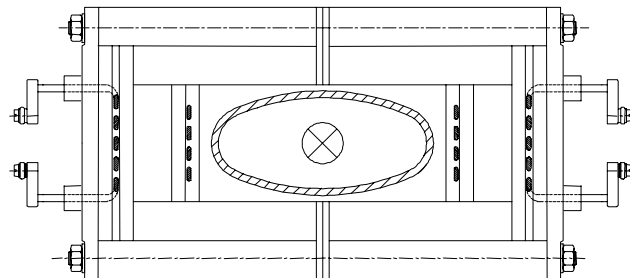


Figure 35.15: Schematic cross-section of the injection bumper magnet featuring 4-turns.

Since the magnet is designed to be installed outside the machine vacuum, the use of a ceramic vacuum chamber is required, because a metal chamber would seriously attenuate and disperse the pulsed magnetic fields. However, a small electrical conductivity is necessary to avoid a large coupling impedance seen by the beam. Therefore, the ceramic vacuum chamber is coated with a metallic layer, thick enough to ensure that the coupling impedance remains small and sufficiently thin to allow a good penetration of the magnetic field provided by the bumper.

The horizontal field-distribution on the median plane has been calculated for nominal excitation and measured at very low excitation with a strip-line probe; both curves are presented in Fig. 35.16.

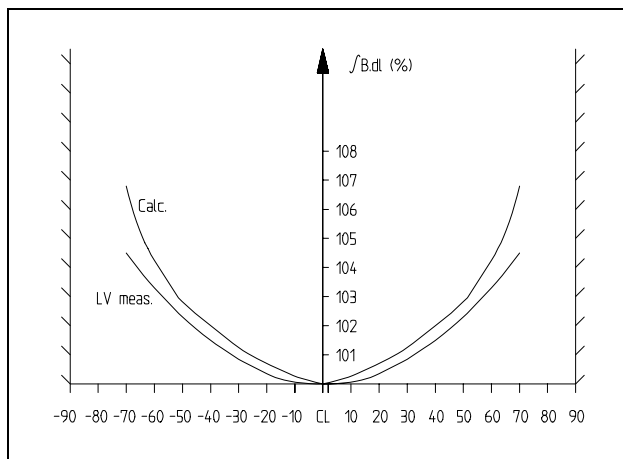


Figure 35.16: Horizontal field distribution across the injection bumper aperture. The principal design data for the magnet are given in Tab. 35.6.

Table 35.6: Principal design data for the injection bumper magnets.

Number of magnets/section		One	
Type		Lumped inductance	
Construction		Double C-core with one 4-turn back-leg winding each. Windings connected in series	
Ferrite types		Philips 4A4 / CMD5005	
Magnet box size	w	351	mm
	h	197	mm
	l	225	mm
Physical aperture	w	180	mm
	h	85	mm
	l	225	mm
Inductance	total	13.77	μH
	strays	4.77	μH
	effective	9	μH
Ferrite length		150	mm
Effective magnetic length		190	mm
Useful horizontal field region	$\pm 1\%$	± 40	mm
	$\pm 0.5\%$	± 24	mm
Nominal kicker strength		110	G.m
Nominal excitation		1100×4	A.turns
Corresponding air gap flux density		641.1	G
Mean ferrite flux density		2611	G
Mean remanent $\int B dl$		> 0.5	G.m
Pulse collapse time		120-300	μs

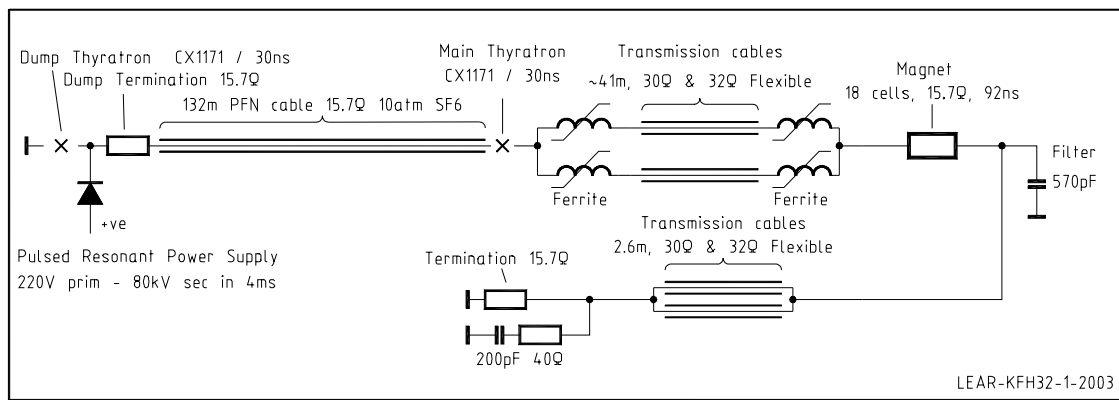
The required nominal $\int B dl$ per bumper of 110 G.m corresponds to a peak magnet current of 1100 A. Four individual pulsed power supplies will excite the four bumpers. The decreasing injection ramp will be variable between 120 μs and 300 μs ; with a nominal value of 210 μs . Linearity of the injection ramp will be $\pm 2\%$. Compensation for the finite particle flight time between the four bumpers can be achieved by differential timing of the four pulsed power supplies.

35.5.2 Extraction Kicker

The extraction kicker system is based on a magnetic rigidity of 4.8 Tm. A kick of 6.4 mrad is required to place the beam in the extraction septum high field region. This corresponds to a kick strength of 309 Gm. A maximum total kick strength of 440 G.m can be achieved with the use of two delay-line type magnets that were previously used in LEAR as injection kickers.

The two identical modules are of cellular closed aperture C ferrite-loaded transmission line construction of characteristic impedance 15.7Ω . They are mounted in a single vacuum tank, ER.KFH32/34 and can be baked in situ up to 300 °C in order to satisfy the machine vacuum quality requirements.

A further single kicker module, formerly used for LEAR extraction, is available for possible use as a diagnostic kicker.



35.6 ELECTRON COOLING

35.6.1 Phase Space Cooling

Tests in 1997 have shown that it is possible to cool a Pb⁵⁴⁺ beam of a total $\Delta p/p = 5 \times 10^{-3}$ (maximum offset between ions of the injected beam and the stack) and emittances of more than 50 mm mrad in less than 400 ms using a 3 m long electron cooler providing a 100 mA electron beam with a transverse temperature of 150 meV. The electron cooler used for these tests has been installed on the AD machine; therefore a new device has to be built. The objective is to cool the ion beam as fast as possible (0.2 s and even faster) by using all the modern features of an electron cooler.

The cooling down times have been discussed in many papers [5]. The problem is somewhat different from the cooling of a normal beam as pulses injected at a relatively large amplitude and large momentum spread have to be cooled and transported into the stack. To estimate the time for this we write the cooling rate as

$$\frac{1}{\tau} = \frac{1}{k} \frac{Q^2}{A} \eta_c L_c r_e r_p \frac{j}{e} \frac{1}{\beta^4 \gamma^5 \Theta^3}$$

with :

$k=0.16$	a constant depending on the distributions of ions and electrons,
$Q=54, A=208$	the charge and mass number of the ions, here Lead 54+,
$\eta_c=(0.037)$	the fraction of the circumference occupied by the cooling device (3m over 78.5 m at LEIR),
$L_c \approx 10$	the Coulomb logarithm,
$r_e=2.8 \cdot 10^{-15} \text{ m}$	the classical electron radius
$r_p=1.54 \cdot 10^{-18} \text{ m}$	the classical proton radius
$j[\text{A/m}^2]$	the current density of the electron beam,
Θ	the rms angular spread between the electron and the ion beam (given by the ion and electron transverse temperatures and misalignments).

By assuming that cooling is completed (i.e. the required emittances obtained) after three time constants and that the starting emittance is 80 mm mrad, the measurements from 1997 agree well with theory. Probably due to the length of the cooler section, the relation with the current density (see Fig. 35.18) is likely to be $j^{0.7}$. Using these measurements, the same Twiss parameters at the electron cooler ($D = 0 \text{ m}$, $\beta = 5 \text{ m}$) and the same interaction length (3 m), it follows that the electron cooler should be able to provide a current of $\sim 300 \text{ mA}$ to cool the beam down to the foreseen emittances in 200 ms. In 1997 it was also shown that β function values around 5 m are suitable for the best possible cooling rate, but also that a non-zero dispersion improves the cooling rate. For ease of daily operation it has been chosen to use zero dispersion at the cooler. The ion beam is then at the same position in the electron cooler whatever the momentum of the particles.

35.6.2 Electron Cooler Device

The proposed electron cooler will be built by a collaboration between the BINP Novosibirsk and CERN. It is a modern version of devices which are presently in use in many laboratories worldwide and also at CERN on the AD machine. The principal parts of an electron cooler are shown in Fig. 35.19.

- A gun provides a dense quasi-monoenergetic electron beam. By monoenergetic we suppose that the longitudinal ($\Delta e\sigma$) and transverse ($\Delta e\perp$) electron energy spreads at the gun exit are much smaller than the corresponding ion energy spreads.
- The beam is expanded by a dedicated solenoid and is bent by a toroid in order to merge with the ion beam to be cooled in the drift space.
- At the end of the drift space the electron beam is bent away from the ion beam and finally collected.
- The overall system is embedded in a longitudinal magnetic field to counteract the electron beam space charge forces and to “magnetise” the electrons (the electrons execute Larmor circles around

the magnetic field lines and this in turn has significant impact on the cooling forces experienced by an ion in the cooler).

The electron cooler developed by BINP for IMP Lanzhou in China [11], shown in Fig. 35.20, has the performance requested for LEIR and has served as a basis for our design and cost estimate. Detailed specifications of the overall LEIR electron cooler are given in [12].

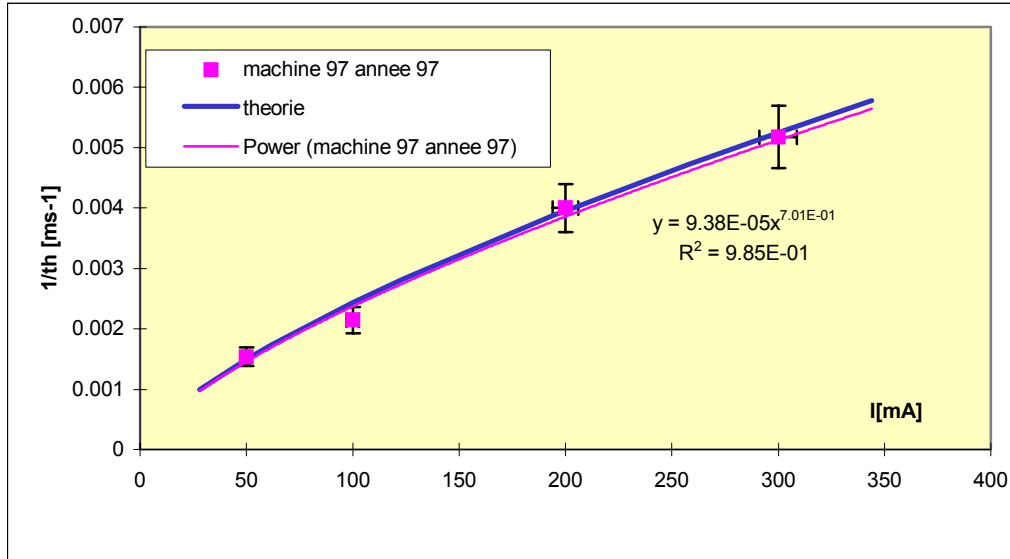


Figure 35.18: Cooling rate measurements made in 1997 in LEAR with an electron cooler with an interaction length of 3 m and a lattice which provides the same Twiss parameters as foreseen in LEIR. A theoretical line (thick) is drawn using the formulae explained in the text and a trend line (thin line) shows the best fit.

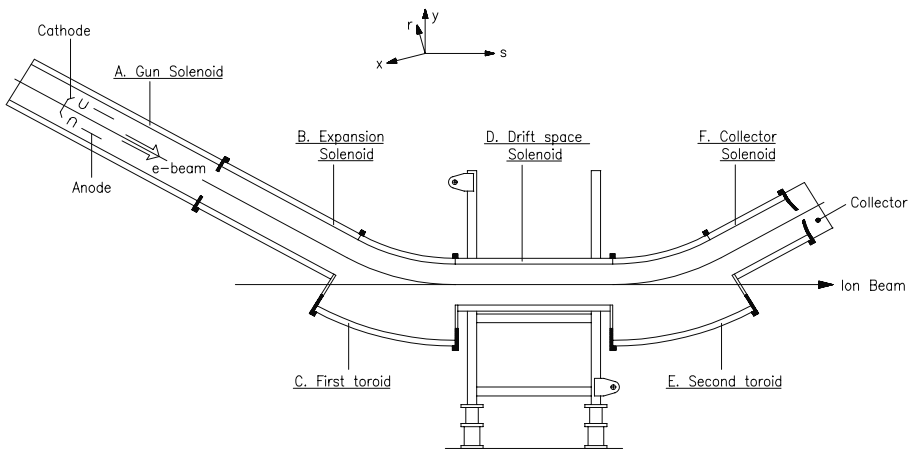


Figure 35.19: Electron cooler general layout.



Figure 35.20: IMP Lanzhou electron cooler, general view.

35.6.3 Special Features for the LEIR Electron Cooler

Taking into account recent improvements tested on various electron coolers during the last decade, it is planned to use a high permeance, variable density gun followed by an adiabatic expansion provided by an additional solenoid (Fig. 35.19).

The high permeance aims at providing an electron beam with a high density in order to decrease the cooling rate (see Sec. 35.6.1). However, increasing the electron density induces first an increase of the recombination rate (ions may capture an electron from the cooler and, finally be lost hitting the vacuum chamber) which is detrimental to the ion beam lifetime [5] and secondly increases the electron azimuthal drift velocity and thus increases the cooling time. For these reasons the electron gun will incorporate a “control electrode” which will be used to vary the density distribution of the electron beam [13, 14]. In this way the lifetime of the cooled ion beam will be increased by a reduction of the recombination rate of the ions with the electron beam. The electron beam profile is adjusted so that the density at the centre, where the stack sits, is smaller and thus the recombination rate is reduced. At larger radii, the density is large and allows efficient cooling of the injected beam executing large betatron oscillations.

The principles of a high permeance ($6 \mu\text{P}$) gun are given in [15]. Details of a possible gun for LEIR based on [15] are given in [16] where it is shown that to obtain such densities it is mandatory to use a convex cathode embedded in a strong magnetic field which, in the case of the study, was of the order of 0.6 T. With a magnetic field of 0.6 T the induced kick on the ion trajectory, at the level of the toroid, would be difficult to compensate. For this reason it is planned to have a dedicated solenoid to provide an adiabatic magnetic field decrease, by a factor k , between the gun and the toroid. As a consequence, the electron beam radius at the cathode “ r_c ” will be multiplied by $k^{1/2}$ at the end of the adiabatic solenoid. With such an expansion, the cooling force is also optimised as the electron beam size is adapted to the dimensions of the ion beam and the transverse velocity of the electron beam is reduced by the factor $k^{1/2}$.

35.6.4 Main Parameters

The main parameters of the electron cooler are given in Tab. 35.8. Two operational regimes will be used depending on the momentum of the ions to be cooled. If the small normalised emittances required cannot be reached at injection energy e.g. due to direct space charge detuning, operation of the electron cooler at higher energy allows cooling again at higher energy. In this scenario (unlikely for Pb ion operation, but a possible option for an eventual later upgrade to lighter ions) the cycle must contain an additional plateau at a suitable higher energy.

Table 35.8: Main characteristics of the electron cooling device

Electron beam energy	2.3 keV to 6 keV	6 keV to 40 keV
Electron beam intensity	0.05 A to 0.6 A	up to 3 A
Ion beam momentum·c	88.6 MeV/u to 143 MeV/u	143 MeV/u to 378 MeV/u
Adiabatic factor k		1 to 3
Electron beam radius		14 mm to 25 mm
Maximum B field at the gun		0.235 T
Relative current losses		<10 ⁻⁴
Collector permeance		25·10 ⁻⁶ A·V ^{-3/2} or 25 μP
Maximum energy spreads		$\Delta_{e\sigma} = 1 \text{ meV}$, $\Delta_{e\perp} = 100 \text{ meV}$
Drift space length		2.5 m
LEIR machine Twiss parameters at the cooler		$\beta_h = \beta_v = 5 \text{ m}$, $D = 0 \text{ m}$

35.6.5 Electron Cooler Magnetic System.

The magnetic field B must be uniform in order to ensure good cooling efficiency. Accurate measurements have to be done in order to fulfil the required parameters detailed in [17]. Independent of the gun requirements, a high magnetic field is welcome for improving the cooling process. On the other hand, as mentioned before, the vertical component of the magnetic field in the toroids induces a horizontal kick on the ion beam. The maximum field will therefore be 0.1 T in the toroids and the drift space. The transverse component B_\perp must be kept very small so that the ratio B_\perp/B never exceeds 10^{-4} all along the electron trajectory. To achieve this field quality, careful adjustment of the “pancake” structure of the solenoids needs to be made before final installation in the ring. Some emphasis has to be put on the adiabatic solenoid and on the toroids which might induce an unacceptable transverse magnetic field component and therefore increase the electron transverse temperature.

35.6.6 Collector.

An efficient collector is mandatory in order to obtain very small electron losses and therefore a small vacuum pressure increase. The system designed for the IMP Lanzhou cooler, making use of a repeller, a collector cup and an electrostatic deflection in the toroid chamber has given promising results and has been retained for the LEIR electron cooler.

35.6.7 Beam Diagnostics Associated with the Electron Cooler

To optimise the cooling process, some emphasis has to be put on the beam monitoring system (see Sec. 35.10). It is planned to install:

- Two H+V position pickups placed at opposite ends of the drift space. The aim is to measure the electron and ion trajectories, if possible simultaneously. The expected resolution is 0.1 mm to ensure that electron and ion beams are aligned within an angle less than 0.05 mrad.
- A recombination detector placed in the first dipole following the electron cooler. It will enable the evaluation of the radiative and dielectric recombination rates between the ions and the electrons.
- Ionisation profile monitors for both transverse planes. Their spatial resolution should be 1 mm and their time resolution 20 ms.
- Longitudinal and transverse Schottky pickups.

35.7 ACCELERATION AND FEEDBACK SYSTEMS

35.7.1 RF Overview

The role of the LEIR RF is to bunch the accumulated lead ions and accelerate them to a point where they can be injected into the PS machine. The moderate ramp rate envisaged leads directly to a (peak) RF voltage requirement of only 4 kV. However, the momentum spread of the beam at the end of cooling implies capture

voltages some three orders of magnitude smaller than this and hence the voltage resolution has been specified at 60 dB. The bandwidth requirement of the system is also large. The frequency swing from injection (at a magnetic rigidity of 1.1 Tm) to extraction (at 4.8 Tm) is 0.72 to 2.84 MHz for operation on harmonic $h=2$. The early scheme employing $h=1$ in the initial stages of operation extends the lower frequency requirement down to 0.36 MHz. Two identical RF systems will be installed in LEIR. They will be driven by low-level hardware making extensive use of digital signal processing.

LEIR must deliver a total of 9×10^8 in 2 bunches of 0.05 eVs/u each or, in the early scheme, 2.25×10^8 ions in a single bunch of 0.025 eVs/u.

35.7.2 High-power RF System

The LEIR RF system is mainly characterised by its wide frequency range. This and the small space available for installation, suggest the use of high-permeability materials like magnetic alloys. The relatively low gap voltage makes for a system of reasonable scale.

Finemet® is the magnetic alloy material of choice because of the high value of its figure of merit, $\mu_p Q f$, which is not affected by any change in magnetic flux density, B_{RF} , at least up to 200 mT. In addition, its very low quality factor (see Fig. 35.21), Q , allows the entire frequency range to be covered without any external tuning system. It has a nanocrystalline structure which is obtained by melting Fe, Si, B, Cu and Nb together and subsequently cooling them in the shape of a ribbon, which is then annealed. The ribbon is formed on a SiO_2 support that electrically isolates neighbouring layers when the ribbon is wound on toroidal frames to form the flat ring magnetic cores. The Curie temperature (570°C) of Finemet® is considerably higher than that ($\sim 200^\circ\text{C}$) of NiZn ferrites and Fe-based amorphous materials. This characteristic allows a much higher power dissipation inside the cores without any risk of non-linearity. The maximum acceptable power dissipation, P_d , is about 10 W/cm^3 .

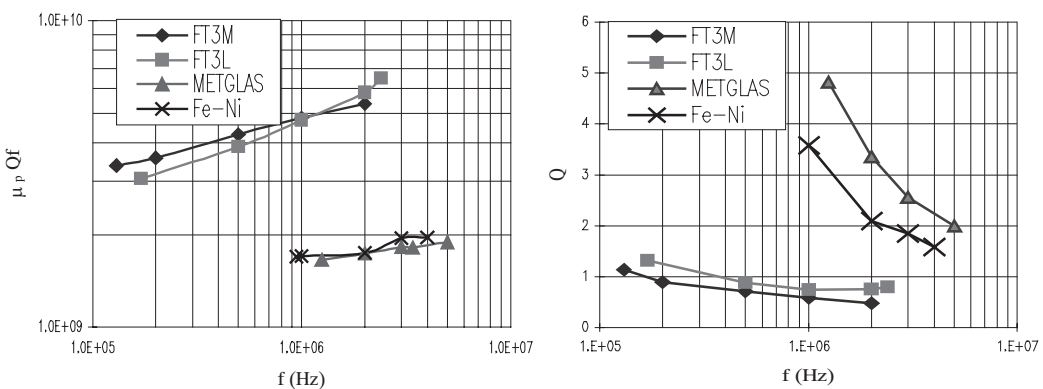


Figure 35.21: Figure of merit and quality factor for Finemet® FT-3L (polarised) and FT-3M (unpolarised) core types compared with two amorphous soft magnetic alloys (courtesy of C. Ohmori).

A collaboration established with the KEK laboratory in Tsukuba (which has already manufactured Finemet® cavities) provides support in terms of R&D and reduces risks and manpower requirements. According to extensive studies performed at KEK [18], the best choice of Finemet® material is the FT-3M type.

The RF cavity is a coaxial resonator with the accelerating gap in the centre (see Fig. 35.22). Its impedance is strongly affected by the number of magnetic cores, the amplifier output impedance and the way in which the amplifier is connected to the cavity. A dedicated study [19] has led to the adoption of 6 cores per cavity and to the connection scheme of Fig. 35.23. This assures the coverage of the full frequency range at the required gap voltage with the selected RF tube. The most efficient way of cooling the cores is by immersion in demineralised water. For this reason, two separate water tanks, each containing three cores, are used and the Finemet® surface is protected against degradation by means of an epoxy coating and vinyl ester painting. The RF path inside the cavity has been designed to allow the heating jackets for the vacuum chamber bake-out to remain in place during operation. A gap relay allowing switching within about 20 ms is planned in order to short circuit the gap when the cavity is not in use. During accumulation, the gap will be closed and,

thus, the additional coupling impedance seen by the circulating beam is negligible during that time. When the gap relay is opened for bunching and acceleration, a significant contribution to the longitudinal coupling impedance is expected (the largest value of Z_n/n is expected for $n = 1$ with an upper limit $Z_l < 300 \Omega$). The main cavity parameters are summarised in Tab. 35.9.

Table 35.9: Cavity parameters at various frequencies.

	0.35 MHz	0.70 MHz	3.50 MHz	5.00 MHz
V_{gap} (max) [kV]	1	4	4	4
P_{cavity} [kW]	2.6	33.4	25	24.6
B_{RF} [mT]	16	33	6.6	4.6
P_d [W/cm ³]	0.06	0.8	0.6	0.6
Cavity impedance [Ω]	195	240	320	325
Cavity length [m]			0.4	

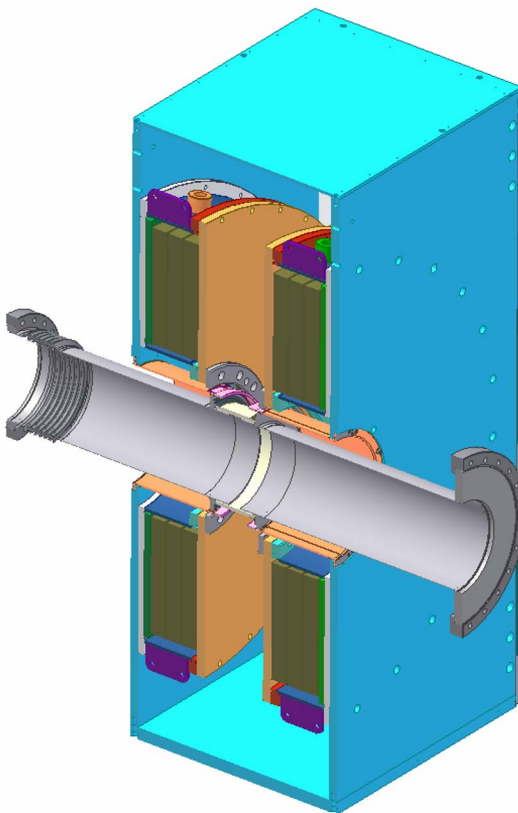


Figure 35.22: LEIR RF Cavity.

The LEIR RF cavity is basically a push-pull device. The very loose coupling between the two cavity halves imposes a differential drive and thus a push-pull configuration for the final amplifier. Due to the wide bandwidth response, the gap voltage harmonic content will be very much dependent on the form of the anode current of the tube. Nevertheless, the beam will experience the differential voltage existing between the two gap sides and cancellation will occur for even harmonics. The amplifier linearity can thus be treated as for a usual class AB device.

The frequency response of the system strongly depends on the additional capacitance introduced in parallel to the cavity gap. This is mainly dominated by the output capacitance of the tube and the characteristic impedance of the connection lines. The latter have been chosen at the high end of practical dimensions. The low-frequency response is mainly affected by the final tube anode chokes, whose inductance has to be

maximised. Unfortunately, this requirement clashes with the need to place the first series resonance of the choke above the maximum working frequency and requires some compromise.

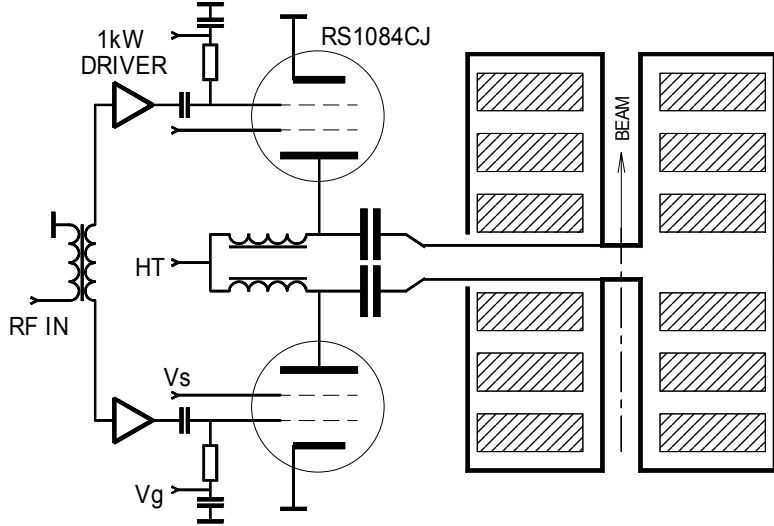


Figure 35.23: Final amplifier schematic diagram.

The RS1084CJ tube has been selected for this application from those already used in the PS Complex, as it can provide a peak current of 40 A and can dissipate 70 kW [19]. Each side of the amplifier is driven by a specially developed wideband 1 kW solid-state amplifier, which provides a gain of $58 \text{ dB} \pm 1.5 \text{ dB}$ in the frequency range 0.2 to 10 MHz. The behaviour of the whole system has been extensively simulated by means of the code Spice and the results are summarised in Tab. 35.10.

Table 35.10: RF Amplifier parameters (per tube) at various frequencies.

	0.35 MHz ($V_{\text{gap}} = 1\text{kV}$)	0.70 MHz ($V_{\text{gap}} = 4\text{kV}$)	3.50 MHz ($V_{\text{gap}} = 4\text{kV}$)	5.00 MHz ($V_{\text{gap}} = 4\text{kV}$)
V_{HV} [kV]		5.5		
V_{grid} [V]		-215		
V_{screen} [V]		1500		
I_{anode} [A]		3		
I_{anode} (peak) [A]	6.9	20.8	16.7	23.9
P_{anode} [kW]	17.4	21.8	21.6	35
$I_{\text{power supply}}$ (rms) [A]	3.4	7.0	6.2	8.6

35.7.3 Low Level RF System

The low-level RF system makes use of electronic circuits developed at the Brookhaven National Laboratory. The architecture is based on a DSP motherboard employing the VME standard. Three different types of daughter board can be attached (4-channel modulator, 4-channel receiver, master DDS). The daughter boards also have some inherent flexibility as they include programmable logic. The complete low-level system will comprise three DSP boards: one that computes the frequency program from the measured magnetic field and includes the radial loop, a second providing the master clock together with the phase and synchronisation loop and a third for the cavity servo (amplitude and phase control). This set-up will condense the entire low-level hardware into a single VME crate, with more remote control capabilities than ever before. Tests of a prototype have only been partial; work still needs to be done on both the hardware and software sides.

35.7.4 Transverse Damper

The transverse damper system is largely a copy of the one presently in use at the CERN PS Booster. It is a wideband (100 MHz) system with an analogue electronic chain between pick-up and kicker. It includes a variable gain pick-up amplifier, a beam offset suppression unit that acts on the differential gain of the pick-ups, an automatic variable delay (switched coaxial cables) that tracks the flight time of the particles and a power amplifier.

35.8 POWER CONVERTERS

Table 35.11: Power converters for the LEIR magnet system

Converter type	Nominal current(A)	Nominal Voltage(V)	Mode of operation	Topology	Origin (comm.=commercial)	Tolerances, (reproducibility Voltage ripple)	Quantity	Use
SM2K	1500	46	DC	1 quadrant Thyr. 12P//	LEAR	$5 \cdot 10^{-3}$ at 50Hz 10^{-2} at 300Hz	1	ER.SMH11 Inj. septum
R121	3300	+500 -450	Function	2 quadrant Thyr. 12P//	Exper. area	$2 \cdot 10^{-3}$ at 50Hz ¹ $3 \cdot 10^{-3}$ at 600Hz 10ppm ²	1	LEIR Bends
RB2	300	+200 -180	Function	2 quadrant Thyr. 6P	LEP	$2 \cdot 10^{-3}$ at 50Hz 10^{-2} at 300Hz 10ppm ²	1	Main Quads ER.QFN10 ..
RB10	400	+ 250 -225	Function	2 quadrant Thyr. 6P	LEP	$2 \cdot 10^{-3}$ at 50Hz 10^{-2} at 300Hz 10ppm ²	4	Main Quads
C6x2s	\pm 20	\pm 150	Function	4-quadrant, linear mode	New, comm.	50ppm (ripple with 200mH load)	12	Sextupoles (normal and 2 skew)
C6	\pm 20	\pm 75	Function	4-quadrant, linear mode	New, comm.	50ppm (ripple with 200mH load)	4	Skew quadrupoles, Vert. dipoles in SS20
S50T	\pm 50	\pm 40	Function	4-quadrant, switch mode	LEAR	120mV at 20kHz	4	Trims on main quadrupoles
S100	\pm 100	\pm 30	Function	4-quadrant, switch. mode	LEAR	270mV at 20kHz	14	ER.DEH21,22, ER.DVN12,31,41,42, Back leg for hor. dips
S150 LV	\pm 150	\pm 20	Function	4-quadrant, switch. mode	LEAR	120mV at 20kHz	8	Pole face windings for vertical dip. comp.
S150 HV	\pm 150	\pm 70	Function	4-quadrant, switch mode	LEAR	270mV at 20kHz	2	Pole face windings for sextupole comps
S250	\pm 250	\pm 30	Function	4-quadrant, switch mode	LEAR	120mV at 20kHz	4	Hor. dipoles
Ejection Septum	30400	2000	Pulsed	Capacitor discharge	New	<100 ppm	1	ER.SMH40 Ej. septum
Total							56	

¹⁾ figures valid for maximum current, at lower currents the voltage ripple is smaller by a factor ~2

²⁾ ½ hour cycle to cycle reproducibility

35.8.1 Introduction

The powering system for the I-LHC project has a diversity of converter types due to the vast range of power converters and the constraint to re-use existing equipments within a minimum cost.

Different technologies and topologies of power converters will be implemented depending on the characteristics and performances required. Thyristor line commutated technology will be used for the power converters above 50 kW and up to 1.7 MW needed for the main magnets of the LEIR machine. Switching technology will be used for the low power requirements. Power converters based on capacitor discharge technology with flat-top currents up to 30.4 kA are required for the ejection septum and fast magnets. High voltage power converters up to 7.5 kV, 25 A for RF or 6500V, 5mA for electron cooling complete the wide range of converters needed for the I-LHC project.

Table 35.12 Power converters for the LEIR Electron Cooler

Converter type	Nominal Current (A)	Nominal Voltage (V)	Mode of operation	Topology	Origin (comm.=commercial)	Tolerances	Quantity	Use
RB2	300	200	DC	1 quadrant Thy. 6P	LEP	$2 \cdot 10^{-3}$ at 50Hz 10^{-2} at 300 Hz 100 ppm ¹	1	Main solenoid (along drift tube)
R14	500	300	DC	1 quadrant Thy. 6P	SPS	$2 \cdot 10^{-3}$ at 50Hz 10^{-2} at 300 Hz 100 ppm ¹	1	Electron gun and collector solenoid
RB9	720	350	DC	1 quadrant Thy. 12P//	LEP	$2 \cdot 10^{-3}$ at 50Hz $5 \cdot 10^{-3}$ at 300 Hz 100 ppm ¹	1	Toroid coils
R2E	1000	110	DC	1 quadrant Thy. 12P//	LEAR	$2 \cdot 10^{-3}$ at 50Hz $5 \cdot 10^{-3}$ at 300 Hz 100 ppm ¹	1	Compensation solenoids
C4	20	35	DC	1 quadrant switch mode	New comm.	100 ppm ¹	1	Cathode heating
C6	± 20	± 75	DC	4 quadrant Lin. mode	New, comm.	50 ppm current ripple with 200 mH load	22	Dipoles
B1	0.02	6500	Function	1 quadrant switch mode	New, comm.	10 ppm ¹	2	Cathode and “grid” of the gun
B2	0.005	6500	DC	1 quadrant switch mode	New, comm.	100 ppm ¹	4	Electrostatic “bends” in toroids
B3	0.04	3500	DC	1 quadrant switch mode	New, comm.	100 ppm ¹	1	Repeller
B5	± 0.01	± 2000	Function	bipolar linear	New, comm.	100 ppm ¹	1	Control electrode (generating hollow beams)
A3	5	5000	Dc	1 quadrant switch mode	New, comm.	100 ppm ¹	1	Collector
Total							36	

¹ 8 hours stability

Table 35.13: Power converters for the LEIR RF system

Converter type	Nominal current (A)	Nominal Voltage(V)	Mode of operation	Topology	Origin (comm.=commercial)	Tolerances (Voltage ripple, Stability)	Quantity	Use
RF1	25	7500	DC	Resonant switching	New CERN spec	<1% for <1kHz <0.1% for 1kHz to 100 kHz $<10^{-4}$ for > 100kHz	2	High power for final amplifier tube
B4	1	2000	DC	1 quad. switch mode	New comm.	<15mV for 50Hz to 100 kHz <1% ¹⁾	3	Screen bias for final amplifier tube
B7	0.5	500	DC	1 quad. Switch mode	New comm.	<15mV for 50Hz to 100 kHz <1% ¹⁾	3	Grid bias for final amplifier tube
C2	100	40	DC	1 quad switch mode	New comm.	<15mV for 50Hz to 100 kHz <1% ¹⁾	6	RF driver power supply
Total							14	

¹⁾ 8 hours stability

In general, the global overall precision on the current or the voltage, depending of the physical use of the power converters, is 100 ppm. The medium and high power converters will be re-used from LEAR, PS, SPS and LEP. The equipment will be refurbished and adapted to the PS type standard 1553. The refurbishment will also include a modernisation of the topology. Despite the various sources of equipment, optimum standardisation will be applied to facilitate operation and converters maintenance. To avoid supplementary interface costs, the RS 422 control for the commercial "off the shelf" power converters will be used. Industrial PLC will be used for the special control systems for RF and electron-cooling.

The existing housing infrastructure will be reused, e.g. the South generator building (250) and the so-called "zone H" in building 150.

35.8.2 Power converter overview

The 172 converters needed for the project have been classified by their functionality in the system. Their main characteristics, mode of operation, topology and origin are summarised in the following five Tabs. 35.11 LEIR Magnet System, 35.12 LEIR Electron Cooling, 35.13 LEIR RF system, 35.14 Injection and Transfer Lines, 35.15 PS and TT2. For each circuit, detailed information can be found in the Power Group database.

Table 35.14: Power converters for Linac 3 (those to be replaced) and the Linac 3 – LEIR – PS transfer lines

Converter Type	Nominal Current (A)	Nominal Voltage (V)	Operation Mode	Topology	Origin (comm.=commercial)	Tolerance (drift, ripple or reproducibility)	Quantity	Functionality
Mini-discap	20	600	Pulsed	Capacitor discharge	New	0.1 % Pulse to pulse	14	Dipoles Linac 3
Maxi-discap	320	1000	Pulsed	Capacitor discharge	New	0.1 % Pulse to pulse	10	Quadrupoles Linac 3 and ITE except ITE.QFN03
SM2K	2000	46	DC	1 quadrant Thyr. 12PP	LEAR	2×10^{-3} at 50Hz 5×10^{-3} at 600Hz	1	IP.SOLINJ Ion source solenoid
R2E	1000	110	DC	1 quadrant Thyr. 12PP	LEAR	2×10^{-3} at 50Hz 5×10^{-3} at 600Hz	5	ITE.BHN10, 20 and 30, EE.QFN10 and QDN20
N02	± 400	± 650	Inj/Ext ¹⁾	4 quadrant Th 6P circulation	New	2×10^{-3} at 50Hz 10^{-2} at 600Hz	1	ETL.BHN10
N05	1600	+35 -30	Inj/Ext ¹⁾	2 quadrant Thyr. 6P	New	2×10^{-3} at 50Hz 10^{-2} at 600Hz	1	ITE.BHN40
R14	500	300	DC	1 quadrant Thyr. 6P	SPS	2×10^{-3} at 50Hz 10^{-2} at 600Hz	1	EE.QFN30
RB2	300	+200 -180	Inj/Ext ¹⁾ DC	2 quadrant thyristor 6P	LEP	2×10^{-3} at 50Hz 10^{-2} at 600Hz	2	ETL.BHN20, EI.BHN10
RB9	720	350	DC	1 quadrant Thyr. 12PP	LEP	2×10^{-3} at 50Hz 5×10^{-3} at 600Hz	1	EE.BHN10 and 20 in series
C2 x2P	200	50	DC	1 quadrant switch mode	New, comm.	0.2 % 25mV at 50 Hz	2	ITE.QFN03, EI.BVN20
C3	70	40	DC	1 quadrant switch mode	New, comm.	0.2 % 25mV at 50 Hz	5	Quad's ETP, EI.BVN10, EI.QDN30, EI.QFN40
C4	20	35	DC	1 quadrant switch mode	New, comm.	0.2 % 25mV at 50 Hz	2	EI.QFN10 and EI.QDN20
C5 x3P	600	60	DC	1 quadrant switch mode	New, comm.		1	ETP.BHN10
C6	± 20	± 75	DC Inj/Ext ¹⁾	4-quadrant, linear mode	New, comm.	25 mV at 50 Hz	4	ETL.DHN10, EE.DHN10, EE.DVN10 and ETP.DVN10
C6 x3P	± 40	± 75	Inj/Ext ¹⁾	4-quadrant, linear mode	New, comm.	25 mV at 50 Hz	5	ETL.QNN10, 20, 40, ETL.BVN10 and 20
C6 x4P	± 60	± 75	Inj/Ext ¹⁾	4-quadrant, linear mode	New, comm.	25 mV at 50 Hz	3	ETL.QNN30, 50 and 60
Total							58	

¹⁾ Two distinct currents (for injection and extraction) will be provided at different moments within the same cycle.

Table 35.15: Power converter for the PS and the TT2 line

Converter type	Nominal Current (A)	Nominal Voltage (V)	Mode of operation	Topology	Origin	Tolerances (Voltage ripple, Precision, Stability)	Quantity	Functionality
Septum	18000	1700	Pulsed	Capacitor discharge	PS	100 ppm	1	PI.SMH26
Bump	100	2000	Pulsed	1 quad. switch. mode	PS	0.1 %	1	PS injection bumper
RB10	400	+250 -225	PPM degauss ¹⁾	2 quad. Thyr. 6P	LEP	5×10^{-3} at 50Hz 5×10^{-2} at 600Hz	5	TT2 line Quadrupoles
R14	500	+300 -270	PPM degauss ¹⁾	2 quad. Thyr. 6P	SPS	5×10^{-3} at 50Hz 5×10^{-2} at 600Hz	1	TT2 Quadrupole
Total							8	

¹⁾ Well defined cycling procedure in order to avoid shot-to-shot variations of the magnetic field due to remanence effects.

35.8.3 Power Converter for the LEIR Magnetic System

The power converter system for the LEIR machine is composed of 4 distinct families :

- Thyristor technology power converters will supply the main dipoles, the main quadrupoles and the injection septum.
- Re-used switching mode power converters will supply the majority of small correction circuits (trims on some quadrupoles, dipoles, sextupoles, pole face windings providing dipolar and sextupolar fields).
- Commercial converters used for sextupoles.
- Pulsed power converter for the ejection septum.

A global overall precision of 100 ppm is for all circuits is planned. For those converters working in function mode, the cycle-to-cycle reproducibility over a period of half an hour is 10 ppm. The dynamic behaviour is a compromise between the overshoot at the end of the ramp and the following error during the ramp. Typically, zero following time delay obtained by feed-forward compensation will lead to an overshoot of $\sim 10^{-3}$, while a following time delay of 2 to 20 ms will allow a non-overshooting response. Machine components like magnets and vacuum chambers also introduce sources of error resulting in additional time constants of the field. Therefore a global dynamic model of the machine will be established from experimental measurements. Depending on the results, appropriate corrections will be applied to the power converter current regulators.

Note that the power supply for the electrostatic injection septum ER.SEH10 is under the responsibility of the team constructing this hardware and, thus, described in Sec. 35.4.2.

Main dipole, quadrupole and injection septum converters

The main dipole (type R121) and the five quadrupoles (type RB10, RB2) converters consist of thyristor, line-commutated technology. The operation mode requires two quadrants insuring voltage bipolarity for rapid magnet current change between beam ejection and the next injection. The dipole converter is re-used from the North experimental area, while the quadrupole ones are re-used from LEP.

- Main dipole power converter :
12 Pulses Parallel (12PP) topology (Fig. 35.24) is used consisting of two sub-converters, each one composed of an 18 kV, 1.9 MVA oil immersed transformer, a six-pulse thyristor rectifier and a passive filter. The rectifiers are phase-shifted by 30° and connected in parallel resulting in a 12 pulse configuration. The two transformers are located in the same oil tank and will be installed in

an existing pit outside building 250. The two thyristor bridges are housed in one module adjacent to the two chokes containing the current measurement transducer module. A capacitor module completes the rectifier passive filter assembly located in building 250. The thyristor bridges and the filter chokes are water-cooled, while the rest of the equipment is air-cooled. The r.m.s. water losses over the LEIR cycle are ~ 15 kW, while the air losses are ~ 2 kW.

- Quadrupole power converters:
Power converters with classical 6 Pulse topology will supply the main LEIR quadrupoles. This topology is similar to that employed for the main dipoles, but using only one single sub-converter. Each air cooled converter is composed of a circuit breaker, a 400 V 50 Hz transformer, a thyristor bridge and passive filter assembled in one cubicle.
- Injection septum ER.SMH11 power converter :
A thyristor 12-P parallel topology power converter with passive filter (as the main dipole power converter) will supply the magnetic injection septum. It is supplied from the 400 V network via two transformers with secondaries phase shifted by means of dog leg windings. The use in DC mode requires one quadrant operation.

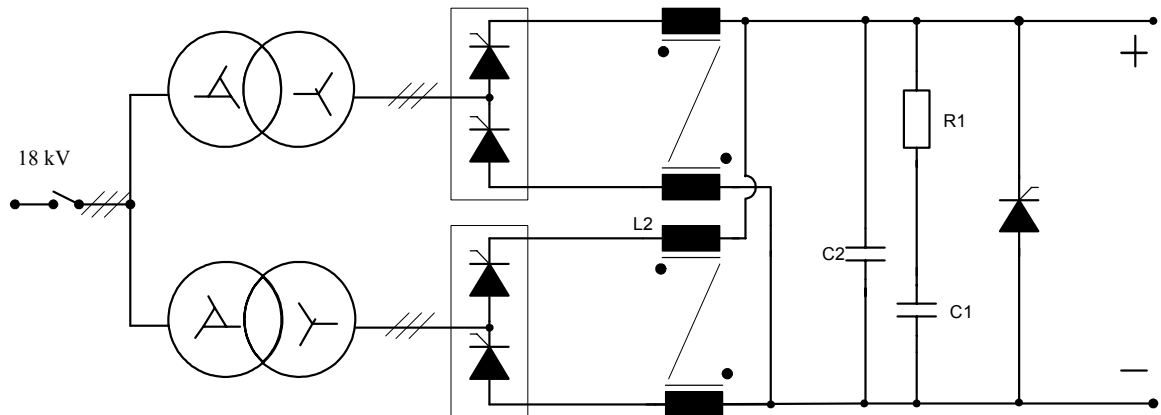


Figure 35.24: Thyristor power converter with 12PP topology

Power supplies for small correction magnets

Power converters installed to add small corrections on top of the basic lattice (i.e. trim power supplies, dipoles used for orbit correction and to create bumps for electron cooling and extraction and sextupoles) are divided into two groups :

- Recuperated power converters of types S50T, S100, S150-LV, S150-HV and S250 will serve as trim power supplies connected to quadrupoles around the electron cooler and to supply correction circuits. These auxiliary converters are transformed into switching mode, having 4-quadrant capability in the output voltage/current plane. Even though there are limiting power boundaries in the regenerative mode (2nd and 4th quadrants), these power limitations are compatible with the LEIR magnet characteristics in all cases. The converter topology is based on a 4-quadrant chopper bridge fed by a full bridge diode rectifier unit (Fig. 35.25).
- Some commercial power supplies (of type C6) needed for correction circuits will have to be bought “from-the-shelf” from industry. Output ratings required for these industrial modules are ± 20 A, ± 75 V with an overall precision of 100 ppm. The current ripple with a 200 mH load inductance is 50 ppm. The standard RS 422 will be used to interface with the PS control system. The type C6 x2s is a series association of 2 C6 type converters actually under study and will supply the sextupole circuits.

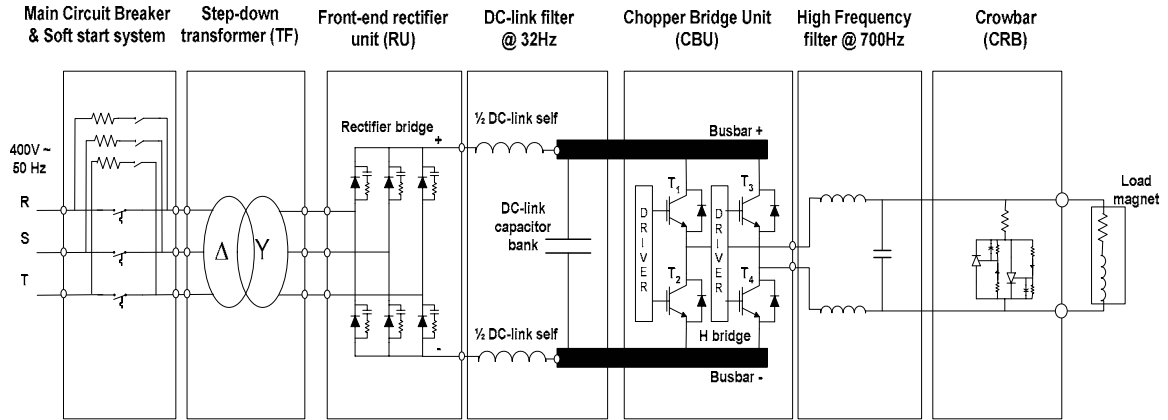


Figure 35.25: Simplified schematics of switch mode power converters supplying various correction circuits.

Power converter for the new ejection septum, ER.SMH40

The new LEIR extraction septum (see Sec. 35.4.3 for a description and Tab. 35.5 for design data) needs a current pulse of nominal 30.4 kA with a pulse-to-pulse reproducibility in the 100 ppm range. This is achieved, as sketched in Fig. 35.26, by a capacity discharge power converter (providing a primary current pulse with a total length of ~5ms with a flattop current of up to 3.3 kA) in combination with a matching transformer (increasing the current by a factor ~12) installed close to the magnet inside the LEIR enclosure. The principle of the power supply is based on the charge and discharge of capacitor banks with a third harmonic circuit. The current flat-top stability of 100 ppm during 500 μ s is achieved using an active filter power circuit. To reduce the cost of the spare parts, the power converter installed will be similar to the existing one [20] in the PS with some modifications (increase of the total capacitance, change of the 3rd harmonic choke, etc...).

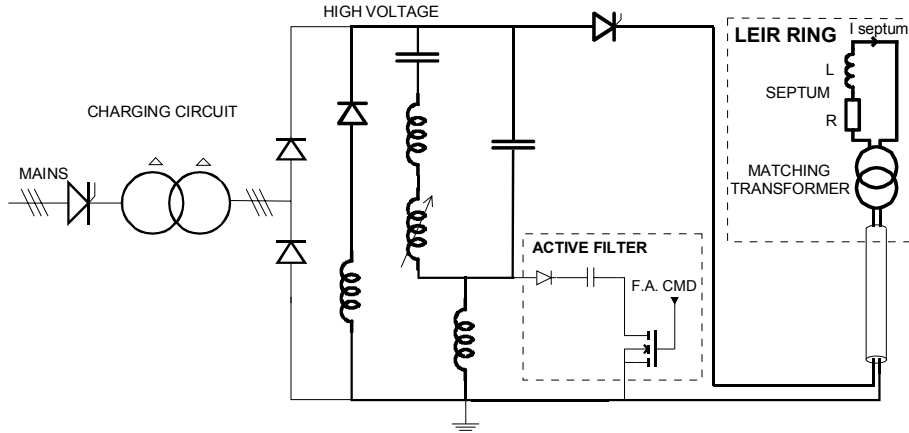


Figure 35.26: Sketch of the power converter for the extraction septum magnet ER.SMH40.

35.8.4 Electron Cooling Converters

Some relevant parameters for the power converters necessary for the LEIR electron cooler are compiled in Tab. 35.12. The main aspects are :

- Solenoid converters :

Thyristor line commutated converters will supply the 3 electron cooling solenoids and the compensation solenoids. They are of 6 P topology for type RB2, R14 and of the 12PP topology (Fig. 35.24) for the type RB9 and R2E. See Sec. 35.8.3 for general descriptions. The type RB9 and R2E are also supplied from the 400 V network, in this case via a single transformer with 2 secondaries phase-shifted by means of dog leg winding.

- Dipole power converter :
22 correction dipoles, which allow adjustment of the magnetic field direction of the cooler will be supplied by commercial type C6 power converters (already described in Sec. 35.8.3). The power converters will be controlled via RS 422 interfaces.
- High voltage power supplies at ground potential :
High voltage power supplies are necessary for the cathode and the electrostatic deflectors in the toroids. Commercial power supplies of types B1 (described in detail in [21]) and B2 will be operated in voltage controlled mode. These converters will be controlled by a PLC via a Profibus network.
- Power supplies at high potential (and isolated w.r.t. ground potential):
Several high voltage power converters will polarise various electrodes with respect to the cathode potential and one low voltage power supply will heat the cathode. These power converters must be floating and working at a potential of up to 4000 V and, thus, be installed in a Faraday cage. The PLC control system (Profibus) will be isolated by an optical link and the connection to the mains network will be done via an insulated transformer. In total, 5 such power converters (of type C4, B1, B3 and B5) will be installed.

35.8.5 Power Converters for the LEIR RF System

The LEIR RF system will be composed of two cavities working in the frequency range of 0.35 MHz to 5 MHz. An independent amplification chain will drive each cavity and the final power stage will be composed of two tetrodes mounted in push-pull configuration and working in class AB. The power converters needed to supply the RF system fall into two families :

- High voltage high power converters to supply the anode :
High voltage power converters will be built to a customer specification [22] and a CERN electronics control crate will be used. Two units are needed, each one driving two RF tubes each. A crowbar will be used to avoid an anode breakdown in case of a flash over inside the RF tube. These power supplies must provide a current of 25 A during a time interval of 2.4 s (out of a cycle lasting 3.6 s). The voltage is continuously adjustable up to a maximum of 7.5 kV. A resonant topology is well adapted at this voltage level.
- Low voltage, low power converters :
Off-the-shelf power converters [23] type B4, B7 and C2 will be used to supply the different RF auxiliary systems (preamplifier, screen and grid of the RF tubes). See Tab. 35.13 for the main data. Each power converter will be interfaced with the RF interlock system.

35.8.6 Power Converters for Linac 3 and the Linac 3 – LEIR - PS Transfer Lines

In this section, power converters to be replaced in Linac 3 and power converters to be installed for the transfer lines from Linac 3 to LEIR and to PS are described. An overview is given in Tab. 35.14. The magnet currents in the line ETL (see Chap. 36 for details) change in less than one second between injection and extraction and again after extraction and the next injection. Therefore power converters with 4 quadrant and 2 quadrant capabilities must be installed for the magnets concerned.

The main modifications and installations necessary are :

- Solenoid of the Linac 3 ion source :
The upgrade of the ECR ion source needs an increase of the magnetic field in the solenoid above the currently achievable level. A power converter previously used for one of the LEAR septa will be refurbished and used.
- Linac 3 dipoles :
The pulsed power supplies connected to these dipoles are not compatible with an increase of the repetition rate up to 5 Hz and thus have to be replaced. Despite the varying magnet characteristics (inductances vary from 6.53 mH to 12.0 mH and resistances from 2.60Ω to 4.36Ω) all Linac 3 dipoles can be supplied by identical power supplies of type MINIDISCAP. These capacity discharge power supplies (for a sketch see Fig. 35.27) use a power correction circuit, a switching capacity charger and an output stage which allows bipolar discharge currents with current flat-top. They will be controlled using MIL 1553 interfaces.

- Linac 3 and ITE quadrupoles (except ITE.QFN03) :

The pulsed power supplies of the quadrupoles in Linac 3 and in the ITE line have to be replaced in order to be compatible with the increase of the Linac 3 repetition rate to 5 Hz. It is important to keep the RMS current small to reduce the dissipated power to acceptable values. This has been achieved by adopting a trapezoidal pulse shape with steep current rise and fall (lasting about 500 μ s) and a useful flat-top of length ~500 μ s. Capacitor discharge power converters of type MAXIDISCAP (see Fig. 35.28 for a sketch) will be installed. A capacitor bank behaves as a DC voltage source during the rise and the fall of the current. The output bridge performs the voltage inversion and the current flat-top is achieved with a high power IGBT module. They will be controlled using MIL 1553 interfaces.

- Thyristor converters in the transfer line:

Several thyristor power converters (both recuperated ones and new ones) will be installed for magnets requiring relatively large power. For the magnets of the ETL line 4 quadrant (ETL.BHN10) and 2 quadrant (ETL.BHN20 and ITE.BHN40) capabilities are necessary to achieve fast current changes between injection and extraction settings. The topology employed is either 6 pulse or 12 pulse for one and two quadrant operation. The 4 quadrant is achieved using two 6 pulse systems with circulating current.

- Low power commercial power converters:

For several magnets with low power requirements, new commercial power converters will be installed. In general, several low power units will be combined to obtain the output power needed. Depending on the requirements (4 quadrant capabilities for magnets installed in the ETL line and one quadrant for the rest) switching mode and switch mode with linear output stage topologies will be employed. These converters will be controlled either by LPS2 interfaces via the MIL 1553 standard, or with RS 422 interfaces.

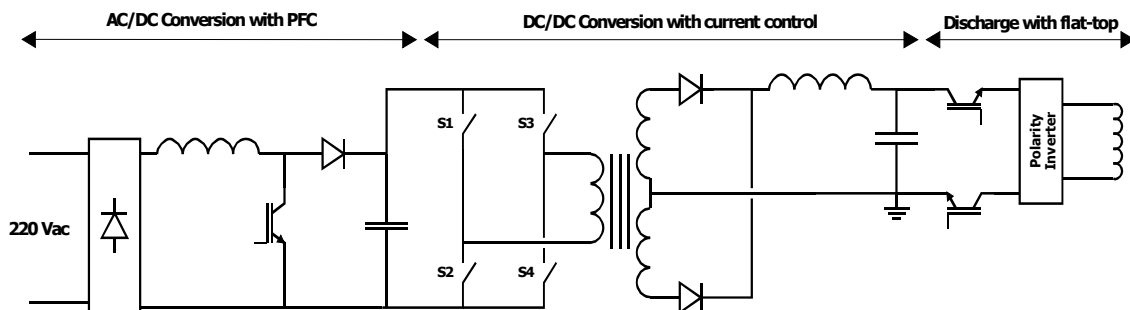


Figure 35.27: Sketch of a capacity discharge power supply of MINIDISCAP type.

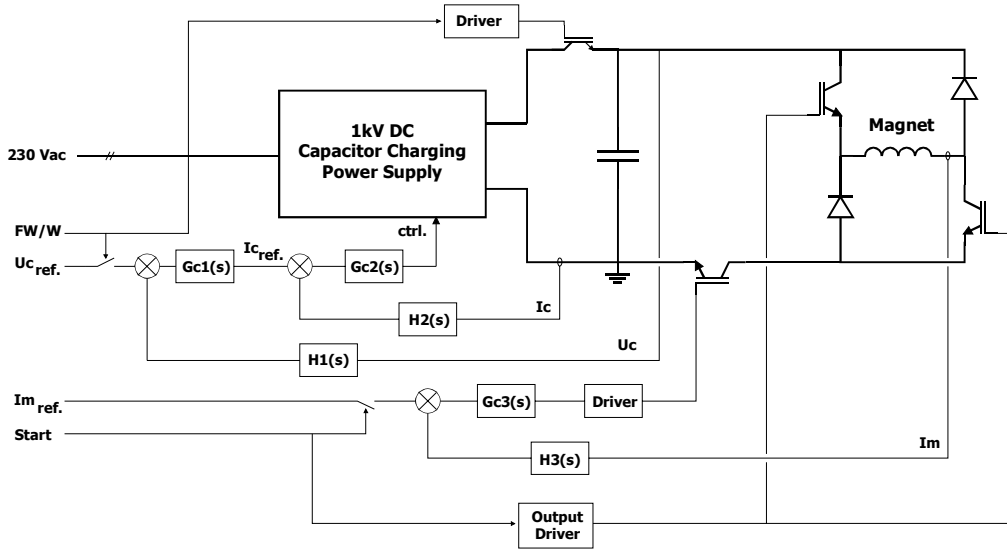


Figure 35.28: Sketch of a capacity discharge power supply of MAXIDISCAP type.

35.8.7 Converters for the PS and the TT2 Line

The main modifications of the PS machine and the TT2/TT10 transfer line (see Chap. 37) with implications for the power converters to be provided are (i) the new injection at a higher beam rigidity necessitating an orbit bump and an upgrade of the septum and (ii) the new low beta insertion for final stripping of the ions. The power supplies to be installed to cope with these requirements are listed in Tab. 35.15. The main aspects are :

- PS injection septum :
The principle employed (a combination of a capacity discharge power supply and a matching transformer) to reach the nominal current of 16 kA is similar to the one of the LEIR extraction septum described in Sec. 35.8.3, but with a different third harmonics circuit as sketched in Fig. 35.29. To reduce cost, two power supplies (one connected to the magnet and one spare) that have been used for lepton injection in the PS will be refurbished. The rectifier's diodes have to be replaced, the low voltage distribution and the relay system have to be checked and updated. The active filter and the electronic crate will be changed if necessary. The power converter will be synchronised with the PS complex using standard timing pulses and the control interface used will be MIL 1553.
- PS injection bump :
Two magnets will be powered in series by one capacity discharge power converter. The waveform is a simple half sine pulse with a maximum of 100 A and a duration of about 5 ms.
- Power supplies for the “low beta insertion” in TT2 :
In the framework of the implementation of a “low beta insertion” for final stripping of the ions in the TT2 line, two quadrupoles will be removed from their respective circuits and powered individually and four quadrupoles will be added. The latter four quadrupoles must deliver zero current for proton operation. In order to supply the six quadrupoles mentioned above, five power converters of type RB10 and one of type R14 will be installed. These power converters are of Thyristor type with 6P topology, each one housed in one cubicle and cooled by natural air convection and will be installed in building 250.

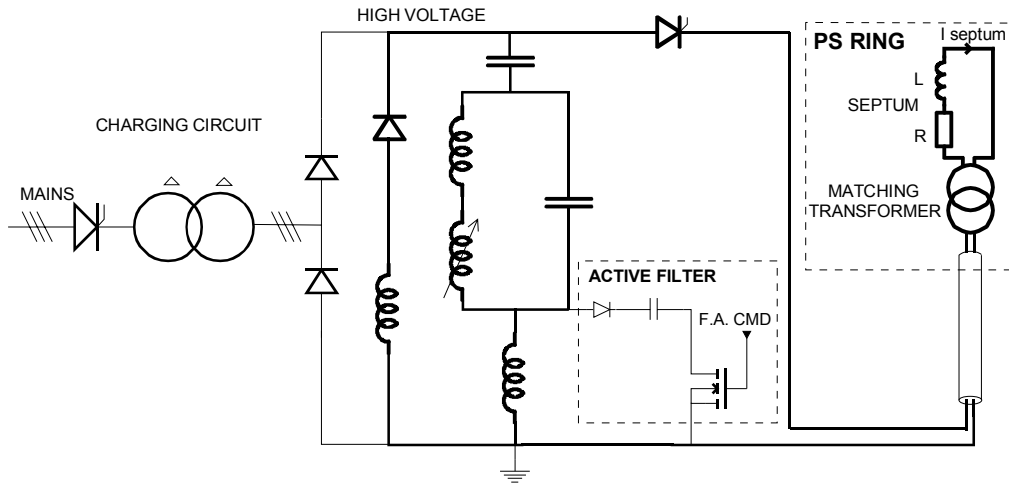


Figure 35.29: Sketch of the power converter for the PS injection septum magnet PI.SMH26.

35.8.8 Power Converter Control Electronics

Electronics for thyristor and switched mode converters

The General Regulation system (GEREG) is a versatile hardware system that can be adapted to control Power Converters of switching or thyristor type (6 or 12 pulse bridge).

It performs three main functions:

- Regulation:
 - Analogue mode, via a specific Regulation Loop card
 - Digital mode via a Digital Signal Processor card.
- Supervision:
 - Communication with the control room via MIL 1553 fieldbus for reference signal, command control and status information
 - Main Machine Interface: via a built-in Keyboard and display unit. The general status, output variables display, local control and constant settings are possible for each converter.
 - Fault logging: detection and storage of present and past faults for easier maintenance
- Fault Detection:
 - A hard-wired protection circuit controls the PC hardware via analogue and digital inputs and the Main Circuit Breaker is opened if unacceptable working conditions are detected.

The reference signal, usually the Load current, can be set via:

- GFAS: for function generation
- MIL 1553: for PPM or constant set-point
- Via Local keyboard for constant actions or tests

Because the GEREc has been designed almost independently of the PC hardware, it can be adapted to converters of any power level. Most of the cards, except the regulation ones, are common to both types of PC hardware.

Pulsed converter electronics

Capacitor voltage and charging current are regulated with a specific control system. For pulsed septum converters, temperature variations and magnetic effects are regulated by special electronics that slightly increases or decreases the capacitor voltage. Current flat top stability is achieved by the use of an active filter power circuit with a regulation control loop.

The electronics for this type of power converter uses MIL 1553 and a G64 interface for timing and controls. Different electronic regulation loops have been specifically designed for this type of power converter. Other electronic cards are PS standard.

35.8.9 B-Train of the LEIR Machine

Existing coils of the LEAR B-train will be reused. The associated electronics will be replaced with standard PS equipment. Two independent systems on different magnets will have their electronics housed in one rack located in the LEIR control room. The second system is a hot spare of the first one.

35.9 VACUUM SYSTEM

35.9.1 Introduction

During LEAR studies in 1997 the static vacuum pressure was about 5×10^{-12} Torr, but during continuous injection, a dynamic pressure increase by a factor five to 2.5×10^{-11} Torr (with local pressure bumps up to 10^{-9} Torr) was observed. This effect increased with beam intensity and limited the maximum intensity that could be accumulated. It has been attributed to the outgassing of vacuum equipment due to the impact of lost lead ions.

An intensive experimental programme on ion-induced gas desorption and its dependence on the surface preparation of stainless steel vacuum chambers started in 2001 in Linac3 [25, 26]. The experiments led to a good quantitative understanding of the phenomena observed at LEAR [27] and, in addition, allowed the demonstration of a “scrubbing” effect (reduction of the ion loss induced outgassing yield after continuous bombardment). The results obtained so far have been used as main input parameters for the design of the LEIR vacuum system.

To satisfy the requested 30 s beam lifetime, an average dynamic pressure of about 3×10^{-12} Torr is required around the LEIR ring [28]. Therefore, ultrahigh vacuum (UHV) technologies, that were developed for the Intersecting Storage Rings (ISR) and the Large Electron Positron Collider (LEP) and which have also been successfully applied to the LEAR machine, must be applied. In particular, a very strict choice of materials, vacuum pumps and instrumentation, cleaning procedures and an elaborate bakeout system are necessary to reduce the total dynamic outgassing rate to the 10^{-13} Torr $1\text{ s}^{-1}\text{ cm}^{-2}$ range and to have a negligible amount of leaks.

35.9.2 LEIR Vacuum Requirements

Beam Lifetime

A dominant contribution of the loss rate is charge-exchange (a Pb^{54+} ion captures or loses one electron) due to interactions with the residual gas. The beam lifetime due to this effect (hence disregarding losses due to other effects like recombination with electrons in the electron cooler) is specified to be 30 s. This beam lifetime can be expressed in the following way :

$$\frac{1}{\tau_{total}} = \frac{1}{\tau_{H_2}} + \frac{1}{\tau_{CH_4}} + \frac{1}{\tau_{CO}} + \frac{1}{\tau_{CO_2}} + \dots,$$

where $1/\tau_{total}$ is the loss rate due to interactions with the rest gas. Gas densities and pressures yielding a life-time of $\tau = 30$ s, if only one species is present in the rest gas, are calculated using Franzke’s [29] and Schlachter’s [30] formulae for estimating the charge exchange cross sections [28] for Pb^{54+} at 4.2 MeV/u. The results are summarised in Tab. 35.16.

During ion-induced desorption experiments in Linac3 it was found that the bulk of the molecules desorbed were CO (70-80%) [25] as had been observed qualitatively during the 1997 tests [5]. CO_2 and H_2 were the second most abundant species in the desorbed gas. Taking typical values (measurements in Linac3, Tab. 35.17) for the gas composition under heavy ion bombardment, an average dynamic pressure of $P_{dynamic} \approx 3 \times 10^{-12}$ Torr is necessary around the LEIR ring for a beam lifetime of 30 s.

Table 35.16: Required gas densities and corresponding pressures for a 30 s beam lifetime of Pb^{54+} ions at 4.2 MeV/u in LEIR. It is assumed that only one type of ion is present. The total cross sections (for electron capture and loss) were calculated with Franzke's [29] and Schlachter's [30] formulae.

Gas	<i>Franzke</i>	<i>Schlachter</i>	<i>Franzke</i>	<i>Schlachter</i>
	$\tau = 30 \text{ s}$			
	$n [\text{m}^{-3}]$	$n [\text{m}^{-3}]$	$P [\text{Torr}]$	$P [\text{Torr}]$
			@20°C	@20°C
H_2	$7.22 \times 10^{+11}$	$2.71 \times 10^{+13}$	2.20×10^{-11}	8.24×10^{-10}
He	$7.23 \times 10^{+11}$	$2.98 \times 10^{+12}$	2.20×10^{-11}	9.05×10^{-11}
CH_4	$1.46 \times 10^{+11}$	$2.30 \times 10^{+11}$	4.45×10^{-12}	6.99×10^{-12}
H_2O	$1.49 \times 10^{+11}$	$1.70 \times 10^{+11}$	4.54×10^{-12}	5.17×10^{-12}
N_2	$1.06 \times 10^{+11}$	$9.88 \times 10^{+10}$	3.23×10^{-12}	3.01×10^{-12}
CO	$1.07 \times 10^{+11}$	$9.88 \times 10^{+10}$	3.24×10^{-12}	3.00×10^{-12}
Ar	$9.50 \times 10^{+10}$	$8.33 \times 10^{+10}$	2.89×10^{-12}	2.53×10^{-12}
CO_2	$6.81 \times 10^{+10}$	$6.26 \times 10^{+10}$	2.07×10^{-12}	1.90×10^{-12}

Dynamic Pressure Calculations

To calculate the pumping configuration to fulfil the 30 s beam lifetime, the results obtained in Linac3 will be used as input parameters for the ion-induced desorption part of the outgassing of the vacuum chamber walls. One can distinguish between two scenarios of losses:

- If a lead ion changes its charge state in a straight section, it will be lost at the end of the following bending magnet and will impact under grazing incidence on the vacuum chamber wall. Since the capture cross section is about one order of magnitude larger than the loss cross sections [28], roughly 90% of the lost ions will impact on the 'outer part' (larger radius) of the vacuum chamber in the bending magnets.
- If the charge state is changed inside a bending magnet, in most cases the ion will be lost in the following straight section. In both cases the exact position of the lost ions depends on the optics of the machine.

The average dynamic pressure was calculated assuming that, to a first order approximation, lead ions will be lost continuously around the LEIR ring. It should be mentioned that due to the absence of residual gas ionisation [28], the assumption of 'homogenous' ion losses around the LEIR ring can be justified, because 'pressure bumps' of the ISR type will not limit the beam lifetime in LEIR.

In Tab. 35.17 the relevant LEIR parameters are listed together with some assumptions made for the losses of lead ions around the machine [31] and results from ion-induced desorption tests are also given there. If one takes the measured desorption yield of $\eta_{\text{tot}} = 2 \times 10^4 \text{ molec./ion}$ and the number of lost ions ($1.5 \times 10^9 \text{ s}^{-1}$), one finds a dynamic gas load of $3 \times 10^{13} \text{ molec s}^{-1}$ at 20°C which corresponds to about $10^{-6} \text{ Torr l s}^{-1}$. With an average vacuum chamber diameter of 150 mm the total dynamic outgassing rate is estimated to be about $3 \times 10^{-12} \text{ Torr l s}^{-1} \text{ cm}^{-2}$.

It is interesting to note that at the beginning of beam "scrubbing" the gas composition is dominated by CO and CO_2 , the molecules 'strongly' limiting the beam lifetime. It has been found that during scrubbing not only is the desorption yield reduced with time but also the gas composition is changed and that H_2 dominates at the end of beam scrubbing.

Table 35.17: Parameters of the LEIR machine relevant to estimate the dynamic pressure. Results from ion-induced desorption tests at Linac 3, used for dynamic pressure simulations of the LEIR vacuum system, are given.

Parameter	LEIR
Circumference	~ 80 m
Vacuum chamber cross sections:	
– in bending magnets	$\sim 180 \times 55 \times 6110$ mm ³
– in straight sections	~ 150 mm (average diameter)
Total surface	~ 40 m ²
Total volume	~ 1.5 m ³
Ion characteristics:	
– Pb ⁵⁴⁺ ions stored	up to 1×10^9
– Pb ⁵⁴⁺ ions lost	$\sim 3 \times 10^8$ every 0.2 s
– Revolution time	~ 2.8 μ s
Integrated loss area:	
– bending magnets (~ 24.5 m)	≈ 6500 cm ²
– straight sections (~ 55.5 m)	$\approx 4 \times 150 \times 3.3 \approx 2000$ cm ²
– straight sections (~ 55.5 m)	≈ 4500 cm ²
Ion induced desorption:	
– η_{tot} (measured at Linac3)	2×10^4 molec./Pb ⁵³⁺ ion
Typical gas composition:	
– start of beam scrubbing	H ₂ (3%), CH ₄ (7%), CO(72%), CO ₂ (18%)
– end of beam scrubbing	H ₂ (74%), CH ₄ (7%), CO(15%), CO ₂ (4%)

It is sufficient to study a quarter of the LEIR vacuum system due to the symmetry of the LEIR ring and the assumption of homogeneous Pb⁵⁴⁺ losses. Parts of sector 3 & 4 together with bending magnet BHN 30 (LEAR naming) have been chosen for the dynamic pressure simulations. The system was parameterised using the existing vacuum envelope and the installed pumping system.

The results are shown in Fig. 35.30 for two cases studied :

- Without any upgrade programme, the average dynamic pressure in LEIR will be about 3×10^{-11} Torr (before beam cleaning) a factor of ≈ 10 too high for the beam lifetime of 30 s. The simulated dynamic pressure fits remarkably well with the value of 2.5×10^{-11} Torr, measured in 1997 with continuous beam in LEAR [5]. In addition, this confirmation highlights the validity and importance of the ion-induced desorption experiments performed in Linac3.
- Non-evaporable getters (NEG's) provide an ideal linear pump for conductance limited vacuum systems like LEIR. A linear pump in the form of a NEG coated strip (St707, 30 mm width) provides very large pumping speeds of about $1000 \text{ l s}^{-1} \text{ m}^{-1}$ for H₂, $2000 \text{ l s}^{-1} \text{ m}^{-1}$ for CO, $\sim 1500 \text{ l s}^{-1} \text{ m}^{-1}$ for CO₂ and $450 \text{ l s}^{-1} \text{ m}^{-1}$ for N₂ [32]. The dynamic pressure simulations have been extended by adding one NEG strip over the whole length (15 m) of the vacuum system being simulated. The results are also shown in Fig. 35.30. With this simple modification made, the dynamic pressure can be reduced from 3×10^{-11} Torr to 5×10^{-12} Torr, a value which is very close to the design value. With a second NEG getter strip (space requirements should allow this) the target figure of 3×10^{-12} Torr would be reached. It should be mentioned that the St707 getter and sputter-coated NEG's are a very interesting choices for the LEIR vacuum system. However, since access to the vacuum chambers of the bending magnets is restricted, getter coatings will only be added in the straight sections and additional measures are necessary to meet the required dynamic vacuum.

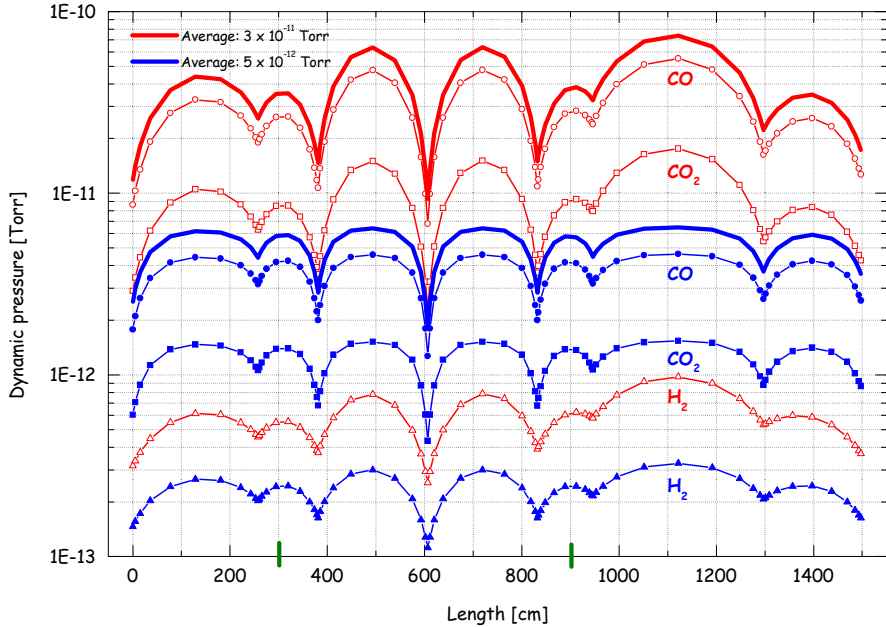


Figure 35.30: Dynamic pressure simulation for a 15 m long part of the LEIR vacuum system, including a bending magnet. As input parameters the measured (in Linac3) desorption yield of $\eta_{tot} = 2 \times 10^4$ molec./ion and a typical gas composition at the beginning of beam scrubbing has been chosen. Two scenarios are displayed: a) open symbols: lumped pumps (existing from LEAR) resulting in an average pressure of 3×10^{-11} Torr, b) closed symbols: lumped pumps plus linear getter (St707 strips) giving an average dynamic pressure of about 5×10^{-12} Torr, a number very close to the design value. The position of the vacuum chamber (about 6 m long) inside the bending magnet is indicated on the horizontal axis.

Design Principles

Dynamic pressure simulations and experience gained during the 1997 tests have clearly shown that the gas density necessary for a 30 s beam lifetime cannot be reached without additional efforts. The following measures will be implemented to improve the dynamic pressure in LEIR:

- Additional linear pumping will be installed in the injection/ejection lines and at all easily accessible locations of the LEIR ring in order to decrease the dynamic gas load by a factor 10 or even more. Non-evaporable getter pumps (coatings or St707 strips) are the only choice for this scenario.
- The vacuum system will also be equipped with low outgassing absorbers [33], positioned at locations where increased losses of heavy ions are expected and no getter coating of the entire vacuum chamber (e.g. bending magnets) is possible. These absorbers will be saw-toothed 316LN stainless steel sheets coated with Au, Ag, Pd, or TiZrV.
- A further reduction of the dynamic pressure after some operation will result from the cleaning effect of the lead ions (scrubbing). The feasibility of beam scrubbing has been demonstrated with various vacuum chambers tested in Linac3 [27, 33]. A factor 10 improvement of the dynamic pressure should be feasible without major difficulties. An example of Linac3 beam scrubbing results is shown in Fig. 35.31.

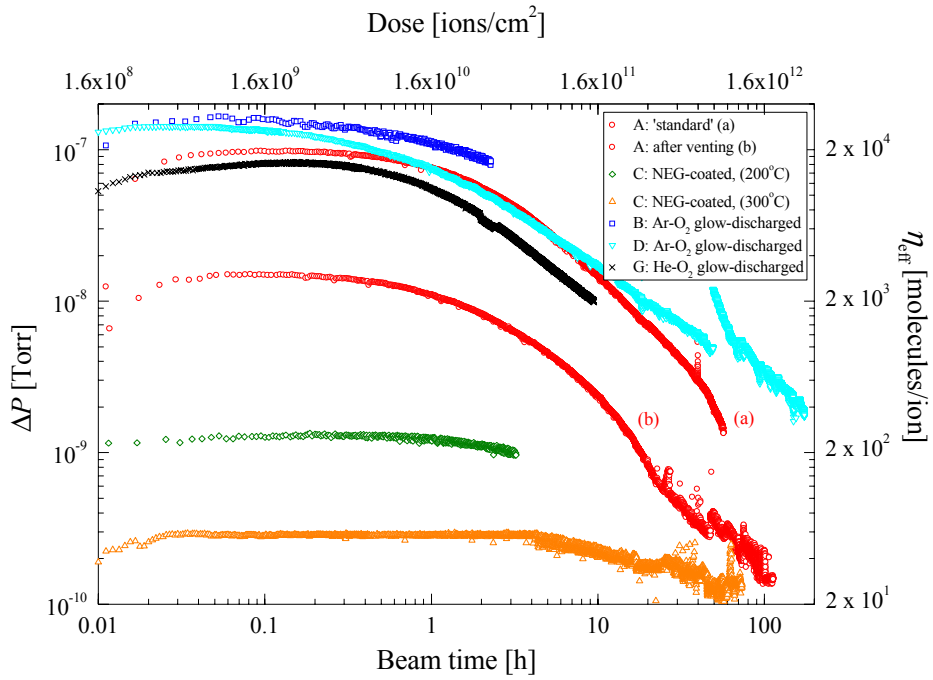


Figure 35.31: Beam cleaning measurements for five different stainless steel vacuum chambers continuously bombarded with $1.5 \times 10^9 \text{ Pb}^{53+}$ ions under $\theta = 89.2^\circ$ grazing incidence. The results obtained for Ar-O₂ and He-O₂ glow discharged vacuum chambers and a NEG-coated chamber, activated at 200°C and 300°C, are compared with an untreated ('standard') vacuum chamber.

35.9.3 The LEIR Vacuum System

Vacuum Envelope

The existing LEAR vacuum system was built between 1980 and 1982. Last experiments at LEAR were done in 1997 and since then the vacuum system was not maintained. Unfortunately, LEAR has not been kept under vacuum all the time, the ring has been vented for more than three years and at some locations the vacuum system is only protected with plastic flange covers. Therefore, the UHV performance may be 'lost' today, but even worse, dust contamination of the LEAR vacuum is very probable.

In any case, the whole vacuum system will be dismantled and then an inspection of its components will be performed. In particular, a detailed verification that all installed components are compatible with UHV requirements is mandatory and, all problematic materials will be removed. Limit pressure tests of the existing ion pumps, inspection of flanges, vacuum gauges and materials used are mandatory in order to take a decision if the vacuum equipment can still be used for LEIR or not. Many bellows are damaged and must be replaced by new ones.

If new chambers are required for the vacuum envelope of the LEIR ring as well as the injection and ejection lines, they will be made out of stainless steel AISI 316L or 316LN. All components must be cleaned according to the CERN procedure [34] and subsequently vacuum fired at 950°C for 2 hours. Wherever possible, a NEG coating will be performed to obtain a low dynamic gas load under heavy ion impact. Due to the UHV requirements, a bakeable all-metal vacuum system using Conflat flanges with silver-coated copper seals is mandatory.

Pumping System

The evacuation of the LEIR vacuum system from atmospheric pressure down to about 10^{-8} Torr will be done with primary and turbo molecular pumps. The same pumping groups, separated by full metal valves, will be used during the bakeouts. Sputter ion pumps and getter pumps (sublimation (SU) and NEG's) will be

distributed around the LEIR ring. A scenario to put linear pumping (non-evaporable getter) is being considered for all parts of the LEIR machine. Special attention has to be given to vacuum components (septa, kicker) where the use of NEG pumping (sputter-coated or strips) is currently being studied.

Since the dynamic vacuum is a challenge for the LEIR vacuum system, a very careful distribution of pumps and vacuum diagnostics (gauges, residual gas analysers) is mandatory. The final pump layout will be done as soon as the vacuum envelope is known for the whole LEIR ring, the injection and ejection lines are currently under study.

Full-metal valves, bakeable at 300°C in their open or closed position, must be used for sectorisation of the LEIR vacuum system. The vacuum envelope of the LEIR machine will be divided into five or six sectors.

Instrumentation

Due to the UHV requirements, vacuum gauges with a very low X-ray limit are the only choice for LEIR (for more details see [28]). Today, there are two possibilities: the commercially available Bayard-Alpert gauge (SVT 305), which has been used extensively at CERN, or, the modified Helmer gauge [35], never used so far in a particle accelerator, but which provides the best performance available today. If the modified Helmer gauge is used in combination with a ‘simplified’ power supply, a pressure of 10^{-13} Torr could be measured [36], thus avoiding the X-ray limit of the modulated Bayard-Alpert gauge. One could argue that the beam lifetime represents a good measurement of the average gas density in the LEIR ring. This statement is of course true, but it would not allow the identification of vacuum regions with higher outgassing rates or small leaks after bakeout. Thus, local improvements of the LEIR vacuum system would be very difficult or even impossible. Therefore, about 30 Bayard-Alpert gauges (SVT 305) will be installed in the LEIR machine. In addition, it is proposed to install a few Helmer gauges equipped with a simplified power supply for test purposes.

In addition, bakeable Pirani and Penning type gauges are necessary to measure the vacuum during pump-down and bakeout when the UHV gauges are still switched off.

Residual gas analysers (RGAs) will be used in LEIR for in situ leak detection and to evaluate the gas composition during beam cleaning. RGAs with a detection limit of 10^{-15} Torr will be used. Individual components of the analyser should be vacuum fired at 950°C to minimise the outgassing rate (often not quoted by the supplier). Four to six RGAs will be installed at locations where an enhanced outgassing due to losses of ions is expected.

Bakeout System

The success of the LEIR vacuum system strongly depends on the reliability of the bakeout system, a strong emphasis will be placed on the homogeneity ($\leq 20^\circ\text{C}$) of the bakeout temperature (maximum 5°C deviation from nominal bakeout temperature) along the whole ring. Baking at 300°C for at least 24 hours will be necessary to obtain a stainless steel outgassing rate of low 10^{-13} to 10^{-14} Torr $\text{l s}^{-1} \text{cm}^{-2}$. Special shaped vacuum envelopes, tanks, ion and sublimation pumps and valves will be surrounded by heating jackets that have to be specially manufactured. The bakeout system will guarantee a temperature gradient of 50°C/h .

The vacuum chambers in the four bending magnets must be all dismantled to install a new bakeout system. They will be equipped with a second (spare) heating system to be used in case of failure of the normal one. As usual, thermocouples will be installed around the machine for temperature control and monitoring. The whole bakeout system will have to be computer controlled and interlocked with the vacuum system. High priority will be given to the security of the bakeout system to avoid uncontrolled baking which would destroy machine and vacuum components.

Control System

The old vacuum control system of LEAR cannot be used for LEIR. A new PLC Simatic-type system will be implemented. The power supplies for the ion and sublimation pumps and the gauges are old models for which no spares are available and which cannot be repaired. The high voltage cables (ion pumps) and boxes do not meet CERN safety standards and, thus, they will be replaced. The pumping groups will be either locally or remotely controlled, using a Simatic-type system that has been adopted as the standard at CERN.

Electron Cooler

The electron cooler represents one of the key components for the LEIR accumulator. The whole layout and construction of the cooler will be done at Novosibirsk, in collaboration with CERN. In order to reach the required dynamic pressure of a few 10^{-12} Torr during operation the vacuum system will be constructed according to the same stringent UHV standards as the rest of the LEIR machine. In particular:

- Materials: Stainless steel AISI 316L or 316LN, cleaned and vacuum fired at CERN, will be used. Materials in question must be tested for outgassing and limit pressure after a bakeout at 300°C for 24 hours.
- Pumping system: Only primary pumps, bakeable turbo molecular, sputter ion and getter pumps (SU, NEG's) will be used. The whole vacuum system will be metal-sealed with standard Conflat flanges and equipped with valves of the full-metal type.
- The electron cooler vacuum system will be fully bakeable at 300°C, with maximum 5°C temperature variation at 300°C.
- Modulated Bayard-Alpert gauges of the CERN-type and low outgassing residual gas analyser(s) will be used for static and dynamic pressure measurements during cooler operation. Their exact position is layout dependent and will be decided during the construction.
- In general, the vacuum controls and the bakeout system of the cooler will be compatible with the equipment used for the LEIR machine. These issues will be settled in close collaboration between the Novosibirsk specialists and the vacuum group at CERN.

35.10 INSTRUMENTATION

Most of the instrumentation needed already existed in LEAR, but has to be adapted for ion operation and to the new PS standards for electronics and controls in order to improve performance and maintenance. All systems are based on having about 10^{10} to 10^{11} charges circulating in LEIR as coasting or bunched beam. There could be 1 to 4 bunches in the machine (but most of the time 2 bunches are expected) having a length (at 4σ) of 700 ns to 200 ns. The beam will be coasting during accumulation, but it will be bunched during acceleration up to extraction.

35.10.1 Intensity Measurements

For measurements of the beam current, an existing continuous current transformer will be reused and installed at a location where no magnetic field can perturb it. A new magnetic shielding will be designed and the water cooling system, used during the bake-out, will be renovated. Electronics, similar to the one used in the PSB and PS, will be adapted to the existing transformer, which is from a previous generation.

The β normaliser, based on the 0.1 Gauss B train counting, will be adapted to the various types of ions expected. The relativistic β will range from 0.09 to 0.37 for Pb^{54+} operation, but later may rise to 0.61 for operation with lighter ions.

Three ranges available in parallel will cover the intensity and charge dynamics. The acquisition of the 3 ranges will be made with a 1 kHz sampling rate by an 11 bit+sign ADC. A post-acquisition selection is performed to choose the best range, i.e. the highest non-saturated range. Performance figures are compiled in Tab. 35.18

In order to observe the intensity build-up (looking like a staircase with one step after every revolution) during multi-turn injection, a special transformer is requested [37]. It should allow measurement of the injection stairs with a precision of 1 %, but 200 ms later it should be ready to measure the next injection, starting without current offset. This translates into a frequency bandwidth from 8 Hz to 500 kHz. The transformer used in the old E5 line will be refurbished for this purpose.

Table 35.18: Expected characteristics of the continuous current transformer

Maximum current	50	mA
Resolution (on the highest sensitivity range)	2	μA
Noise (rms value on the highest sensitivity range)	2	μA
Temperature dependence	5	$\mu\text{A}/^\circ\text{C}$
High frequency cut-off (on the lowest sensitivity range)	3	kHz

For monitoring of the last part of the injection line (with the $\sim 200 \mu\text{s}$ long Linac3 pulse, up to $50 \mu\text{A}$) two old transformers and their electronics will be used and serve as ETL.MTR20 and EI.MTR10. For extraction, three existing transformers will be refurbished to the PS standard.

35.10.2 Orbit Measurements

All 14 existing pick-up stations (H+V) are reused and the 2 stations in the electron cooler are also included in the orbit measurement system but should be made compatible with the electron trajectory measurement (see Sec. 35.5.6). They are made of metal-coated ceramic tubes onto which electrodes are formed. The system should be able to measure the beam orbit every 10 ms during ramping and “on request” when the beam is on the flat tops (a special bunching process should be available). To decrease the noise level, an AD type head amplifier will be used, for which 3 different gains will be necessary to handle the high intensity range. Either a normaliser of PSB style, followed by “slow” digitisation or FADC’s followed by digital receivers will ensure fast orbit measurement.

Table 35.19 Characteristics of the ring pick-ups

Ring pick-up diameter	180	mm
Electrical length (H, V)	40	mm
Capacity	500	pF
Position resolution for a bunch 10^8 charges, 700 ns	2	mm
Position resolution for a bunch $\geq 10^9$ charges, 700 ns	0.1	mm
Relative precision	1	%

35.10.3 Tune Measurements

Coasting beam

The use of Beam Transfer Function technique allows precise tune measurement even with a small number of circulating particles (down to 10^6 charges). An existing resonant pick-up and kicker will be re-used. Software for automatic treatment of the data needs to be implemented.

The Schottky pick-ups which are described below will allow measurement of the tunes of coasting beams as well.

Bunched beam

The usual method (kick + oscillation acquisition + Fourier transform) is planned. Tune measurement “on request”, i.e. allowing measurement at one predefined timing inside the cycle, is required for the commissioning. Measurements every 10 ms may be added later but will require the construction of a new kicker magnet.

35.10.4 Schottky Signals (Σ, H_β, V_β)

The Schottky pick-ups will serve on the one hand for diagnostics purposes like measurements of tunes, of transverse emittances, the momentum distribution of coasting beams and on the other hand as pick-up for a broadband active transverse feedback (damper) in case this turns out to be necessary. Two Schottky pick-ups for low beta (0.095) and two pickups for beta > 0.15 exist and will be brought back to operation. A Spectrum analyzer or FFT software is needed and the controls will be rejuvenated.

All Schottky pick-ups, which had been initially constructed for stochastic cooling in LEAR, consist of a succession of short strip-line pick-ups. They differ mainly by the way the signal from the individual strip-line pick-ups are combined :

- Travelling wave pickup :

For slow velocities near injection energy, i.e. at a relativistic $\beta = 0.095$ up to $\beta = 0.15$, the individual strip-line pick-ups are connected in series with appropriate time delays in between. The signal is extracted at the last strip-line downstream, amplified and further treated. One horizontal and one vertical Schottky pick-up of this type, both yielding longitudinal signals as well, will give a very low signal to noise ratio. However, this scheme is not suitable for larger beam velocities.

- Direct summing of individual strip-lines:

For $\beta > 0.15$, the signal of every individual strip-line is amplified. Then the signals of the different strip-lines are summed up after inserting the appropriate velocity dependent delays. This scheme is possible for any velocity, but yields a smaller signal to noise ratio.

In order to extract useful information (e.g. tunes, emittances ...) from noise measured with these Schottky pick-ups, a spectrum analyzer (or equivalent) and down-mixing to low frequency is necessary to follow the evolution of the beam characteristics during cooling.

35.10.5 Wide Band Pickup

The existing 300 MHz wide-band pick-up will be reused in order to measure the longitudinal bunch shape. The same electronics and data treatment (high-speed scope and digital transfer to MCR) as for the PSB and PS is planned. A fast digital scope will be used to monitor the bunched beam, as in the other machine of the PS Complex (Bunch Shape Monitor).

35.10.6 Transverse Beam Dimension Measurements in LEIR

Calibrated transverse Schottky signals can be used to determine transverse emittances, when the beam is not too dense, otherwise the signals suffer from large coherent lines.

For observing the transverse dimensions of the beam during the cooling down process, two Beam Ionisation Profile Monitors (BIPM), one to measure in the horizontal plane and one for the vertical plane, will be installed. The principle, sketched in Fig. 35.32, is to make use of the fact that the circulating beam ionises the residual gas. The ions created are accelerated by an electric field towards the cathode where they impact on a Micro Channel Plate (MCP) and create secondary electrons. Two MCPs mounted in chevron increase the electron current by a factor 10^5 to 10^6 and finally, the electrons are collected on a grid which gives the measurement of the profile of the beam. It should be possible to measure beams of $(\epsilon_h, \epsilon_v) = (100, 50)$ mm mrad for 10^9 charges in a vacuum in the 10^{-12} T (95 % H₂) range every 20 ms with a good resolution (10^8 charges every 50 ms).

In addition, the existing horizontal and vertical scrapers are reused for amplitude distribution measurements and also for calibration of other systems like the Schottky signals.

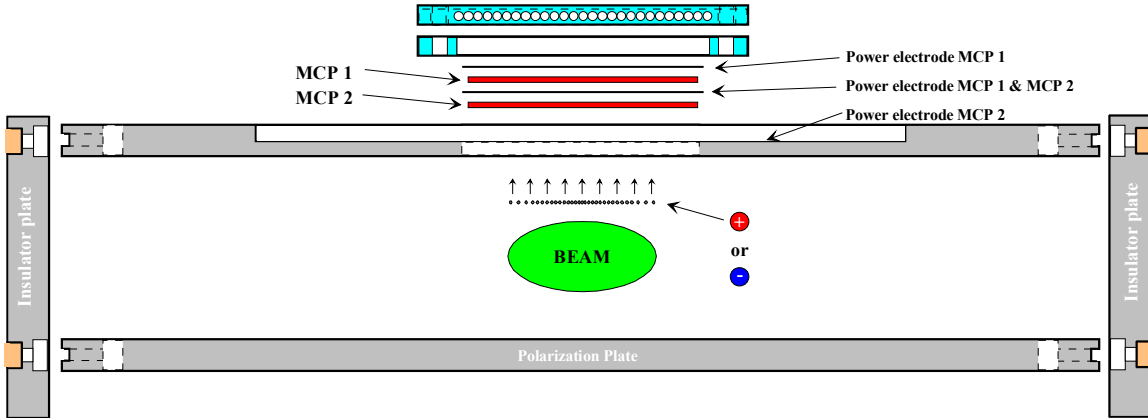


Figure 35.32: Principle of a BIPM.

35.10.7 Quadrupolar Pickup.

The existing quadrupolar pick-up and kicker allows the measurement of the incoherent tune shift by the BTFQ method [38] of the very dense beam obtained after cooling. This pickup is not expected to be used during the commissioning phase and may be made available later.

35.10.8 Electron-ion Recombination

In the bending magnet following the electron cooler, the existing movable scintillator will be used to measure the electron-ion recombination in the electron cooler. Data acquisition and position control electronics including software must be made available.

35.11 CONTROL SYSTEM

35.11.1 Introduction

The LEIR machine will be operated from the CERN Control Centre (CCC) like the PS Complex and SPS machines. A local control room for equipment tests, commissioning and possibly machine development will be set up with the appropriate infrastructure, replacing the former LEAR control room. The latter will be equipped with the same operation consoles as the ones in the CCC.

The LEIR control system will basically make use of the standard distributed architecture already implemented for the other PS Complex machines. The same software and hardware components will be deployed, in particular the recently introduced hardware and software items, namely:

Hardware :

- PLCs (Programmable Logic Controller) to interface specific power converters as a complement to the usual G64/MIL1553 interface.
- Linux front-end computers as a complement to the usual VME-LynxOS machines.
- CompactPCI computers for the analog signal observation system.

Software :

- “Middleware” communication layer to link the equipment layer to the desktop control layer.
- Java applications to operate the machine.

35.11.2 General Implementation

The control system will be made of the following parts :

- Extension of the PS secured mains to power the workstations, the front-end computers and the communication network using the UPS located in building 259.
- Extension of the Controls structured network in the relevant buildings.

- Dedicated timing system to drive the LEIR pulsed equipment and to synchronise the control system with the beam. The LEIR machine will be PPM (Pulse to Pulse Modulated), in order to provide more flexibility for machine development and future operation with other ion types. Linac3 and LEIR will be piloted by a dedicated telegram and their timing system subordinate to the CPS injection timing. The LEIR sequencing, like the PS Complex and SPS machines, will be handled by the Central Beam and Cycle Management (CBCM) system.
- The front-end computers to connect to the equipment:
 - Power converters and associated function generators.
 - Electron cooling.
 - Beam instrumentation and diagnostics.
 - RF (beam control and high power).
- Front-end hardware (VME or PLC like modules) to interface the various types of equipment :
- Front-end software:
 - Drivers, real time tasks and control modules to drive the equipment
 - “Middleware” communication layer
- Communication to the vacuum control system in order to display vacuum alarms and status.
- Back-end infrastructure (database and file servers) based upon the currently operational machines as these can easily support the additional load for LEIR
- Desktop equipment to operate the machine from the CCC, as well as from LEIR equipment room (former LEAR control room) and from a few places close to the machine
- The Java environment and application software to commission and run LEIR

35.11.3 Proposal for LEIR Timing and Sequencing

A dedicated timing system will be implemented to drive the LEIR pulsed equipment and to synchronise the control system with the beam.

- The LEIR machine will be PPM (Pulse to Pulse Modulated), in order to provide more flexibility to machine development or future operation with other ion types.
 - Linac3 and LEIR will be piloted by a dedicated *telegram* and their timing system subordinate to the CPS injection timing. Assuming that there will be no ion beams extracted from Linac3 into the PS Booster, the Linac3-LEIR telegram will be dedicated to the production of ion beams while the Linac2-PSB telegram will be responsible for driving proton beams. Thus, both telegrams are intended to be made completely independent.
 - Like the PS Complex and SPS machines, the LEIR sequencing will be handled by the Central Beam and Cycle Management system and programmed with the standard tools, namely the BCD Editor/Manager program.
 - Two operational modes are foreseen for the LEIR machine:
 - a) Pulsed mode :
This mode will be used operationally to prepare ion bunches to be delivered to the machines further downstream in the ion acceleration chain. The LEIR sequencing will be driven by cycles; each one handling the overall process, i.e. accumulation, acceleration and extraction. The length of the cycles must a multiple of the basic period (1.2 s at present) used for timing in the PS complex. The 3.6 s nominal LEIR cycle will correspond to three basic periods. For early operation, shorter cycles corresponding to two basic periods are envisaged.
 - b) Test (*machine development*) mode :
In this mode, needed for setting up and commissioning of the multi-turn injection and the cooler, the injection plateau is extended for an arbitrary duration. This mode will be requested for LEIR running in.
- Furthermore, switching from one mode to the other should be simple and fast.

A preliminary scheme is proposed to allow for the two operational modes needed for LEIR. The solution is based on the Normal/Spare supercycle switching mechanism, which is a standard functionality presently implemented in the CBCM.

In nominal mode, the active supercycle will be filled with cycles (cf. upper drawing in Fig. 35.33, “USER Nom”) of 3.6 s in the example depicted for nominal operation. The test mode has to be anticipated, resulting in the definition of two specific supercycles as shown below (cf. lower drawing in Fig. 35.33). The removal of the request on the programmed cycles in the Normal supercycle will trigger the switch to the Spare supercycle. Power supply constraints (in terms of current’s variation as function of time) may cause switching at specific points to be forbidden by the BCD Editor/Manager program.

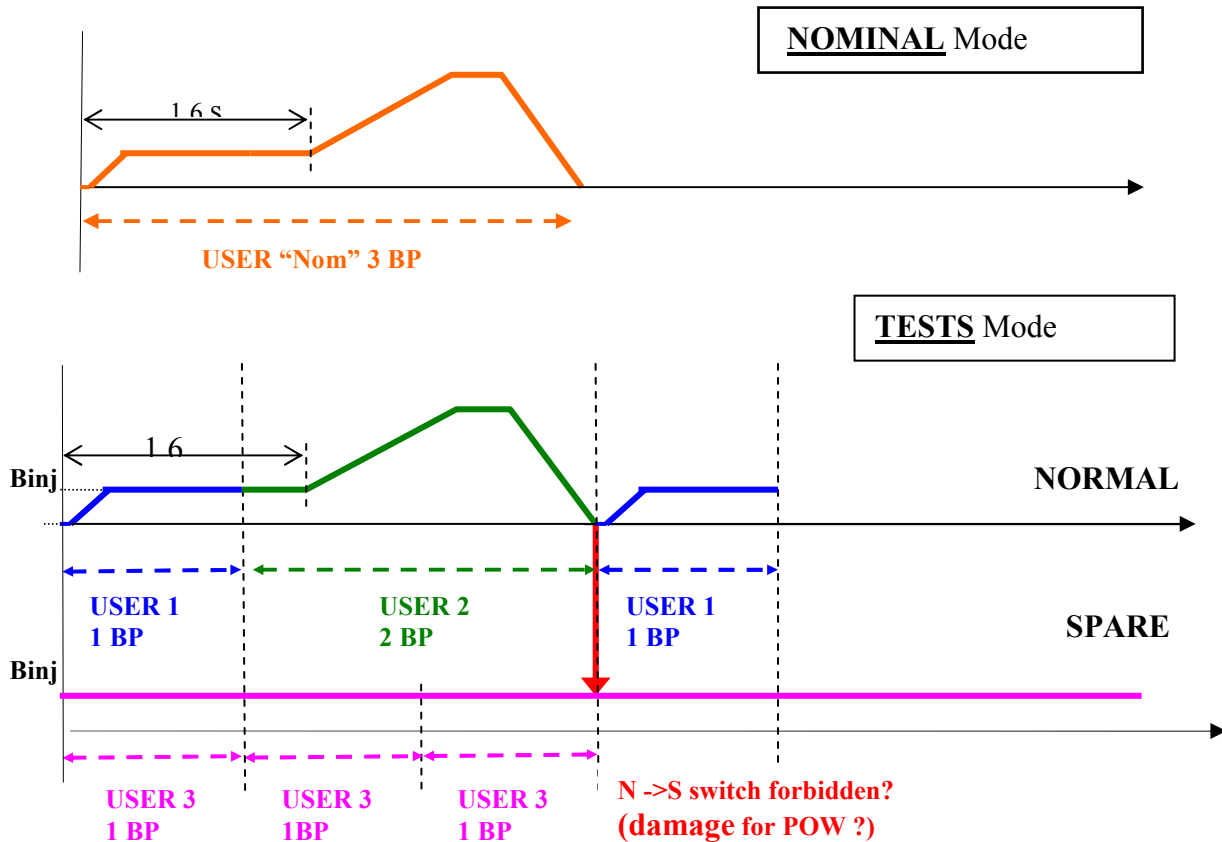


Figure 35.33: LEIR operation modes

35.12 INFRASTRUCTURE, SAFETY AND RADIATION PROTECTION

35.12.1 Technical Infrastructure

The existing technical infrastructure will be adapted to the needs of the LEIR machine.

Electrical Infrastructure

Electrical installations for LEIR are located in buildings 150, 233, 249, 250 and 363. Many of the existing switchboards are obsolete and dangerous to operate. Several of these old switchboards will be grouped together and replaced, to simplify also the LV distribution system in the LEIR zone. The installed power of the LEIR equipment is as follows:

- building 150: 1.2 MVA
- building 249: 750 kVA
- building 250: 2.5 MVA
- other buildings: 250 kVA (total)

There are about 250 km of existing cables installed in the LEIR zone, a large portion of them being of the PVC type. It was decided to re-use and adapt the existing cables whenever possible.

Cooling System

To ensure a sufficient supply of cooling water to LEIR, the existing 2.5 MW cooling station 234 will receive larger pumps and heat exchanger, increasing the flow rate of the demineralised water circuit by about 30 % to 200 m³/h. In addition, the demineralised water distribution circuit will be adapted to the LEIR equipment.

Fire Detection, Monitoring and Access

A number of fire detectors will be installed in the buildings used for LEIR equipment in order to limit the potential risks of fire in a zone where large quantities of PVC type cable are installed. The existing access system will be modified for LEIR. All signals and alarms critical for LEIR operation will be defined and transmitted to the Technical Control Room.

35.12.2 Shielding of LEIR

Given the expected beam intensity in LEIR, the 1.6 m think concrete walls enclosing the accelerator are sufficient to shield LEIR sideways and allow access to the rest of the East Hall during operation. The open question is whether or not a top shielding is required and whether or not the gangway (which is at a distance of approximately 5-6 m from the closest section of the machine) from which LEIR can be viewed by visitors could be made accessible during acceleration and extraction. This depends on the rate and position of beam losses.

Losses at the injection energy of 4.2 MeV/u will pose no major radiation problems. The estimate of the dose equivalent rate made for the dump at the end of Linac 3 indicates that even if 50% of the beam is lost at injection, the radiation level will remain below a few $\mu\text{Sv}/\text{h}$. Under these conditions the gangway can remain accessible.

On the other hand, there are very few data for radiation shielding of low to intermediate energy (up to a few hundreds MeV/u) ion accelerators and practically no data for lead ions in the LEIR energy range. The approach of considering an ion of mass number A, equivalent to a group of A protons is not a good approximation in the LEIR energy range. This is correct at SPS energies, i.e. hundreds of GeV/u and has been experimentally verified in recent years [39, 40, 41, 42], but at lower energies assuming the ion as a bunch of free protons generally leads to an underestimate of the shielding requirement, by a factor that becomes increasingly large with increasing shielding thickness, especially at forward angles. This is because secondary neutrons generated from ion interaction have a spectrum that extends to a maximum energy which is about twice the projectile energy per nucleon. This penetrating component would dominate the radiation dose past a thick shield.

Experimental data exist [43, 44, 45] on neutron production from 100-400 MeV/u He, C, Ne, Si, Fe and Xe ions on thick Al, C, Cu and Pb targets. An extensive set of Monte Carlo calculations was performed to convert these neutron energy distributions into shielding data (i.e., attenuation curves of neutrons in concrete) [46]. However, these calculations still do not yield data directly applicable to the case of lead ions in LEIR, so that extrapolations are nonetheless required. A simple model developed at GANIL (Caen, France) for ion energies in the range 30-100 MeV/u was compared with the Monte Carlo data at 100 MeV/u [46]. The model seems to provide a reasonable estimate of the Monte Carlo results at this specific energy, with some important overestimates at large depths in the shield (which is not a matter of concern in the present case).

LEIR will extract about 10^9 $^{208}\text{Pb}^{54+}$ ions at 72 MeV/u every 3.6 s. Apart from the losses at injection as discussed above, no significant losses are expected in the course of the acceleration process during normal operation. Thus the only case considered here is an accident scenario with loss of the entire beam at maximum energy. Two cases were investigated: 1) 10^9 Pb-ions lost at 72 MeV/u every 3.6 s in a single, unshielded point in the extraction region, at a distance of approximately 25 m from the gangway; 2) 10^9 Pb-ions lost at 72 MeV/u every 3.6 s uniformly around the ring. In this case losses occurring in the fraction of the machine closest to the gangway (approximately 5 m distance) are the major concern. Losses can occur in

a straight section (where no shielding is provided by the machine) or inside a magnet (where some shielding is provided by the magnet yoke, assumed here as 10 cm iron).

Estimates of the expected dose equivalent rate at the gangway were made using the GANIL model for the two cases mentioned above [47]. These estimates indicate that a maximum dose equivalent rate of a few tens of $\mu\text{Sv/h}$ can be expected under accidental conditions. Cutting the beam within – say – ten machine pulses will give an integral dose of the order of 1 μSv . If this beam abort time can be guaranteed, no special precautions need to be taken.

During the commissioning phase it is planned to operate LEIR with $^{16}\text{O}^{4+}$ ions at 67 MeV/u at a higher intensity than with $^{208}\text{Pb}^{54+}$ ions, i.e. extracting 2×10^{10} ions every 2.4 s. With such a beam and under the same accidental conditions as above, a full beam loss may induce a dose equivalent rate at the gangway of the order of 1 mSv/h. Cutting the beam within ten pulses will give an integral dose of the order of 10 μSv (a few tens of μSv maximum). A radiation monitor providing a local alarm will most likely suffice, but access to the gangway by visitors during the commissioning phase will probably be forbidden.

It will be useful to perform dose rate measurements during commissioning to verify the present estimates and to decide if and where any additional shield is needed and if the gangway can be left open during routine operation. In the worst case scenario that LEIR will have to be top-shielded, it will probably be more economical to build a tunnel structure around the ring rather than covering the entire accelerator hall. It is also possible that some local shielding at the major loss points will suffice.

35.13 LEIR PARAMETER LIST

Table 35.20: LEIR parameter for nominal and early scheme Pb^{54+} operation.

Parameter	Value	
	Nominal	Early stage scheme
Circumference	$25 \pi \text{ m}$	
Basic structure	“Square” with four straight section ($\sim 12.5 \text{ m}$) and four 90° bending magnets	
Focussing structure :		
In ER.SS10 (injection) and ER.SS30	doublets on either side of the section	
In ER.SS20 (electron cooler) and ER.SS40	triplets on either side of the section	
Nominal Tunes : horizontal/vertical	1.82/2.72	
Maximum direct space charge tune shifts (after bunching and at beginning of ramp)	0.06	0.04
Relativistic γ factor at transition γ_{tr}		2.84
Injection energy per nucleon	4.2 MeV/nucleon	
momentum per nucleon/per charge	88.6 MeV/c/nucleon / 342.1 MeV/c/charge	
beam rigidity	1.138 Tm	
revolution period	2.76 μs	
Extraction energy per nucleon	72.2 MeV/nucleon	
momentum per nucleon/charge	374 MeV/c/nucleon / 1439 MeV/c/charge	
beam rigidity	4.8 Tm	
revolution period	704 ns	
Repetition period	3.6 s	2.4 s
Intensities: injected from one linac pulse (25 to $50 \mu\text{A}$, 200 μs , efficiency $\sim 50\%$)	$3 \text{ to } 6 \cdot 10^8 \text{ Pb}^{54+}$	$3 \text{ to } 6 \cdot 10^8 \text{ Pb}^{54+}$
after accumulation	$10 \cdot 10^8 \text{ Pb}^{54+}$	$2.5 \cdot 10^8 \text{ Pb}^{54+}$
extracted and transferred to PS	$9 \cdot 10^8 \text{ Pb}^{54+}$	$2.25 \cdot 10^8 \text{ Pb}^{54+}$
Injected beam :		
total emittances horizontal/vertical	$60 \mu\text{m}/40 \mu\text{m}$	
momentum range	$-0.4 \cdot 10^{-3} \text{ to } 3.6 \cdot 10^{-3}$	up to $\pm 4 \cdot 10^{-3}$
Accumulated beam (stack) :		
transverse. rms emittances ($\sigma^2/\beta_{\text{twiss}}$)	$\sim 7 \mu\text{m}$ ¹⁾	$< 7 \mu\text{m}$
momentum offset	$-2 \cdot 10^{-3}$	$0 \text{ to } -2 \cdot 10^{-3}$?
relative rms Momentum spread	$\sim 0.2 \cdot 10^{-3}$	
total long, emittance		$\sim 0.015 \text{ eVs/u}$
Harmonic number h (bunching, acceleration ...)	2	1
After bunching :		
transverse emittances ($\sigma^2/\beta_{\text{twiss}}$)	$\sim 7 \mu\text{m}$ ¹⁾	$< 7 \mu\text{m}$
relative rms momentum spread	$2.0 \cdot 10^{-3}$	$1.3 \cdot 10^{-3}$
bunch length (4 rms)	$\sim 800 \text{ ns}$	$\sim 580 \text{ ns}$
total long, emittance ($\epsilon_{\text{long}} = h \times 4\pi \sigma_E \sigma_t$)	$\sim 0.08 \text{ eVs/u}$	$\sim 0.020 \text{ eVs/u}$
RF voltage	$\sim 2200 \text{ V}$	$\sim 3000 \text{ V}$
synchrotron frequency	$\sim 1570 \text{ Hz}$	$\sim 1300 \text{ Hz}$
Extraction :		
ϵ_{rms}^* ($= (\beta\gamma)_{\text{rel}} \sigma^2/\beta_{\text{twiss}}$)	$0.7 \mu\text{m}$ ²⁾	$< 0.7 \mu\text{m}$
total Long, emittance ($\epsilon_{\text{long}} = h \times 4\pi \sigma_E \sigma_t$)	0.10 eVs/u	0.025 eVs/u
relative rms momentum spread	$0.6 \cdot 10^{-3}$	$0.3 \cdot 10^{-3}$
bunch length (4 rms)	200 ns	200 ns
bunch spacing	352 ns	
RF Voltage	2900 V	1100 V
synchrotron frequency	1600 Hz	700 Hz

1) This figure denotes the mean value of the two transverse emittances. Due to different IBS growth rates in the two transverse phase spaces, unequal emittances (of e.g. $9 \mu\text{m}$ and $5 \mu\text{m}$ for the horizontal and the vertical phase space respectively) are expected.

2) Denotes the mean value of the two normalised rms emittances. Different emittances (of e.g. $0.9 \mu\text{m}$ and $0.5 \mu\text{m}$ for the horizontal and the vertical phase space respectively) are expected

REFERENCES

- [1] M. Chanel, *LEIR: The Low Energy Ion Ring at CERN*, Proc. 8th EPAC, Paris, June 2002, CERN/PS 2002-015 (AE).
- [2] C. Carli, M. Chanel, S. Maury (editors), *PS Ions for LHC design report*, (unpublished draft).
- [3] S. Maury, D. Möhl, *Combined Longitudinal and Transverse Multiturn Injection into a Heavy Ion Accumulator Ring*, PS/AR>Note 94-12.
- [4] C. Carli, S. Maury, D. Möhl, *Combined Longitudinal and Transverse Multiturn Injection in a Heavy Ion Accumulator*, PAC, Vancouver, B.C., May 1997 and CERN/PS 97-27 (HP).
- [5] J. Bosser, C. Carli, M. Chanel, C. Hill, A. Lombardi, R. Maccaferri, S. Maury, D. Möhl, G. Molinari, S. Rossi, E. Tanke, G. Tranquille, M. Vretenar, *Experimental Investigations of Electron Cooling and Stacking of Lead Ions in a Low Energy Accumulation Ring*, CERN/PS 99-033 (DI) and Particle Accelerators, Vol. 63, p. 171-210, 1999.
- [6] J. Bosser et al., *Results on Lead Ion Accumulation in LEAR for the LHC*, Proc. 6th EPAC, Stockholm, June 1998, CERN/PS 98-033(CA).
- [7] P. Lefèvre, D. Möhl, *A Low Energy Accumulation Ring of Ions for LHC (A Feasibility Study)*, CERN/PS 93-62(DI), LHC Note 259, 1993.
- [8] M. Chanel, Private communications on unpublished LEAR results.
- [9] L. Hermansson, D. Reistad, *Electron cooling at CELSIUS*, Proceedings of the Workshop on Electron and Related Topics, Uppsala, Sweden, May 19-22, 1999, NIM A 441 (2000).
- [10] I. Hofmann, *Density Limitations in Cooled Beams*, Proceedings of the third LEAR workshop on Physics with Antiprotons at LEAR in the ACOL era, Tignes, 1985.
- [11] H. Zhao et al., *Highlights of HIRFL CSR electron coolers at IMP*, to be published in the proceedings of the 2003 Workshop on Beam Cooling and Related Topics, COOL03.
- [12] J. Bosser, C. Dimopoulou, G. Tranquille, *LEIR Electron Cooler Conceptual Study* PS/BD/Note 2001-017.
- [13] A.V. Ivanov, V.V. Parkhomchuk, B.N. Sukhina, M.A. Tiunov, *The Hollow Electron Beam – The new opportunities in electron cooling*, Proceedings of the 2001 Workshop on Cooling and Related Topics, Cool01.
- [14] V.V. Parkhochuk et al, *The electron gun with variable beam profile for optimized electron cooling*, Proceedings of the 2002 European Particle Accelerator Conference, EPAC2002.
- [15] A.N. Sharapa, A.V. Grudiev, D.G. Myakishev, A.V. Shemyakin, *A high perveance electron gun for the electron cooling*, NIM A 406 (1998) 169-171.
- [16] C. Dimopoulou, *General parameters of the high perveance gun for the LEIR electron cooler*, CERN/PS/2002-004 (BD).
- [17] J. Bosser, V. Prieto, G. Tranquille, *Specifications of the LEIR electron cooler magnetic components*, PS/BD/Note 2001-018.
- [18] Y. Tanabe et al., “Evaluation of magnetic alloys for JHF RF cavity”, in Proc. APAC1998 Conference, Tsukuba, 23–27 March 1998.
- [19] M. Paoluzzi, “LEIR RF power amplifier design”, CERN-AB-Note-2003-029 RF (2003).
- [20] J.M. Cravero, J.P. Royer, *The new pulsed power converter for the septum magnet in the straight section 42*, PS/PO/ Note 97-03, 1997.
- [21] J.Lahaye, G.Simonet, W.Hofle, *Technical Specification for Power Converters for the Ions for LHC Project and the LHC Transverse Damper System*, IT-3225/AB/LHC August 2003.
- [22] J.Lahaye, G.Simonet, *Technical Specification for High Voltage Power Converters for the Ions for LHC Project*, IT-3257/AB/LHC September 2003.
- [23] J.Lahaye, G.Simonet, *Technical Specification for Power Converters for the Ions for LHC Project*, PE-21785/AB/LHC August 2003.
- [24] K.Fischer, M.Royer, *Technical Specification for the Power Part of 26 Thyristors Pulsed Converters for the SPS magnet system*, IT/2353B/SL January 1998.
- [25] J. Hansen, J.-M. Laurent, N. Madsen, E. Mahner, CERN, LHC/VAC-TN-2001-07 (2001).
- [26] M. Chanel, J. Hansen, J.-M. Laurent, N. Madsen, E. Mahner, *Experimental Investigation of Impact-Induced Molecular Desorption by 4.2 MeV/u Pb ions*, Proceedings of Particle Accelerator Conference, Chicago, 2001, p. 2165 and CERN, PS-2001-040-AE.

- [27] E. Mahner, J. Hansen, J.-M. Laurent, N. Madsen, *Molecular desorption of stainless steel vacuum chambers irradiated with 4.2 MeV/u lead ions*, Phys. Rev. ST-AB 6, 013201 (2003).
- [28] E. Mahner, *Technical Design of the LEIR Vacuum System*, CERN, LHC/VAC-TN-2002-04 (2002).
- [29] B. Franzke, *Vacuum requirements for heavy ion synchrotrons*, Proceedings of the 1981 Particle Accelerator Conference, IEEE Trans. Nucl. Sci. NS-28, p. 2116 (1981).
- [30] A.S. Schlachter, J.W. Stearns, W.G. Graham, K.H. Berkner, R.V. Pyle, J.A. Tanis, *Electron capture for fast charged ions in gas targets: An empirical scaling rule*, Phys. Rev. A 27, p 3372 (1983).
- [31] M. Chanel, *private communication*, March 2002.
- [32] C. Benvenuti, P. Chiggiato, *Pumping characteristics of the St707 non-evaporable getter (Zr 70-V 24.6-Fe 5.4wt%)*, J. Vac. Sci. Technol. A14, p 3278 (1996) and CERN-MT-95-10 SM.
- [33] E. Mahner, J. Hansen, D. Küchler, M. Malabaila, M. Taborelli, *Ion-stimulated gas desorption yields of coated (Au, Ag, Pd) stainless steel vacuum chambers irradiated with 4.2 MeV/u lead ions*, CERN Divisional Report AT/2003-6 (VAC).
- [34] CERN cleaning procedure: ‘Reference Technique TR-01’.
- [35] J.C. Helmer, *History and development of the UHV Helmer gauge as an analytic instrument*, Vacuum 51, p. 7 (1998).
- [36] C. Benvenuti, *private communication*, October 2001.
- [37] F. Lenardon, P. Odier, S. Tirard, *Un transformateur semi-lent pour LEIR*, PS/BD/Note 2001-011 (tech).
- [38] M. Chanel, *Study of beam envelope oscillations by measuring the beam transfer function with quadrupolar pick-up and kicker*, Proceedings of the 1996 European Particle Accelerator Conference EPAC96, June 1996.
- [39] S. Agosteo, C. Birattari, A. Foglio Para, E. Nava, M. Silari and L. Ulrici, *Neutron measurements in the stray field produced by 158 GeV/c lead ion beams*, Health Physics 75, 619-629, 1998.
- [40] S. Agosteo, C. Birattari, A. Foglio Para, M. Silari and L. Ulrici, *Neutron measurements around a beam dump bombarded by high energy protons and lead ions*, Nuclear Instruments and Methods A 459, 58-65, 2001.
- [41] S. Agosteo, C. Birattari, A. Foglio Para, A. Mitaroff, M. Silari and L. Ulrici, *90° neutron emission from high energy protons and lead ions on a thin lead target*, Nuclear Instruments and Methods A 476, 63-68, 2002.
- [42] S. Agosteo, C. Birattari, A. Foglio Para, L. Gini, A. Mitaroff, M. Silari and L. Ulrici, *Neutron production from 158 GeV/c per nucleon lead ions on thin copper and lead targets in the angular range 30°–135°*, Nuclear Instruments and Methods B 194, 399-408, 2002.
- [43] T. Kurosawa, N. Nakao, T. Nakamura, Y. Uwamino, T. Shibata, N. Nakanishi, A. Fukumura and K. Murakami, *Measurements of secondary neutrons produced from thick targets bombarded by high-energy helium and carbon ions*, Nuclear Science and Engineering 132, 30-57, 1999.
- [44] T. Kurosawa, N. Nakao, T. Nakamura, Y. Uwamino, T. Shibata, A. Fukumura and K. Murakami, *Measurements of secondary neutrons produced from thick targets bombarded by high energy neon ions*, Journal of nuclear science and technology, 36, 41-53, 1999.
- [45] T. Kurosawa, N. Nakao, T. Nakamura, H. Iwase, H. Sato, Y. Uwamino and A. Fukumura, *Neutron yields from thick C, Al, Cu and Pb targets bombarded by 400 MeV/nucleon Ar, Fe, Xe and 800 MeV/nucleon Si ions*, Physical Review C 62, Third series, No. 4, 2000.
- [46] S. Agosteo, T. Nakamura, M. Silari and Z. Zajacova, *Attenuation curves in concrete of neutrons from 100-400 MeV per nucleon He, C, Ne, Ar, Fe and Xe ions on various targets*, submitted for publication in Nuclear Instruments and Methods B.
- [47] M. Silari, *Shielding Requirements for LEIR as LHC Injector*, Technical Note CERN TIS 2003-022-RP-TN.

CHAPTER 36

LINAC3-LEIR-PS LINES

36.1 OVERVIEW AND LAYOUT

The Linac3-LEIR-PS transfer lines transport the beam from Linac 3 to the LEIR injection and, after accumulation and acceleration, from the LEIR extraction to the PS. The existing transfer lines (used in the past to transfer antiprotons from the PS to LEAR and protons and ions from the linacs to LEAR) are not compatible with the LEIR requirements since :

- A part of the line (namely the ETL line) will be used both for LEIR injection and LEIR extraction, but in opposite direction (Fig. 36.1 shows the new layout and definition of acronyms). Furthermore, the beam rigidity for these two operations differs by a factor of about 4 (in case of Pb ions). Therefore, all magnets in this common line ETL (including ITE.BHN40) must be pulsed and feature laminated yokes.
- For beams extracted from LEIR and transferred to the PS, the new transfer line must cope with an increased beam rigidity of 4.8 Tm, not compatible with the available strength of some magnets of the existing lines.
- The LEIR injection and extraction systems will be completely rebuilt, requiring reconstruction of the EI and EE lines as well.

Thus, a significant part of the transfer lines connecting Linac 3, LEIR and the PS has to be reconstructed to meet the new requirements.

Most of the ITE loop can be recuperated from the previous line. As already mentioned above, only the last dipole ITE.BHN40 must be replaced by a laminated magnet. A quadrupole will be added for a better control of the matching in the last part of the transfer line towards the PS (ETP line). The ETL line has to be constructed from scratch, primarily to replace solid-core magnets by laminated ones, allowing pulsing between injection and extraction. Polarity changes of the power supplies of the bending magnets are unavoidable (except ETL.BHN20). Naively, one would assume that the ETL line quadrupoles also have to change their polarity. However, by a clever design of both the injection and the extraction optics, none of the quadrupole power supplies has to be bipolar.

The LEIR machine is located at a level 40 cm higher than Linac 3 and the PS machine. In order to bring the beam from one level to the other, a long part of the ETL line has a slope of about 9 mrad (upwards for the beam transferred towards LEIR) produced by two vertical bending magnets.

The special injection process requires a tilted electrostatic injection septum. Thus, the beam will undergo an unavoidable vertical deflection in this injection septum. This implies a slope of the magnetic septum installed upstream from the electrostatic septum and complicates geometry of the injection EI line upstream of the injection region. Two additional vertical bending magnets will be installed to provide the correct vertical position and slope at the entrance to the two (upright magnetic and tilted electrostatic) septa.

An additional requirement for the optics design of the extraction line was to allow emittance measurements with the “3 profile monitor” method. To this end, three appropriate locations (with suitable betatron phase advances in both planes) to install Secondary Emission Monitors have been determined in the ETL line.

36.2 OPTICS

The optics presented in this section is an updated version of the one described in [1], taking small changes of the geometry into account.

The injection line considered here starts at a hand-over point located inside the shielding wall separating the Linac 3 from the PS tunnel (see Fig. 36.1). Two quadrupole triplets, belonging to the Linac3 transfer line IT and located between the hand-over point and the first bend of the ITE line, have been integrated into the modelling of the injection, in order to adjust the matching at the entrance into the loop ITE. At the end of the line at the LEIR injection, a moderate (by a factor of about 1/2) betatron mismatch w.r.t. the beam circulating in LEIR enhances the multi-turn injection efficiency. A very stringent requirement is that the dispersion of the beam arriving in the LEIR machine must vanish (note that the LEIR machine itself has a relatively large dispersion of about 10 m at the injection point). Otherwise the arriving beam would move during one linac

pulse due to the momentum ramping and, thus, a finite dispersion is not compatible with the special injection process. The line has been matched to $\beta_H = 1$ m, $\beta_V = 2$ m and $D = 0$ m.

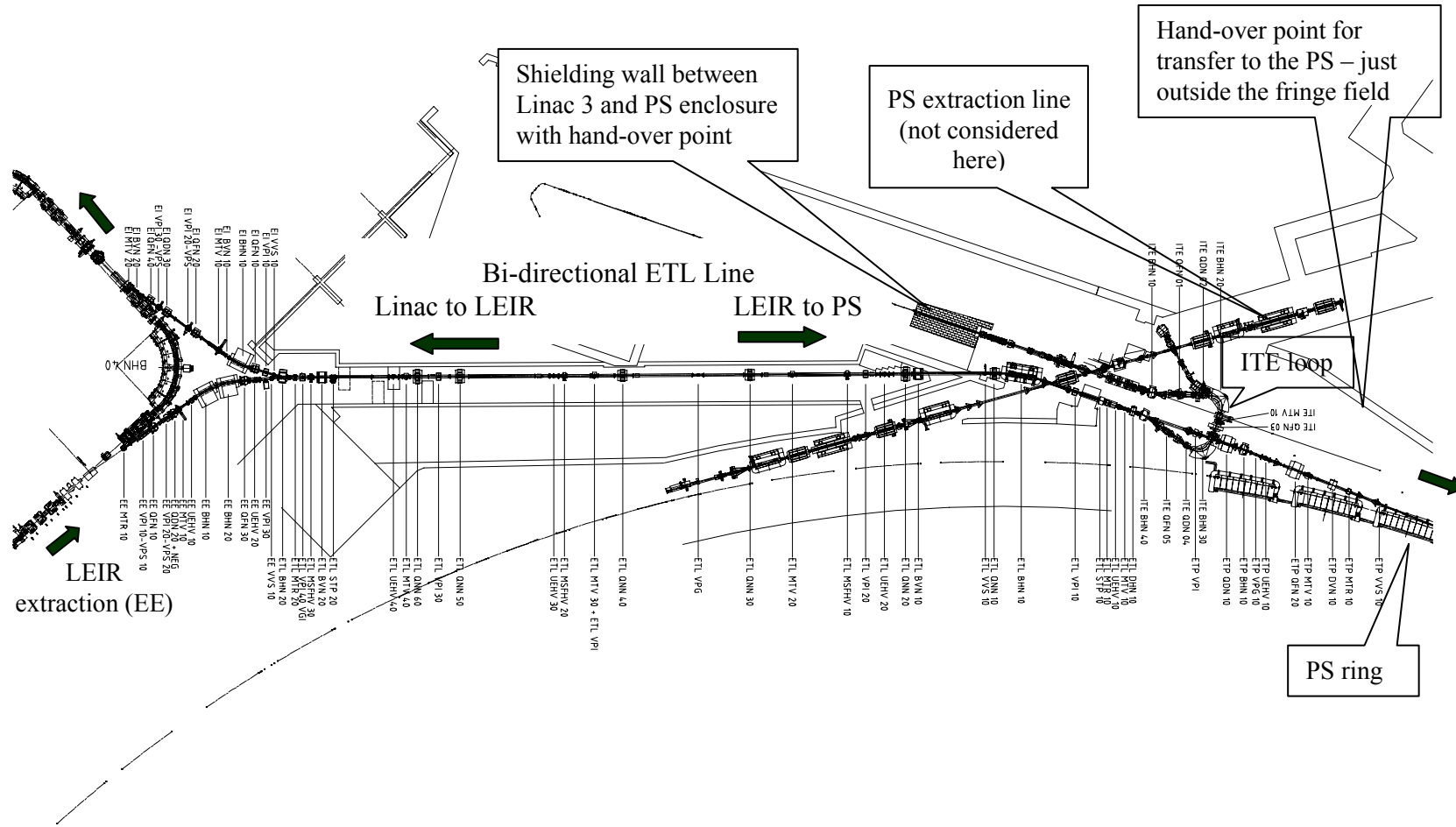


Figure 36.1: Geometry of the Linac3, LEIR and PS accelerators and the transfer lines between them.

The extraction line considered here starts at the centre of the LEIR extraction section (with $\beta_H = \beta_V = 5$ m and $D = 0$ m) and ends at a hand-over point just outside the stray field of one of the PS main bending magnets. The Twiss parameters at this hand-over have been determined by tracking the PS lattice functions at the centre of the injection section through the main magnet fringe field using a transfer matrix given in reference [2].

In order to limit the number of bipolar power supplies necessary for the ETL line, the optics of the line has been designed in such a manner that the polarity of the quadrupole power supplies does not change between injection and extraction. Since the beam travels through this line in opposite directions for injection and extraction, the gradients used in a beam optics program have to change sign, i.e. a quadrupole focusing for injection becomes defocusing for extraction and vice versa.

Lattice functions along the line for transfer from Linac3 to the LEIR machine are shown in Fig. 36.2. Two triplets in the IT line (belonging to Linac3) allow matching of the beam at the entrance of the loop ITE. Inside this loop (which changes the beam direction by 180° and directs the beam towards LEIR), the lattice functions are symmetric. In order to achieve vanishing dispersion at injection, a relatively large betatron phase advance in the ETL line is necessary, giving rise to fairly large fluctuations of the betatron functions and small spot-sizes at some locations. The last triplet in the EI line has been shifted as close as possible to the injection septa, in order to facilitate focusing the beam at the injection point. The space occupied by the beam (assuming a perfect trajectory) is depicted in Fig. 36.3 for relative momentum offsets of -2% and $2\%^1$, corresponding to the beginning and the end of the injection. The beam parameters used for the computation are transverse physical RMS emittances of $\epsilon_H = \epsilon_V = 2.5 \mu\text{m}$ and an RMS relative momentum spread $\sigma_p/p = 0.2 \times 10^{-3}$.

Lattice functions along the extraction line are shown in Fig. 36.4. The most delicate location is around the doublet at the very beginning of the line, where the extracted beam has to be refocused. The first quadrupole EE.QFN10 has been shifted as close as possible to the extraction septum. The position of the second quadrupole EE.QDN20 is a compromise avoiding excessive gradients of both quadrupoles on the one hand and large vertical betatron functions on the other hand. Rather smooth FODO like focusing has been achieved in the ETL line. Two quadrupoles (one more than in the line previously installed at this location) are available in the ETP line and allow matching the beam to the PS while keeping the betatron functions at moderate levels. The space occupied by the beam, assuming transverse physical RMS emittances of $\epsilon_H = \epsilon_V = 1.75 \mu\text{m}$ and an RMS relative momentum spread of $\sigma_p/p = 0.7 \times 10^{-3}$, is depicted in Fig. 36.5. Magnet parameters (e.g. strengths and currents) are given Tab. 36.1 and Tab. 36.2.

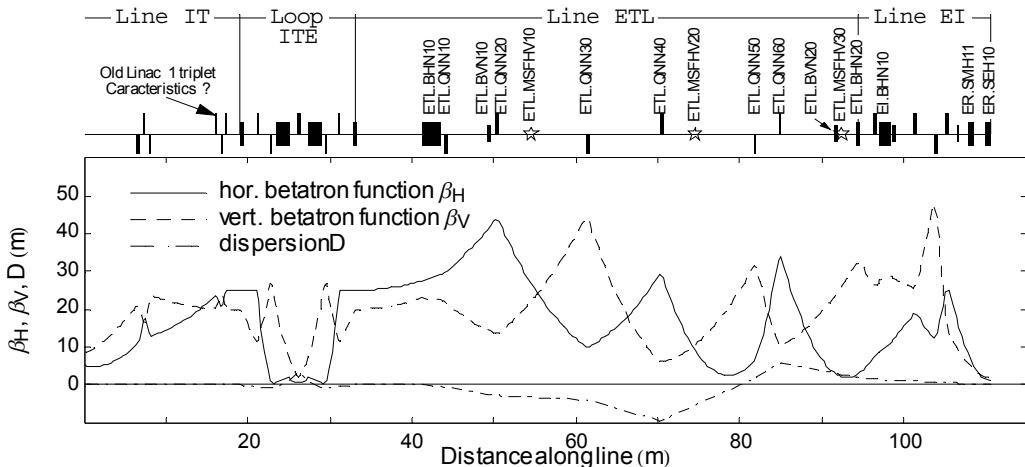


Figure 36.2 : Optics functions along the line for beam transfer from the ion Linac 3 to LEIR injection.

¹ This momentum range translates to a momentum ramp between about -1% and 3% in the LEIR machine.

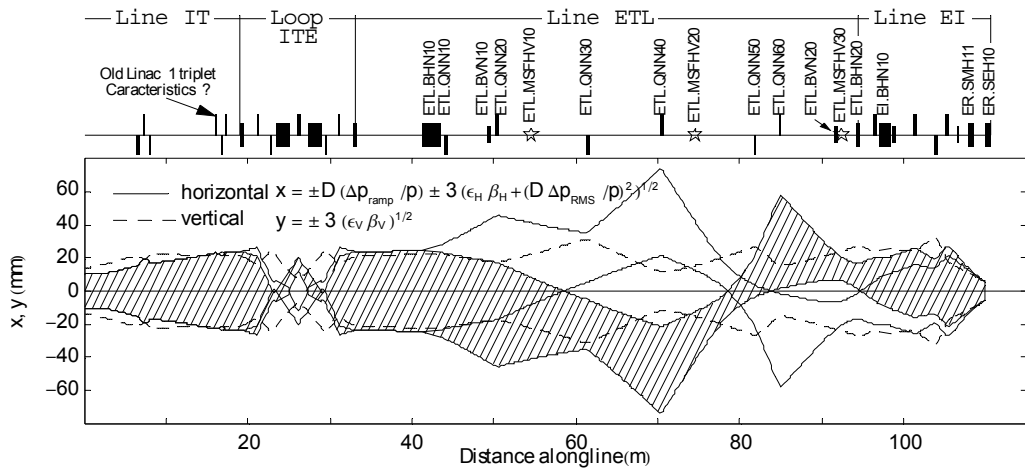


Figure 36.3 : 3σ size of the beam transferred from ion Linac 3 to LEIR injection. The hatched area shows the horizontal beam size for a momentum offset of 2 %.

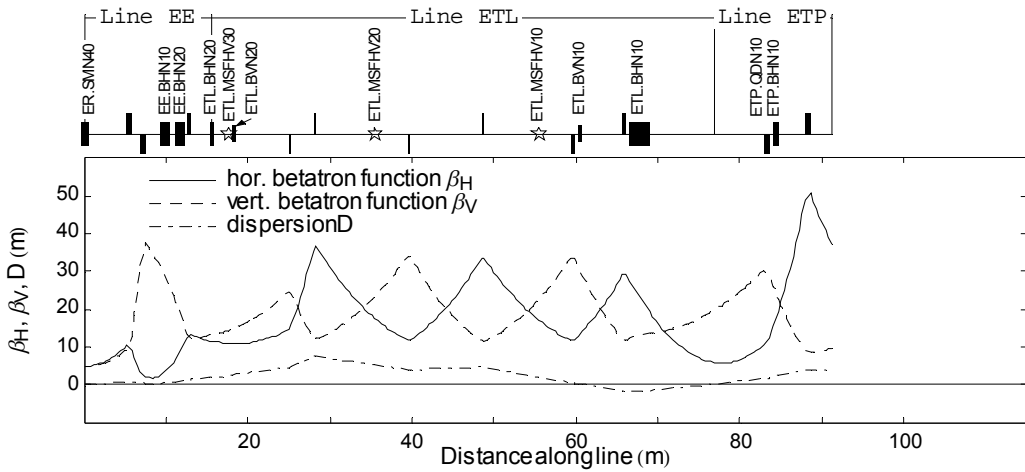


Figure 36.4 : Optics functions along the line from LEIR extraction to PS injection.

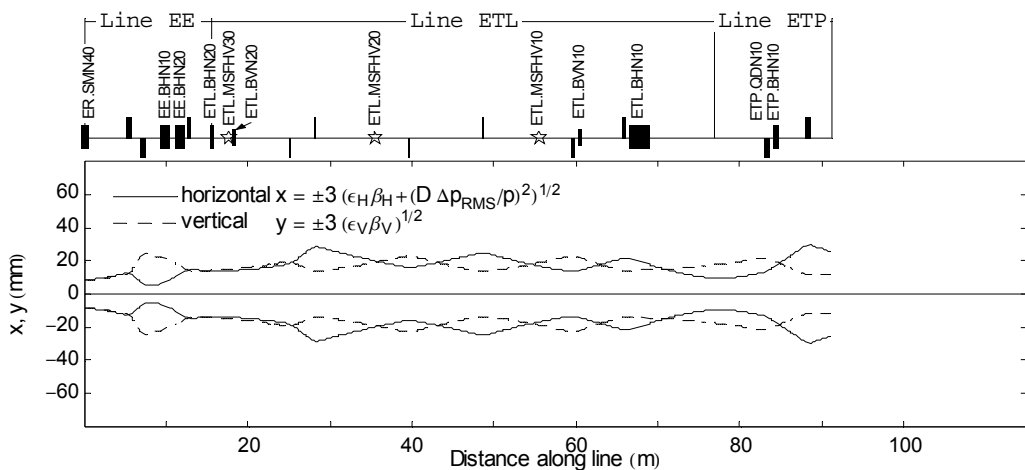


Figure 36.5 : 3σ size of the beam transferred from LEIR extraction to PS injection.

Table 36.1 : Characteristics of the Linac 3 – LEIR – PS transfer line quadrupoles.

			Injection		Extraction			
Quadrupole	Type	L _{Mag} (m)	Strength k×L _{Mag} (m ⁻¹)	I (A)	Strength k×L _{Mag} (m ⁻¹)	I (A)	R (Ohm)	L (H)
IT.QN08/10	Linac 7	0.255	-0.2583	72.74	not used		0.068	0.00122
IT.QN09	Linac 7	0.255	0.4960	139.67	not used		0.068	0.00122
IT.QN11/13	Unknown	Unknown	0.1801	Unknown	not used			
IT.QN12	Unknown	Unknown	-0.3371	Unknown	not used			
ITE.QFN01	Linac 7	0.255	0.5098	143.58	not used		0.068	0.00122
ITE.QDN02	Linac 7	0.255	-0.5088	143.27	not used		0.068	0.00122
ITE.QFN03	Q22	0.326	1.2143	129.43	not used		0.21	0.060
ITE.QDN04	Linac 7	0.255	-0.5088	143.27	not used		0.068	0.00122
ITE.QFN05	Linac 7	0.255	0.5098	143.58	not used		0.068	0.00122
ETL.QNN10	QTN	0.385	-0.0176	1.457	0.1353	47.28	0.23	0.20
ETL.QNN20	QTN	0.385	0.0854	7.073	-0.1192	41.67	0.23	0.20
ETL.QNN30	QTS	0.385	-0.1239	10.266	0.1003	35.05	0.25	0.31
ETL.QNN40	QTS	0.385	0.1694	14.035	-0.0994	34.74	0.25	0.31
ETL.QNN50	QTS	0.385	-0.2199	18.22	0.1724	60.26	0.25	0.31
ETL.QNN60	QTN	0.385	0.3127	25.90	-0.1475	51.55	0.23	0.20
EI.QFN10	air cooled SMIT (PSB)	0.462	0.1338	4.642	not used		0.95	0.31
EI.QFN20	air cooled SMIT (PSB)	0.462	0.1837	6.373	not used		0.95	0.31
EI.QDN30	water cooled SMIT (PSB)	0.462	-0.4541	44.69	not used		0.20	0.04
EI.QFN40	water cooled SMIT (PSB)	0.462	0.4408	43.39	not used		0.20	0.04
EE.QFN10	QLC	0.499	not used		0.4495	687.1	0.09	0.00072
EE.QDN20	QLC	0.499	not used		-0.3505	535.2	0.09	0.00072
EE.QFN30	QLC	0.499	not used		0.2353	359.1	0.09	0.00072
ETP.QDN10	Q500	0.656	not used		-0.1356	37.83	0.0195	0.254
ETP.QFN20	Q500	0.656	not used		0.1673	46.68	0.0195	0.254

36.3 MAGNETS

As mentioned in Sec. 36.1, a major part of the transfer lines between Linac3, LEIR and the PS have to be rebuilt in order to satisfy the requirements of the I-LHC project. To this end, a large number of the existing magnets have to be replaced. Fortunately, it has been possible to find nearly all required magnets within CERN, thus reducing cost. They have been recuperated from other accelerators and transfer lines. Before installation in the tunnel, all recuperated magnets will be carefully refurbished and upgraded if necessary. In total, around 30 magnets have to be repaired and modified until the end of 2004. The refurbishment typically includes:

- Visual inspection.
- Insulation tests, leakage tests and water flow measurements.
- Cleaning of yoke and coils.
- Repair of degraded coil clamps (usually polyurethane pads).
- Modification and upgrade of the cooling circuit: replacement of rubber hoses by stainless steel tubes and glass fibre insulators (if applicable).

- Replacement of Thermo-switches.
- Final tests (insulation resistance, leakage, water flow, interlock).

The modifications of each part of the transfer line (the magnets are compiled in Tab. 36.1 and Tab. 36.2) are described in detail below.

Table 36.2: Characteristics of the Linac 3 – LEIR – PS transfer line deflection magnets (dipoles and septa).

Bending	Type	L_{Mag} (m)	Injection		Extraction		R (Ohm)	L (H)
ITE.BHN10	Special	0.48	-16°	736.3	not used		0.012	0.006
ITE.BHN20	Special	$0.80 \times 106^\circ$	106°	928.6	not used		0.040	0.10
ITE.BHN30	Special	$0.80 \times 106^\circ$	106°	928.6	not used		0.040	0.10
ITE.BHN40	Special	0.48	-16°	736.3	not used		0.012	0.006
ETL.BHN10	VB4	2.34	-336.75 mrad	-68.21	336.75 mrad	289.09	0.15	0.47
ETL.BVN10	MEA43	0.558	9.56 mrad (upwards)	-8.77	9.56 mrad (upwards)	37.00	0.33	0.31
ETL.BVN20	MEA43	0.558	-9.56 mrad (downwards)	-8.77	-9.56 mrad (downwards)	37.00	0.33	0.31
ETL.BHN20	Special	0.610	17°	195.3	4.5°	217.3	0.166	0.080
EI.BHN10	MC100	1.175	330.03	160.8	not used		0.18	0.22
EI.BVN10	PSB type A water cooled	0.350	7.86 mrad	34.1	not used		0.075	0.003
EI.BVN20	PSB type A water cooled	0.350	-22.08 mrad	95.4	not used		0.075	0.003
ER.SMH11	Special	0.825	175 mrad	1055	not used		0.0115	0.000315
ER.SMH40	Special	0.850	not used		130 mrad	30400	0.00015	2.7×10^{-6}
EE.BHN10	MC100	1.175	not used		267.76 mrad	556.8	0.18	0.22
EE.BHN20	MC100	1.175	not used		267.76 mrad	556.8	0.18	0.22
ETP.BHN10	Special	0.48	not used		47.88 mrad	531	0.012	0.006

36.3.1 ITE Loop (former E0 Line)

This line will keep its present configuration and will remain unmodified apart from the last magnet ITE.BHN40. Since both the injected and the extracted beam have to pass through this bending magnet, the currently installed magnet cannot be re-used due to its massive yoke. It will be replaced by a new laminated magnet which is under construction in industry. The magnetic characteristics will be identical to the massive magnet; only a few modifications and improvements to facilitate the maintenance as well as the mounting of the coils and the vacuum chamber are planned. In fact, this laminated M16 dipole is the only magnet which could not be found at CERN and which has to be fabricated. The quadrupole of type Q22-01 in position ITE.QFN03 will be replaced by a refurbished magnet of the same type.

36.3.2 ETL Line (former E2 Line)

As mentioned earlier, all massive magnets currently installed in this transfer line have to be replaced by magnets with laminated yokes to cope with the new requirements. The former E2.BHN02 has been taken out due to lack of strength and has been replaced by a bending magnet of type VB4. This magnet has been modified (rotated by 90°) and completely rebuilt; all rubber hoses have been replaced by stainless steel pipes. Recuperated and upgraded quadrupoles of type QTN will be installed on positions ETL.QNN10, ETL.QNN20 and ETL.QNN60, those of type QTS at positions ETL.QNN30, ETL.QNN40 and ETL.QNN50 during the winter shut-down 2003-04. They all have been equipped with new stainless steel cooling circuits. Two magnets of type MEA43 will be installed at positions ETL.BVN10 and ETL.BVN20 to bring the beam from the Linac3 – PS level to the LEIR level and vice versa. Their maintenance and installation is planned for 2004. At the end of the ETL line, where the line splits up into the EI (injection) line to LEIR and the EE (extraction) line coming from LEIR, the bending magnet recuperated from the former position E2.BHN02

will be installed. Since the coil insulation is in a rather doubtful condition, the replacement of the coils is being considered.

36.3.3 EI and EE Lines

Magnets for both the injection and the extraction lines do not need to be laminated. Nevertheless, a reshuffling and upgrade of both EI and EE lines is required. Four massive quadrupoles of type SMIT recuperated from the former PSB injection line have been refurbished. Two air-cooled SMIT will be installed in EI.QFN10 and EI.QFN20, whereas the two water-cooled magnets of the same type will be placed at EI.QDN30 and EI.QDN40. Three massive bending dipoles of type MC100 will be placed on EI.BHN10, EE.BHN10 and EE.BHN20. All three magnets will be equipped with new stainless steel water pipes. The vertical deflection of the inclined injection septum leads to the need for two vertical bending magnets in the injection line. Water cooled “type A” dipoles, originally constructed for the PSB transfer lines, are recuperated and will be installed in positions EI.BVN10 and EI.BVN20, respectively. Three quadrupoles of type QLC currently installed in both lines will be taken out, refurbished and re-installed in the extraction line during 2004 (EE.QFN10, EE.QDN20 and EE.QFN30).

36.3.4 ETP Line

The modification of the ETP line includes the installation of two refurbished quadrupoles of type Q500 (ETP.QDN10 and ETP.QFN20) and one massive bending magnet of type M16, which has been taken from ITE.BHN40 (see above) to replace an obsolete magnet of type MNPA50 previously situated at ETP.BHN10. The MNPA25 type magnet presently installed at ETP.DVN10 will remain as corrector magnet on its current position.

36.4 POWER CONVERTERS

New and upgraded power converters are required for the Linac3 – LEIR – PS transfer lines. Their description is included in Chap. 35 (on the LEIR machine) in Tab. 35.17 and Sec. 35.8.6.

36.5 INSTRUMENTATION

The beam pulse coming from Linac 3 has a length of up to 450 μ s (out of this maximum length, only a part of \sim 200 μ s will be injected into LEIR). Its intensity will be upgraded from 25 μ A at present to 50 μ A at the start of LEIR. The nominal Pb⁵⁴⁺ beam extracted from LEIR is composed of two bunches each one 200ns long and with a maximum intensity of 5×10^{10} charges.

36.5.1 Intensity Measurements

The intensity of the beam transferred from Linac3 to LEIR will be monitored using two existing transformers (ITH.MTR41 and EI.MTR10). Two existing transformers will be refurbished (EE.MTR10 and ETP.MTR10) and 3 additional transformers are available in the PS for observing the beam extracted from LEIR and transferred to the PS,. Two transformers will be installed in the common injection/ejection line and will therefore see both beams (ETL.MTR10 and ETL.MTR20). Due to the different pulse length (up to 450 μ s at injection, 200 ns at ejection) different analogue treatment is needed. Three amplifier chains will be provided: one for the slow injected beam and two chains with different gains for the fast ejected pulse. Tests have been made confirming that this scheme is feasible. Each transformer will be equipped with a fast sampling ADC where the injected beam will be sampled at 10 MHz while the ejected one will use a sampling frequency of 100 MHz (yielding about 20 samples per bunch). Each of the transformers is equipped with a calibration winding generating a calibration pulse in front of each beam pulse to be measured. The digital pulse form will be available as well as the digitally integrated total charge in the bunch.

36.5.2 Trajectory Measurements

Owing to the very low intensity of the ions, no pick-up stations will be available to measure the position of the beam transferred from Linac3 to LEIR. Thus, the seven scintillating screens (see also Sec. 36.5.3) must be used to determine the trajectory as well.

For ejection trajectory measurements, seven pick-up stations (H+V), the same number as before, in the transfer line (2 EE, 4 ETL and 1 ETP) to the PS are used. The pick-ups consist of 1 Σ -electrode and 2 Δ -electrodes formed from stainless steel sheets. Four of them have to be rebuilt as they have been taken for the AD. The front-end electronics is obsolete and new head amplifiers will have to be developed. The present acquisition chain (analogue integrators followed by slow digitisation) will be replaced by a system using fast digitisation (100 MH) and digital integration as in other transfer lines of the PS complex. Details are given in Tab. 36.3.

Table 36.3: Characteristics of the seven Pick-ups in the line from LEIR to PS.

Pick-up diameter	140/172/243	mm
Electrical length (H, V) / Σ	71 / 53	mm
Capacity	200	pF
Position resolution for a bunch of 10^9 charges, 200ns	1.0	mm
Position resolution for a bunch $\geq 10^{10}$ charges, 200ns	0.1	mm
Relative precision	1	%

36.5.3 Beam Size Measurements.

A total of 9 TV stations will be installed in the Linac3 – LEIR – PS transfer lines. Each TV station will consist of a scintillating screen with its associated in/out mechanism, a TV camera and the necessary control electronics. VME based control and acquisition modules will contain everything needed to control the camera and the in/out mechanism and will also provide a frame grabber for digitization of the video image. CCD cameras will be used wherever the radiation level permits.

These 9 TV stations will be installed as follows :

- ITE loop :
One TV station will be installed and replace a SEMGrid currently installed there.
- ETL line :
Four TV stations will be installed in the ETL line to observe the injected and the extracted beam. In order to observe the beam extracted from LEIR, the support mechanism must allow the scintillating screen to be inserted between the last injection and the extraction and to retract it again before the next injection (in and out movement of the scintillating screen within about 1 s).
- EI line :
Two TV stations will be installed in the EI line.
- EE line :
One TV station will be available in the EE line.
- ETP line :
One TV station will be installed in the ETP line.

In order to measure the emittance of the ion beam prepared in LEIR using the "3 profile method", three new secondary emission monitor stations (each one equipped with two sets of wires, allowing the horizontal and vertical profile to be measured) will be built and installed at suitable locations.

REFERENCES

- [1] C. Carli, M. Chanel, J.-Y. Hémery, *Design of the LEIR Transfer Lines*, PS/AE Note 2002-218 and PIL/LEIR Note 011.
- [2] G. Tranquille, Input File for Beam Optics Simulations of the Transfer of Antiprotons from the PS to LEAR.

CHAPTER 37

THE PS AND TRANSFER LINE TO SPS

37.1 INJECTION: TRAJECTORIES AND OPTICS

Partially stripped Pb^{54+} ion beam will be injected into the PS ring at 72.2 MeV/u. The selected LEIR extraction energy is a compromise between the incoherent tune shift limit at PS injection ($\Delta Q_{\text{inc}} < 0.25$), the bunch spacing needed for the ejection kicker rise time, the cycle length in LEIR and the minimum frequency attainable with the PS RF system [1, 2]. Tab. 37.1 summarizes the main parameters of lead ion beams at transfer between LEIR and PS and at PS extraction for the sake of completeness.

Table 37.1: Summary of lead ion beam characteristics at PS input and output.

Parameter at PS	Injection	Ejection
Kinetic energy	72.16 MeV/u	5.88 GeV/u
Proton kinetic energy for equal B_p	779.60 MeV	25.06 GeV
γ	1.077	7.312
β	0.372	0.991
Beam rigidity (B_p)	4.80 Tm	86.67 Tm
Magnetic field in PS dipoles	0.0685 T	1.237 T
Number of injected bunches	2 every 3.6 s	8 “bunchlets”
Number of Pb^{54+} ions per batch	9.0×10^8	4.8×10^8
Normalised transverse emittance (1σ)	0.7 μm	1.0 μm

37.1.1 Layout of the Former Antiproton PS Extraction towards LEAR

The former PS antiproton ejection to LEAR took place in the long PS straight-section 26 as depicted in Fig. 37.1.

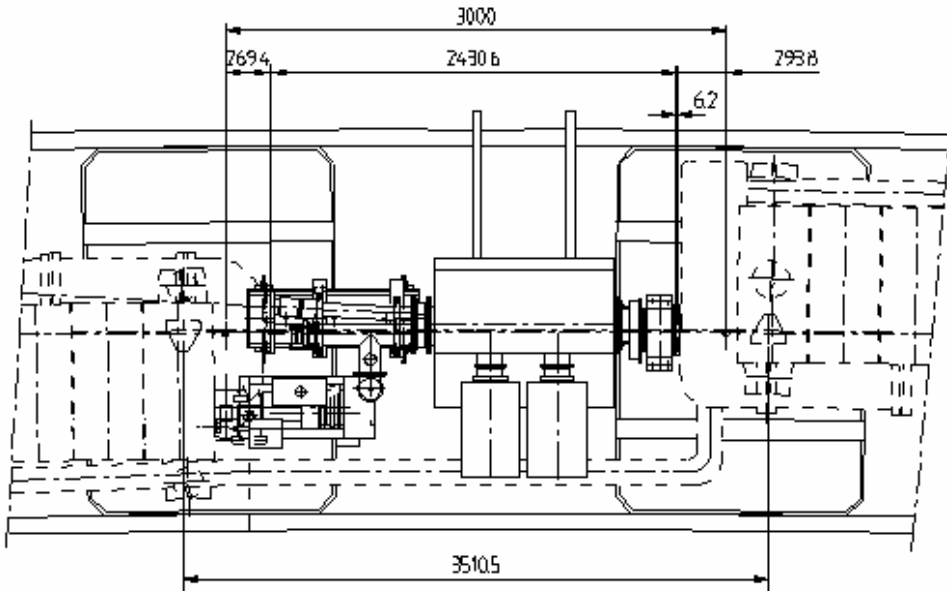


Figure 37.1: Layout of the PS straight-section 26 with the antiproton extraction septum.

Antiprotons were fast extracted from the PS at 2.0 Tm beam rigidity using kicker and septum magnets located in straight-sections 28 and 26. The septum strength used in operation to extract the beam ($\int B dl = 0.105$ Tm gave a deflection angle of 51.5 mrad) did not exceed the maximum attainable value of 0.117 Tm. No local closed orbit distortion was needed since the kicker strength necessary to eject directly

from the central orbit ($\int B dl = 192.6$ Gm yielding a kick of 9.5 mrad) was below the maximum kicker value of 232.4 Gm. Beam position and angle at the septum were 80.6 mm and 6.7 mrad respectively. The septum was positioned at 53 mm from the central orbit; its thickness varies between 1.5 mm and 18 mm. Fig. 37.2 shows the Y shape vacuum chamber adjacent to the ejection septum tank used to take the antiproton beam out of the PS ring.

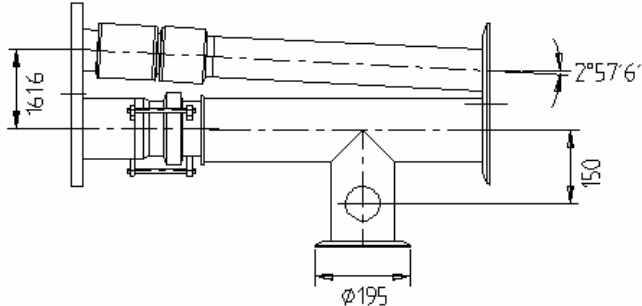


Figure 37.2: Y shape vacuum chamber adjacent to the extraction septum 26. The angle between the two pipes is $2^{\circ}57'6''$ or 51.5 mrad, the nominal extracted antiproton deflection angle.

37.1.2 Lead Ion Injection Scenario into the PS

The lead ion beams from LEIR will follow the geometry of the former antiproton transfer line in the reverse direction. The higher ion beam rigidity (4.8 Tm) would require septum magnet strength of 0.247 Tm to handle the 51.5 mrad beam deflection, which is beyond the maximum strength of the present septum (0.117 Tm). A new septum for ion injection with a maximum strength of 0.264 Tm has then been proposed (with a septum thickness of 5 mm). From the geometry of the Y shaped injection pipe the beam position at the septum 26 centre is evaluated to be 84.3 mm. Pushing the beam onto the reference orbit from the 84.3 mm beam position at the septum would need a kicker strength of 469.8 Gm (9.8 mrad kick), a little bit too high even if the present kicker strength is upgraded ($Bdl_{max} = 464.8$ Gm).

A local closed orbit bump is proposed to push the beam towards the septum. With the upgraded kicker a local closed orbit bump is not strictly needed but still recommended in order to keep some margin. The bump must not exceed the distance of the septum from the central orbit minus the half-width of the injected beam and possible orbit distortions. The horizontal beam size (at 6σ) near the septum is of the order of 30 mm. Assuming the same 53 mm septum position used for the former antiproton extraction, and taking a 13 mm safety margin for orbit distortions and kicker tuning, the bump at the septum is found to be 25 mm. A three-magnet bump creates the needed orbit displacement without residual orbit deformation outside the injection region. This bump can be reduced to an almost half-wavelength two-magnet bump if a small residual orbit distortion outside the bump is permitted.

Three-magnet bump

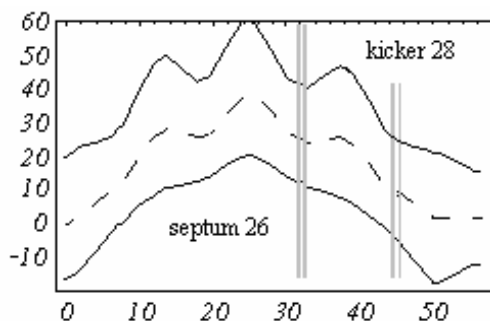


Figure 37.3: Three-dipole bump with 6σ -beam envelope [mm] in PS straight-sections 21, 25, 29. The dipoles are at 0.2 m, 25.1 m, 50.0 m from the centre of straight-section 21.

Fig. 37.3 shows a three-magnet bump with 25 mm amplitude at the septum. The phase advance between the dipoles 29 and 21 is very close to π . The three kicks producing the bump are below 2 mrad, the maximum strength of the deflecting dipoles being 86 Gm. The kicker 28 is inside the bump extension so that the orbit is displaced by 10 mm in the kicker tank.

Fig. 37.4 shows the injected beam envelope (at 6σ) from a matching point in the LEIR to PS transfer line (located 6.5 m upstream from the septum centre) to the kicker 28, together with that of the circulating beam over the range of the bump. The 38 mm maximum displacement of the beam is reached in straight-section 25, at about 25 m from the beginning of the bump while the maximum beam size coordinate on the outside is 58 mm within straight-section 25. The kicker 28 strength has to be enhanced from 232.4 to 330.4 Gm.

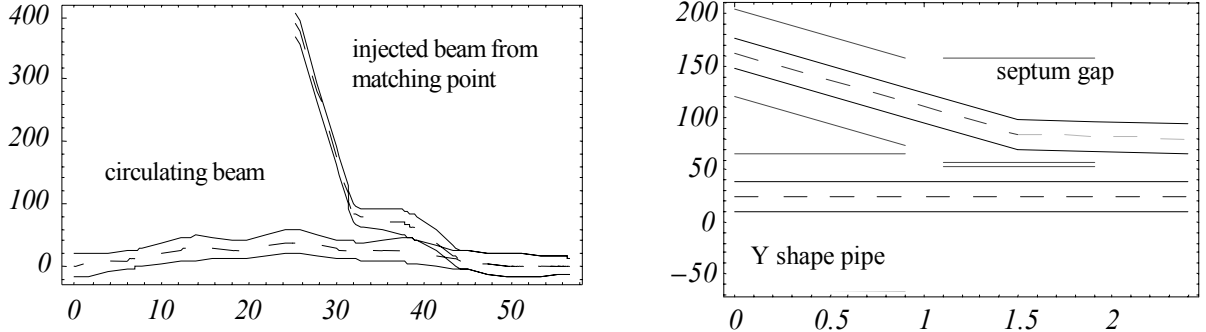


Figure 37.4: Left: horizontal injected and circulating 6σ -beam envelopes over the full bump range [mm]. Right: horizontal 6σ -beam envelopes in PS straight-section 26 [mm].

Two-magnet bump

The best configuration for the position of the dipoles, given the smaller residual orbit distortion outside the bump region, is a symmetric two-magnet bump with dipoles in straight-sections 22 and 30. The phase difference between the dipoles is very close to π . The required kick is 2.1 mrad per dipole yielding a residual orbit distortion of about 2 mm.

37.1.3 Matching Conditions between LEIR Output and PS Input

The PS magnet unit 25 adjacent to septum 26 is made of a closed half-unit followed by an open half-unit. The incoming beam trajectories pass far from the central orbit of the closed half-unit (at about 430 mm on average), where the gradient has a reverse polarity, and about 250 mm away from the open half-unit. The incoming beam will thus experience the stray field of the magnet.

PS magnet field map values have been obtained from magnetic measurements at 3.5 GeV/c [3]. The gradient and thus the deflecting field away from the central orbit may be derived from these data by interpolation and extrapolation using approximation formulas for the fringe field [4]. The mean gradient and deflection angle seen by the input beam in the closed and open half-units are -0.008 m^{-2} , 2.2 mrad and -0.020 m^{-2} , 5.1 mrad, respectively. These values have to be compared to the nominal $\pm 0.059 \text{ m}^{-2}$ and 31.4 mrad gradient and angle on the central orbit. The resulting transfer matrices in the LEIR to PS transfer line, from the magnet unit 25 stray field entry (matching point M) to septum 26 centre have been derived accordingly. Optical parameters at point M are obtained propagating back the required optical parameters at injection point (septum centre) through the transfer line from the septum up to point M (Tab. 37.2).

Table 37.2: Parameters at PS septum and LEIR to PS transfer line point M (located 6.5 m away).

Optical parameters	β_x [m]	α_x	β_y [m]	α_y	D_x [m]	D'_x	D_y [m]	D'_y
PS septum 26 centre	12.48	0	19.71	0	2.21	-0.02	0	0
LEIR-PS matching point	21.50	1.62	15.21	-0.71	2.78	-0.17	0	0

37.1.4 Hardware for PS Ion Injection

The three-magnet orbit bump as well as the simpler two-magnet bump (using one power supply only) are presented in Tab. 37.3. The two-magnet bump will be implemented first with the possibility to install a 3-magnet bump later if needed. A new injection septum has to be built and the present kicker 28 must be upgraded to handle ion beams with 4.8 Tm beam rigidity (Tab. 37.4).

Table 37.3: PS injection dipole bump characteristics.

Dipole location in PS straight-sections	Dipole deflection angle	Maximum bump amplitude	Remarks
3-dipole bump in PS sections 21-25-29	1.8, -0.1, 1.7 mrad (max 86 Gm)	38 mm in straight section 25	no residual orbit, needs 3 power supplies
2-dipole bump in PS sections 22-30	2.1, 2.1 mrad (max 100 Gm)	32 mm in straight sections 25-27	about 2 mm residual closed orbit, needs 1 power supply

Table 37.4: PS injection septum and kicker characteristics.

Magnet type	Integrated magnetic field for 4.8 Tm lead ion injection	Foreseen maximum integrated magnetic field
Septum 26	0.247 Tm (51.5 mrad)	0.264 Tm
Kicker 28 with a 25 mm bump	330.4 Gm (6.9 mrad)	464.8 Gm (2×232.4)

37.2 NEW PULSED INJECTION SEPTUM

The LEIR extraction energy requires a new magnetic septum in the PS for the injection of the ions. The main parameters of the septum for a particle beam with a magnetic rigidity of $B_p = 4.8$ Tm are indicated in Tab. 37.5. The vacuum tank, the mechanical support structure, the vacuum equipment and the magnet displacement systems, together with their spare, are recovered from the “PE.SMH58” device (previously used for electron extraction in the PS ring) to reduce the cost. The spare has never been installed in the PS, and thus is not radioactive. These existing vacuum tanks are modified to contain the magnet and to fit into straight section 26. New magnets have been constructed and their design is based on the septa previously developed for the PSB to PS transfer line, keeping their cross section, but modifying the length to suit the present application. However, the modification of the existing vacuum vessel that has been installed in the PS ring from 1994 to early 2003 was done very carefully, because it is slightly radioactive. Modifications are required to ensure compatibility between the tank and the existing PS vacuum chamber.

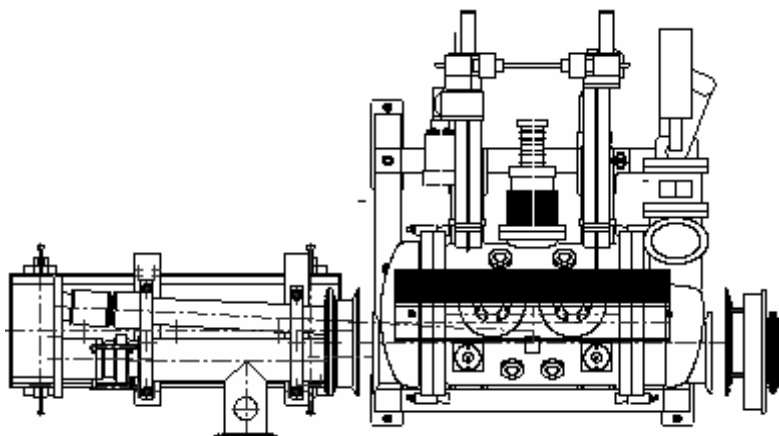


Figure 37.5: Layout of the PS straight-section 26 with the future ion injection septum

The connecting flange and flange aperture on the vacuum vessel will be increased, at least on the upstream side, to allow the injected beam to pass. In Fig. 37.5 the layout of the septum magnet and its vacuum vessel are illustrated. Experience with magnets of the same design has shown that the fringe field at the axis of the orbiting beam (approximately 50 mm from the septum) is below 0.15 % of the integrated gap field.

Table 37.5: Main parameters for PI.SMH26.

Deflection angle (maximum)	55 mrad
Integrated magnetic field (J _{Bdl})	0.264 Tm
Gap field	0.336 T
Gap height	60 mm
Gap width between conductors	102 mm
Length (physical)	850 mm
Length (magnetic)	785 mm
Septum thickness	5 mm
Number of conductor turns	1
Peak current	16 kA
Half sine pulse base width	3 ms
Magnet inductance	1.8 μ H
Magnet resistance	0.1 m Ω

The vacuum design relies on standard PS equipment, such as vacuum seals, vacuum pumps, and an under-vacuum bake out system. A vacuum in the low 10^{-9} mbar range is expected after a 5-day bake out period (of which 24 hours at 200 °C for the magnet core). The magnet is built as a modular plug-in unit, and can be exchanged for its spare within one day in the event of a failure. On the downstream side, space is available in the vacuum tank to insert a beam observation system (for example a scintillator screen). The mechanical displacement system will be recovered from the old “PE.SMH58” device. This system is of the same type as the standard systems used for septa in the PS Complex. This allows the magnet position to be adjusted with ± 10 mm with respect to the nominal position of 53 mm from the circulating beam. Also the septum angle can be adjusted from the nominal zero to 10 mrad angle with respect to the circulating beam.

The power converter (including the step-up transformer in the tunnel) for the new pulsed injection septum magnet is discussed in Sec. 35.8.

37.3 UPGRADED INJECTION KICKER AND BUMPERS

Table 37.6: PS KFA28 System – Principal parameters after upgrading for ions

HV modulator:	Generator impedance:	12.5 Ω
	PFN:	4 RG220, 50 Ω , ~220m cables in parallel
	Transmission:	4 RG220, 50 Ω , ~150m cables in parallel
	Main Switch:	E2V CX1573
	Dump Switch:	E2V CX1573
	Max. PFN voltage:	35 kV (positive)
	Max. load current:	2800 A
Magnet:	Type:	lumped inductance
	Aperture w×h:	159 mm×70 mm
	Aperture centre shift:	25 mm outside from circulating beam centre line
	Effective length:	954 mm
	Useful field region	$\pm 0.5\%$: w= ± 62 mm, h= ± 27 mm from centre
	Inductance:	2.9 μ H
Kick:	$\int B_{dl}$ max:	46.5 mTm
	$\int B_{dl}$ flat top uniformity:	$\pm 0.5\%$
	$\int B_{dl}$ post pulse ripple	$\pm 1\%$
	Deflection angle:	9.7 mrad
	Rise time (1-99 %):	1.1 μ s
	Fall time (99-1 %):	1.15 μ s
	Fall time (98-2 %):	940 ns
	Length (max):	$\sim 1 \mu$ s (variable)

The ion beam arriving from LEIR will be injected into the PS using the existing KFA28 kicker magnet. This is a lumped inductance single turn device using a window frame magnetic circuit, the bottom block of which is interrupted at the vertical median plane to reduce the inductive coupling between beams and magnet. The magnet is installed in the machine vacuum. It is connected to its high voltage generator via parallel strip lines within the vacuum tank and a coaxial vacuum feed-through at the tank wall. The magnet is short circuited at its other end inside the tank. This magnet was originally built for the antiproton beam extraction from PS to LEAR at $B_p = 2.0$ Tm [5]. Injection at $B_p = 4.8$ Tm requires an increase in the nominal integrated magnetic field to 330.4 Gm. This is possible as the ferrite magnetic circuit has sufficient cross section to avoid saturation, except in the magnet extremities where the effect is unimportant. The main data and performance of the PS ion injection kicker system are summarized in Tab. 37.6.

The increase in kick requires a new pulse generator. The proposed new system is shown in Fig. 37.6. The pulse-forming network (PFN) is charged to a maximum voltage of 35 kV and discharged by a thyratron switch into the magnet via a transmission line. A second thyratron switch is connected at the other end of the PFN to allow for pulse length adjustment.

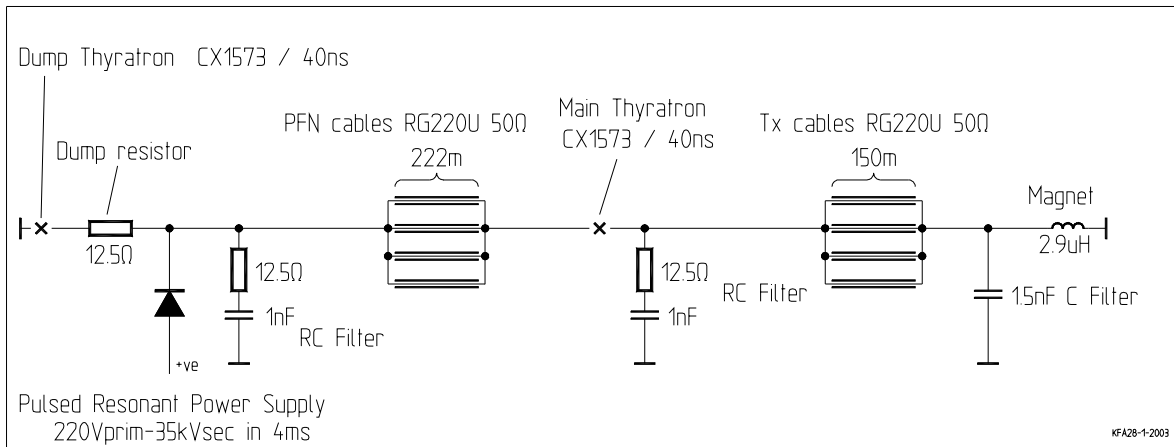


Figure 37.6: PS KFA28 system after upgrading for ions.

37.4 PS RF MANIPULATIONS FOR LEAD IONS

37.4.1 Overview

The role of the PS is to adapt the beam from LEIR according to a variety of constraints imposed by the downstream machines. Principally, the charge per bunch must be below the threshold for problems at injection in the SPS. But, in addition, it is the PS machine that imposes the bunch spacing required by LHC experiments, while the bunch length and repetition frequency at PS ejection must lie within the narrow ranges acceptable by the RF system of the SPS. The frequency window of the 200 MHz system of the SPS is shown in Fig. 37.7.

LHC experiments require that the bunch separation be some multiple of the 25 ns established for protons. If every m^{th} SPS bucket is filled, then m must be a multiple of 5. Consequently, previously published scenarios concentrate on $m = 25$ with acceleration on PS harmonic $h = 17$ and extraction close to transition ($\gamma_t = 6.1$) to obtain sufficiently short bunches. This is indicated by the point labeled "O" in Fig. 37.8. However, such schemes do not overcome the severe space charge problems at SPS injection so that a higher transfer energy and fewer charges per bunch are necessary. The point labeled "A" corresponds to the highest PS energy and also involves a factor of 5 in m . It may be reached by accelerating on $h = 21$, with $m = 20$ corresponding to a bunch spacing of 100 ns in the LHC. This spacing is preferable to 125 ns ($m = 25$) because the LHC bunch harmonic is then an integer, removing the need for turn-by-turn resynchronization by the experiments. Rebucketing from $h = 21$ to $h = 169$ using the PS 80 MHz cavities shifts the bunch repetition frequency within the scope of the SPS cavities (point "B"). Finally, bunch splitting from $h = 169$ to $h = 423$ using the PS 200 MHz cavities halves the number of charges per bunch and produces a beam ("C") that can be digested by the SPS. Of course, the resultant bunch pairs must be recombined at high energy in the SPS in order to re-establish both the 100 ns spacing and the intensity per bunch required for collisions in the LHC. In order to keep the total filling time reasonable, four bunch pairs are expected per PS cycle.

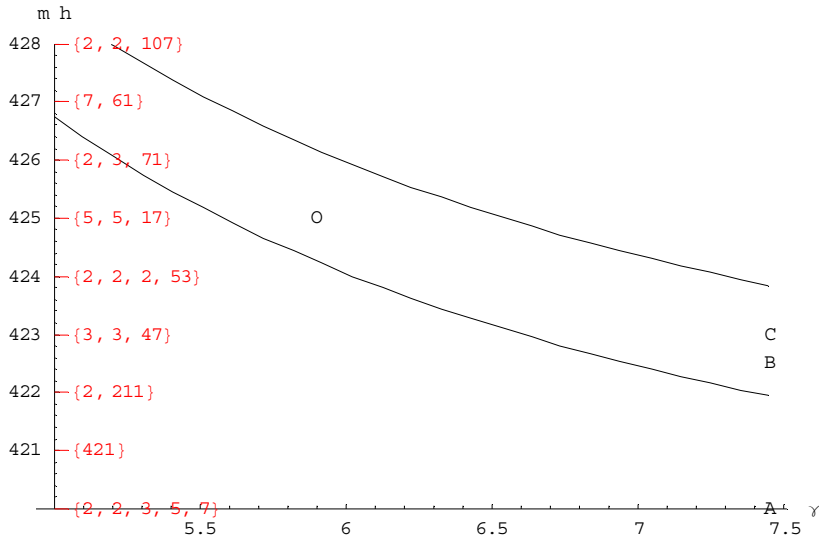


Figure 37.7: Upper and lower frequency limits of the SPS RF system as a function of relativistic factor γ for Pb^{54+} ions at PS extraction. The vertical scale gives the equivalent PS harmonic at 200 MHz and its prime factors.

37.4.2 Injection

The LEIR machine, operating on $h = 2$, delivers two bunches of lead ions to the PS at a magnetic rigidity of 4.8 Tm. This is just sufficient to allow the ferrite cavities of the PS to operate above their lower frequency limit (2.8 MHz) on $h = 16$ and hence for a bunch-to-bucket transfer between the two machines, whose size ratio is 8.

An injected bunch duration must not exceed 200 ns because a kicker gap of 150 ns between the two bunches at LEIR ejection is needed. A total (sum of all bunches) emittance of 0.1 eVs per nucleon allows a factor of 2 blow-up in the PS (Tab. 37.7). Under stationary transfer conditions, an RF voltage of 2.8 kV is then required in LEIR and is matched by 25 kV in the PS. Injecting into a moving bucket could also be considered in order to improve the energy reproducibility of the PS at transfer. Accelerating at a moderate 0.2 T/s, the bunches from LEIR could still be quite matched in the PS, but with insufficient longitudinal acceptance margin unless the LEIR RF voltage is raised to the 4 kV maximum available from one cavity. The shorter bunches imply 39 kV in the PS. At higher ramp rates, the spare LEIR cavity would have to be brought into operation.

37.4.3 Intermediate Energy Gymnastics

The beam is first accelerated on $h = 16$ to escape the space charge regime near injection ($\beta\gamma^2 = 0.43$). Then, on a magnetic plateau at around 22 Tm ($\beta\gamma^2 = 3.8$), the harmonic number is changed to 21 in a series of quasi-adiabatic steps while the number of bunches is doubled to four. The bunch spacing is initially increased during this “batch expansion” process, which is possible because the full circumference of the machine is not occupied.

The steps involved are harmonic number changes from $h = 16$ to $h = 14$ to $h = 12$ (each at 10 kV), then bunch splitting to $h = 24$ (at 15 kV) and, finally, to $h = 21$ (at 15 kV). All of this can be achieved in roughly 100 ms. The use of $h = 24$ means that the upper frequency limit (10.1 MHz) of the ferrite cavities precludes a higher intermediate energy.

37.4.4 Transition Crossing

A fast transition jump with a quasi-zero tune shift is a routine operation for proton beams in the PS to prevent particle loss and emittance growth triggered by instabilities. The elements in the ring comprise two “gamma jump cells”, each consisting of four quadrupole doublets separated into two families (the two central doublets of a cell together form a quadrupole triplet). Fig. 37.8 depicts the present layout [6].

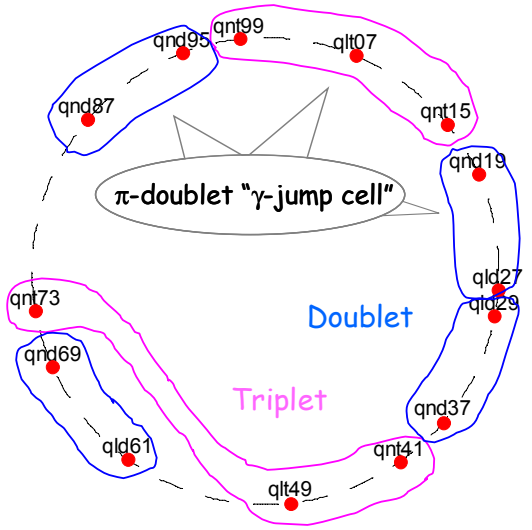


Figure 37.8: Quadrupole layout of the PS transition jump scheme.

At the ion intensities required for the LHC, neither longitudinal nor transverse microwave instabilities caused by the longitudinal broadband impedance are expected close to transition ($\gamma_t = 6.12$) [7]. Nevertheless, the transition jump system will still be used as a precautionary measure. Since the quadrupoles can only be powered with the currents used for protons, a gamma transition excursion of less than 0.1 is the maximum that can be achieved at the 72 Tm magnetic rigidity of lead ions at transition. A simulation of the transition jump process is shown in Fig. 37.9.

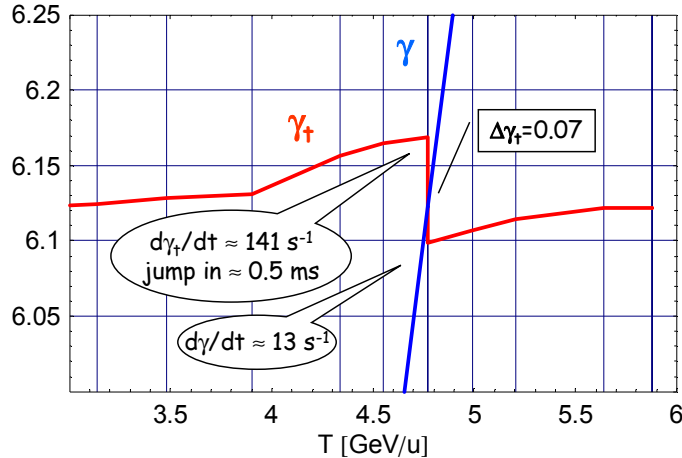


Figure 37.9: Relativistic γ versus kinetic energy for lead ions crossing transition in the PS ($\gamma=6.12$).

37.4.5 High-Energy Gymnastics

At top energy (86.7 Tm), the four bunches in consecutive $h = 21$ buckets are transferred from the ferrite cavity system (at 20 kV) to the fixed-frequency 80 MHz one (at 50 kV). In 80 MHz terms, there is a harmonic number change from $h = 168$ to $h = 169$ and the bunches are 8 buckets apart.

Optionally, if space charge proves problematic at injection in the SPS, the bunches could be split into pairs of consecutive buckets of the 200 MHz system (at 75 kV). In 200 MHz terms, there is a slight shift from $h = 422.5$ to $h = 423$, but this is insufficient to seriously bias the splitting equality. The final bunch pattern sees 5 ns between the ‘‘bunchlets’’ of each pair and 95 ns between the nearest neighbours of consecutive pairs. Note that $h = 21$ to 423 cannot be done in a single step because splitting requires that the ratio of harmonics be fairly close to 2.

The flat-top required for these manipulations is of the order of 125 ms, not including synchronisation with the SPS.

37.4.6 PS Longitudinal Parameters

Table 37.7: Summary of longitudinal beam characteristics at PS input and output.

Parameter at PS	Injection	Ejection 8 bunchlets	Ejection 4 bunches
Total number of ions	9×10^8	4.8×10^8	4.8×10^8
Number of bunches	2	4×2	4
Harmonic number	16	423	169
Total emittance [eVs per nucleon]	2×0.05	8×0.025	4×0.05
Bunch spacing [ns]	352	5+95	100
Bunch duration [ns]	202	3.9	3.9
RF voltage [kV]	25	75	75
RF frequency [MHz]	2.842	200	80
Dipole magnetic field [T]	0.0685	1.237	1.237
Equivalent proton momentum [GeV/c]	1.44	25.98	25.98

37.4.7 Early Lead Ion Operation Scheme

A simplified scheme has been proposed [8] for the first LHC ion run in which only one bunch of 2.25×10^8 ions in 0.025 eVs per nucleon is supplied to the PS by LEIR, which would operate on $h=1$ instead of $h=2$. The beam must be cooled to the same longitudinal density as before, but the lower intensity implies a shortening of the LEIR cycle from 3.6 to 2.4 s. The ramp rate at injection in the PS could be increased up to 0.6 Ts^{-1} without requiring the spare LEIR cavity. More significantly, no complicated RF gymnastics would have to be set up in the PS. Acceleration would take place uninterrupted on $h = 16$ and, after rebucketing at 80 MHz, a single bunch of 1.2×10^8 ions in 0.05 eVs per nucleon (again allowing a factor of 2 blow-up margin) would be extracted towards the SPS.

37.5 PS-SPS LINE STRIPPING WITH LOW-BETA INSERTION

The Pb^{54+} ion beams will be accelerated in the PS to 5.9 GeV/u (beam rigidity $B\beta = 86.7 \text{ Tm}$) and then ejected and fully stripped to Pb^{82+} ($B\beta = 57.1 \text{ Tm}$) in the TT2/TT10 transport channel between PS and SPS. This PS extraction energy, higher than the existing fixed target ion programme requires, has been chosen to avoid the limitations of space charge and of intra beam scattering at SPS injection. The implementation of a low- β insertion to minimise transverse emittance blow-up due to multiple Coulomb scattering in the stripping foil has been studied. In the presence of non-zero dispersion at the foil, the stripping process also leads to additional emittance increase due to energy straggling of the ions [9, 10]. The performance of the new low- β stripping insertion is compared to the current situation where the stripper is at a location with a relatively large betatron function and with the energy of 4.25 GeV/u instead of 5.9 GeV/u.

37.5.1 Emittance Budget of the LHC Lead Ion Beam

The transverse emittance budget of the ion beams to obtain the required luminosity for the lead experimental programme in the LHC is listed in Tab. 37.8.

Table 37.8: Normalized r.m.s emittance budget for the LHC ion and proton programmes and for the present operational beams.

MACHINE (at top energy)	Ions for LHC $\epsilon_{h,v}^* [\mu\text{m}]$	Protons for LHC $\epsilon_{h,v}^* [\mu\text{m}]$	Ions for SPS fixed target exp. $\epsilon_{h,v}^* [\mu\text{m}]$
LHC	1.5	3.75	-
SPS	1.2	3.5	4.0
PS	1.0	3.0	3.8
LEIR	0.7	-	-
BOOSTER	-	2.5	3.0

The PS emittance of $\epsilon_{h,v}^* = 1.0 \mu\text{m}$ (normalized r.m.s emittance $\epsilon_{h,v}^* = \beta\gamma\sigma_{h,v}^2/\beta_{h,v}$, where $\sigma_{h,v}$ is the standard deviation of the projected distribution), or $\epsilon_{h,v} = 0.18 \mu\text{m}$ (physical r.m.s), refers to the value at the end of the TT2 transfer line after the stripping process. Small emittances (about 1/4 to 1/3 of the present lead ion beam emittances) are required. Thus emittance preservation is of great importance.

37.5.2 Present Situation in TT2

In the fixed-target lead ion runs performed up to now the charge state of the ions is changed from 53+ to 82+ in TT2 at 4.25 GeV/u ($B_p = 66.7 \text{ Tm}$ for 53+) using a 0.8 mm thick aluminium stripping foil installed at about 302 m from the entrance of TT2. The betatron and dispersion functions of the entire TT2 transfer line for the present optics are shown in Fig. 37.10.

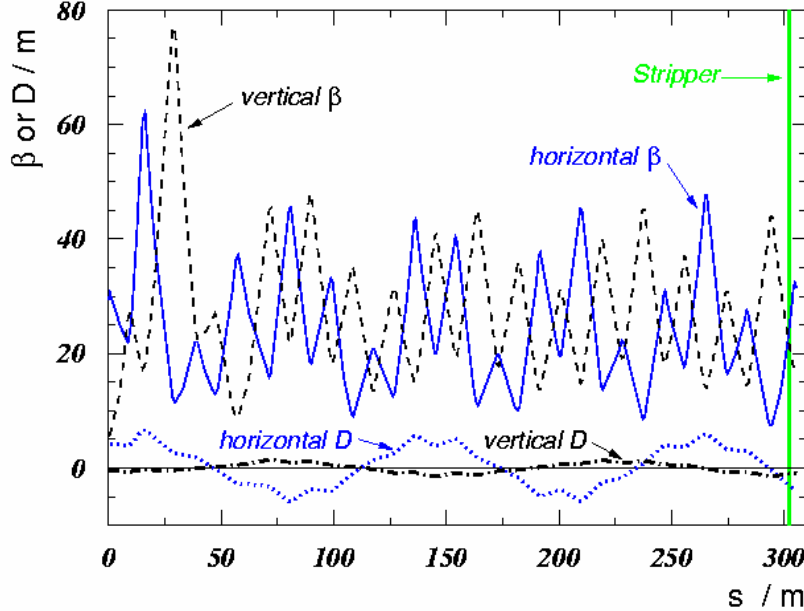


Figure 37.10: Horizontal and vertical betatron and dispersion functions of the present lead ion optics in TT2 transfer line (distance from entrance of TT2).

The quadrupole setting yielding the present optics has been kept in operation since the 1999 lead ion run following the 1998 matching campaign of the TT2/TT10 transfer line optics. A further re-matching was not retained because no conclusive result could be drawn from the measurements collected [11].

Measurements of the emittance growth due to stripping were performed in 1995 for a 0.8 mm thick aluminium foil. The measured transverse normalized r.m.s emittance increases at 4.25 GeV/u were about 0.59 to 0.77 μm [12] while calculations for this situation give about 0.42 to 0.45 μm (Tab. 37.11). While tolerable in the present fixed target runs ($\epsilon_{h,v}^* = 4 \mu\text{m}$ as shown in Tab. 37.8), this blow-up is unacceptable compared to the $\epsilon_{h,v}^* = 1.5 \mu\text{m}$ required at LHC collision energy.

37.5.3 The Proposed Low- β Insertion in TT2

A low- β insertion is proposed at about 70 m from the entrance of TT2, just before the beginning of the quadrupole string (families QDE210.S and QFO215.S). Detailed studies show that the existing quadrupoles are insufficient to match Twiss parameters and dispersion functions. To create the insertion, four quadrupoles are added and in addition the first two quadrupoles of the string have to be powered individually. Fig. 37.11 depicts betatron and dispersion functions of the proposed lead ion optics for the TT2 line. The optical functions at the new stripper (STRN) and at present stripper (STR373) are given in Tab. 37.9.

Since the optics parameters at TT2 entrance have been derived from measurements [11] they are subject to intrinsic uncertainties. However the proposed optics is flexible enough to guarantee stable conditions at the stripper for a reasonable range of initial parameters. Furthermore it has been shown that the emittance blow-up due to an imperfect re-matching of TT10 is small [10]. The betatron functions and therefore the emittance

blow-up due to multiple Coulomb scattering are reduced by about a factor five (Tab. 37.9) compared to the present optics.

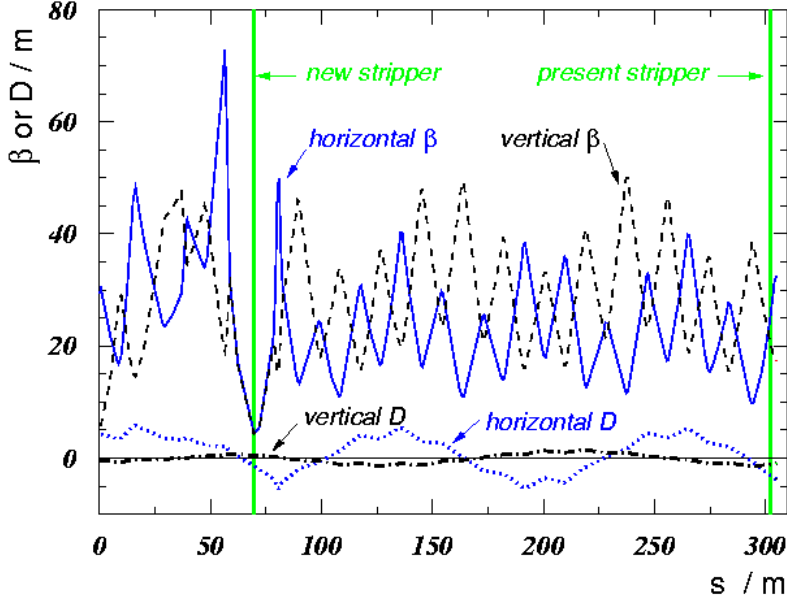


Figure 37.11: Betatron and dispersion functions of the new lead ion optics in the TT2 line with a low- β insertion (distance from entrance of TT2).

Table 37.9: Optical parameters at the present (STR273) and new stripper position (STRN)

Location	Horizontal				Vertical			
	β_h [m]	α_h	D_h [m]	D'_h	β_v [m]	α_v	D_v [m]	D'_v
Entry TT2	29.42	-2.51	4.13	0.41	5.71	0.29	-0.47	0.03
Present STR373	23.56	-1.70	-2.94	-0.34	22.05	1.12	-1.03	0.06
New STRN	4.92	-0.04	-1.33	-0.29	4.37	0.007	0.20	-0.08

Together with the increase of the PS extraction kinetic energy from 4.25 to 5.9 GeV/u the emittance growth due to the stripping process is reduced by roughly a factor six compared to the present optics. The impact of a thinner stripper foil (e.g. 0.5 instead of 0.8 mm) is shown in Tab. 37.10, the gain in emittance blow-up is about a factor two, at the expense of a drop in the stripping efficiency (96% to 83%) [12]. Thus, this is not an alternative to the low- β insertion.

Table 37.10: Scaling of normalized emittance blow up when stripping from Pb^{54+} to Pb^{82+} .

Kinetic energy	4.25 GeV/u	5.9 GeV/u	5.9 GeV/u
Stripper thickness d	0.8 mm	0.8 mm	0.5 mm
Emittance blow up ratio $\frac{d}{\beta^3 \gamma} \left/ \left(\frac{d}{\beta^3 \gamma} \right)_{at 4.25 \text{ GeV/u}} \right.$	1	0.745	0.466

The influence of the non-zero dispersion at the stripper may lead to an additional emittance contribution after filamentation due to coherent energy loss of the ions crossing the stripper. This effect can be avoided by adjusting the optics downstream of the stripper for the lower reference momentum. Finally, the energy spread introduced by the straggling process for the thick aluminium foil (0.8 mm) yields a relative momentum spread of only $\sigma_p/p \approx 4 \times 10^{-5}$ at 5.9 GeV/u and is negligible.

Tab. 37.11 shows the calculated emittance growth for the present and the proposed low- β optics (assuming fully stripped lead ions) and for the measured [12] and “scaled” low- β optics.

Table 37.11: Increase in normalized r.m.s emittances in the stripper foil (0.8 mm Al) for the present optics of lead ions (4.25 GeV/u) and new low- β optics (5.9 GeV/u).

Optics	$\Delta \varepsilon^*_h$ [mm]		$\Delta \varepsilon^*_v$ [mm]	
	Scattering	Straggling	Scattering	Straggling
Calculated present	0.447	0.003	0.418	0.0002
Calculated low- β	0.069	0.004	0.062	0.0003
	Scattering + straggling		Scattering + straggling	
Measured present	0.766		0.584	
“Scaled” low- β	0.119		0.086	

37.6 STRIPPING IN THE PS-SPS LINE: HARDWARE ASPECTS

37.6.1 Quadrupole Layout for the Present Situation

The quadrupoles used for the present optics with their characteristics are listed in Tab. 37.12. QDE210.S and QFO215.S denote a string made of two families of quadrupoles arranged as a FODO lattice, each family being powered by a single power supply. Families QDE210.S and QFO215.S comprise 14 and 13 quadrupoles, respectively. The first seven quadrupoles in TT2 are used for matching purpose.

Table 37.12: TT2 quadrupole characteristics for the present optics and low- β optics, ⁽¹⁾ indicates new quadrupoles, ⁽²⁾ new power supplies.

Quadrupole	Type	Present optics		Low- β optics		Comments
		Strength	Current	Strength	Current	
QF0105	-	7.26 T	345.7 A	10.72 T	510.4 A	
QDE120	QFL	-8.23 T	-160.4 A	-10.81 T	-208.1 A	
QFO135	QFL	7.91 T	154.2 A	7.46 T	145.0 A	
QDE150	QFL	-6.32 T	-123.1 A	-5.56 T	-108.2 A	
QNO01 ⁽¹⁾⁽²⁾	QFS			-3.18 T	-91.2 A	In stock
QFO165	QFL	5.85 T	114.1 A	9.32 T	181.0 A	
QDE180	QFL	-5.30 T	-103.3 A	-7.38 T	-143.5 A	
QFO205	QFL	5.80 T	113.1 A	20.81 T	422.9 A	
QNO02 ⁽¹⁾⁽²⁾	QFL			-19.48 T	389.7 A	In stock
New stripper						
QDE210 ⁽²⁾	QD	-6.02 T	-169.1 A	-0.40 T	-11.3 A	
QNO03 ⁽¹⁾⁽²⁾	QFS			-11.95 T	-347.5 A	In stock
<u>QFO215</u>	<u>QFS</u>	6.56 T	188.6 A	<u>20.36 T</u>	<u>Overflow</u>	<u>To be moved</u>
QFO215 ⁽²⁾	QFL			20.36 T	411.3 A	New: in stock
QNO04 ⁽¹⁾⁽²⁾	QFS			-7.82 T	-223.4 A	Old QFO215
QDE210.S	QD	-6.02 T	-169.1 A	-4.80 T	-134.7 A	
QFO215.S	QFS	6.56 T	188.6 A	5.37 T	153.5 A	
Present stripper						
QFO375	QFS	3.70 T	106.2 A	4.40 T	125.9 A	

37.6.2 Quadrupole Characteristics for the Low- β Insertion

The proposed layout for the low- β insertion with its characteristics is given in Tab. 37.12. The maximum strengths for the three types of quadrupoles proposed QFS ($L = 0.8$ m), QD ($L = 0.82$ m) and QFL ($L = 1.2$ m) are 15.64, 16.66 and 23.20 T, respectively. QFO215 (to be disconnected from family QFO215.S) will be

transferred to the QNO04 location where a lower gradient is required and replaced by a longer quadrupole. The characteristics of the six new power converters needed for TT2 are described in Sec. 36.4. The location of the new quadrupoles in TT2 is given in Tab. 37.13.

Table 37.13: TT2 new quadrupole positions (values refer to the quadrupole entry). The new stripper foil (STRN) will be located at 69.59 m from the entry of QF0105.

New quadrupole	QNO01	QNO02	QNO03	QNO04
Position from entry QF0105	37.00 m	58.52 m	78.29 m	81.75 m

The new magnetic structure and optics are shown in Fig. 37.12 which is a zoom into the first 90 m of TT2. The shaded elements represent the additional four quadrupoles required.

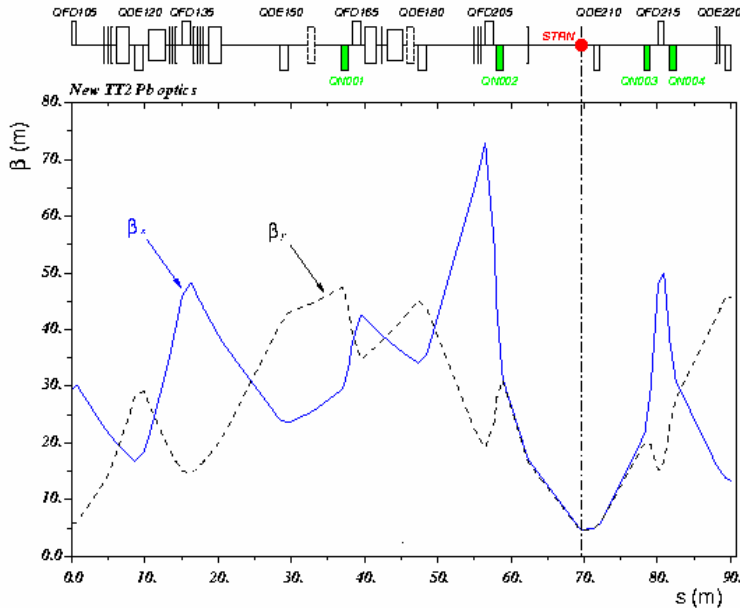


Figure 37.12: A zoom on the first 90 m of the TT2 line with the low- β insertion optics.

REFERENCES

- [1] M. Martini, *Injection of the lead ion beam for LHC into the PS*, PS/AE Note 2001-012, 2001.
- [2] R. Garoby, S. Hancock, *LHC Ion Bunch Generation in the PS*, Proc. CERN/PS/RF/Note 2002-10.
- [3] D. Cornuet, Z. Sharifullin, *Magnetic Measurements on the PS Magnet Unit U17 with Hall Probes*, AT/MA Note 92-23, 1992.
- [4] H.H. Umstätter, *Simple Formulas for Fringe Field of PS-Magnet*, PS/SM/Note 77-12, 1977.
- [5] D.C. Fiander, K.D. Metzmacher, D. Grier, *Simple proposal for a kicker for the fast extraction of antiprotons from SS 26*, PS/EI/Note 80-9.
- [6] T. Risselada, “Gamma transition jump schemes”, CERN 94-01, pp313–327 (1994).
- [7] A.W. Chao and M. Tigner (Editors), “Handbook for Accelerator Physics and Engineering”, pp281–283 (1999).
- [8] J. Poole (Editor), “Proceedings of the workshop on LHC performance – Chamonix XII”, pp11–12, CERN-AB-2003-008 ADM (2003).
- [9] L. Durieu, M. Martini, S. Maury, D. Möhl, A-S Müller, *A Low- β stripping insertion in the PS-SPS transfer line to limit emittance blow-up due to stripping of lead ions for LHC*, CERN-PS-2001-006 (AE).
- [10] M. Giovannozzi, M. Martini, A-S Müller, *A Low- β stripping insertion in the CERN PS to SPS transfer line for the LHC ion programme*, Proc. PAC’01, Chicago, June 2001, CERN-PS-2001-036 (AE).
- [11] G. Arduini et al., *Betatron and dispersion matching of the TT2/TT10 transfer line for the fixed target lead ion beam*, CERN PS/CA Note 99-009.
- [12] G. Arduini et al., *Lead ion beam emittance and transmission studies in the PS-SPS complex at CERN*, Proc. EPAC’96 Sitges, Spain, 1996.

CHAPTER 38

SPS

38.1 INJECTION

The SPS is the last link before the LHC in the ion injector chain. The LHC filling scheme, described in detail in Chap. 33, implies that each injected PS batch will have to stay a long time, up to 43.2 seconds, on the SPS front porch. This important feature will dictate the choice of the injection parameters [1, 2].

38.1.1 Choice of Injection Energy

In order to minimise the space-charge tune spread on the long injection plateau of the SPS, the highest possible injection energy has been chosen. It corresponds to the maximum PS ejection momentum, 26 GeV/c/charge before stripping, which for Pb⁵⁴⁺ lead ions yields a kinetic energy $K = 5.9 \text{ GeV/u}$ ($\gamma = 7.31$). After stripping in TT2 the beam rigidity drops to 17.1 GeV/c/charge, see Chap. 37.

The SPS injection kickers had originally been upgraded to accommodate for as short a rise time as 115 ns, for an energy $\gamma = 5.45$, fitting a batch spacing of 125 ns [3]. The higher injection energy of $\gamma = 7.31$ imposes a minimum rise time of 225 ns, which becomes the minimum spacing between PS batches.

The long injection plateau is also the reason of the bunch splitting into bunchlets in the PS as it allows the line density of the beam to be decreased, while preserving its transverse emittances, yielding a much longer longitudinal IBS growth time.

The beam parameters are summarised in Tab. 38.1. IBS calculations have been performed with the Windows version of MAD8 [4], using the Bjorken-Mtingwa formalism [5]

Table 38.1: Summary of injection parameters into the SPS

Momentum per charge	p/Q	17.10	GeV/c/charge
Kinetic energy per nucleon	K/A	5.87	GeV/u
Magnetic rigidity	Bp	57.03	T.m
Reduced energy	γ	7.31	
Reduced velocity	β	0.9906	
Revolution frequency	f_{rev}	42.968	kHz
Bunchlet ion intensity	N_I	6.0×10^7	Ions
Bunchlet charge intensity	N_Q	4.9×10^9	Charges
Longitudinal emittance per nucleon (2 r.m.s.)	ϵ_{\parallel}	0.025	eV.s/u
Bunchlet length (4 r.m.s.)	τ_b	4.0	ns
Relative momentum spread (2 r.m.s)	$\Delta p/p$	6.5×10^{-4}	
Transverse normalised r.m.s. emittance	$\epsilon_{H,V}$	1.0	μm
RF frequency ($h = 4620$, average)	f_{RF}	198.51	MHz
RF frequency ($h = 4653$, beam passage)	f_{RF}	199.93	MHz
RF voltage	V_{RF}	1.0	MV
Space charge detuning	ΔQ	0.041	
IBS longitudinal growth time	τ_{\parallel}	570	s
IBS horizontal growth time	τ_H	1450	s
IBS vertical growth time	τ_V	2260	s
Duration of injection plateau		43.2	s

38.1.2 Longitudinal Parameters

When filling the LHC, the SPS receives 8, 12 or 13 injections of 8 pairs of bunchlets. The separation between two pairs is 100 ns, while the bunchlets are 5 ns apart.

At injection, a bunch-to-bucket transfer using the existing 200 MHz travelling wave RF system is planned. The nominal longitudinal emittance of the injected bunchlets is 0.025 eVs/u. Below it is assumed that this

emittance increases to 0.04 eVs/u along the long flat bottom and during acceleration up to and across transition. The bunch spacing at injection, which corresponds to harmonic number 4653, can be accommodated in the SPS using the technique of fixed-frequency acceleration (see next section).

In the present baseline scheme the injection energy is increased to $\gamma = 7.31$ from the lower value $\gamma = 5.58$ [6] proposed in the previous scheme. This allows a larger emittance at injection for the same RF voltage, which is also advantageous for IBS growth rates. With 8 MV at 200 MHz the maximum possible emittance at injection is now 0.065 eVs/u. A limitation in emittance also comes from the front porch of the accelerating cycle, see next section.

A decrease in peak line density, which can be important for the transverse space charge tune shift can be provided by flattening the bunches using the existing fourth harmonic RF system in the SPS (800 MHz) in the so called bunch lengthening mode.

38.2 ACCELERATION AND RECOMBINATION OF BUNCHLETS

38.2.1 Acceleration

During acceleration the RF frequency for a constant harmonic number changes from 198.51 MHz to 200.39 MHz, while the tuning range of the 200 MHz TW cavities is only (199.5 - 200.4) MHz. The fact that the beam occupies only a part of the ring (6.6 out of 23.1 μ s) and that the cavity-amplifier rise-time is about 1 μ s allows one to use the technique of fixed frequency acceleration [7]. The idea is to use a non-integer harmonic number by pulsing the RF on at the cavity centre frequency during the beam passage and switching it off in the beam holes to correct the RF phase ready for the next beam passage in the cavities. The phase is adjusted by modulating the frequency via the VCO. At higher energies when the RF frequency is already inside the bandwidth of the cavities, this technique is replaced by normal fixed harmonic number acceleration.

This method has been successfully used for ion acceleration in the SPS fixed target programme since the first lead ion run in 1994 [8].

The length of the acceleration cycle is 10 s. The voltage programmes calculated for emittances of 0.025 eVs/u and 0.05 eVs/u with a filling factor in momentum of 0.95 are shown in Fig. 38.1. As usual the voltage amplitude is decreased during transition crossing ($\gamma_t = 22.8$) to improve transmission. On the flat top the 4 pairs of bunchlets must be recombined into 4 bunches before extraction to the LHC. With a 100 ns bunch spacing this can be done using the 100 MHz RF system installed in the SPS in the past for both p-pbar and lepton acceleration. The small frequency bandwidth (150 kHz) of these cavities limits their application for ions to fairly high energies and in practice to the flat top energy. Three cavities are available and each can provide 330 kV.

38.2.2 Flat Top

To avoid capture losses in the absence of a 200 MHz RF capture system in the LHC (at least in the early stages), the bunch length should be less than 2 ns for the bunch into bucket transfer provided by the main 400 MHz RF system in the LHC.

The corresponding longitudinal emittance at injection into the LHC should then be less than 1.0 eVs/charge or 0.4 eVs/u. The lower limit, 0.7 eVs/charge, is defined in Vol. I, Chap. 21 by the IBS growth rates on the flat bottom in the LHC. If the bunch emittance after all gymnastics is smaller than this low limit, additional controlled emittance blow-up should be planned. Experimental studies with proton beams have shown that the best results (required blow-up efficiency with a minimum loss of particles at the time of excitation) can be obtained using one of the following methods: resonant phase modulation of the 800 MHz voltage, or band-limited phase modulation of the main 200 MHz voltage [9]. In the following paragraphs, two possible schemes for bunchlet recombination which can provide a final bunch emittance in the range (0.24-0.36) eVs/u are considered.

Bunch rotation

In this scheme the voltage of the 100 MHz RF system is used to rotate the bunchlets in longitudinal phase space by 90°. This can be done using two or three cavities with the maximum available RF voltage. This bunch is then recaptured by the 200 MHz RF system. The voltage is increased to 8 MV to shorten the bunch

before extraction to the LHC. With two cavities, from simulations with ESME [10], the final emittance (95 % particles) is around 0.36 eVs/u and the rms bunch length is 0.46 ns. The final bunch distribution has two peaks. The time necessary for these manipulations is less than 150 ms.

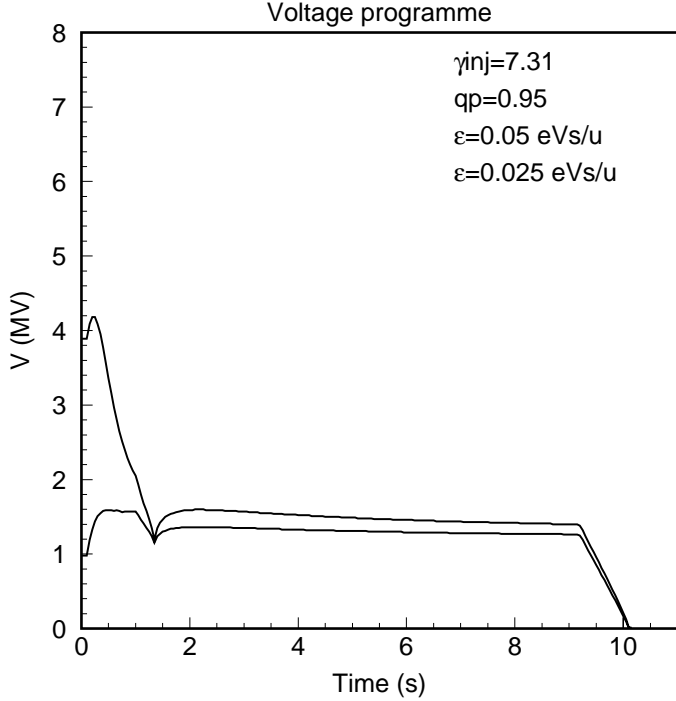


Figure 38.1: Voltage programmes during ion acceleration in the SPS for emittances of 0.025 eVs/u (lower curve) and 0.05 eVs/u (upper curve) with filling factor in momentum of 0.95.

Adiabatic process

In this scheme the voltage of the 200 MHz RF system, used for acceleration, is adiabatically reduced on the flat top to zero or some small amplitude (see below) while the voltage of the 100 MHz is increased to a value sufficient to provide capture of the bunchlet pair with the given initial emittances. The total time necessary for bunch recombination is much longer than for bunch rotation and is around 1.5 s. If no intensity effects are taken into account the total emittance increase in this scheme is very small.

For the LHC beam in the SPS, top energy is known to be the most critical area for beam stability [11] (this has been observed in measurements with proton beams). Even for the relatively low intensity of the LHC ion beam, the impedance of the 200 MHz RF system in the absence of a cavity servo-control system (the RF feedback and feed-forward being switched off) is sufficient to drive the beam unstable leading to rebunching at 200 MHz and some uncontrolled emittance blow-up. This is why in this (adiabatic) scheme it will be necessary to have some controlled emittance blow-up before recombination and to keep the cavity servo-control of the 200 MHz RF system on with some small residual voltage amplitude (for example 100 kV). Starting with an emittance of 0.1 eVs/u per bunchlet (after the controlled emittance blow-up), one gets 0.22 eVs/u for the final bunch emittance (for 95 % of particles). One 100 MHz cavity with 0.33 MV is sufficient. The RF gymnastics for both methods are shown schematically in Fig. 38.2.

38.2.3 The 100 MHz RF System

The 100 MHz RF system was dismantled and removed from the machine following the end of LEP operation as part of the SPS impedance reduction programme and should now be re-installed in the ring. Three 100 MHz RF cavities exist together with the 20 kW final RF amplifiers. All other equipment (infrastructure) should be rebuilt. Each cavity has an $R/Q = 230 \Omega$ and an undamped $Q = 28000$. The damping loops give a reduction in impedance of 40 dB on the fundamental frequency. Beam loading is not

important for ion intensities. However to be sure that the fundamental and HOM impedances will not create problems for the high intensity LHC proton beam it is planned to install two non-active cavities in the ring already during the 2003/2004 shutdown for tests. Estimations show that the HOM couplers should be able to cope with the power induced by the high intensity LHC proton beam without additional hardware modifications.

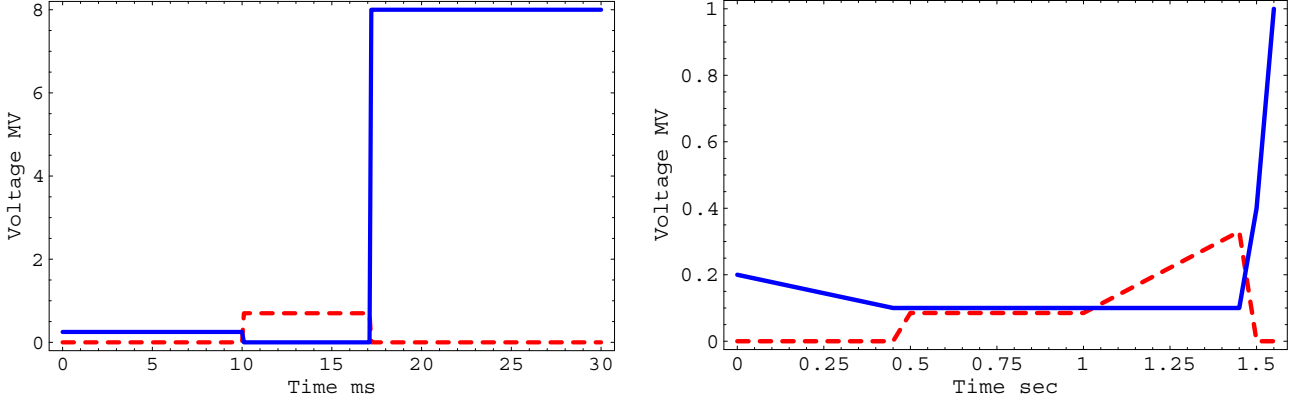


Figure 38.2: Voltage programmes for the 100 MHz (dashed line) and 200 MHz (solid line) RF systems during bunchlet recombination on the flat top for the two schemes: bunch rotation (left) and adiabatic process (right).

38.2.4 Synchronisation

Bunch into bucket transfer was not used in the past for ion injection into the SPS and some new electronics must be built for this purpose to provide synchronisation with the PS [12]. The problem is the same as for acceleration and is connected with the fact, discussed above, that the RF frequency corresponding to the bunch spacing must lie within the 200 MHz cavity bandwidth. Thus, to capture the injected beam, the cavity RF frequency should be locked to the injection frequency while the mean RF frequency is locked to the revolution frequency. For extraction to the correct position in the LHC the beam should be in the right place in the SPS. The time it takes to position the batch in the SPS including fine synchronisation (centring the bunch accurately in the bucket) is about 300 ms. This time can be reduced to 50 ms, in the same way as for LHC protons [13], if the PS batch is injected into the SPS in the position predicted to give the correct position on the flat top. This assumes sufficient reproducibility of the B-field.

38.2.5 Parameters for the Ejected Beam

Taking into account 20 % transverse emittance blow-up and 25 % beam losses, the parameters for the ejected beam are listed in Tab. 38.2 below.

Table 38.2: Parameters of the ejected beam

Bunch ion intensity	N_I	9.0×10^7	Ions
Bunch charge intensity	N_Q	7.4×10^9	Charges
Longitudinal emittance per nucleon (2 r.m.s.)	ϵ_{\parallel}	0.28	eV.s/u
Bunch length (4 r.m.s.)	τ_b	1.8	ns
Relative momentum spread (2 r.m.s)	$\Delta p/p$	6.3×10^{-4}	
Transverse normalised r.m.s. emittance	$\epsilon_{H,V}$	1.2	μm
Momentum per charge	p/Q	449.85	GeV/c/charge
Kinetic energy per nucleon	K/A	176.4	GeV/u
Magnetic rigidity	Bp	1500.3	T.m
Reduced energy	γ	190.4	
Revolution frequency	f_{rev}	43.375	kHz
RF frequency ($h = 4620$)	f_{RF}	200.39	MHz
RF voltage	V_{RF}	7.0	MV

38.3 OTHER ISSUES

38.3.1 Instrumentation

The SPS instrumentation is up-to-date to measure the ion beams needed for the LHC as it is already now able to measure the lower intensity fixed target indium or lead ion beams. This is in particular true for the orbit measurement systems, beam current transformer and transverse damper [14].

38.3.2 Early Phase Scheme

The early lead ion scheme introduced in 33.1 implies a modification of the parameters for the injection plateau of the SPS. This plateau is now shortened down to 7.2 seconds and one can relax the constraints on the IBS growth times and on the space charge detuning. Although the conservative value of 0.07, dating from the p-pbar era, had originally been retained for the maximum allowed value of the space-charge detuning [15], recent machine developments indicate that much higher values, over 0.15, can be tolerated [16].

Tab. 38.3 gives a list of the injection parameters for the early phase scheme, respectively with a longitudinal emittance of 0.025 and 0.05 eVs/u. Since the longitudinal parameters are unchanged, the discussions on acceleration, flat top and synchronisation presented in section 38.2 above stay valid. The simplification of the early phase scheme in the SPS is the absence of bunchlet merging.

Table 38.3: Injection parameters into the SPS for the early phase scheme

Bunch ion intensity	N_I	1.2×10^8		Ions
Bunch charge intensity	N_Q	9.8×10^9		Charges
Longitudinal emittance per nucleon (2 r.m.s.)	ϵ_{\parallel}	0.025	0.05	eV.s/u
RF voltage	V_{RF}	1.0	4.0	MV
Bunch length (4 r.m.s.)	τ_b	4.0		ns
Relative momentum spread (2 r.m.s)	$\Delta p/p$	6.5×10^{-4}	1.3×10^{-3}	
Transverse normalised r.m.s. emittance	$\epsilon_{H,V}^*$	1.0		μm
Space charge detuning	ΔQ	0.081		
Number of bunches per PS cycle		1		
Number of PS injections per SPS cycle		3-4		
Bunch spacing		1.35		μs
IBS longitudinal growth time	τ_{\parallel}	285	-880 (damping)	s
IBS horizontal growth time	τ_H	725	290	s
IBS vertical growth time	τ_V	1130	290	s
Duration of injection plateau		7.2		s

REFERENCES

- [1] L. Vos, Considerations about Pb ions at injection plateau of the SPS, Beam Physics Note 60, august 8, 2001
- [2] D. Manglunki, Status of what has been and what has to be done on SPS, Proc. of the Workshop on LHC performance, Chamonix XII, CERN-AB-2003-008 ADM, 2003.
- [3] J. Uythoven, The New SPS Injection Channel, Proc. of the Workshop on LEP-SPS performance, Chamonix IX, CERN-SL-99-007 DI, 1999.
- [4] <http://cern.ch/mad/mad8onWindows.html>
- [5] J.D. Bjorken and S.K. Mtingwa, Intrabeam Scattering, FERMILAB-Pub-82/47-THY, July 1982.
- [6] P. Collier (ed), The SPS as Injector for LHC. Conceptual Design. CERN-SL-97-07 DI, 1997.
- [7] D. Boussard, J. M. Brennan, T. P. R. Linnecar, Fixed frequency acceleration in the SPS, CERN SPS/89-49 (ARF), 1989.
- [8] D. Boussard, T. Bohl, T. Linnecar, U. Werhle, Non integer harmonic number acceleration of lead ions in the CERN SPS, PAC95, Dallas, 1995 and CERN SL-95-022.
- [9] T. Bohl, T. Linnecar, J. Tuckmantel, E. Shaposhnikova Controlled longitudinal emittance blow-up in the SPS as injector and LHC test-bed, CERN AB-Note-03-084 MD
- [10] J. MacLachlan, code ESME, <http://www-ap.fnal.gov/ESME>.
- [11] E. Shaposhnikova, LHC beams in the SPS: longitudinal plane, Proc. of the Workshop on LHC performance, Chamonix XII, CERN-AB-2003-008 ADM, p. 44, 2003.
- [12] T. Linnecar, SPS RF hardware, I-LHC/LEIR Review, 26-28 March 2003, CERN.
- [13] P. Baudrenghien, Beam control for protons and ions, Proc. of the Workshop on LEP-SPS performance, Chamonix IX, CERN-SL-99-007 DI, p. 116, 1999. Synchronisation of the SPS beam with LHC
- [14] G. Arduini, private communication
- [15] P. Collier, LHC ions in the SPS, 20th LCC meeting, http://cern.ch/lhcp/LCC/LCC_2002-05.html#main2c
- [16] H. Burkhardt, G. Rumolo, F. Zimmermann, Investigation of Space Charge Effects in the SPS, Proc. Particle Accelerator Conference PAC'2003, 12-16 May 2003, Portland, Oregon, USA.